RECENT ADVANCES IN ELECTRORECEPTION AND ELECTROGENERATION

EDITED BY: Maurice Chacron and Michael R. Markham

PUBLISHED IN: Frontiers in Integrative Neuroscience and Frontiers in Neural Circuits

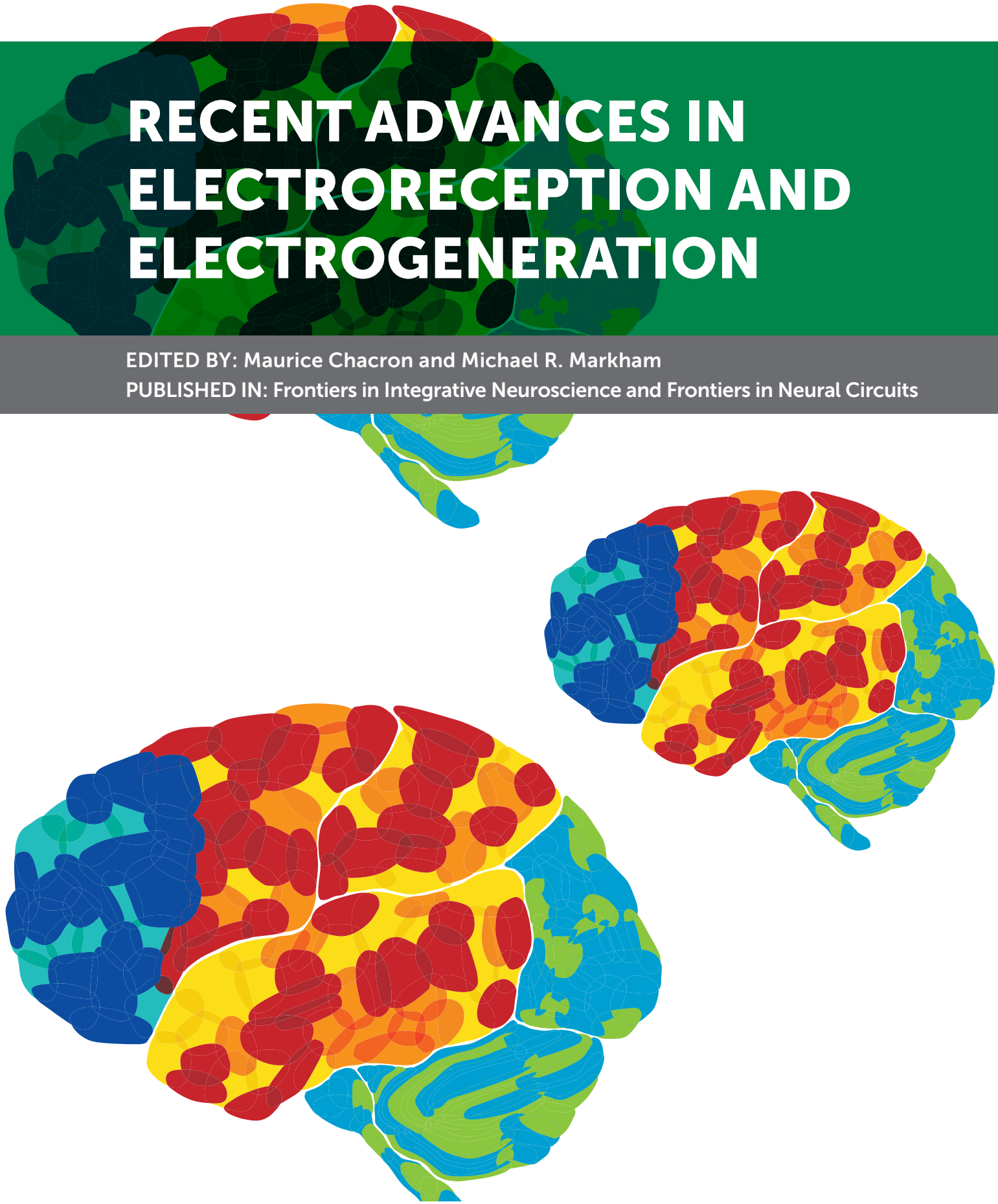

frontiers Research Topics

ISSN 1664-8714
ISBN 978-2-88966-732-1
DOI 10.3389/978-2-88966-732-1

About Frontiers

Frontiers is more than just an open-access publisher of scholarly articles: it is a pioneering approach to the world of academia, radically improving the way scholarly research is managed. The grand vision of Frontiers is a world where all people have an equal opportunity to seek, share and generate knowledge. Frontiers provides immediate and permanent online open access to all its publications, but this alone is not enough to realize our grand goals.

Frontiers Journal Series

The Frontiers Journal Series is a multi-tier and interdisciplinary set of open-access, online journals, promising a paradigm shift from the current review, selection and dissemination processes in academic publishing. All Frontiers journals are driven by researchers for researchers; therefore, they constitute a service to the scholarly community. At the same time, the Frontiers Journal Series operates on a revolutionary invention, the tiered publishing system, initially addressing specific communities of scholars, and gradually climbing up to broader public understanding, thus serving the interests of the lay society, too.

Dedication to Quality

Each Frontiers article is a landmark of the highest quality, thanks to genuinely collaborative interactions between authors and review editors, who include some of the world's best academicians. Research must be certified by peers before entering a stream of knowledge that may eventually reach the public - and shape society; therefore, Frontiers only applies the most rigorous and unbiased reviews.
Frontiers revolutionizes research publishing by freely delivering the most outstanding research, evaluated with no bias from both the academic and social point of view. By applying the most advanced information technologies, Frontiers is catapulting scholarly publishing into a new generation.

What are Frontiers Research Topics?

Frontiers Research Topics are very popular trademarks of the Frontiers Journals Series: they are collections of at least ten articles, all centered on a particular subject. With their unique mix of varied contributions from Original Research to Review Articles, Frontiers Research Topics unify the most influential researchers, the latest key findings and historical advances in a hot research area! Find out more on how to host your own Frontiers Research Topic or contribute to one as an author by contacting the Frontiers Editorial Office: frontiersin.org/about/contact

RECENT ADVANCES IN ELECTRORECEPTION AND ELECTROGENERATION

Topic Editors:
Maurice Chacron, McGill University, Canada
Michael R. Markham, University of Oklahoma, United States

Citation: Chacron, M., Markham, M. R., eds. (2021). Recent Advances in Electroreception and Electrogeneration. Lausanne: Frontiers Media SA.
doi: 10.3389/978-2-88966-732-1

Table of Contents

frontiers in Integrative Neuroscience

EDITORIAL
published: 11 March 2021
doi: 10.3389/fnint.2021.668677

Editorial: Recent Advances in Electroreception and Electrogeneration

Maurice J. Chacron[1]* *and Michael R. Markham*[2]

[1] Department of Physiology, McGill University, Montreal, QC, Canada, [2] Department of Biology, University of Oklahoma, Norman, OK, United States

Keywords: neuroscience, weakly electric fishes, neuroethology, electrogeneration, electroreception

Editorial on the Research Topic

Recent Advances in Electroreception and Electrogeneration

The study of fish that generate electric fields around their bodies in order to interact with their environment continues to generate intense interest in the research community. While it has been known since ancient times that some fish can generate electricity (Gaillard, 1923), the fact that some of these animals use the resulting electric field to detect objects and communicate with conspecifics has been discovered far more recently (Lismann and Machin, 1958; Lissmann, 1958). These animals have led to key discoveries in cholinergic transmission as well as the development of modern electrophysiology (Wu, 1984). Today, studies of electric fishes continue to generate important discoveries. This issue contains 11 articles (3 review and 8 original research) that highlight the diversity of recent research progress using electric fishes that range from studying the effects of changes in hormonal levels and the natural environment on electrosensory behaviors, to understanding how the brains of electric fishes process natural stimuli. This issue not only reviews the contributions that studies of electric fish have made toward understanding key problems in sensory processing (e.g., how does the brain distinguish sensory input that is self vs. externally-generated; Heiligenberg, 1991), but also provides novel functions for some of behavioral responses displayed by electric fishes such as natural electrocommunication stimuli as well as the jamming avoidance response that has been studied for over 40 years (Heiligenberg, 1991; Zakon et al., 2002).

Fukutomi and Carlson provide a very nice historical review of the contribution of mormyrid weakly electric fish toward understanding the function of the corollary discharge in distinguishing the sensory consequences of self vs. externally generated stimuli. This is a general problem that every animal must solve in order to successfully interact with its environment and common mechanisms have emerged across species (Cullen, 2004). It has furthermore become clear that the brain is not a simple input-output device but that the brain's internal state strongly influences perception and behavior (Hurley et al., 2004). Toward that end, Marquez and Chacron investigate the effects of serotonergic neuromodulation on sensory processing.

In general, processing of sensory input by the brain is achieved through a combination of neural circuits as well as ion channels embedded in the cell membrane. Toward the former end, Hofmann and Chacron review recent findings on the role of descending pathways from higher brain areas to more peripheral ones, which are found ubiquitously in the CNS of vertebrates (Cajal, 1909), on actually generating neural responses to sensory input. Toward the latter end, Motipally et al. investigate the expression of sodium channels across parallel sensory maps, with functional implications for differential coding of behaviorally relevant stimulus features by bursts (i.e., packets of action potentials followed by quiescence). Such bursts have been shown to reliably encode

OPEN ACCESS

Edited and reviewed by:
Elizabeth B. Torres, Rutgers, The State University of New Jersey, United States

***Correspondence:**
Maurice J. Chacron
maurice.chacron@mcgill.ca

Received: *16 February 2021*
Accepted: *19 February 2021*
Published: *11 March 2021*

Citation:
Chacron MJ and Markham MR (2021) Editorial: Recent Advances in Electroreception and Electrogeneration. Front. Integr. Neurosci. 15:668677. doi: 10.3389/fnint.2021.668677

electro-communication stimuli that occur during agonistic encounters (Marsat et al., 2009). Metzen provides a review of how natural electrocommunication stimuli are processed across successive brain areas in order to give rise to perception and behavioral responses. Interestingly, Field et al. suggest an important new function for natural electro-communication stimuli toward actually avoiding the deleterious effects of jamming stimuli, a function that was previously thought to be carried out by the jamming avoidance response. Specifically, when two fish are located within close proximity of one another, interference between their electric fields can create a jamming signal that interferes with the animal's ability to electrolocate other relevant stimuli such as prey or object boundaries (Ramcharitar et al., 2005). The animal solves this problem by changing its EOD characteristics in order to increase the frequency content of the jamming signal away from that of other electrosensory stimuli that it must detect (Heiligenberg, 1991). This so-called "classical function" of the jamming avoidance response is also being questioned by Fortune et al. in their investigation of how evolutionary loss of vision affects electroreception in different species of glass knifefishes and, in particular, demonstrate lack of jamming avoidance responses despite social conditions that would normally trigger such behavior based on previous studies.

Interestingly, Fortune et al. also demonstrate that blind electric fish display more territoriality and dominance than their seeing cousins. Raab et al. provide some critical field data as to dominance and exploration behavior. Such field data will no doubt be key toward guiding future studies as to how these animals actively acquire information about their environments in natural settings. A study by Yu et al. investigates how an important aspect of electrosensory stimuli experienced by electric fish during social interactions, namely contrast, strongly depends on the relative distance and orientation between animals. In particular, Yu et al. reveal that contrast routinely reaches much higher values than are typically used in laboratory settings (see e.g., Marsat et al., 2009). An important aspect of electrosensory research is that laboratory studies of sensory processing have often focused on recording from immobilized animals. Future studies are needed where recordings are instead obtained from freely moving animals in order to better mimic natural conditions where animals actively sense their environment (Schroeder et al., 2010). Such approaches have recently been applied to record neural activity from forebrain in weakly electric fish (Fotowat et al., 2019) and are becoming increasingly common in aquatic species (Cohen et al., 2019).

In addition to research on the sensory processing of electric signals during social encounters, it is also critical to investigate the central networks and peripheral mechanisms that regulate electric signaling in social contexts to fully understand the social communication functions of electric signals. Toward this end, Pouso et al. report, for the first time in electric fish, that distinct classes of vasotocin neurons within the pre-optic area are preferentially activated by social stimuli in courting males, and that these changes are associated with the production of electric courtship signals as well as locomotor activity related to courtship.

Finally, it is important to remember that the most widely recognized electric fish, the Electric Eel, not only uses weak electric fields to sense the environment but also uses strong electric fields as a weapon to stun and capture prey. Catania reviews recent advances showing how electric eels adapt the characteristics of their strongly electric fields for different behavioral contexts ranging from stunning prey to self-defense. Interestingly, electric eels also use their strong electric field to actually track prey, which was until recently thought to be achieved exclusively through the weak electric field.

Taken together, the manuscripts in this collection help to illustrate the many historical advances and current progress that research with electric fish contributes to neuroethology and integrative neurobiology. This collection also serves to highlight the vast range of unresolved questions yet to be experimentally addressed.

AUTHOR CONTRIBUTIONS

MC and MM wrote the manuscript. All authors contributed to the article and approved the submitted version.

REFERENCES

Cajal, R. S. (1909). *Histologie du système nerveux de l'Homme et des vertébrés.* Paris: Maloine.

Cohen, L., Vinepinsky, E., and Segev, R. (2019). Wireless electrophysiological recording of neurons by movable tetrodes in freely swimming fish. *J. Vis. Exp*. 153. doi: 10.3791/60524

Cullen, K. E. (2004). Sensory signals during active versus passive movement. *Curr. Opin. Neurobiol.* 14, 698–706. doi: 10.1016/j.conb.2004.10.002

Fotowat, H., Lee, C., Jun, J. J., and Maler, L. (2019). Neural activity in a hippocampus-like region of the teleost pallium is associated with active sensing and navigation. *Elife* 8:e44119. doi: 10.7554/eLife.44119

Gaillard, M. C. (1923). "Faune Égyptienne Antique. Recherches sur les poissons représentés dans quelques tombeaux égyptiens de l'Ancien Empire," in *Memoires de l'Institut Français d'Archéologie Orientale*, eds V. Loret and C. Kuentz (Cairo: Imprimerie de l'Institut Français d'Archéologie Orientale), 75–78.

Heiligenberg, W. (1991). *Neural Nets in Electric Fish.* Cambridge, MA: MIT Press.

Hurley, L. M., Devilbiss, D. M., and Waterhouse, B. D. (2004). A matter of focus: monoaminergic modulation of stimulus coding in mammalian sensory networks. *Curr. Opin. Neurobiol.* 14, 488–495. doi: 10.1016/j.conb.2004.06.007

Lismann, H. W., and Machin, K. E. (1958). The mechanism of object location in *Gymnarchus niloticus* and similar fish. *J. Exp. Biol.* 35, 451–486.

Lissmann, H. W. (1958). On the function and evolution of electric organs in fish. *J. Exp. Biol.* 35, 156–191.

Marsat, G., Proville, R. D., and Maler, L. (2009). Transient signals trigger synchronous bursts in an identified population of neurons. *J. Neurophysiol.* 102, 714–723. doi: 10.1152/jn.91366.2008

Ramcharitar, J. U., Tan, E. W., and Fortune, E. S. (2005). Effects of global electrosensory signals on motion processing in the midbrain of Eigenmannia. *J. Comp. Physiol. A Sens. Neural Behav. Physiol.* 191, 865–872. doi: 10.1007/s00359-005-0008-2

Schroeder, C. E., Wilson, D. A., Radman, T., Scharfman, H., and Lakatos, P. (2010). Dynamics of active sensing and perceptual selection.

Curr. Opin. Neurobiol. 20, 172–176. doi: 10.1016/j.conb.2010.02.010

Wu, C. H. (1984). Electric Fish and the discovery of animal electricity: the mystery of the electric fish motivated research into electricity and was instrumental in the emergence of electrophysiology. *Am. Sci.* 72, 598–607.

Zakon, H., Oestreich, J., Tallarovic, S., and Triefenbach, F. (2002). EOD modulations of brown ghost electric fish: JARs, chirps, rises, and dips. *J. Physiol. Paris* 96, 451–458. doi: 10.1016/S0928-4257(03)00012-3

Conflict of Interest: The authors declare that the research was conducted in the absence of any commercial or financial relationships that could be construed as a potential conflict of interest.

frontiers in Neural Circuits

ORIGINAL RESEARCH
published: 04 June 2019
doi: 10.3389/fncir.2019.00041

Differences in Sodium Channel Densities in the Apical Dendrites of Pyramidal Cells of the Electrosensory Lateral Line Lobe

*Sree I. Motipally, Kathryne M. Allen, Daniel K. Williamson and Gary Marsat**

Department of Biology, West Virginia University, Morgantown, WV, United States

Heterogeneity of neural properties within a given neural class is ubiquitous in the nervous system and permits different sub-classes of neurons to specialize for specific purposes. This principle has been thoroughly investigated in the hindbrain of the weakly electric fish *A. leptorhynchus* in the primary electrosensory area, the Electrosensory Lateral Line lobe (ELL). The pyramidal cells (PCs) that receive inputs from tuberous electroreceptors are organized in three maps in distinct segments of the ELL. The properties of these cells vary greatly across maps due to differences in connectivity, receptor expression, and ion channel composition. These cells are a seminal example of bursting neurons and their bursting dynamic relies on the presence of voltage-gated Na^+ channels in the extensive apical dendrites of the superficial PCs. Other ion channels can affect burst generation and their expression varies across ELL neurons and segments. For example, SK channels cause hyperpolarizing after-potentials decreasing the likelihood of bursting, yet bursting propensity is similar across segments. We question whether the depolarizing mechanism that generates the bursts presents quantitative differences across segments that could counterbalance other differences having the opposite effect. Although their presence and role are established, the distribution and density of the apical dendrites' Na^+ channels have not been quantified and compared across ELL maps. Therefore, we test the hypothesis that Na^+ channel density varies across segment by quantifying their distribution in the apical dendrites of immunolabeled ELL sections. We found the Na^+ channels to be two-fold denser in the lateral segment (LS) than in the centro-medial segment (CMS), the centro-lateral segment (CLS) being intermediate. Our results imply that this differential expression of voltage-gated Na^+ channels could counterbalance or interact with other aspects of neuronal physiology that vary across segments (e.g., SK channels). We argue that burst coding of sensory signals, and the way the network regulates bursting, should be influenced by these variations in Na^+ channel density.

Keywords: sodium channels, bursting, weakly electric fish, feature detection, apical dendrites, backpropagation

OPEN ACCESS

Edited by:
Maurice Chacron, McGill University, Canada

Reviewed by:
Leonard Maler, University of Ottawa, Canada
Harold H. Zakon, University of Texas at Austin, United States

***Correspondence:**
Gary Marsat
gary.marsat@mail.wvu.edu

Received: *28 March 2019*
Accepted: *20 May 2019*
Published: *04 June 2019*

Citation:
Motipally SI, Allen KM, Williamson DK and Marsat G (2019) Differences in Sodium Channel Densities in the Apical Dendrites of Pyramidal Cells of the Electrosensory Lateral Line Lobe. Front. Neural Circuits 13:41. doi: 10.3389/fncir.2019.00041

INTRODUCTION

Neurons possess a variety of ion channels and membrane proteins that shape their response properties, from the classical Na^+ and K^+ ion channels generating action potentials to G-protein coupled receptors (e.g., Prešern et al., 2015; Duménieu et al., 2017; Lizbinski et al., 2018). Heterogeneity in neuronal physiology can be understood through two complementary principles. One perspective stresses that a given neural output can result from various composition of channels and receptors. This principle was most obviously demonstrated in the stomatogastric ganglion of crabs, where an identical motor output pattern could be generated using networks which neurons differed widely in their channel composition (Prinz et al., 2004). This work highlighted that a change in one element of the neuron's physiology can be compensated by changes in another element.

The complementary, but non-exclusive, principle is also a basic concept in neuroscience. This principle argues that changes in membrane proteins (e.g., voltage gated ions channels) are necessary for specialization of neurons, and result in different neural outputs (Hille, 2001). An example of this principle, central to the subject of our study, comes from neurons that possess specific ionic conductances responsible for generating burst firing (Krahe and Gabbiani, 2004). The neuron's bursting dynamic could not be possible without these specific ion channels and thus their role in neural coding is changed by this bursting dynamic.

Bursting is observed in various sensory systems and typically fulfills the same function: signaling the occurrence of specific spatio-temporal patterns of inputs (Gabbiani et al., 1996; Kepecs et al., 2002). In the visual system, bursts signal edges and sharp contrasts (Lesica and Stanley, 2004), in the cricket auditory system they signal salient ultrasound pulses typical of insectivorous bats (Marsat and Pollack, 2006, 2012) and in the electrosensory system they signal prey-like peaks in signal amplitude or communication signals (Gabbiani et al., 1996; Oswald et al., 2004; Marsat et al., 2009). The presence of a bursting mechanism is key in shaping the neuron's role in the sensory pathway. The present study focuses on this bursting property and investigates variations in the ion channels responsible for burst generation in the sensory system of weakly electric fish.

The electrosensory lateral line lobe (ELL) is the primary sensory area in the hindbrain of gymnotid weakly electric fish and the main output neurons, pyramidal cells (PCs), possess a well characterized bursting mechanism (Turner et al., 1994; Doiron et al., 2002). PCs, particularly the more superficial ones, have extensive apical dendrites dedicated to receiving feedback inputs, but these dendrites also support the generation of bursts. These apical dendrites extend several 100 μm into the molecular layer (**Figure 1A**) dorsal to the PC layer (PCL; Bastian and Courtright, 1991). They contain TTX-sensitive voltage-gated sodium channels (Nav channels). When an action potential is initiated in the cell, the somatic potential backpropagates actively ∼200 μm up the apical dendrites due to the Nav conductance. Current from the backpropagating action potential then flows back down to the soma passively causing a depolarizing after-potential (DAP) after each spike (**Figure 1B**; Turner et al., 1994). In slices and in models, this backpropagation mechanism

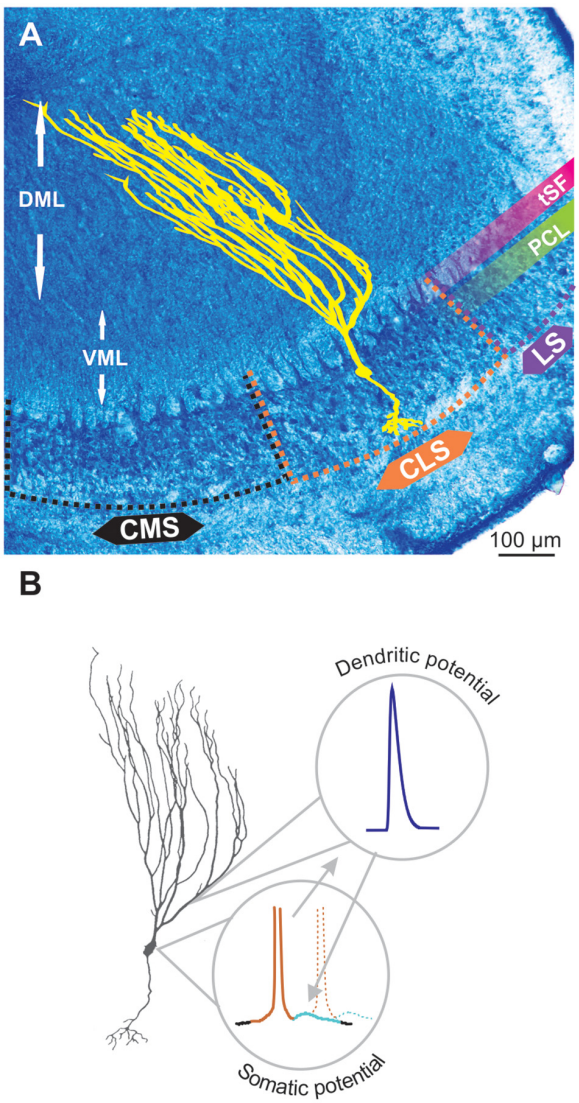

FIGURE 1 | Pyramidal cell (PC) and backpropagation. **(A)** Transverse section through the electrosensory lateral line lobe (ELL), the primary sensory area located in the hindbrain of gymnotid weakly electric fish. The structure is layered and the main output neurons-PCs (yellow schematic) are organized in several topographic maps: medial, centro-medial, centro-lateral and lateral segments (MS, CMS, CLS and LS, respectively). The latter three segments receive inputs from tuberous electroreceptors. The PC layer (PCL) contains the soma of these neurons whereas the ventral and dorsal molecular layers (VML and DML, respectively) contain the extensive apical dendrites of the PCs (illustrated in yellow). The tractus stratum fibrosum (tSF) is an easily identifiable band (see also **Figure 2**) separating the PCL from DML. **(B)** Backpropagation and bursting. The ON PCs possess a small basilar dendritic bush receiving feedforward inputs, extensive apical dendrites (particularly long in superficial PCs) receiving feedback and an axon (not depicted here). Apical dendrites contain Nav channels such that, when an action potential is elicited in the soma (brown portion of the voltage schematic), it propagates up and back down the apical dendrites causing a depolarizing after potential (DAP; light blue) at the soma. The DAP increases the probability that subsequent action potentials (e.g., dashed line) are fired immediately after the first one thus leading to bursting.

can trigger a sequence of several spikes with increasingly shorter interspike intervals (ISIs). This stereotyped bursting dynamic, named ghostbursting (Doiron et al., 2002), might not unfold in the same way *in vivo*, where bursts are typically truncated to be only a few spikes-long. Nevertheless, backpropagation and the DAP are an integral part of the bursting dynamic and enable burst-coding of sensory signals (Oswald et al., 2007).

Response properties of ELL PCs are shaped by a variety of additional factors that vary across cell subtypes (Maler, 2007; Chacron et al., 2011). PCs are classified based on their location in the ELL layer. Superficial and intermediate PCs have extensive apical dendrites while deep PCs have short apical dendrites and fulfil a different role in the circuit (Bastian and Nguyenkim, 2001; Bastian et al., 2004). PCs receive inputs from receptors either directly or through an inverting interneuron. This leads to response patterns typical of ON-cells and OFF-cells, respectively (Maler, 1979; Clarke et al., 2015). Both types have the same burst dynamic. The ELL is organized in several topographic maps. While the map of the medial segment is driven by a separate category of passive ampullary electroreceptors, the centro-medial, centro-lateral and lateral segments (CMS, CLS and LS, respectively) receive inputs from the tuberous receptors sensitive to the fish's self-generated electric signal (Kawasaki, 2005). These areas each play a critical role in prey detection, communication, and navigation. In this study, we focus on those three ELL maps responsible for processing this actively-generated electrosensory signal.

PCs from the three maps vary widely in their response properties. These differences are due to variations in network connectivity, ion channels composition, expression of neuromodulator receptors and more (Ellis et al., 2008; Maler, 2009; Krahe and Maler, 2014). These differences in properties allow the specialization of the three maps for different purposes: whereas the CMS is well suited for the localization of small near-by objects such as prey, the more lateral segments (CLS and especially LS) might specialize for processing communication signals (Metzner and Juranek, 1997; Marsat et al., 2009). Despite these differences in properties and function, all segments display similar bursting rates (Krahe et al., 2008). Although some small differences in burst patterns have been noted (Turner et al., 1996; Metzner et al., 1998; Mehaffey et al., 2008), it is unclear to what extent burst dynamics varies across segments since no fundamental differences have been documented in burst coding (Metzner et al., 1998; Oswald et al., 2004; Krahe et al., 2008). Large differences, particularly in bursting rates, could have been expected across different segments given the known differences in conductances affecting bursting. SK channels, which generate a hyperpolarizing after-potential, vary in expression across PCs subtypes and segments. They are particularly prevalent in the LS where they oppose the DAP-based burst generation mechanism (Ellis et al., 2007a, 2008). Serotonin receptors are also expressed differently, with LS cells expressing more, and when activated serotonergic inputs can enhance bursting propensity (Johnston et al., 1990; Deemyad et al., 2011, 2013). It is clear that many factors interact to shape bursting and it is possible that similarities in burst coding across PC subtypes and segments happens despite differences in intrinsic configurations, rather than because they have identical physiology.

Variation in one element central to the burst-generation mechanism has not been examined yet: Nav channel expression in the apical dendrites of PCs. Considering the differences related to the burst mechanism noted above, we hypothesize that variations in the expression of Nav channels will also be observed across segments. To test this hypothesis, we performed immunocytochemistry on ELL slice labeling Nav channels in the molecular layer of the three segments of the ELL. We observed Nav expression throughout the molecular layer and we show that it is denser in LS than CMS. We argue that this differential expression should have functional consequences on response properties but that it is hard to determine how it interacts with the many other differences seen across segments.

MATERIALS AND METHODS

Brain Slices Preparation

Apteronotus leptorhynchus fish used for experiments were wild-caught and purchased from a tropical fish supplier. They were maintained in home tanks (61 × 30.5 × 50.8 cm) at 26–27°C, 250–300 μS on inverted light cycles, fed *ad libitum* and were provided with environmental enrichment. Fish of either sex were anesthetized in tank water with MS-222 (3-amino benzoic acid ethyl ester, Western Chemicals Inc.) and respirated with oxygen bubbled MS-222 water during perfusion. All chemicals were obtained from Fisher Scientific (Hampton, NH, USA) unless otherwise noted. Heart was surgically exposed and intracardial perfusion was performed *via* the Conus arteriosus with 5 ml of cold 0.9% saline containing Heparin (#9041-08-1), $NaNO_2$ (#S25560) and NaCl (#7647-14-5) which is followed by perfusion with 40 mL of cold 4% paraformaldehyde (PFA; Electron Microscopy Sciences, #RT-15714) in 1×-phosphate buffered saline (PBS), pH-7.3. Whole brains were surgically removed and post-fixed in 4% PFA in 1× PBS for 4 h at 4°C and were washed three times for 15 min each in 1× PBS at 4°C. Brains were sequentially cryoprotected in 20% and 30% sucrose (#S25590) in 1×-PBS, pH-7.3 until they were completely saturated and later incubated in 1:1 mixture of 30% sucrose solution and optical cutting temperature (OCT) compound (Electron Microscopy Sciences, #62550-01) for 1–2 h before embedding in OCT. Dry-ice chilled 100% ethanol was used to freeze the brain in OCT in a cryomold and the mold was incubated at −80°C for 1–2 h before sectioning. 15–20 μm thick true-transverse brain sections were obtained using cryostat (Leica 1850) and the slides were stored at 4°C for immediate processing or stored at −20°C until use.

Immunohistochemistry

Brain sections were immunoreacted for Nav *in situ* through the following procedure. Sections were washed three times with 1×-PBS, pH-7.3 for 5 min each and were blocked for 1 h in 5% normal goat serum (#005-000-121, Jackson Immuno Research) in PBSAT (1× PBS, 5 mM Sodium Azide and 0.1% Triton X-100). Blocking was followed by 1-h incubation with Anti-Pan Nav

(Alomone labs, #ASC003; 1:50) and purified Mouse Anti-MAP II (BD Biosciences, #556320; 1:400) primary antibodies in blocking buffer at room temperature. The Anti-Pan Nav antibody was raised in rabbits and was shown to selectively bind to the Na channels in apteronitids' electric organ with a protein size of 250–260 kDa (Ban et al., 2015). Later, brain sections were transferred to 4°C for overnight incubation. Note that the MAP2 antibody used in the current study only stains the high molecular weight isoforms of MAP2 and does not recognize low molecular weight MAP2 isoforms or other microtubule proteins. In addition, MAP2 is mainly concentrated in the dendritic part of the nerve cells (Olesen, 1994), this might possibly explain the comparatively fainter MAP2 labeling observed in the cell bodies.

Sections were washed four times with 1×-PBST (1× PBS and 0.1% Triton X-100), pH-7.3 for 15 min each and were incubated with Goat anti-rabbit Alexa 488 (Life Technologies, #A-11008; 1:500) and Goat anti Mouse Alexa 546 (Thermofisher, #A-11030; 1:500) secondary antibodies for 3 h at room temperature in an enclosed moist chamber. Sections were washed four times with 1×-PBS, pH-7.3 for 15 min each and were mounted in Vectashield (Vector Laboratories, #H-1000) and coverslipped. Selectivity of the labeling was confirmed with several controls: an absorption control where the Nav antibody is incubated with the immunogen (**Supplementary Figure S1**), a control with no primary antibody (**Supplementary Figure S2**) and a quantification of Nav labeling in regions where no Nav channels are expected to be found. For this last control, we selected 27 different 10 × 10 μm areas in the gaps between dendrite in the tractus stratum fibrosum (tSF) layer (where we do not expect Nav channels to be present; see **Figure 2D**) and compared the Nav labeling to 27 areas selected randomly on the same scans but in the middle of the dendritic arbors in the molecular layer. As expected, minimal staining was found (gaps in tSF: 0.009 puncta/μm^2; molecular layer: 0.1 puncta/μm^2; *T*-Test: $p < 10^{-6}$) proving that puncta of labeling are not simply an artifact and randomly distributed on the tissue.

Western Blot

The specificity of polyclonal Anti Pan-Nav antibody was evaluated using western blot analysis (**Figure 3F**). Unperfused whole brain was surgically removed and freezed in liquid nitrogen and immediately homogenized with cold homogenization buffer containing 250 mM Sucrose, 1 mM EDTA, 10 mM Tris HCL and protease inhibitor cocktail (#4693132001, Sigma Aldrich), pH-7.2, on pre-chilled mortar and pestle. Tissue sample was sonicated using two 10 s pulses with 30-s interval between each sonication. Sample was centrifuged at 500× *g* for 10 min to remove intact cells, nuclei and cell debris, and the supernatant was centrifuged at 100,000× *g* for 1 h at 4°C. Supernatant was discarded, and the pellet was resuspended in homogenization buffer and centrifuged at 100,000× at 4°C for 1 h. Resultant supernatant was discarded and the pellet containing the membrane fractions was used to run western blot.

For western blot, 1× LDS (#NP0008, Thermofisher) was added to the protein samples which was then heated for 10 min at 70°C. Five microliter of the sample was loaded into 4%–6% polyacrylamide gel along with Precision Plus Protein™ Dual Color Standard (#1610374S, Bio-Rad) and was run at 120 V. Transfer was done at 100 mA for 22 h at 4°C and the nitrocellulose membrane (#162-0094, Bio-Rad) was blocked for 1 h with 5% BSA and 0.05% NaN 3 in 1× TBST (1× TBS, 0.1% Tween) under agitation. Primary antibody diluted in the blocking buffer (1:200) was applied to the membrane and incubated overnight at 4°C under gentle agitation. After incubation, membrane was washed three times with 1× TBST for 15 min each. HRP conjugated anti-rabbit secondary antibody (#A0545, Sigma) was applied at 1:10,000 dilution and agitated for 1 h at room temperature, which was followed by three 15-min washes with 1× TBST. ECL substrate (#RPN2109, GE Healthcare) was added and the membrane was imaged on FluorChemQ system (Protein Simple).

Nav Puncta Density Quantification

Scans were obtained on FV-1000 Fluoview confocal microscope and minor brightness adjustments were made using Fluoview software. All of the scans were imaged using 60× oil immersion lens at 2× digital zoom unless otherwise noted. Scan size X*Y is set at 105.4*105.4 μm with Z at 0.5 μm. Differences in the spatial distribution across the brain maps are assessed by quantitative image analysis using VAA-3D software. ImageJ software was used to perform image normalization. To measure the spatial distribution of dendritic Nav channels across different ELL maps (LS, CLS and CMS), the dorsal edge of the tSF layer is chosen as reference location (0 μm). Scans covered the first 600–800 μm of apical dendrites as they project dorsally through the ventral molecular layer (VML) and dorsal molecular layer (DML) layers.

In each scan, 2–4 portions of dendrites with clear MAP2 labeling were chosen prior to looking at the Nav labeling to prevent biased choice of dendrite based on expected channel density. Nav labeling was quantified by manually marking each punctum visually identified on the chosen dendrites. XY coordinates of each punctum and dendrites were stored for analysis. We were conservative in assigning a punctum as belonging to a dendrite and the numbers presented in this article should be viewed as a lower-bound estimate. Note that any bias in quantifying puncta within a segment is also inherent to the quantifications done across segments, and therefore, the differences observed in Nav density across the segments are unlikely to be affected by such biases.

To standardize the identification of the edge of the tSF layer (defined as location 0 μm) a Matlab (Mathworks, Natick, MA, USA) program was created to plot the density profile of the gaps present in the tSF layer along with the pixel intensity profile of the scan (see **Figure 2D** and explanation in the legend).

A series of slightly overlapping scans of the entire extent of each map were obtained (**Figure 2A**) and the bleached area from the overlapped portion as well as a local landmark was used to obtain the start point x-coordinate of each subsequent scan of the map. This allowed us to determine the orthogonal distance of each scan, dendrite and punctum from the tSF edge. Since dendrites do not travel orthogonally to the tSF edge and the scan orientation (**Figures 2B,C**), we had to correct the distances using dendrites' angles. To do so, in each scan we

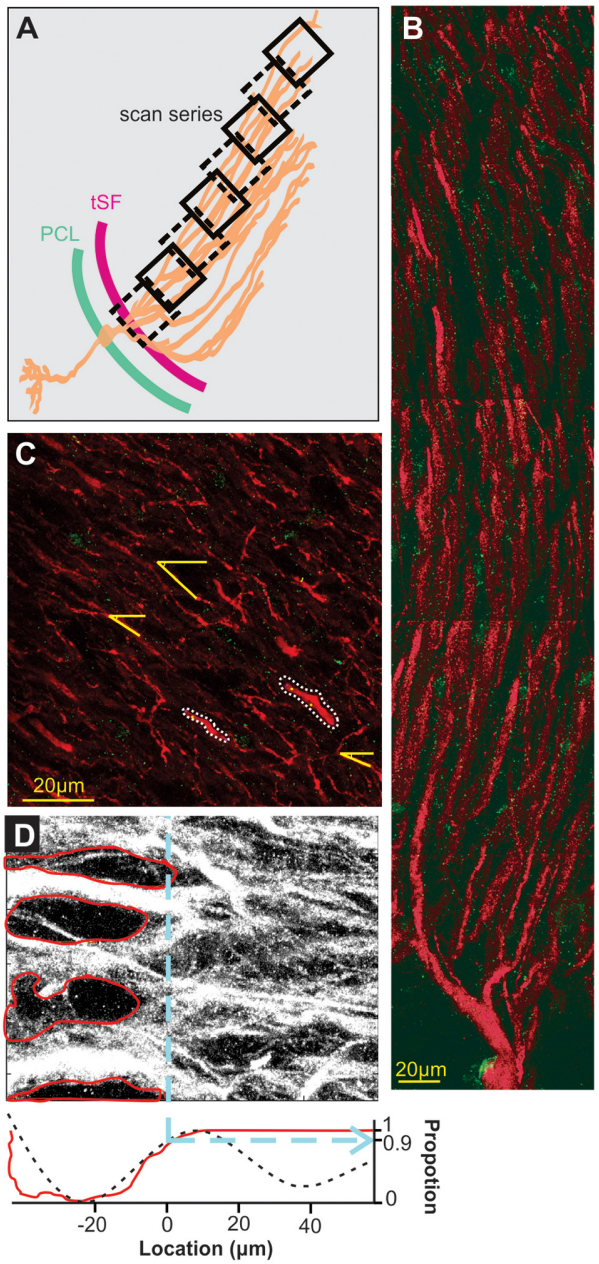

FIGURE 2 | Scanning and localization procedure. **(A)** Scans arrangement. Each 105 × 105 μm scan is positioned relative to the transverse section of the ELL so that the first one of a series contains the tSF layer and subsequent ones overlap the previous and follow the orientation of dendrites in the molecular layer. Eight successive scans or more were performed to cover at least 600 μm of apical dendrites. **(B)** A series of scans showing the extensive apical dendritic bush in the molecular layer. Although we did not attempt to reconstruct and isolate single PC, our successive scans follow the apical dendrites of PCs. Red MAP2 labeling marks the inside of the dendrites and green labeling highlights the position of Nav channels. Since no distinction could be made between ON and OFF cells based on the immunolabeling used, all the dendrites quantified in the study are mixed, either ON or OFF-cells, and possibly VML interneurons (although it is unknown if they express dendritic Nav). **(C)** Dendrite selection and angle. Based solely on the MAP2 labeling (Nav labeling not displayed) we selected several clearly defined

(*Continued*)

FIGURE 2 | Continued

dendrites per scans for quantification (e.g., outlined with white dashes). Since dendrite orientation relative to the scan orientation is not orthogonal, we measured, in each scan, the average relative orientation of dendrites based on several dendrites per scan (yellow lines). This allowed us, using the position on the x-axis of the scan, the angle of dendrites and trigonometry, to determine a more accurate position of dendrites along the dendritic bush. **(D)** Determination of tSF dorsal edge to set it as location "0 μm". The stratum fibrosum tract is characterized by large circular areas without MAP2 labeling between the large proximal apical dendrite shafts. We determined the dorsal edge of this layer by first highlighting the visible holes in labeling (red in the top image) and constructing a pixel histogram (red curve, bottom plot) along the x-axis based on the pixels outside these areas. Second, we used the raw pixel intensity values to build a histogram along the x-axis and smoothed it by fitting a triple sinusoid function (black dashes, bottom plot). Both histograms were normalized between 0 and 1 and we took the 0.9 mark of the rising slope to determine the 0 μm location (dashed blue line). We confirmed both histograms gave similar results and used the average of the two calculated values to set the 0-mark.

selected randomly five clear portions of dendrites and measured their angle relative to the scan's frame (**Figure 2C**). Using the average angle of the selected dendrites in each scan and trigonometry, orthogonal distances could be converted into the estimated distance (i.e., distances that take into account the general curvature of dendrites). This estimate is still an underestimation of actual distance along the dendritic tree since dendrites are often not completely straight over one scan, and also any z-plane curvature was ignored. Note that we sectioned the hindbrain in a true-transverse orientation minimizing the curvature of dendrites in the z-plane over the proximal apical dendrites. This underestimation does not affect our conclusions but should be noted. Data analysis was performed with Matlab (Mathworks, Naticks, MA, USA) and statistics with JMP (SAS Institute Inc., Cary, NC, USA).

Burst ISI Characterization

Fish were prepared for *in vivo* electrophysiological recordings as described in Marsat et al. (2009) where recording and analysis methods are also described in detail. Briefly, superficial ON and OFF-cells of the three segments were targeted and spontaneous activity was recorded for 60 s. Recorded spike trains were binarized and burst identified by first constructing an ISI histogram of the entire spike train and identifying the upper interval limit characteristic of the cell's burst ISIs (for more details see Marsat and Pollack, 2012). Identified bursts were then used to calculate their ISI distribution. All procedures on animals were authorized by West Virginia University's IACUC (protocol #13-0103).

RESULTS

To study the distribution of Nav channels along the apical dendrites of PCs we used a pan-Nav antibody known to bind selectively to these channels in other tissues of this species (Ban et al., 2015). We confirmed the selectivity of the antibody in brain tissue by performing a Western blot (**Figure 3F**). To identify the position of the labeled channels relative to the dendrites, we also used a MAP2 antibody that densely labels the

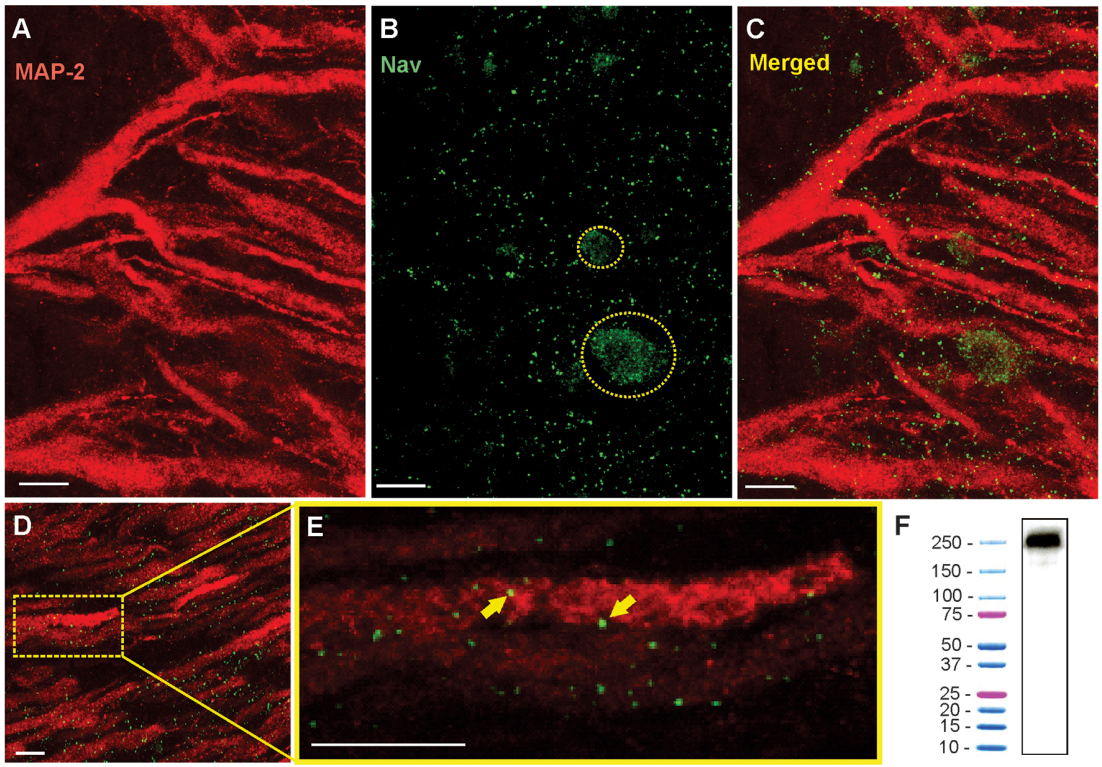

FIGURE 3 | Immunohistochemistry shows the punctate expression of Nav channels on the apical dendrites. **(A)** Confocal image of a 16 μm section of ELL showing the red Anti-MAP2 labeled apical dendrites projecting through tSF and VML. White scale bars are 10 μm in all panels. **(B)** Nav channel punctate distribution (green dots). Nav label was also found on the surface membranes of interneurons (e.g., VML cells) where their distribution is more uniform. Two interneuron cell bodies are outlined with a dashed yellow line. **(C)** Merged MAP2 and Nav labeling. Note that these images show the combined z-layers of the scan through the 16 μm slice but that looking through the individual successive scans at varying depth (0.5 μm apart) can help determine the proximity between MAP2 and Nav labeling. **(D)** Nav and MAP2 labeling in a more distal portion of VML (∼200 μm from tSF boundary). **(E)** Enlarged view of one dendrite in the image displayed in **(D)** selected for quantification of Nav channels. The proximity between the labeled Nav channels and the labeled MAP2 inside dendrites allows us to confirm that the channels were in the membrane of a PC dendrite. Two puncta are indicated with yellow arrows. Note that the Nav and MAP2 labeling does not need to overlap directly since MAP2 is located inside the dendrite and Nav channels are in the membrane. We thus expect some of the puncta to be slightly separated (in the x-y plane or the z plane) from the MAP2 labeling. **(F)** Western blot analysis of brain tissue demonstrating the specificity of Anti-pan Nav antibody. The western blot of the tissue processed along with a protein ladder displayed a single band at ∼250–260 kDa.

microtubules inside dendrites (Deng et al., 2005). By using thin brain slices (15–20 μm) and high-resolution confocal scans we were able to precisely localize the labeled channels relative to PCs apical dendrites (**Figures 3A–E**). The pattern of expression of Nav channels in the dendrites followed a punctate pattern, as described previously (Turner et al., 1994), that is visibly different from the more uniform expression pattern in the soma of interneurons (**Figure 3B**) or in axons. Prior to visualizing the Nav labeling, we selected in each scan 2–4 portions of dendrites that are clearly delineated by the MAP2 labeling. We then visualized in 3D (moving through the z-plane with the imaging software) the position of each punctum in the vicinity of the dendrite portion selected for quantification. Since Nav channels are in the membrane of the dendrites and MAP2 proteins are inside the dendrite, Nav puncta were immediately adjacent (in the x-y plane or the z-plane) to the MAP2 labeling or overlapping.

Our dataset is based on images from 15 brain slices (five slices each from three fish). In each slice, all three segments were scanned and quantified thereby assuring that differences in immunolabeling clarity from slice to slice could not cause a bias in quantification across segments. Scans starting at the tSF layer and tiled to extend beyond 600 μm into the molecular layer (**Figure 4**) allowed us to evaluate Nav expression as a function of segment and location along the ventral-dorsal axis (i.e., proximal-distal to the soma). We localized and counted Nav puncta on 727 portions of dendrites representing over 21,400 μm of dendrites (**Figure 5**). We found a large dendrite-to-dendrite variability in puncta density with some long portions of dendrites containing no puncta and others being densely populated with puncta. This variability could be observed even between dendrites located side-by-side on the same scan precluding the possibility that variations in the immunolabeling process could account for this variability.

PCs can be classified in several subcategories (deep, intermediate or superficial PCs and ON-cells or OFF-cells) organized in microcolumns and their apical dendrites can overlap at the same location in the molecular layer. Our method cannot determine to which type of PC a dendrite belongs and

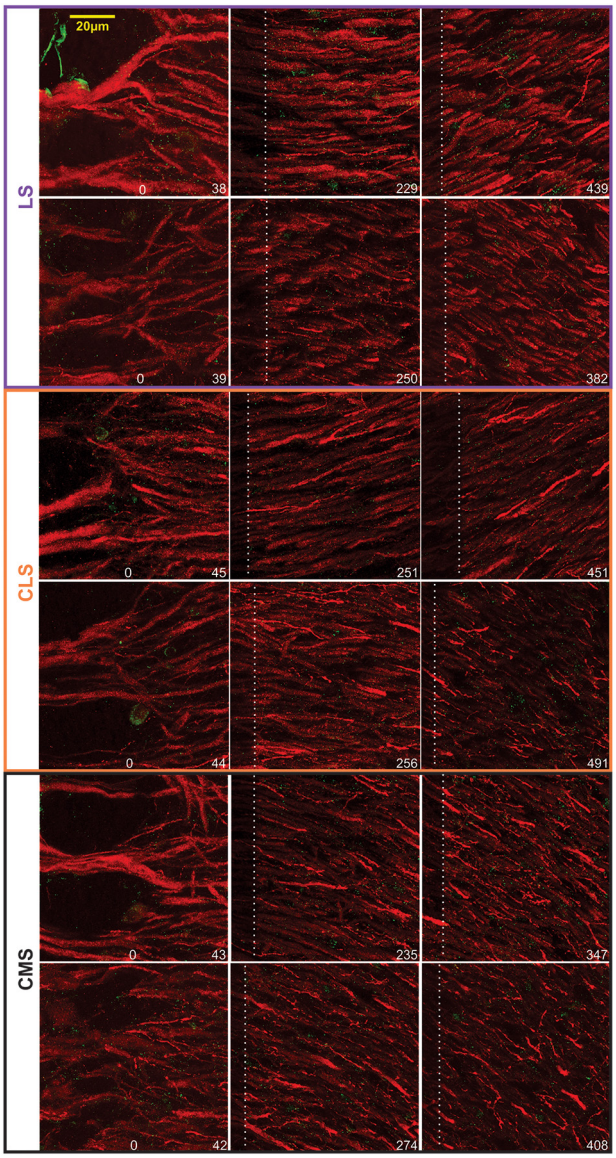

FIGURE 4 | Examples of Nav-Map 2 expression in the ELL. Confocal images from two brains (top vs. bottom rows for each map) taken at different distances from the tSF. The location of the distal edge of the image is specified in μm at the bottom right of each image. The white dashed lines indicate the edge of the previous—overlapping—scan and thus the pixels on the left of this line are bleached from the previous scan.

thus we cannot determine to what extent the variability observed is due to variations across—vs. within—subcategories.

The density of puncta per μm of dendrite was calculated for each of the ∼250 dendrites per segment and we first visualize in a 3D histogram the proportion of dendrites with various densities as a function of dendrite position along the molecular layer (**Figure 6A**). The pattern of Nav expression clearly differs across segments. In LS, a large proportion of dendrites have puncta densities higher than 0.1 puncta/μm whereas CMS dendrites have densities mostly below 0.1 puncta/μm. Our data also shows that density stays similar throughout the molecular layer up to at least 600 μm away for tSF. Our data beyond 600 μm are more sparse, nevertheless, the data we do have suggest that more distal dendrites express Nav channels with a density similar to the more proximal dendrites (see **Figures 5**, **6A**). Our data demonstrate that dendrites in the LS have Nav puncta densities about twice as high as CMS dendrites and 1.4 times higher than CLS dendrites (**Figures 6B,C**). The distribution of Nav puncta along the first 600 μm of dendrites (for which we have most data) was not very different across segments. Specifically, we see similar densities over the length of the dendrites in LS and CLS but channel density increased slightly in CMS for dendrites located further from tSF (**Figure 6D**). Therefore, our data show that, despite small differences across segments, we see a qualitatively similar distribution of Nav puncta over the entire length of dendrites considered here (0–600 μm from tSF dorsal edge; **Figure 6E**).

The differences in Nav channel density across segments could have a significant impact on the neuron response properties. The impact on neural dynamic and sensory processing is hard to gauge because PCs differ in many aspects between segments. Differences in ion channel composition, tuning, connectivity and more, interact intricately with the dynamics imposed by Nav channels. Even potential studies using modeling, where a single parameter can be altered (e.g., Nav channels density), presents important challenges. Indeed, all the elements of the neurons and of the network known to influence the neuron's response dynamic would need to be included to understand the effect of changing Nav density and determine if it can explain differences observed across segments. Such modeling effort is beyond the scope of this manuscript.

Nevertheless, we suggest that looking at the spontaneous activity of the neurons could give us useful insight into the effects of differences in Nav density on bursting. ISIs during spontaneous activity are largely determined by the neuron's intrinsic mechanisms since excitation is weak and relatively constant. Furthermore, burst ISIs are heavily influenced by only a few ion channels, first and foremost the Nav channels in apical dendrites. Therefore, we investigated potential differences across segments in burst ISIs during spontaneous activity. Focusing on superficial PCs, we show that burst ISIs tend to be shorter in LS than in CMS; CLS being intermediate (**Figure 7**; average ISIs ± SE: LS = 3.2 ± 0.6; CLS = 3.8 ± 0.5; CMS = 6.2 ± 0.3. Wilcoxon test: LS-CLS, $p < 0.0001$; LS-CMS, $p < 10^{-9}$; CLS-CMS, $p < 10^{-7}$. $n = 13$–19 neurons). This trend is consistent with a previous observations (Turner et al., 1996; Mehaffey et al., 2008) and could potentially be attributed in part to the higher density of Nav channels in LS (see "Discussion" section).

DISCUSSION

Dendritic Nav Channel Expression and Firing Patterns

The principal finding of the present experiment was that LS exhibits the highest dendritic Nav channel density, followed by CLS and CMS. The difference was obvious in the proximal dendritic regions of apical dendrites that support

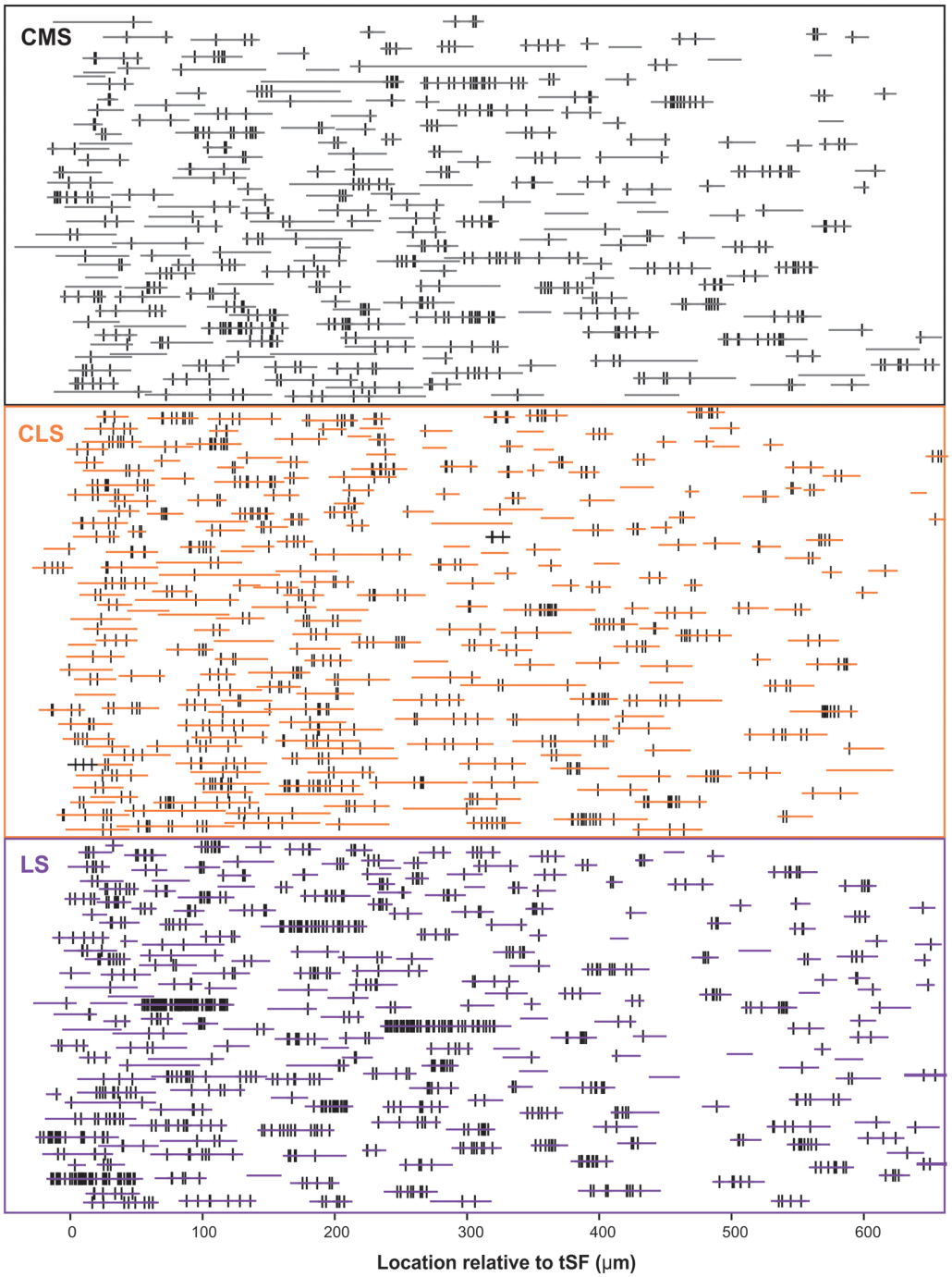

FIGURE 5 | Schematic representation of the entire dataset. The position and length of each dendrite quantified is depicted by the horizontal colored lines. The position of each Nav punctum identified is marked by a vertical black line. The vertically stacked arrangement of the dendrites loosely follows the order of processing and thus data from a given slice/brain are found in adjacent rows of the stack. We quantified 727 dendrites in 15 brain slices, totaling >21,400 μm of dendrite, and identified 2,435 puncta of Nav labeling across segments/locations.

active backpropagation. Nav channel densities remain relatively constant along the proximo-distal axes of the apical dendrites in all segments.

Previous studies have established the subcellular distribution and function of TTX sensitive Nav channels using immunocytochemistry and electrophysiology techniques (Turner et al., 1994). Punctate regions of Nav immunolabel were detected in PC somata, basal and apical dendrites. The previous EM study (Turner et al., 1994) pointed out that regions of denser labeling along a dendrite could be separated by longer portions

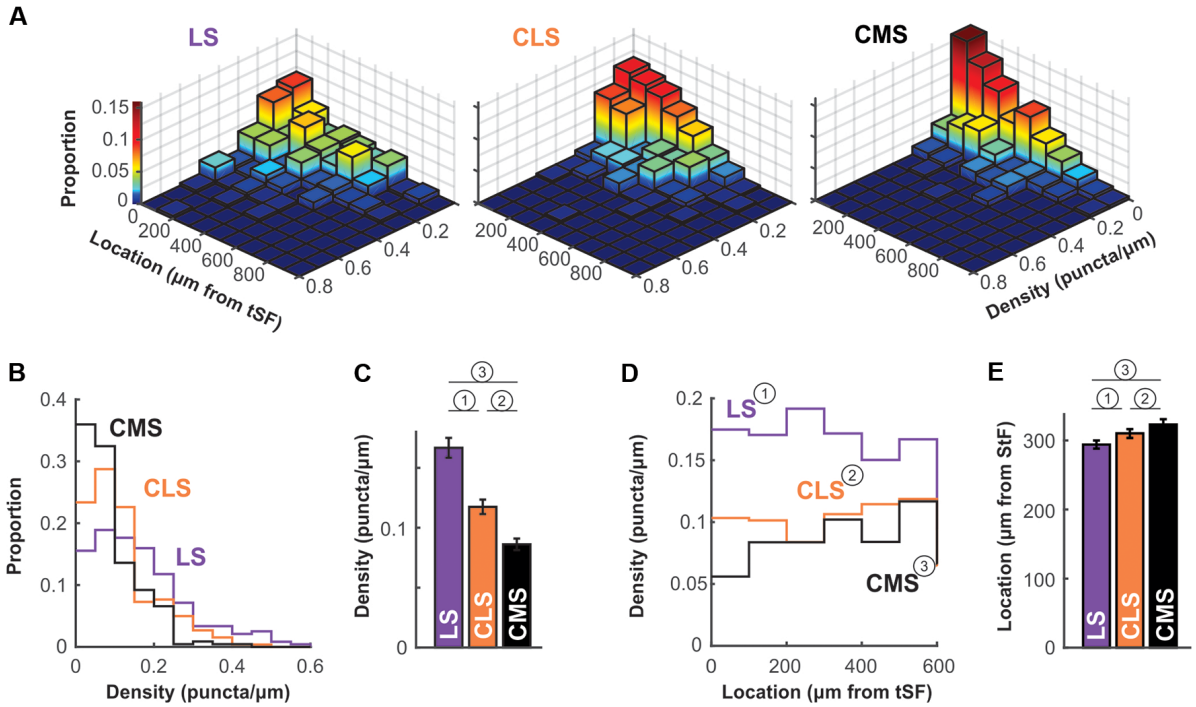

FIGURE 6 | Nav channel expression density differs across maps. **(A)** Histogram of channel density per dendrite as a function of location. For each dendrite (LS, $n = 238$; CLS, $n = 261$; CMS, $n = 228$) channel density (puncta/µm) was calculated. The z-axis (also color-mapped) shows the proportion of dendrites in each location/density bin (i.e., sum of all bin heights is 1 in each panel). These data show that densities in CMS are largely constrained to the 0–0.1 puncta/µm range whereas densities are equally distributed in the 0–0.1 and 0.1–0.2 range (and higher) for LS (see panels **B,C**). Also, channel density seems to be equally distributed along at least the first 600 µm of the molecular layer (see panels **D,E**). Note that overall height of the bins tends to decrease with increasing distance from tSF simply because fewer dendrites were quantified distally compared to proximal locations. **(B)** Histogram of channel density across maps. The data displayed in **(A)** were collapsed across all locations to clearly show the differences in puncta density across maps. LS clearly has a higher proportion of dendrites with high density (>0.1 puncta/µm) compared with CMS and thus a lower proportion of dendrites with low density (<0.1 puncta/µm). See panel **(C)** for a listing of statistical differences. **(C)** Average puncta density is significantly different across segments and decreases from LS to CMS. Since the data are not normally distributed (see panel **B**) we tested pairwise differences using a Wilcoxon test: (1) $p = 0.000004$; (2) $p = 0.0002$; and (3) $p = 10^{-15}$. **(D)** Channel density is similar across location in the molecular layer. Average channel density was calculated for dendrite positioned at various distances for tSF. Location does not influence the observed puncta density in LS and CLS [One-way ANOVA: (1) $p = 0.82$; (2) $p = 0.1$] but density increases slightly with distance in CMS [One-way ANOVA: (3) $p = 0.005$]. The analysis shown in this panel and in panel **(E)** took into account dendrites located <600 µm only since our data for locations >600 µm is sparse. **(E)** Nav channel distribution across the molecular layer is similar for all three maps. We calculated an average channel location across the 600 µm of the molecular layer considered here to compare the distribution of channels along the dendrites for the three maps. To do so, we normalized our puncta counts to account for the length of dendrites quantified in each location bin. Therefore, an average location of 300 µm indicates that channels are uniformly distributed across the dendritic length considered here. This average is similar for all three maps ranging from 294 µm to 323 µm but the small differences are significant [Wilcoxon: (1) $p = 0.0001$; (2) $p = 0.003$; and (3) $p = 10^{-11}$].

of dendrites with little labeling. Our study confirms that channel density varied widely from one portion of the dendrite to the next. Note that our study does not distinguish between dendrites belonging to ON-cell, OFF-cells or interneurons. Part of the variability observed could be due to differences across cell types If this was the case, you would expect to see two or three clusters of channels densities (one for each cell types) but we observe a mono-modal distribution instead. Future studies labeling for cell identity and for Nav could test this hypothesis.

Dendritic Nav channels allow the active propagation of an antidromic spike over around 200 µm of proximal apical dendrite. The resulting DAP at the soma after each somatic spike underlies the production of burst discharge. Focal ejections of TTX inactivates Nav channels, decreasing spike frequency (Turner et al., 1994; Oswald et al., 2004). However, higher conductance from Nav channels does not necessarily lead to an increase in spike frequency. Decreased Na^+ conductance in dendrites can increase the excitability of the soma by delaying the DAP thereby enhancing the so-called "ping-pong" dendro-somatic dynamics that underlies burst generation (Fernandez et al., 2005). There is thus a non-monotonic relationship between Na^+ conductance and cell excitability (Fernandez et al., 2005) or the amount of information carried by bursts (Doiron et al., 2007) with a maximum at intermediate values. Nevertheless, modeling studies indicate that an increase in dendritic conductance from Nav channels systematically causes increased burst rates (Doiron et al., 2007).

Backpropagation has been characterized as traveling up 200 µm before the active propagation is not detected. Our results, and the original study that identified the Nav channel's presence in the dendrites (Turner et al., 1994), show that the channels are distributed along the majority of the dendritic

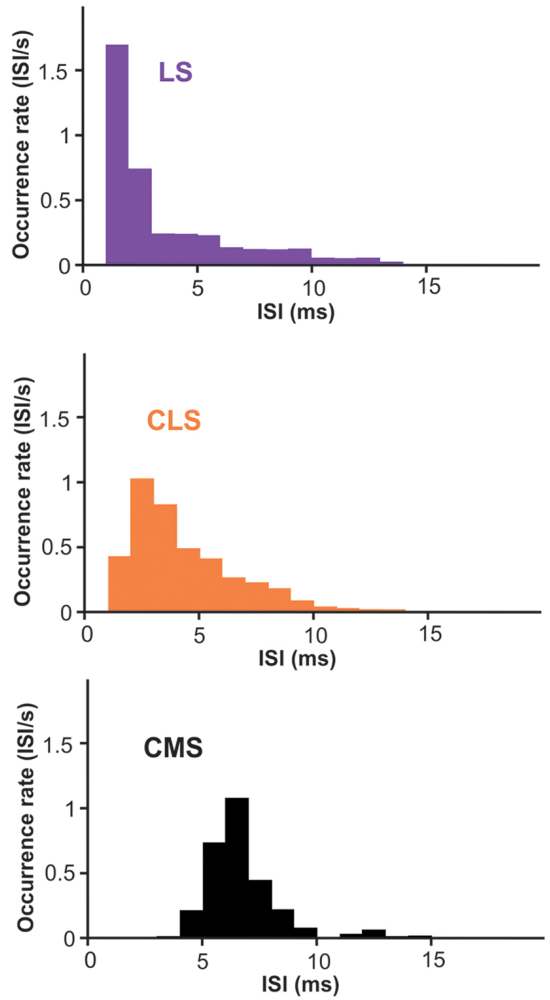

FIGURE 7 | Inter-spike intervals (ISIs) histogram for burst-spikes during spontaneous activity. Burst of spikes was identified as described in the methods and the interval between the spikes in each burst contributed to the histograms displayed. The average interval is shorter in LS than CMS with significant differences across all three segments (averages ± SE: LS = 3.2 ± 0.6; CLS = 3.8 ± 0.5; CMS = 6.2 ± 0.3. Wilcoxon test: LS-CLS, $p < 0.0001$; LS-CMS, $p < 10^{-9}$; CLS-CMS, $p < 10^{-7}$. n = 13–19 neurons).

tree. The role of these channels, past the 200 μm where backpropagation is evident, is unknown. One possibility is that they contribute to the DAP but the current they generate in the more distal dendrites is too small to be clearly identified. The DAP is indeed likely to be reduced in distal apical dendrites due to the presence of Kv3.3 channels (Deng et al., 2005) producing an after-hyperpolarization. Another possibility involves an interaction between the channels and synaptic inputs. GABAergic inputs have been shown to influence the DAP generation (Mehaffey et al., 2005), it is therefore not unlikely that the Na+ current in the distal dendrites shapes and affects the dynamics of synaptic inputs. Given the important role of feedback inputs onto these apical dendrites the presence of the channels near these synapses could alter the neuron's response properties significantly.

Segment-Specific Regulation of Bursting Mechanisms

The effect of variations in the DAP current is particularly hard to predict because several other currents overlap with the depolarization from dendritic Nav channels. K channels, muscarinic or 5HT receptors, and GABAergic inputs can influence the after-potential (Márquez et al., 2013). In particular, somatic spikes are followed by both fast and slow AHPs that help repolarize the cell and lengthen the interval to the next spikes (Turner et al., 2002). Therefore, the DAP and the AHP have opposite influences on bursting. ELL expresses two different subtypes of SK channels (SK1: dendrites; SK2: soma) that cause AHPs (Ellis et al., 2007b, 2008) following a gradient where LS has a denser distribution than CMS. The relatively short DAP (8–10 ms) temporally overlaps with the longer AHP and their strength varies with PC subtype. It is possible that higher expression of dendritic Nav channels may partially compensate higher hyperpolarizing currents and allow these currents to be modulated with different gains.

Several mechanisms for external modulation of these hyperpolarizing and depolarizing currents have been characterized. Inhibitory interneurons are prevalent in the ELL (e.g., VML cells or granular cells) and synapse both on PC's soma and dendritic arbor (Berman and Maler, 1999). Dendritic application of $GABA_A$ agonist can affect the dendritic leak conductance leading to a DAP reduction and thus have a divisive effect on the cell's input-output relationship (Mehaffey et al., 2005). In contrast, somatic inhibition has a subtractive effect in suprathreshold regime and divisive in subthreshold regime since the reversal potential of $GABA_A$ channels is close to the neuron's resting potential (Doiron et al., 2002). Therefore, somatic inhibition could also potentially interact with the subthreshold dynamic influenced by the DAP and AHPs. Since the inhibitory surround input onto PCs varies across segments (Hofmann and Chacron, 2017) and the proportion of inhibitory interneurons (**Supplementary Figure S3**) also varies across segments, GABAergic inhibition is another segment-specific factor that could interact with the current from dendritic Nav channels.

5-HT is an important modulator of social behavior that is released during communication and LS shows the highest 5-HT innervation (Johnston et al., 1990). Interestingly, the innervation pattern is also layer specific across segments, where LS shows dense expression in the PCL and VML. 5-HT increases burst firing across segments with the greatest effect in the LS which is consistent with its expression density (Deemyad et al., 2011). These effects are mediated by 5-HT2 receptors (Larson et al., 2014) that increase PC excitability and bursting *via* downregulation of SK channel and M-type potassium channel currents that contribute to the AHP (Deemyad et al., 2013).

Given that several factors affect the shape of spike's after-potential and the bursting dynamic, we cannot be certain that the shorter burst ISIs we observed in LS is due to the denser Nav expression but it is a plausible factor. A strong DAP, that peaks a few ms after the spike, could explain the relatively high probability of having 2–4 ms ISIs in LS whereas the

longer-lasting AHPs strongly influencing LS ON-cells could lead to the relatively low probability of ISIs longer than 5 ms. The longer burst ISIs observed in CMS could result from the lower Nav current since it can delay the DAP (Fernandez et al., 2005) and is not opposed by a strong AHP in superficial PCs. We, therefore, propose that differences in Nav channel expression interact with other aspects of the neuron's dynamic to influence the spiking patterns.

Bursts and Neural Coding

Bursts have a well-defined role in coding for specific temporal features of sensory signals. The relationship between patterns of spikes within a burst can further signal details about the feature that triggered the burst (Oswald et al., 2007). Specifically, the ISI within the burst is correlated with the amplitude and slope of the upstroke it signals. Studies in several sensory systems have shown that burst structure can carry information about the stimulus (Guido et al., 1995; Lesica and Stanley, 2004) and that this information is behaviorally relevant (Marsat and Pollack, 2010). Our results point to the possibility that variations in Nav channels may influence the burst dynamic to adjust the correlation between burst ISI and stimulus features. By adjusting the range of ISI coding for specific portions of stimulus space, each ELL segment could have its burst-code adjusted for slightly different stimulus features. We already know that bursts are involved in processing different signals across segments since bursts signal the presence of certain types of chirps in LS but not the other segments (Marsat et al., 2009). Also, bursts in CLS and CMS might be more specifically dedicated to signaling prey-like stimuli (Nelson and Maciver, 1999). Differences in Nav expression we describe could contribute to these different roles of burst coding across segments.

We started this article by pointing out two perspectives on neural heterogeneity. One highlights how similar neural outputs can arise from diverse combinations of neural properties. The other focuses on the need to vary neural physiology in order to adjust and specialize cells for different purposes. Our study does not determine what role the variability in dendritic Nav channel expression plays: compensating for other neural properties to keep burst coding functioning similarly across segments or on the contrary adjusting burst coding for specific roles. Since these two possibilities are not exclusive, we speculate both may be at work. The differences we describe in our study could partly compensate for other variations in PC properties while at the same time influence burst structure and coding to improve the ability of different segments to perform specific tasks.

DATA AVAILABILITY

All datasets generated for this study are included in the manuscript and/or the **Supplementary Files**.

ETHICS STATEMENT

This study was carried out in accordance with the recommendations of Animal Welfare Act, the Public Health Service Policy on Humane Care and Use of Laboratory Animals, the Guide for the Care and Use of Laboratory Animals established by the Office of Laboratory Animal Welfare. The protocol was approved by the West Virginia University Institutional Animal Care and Use Committee.

AUTHOR CONTRIBUTIONS

GM designed the research, supervised the experiments and data analysis and wrote the article. SM performed the Nav immunolabeling experiments and analyzed them and wrote the article. KA performed the GABA immunolabeling experiments and analyzed them and wrote the article. DW performed the electrophysiological recordings and analyzed them.

FUNDING

This research was supported by an National Science Foundation (NSF; IOS #1557846) and West Virginia University Research Corporation.

ACKNOWLEDGMENTS

We thank Dr Andrew Dacks and Dr Saravanan Kolandaivelu for offering their time, resources and guidance to help with some of the experimental procedures. Dr Michael Markham and Dr Vielka Salazar and their lab members were helpful in establishing the immunolabeling protocol. We also thank Dr Maurice Chacron and Dr Len Maler for useful discussions about this project.

SUPPLEMENTARY MATERIAL

The Supplementary Material for this article can be found online at: https://www.frontiersin.org/articles/10.3389/fncir.2019.00041/full#supplementary-material

REFERENCES

Ban, Y., Smith, B. E., and Markham, M. R. (2015). A highly polarized excitable cell separates sodium channels from sodium-activated potassium channels by more than a millimeter. *J. Neurophysiol.* 114, 520–530. doi: 10.1152/jn.00475.2014

Bastian, J., Chacron, M. J., and Maler, L. (2004). Plastic and nonplastic pyramidal cells perform unique roles in a network capable of adaptive redundancy reduction. *Neuron* 41, 767–779. doi: 10.1016/s0896-6273(04)00071-6

Bastian, J., and Courtright, J. (1991). Morphological correlates of pyramidal cell adaptation rate in the electrosensory lateral line lobe of weakly electric fish. *J. Comp. Physiol. A* 168, 393–407. doi: 10.1007/bf00199600

Bastian, J., and Nguyenkim, J. (2001). Dendritic modulation of burst-like firing in sensory neurons. *J. Neurophysiol.* 85, 10–22. doi: 10.1152/jn.2001.85.1.10

Berman, N. J., and Maler, L. (1999). Neural architecture of the electrosensory lateral line lobe: adaptations for coincidence detection, a sensory searchlight and frequency-dependent adaptive filtering. *Neuron* 202, 1243–1253.

Chacron, M. J., Longtin, A., and Maler, L. (2011). Efficient computation via sparse coding in electrosensory neural networks. *Curr. Opin. Neurobiol.* 21, 752–760. doi: 10.1016/j.conb.2011.05.016

Clarke, S. E., Longtin, A., and Maler, L. (2015). Contrast coding in the electrosensory system: parallels with visual computation. *Nat. Rev. Neurosci.* 16, 733–744. doi: 10.1038/nrn4037

Deemyad, T., Maler, L., and Chacron, M. J. (2011). Inhibition of SK and M channel-mediated currents by 5-HT enables parallel processing by bursts and isolated spikes. *J. Neurophysiol.* 105, 1276–1294. doi: 10.1152/jn.00792.2010

Deemyad, T., Metzen, M. G., Pan, Y., and Chacron, M. J. (2013). Serotonin selectively enhances perception and sensory neural responses to stimuli generated by same-sex conspecifics. *Proc. Natl. Acad. Sci. U S A* 110, 19609–19614. doi: 10.1073/pnas.1314008110

Deng, Q., Rashid, A. J., Fernandez, F. R., Turner, R. W., Maler, L., and Dunn, R. J. (2005). A C-terminal domain directs Kv3.3 channels to dendrites. *J. Neurosci.* 25, 11531–11541. doi: 10.1523/JNEUROSCI.3672-05.2005

Doiron, B., Laing, C., Longtin, A., and Maler, L. (2002). Ghostbursting: a novel neuronal burst mechanism. *J. Comput. Neurosci.* 12, 5–25. doi: 10.1023/A:1014921628797

Doiron, B., Oswald, A.-M. M., and Maler, L. (2007). Interval coding. II. Dendrite-dependent mechanisms. *J. Neurophysiol.* 97, 2744–2757. doi: 10.1152/jn.00988.2006

Duménieu, M., Oulé, M., Kreutz, M. R., and Lopez-Rojas, J. (2017). The segregated expression of voltage-gated potassium and sodium channels in neuronal membranes: functional implications and regulatory mechanisms. *Front. Cell. Neurosci.* 11:115. doi: 10.3389/fncel.2017.00115

Ellis, L. D., Krahe, R., Bourque, C. W., Dunn, R. J., and Chacron, M. J. (2007a). Muscarinic receptors control frequency tuning through the downregulation of an a-type potassium current. *J. Neurophysiol.* 98, 1526–1537. doi: 10.1152/jn.00564.2007

Ellis, L. D., Mehaffey, W. H., Harvey-Girard, E., Turner, R. W., Maler, L., and Dunn, R. J. (2007b). SK channels provide a novel mechanism for the control of frequency tuning in electrosensory neurons. *J. Neurosci.* 27, 9491–9502. doi: 10.1523/JNEUROSCI.1106-07.2007

Ellis, L. D., Maler, L., and Dunn, R. J. (2008). Differential distribution of SK channel subtypes in the brain of the weakly electric fish Apteronotus leptorhynchus. *J. Comp. Neurol.* 507, 1964–1978. doi: 10.1002/cne.21597

Fernandez, F. R., Mehaffey, W. H., and Turner, R. W. (2005). Dendritic Na^+ current inactivation can increase cell excitability by delaying a somatic depolarizing afterpotential. *J. Neurophysiol.* 94, 3836–3848. doi: 10.1152/jn.00653.2005

Gabbiani, F., Metzner, W., Wessel, R., and Koch, C. (1996). From stimulus encoding to feature extraction in weakly electric fish. *Nature* 384, 564–567. doi: 10.1038/384564a0

Guido, W., Lu, S. M., Vaughan, J. W., Godwin, D. W., and Sherman, S. M. (1995). Receiver operating characteristic (ROC) analysis of neurons in the cat's lateral geniculate nucleus during tonic and burst response mode. *Vis. Neurosci.* 12, 723–741. doi: 10.1017/s0952523800008993

Hille, B. (2001). *Ion Channels of Excitable Membranes.* 3rd Edn. Sunderland, Massachusetts, USA: Sinauer Associates.

Hofmann, V., and Chacron, M. J. (2017). Differential receptive field organizations give rise to nearly identical neural correlations across three parallel sensory maps in weakly electric fish. *PLoS Comput. Biol.* 13:e1005716. doi: 10.1371/journal.pcbi.1005716

Johnston, S. A., Maler, L., and Tinner, B. (1990). The distribution of serotonin in the brain of Apteronotus leptorhynchus: an immunohistochemical study. *J. Chem. Neuroanat.* 3, 429–465.

Kawasaki, M. (2005). "Physiology of tuberous electrosensory systems," in *Electroreception*, eds T. H. Bullock, C. D. Hopkins, A. N. Popper and R. R. Fay (New York, NY: Springer), 154–194.

Kepecs, A., Wang, X.-J., and Lisman, J. (2002). Bursting neurons signal input slope. *J. Neurosci.* 22, 9053–9062. doi: 10.1523/JNEUROSCI.22-20-09053.2002

Krahe, R., Bastian, J., and Chacron, M. J. (2008). Temporal processing across multiple topographic maps in the electrosensory system. *J. Neurophysiol.* 100, 852–867. doi: 10.1152/jn.90300.2008

Krahe, R., and Gabbiani, F. (2004). Burst firing in sensory systems. *Nat. Rev. Neurosci.* 5, 13–23. doi: 10.1038/nrn1296

Krahe, R., and Maler, L. (2014). Neural maps in the electrosensory system of weakly electric fish. *Curr. Opin. Neurobiol.* 24, 13–21. doi: 10.1016/j.conb.2013.08.013

Larson, E. A., Metzen, M. G., and Chacron, M. J. (2014). Serotonin modulates electrosensory processing and behavior via 5-HT2-like receptors. *Neuroscience* 271, 108–118. doi: 10.1016/j.neuroscience.2014.04.033

Lesica, N. A., and Stanley, G. B. (2004). Encoding of natural scene movies by tonic and burst spikes in the lateral geniculate nucleus. *J. Neurosci.* 24, 10731–10740. doi: 10.1523/JNEUROSCI.3059-04.2004

Lizbinski, K. M., Marsat, G., and Dacks, A. M. (2018). Systematic analysis of transmitter coexpression reveals organizing principles of local interneuron heterogeneity. *eNeuro* 5:ENEURO.0212–18.2018. doi: 10.1523/eneuro.0212-18.2018

Maler, L. (1979). The posterior lateral line lobe of certain gymnotoid fish: quantitative light microscopy. *J. Comp. Neurol.* 183, 323–363. doi: 10.1002/cne.901830208

Maler, L. (2007). Neural strategies for optimal processing of sensory signals. *Prog. Brain Res.* 165, 135–154. doi: 10.1016/S0079-6123(06)65009-7

Maler, L. (2009). Receptive field organization across multiple electrosensory maps. I. Columnar organization and estimation of receptive field size. *J. Comp. Neurol.* 516, 376–393. doi: 10.1002/cne.22124

Márquez, B. T., Krahe, R., and Chacron, M. J. (2013). Neuromodulation of early electrosensory processing in gymnotiform weakly electric fish. *J. Exp. Biol.* 216, 2442–2450. doi: 10.1242/jeb.082370

Marsat, G., and Pollack, G. S. (2006). A behavioral role for feature detection by sensory bursts. *J. Neurosci.* 26, 10542–10547. doi: 10.1523/JNEUROSCI.2221-06.2006

Marsat, G., and Pollack, G. S. (2010). The structure and size of sensory bursts encode stimulus information but only size affects behavior. *J. Comp. Physiol. A* 196, 315–320. doi: 10.1007/s00359-010-0514-8

Marsat, G., and Pollack, G. S. (2012). Bursting neurons and ultrasound avoidance in crickets. *Front. Neurosci.* 6:95. doi: 10.3389/fnins.2012.00095

Marsat, G., Proville, R. D., and Maler, L. (2009). Transient signals trigger synchronous bursts in an identified population of neurons. *J. Neurophysiol.* 102, 714–723. doi: 10.1152/jn.91366.2008

Mehaffey, W. H., Doiron, B., Maler, L., and Turner, R. W. (2005). Deterministic multiplicative gain control with active dendrites. *J. Neurosci.* 25, 9968–9977. doi: 10.1523/JNEUROSCI.2682-05.2005

Mehaffey, W. H., Maler, L., and Turner, R. W. (2008). Intrinsic frequency tuning in ELL pyramidal cells varies across electrosensory maps. *J. Neurophysiol.* 99, 2641–2655. doi: 10.1152/jn.00028.2008

Metzner, W., and Juranek, J. (1997). A sensory brain map for each behavior? *Proc. Natl. Acad. Sci. U S A* 94, 14798–14803. doi: 10.1073/pnas.94.26.14798

Metzner, W., Koch, C., Wessel, R., and Gabbiani, F. (1998). Feature extraction by burst-like spike patterns in multiple sensory maps. *J. Neurosci.* 18, 2283–2300. doi: 10.1523/JNEUROSCI.18-06-02283.1998

Nelson, M. E., and Maciver, M. A. (1999). Prey capture in the weakly electric fish Apteronotus albifrons: sensory acquisition strategies and electrosensory consequences. *J. Exp. Biol.* 202, 1195–1203.

Olesen, O. F. (1994). Expression of low molecular weight isoforms of microtubule-associated protein 2. Phosphorylation and induction of microtubule assembly *in vitro*. *J. Biol. Chem.* 269, 32904–32908.

Oswald, A.-M. M., Chacron, M. J., Doiron, B., Bastian, J., and Maler, L. (2004). Parallel processing of sensory input by bursts and isolated spikes. *J. Neurosci.* 24, 4351–4362. doi: 10.1523/JNEUROSCI.0459-04.2004

Oswald, A.-M. M., Doiron, B., and Maler, L. (2007). Interval coding. I. Burst interspike intervals as indicators of stimulus intensity. *J. Neurophysiol.* 97, 2731–2743. doi: 10.1152/jn.00987.2006

Prešern, J., Triblehorn, J. D., and Schul, J. (2015). Dynamic dendritic compartmentalization underlies stimulus-specific adaptation in an insect neuron. *J. Neurophysiol.* 113, 3787–3797. doi: 10.1152/jn.00945.2014

Prinz, A. A., Bucher, D., and Marder, E. (2004). Similar network activity from disparate circuit parameters. *Nat. Neurosci.* 7, 1345–1352. doi: 10.1038/nn1352

Turner, R. W., Lemon, N., Doiron, B., Rashid, A. J., Morales, E., Longtin, A., et al. (2002). Oscillatory burst discharge generated through conditional backpropagation of dendritic spikes. *J. Physiol.* 96, 517–530. doi: 10.1016/s0928-4257(03)00007-x

Turner, R., Maler, L., Deerinck, T., Levinson, S., and Ellisman, M. (1994). TTX-sensitive dendritic sodium channels underlie oscillatory discharge in a vertebrate sensory neuron. *J. Neurosci.* 14, 6453–6471. doi: 10.1523/JNEUROSCI.14-11-06453.1994

Turner, R. W., Plant, J. R., and Maler, L. (1996). Oscillatory and burst discharge across electrosensory topographic maps. *J. Neurophysiol.* 76, 2364–2382. doi: 10.1152/jn.1996.76.4.2364

Conflict of Interest Statement: The authors declare that the research was conducted in the absence of any commercial or financial relationships that could be construed as a potential conflict of interest.

frontiers in Integrative Neuroscience

BRIEF RESEARCH REPORT
published: 05 July 2019
doi: 10.3389/fnint.2019.00021

Dominance in Habitat Preference and Diurnal Explorative Behavior of the Weakly Electric Fish *Apteronotus leptorhynchus*

*Till Raab, Laura Linhart, Anna Wurm and Jan Benda**

Institute for Neurobiology, Eberhard Karls Universität, Tübingen, Germany

Electrocommunication and -localization behaviors of weakly electric fish have been studied extensively in the lab, mostly by means of short-term observations on constrained fish. Far less is known about their behaviors in more natural-like settings, where fish are less constrained in space and time. We tracked individual fish in a population of fourteen brown ghost knifefish (*Apteronotus leptorhynchus*) housed in a large 2 m^3 indoor tank based on their electric organ discharges (EOD). The tank contained four different natural-like microhabitats (gravel, plants, isolated stones, stacked stones). In particular during the day individual fish showed preferences for specific habitats which provided appropriate shelter. Male fish with higher EOD frequencies spent more time in their preferred habitat during the day, moved more often between habitats during the night, and less often during the day in comparison to low-frequency males. Our data thus revealed a link between dominance indicated by higher EOD frequency, territoriality, and a more explorative personality in male *A. leptorhynchus*. In females, movement activity during both day and night correlated positively with EOD frequency. In the night, fish of either sex moved to another habitat after about 6 s on average. During the day, the average transition time was also very short at about 20 s. However, these activity phases were interrupted by phases of inactivity that lasted on average about 20 min during the day, but only 3 min in the night. The individual preference for daytime retreat sites did not reflect the frequent explorative movements at night.

Keywords: animal behavior, weakly electric fish, dominance, diurnal activity, habitat selection

OPEN ACCESS

Edited by:
Maurice Chacron, McGill University, Canada

Reviewed by:
G. Troy Smith, Indiana University Bloomington, United States
John E. Lewis, University of Ottawa, Canada

****Correspondence:***
Jan Benda
jan.benda@uni-tuebingen.de

Received: *29 March 2019*
Accepted: *19 June 2019*
Published: *05 July 2019*

Citation:
Raab T, Linhart L, Wurm A and Benda J (2019) Dominance in Habitat Preference and Diurnal Explorative Behavior of the Weakly Electric Fish Apteronotus leptorhynchus. Front. Integr. Neurosci. 13:21. doi: 10.3389/fnint.2019.00021

1. INTRODUCTION

Weakly electric fish are nocturnally active. In the night, many pulse-type fish increase the rate of their electric organ discharges (EOD) (Lissmann and Schwassmann, 1965; Stoddard et al., 2007), wave-type fish emit various kinds of electrocommunication signals more frequently (Zupanc et al., 2001; Henninger et al., 2018), and gymnotids have been shown to move from deep waters up to the shore (Steinbach, 1970). During the day, weakly electric fish hide under submerged logs (*Gymnotus*, Westby, 1988), between roots (*Eigenmannia*, Hopkins, 1974), in leaf litter (*Brachyhypopomus*, Hagedorn, 1988), or bury themselves in sand (*Gymnorhamphichthys*, Lissmann and Schwassmann, 1965).

EOD frequencies of the gymnotiform brown ghost knifefish *A. leptorhynchus* are sexually dimorphic with males having higher EOD frequencies than females (Meyer et al., 1987). In playback experiments with restrained fish, males more frequently produced aggressive communication signals (chirps) than females (Zupanc and Maler, 1993; Bastian et al., 2001) and in experiments of free swimming fish, male *A. leptorhynchus* showed a higher overall chirp rate compared to females (Dunlap and Oliveri, 2002; Hupé and Lewis, 2008). However, during courtship in the field females produced almost as many chirps as males (Henninger et al., 2018), and both sexes jammed rivals by approaching their EOD frequencies (Tallarovic and Zakon, 2002). In competition experiments, male *A. leptorhynchus* were more likely to inhabit tubes alone, whereas females cohabited tubes more often (Dunlap and Oliveri, 2002).

Several studies suggest higher EOD frequencies in males as an indicator of dominance. Additionally, body size correlated with EOD frequency in males (Triefenbach and Zakon, 2008; Fugère et al., 2011) but not in females (Dunlap and Oliveri, 2002). Dominant males with higher EOD frequencies were more aggressive (Fugère et al., 2011) and participated more in mating (Hagedorn and Heiligenberg, 1985; Henninger et al., 2018). In competition experiments, males with higher EOD frequencies occupied the most preferred tubes, whereas females did not distribute according to EOD frequency (Dunlap and Oliveri, 2002). In summary, these laboratory studies suggest that male brown ghost knifefish are territorial at their preferred retreat site during the day, and that males with higher EOD frequencies are more dominant.

Observations on aggression and dominance have previously been limited to studies in the lab in small tanks, and mostly to short observation times (e.g., Hopkins, 1974; Hagedorn and Heiligenberg, 1985; Nelson and MacIver, 1999; Tallarovic and Zakon, 2005; Hupé and Lewis, 2008; Triefenbach and Zakon, 2008). Recent technological advances allow for long-term observations of electric activity of these fish in the lab and in the field (Henninger et al., 2018; Madhav et al., 2018). Here, we take advantage of these methods and describe diurnal activity patterns of a community of *A. leptorhynchus* competing for different microhabitats in a large indoor tank over 10 days.

2. METHODS

Six male and eight female *A. leptorhynchus*, obtained from a tropical fish supplier, were housed in a $2.5 \times 1 \times 0.8\,m^3$ indoor tank with a water conductivity of 320 µS/cm at a 12 h/12 h light cycle. Initially, four fish inhabited the tank. Starting at day 4 we introduced two additional fish per day. Fish were selected for approximately equal size to minimize effects based on physical differences as far as possible. All fish were mature and not in breeding condition. EOD frequency is sexually dimorphic in *A. leptorhynchus* (Meyer et al., 1987). We identified fish with EOD frequencies lower than 750 Hz as females, and fish with higher EOD frequencies as males (Henninger et al., 2018). Four natural-like habitats in $60 \times 45 \times 10\,cm^3$ PVC-containers were arranged next to each other in the tank: stacked stones, quartz gravel (few millimeters diameter), isolated stones, and aquatic plants (*Vallisneria spec.*) (**Figure 1A**). Fish were fed frozen *Chironomus plumosus* on the gravel habitat every day at about 8 h after lights were switched on. Animal housing complied with national and European law and was approved by the Regierungspräsidium Tübingen (permit no: 35/9185.46/UniTÜ). Approval by an ethics committee was not required because our study was purely observational.

We continuously recorded EODs for 10 days and nights using 16 monopolar electrodes at low-noise headstages, and digitized at 20 kHz per channel with 16 bit resolution (see Henninger et al., 2018 for details). For each of the four habitats, two electrodes were placed at the bottom of the habitat 35 cm apart and two electrodes 35 cm above the respective electrodes in the habitats in the open water (**Figures 1A,B**). Water temperature was measured once a day. During the course of the experiment, water temperature steadily dropped from 26.3°C to 24.8°C. Fish were identified by their specific peaks in the spectrogram of the recordings (nfft = 2^{16}, overlap = 90%) and tracked using a custom tracking algorithm comparing fundamental EOD frequency and the corresponding power pattern in the spectrograms of the different electrodes (see Henninger et al., 2018 and Madhav et al., 2018 for details).

Every 0.328 ms (temporal resolution of the spectrogram), fish were assigned to habitats by means of the electrode with the largest power at the fish's EOD frequency. Based on this spatial information we analyzed how the fish occupied the habitats. For each day and night, we computed the fraction of fish in each habitat by dividing the detections within one habitat by the total number of detections on that day or night (**Figure 1E**). Likewise, individual habitat preferences were computed separately based on the detections of each fish (**Figure 2A**). To assess the number and composition of fish in each habitat we counted the number of males and females detected in each habitat for every time step (**Figure 2C**). The male ratio is the number of males in a habitat divided by the total number of detected fish in that habitat (**Figure 2D**).

The preferred habitat of a fish was defined as the habitat where the fish spent most of the time, i.e., had the most detections, for each day and night. Relative time spent in the preferred habitat was computed as the ratio between detections in the preferred habitat and the number of detections per day or night (12 h $\times$ 3,600 s/h $\times$ 3.05 detections per second $\approx$ 131,827 detections per 12 h) for every day and night (**Figure 2B**). The stability of individual habitat preferences were evaluated using preference change rates, i.e., the probability of a fish to change its preferred habitat from one day or night to another one, computed as the number of days (or nights) on which the fish preferred a different habitat as on the previous day (or night) divided by the number of days the fish was in the tank minus one (**Figures 3A,C**).

Transitions of fish between habitats were characterized by the number of transitions of detections from electrodes of one habitat to electrodes from another habitat (**Figures 3B,D**). The distributions of transition times Δt, i.e., the time spans a fish spent in one habitat between two habitat changes, were

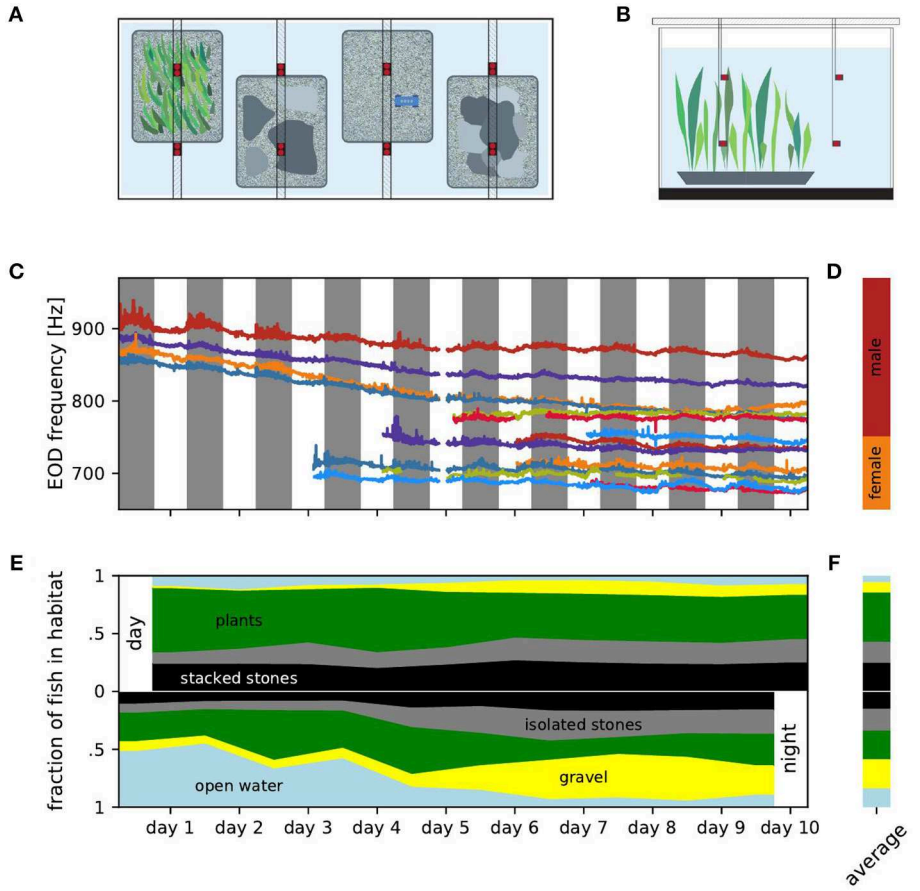

FIGURE 1 | Experimental setup, EOD frequencies and distribution of fish over habitats. **(A)** Top view of the experimental setup with four different micro habitats (plants, isolated stones, gravel, stacked stones). Electrodes (red) were fixed in location by PVC poles positioned above the tank. Fish were fed on a daily basis on the gravel habitat using a custom PCV feeder (blue). **(B)** Side view of the experimental setup showing the electrodes positioned in two levels over the habitats. **(C)** EOD frequency traces tracked over the entire duration of the experiment. Individual fish are marked by the same color in all figures. **(D)** Ranges of male (red) and female (orange) EOD frequencies. **(E)** Fraction of fish detected within each of the five habitats for consecutive days (top) and nights (bottom). **(F)** Relative occupation of the habitats averaged over all days (top) and nights (bottom).

exponentially distributed (**Figure 4A**):

$$p(\Delta t) = \lambda e^{-\lambda \Delta t}. \tag{1}$$

The number of transitions per time (**Figure 3B**) is the transition rate. In **Figure 4B** the transition rate $\lambda = 1/\tau$ was estimated from the average transition time $\tau = \frac{1}{n}\sum_{i=1}^{n} \Delta t_i$ for each fish separately for days and nights.

The tails in the distributions of transition times dominate the activity patterns of the fish because a single long transition time implies a non-moving fish for exactly this time. During the same time, however, many more short transitions can occur. Short transition times are thus overrepresented when taking the average. To account for this we also computed a weighted average $\overline{\Delta t_i}$, where we weighted each transition time Δt_i by its duration Δt_i (**Figure 4C**):

$$\overline{\Delta t_i} = \frac{\sum_{i=1}^{n} \Delta t_i^2}{\sum_{i=1}^{n} \Delta t_i} \tag{2}$$

Finally, we investigated if individual habitat changes were independent of each other by calculating the time differences between a fish entering a habitat and the other fish leaving the respective habitat. We compared these distributions to boot strapped distributions where entering times to a random habitat were set randomly throughout the whole recording period.

Because fish were in similar physical condition and their sexes were determined using only a hard EOD frequency cutoff at 750 Hz we performed a sensitivity analysis for all corresponding results, i.e., additionally to the original sex assignments, all statistics were calculated with up to ±2 males or females, where the individuals closest to the cutoff were assigned to the opposite sex.

For quantifying differences between groups we used Cohen's d for unequal group sizes:

$$d = \left| \frac{\mu_1 - \mu_2}{\frac{n-1}{n+m-2}\sigma_1^2 + \frac{m-1}{n+m-2}\sigma_2^2} \right| \tag{3}$$

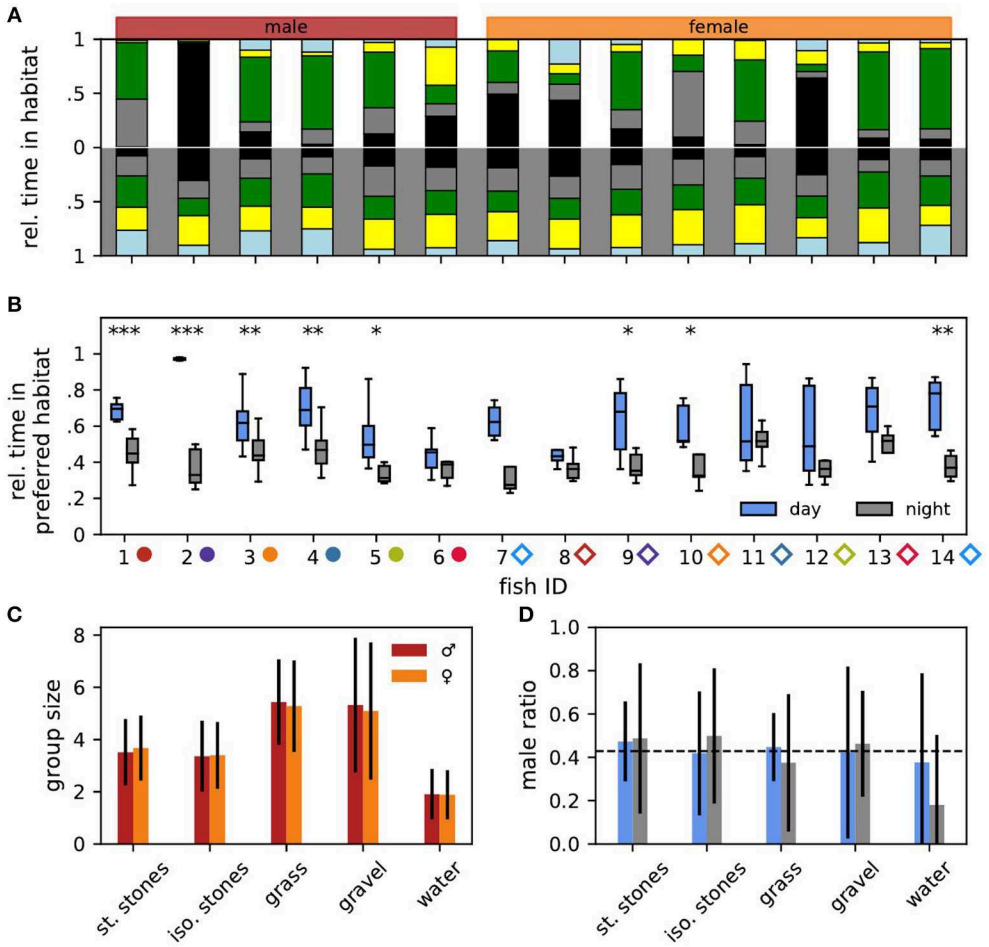

FIGURE 2 | Habitat preference. **(A)** Relative time each individual fish spent in the different habitats (same color code as in **Figure 1E**) averaged over all days (top) and nights (bottom). Males (fish IDs 1–6) are indicated in red, females (fish IDs 7–14) in orange. Male and female fish IDs are sorted according to descending EOD frequency in all figures. **(B)** For each fish and day (blue) or night (gray) the fraction of time the fish spent in its currently preferred habitat. Asterisks indicate significant differences: $^{***}p < 0.001$, $^{**}p < 0.01$, and $^{*}p < 0.05$. **(C)** For each habitat the mean group size with standard deviation in which males (red) and females (orange) were found after the maximum of 14 fish had been reached. **(D)** For each habitat the average male ratio with standard deviation during the day (blue) and night (gray) after the maximum of 14 fish had been reached.

where μ_1 and μ_2 are the means, σ_1 and σ_2 the standard deviations, and n and m the group sizes, respectively.

3. RESULTS

We observed the movements of six male and eight female *A. leptorhynchus* between four microhabitats and the open water in a two cubic meter tank over 10 days. We tracked individual fish based on EOD frequency and power on 16 recording electrodes (**Figure 1C**). EOD frequency is known to be sexually dimorphic in *A. leptorhynchus* (Meyer et al., 1987). Fish with an EOD frequency above 750 Hz are defined as males, fish below 750 Hz as females (**Figure 1D**, Henninger et al., 2018). The overall decline of EOD frequencies followed the water temperature, which decreased by 1.5°C over the course of the experiment. In fact, the Q_{10} values computed for each fish from daily temperature measurements and the corresponding EOD frequencies (median $Q_{10} = 1.54$) were close to typical Q_{10} values reported for these fish in the literature (Dunlap et al., 2000; Stöckl et al., 2014). Additionally, circadian modulations of each fish's EOD frequency followed similar patterns and can also be best explained by periodic diurnal water temperature changes (Dunlap et al., 2000). On top of these exogenous influences, the fish actively changed their EOD frequency, approaching and evading EOD frequencies of other fish. For example, the EOD frequencies of the males indicated in orange and blue approached each other and got closer to the males indicated in red and green. Female fish also approached each other in their EOD frequency and even switched order (e.g., the females indicated in red and light blue at the bottom of **Figure 1C**). In the following we do not analyze these modulations of EOD frequency but rather focus on diurnal movement patterns.

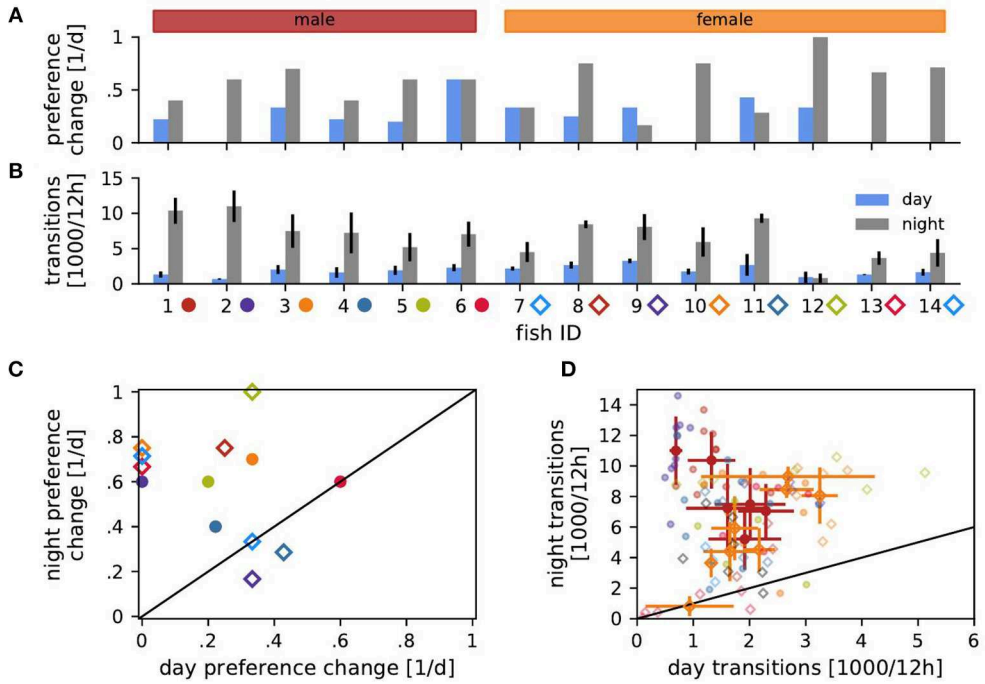

FIGURE 3 | Transitions of habitat preference and between habitats. **(A)** Probability of changing the preferred habitat from one day (blue) or night (gray) to the next for each fish. **(B)** Transition rates, i.e., number of detected transitions between habitats per 12 h, averaged over days (blue) or nights (gray) with standard deviation. **(C)** Probabilities of changing preference of night habitats vs. preference changes of day habitats from **(A)**. **(D)** Transition rates during the day vs. transition rates at night from **(B)**. Transition counts averaged over days and nights with standard deviation are shown for each male (red) and female (orange). Symbols in **(C,D)** indicate fish ID as in **(B)**.

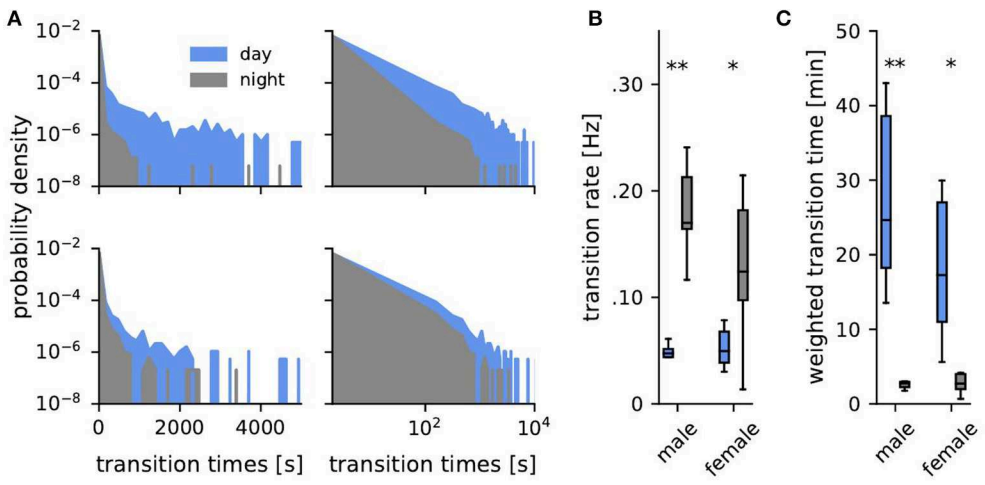

FIGURE 4 | Transition times. **(A)** Probability density of transition times (time span spent consecutively within one habitat) during the day (blue) and the night (gray) for one example male (top, fish ID 4) and female (bottom, fish ID 10). **(B)** Corresponding transition rates obtained from fitting an exponential to the distributions of transition times. **(C)** Averaged weighted transition times (Equation 2). Asterisks indicate significant differences: $^{**}p < 0.01$ and $^{*}p < 0.05$.

3.1. Habitat Occupation

The tank offered the fish four different 0.25 m^2 habitats that contained either stacked stones, quartz gravel, isolated stones, or aquatic plants. We counted the open water above the habitats as a fifth habitat. For each time point we assigned each fish to one of these habitats according to the electrode with the largest power at its EOD frequency.

During the days, i.e., the presumably inactive phases of the fish, most fish were located within the aquatic plants followed by the stacked stones and the isolated stones. Fish were rarely

found in the gravel habitat or in the open water (**Figures 1E,F**, top). At night, no habitat seemed to be preferred on average (**Figures 1E,F**, bottom).

During the days, the addition of fish did not influence the distribution of fish in the habitats by a lot (**Figure 1E**, top). The standard deviation of the fraction of fish occupying a habitat was below 6.5 % for all habitats. Nevertheless, the fraction of fish occupying isolated stones or gravel increased slightly throughout the experiment (Spearman's rank correlation: $r = 0.76, p = 0.005$ and $r = 0.88, p < 0.001$, respectively), whereas the occupation of the aquatic plants and the open water slightly decreased within the 10 days (Spearman's rank correlation: $r = -0.76$, $p < 0.05$ and $r = -0.65$, $p < 0.05$, respectively). The occupation of the stacked stones habitat was unaffected by the increasing fish count and did not change over the days of the experiment (Spearman's rank correlation: $r = 0.37, p = 0.30$). Consequently, the increasing total fish count lead to an almost uniform increase in the number of fish occupying each habitat. None of the habitats was claimed exclusively by a dominant fish as a retreat site during the days.

In contrast, at nights the increased fish count seemed to influence the distribution of the fish over the habitats more strongly (**Figure 1E**, bottom). The occupation of both the isolated and stacked stones habitats increased slightly during the course of the experiment (Spearman's rank correlation: $r = 0.84, p < 0.01$ and $r = 0.79, p < 0.01$, respectively), whereas the fraction of fish in the open water clearly decreased (Spearman's rank correlation: $r = -0.90, p < 0.001$) and the occupation of the gravel habitat increased (Spearman's rank correlation: $r = 0.95, p < 0.001$). The latter could be attributed to the experimental design. Food was supplied daily at the gravel habitat and gymnotiform fish have been shown to learn the location of food (Jun et al., 2013).

3.2. Habitat Preferences

Let us now turn to the habitat preferences of individual fish (**Figures 2A,B**). Even during the day fish did not stay at the same habitat. Male no. 2 was the only exception, which throughout the experiment stayed in the stacked stones at daytime (**Figure 2A**, top). The preferred daytime habitat, i.e., the habitat the fish stayed the longest during the day, varied between individuals. Some fish preferred the stacked stones, whereas others preferred the isolated stones or the plants. Only male no. 6 had a slight preference for the gravel habitat. In the night, individual fish had less obvious preferences for specific habitats on average (Wilcoxon: $W = 0, p = 0.001$, **Figure 2A**, bottom).

The fish sometimes changed their preferred habitat from one day to another (**Figure 3A**). Preferred nighttime habitats were changed more often than daytime habitats (Wilcoxon: $W = 3$, $p = 0.005$) (**Figure 3C**). The probability of changing the preferred habitat from one day to the next did not significantly correlate with EOD frequency, neither for males nor for females (Spearman's rank correlation: $p > 0.2$).

In particular males stayed significantly longer in their preferred daytime habitat than in their preferred nighttime habitat (**Figure 2B**). Furthermore, males with higher EOD frequencies spent more time in their preferred daytime habitat than low-frequency males (Spearman's rank correlation: $r = 0.49$, $p < 0.001$). For males at night and females no such correlation was significant (Spearman's rank correlation: $p > 0.1$).

To summarize, with the exception of male no. 2, the notion of a "preferred habitat" turns out to be misleading. Of course there is always a habitat where a fish spends most time during a day or night simply by definition. However, other habitats are visited as well (**Figures 2A,B**) and even the preferred habitat is changed within a few days (**Figure 3A**).

3.3. Group Sizes and Composition

Many fish had similar habitat preferences. This should be reflected in the number of fish found in each habitat. For quantifying group sizes and compositions in the different habitats we analyzed the final 78 h where all fourteen fish were present in the tank. The mean group size differed between the habitats (**Figure 2C**). Significantly less fish were simultaneously detected in the open water (1.89 ± 0.95) than in the isolated stones (3.39 ± 1.32, Mann-Whitney U: $p < 0.001$, Cohen's $d = 1.20$), and stacked stones (3.61 ± 1.26, Mann-Whitney U: $p < 0.001$, Cohen's $d = 1.43$). Group sizes in the gravel (5.21 ± 2.61) and plant habitat were significantly larger than in both stone habitats and the open water (Mann-Whitney U: $p < 0.001$, Cohen's d: $0.78 < d < 2.16$).

Interestingly, male ratios in all habitats were close to the expected 0.43 given by the overall number of six males and eight females (dashed line in **Figure 2D**, Cohen's $d < 0.24$). There was no difference in habitat preferences between the sexes. Only in the open water at night the male ratio was considerably lower than expected (Cohen's $d = 0.77$).

3.4. Transitions Between Habitats

Fish frequently moved between habitats (**Figure 3B**). The EOD frequency of males correlated negatively with the number of transitions between habitats during the day and positively during the night (Spearman's rank correlation: $r = -0.47$, $p < 0.01$ and $r = 0.55$, $p < 0.001$, respectively). That is, high-frequency males were more territorial during the day and more explorative at night than low-frequency males. In females, transition counts correlated positively with EOD frequency during both day and night (Spearman's rank correlation: $r = 0.55$, $p < 0.001$ and $r = 0.45$, $p < 0.01$). Therefore, females with higher EOD frequency were more active.

Both males and females switched habitats significantly more often during the night than during the day (**Figure 3D**). The more stationary males were during the day, the more explorative they were at night (Spearman's rank correlation: $r = -0.49$, $p < 0.001$). On the other hand, female transition counts during day and night were positively correlated ($r = 0.53, p < 0.001$). No such correlations existed for individual fish.

Transition times, i.e., the time intervals between habitat transitions, were approximately exponentially distributed (Equation 1, **Figure 4A**). Such exponential distributions are generated by Poisson point processes where the probability of an event (here a transition to another habitat) is the same for each time point and independent of previous events, like for example radioactive decay or state transitions of ion channels.

There was no distinguished time scale that separated activity phases from resting phases. Transition rates (**Figures 3B**, **4B**) were generally quite high and average to 0.1 Hz. They were significantly larger during the night than during the day for both, males (Mann-Whitney U: $U = 0, p < 0.01, d = 4.05$) and females (Mann-Whitney U: $U = 8, p < 0.05, d = 1.58$), and were independent of sex (**Figure 4B**).

Averaged weighted transition times, Equation (2), better capture differences on long time scales, reflecting non-moving fish. On average weighted transition times were 20 min during the day and 3 min at night (**Figure 4C**, Mann-Whitney U: males $U = 0, p < 0.01, d = 1.41$, females $U = 8, p < 0.05, d = 0.34$).

Transitions of individual fish were independent from other fish entering the habitat (not shown). The distribution of times between a fish entering a habitat and another fish leaving the same habitat showed statistically significant (Kolmogorov-Smirnov test, $p < 0.001$) but small differences to a distribution generated for times of a fish entering a randomly chosen habitat drawn from a uniform distribution (Cohen's d: $0.02 < d < 0.08$).

3.5. Sensitivity Analysis

Since we based the sex of the fish on EOD frequency only, we repeated all analysis for different EOD frequency thresholds separating males from females. For up to two males reassigned to females and vice versa the sex dependent results in the contexts of **Figures 3C,D**, **4B,C** did not change. All significant levels as well as effect sizes stayed in the same range.

4. DISCUSSION

We observed movement patterns and habitat preferences in a population of fourteen brown ghost knifefish, *A. leptorhynchus*, in a large indoor tank over 10 days. During the day, these nocturnal fish distributed themselves quite uniformly in habitats providing appropriate retreat sites between stones or plants. Activity at night was characterized by strong explorative movements where fish frequently changed between habitats and the open water. In male fish, high EOD frequency correlated with more territorial behavior during days and a more explorative personality at night, whereas in female fish EOD frequency was positively correlated with movement activity during both day and night.

4.1. Nocturnal Activity

Despite the well supported common notion of weakly electric fish being nocturnally active (Lissmann and Schwassmann, 1965; Zupanc et al., 2001; Henninger et al., 2018), our data show that phases of activity, as indicated by short transition times between the habitats, occurred in similar ways both at night and during the day (**Figure 4A**). There was no qualitative difference between day and night. During the day, phases of inactivity were prolonged about ten-fold in comparison to the ones at night (**Figures 4B,C**). Otherwise, activity, as quantified by transitions between habitats, occurred randomly and independently of each other. This fits well with the description of stochastic onsets of activity phases in *Gymnotus* (Jun et al., 2014).

4.2. Retreat Site Selection

Selection of an appropriate retreat site has profound effects on the animal's physiological condition and fitness (Rosenzweig, 1981; Huey, 1991). All of the preferred retreat sites in our experiment offered appropriate places where fish could hide. This fits well to field observations where fish were also found hiding under submerged logs, between roots, or in leaf litter during the day (Hopkins, 1974; Hagedorn, 1988; Westby, 1988). Our data demonstrates that, at least in captivity, most fish do not depend on specific retreat sites, like for example stacked stones, but rather change between many available types of microhabitats.

In small tanks in the laboratory males often compete over tubes provided for refuge (Hopkins, 1974; Hagedorn, 1988; Fugère et al., 2011). In the presence of enough tubes, male *A. leptorhynchus* preferred to occupy tubes alone, but females were sometimes found together in single tubes (Dunlap and Oliveri, 2002). Fish had clear preferences when presented with a variety of tubes of different dimensions and opacity (Dunlap and Oliveri, 2002).

In our study fish showed individual preferences for different habitats (**Figure 2A**). The grass and gravel habitat accommodated the most individuals simultaneously, and the open water the least (**Figure 2C**). This indicates either differences in general habitat quality or differences in the actual number of available suitable retreat sites in each of the habitats. The fraction of males found in each habitat on average did not deviate from the expectation given the total number of males and females (**Figure 2D**). Thus, group composition on the scale of a whole habitat was not influenced by the hierarchical status of individual fish. However, our experimental design did not allow to resolve group compositions on a finer spatial scale of specific retreat sites within each habitat. Our data therefore do not contradict an influence of hierarchical status on retreat site selection as reported by Dunlap and Oliveri (2002).

4.3. Social Dominance

The EOD and its modulations convey information about species, sex, status and intent of individuals (e.g., Hagedorn and Heiligenberg, 1985; Stamper et al., 2010; Fugère et al., 2011). In *A. leptorhynchus* EOD frequency correlates with body size (Dunlap, 2002; Triefenbach and Zakon, 2003). Furthermore, dominant males in breeding contexts in the laboratory (Hagedorn and Heiligenberg, 1985) as well as in the field (Henninger et al., 2018), and in tube selection contexts (Dunlap and Oliveri, 2002; Fugère et al., 2011) had higher EOD frequencies. We here reported a more subtle variant of dominance. Male fish with higher EOD frequency moved less between habitats during the day and showed increased movement activity at night compared to males with lower EOD frequency. These increased nocturnal movement activities could reflect frequent fights for dominance (Tallarovic and Zakon, 2005), as the approaching EOD frequencies of the fish suggest (**Figure 1C**). Contrary to the expectation of fish fighting for dominance, the time points of fish leaving a habitat were independent from fish entering the respective habitat. A closer inspection of the EOD frequency traces for communication signals like rises and chirps (Zakon et al., 2002) could help classify different types of

movement activities and interactions in the future (Triefenbach and Zakon, 2008). In females, EOD frequency did not appear to be correlated with dominance (Dunlap and Oliveri, 2002). However, we found that EOD frequencies of females were positively correlated with movement activity during both day and night. Rather than an indication of hierarchical status, EOD frequency seems to indicate individual activity personalities (Sih et al., 2004).

5. CONCLUSION

Many laboratory studies on the behavior of weakly electric fish focused on specific questions that were tested in temporally and spatially limited experimental settings (Hopkins, 1974; Hagedorn and Heiligenberg, 1985; Nelson and MacIver, 1999; Tallarovic and Zakon, 2002; Hupé and Lewis, 2008; Triefenbach and Zakon, 2008). Recent advances in recording techniques (Henninger et al., 2018; Madhav et al., 2018) allowed us to continuously monitor a population of weakly electric fish in a large tank with a more natural-like setting for many days. In particular, we did not force the fish into specific behaviors, but rather, extracted behavioral activity patterns from the data (Gomez-Marin et al., 2014). In this way, we revealed personality like differences in territoriality and explorative movements (Sih et al., 2004). In both males and females these were correlated with EOD frequency, suggesting EOD frequency as an indicator for more explorative personalities in both sexes, and territoriality in males.

DATA AVAILABILITY

The datasets generated for this study are available on request to the corresponding author.

ETHICS STATEMENT

Pure observational study on weakly electric fish.

AUTHOR CONTRIBUTIONS

TR: designed the experiment, analyzed data, and wrote the manuscript. LL and AW: measured and analyzed the data. JB: discussed the experiment and advised data analysis and wrote the manuscript.

ACKNOWLEDGMENTS

Supported by Deutsche Forschungsgemeinschaft, Open Access Publishing Fund of University of Tübingen, and the Center of Integrative Neuroscience at the University of Tübingen through the mini RTG Sensory Flow Processing across Modalities and Species.

REFERENCES

Bastian, J., Schniederjan, S., and Nguyenkim, J. (2001). Arginine vasotocin modulates a sexually dimorphic communication behavior in the weakly electric fish *Apteronotus leptorhynchus*. *J. Exp. Biol.* 204, 1909–1923.

Dunlap, K. D. (2002). Hormonal and body size correlates of electrocommunication behavior during dyadic interactions in a weakly electric fish, *Apteronotus leptorhynchus*. *Hormon. Behav.* 41, 187–194. doi: 10.1006/hbeh.2001.1744

Dunlap, K. D., and Oliveri, L. M. (2002). Retreat site selection and social organization in captive electric fish, *Apteronotus leptorhynchus*. *J. Comp. Physiol. A* 188, 469–477. doi: 10.1007/s00359-002-0319-5

Dunlap, K. D., Smith, G. T., and Yekta, A. (2000). Temperature dependence of electrocommunication signals and their underlying neural rhythms in the weakly electric fish, *Apteronotus leptorhynchus*. *Brain Behav. Evol.* 55, 152–162. doi: 10.1159/000006649

Fugère, V., Ortega, H., and Krahe, R. (2011). Electrical signalling of dominance in a wild population of electric fish. *Biol. Lett.* 7, 197–200. doi: 10.1098/rsbl.2010.0804

Gomez-Marin, A., Paton, J. J., Kampff, A. R., Costa, R. M., and Mainen, Z. F. (2014). Big behavioral data: psychology, ethology and the foundations of neuroscience. *Nat. Neurosci.* 17, 1455–1462. doi: 10.1038/nn.3812

Hagedorn, M. (1988). Ecology and behavior of a pulse-type electric fish, *Hypopomus occidentalis* (Gymnotiformes, Hypopomidae), in a fresh-water stream in Panama. *Copeia* 1988, 324–335. doi: 10.2307/1445872

Hagedorn, M., and Heiligenberg, W. (1985). Court and spark: electric signals in the courtship and mating of gymnotid fish. *Anim. Behav.* 33, 254–265. doi: 10.1016/S0003-3472(85)80139-1

Henninger, J., Krahe, R., Kirschbaum, F., Grewe, J., and Benda, J. (2018). Statistics of natural communication signals observed in the wild identify important yet neglected stimulus regimes in weakly electric fish. *J. Neurosci.* 38, 5456–5465. doi: 10.1523/JNEUROSCI.0350-18.2018

Hopkins, C. D. (1974). Electric communication: functions in the social behavior of *Eigenmannia virescens*. *Behavior* 50, 270–304. doi: 10.1163/156853974X00499

Huey, R. B. (1991). Physiological consequences of habitat selection. *Amer. Soc. Nat.* 137, 91–115. doi: 10.1086/285141

Hupé, G. J., and Lewis, J. E. (2008). Electrocommunication signals in free swimming brown ghost knifefish, *Apteronotus leptorhynchus*. *J. Exp. Biol.* 211, 1657–1667. doi: 10.1242/jeb.013516

Jun, J. J., Longtin, A., and Maler, L. (2013). Real-time localization of moving dipole sources for tracking multiple free-swimming weakly electric fish. *PLoS ONE* 8:e66596. doi: 10.1371/journal.pone.0066596

Jun, J. J., Longtin, A., and Maler, L. (2014). Enhanced sensory sampling precedes self-initiated locomotion in an electric fish. *J. Exp. Biol.* 217, 3615–3628. doi: 10.1242/jeb.105502

Lissmann, H. W., and Schwassmann, H. O. (1965). Activity rhythm of an electric fish, *Gymnorhamphichtys hypostomus*, ellis. *Z. vergl. Physiol.* 51, 153–171. doi: 10.1007/BF00299291

Madhav, M. S., Jayakumar, R. P., Demir, A., Stamper, S. A., Fortune, E. S., and Cowan, N. J. (2018). High-resolution behavioral mapping of electric fishes in amazonian habitats. *Sci. Rep.* 8:5830. doi: 10.1038/s41598-018-24035-5

Meyer, J. H., Leong, M., and Keller, C. H. (1987). Hormone-induced and maturational changes in electric organ discharges and electroreceptor tuning in the weakly electric fish *Apteronotus*. *J. Comp. Physiol. A* 160, 385–394. doi: 10.1007/BF00613028

Nelson, M. E., and MacIver, M. A. (1999). Prey capture in the weakly electric fish *Apteronotus albifrons*: sensory acquisition strategies and electrosensory consequences. *J. Exp. Biol.* 202, 1195–1203.

Rosenzweig, M. L. (1981). A theory of habitat selection. *Ecology* 62, 327–335. doi: 10.2307/1936707

Sih, A., Bell, A., and Johnson, J. C. (2004). Behavioral syndromes: an ecological and evolutionary overview. *Trends Ecol. Evol.* 19, 372–378. doi: 10.1016/j.tree.2004.04.009

Stamper, S. A., Carrera-G, E., Tan, E. W., Fugére V., Krahe, R., and Fortune, E. S. (2010). Species differences in group size and electrosensory interference in weakly electric fishes: implications for electrosensory processing. *Behav. Brain Res.* 207, 368–376. doi: 10.1016/j.bbr.2009.10.023

Steinbach, A. B. (1970). Diurnal movements and discharge characteristics of electric gymnotid fishes in the Rio Negro, Brazil. *Biol. Bull.* 138, 200–210. doi: 10.2307/1540202

Stöckl, A., Sinz, F., Benda, J., and Grewe, J. (2014). Encoding of social signals in all three electrosensory pathways of eigenmannia virescens. *J. Neurophysiol.* 112, 2076–2091. doi: 10.1152/jn.00116.2014

Stoddard, P. K., Markham, M. R., Salazar, V. L., and Allee, S. (2007). Circadian rhythms in electric waveform structure and rate in the electric fish *Brachyhypopomus pinnicaudatus*. *Physiol. Behav.* 90, 11–20. doi: 10.1016/j.physbeh.2006.08.013

Tallarovic, S. K., and Zakon, H. H. (2002). Electrocommunication signals in female brown ghost electric knifefish, *Apteronotus leptorhynchus*. *J. Comp. Physiol. A* 188, 649–657. doi: 10.1007/s00359-002-0344-4

Tallarovic, S. K., and Zakon, H. H. (2005). Electric organ discharge frequency jamming during social interactions in brown ghost knifefish, *Apteronotus leptorhynchus*. *Anim. Behav.* 70, 1355–1365. doi: 10.1016/j.anbehav.2005.03.020

Triefenbach, F., and Zakon, H. (2003). Effects of sex, sensitivity and status on cue recognition in the weakly electric fish *Apteronotus leptorhynchus*. *Anim. Behav.* 65, 19–28. doi: 10.1006/anbe.2002.2019

Triefenbach, F., and Zakon, H. H. (2008). Changes in signalling during agonistic interactions between male weakly electric knifefish, *Apteronotus leptorhynchus*. *Anim. Behav.* 75, 1263–1272. doi: 10.1016/j.anbehav.2007.09.027

Westby, G. W. M. (1988). The ecology, discharge diversity and predatory behaviour of gymnotiforme electric fish in the coastal streams of french guiana. *Behav. Ecol. Sociobiol.* 22, 341–354.

Zakon, H., Oestreich, J., Tallarovic, S., and Triefenbach, F. (2002). EOD modulations of brown ghost electric fish: JARs, chirps, rises, and dips. *J. Physiol. Paris* 96, 451–458. doi: 10.1016/S0928-4257(03)00012-3

Zupanc, G. K. H., and Maler, L. (1993). Evoked chirping in the weakly electric fish apteronotus leptorhynchus: a quantitative biophysical analysis. *Can. J. Zool.* 71, 2301–2310. doi: 10.1139/z93-323

Zupanc, M. M., Engler, G., Midson, A., Oxberry, H., Hurst, L. A., Symon, M. R., et al. (2001). Lightdark-controlled changes in modulations of the electric organ discharge in the teleost *Apteronotus leptorhynchus*. *Anim. Behav.* 62, 1119–1128. doi: 10.1006/anbe.2001.1867

Conflict of Interest Statement: The authors declare that the research was conducted in the absence of any commercial or financial relationships that could be construed as a potential conflict of interest.

frontiers in Integrative Neuroscience

REVIEW
published: 16 July 2019
doi: 10.3389/fnint.2019.00023

The Astonishing Behavior of Electric Eels

*Kenneth C. Catania**

Department of Biological Sciences, Vanderbilt University, Nashville, TN, United States

The remarkable physiology of the electric eel (*Electrophorus electricus*) made it one of the first model species in science. It was pivotal for understanding animal electricity in the 1700s, was investigated by Humboldt and Faraday in the 1800s, was leveraged to isolate the acetylcholine receptor in the 20th century, and has inspired the design of new power sources and provided insights to electric organ evolution in the 21st century. And yet few studies have investigated the electric eel's behavior. This review focuses on a series of recently discovered behaviors that evolved alongside the eel's extreme physiology. Eels use their high-voltage electric discharge to remotely control prey by transcutaneously activating motor neurons. Hunting eels use this behavior in two different ways. When prey have been detected, eels use high-voltage to cause immobility by inducing sustained, involuntary muscle contractions. On the other hand, when prey are hidden, eels often use brief pulses to induce prey twitch, which causes a water movement detected by the eel's mechanoreceptors. Once grasped in the eel's jaws, difficult prey are often subdued by sandwiching them between the two poles (head and tail) of the eel's powerful electric organ. The resulting concentration of the high-voltage discharge, delivered at high-rates, causes involuntary fatigue in prey muscles. This novel strategy for inactivating muscles is functionally analogous to poisoning the neuromuscular junction with venom. For self-defense, electric eels leap from the water to directly electrify threats, efficiently activating nociceptors to deter their target. The latter behavior supports a legendary account by Alexander von Humboldt who described a battle between electric eels and horses in 1800. Finally, electric eels use high-voltage not only as a weapon, but also to efficiently track fast-moving prey with active electroreception. In conclusion, remarkable behaviors go hand in hand with remarkable physiology.

Keywords: predator, gymnotidae, electrocyte, evolution, electroreception, humboldt, *Electrophorus electricus*

OPEN ACCESS

Edited by:
Michael R. Markham, University of Oklahoma, United States

Reviewed by:
Luis A. Tellez, Universidad Nacional Autónoma de México, Mexico
Matthew H. Perkins, Icahn School of Medicine at Mount Sinai, United States

***Correspondence:**
Kenneth C. Catania
ken.catania@vanderbilt.edu

Received: *31 March 2019*
Accepted: *24 June 2019*
Published: *16 July 2019*

Citation:
Catania KC (2019) The Astonishing Behavior of Electric Eels. Front. Integr. Neurosci. 13:23. doi: 10.3389/fnint.2019.00023

INTRODUCTION

You might say that electric eels need no introduction. Most people have heard of them and are aware of their unusual ability to generate powerful electrical discharges for offense and defense. But it would probably come as some surprise to many readers that electric eels played a pivotal role in the early development of the science of physiology and their anatomy helped inspire Volta to develop the battery, which he called an artificial electric organ similar to the electric eel's (Finger and Piccolino, 2011). In the 1700s, when our understanding

of electricity was in its infancy and the Leyden jar was the primary device for electrical experiments, the question of whether animals could produce electricity was paramount. Strongly electric fish were well-known, but how their mysterious emissions were produced, and whether this was the same "force" produced by a Leyden jar was a matter of intense debate.

In the early 1770s, evidence in favor of animal electricity was tantalizing but inconclusive. Investigators working with the strongly electric torpedo had established that conductors transmit the torpedo's emissions but insulators such as wood or wax did not (Wu, 1984). Both fishermen and philosopher-scientists of the time rated the subjective "shock" from a torpedo and a Leyden jar as the same (Piccolino and Bresadola, 2002). Moreover, if a group of people formed a ring holding hands, each would feel the shock from a Torpedo—as occurred for a Leyden jar. Electric fish fell short in one key area–they could not (as yet) produce the all-important "spark" that typified the electric force.

Enter the electric eel. Because the peak electrical potential of a Torpedo (50 volts) is much lower than that of an eel (400–600 volts) it was very difficult to obtain a gap-crossing spark from the former. In 1775, John Walsh experimented with eels and succeeded in demonstrating the spark repeatedly to colleagues and visitors (Piccolino and Bresadola, 2002). It was a pivotal moment in the history of science and kicked off the field of animal physiology.

But the experiments of John Walsh were by no means the end of the scientific community's obsession with electric eels. Others followed in his footsteps, including Alexander von Humboldt and Michael Faraday. Humboldt reported many details of how and when shocks were conveyed from eels to humans (von Humboldt, 1806) but by far his most famous link to eels was the unconventional way he (supposedly) obtained specimens. While traveling in South America, Humboldt was eager to find eels, but initially could only obtain animals that had been poisoned, and these were useless for study. He eventually succeeded by hiring fishermen who told him they would "fish with horses." As the story goes (von Humboldt, 1807) the fishermen herded about 30 horses and mules into a pool containing eels, and a spectacular battle ensued. The horses were contained within the pool by the fishermen, and the eels attacked. Two horses died within 5 min, and others managed to escape and collapsed on the ground next to the pond. Humboldt thought all the remaining horses would be killed, but before this could happen the eels were exhausted. This was apparently the point of the exercise, as the fishermen were then able to safely collect five specimens for Humboldt. Not everyone believed his story, but it is now supported by recent discoveries that will be reviewed here.

Faraday's much later foray into eel research included a meticulous investigation of the many parallels between electrical phenomena and eel discharges. His results, coming from perhaps the world's foremost electrician of the time, shored up the belief in animal electricity. He also published several prescient observations of eel behavior with interpretations that are, as in the case of Humboldt's reports, supported by recent investigations (Faraday, 1838).

Despite the centuries-long scientific interest in electric eels, there is still much to learn from this species. What follows is a summary of the author's recent work investigating electric eel behavior and the effects of its electric organ discharge (EOD) on nearby animals. This research began simply as a photography project but turned into a multi-year scientific investigation.

NEW INSIGHTS INTO EOD FUNCTION

Electric Eels Have Two Forms of EOD

Electric eels provide an informative example of strongly electric fish because they uniquely emit two different types of EOD (Coates et al., 1940; Bullock, 1969; Bauer, 1979). Each is of the same form, consisting of a roughly 1 ms, monophasic pulse, but one is far stronger than the other. **Figure 1** illustrates these two different outputs in a single trace from a behaving eel—recorded from electrodes in the aquarium. The low-voltage output comes at a low rate in a resting eel but may be emitted at 10–20 Hz when the eel is excited and hunting (Bauer, 1979). The high-voltage EOD is far stronger and is emitted at rates of up to 500 Hz. These two different EOD's have been thought to provide extant examples for two different functions: low-voltage discharges used for active electroreception (and perhaps communication) and high-voltage discharges used as a weapon. As the reader will see below, recent studies shown there is more to this story.

The mechanism by which electric eels generate either a weak EOD or a strong EOD has been determined in some detail (Bennett, 1968, 1970). Given the similar form of the two outputs, it is perhaps not surprising that the weak EOD is emitted by simply activating a subset of the eel's electrocytes (the eel's electrocytes are divided among three different electric organs which are referred to here as the eel's electric organ for simplicity). Surprisingly, an action potential is sent to every electrocyte in the eel's body when the weak EOD is emitted. But for the majority of electrocytes, the excitatory post-synaptic potentials are sub-threshold and do not result in an electrocyte action potential. Thus the weak EOD is the result of a subset of low-threshold electrocytes that can be activated by a single motor neuron action potential. The high-voltage EOD is emitted simply by sending a very high rate of action potentials to all of the same electrocytes. This, in turn, results in temporal summation in the higher-threshold electrocytes such that every electrocyte in the eel's body is activated. As a result of this simple mechanism for generating EODs of two different strengths, every high-voltage volley is (necessarily) immediately preceded by a single low-voltage, weak EOD (Bauer, 1979).

Eel High-Voltage EOD's Temporarily Immobilize Prey

Recent high-speed video recordings of electric eels hunting revealed an unusual reaction of prey fish electrified by high-voltage volleys (Catania, 2014). Within 3–4 ms of the first EOD in the volley, all prey voluntary movement was arrested and the fish floated "statuesque" with fins and body immobile throughout the volley (the fish was invariably captured by the eel shortly thereafter). Even when fish were in the midst of a rapid escape response and bent into a C-shape, the high-voltage froze

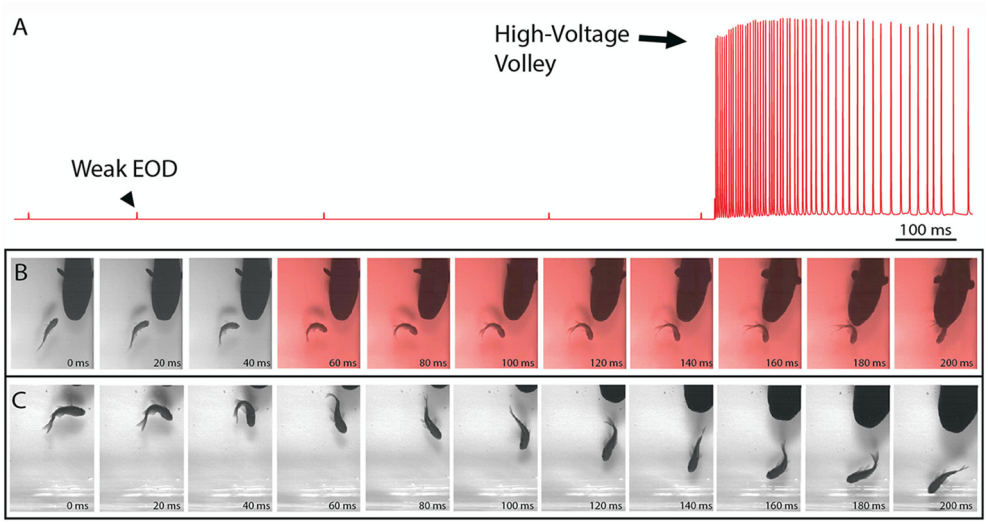

FIGURE 1 | The electric organ discharge (EOD) and its effect on prey. **(A)** Recording showing the two different EODs of an electric eel. Each is a monophasic, head-positive pulse lasting approximately 1 ms. The low voltage output (arrowhead) occurs at a low rate. The high voltage output (arrow) is much stronger and occurs at a much higher rate in volleys of up to 500 Hz during the predatory strike. High-voltage volleys are also used for defense. **(B)** An approaching eel elicits a C-start escape response in a goldfish, but the goldfish is immobilized by a volley of high-voltage pulses (red frames) and captured within 200 ms. **(C)** A similar encounter during which the fish was not immobilized and thus rapidly outpaced the eel. In the final frame (far right) this distance between eel and fish has increased and the prey velocity is greater than the eel velocity (from Catania, 2015a, reproduced with permission).

all subsequent body movements. This was surprising because it is easy to imagine high-voltage electrical impulses inducing some form of movement, rather than immobility. When the eel's strike missed the fish and the high-voltage volley was discontinued, most fish immediately resumed their escape. Thus the prey were usually not killed or disabled.

A potential explanation for this effect was the induction of muscle contraction by the EOD, in a manner analogous to a law-enforcement TASER. This possibility was investigated using a whole-fish preparation immersed in the aquarium with the eel but separated by an electrically permeable agarose barrier (Kalmijn, 1971). **Figure 2** illustrates the preparation that was used. The fish was first anesthetized and pithed to destroy the brain, and the hole was sealed with cyanoacrylate. This preparation, with muscles that remained viable throughout the experiment, was then attached to a force-transducer positioned above the water. High-voltage volleys were easily and repeatedly elicited from the nearby eel simply by feeding it earthworms in the adjacent chamber.

The results of this experiment showed that eels induce massive whole-body muscle contractions (**Figure 2**). By comparing eel induced contractions to those induced by direct stimulation with a Grass SD9 stimulator, it was shown that eels induce massive whole body tension, similar to that induced by a stimulator with leads directly connected to the fish body. Presumably, the statuesque appearance of prey during the eel's volley results from simultaneous contraction of equally powerful trunk muscles on both sides of the fish. The importance of this ability is evident when a successfully escaping fish track is compared to that of an eel-immobilized fish during the attack (**Figures 1B,C**). It is usually obvious that an active fish would have escaped (see also Catania, 2014, 2015a). This is not to say that eel strikes are slow, rather escaping fish are fast.

Eels Cause Muscle Tension by Remotely Activating Prey Motor Neurons

The discovering that electric eel high-voltage volleys cause powerful whole-body muscle contractions in nearby prey immediately raised a follow-up question: what was the mechanism by which muscles were activated? The two most likely possibilities were either the direct depolarization of the prey's muscles or alternatively, activation of the associated motor neurons. This question was addressed using two side-by-side fish preparations attached to force transducers, such that one served as a control and the other could be pharmacologically manipulated (**Figure 2**). When one preparation was injected with curare to block the neuromuscular junction, and the other sham injected, the muscle contractions in response to eel volleys were eliminated in the former but not in the latter (Catania, 2014). This demonstrated that high-voltage volleys were not directly depolarizing prey muscles. The experiment was then extended by pithing the spinal cord of the fish (double-pithing). There was no difference in latency or tension magnitude in double-pithed vs. brain-pithed fish, indicating the spinal cord is not necessary for the fish muscle response. These experiments showed that electric eels immobilize prey by remotely activating the peripheral branches of motor neurons.

As often happens, the experiments described above also revealed unanticipated details about the mechanism. The electric eels used to activate the fish preparation were repeatedly fed earthworms in order to elicit many high-voltage volleys. Over

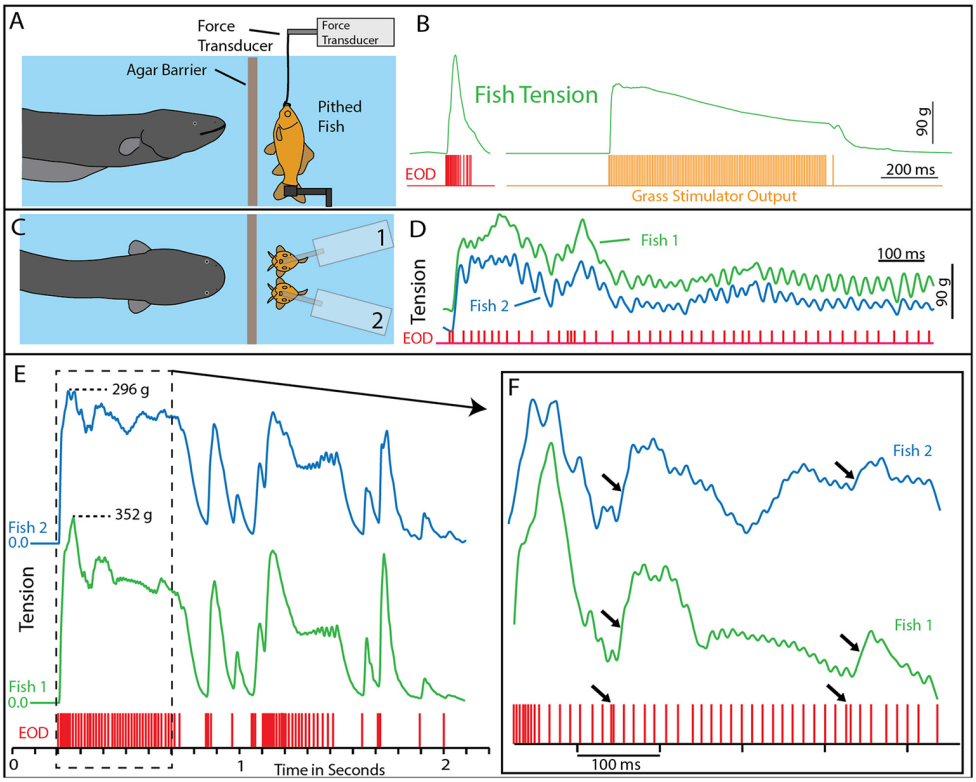

FIGURE 2 | Paradigm and results for eel-induced muscle tension measurements in prey. **(A)** To measure prey muscle tension, a pithed fish was attached to a force transducer while an eel (behind and agar barrier) was fed earthworms (which it shocked with high-voltage volleys). **(B)** Onset of fish tension (green) occurred in roughly 3 ms and was generally similar to the maximum whole-body fish tension that could be induced through direct stimulation (orange trace) with an SD9 Grass stimulator. **(C)** To compare responses of two different fish under various conditions (see Catania, 2014), two force transducers were placed side by side. **(D)** The dual fish paradigm unexpectedly revealed that long eel interpulse intervals result in nearly identical patterns (green and blue traces) of individual twitches in the two, adjacent fish. **(E)** Overall tension responses in two fish were also similar at a more compressed time scale (blue and green traces, different cases from "**D**"). **(F)** An expanded time scale shows the marked effect of eel doublets-closely spaced EODs (arrows) on corresponding fish tension. This suggests that doublets have the same strong tension-inducing effect in fish as shown for other experimental preparations (from Catania, 2015a, reproduced with permission).

time some eels apparently became fatigued, because the rate of their high-voltage EOD slowed and the interpulse interval became variable. In these cases, individual twitches emerged on the tension traces in the nearby experimental fish preparations. Moreover, in the side-by-side fish preparations, the twitch responses were nearly identical (**Figures 2E,F**). These results indicated that each high-voltage EOD from the electric eel typically results in an action potential in the motor neurons of nearby prey. High rates of the EOD result in fused muscle tension, whereas lower rates reveal individual twitches—as would be observed in a muscle physiology laboratory.

The implications of these results are remarkable. Ultimately, the motor neurons in the electric eel are activating the muscles of a nearby animal in a one-to-one fashion. By amplifying the "signal" from its own motor neuron, the eel's electrocytes provide a mechanism for remotely controlling another animal. In a sense, the eel's high-voltage discharge can be viewed as an action potential traveling through the water, destined to activate the motor neurons in any nearby animal.

Though astonishing, in retrospect these results might have been predicted from the analogous mechanism underlying the function of a law-enforcement TASER, or the mechanism of more commonly used transcutaneous electrical nerve stimulation paradigms (TENS) used for human muscle therapy (Sweeney, 2009).

This mechanism for incapacitating prey suggested that new insights might be gained by considering the eel's volley from the perspective of prey motor neurons. For example, **Figure 3** shows the average interpulse interval for the high-voltage volleys of three different electric eels. In each case, a significantly (statistically) shorter interpulse interval was found for the first two discharges in the volley. As it turns out, numerous investigations of neuromuscular systems have found that the rate of muscle contraction can be maximized by including two closely spaced action potentials at the beginning of the motor neuron train. These are called doublets (Celichowski and Grottel, 1998; Cheng et al., 2013; Pedersen et al., 2013). More detailed investigation of the optimal motor neuron train for maximizing muscle tension (Zajac and Young, 1980a,b) reveals a pattern of action potentials that is similar in form to the first part of an electric eel's volley. This raises the possibility that eel volleys have been specifically selected to most efficiently induce

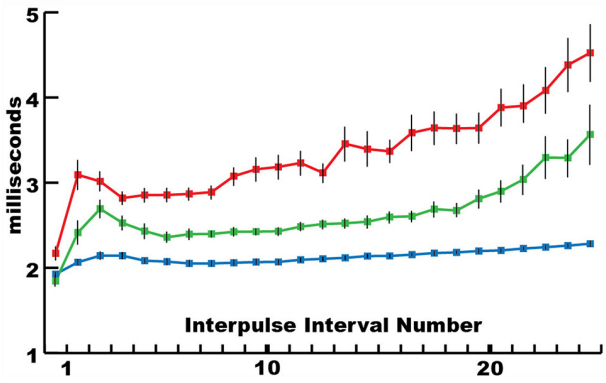

FIGURE 3 | The mean interpulse intervals for differently sized electric eels. The longest interpulse intervals (red) corresponded to the smallest eel (50 cm), intervals of intermediate length corresponded to the intermediate eel (approximately 75 cm), whereas the shortest intervals (blue) corresponded to the largest eel (115 cm). For each specimen, the first interpulse interval was the shortest. Bars are standard error. See Catania (2014) for additional statistics (from Catania, 2015a, reproduced with permission).

rapid and powerful muscle contractions in nearby animals, and hence to most rapidly immobilize animals that might otherwise escape.

Alternatively, because eel electrocytes are derived from muscles and innervated by motor neurons, the eel's motor neuron output (and therefore its EOD) might be constrained in a manner similar to that of a wide range of neuromuscular systems. Put another way, the similarity between the beginning of an eel's EOD and the optimal motor neuron train found for maximal muscle activation could reflect a constraint on both systems at peak power output. And yet this seems unlikely, given the incredible variation in the form and rate of EOD's exhibited by a diversity of electric fish. Moreover, electric eels have another way of remotely controlling prey that also seems to make use of an optimal strategy.

Eels Emit High-Voltage Doublets to Induce Movement in Hidden Prey

In 1979 the results of Bauer's investigation of electric eel hunting behavior and EOD were posthumously published (Bauer, 1979). He reported that: "Introduction of prey into the aquarium arouses the eel, causing it to swim around, but often stopping in a particular corner of the aquarium. During these stops, two high-voltage pulses with an interval of about 2 ms are emitted." He reported this behavior as typical of hunting eels.

Bauer's observations took on new significance in light of the mechanisms described above, by which eels activate motor neurons in nearby prey with each high-voltage discharge (Catania, 2014). This is especially true given that doublets at the beginning of a motor neuron action potential train are particularly efficient and producing powerful muscle contractions. All of the eels used in the recent studies (reviewed here) gave off doublets while hunting, and it was a frequent behavior during the fish muscle-tension experiments described above. As would be predicted, the doublets resulted in a massive whole-body twitch in the nearby fish preparations (**Figure 4A**). In some cases, after giving off a doublet the eel tried to break through the thin agarose barrier (which was reinforced with nylon netting) to reach the fish.

The context during which doublets were emitted, and the preliminary behavioral observations, suggested that doublets might function by causing prey movement that is detected by the eel's neuromasts (mechanoreceptors). Electric eels are extremely sensitive to water movements and often respond with a high-voltage volley and strike. In addition, eels hunting live prey in a complex environment (or when prey were under an agarose barrier) sometimes gave off a doublet, resulting in prey twitch, followed (20–40 ms later) by the eel's full, tetanus inducing high-voltage volley and suction feeding strike (**Figure 4B**).

Determining whether eels use doublets to detect induced prey movements required a paradigm in which the prey's response was under the control of the experimenter. This was achieved using a variation of the pithed fish preparation (**Figures 4C,D**). In this case, a stimulator was connected to the fish, and the preparation was sealed in a plastic bag such that the fish preparation was electrically isolated from the eel. The stimulator was then controlled through a data acquisition unit that monitored the eel's EOD, such that fish twitch could be triggered in response to a doublet (or not triggered, at the discretion of the investigator).

The first question to be addressed was the latency of the eel's response to fish twitch. If eel's were responding to fish twitch in their natural doublet-hunting behavior, then their reaction time would have to be in the 20–40 ms range. This was, in fact, found to be the case. When the eels were close to the fish preparation and the investigator trigger the stimulator, eels responded to the twitch with a high-voltage volley and strike toward the preparation with a delay of 20–40 ms.

When eels gave off doublets near the fish preparation, but no fish twitch was triggered, no attack was elicited. Moreover, eels never gave off doublets, followed by a full volley, in the absence of fish twitch. However, the key experiment was to configure the data acquisition unit to immediately trigger fish twitch when the eel gave of a doublet. When this was arranged, the natural doublet-hunting behavior was recreated (**Figure 4**). Eels gave off a doublet, the fish twitched (as a result of the EOD triggered stimulator) and then the eels attacked with a full volley and strike toward the fish preparation. A number of control experiments confirmed that eels were not responding to visual cues from the moving fish or electrical impulses from the stimulator leads (Catania, 2014).

The remarkable conclusion from these experiments is that eels have dual modes of prey remote control. When a nearby fish is detected, a full volley of high-voltage impulses causes rapid and powerful muscle contractions preventing escape. When prey are hidden, or their identity is uncertain, eels can induce involuntary twitch, revealing their approximate location (**Figure 4E**). In essence, the doublet allows the eel to ask the question of a nearby object: are you alive? Prey have no choice but to respond.

It has been previously suggested, that both strongly electric catfish (Belbenoit et al., 1979) and the strongly electric torpedo might use this kind of hunting strategy as well

(Belbenoit and Bauer, 1972). The former suggestion was inferred from recordings of catfish hunting in the wild, during which some volleys were preceded by brief pre-volleys. It is astonishing, however, that Michael Faraday (using only his hands) inferred the electric eel's ability to detect and attack EOD induced movement in 1838. His description is so prescient as to seem incredible, especially given the limitations of his equipment. I quote his comments in full here: "*The Gymnotus appears to be sensible when he has shocked an animal, being made conscious of it, probably, by the mechanical impulses he receives, caused by the spasms into which he is thrown*" (Faraday, 1838).

Active Electroreception by Electric Eels

As described above, electric eels have both a low voltage and high voltage EOD. Undoubtedly the first observation of active electroreception comes from Walsh's experiments on electric eels in the 1770s (see Wu, 1984). Walsh noticed that when two wires were put into the water with the electric eel and extended some distance from the container, the eel was able to detect when the two wires were connected. The eel responded by giving of its high voltage volley.

At the time, no one was aware of the low voltage EOD that is constantly emitted as eels explore their surroundings (which was almost certainly the basis for the eel's ability). The explanation was not available until Lissmann (1958) showed that weakly electric fish use low-voltage EOD's for active electroreception. Not long after Lissmann's discovery, Hagiwara et al. (1965) investigated the physiological properties of the eel's electroreceptors and concluded that the low-voltage EOD was, in fact, used for active electroreception (see also Keynes and Martins-Ferreira, 1953).

Lissmann's discovery of active electroreception provided the missing, functional intermediate needed to explain the evolution of strongly electric species. Thus for electric eels, the evolutionary trajectory was easy to envision. Their ancestors presumably used an electric organ for navigation, and this was progressively enlarged to provide an electrical weapon (as previously noted, the eel's electrocytes are actually divided among three separate organs). The retention of the low-voltage EOD for active electrolocation seemed to fit well with such a functional bifurcation: low voltage for electrolocation and high-voltage for offense and defense. In the author's view (prior to 2015) a remaining question was how the eel's sensitive electroreceptors dealt with the high-voltage volleys, the presumption being that the electric sense was shut down completely during the high-voltage EOD. Recent data show this is not the case.

The Use of High-Voltage for Active Electroreception

Recall the electric eels did not grasp the electrically insulated prey in the course of doublet hunting experiments described

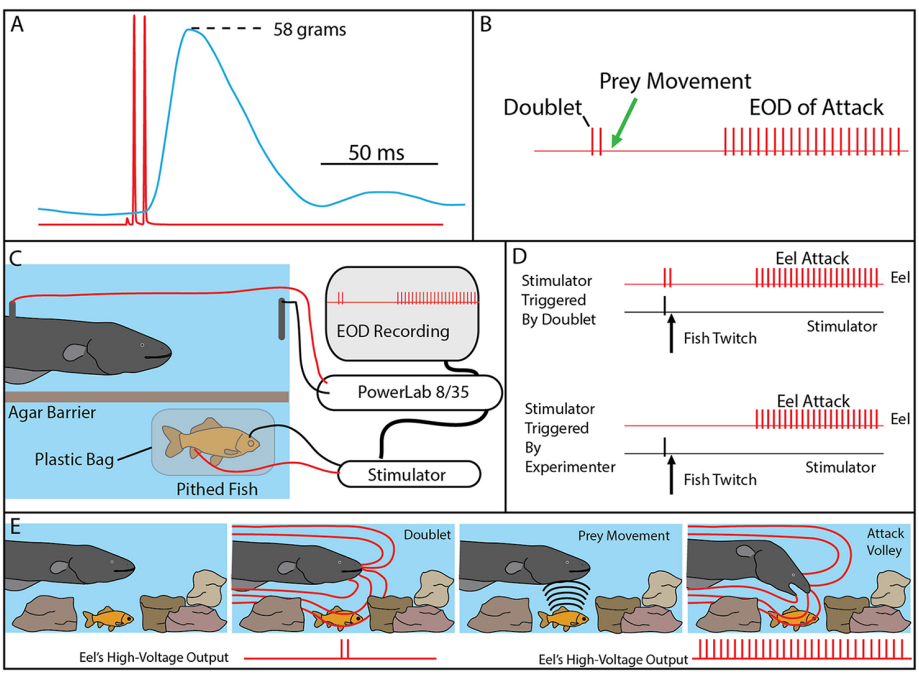

FIGURE 4 | The use of doublets in eel predatory behavior. **(A)** Example of an isolated doublet (red) inducing strong tension (blue) in a nearby pithed fish attached to a force transducer. **(B)** Schematic of the doublet output followed by prey movement (twitch) and then a full high-voltage volley. **(C)** Schematic of the paradigm used to investigate the use of doublets during hunting. A pithed fish was enclosed in a plastic bag, while connected to an SD9 Grass stimulator that could induce twitch when the eel emitted a doublet. **(D)** The doublet was followed by a full volley (and predatory strike) if twitch was immediately triggered through the stimulator (upper trace), but no attacks were elicited in the absence of prey twitch (not shown). In the absence of doublets, full volleys and strikes could be elicited by randomly generated fish twitch (bottom). **(E)** Schematic illustration of the use of doublets to detect prey in normal hunting behavior (from Catania, 2015a, reproduced with permission).

above. Instead, the strikes were aborted without a final "bite." This was obvious because electric eels are air-breathers and they hold air in their mouths between breaths. As a result, their suction feeding is accompanied by sudden expulsion of air from the operculum. This was fortuitous because it made the absence of the final component of the strike more obvious during experiments. Before describing the next experiments, it is import to re-emphasize that electric eel predatory strikes occur in conjunction with the high-voltage volley; there are no low-voltage EOD's emitted during the strike. Thus evidence of ongoing active electroreception during the strike must be attributed to the high-voltage EOD.

As a preliminary test for the possibility that electric eels were using the high-voltage EOD for active electroreception, a conductive carbon rod was placed next to the electrically isolated fish preparation (to interpret this experiment it is important to note that prey are conductors, thus the carbon rod was a "stand-in" for a prey item). The fish was made to twitch by activating the stimulator and the eel then gave off its high-voltage volley and struck toward the electrically isolated fish as previously described. But this time, the eel altered course, moved over the conductor, broke through the agarose barrier, and sucked the conductive rod into its jaws (see movies in Catania, 2015b). This dramatically different response in the presence of a conductor suggested the eels depend on the high-voltage EOD to guide their strikes during normal predatory behavior.

To test this possibility more rigorously, a number of additional experiments were devised. The first was an elaboration of the carbon rod paradigm. An apparatus was made that could hold seven different rods of similar shape and appearance (**Figure 5**). One rod was a carbon conductor (imitation prey), and the other six rods were plastic non-conductors. The pithed fish preparation (electrically insulated in a plastic bag) was then placed below the carbon rods, and the entire apparatus was covered with a thin agarose barrier that did not block mechanosensory cues. Under these conditions, fish twitch could be generated either by the experimenter triggering the stimulator or by having the data acquisition unit trigger the stimulator in response to a doublet. Electric eels responded to fish twitch with a high voltage volley and strike. In each case, the strike was guided, often on a circuitous path, to the conductor, which was then violently attacked with a suction feeding bite (this is a rapid series of events analyzed in slow motion from high-speed video).

These experiments seemed to confirm that electric eels use their high-voltage EOD for active electroreception. However, the conclusion is somewhat extraordinary, and therefore additional experiments were conducted to provide the clearest evidence possible (Catania, 2015b). For these additional experiments, a small (2.5 cm diameter) carbon disk was inserted into a larger (16.5 cm diameter) disk that was mechanically driven to spin below an agarose barrier (**Figure 6**). Three non-conductive plastic disks of the same diameter and appearance were also

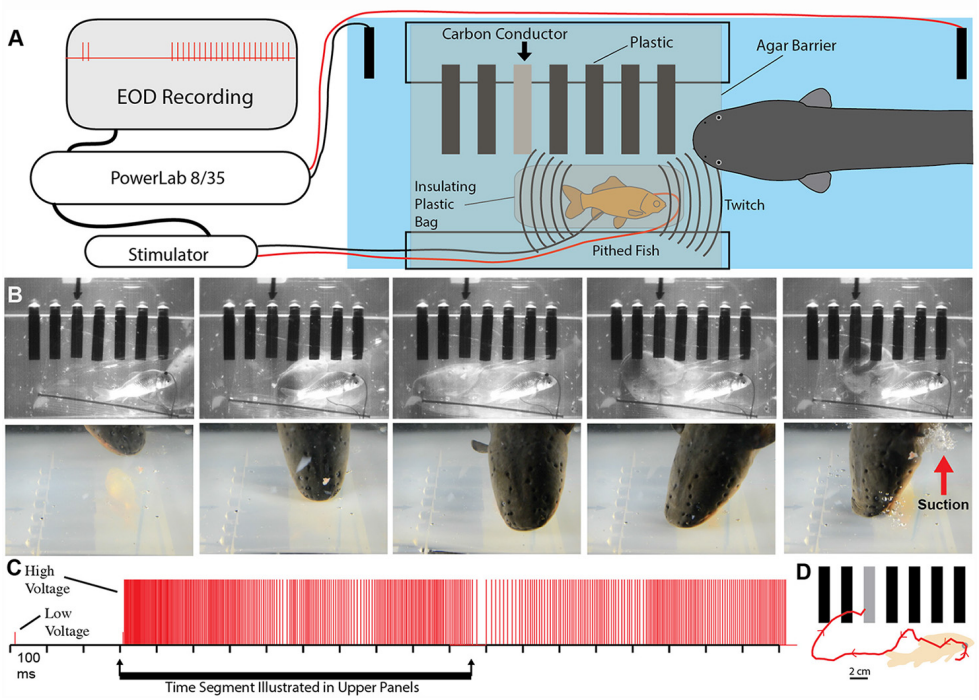

FIGURE 5 | Paradigm showing that electric eels find and attack conductors. **(A)** Recording and stimulator configuration that triggered pithed-fish twitch and eel attack in the presence of six plastic rods and one conductor (arrow). **(B)** Plates from high-speed video (top) and real-time (bottom) of same trial illustrating circuitous path to conductor. **(C)** Eel low and high voltage discharge marked with short, and tall ticks respectively, illustrating the exclusive use of high-voltage during strike movement. **(D)** Eel path to conductor (from Catania, 2015b, reproduced with permission).

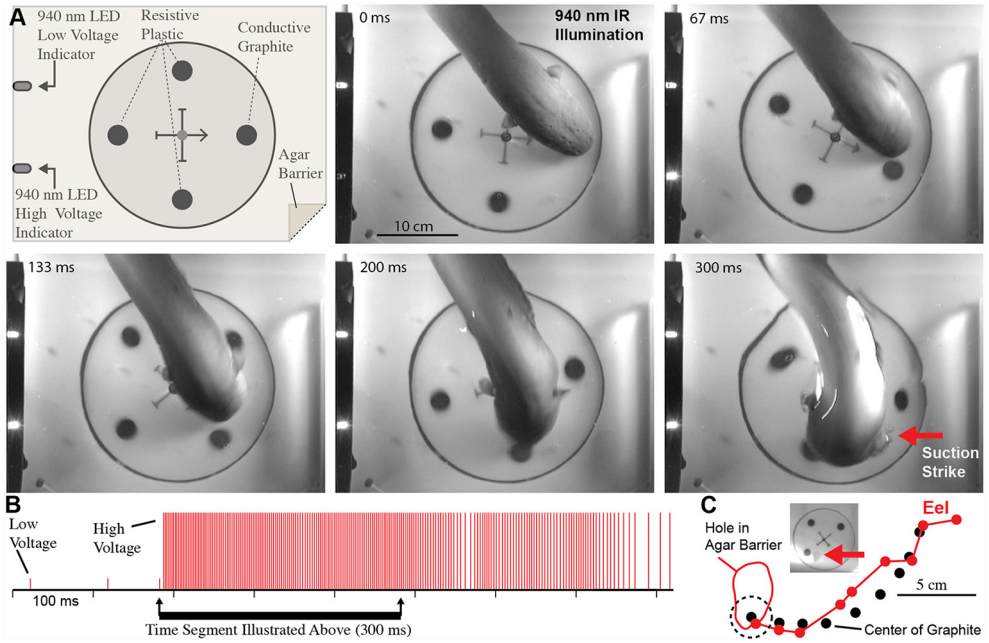

FIGURE 6 | Eel conductor tracking under 940 nm IR illumination. **(A)** Schematic of paradigm and plates showing eel tracking behavior and suction feeding strike to conductor. **(B)** Eel low and high voltage discharge marked with short, and tall ticks respectively, illustrating the exclusive use of high-voltage during strike movement. **(C)** Eel track relative to conductor movement. Inset shows hole in agar (arrow) that was directly over conductor at suction onset (from Catania, 2015b, reproduced with permission).

inserted into the larger spinning disk as control stimuli. The apparatus was illuminated by invisible, 940 nm infrared light, and 940 nm infrared diodes (controlled through a data acquisition unit) were configured to indicated each low voltage EOD and each high-voltage EOD. This paradigm provided redundant control for vision and prevented contact and chemical cues by virtue of the electrically permeable agarose barrier. The eels attacked the moving conductor (the imitation prey) with suction feeding strikes (after initial attacks, eels were rewarded after each strike to maintain the behavior). The results of these and additional experiments clearly showed that electric eels can rapidly track conductors moving on a curved trajectory using their high-voltage EOD. Moreover, the eel's were able to track the conductors at a greater speed than has been previously reported for active electroreception in other species (Maciver et al., 2001).

Details of conductor tracking indicate that active electroreception using high-voltage is integral to the strike. In retrospect, it seems obvious that some form of sensory feedback is necessary for eels to accurately strike. Although the high voltage EOD prevents prey muscle movement, it does not prevent the continued motion of a fast-moving fish through the water after voluntary behavior has been arrested. In addition, the explosive movement of the eel's head through the water toward prey causes much additional water motion. As a result, prey are often fast-moving targets, even after their muscles have been inactivated. Finally, it is unlikely that a brief, distant water movement caused by prey—which often triggers the eel's strike—provides the necessary positional information for an accurate attack. Active electroreception during the strike solves these problems for the eel.

A Revision of the Evolutionary Trajectory

It is worth recounting Darwin's discussion of electric fish under the section in the Origin of Species that dealt with difficulties of the theory (Darwin, 1873). Electric fish were considered a problem, in part, because there was no obvious use for the small electric organs that were intermediate between muscles and the large electric organs of eels and rays. The use of the latter for offense and defense was clear, but bridging the "functional gap" between muscle contraction and high-voltage weapons was problematic. Lissmann's discovery of active electroreception in weakly electric fish seemed to fill in this part of the evolutionary puzzle (Lissmann, 1958). But the present results indicate there was more to the story for eels. Active electroreception using high-voltage shows that, in the case of eels, the electric organ did not simply transition from a sensory role to a weapon. Rather, it most likely added the role as a weapon while retaining its sensory function throughout.

The stages of this evolutionary process are of course lost to history. But it is intriguing to consider, in addition to its role as a weapon, the possibility of the eel's high-voltage being important for sexual selection (courtship), territoriality, or communication. Assunção and Schwassmann (1995) were able to identify nests of breeding eels and found these were built by males and subsequently defended. Although they did not observe possible courtship or territoriality, it seems an interesting possibility to explore in future in the context of the EOD.

DEALING WITH DIFFICULT PREY

The Dipole Attack

So far the predatory behavior of electric eels has been described and illustrated as it typically occurs when feeder goldfish are provided to an eel in an aquarium. But electric eels live in the Amazon, which includes a wide diversity of fish species and other potential prey. Surprisingly little is known about the diets of electric eels in their natural habitat, but it is obvious that feeder goldfish are not their most challenging prey. Moreover, juvenile eels have much smaller, weaker electric organs and can have difficulty handling even small fish.

In cases where difficult prey are encountered, electric eels are uniquely suited for a strategy that increases the intensity of their attack. This is because, unlike strongly electric rays or catfish, the eel's electric organ is linear and extends through its long, thin body. This means the positive and negative poles (the head and tail, respectively) are widely separated in space. During a typical predatory attack, the eel's electrical discharge forms a (roughly) dipole field around the eel. The positive pole is the region around the eel's head and the negative poll is the region around the tail (**Figures 7A,B**). A fish near the eel's head experiences the effect of the positive pole and almost no effect from the more distant negative pole around the tail. In fact, for a fish situated directly in front of an eel—when the eel's body is straight—the effect of the negative pole (tail) would subtract from the effect of the positive pole, reducing the strength of the local field.

This would change drastically, however, if the eel were to curl and bring its tail behind and close to the prey. In such a case, the effect of the tail (the negative pole) would be additive (because the prey would be sandwiched between the two poles) and strong (because the negative pole would be close), rather than subtractive and weak. The theoretical effect of such a curling move would be to double the intensity of the electric field experienced by prey, at virtually no cost to the eel.

In fact, electric eels commonly engage in this curling behavior when handling difficult prey (Catania, 2015c). Juvenile eels frequently curl when attacking any prey item, whereas adults curl when handling difficult, struggling prey, or when they have captured a fish that is being held precariously and might otherwise escape. Although the basic physics of dipole fields predict the effect of this curling behavior, a number of experiments were conducted to directly measure the resulting electric field and its effect on prey (Catania, 2015c).

Measuring Field Strength During the Eel's Curling Behavior

Measuring the changing intensity of an electric field experienced by prey during an eel's attack would seem daunting. The common method of monitoring electric fish EOD's, with electrodes stationary in the aquarium, cannot provide data about the local field strength in and around prey. Nor can an investigator chase a hunting eel with electrodes and hope to get useful data. This problem was solved by leveraging the eel's aggressive predatory attack.

To measure the electric field within prey, the pithed fish preparation was again used. However, in this case, the fish was impaled on a custom-made, plastic electrode holder (**Figure 7C**). The recording electrodes consisted of two wrappings of thin copper wire spaced 1 cm apart on the long projection of the T-shaped electrode holder. The thin insulated leads from the electrodes led to a data acquisition unit that recorded the electrical potential. At the same time, the insulated leads provided a convenient handle—much like a fishing line—that could be manipulated by the investigator. Finally, the upper part of the T-shaped electrode holder prevented the eel from swallowing the preparation.

When this preparation was introduced to a hungry eel, it was attacked, sucked into the eel's mouth, and gripped very tightly (**Figures 7D,E**). This condition likely mimics natural situations during which prey fish with defensive spines have been caught but are difficult to swallow. By manually vibrating the electrode leads, the investigator was able to imitate struggling by the pithed fish-electrode preparation, and this elicited the eel's curling behavior.

The preparation provided data from numerous eels, showing that the intensity of the electric field experienced by prey often more than doubled when the eel curled (**Figures 7F,G**). Recall, that electric eels cannot increase the magnitude of their total power output during the high-voltage volleys, rather every electrocyte is active during each high-voltage EOD (see above). Therefore, the increase in measured field strength resulted from the reconfiguration of the electric field. The electric field was concentrated, so-to-speak, through the prey item, much like focusing the fixed power of a flashlight into a smaller area.

It might seem surprising that, in many cases, the field strength within prey more than doubled when the eel curled. This likely occurred because the tail, containing the negative pole, can be brought very close to the prey (essentially touching), whereas the positive pole of the electric organ is situated at some distance behind the front of the eel's head (to make room for the eel's internal organs). Therefore the negative pole (with an effect that is added to the positive pole) may have a greater effect, based on proximity, than the positive pole during the curling behavior.

What benefit does this behavior provide the eel? Although it intensifies the electric field through prey, a large electric eel would seem to have enough power from just the positive pole. This appeared to be the case when an eel was offered goldfish. But when an electric eel was offered large crayfish, the eel's initial attack sometimes failed and the crayfish executed the appropriate escape response (**Figure 8**). Clearly, some prey are more resistive to electricity than others. Curling provides a mechanism for electrifying prey that are both physically and electrically, more resistive. Still, what is the ultimate function of the eel's curling behavior? The answer seems obvious in retrospect.

The Induction of Involuntary Fatigue

Recall that high-voltage EOD's from electric eels activate motor neuron efferents, and hence muscles in nearby prey. In the pithed-fish preparation, this was measured based on whole-body fish tension. Crayfish provide a different window into this effect because many of their paired muscles are asymmetric: the

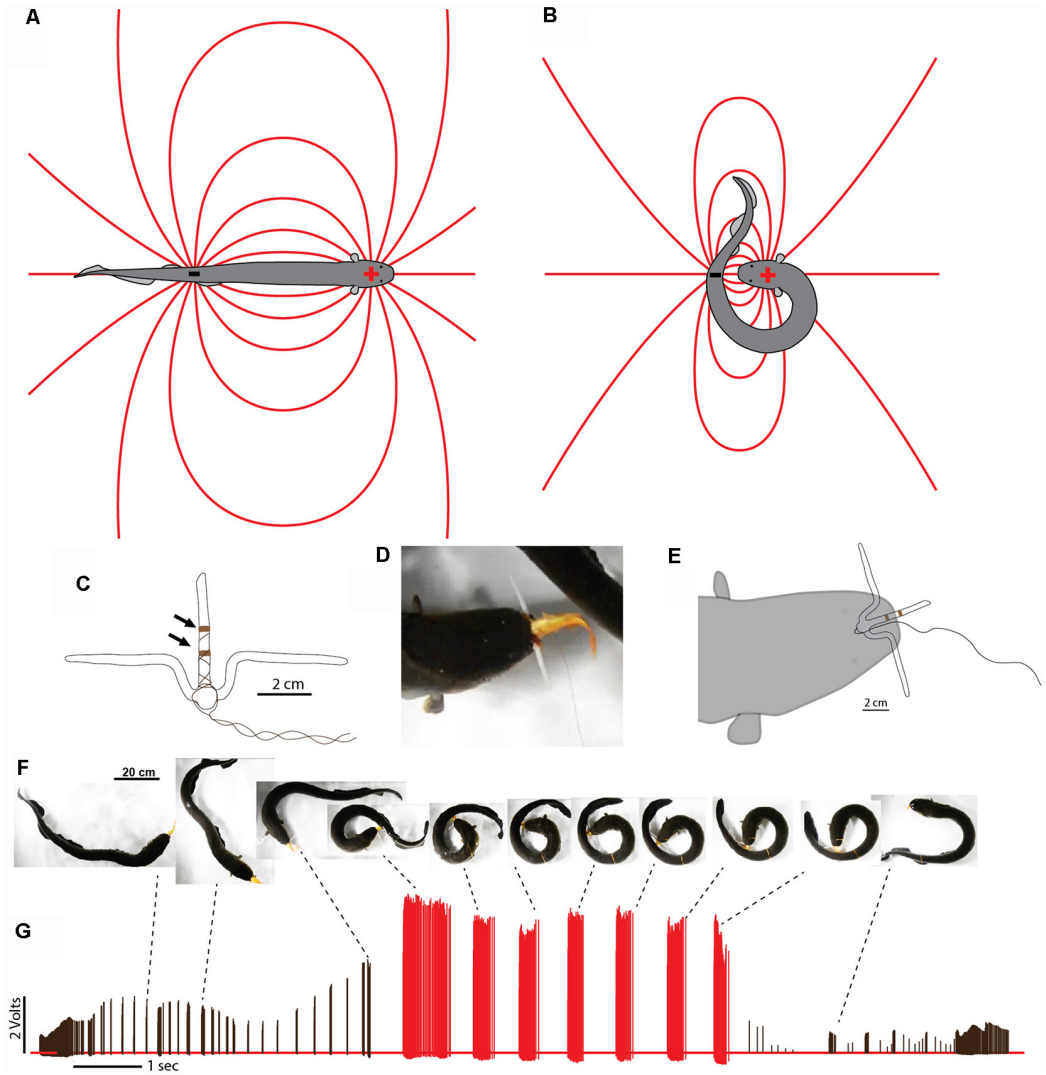

FIGURE 7 | Dipole field and dipole attack. **(A)** Schematic illustration of a dipole field surrounding an electric eel and its change in configuration **(B)** after the eel has brought the two poles close together. Lines indicate electric field lines (a positive test charge would experience a force tangent to the line at any point—in the direction of the negative pole). **(C)** Schematic illustration of electrodes with un-insulated wire (arrows) approximately 1 cm apart. **(D)** View of eel holding electrode-fish preparation tightly. **(E)** Schematic of electrode position during trial. **(F)** Large eel presented with the pithed fish with electrodes. After capture, the experimenter manually jiggled the wire to simulate prey struggling and the eel curled to deliver multiple discharges. **(G)** Voltages recorded from the electrode at different points during the eel's attack. Black tick marks indicate discharges while "uncurled." Red tick marks were all recorded while curled. Note the dramatic increase in recorded voltage, and discharge frequency, during the curl relative to the uncurled configuration (from Catania, 2015c, reproduced with permission).

muscles that close their claws are more powerful than the muscles that open them. As a result, the effect of repeated high-voltage volleys from the eel electrifying a crayfish was readily apparent. Unlike the situation in fish, where contraction of symmetric muscle groups resulted in total immobility, in crayfish it was possible to watch the claws open and close with repeated high voltage volleys (see video in Catania, 2015c).

This observation emphasizes an outcome worth re-emphasizing in the context of the eel's curling behavior. The high-voltage EOD's result in one-to-one activation of prey motor neurons, causing repeated, high rates of muscle contraction in the captured prey. The eel's curling strategy is, therefore, a recipe for quickly fatiguing prey muscles. Indeed, the same procedure is used (with a stimulator) in muscle physiology labs to investigate fatigue.

To investigate this outcome a stimulator was first used to mimic the effects of an electric eel on prey muscle preparations (**Figures 9A–C**). Muscle tension from a single stimulator pulse was first measured. This was followed by five bouts of electrical stimulation, each lasting half a second and consisting of 1 ms electrical pulses delivered at 100 Hz. Half a second after the last stimulation bout, muscle tension was then measured (again) for a single stimulator pulse. In a pithed fish preparation, the muscle tension response had dropped drastically. In a crayfish tail

FIGURE 8 | Frame captured from video showing an eel attacking a crayfish. Note that despite the eel's comparatively large size and ability to cause tetanus in most fish with its high- voltage discharge, the crayfish escape response was not canceled. The appropriate form of the lateral giant escape from the rear-ward attack indicates that the crayfish movement was not caused by arbitrary stimulation from the eel's discharge. This suggests that crayfish are more resistant to electric discharges (from Catania, 2015c, reproduced with permission).

preparation, there was only a slight drop in muscle tension after five bouts of stimulation. However, after extending the number of stimulation bouts to 10 (**Figure 9D**), tension responses in the crayfish tail responses had also dropped drastically. Finally, after a 30 s recovery period, the muscle preparations showed substantial recovery.

These experiments demonstrate the predictable, fatiguing effect of repeated bouts of high-frequency muscle stimulation. The half-second, post-bout testing time for muscle fatigue was chosen because after electric eels engage in this form of behavior while curled, they then reposition the prey for swallowing within a half-second. Thus they need only cause a short period of muscle inactivation to reposition and swallow helpless prey.

To provide more data regarding the effect of eel curling behavior, an additional more elaborate experiment was designed. In this case, the stimulator was configured to be driven by an eel's high voltage EOD while the eel curled around the previously described fish-electrode preparation (**Figures 9E–G**). Thus this paradigm tested the effect of the actual, real-time rate of the high-voltage volley on the muscle preparations (i.e., the eel's EOD drove the stimulator). These cases provided a more realistic view of how eel's induce fatigue over time. As in the previously described paradigm, the repeated bouts of stimulation resulted in a rapid and drastic reduction in muscle contractile force.

Finally, although this was not explicitly investigated for eels, the oral region of most animals is very sensitive. Electric eels are holding the prey in their mouth while they engage in the curling behavior, so there is every reason to suggest the eel can monitor the contractile force of the prey's muscles during the curl. This would explain, for example, why eels sometimes electrify the crayfish, while in the curled position, for over a minute (Catania, 2015c). This is far longer than previously observed for any other prey. By the end of such a bout, the crayfish limbs are invariably completely flaccid, and the eel can swallow its prey at leisure.

To summarize these results, electric eels have a strategy for inactivating the muscles of difficult, struggling prey that have been grasped but not subdued. In these cases, the eels concentrate the electric field by sandwiching the prey between the two poles of their long electric organ. This likely ensures activation of the motor neuron efferents in prey that might have more resistive skin or cutical or in the case of juvenile eels, prey might simply not be affected by the output of their weaker electric organ in a linear configuration. Once curled to amplify the local field through the prey, the eels give off repeated volleys. The resulting effect on prey muscles is remarkably similar to the application of a paralyzing agent, such as curare, that blocks the neuromuscular junction. There is a precipitous drop in muscle function. In essence, the eels have a new method for inactivating muscles, through the induction of involuntary fatigue. The strategy is analogous to the use of paralyzing venom, but it takes effect more rapidly.

SELF DEFENSE BY THE ELECTRIC EEL

Humbolt's Fish Story

In March of 1800, Alexander von Humboldt supposedly observed an extraordinary encounter between electric eels and horses. He had been traveling in South America and one of his goals was to experiment with electric eels. The first eels that fishermen had brought to him had been poisoned with plant roots and they were "much enfeebled" and useless for experiments (von Humboldt, 1807). Later he encountered a group of locals at the village of El Rastro, and they offered to collect eels by "fishing with horses." The ensuing battle between the horses and eels is one of Humboldt's most famous stories of adventure and it has been recounted and illustrated many times in the last 200 years. Most histories of electric fish include an illustration and description of the event. But not everyone believed the story (Catania, 2016). On the other hand, there was no obvious reason for anyone to investigate further. The story had little relevance to the biology of electric eels and it served as an amusing anecdote. It, therefore, came as some surprise when the author discovered a dramatic defensive behavior by electric eels, supporting Humboldt's account.

The Leaping Attack

In the course of many of the experimental investigations described above, electric eels were transferred from a home cage to an experimental cage. Depending on the size of the eel, sometimes the net had a metal rim and handle. Although this may not seem wise, the investigator always wore rubber gloves, such that the composition of the handle was inconsequential (or so it seemed). On many occasions, when the metal net was brought toward a large eel, the eel transitioned from a retreat to an explosive attack targeting the metal part of the net. The eel rapidly approached, followed the metal rim to where it exited the water, and then leaped upward while pressing its lower jaw

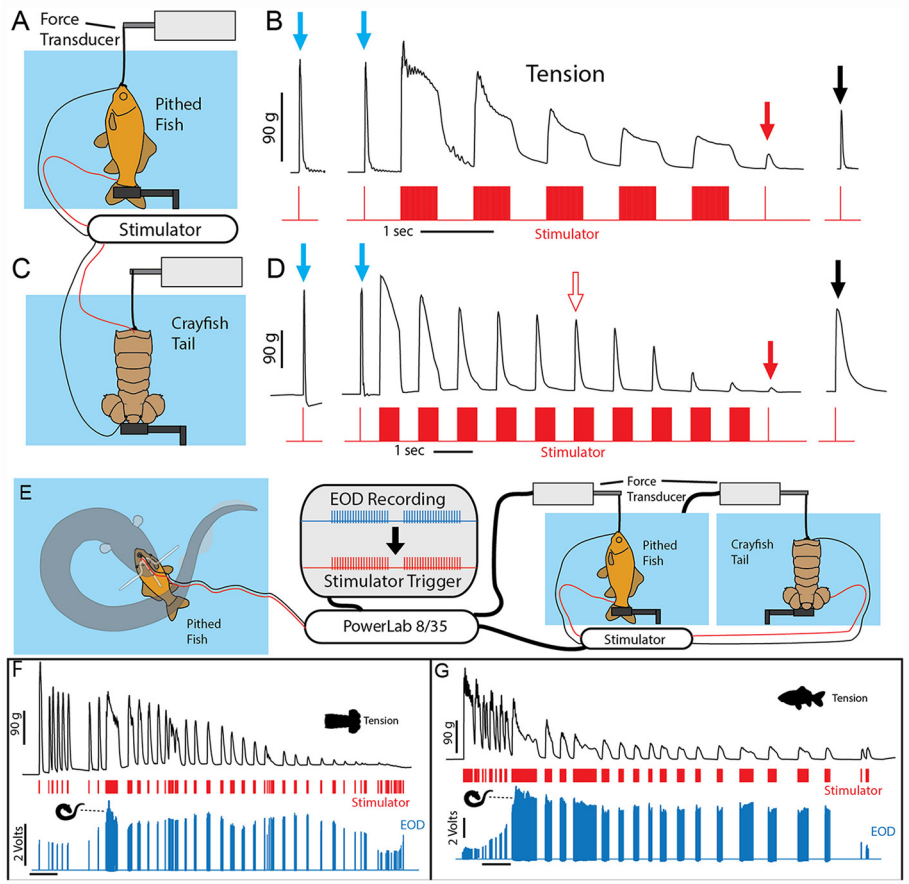

FIGURE 9 | Paradigm used to simulate the effect of eel volleys on prey muscles. **(A)** Pithed fish attached to a force transducer and stimulator. **(B)** Example of whole fish tension responses to single stimulator pulses prior to (blue arrows) a series of 500 ms, 100 Hz volleys, and after (red and black arrows) volleys. Note the dramatic reduction on contractile force following five volleys (red arrow). **(C)** Crayfish tail preparation and stimulator. **(D)** Example of crayfish tail tension responses as described above. Note the difference in time scale, and that more volleys (10) were required to cause a similar reduction in contractile force. **(E)** An electric eel was induced to perform a curling attack on prey-electrode preparation. The recorded high-voltage EOD triggered an SD 9 grass stimulator connected to either a pithed fish preparation, or a crayfish tail preparation connected in turn to a force transducer. **(F)** Tension, stimulator output, and electric eel EOD's were simultaneously recorded (muscle preparation in adjacent aquarium). Tension in each preparation dropped dramatically over time **(F,G)** and particularly quickly when subjected to the continuous high-frequency stimulation that co-occurs with curling (from Catania, 2015c, reproduced with permission).

to the metal handle. In coordination with the upward leap, the eel gave off long volleys of its high-voltage EOD. The behavior was particularly surprising because at no other time were electric eels observed leaping upward from the aquarium. Moreover, the unexpected leap was clearly directed toward the metal handle, and therefore coincidently toward the investigator's hand. Although the rubber glove afforded protection from the eel's EOD, it was easy to imagine the consequences had there been no glove. The behavior gave the impression of a formidable, electrical attack.

Measuring the Potential of Leaping Eels

As was the case for experiments measuring the effect of curling, it was possible to leverage the eel's behavior to further investigate this novel attack. This was accomplished using two flat metal plates attached to a plastic handle. The lower plate was submerged most of the way in the water, separated from the upper plate (which was entirely above the water) by a thin insulator. A voltmeter was then connected between the two plates. When the eels attacked the apparatus, they emerged from the water pressing their lower jaw against the lower plate while giving off their high-voltage volleys. As they rose higher, they crossed from the lower plate to the upper plate, and thus variations in the electrical potential could be recorded as the eels ascended (**Figure 10**).

As might be predicted, the electrical potential (voltage) increased dramatically as the eels ascended to greater heights. This is best appreciated by considering the equivalent circuit that is thought to develop (**Figure 10D**). When fully submerged in the water, the eel's discharges form an approximately dipole electric field around the eel. In this case, the resistances in the circuit include the internal resistance of the eel (r) and the resistance of the surrounding water (Rw). When the eel emerges from the water and presses its lower jaw against an object, the circuit

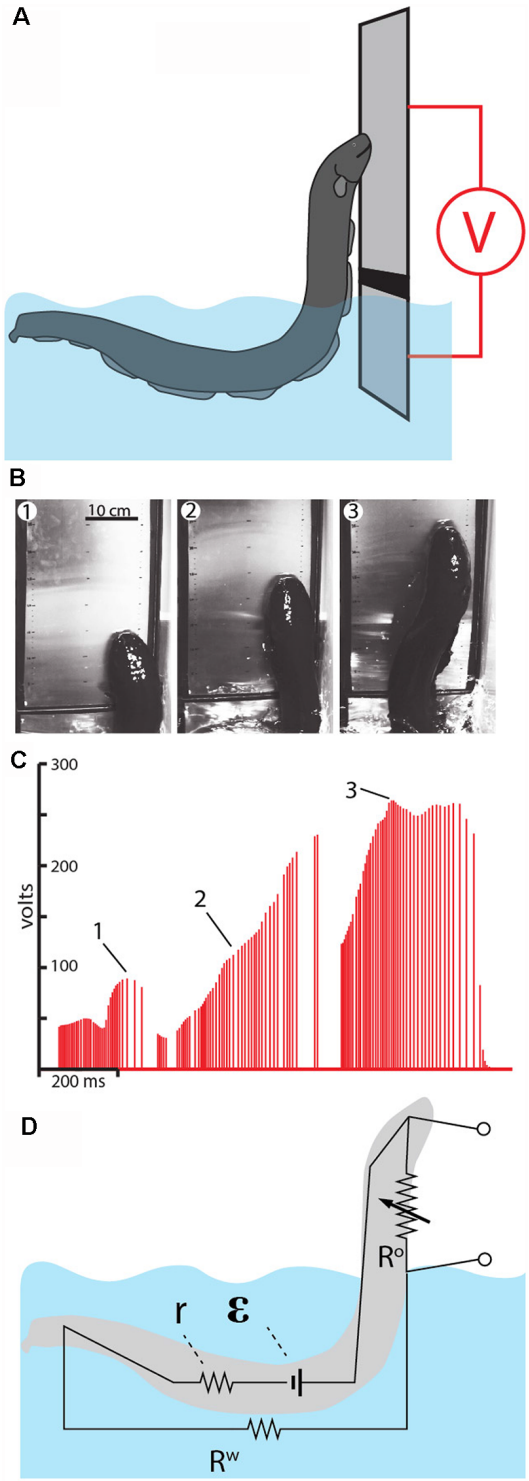

FIGURE 10 | Measurement of voltage during eel leaping defense. **(A)** Schematic of the plate arrangement and voltmeter used to measure the electrical potential as eels ascended the conductor. Black line indicates a non-conductor separating the plates. **(B)** Frames from high-speed video for a shocking leap. **(C)** Voltage measured as the eel ascended. Numbers 1–3 correspond the plates illustrated in **(B)**, indicating the location of the eel at time of discharge. **(D)** The proposed equivalent circuit that develops as the eel emerges from the water. The electromotive force (EMF) of the electrocytes is represented by ε. The resistors include water resistance, the eel's internal resistance (*r*) and the variable resistor (R°) that represents the current path on, or through, the eel back to the main body of water. This path becomes more resistant as the eel ascends to greater heights (from Catania, 2017a, reproduced with permission).

changes such that a new resistance exists above the water. This is the return path to the water along the eel's head and upper body (and perhaps through the eel's body). As the eel ascends to greater heights, the resistance of the return path along the eel increases, hence the measured voltage increases in proportion to height.

Another way to think about this dynamic is to consider the flow of electricity being "pushed" by the eel's electrocytes. The increasing resistance of the return path along the eel means that more current would be "pushed" through the target (if the target was an animal, rather than a high-impedance voltmeter). In other words, the higher the eel leaps, the less pleasant the experience for the target.

The experiment and observations described above seem to support Humboldt's story. Yet it was not entirely clear how similar the behavior described above might be to what Humboldt observed. He reported that the eels emerged from the mud and attacked, with at least some eels pressing themselves against the horses (von Humboldt, 1807). But he did not describe eels as leaping out of the water. Since the first observation of eels leaping in the laboratory, two additional pieces of evidence emerged that, combined with the observations described above, further support Humboldt's story. The first piece of evidence is historical, and comes from a friend of Humboldt's, as described below and illustrated in **Figure 11A**.

Robert Schomburk's Illustration

Humboldt's story of the horses and eels has been recounted in numerous publications and books since he first published his own account in 1807 (von Humboldt, 1807). His original publication did not include an illustration of the events, but many subsequent authors provided their own illustrations. The most significant illustration seems to have been lesser known and the least circulated and re-published. This is the front-piece to The Naturalist Library, Ichthyology, Volume V, Part II, the fishes of Guiana, authored by Robert Schomburgk (Schomburgk, 1843). This particular image stands out for two reasons. First, it is by far the most accurate depiction of the events described by Humboldt. Humboldt described fishermen waving reeds, a fisherman that had climbed an overhanging tree above the pool, horses that had escaped, and horses that had collapsed on the nearby shoreline. All of these details are included in the image.

The second reason for its significance is the author. Robert Schomburgk was a friend and admirer of Humboldt (Schomburgk, 1838). Humboldt helped the Schomburgk brothers obtain funding for their own trip to South America (Payne, 2007) and provided advice (Roth, 1922). Given that they knew each other and were in communication about South

FIGURE 11 | Fishing with horses. **(A)** This illustration depicts the battle between eels and horses observed by Alexander von Humboldt in March of 1800. It was published in 1843 as the front-piece for The Naturalist Library, Ichthyology, Volume V, Part II, the Fishes of Guiana, authored by Robert H. Schomburgk, a friend and protégé of Humboldt's. **(B)** Schematic and plates showing a fisherman being shocked by an electric eel (Plate **A** is in the public domain, **(B)** from Catania, 2017b, reproduced with permission).

American travels in the years prior to the image's production (Roth, 1922) it is possible that Humboldt provided some of his own input for the illustration. Moreover, the illustration shows an electric eel that has emerged from the water to press its lower jaw against one of the horses. There is a remarkable similarity between the eel's behavior depicted in the image

and the behavior observed in recent laboratory experiments (Catania, 2016).

A Leaping Attack in the Field

The second piece of evidence that also supports Humboldt's account from 1,800 is the circulation of a very recent video showing a fisherman being attacked by an electric eel. **Figure 11B** documents this event, which can be viewed from Hawkin (2016). Much can be inferred from the circumstances surrounding this incident. For example, the fisherman wades into a relatively shallow pool while attached to a rope, the other end of which is held by one of his comrades on shore. The fisherman also holds a machete, which is a common means of killing electric eels. The man searches for the eel, but the eel finds him first. The result is a leaping attack onto the man's chest. The predictable effect is instant paralysis from involuntary muscle activation, as previously described for prey. This possibility was obviously anticipated, as evidenced by the rope, which was used to immediately drag the incapacitated fisherman to shore. The man recovered quickly and the eel (which pursued him to shore) was then killed with a machete. The incident supports Humboldt's account because it clearly shows that some electric eels in the wild go on the offensive when a potential predator (a large, partially submerged conductor) enters their territory—as occurred with the horses.

THE EQUIVALENT CIRCUIT

Electromotive Force (EMF), Internal Resistance (r), and Water Resistance (Rw)

When an eel emerges from the water to make direct contact with a potential threat, the circuit that develops is comparatively simple. It was, therefore, possible to investigate most of the variables in the circuit and to estimate how current would flow through different elements (for these measurements and calculations, all values refer to the peak voltages and currents during the high-voltage EOD). The analysis begins with a determination of the (EMF in volts) and internal resistance (r) for each eel. These variables are unique for any given eel at a particular stage of development. As the eel grows and adds electrocytes, its internal resistance and EMF change (the former decreasing, and the latter increasing). Previous investigations of eels (Brown, 1950) and other electric fish (Bell et al., 1976; Caputi et al., 1989; Baffa and Côrrea, 1992) have shown that the electrocytes can be analyzed with methods commonly used for batteries.

One way this can be done is to measure the current (I) that flows for a "short circuited" eel and then measure voltage (V) directly from the skin of an eel that has been removed from the water. Then the resistance (r) can be determined from Ohm's law (r = V/I). But a more accurate method is to add a variable resistor to the circuit and measure V and I (during each high-voltage EOD) as the resistance is varied. When this is done, a plot of V vs. I yields a straight line with a slope equivalent to the negative of the internal resistance (r). The details of the method are given in Catania (2017a). Using this procedure (Catania, 2017a,b), the EMF and internal resistance (r) of five different electric eels of different sizes were recently measured. Once these variables were determined for each eel, it was then possible to design experiments to measure, for any given eel, the approximate water resistance in the circuit, and subsequently, the resistance of the return path from the eel's head to water when it leaped to attack. These determinations require only Ohm's Law, Kirchhoff's Voltage Law, and algebra in conjunction with various voltage and current measurements. Because these details may not interest all readers, they are omitted for brevity but can be reviewed in Catania (2017a).

Figure 12 shows the EMF and internal resistance that were determined for five different eels. The circuit in **Figure 12B** shows the additional resistance of the return path from head to water (Ro). This configuration is often called a voltage divider circuit, and it has many parallels with circuits used to modulate the amplitude of an electric output in a wide range of electrical equipment. In essence, the eel's leaping behavior increases the value of the variable resistor, Ro, in proportion to leap height, thus turning up the "volume" of its attack. This comparison to a volume control knob is useful for considering how the eel's behavior likely evolved. There is no need to imagine a "hopeful monster" scenario in which an ancestral eel suddenly evolved the behavior in one, metaphorical leap. Rather, each successive approximation of the behavior in an ancestor, starting with an approach to the threat in the water, and followed by direct contact, and then by emergence from the water to greater and greater heights (all while giving off the high-voltage EOD), would provide a selective advantage for deterring a predator.

COMPLETING THE CIRCUIT

Many insights can be gained about the dynamics of the electric circuit from the parameters shown in **Figure 12B**. Yet this configuration of resistors for the leaping attack is incomplete because it lacks the resistance of the target. This, in turn, demonstrates a fundamental problem in circuit analysis. Namely, the total current flowing in a circuit is dependent upon the total resistance of the circuit. In the case of the leaping eel, once a target is added, there are two resistors in parallel above the water. Determining their equivalent resistance, and hence the total circuit resistance is required to calculate total current in the circuit. Having spent considerable effort to determine each of the other variables in this circuit, the story seemed incomplete without this final variable.

Target resistance was therefore determined using the small eel illustrated in **Figure 12A** (top eel) and a single human subject's arm. To determine this resistance a device was designed that allowed for measurement of the current through the arm during the small eel's leaping attack. This consisted of a plastic, non-conductive water chamber with a handle. The inside of the water chamber had an area covered with conductive aluminum tape, but not in direct contact with the subject's hand. The outside front portion of the chamber was likewise covered with aluminum tape (but electrically isolated from the inner portion of the chamber by virtue of the plastic container's walls). The inner and outer portions of aluminum tape were then connected with a copper wire through which current could be measured as the eel

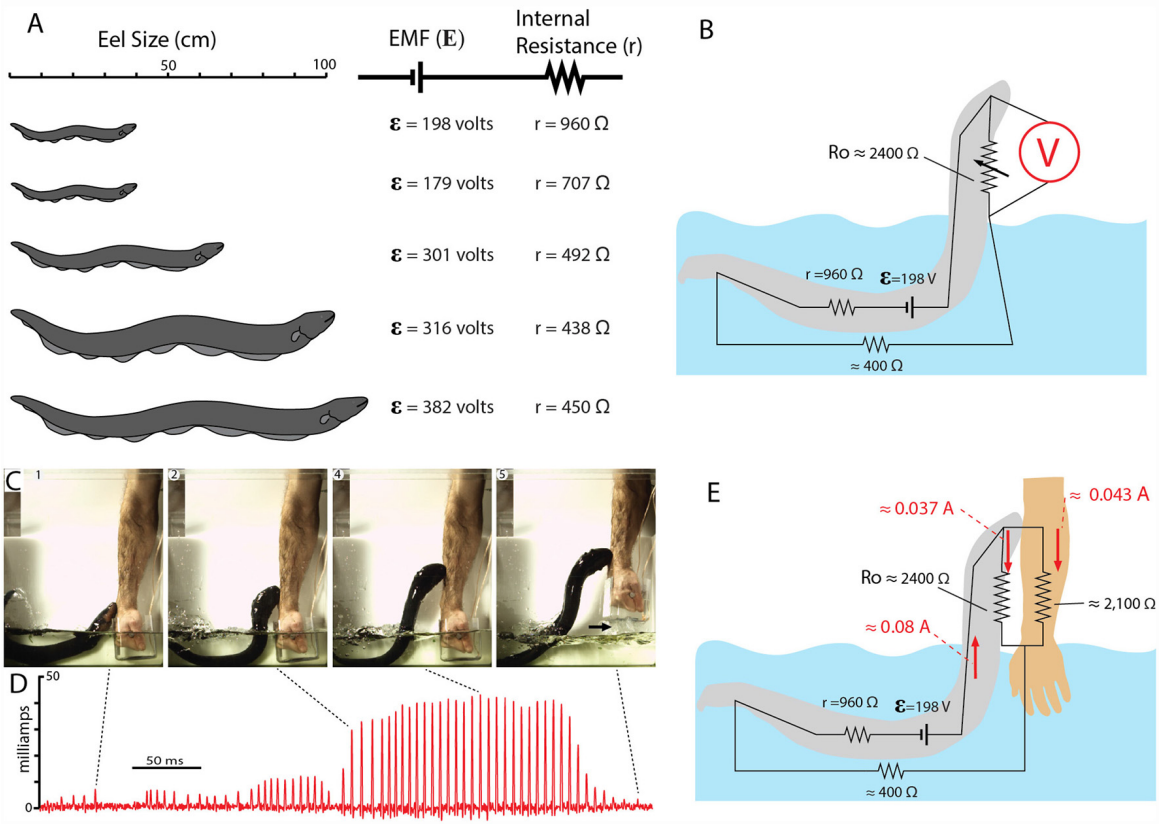

FIGURE 12 | Summary of electromotive force (EMF; ε) internal resistance (*r*), for five different eels and the circuit for the leaping attack. **(A)** Size of each eel in relationship to measured ε and *r*. **(B)** Estimate resistances and the maximum resistance of the return path to the water during the leap by eel shown at the top in (**A**; from data in Catania, 2017b). **(C)** Frames from high-speed video documenting the eel and the subject's arm. Arrow marks break in circuit as arm was withdrawn. **(D)** Current recording during the eel's shocking leap. Current increased as the eel ascended, as predicted from the equivalent circuit in **(B)**. Current peaks were approximately 43 milliamps. **(E)** Resistances and currents for each component of the circuit during the eel's leaping attack on a human arm. Resistances are shown in black, currents are shown in red (plates from Catania, 2017a,b; Copyright K.C. Catania).

made its attack. It was then possible to calculate target resistance based on the measured current (Catania, 2017b). The target (arm) resistance was found to be approximately 2,100 ohms. Of course, other eel targets will have other resistances. Nevertheless, this experiment provided important information by indicating whether the eel-target interface or the target-water interface made a substantial contribution to the circuit. The results suggest they did not, instead, the target resistance was in line with predictions (Catania, 2017a). Finally, this final piece of data, in conjunction with the other circuit components, provides a starting point for similar calculations that can be made for different eels attacking different targets in water with more or less resistance.

SUMMARY

The results of these recent investigations show that electric eels have behaviors that are far more sophisticated than previously thought (at least by the author). The conception of this species as a "one trick pony"—having a powerful weapon that provided the advantage of brute force, without the need for complex behaviors, could not be further from the truth. As is often the case, this seems obvious in retrospect when one considers the eel's anatomy and physiology in an evolutionary context. Clearly, the electric eel has been strongly selected for electrical power. Electrocytes make up an astonishing proportion of its long body. But there is more than one way to increase power. The first is to add electrocytes. The second is to apply the power from existing electrocytes more efficiently. The second option is arguably less costly than expending many resources to develop, maintain, and power more electrocytes. The curling behavior provides the most obvious example—an eel can literally double the power communicated to prey by simply reorienting its tail. Consider the difference in "cost" between evolving this behavior or, alternatively, doubling the number of electrocytes. A similar argument can be made for the leaping defense. In short, it seems inevitable the strong selection for electrical power would act on both physiology and behavior.

In addition to revealing a number of new behaviors, these studies raise many additional questions for future study. Perhaps the most obvious questions relate to other strongly electric species. Are electric rays and catfish activating the motor neurons

in nearby prey? If so, do they use the same strategies for inducing or arresting prey movement? Belbenoit and Bauer (1972) suggested the EOD of the *Torpedo marorata* might serve to startle prey. Similarly, Belbenoit et al. (1979) recorded EOD of hunting electric catfish (*Malapterurus electricus*) and identified frequent pre-volley activity; the investigators specifically suggested these might serve to startle immobile prey. If so, these would be remarkable examples of convergent hunting strategies. Do other strongly electric species also use high-voltage for active electroreception? What are the parallels, from the perspective of sensory processing, between the high rate of an eel's attack volley and the high rate of a bat's feeding buzz while echolocating? What kinds of electroreceptors might mediate sensory transduction of high-voltage? What is the composition of an eel's diet in the wild? Do electric eels specifically target other electric fish (Stoddard, 2002) as suggested from observations of Westby (1988)? How well cloaked are electric fish EOD's as a result of pressure from eels and other electroreceptive predators (Stoddard, 1999; Stoddard and Markham, 2008)? How does the high skin resistance of an electric fish impact the hunting strategy of an eel? Does active electroreception during a high-speed strike allow tracking precision that cannot be obtained with vision or the mechanosensory lateral line? What role does mechanosensory feedback play as the eel induces involuntary fatigue while curling? How does an eel protect its own nervous system from the high-voltage EOD? These are just a few of the many questions that remain to be investigated.

AUTHOR CONTRIBUTIONS

The author confirms being the sole contributor of this work and has approved it for publication.

FUNDING

The work was supported by National Science Foundation (NSF; Grant No. 1456472) award to KC.

REFERENCES

Assunção, M. I. S., and Schwassmann, H. O. (1995). Reproduction and larval development of *Electrophorus electricus* on Marajó Island (Pará, Brazil). *Ichth. Expl. Freshw.* 6, 175–184.

Baffa, O., and Côrrea, S. L. (1992). Magnetic and electric characteristics of the electric fish Gymnotus carapó. *Biophys. J.* 63, 591–593. doi: 10.1016/s0006-3495(92)81633-8

Bauer, R. (1979). Electric organ discharge (EOD) and prey capture behaviour in the electric eel, *Electrophorus electricus*. *Behav. Ecol. Sociobiol.* 4, 311–319. doi: 10.1007/bf00303239

Belbenoit, P., and Bauer, R. (1972). Video recordings of prey capture behaviour and associated electric organ discharge of *Torpedo marmorata* (Chondrichthyes). *Mar. Biol.* 17, 93–99.

Belbenoit, P., Moller, P., Serrier, J., and Push, S. (1979). Ethological observations on the electric organ discharge behaviour of the electric catfish, *Malapterurus electricus* (Pisces). *Behav. Ecol. Sociobiol.* 4, 321–330. doi: 10.1007/bf00303240

Bell, C. C., Bradbury, J., and Russell, C. J. (1976). The electric organ of a mormyrid as a current and voltage source. *J. Comp. Physiol. A* 110, 65–88.

Bennett, M. V. L. (1968). "Neural control of electric organs," in *The Central Nervous System and Fish Behavior*, ed. D. Ingle (Chicago: University of Chicago Press), 147–169.

Bennett, M. V. L. (1970). Comparative physiology: electric organs. *Annu. Rev. Physiol.* 32, 471–528. doi: 10.1146/annurev.ph.32.030170.002351

Brown, M. V. (1950). The electric discharge of the electric EEL. *Electr. Eng.* 69, 145–147. doi: 10.1109/ee.1950.6434151

Bullock, T. H. (1969). Species differences in effect of electroreceptor input on electric organ pacemakers and other aspects of behavior in electric fish; pp. 85–101. *Brain Behav. Evol.* 2, 85–101. doi: 10.1159/000125815

Caputi, A., Macadar, O., and Trujillo-Cenóz, O. (1989). Waveform generation of the electric organ discharge in *Gymnotus carapo*. *J. Comp. Physiol. A* 165, 361–370. doi: 10.1007/bf00619354

Catania, K. (2014). The shocking predatory strike of the electric eel. *Science* 346, 1231–1234. doi: 10.1126/science.1260807

Catania, K. C. (2015a). An optimized biological TASER: electric eels remotely induce or arrest movement in nearby prey. *Brain Behav. Evol.* 86, 38–47. doi: 10.1159/000435945

Catania, K. C. (2015b). Electric eels use high-voltage to track fast moving prey. *Nat. Commun.* 6:8638. doi: 10.1038/ncomms9638

Catania, K. C. (2015c). Electric eels concentrate their electric field to induce involuntary fatigue in struggling prey. *Curr. Biol.* 25, 2889–2898. doi: 10.1016/j.cub.2015.09.036

Catania, K. C. (2016). Leaping eels electrify threats supporting Humboldt's account of a battle with horses. *Proc. Natl. Acad. Sci. U S A* 113, 6979–6984. doi: 10.1073/pnas.1604009113

Catania, K. C. (2017a). Electrical potential of leaping eels. *Brain Behav. Evol.* 89, 262–273. doi: 10.1159/000475743

Catania, K. C. (2017b). Power transfer to a human during an Electric Eel's shocking leap. *Curr. Biol.* 27, 2887.e2–2891.e2. doi: 10.1016/j.cub.2017.08.034

Celichowski, J., and Grottel, K. (1998). The influence of a doublet of stimuli at the beginning of the tetanus on its time course. *Acta Neurobiol. Exp.* 58, 47–54.

Cheng, A. J., Place, N., Bruton, J. D., Holmberg, H. C., and Westerblad, H. (2013). Doublet discharge stimulation increases sarcoplasmic reticulum Ca^{2+} release and improves performance during fatiguing contractions in mouse muscle fibres. *J. Physiol.* 591, 3739–3748. doi: 10.1113/jphysiol.2013.257188

Coates, C. W., Cox, R. T., Rosemblith, W. A., and Brown, M. B. (1940). Propagation of the electric impulse along the organs of the electric eel, *Electrophorus electricus* (Linnaeus). *Zoologica* 25, 249–256.

Darwin, C. (1873). *The Origin of Species by Means of Natural Selection: Or, The Preservation of Favored Races in the Struggle for Life*. 6th Edn. London: John Murray.

Faraday, M. (1838). Experimental researches in electricity. *Philos. Trans. R. Soc. Lond.* 122, 125–162.

Finger, S., and Piccolino, M. (2011). *The Shocking History of Electric Fishes: From Ancient Epochs to the Birth of Modern Neurophysiology*. New York, NY: Oxford University Press.

Hagiwara, S., Szabo, T., and Enger, P. S. (1965). Physiological properties of electroreceptors in the electric eel, *Electrophorus electricus*. *J. Neurophysiol.* 28, 775–783. doi: 10.1152/jn.1965.28.5.775

Hawkin, A. (2016). *Would you act as bait for an electric eel? Brave fisherman wades into swamp to find creature—and gets the shock of his life.* 24 May; Daily Mail; Mailonline.

Kalmijn, A. J. (1971). The electric sense of sharks and rays. *J. Exp. Biol.* 55, 371–383.

Keynes, R. D., and Martins-Ferreira, H. (1953). Membrane potentials in the electroplates of the electric eel. *J. Physiol.* 119, 315–351. doi: 10.1113/jphysiol.1953.sp004849

Lissmann, H. W. (1958). On the function and evolution of electric organs in fish. *J. Exp. Biol.* 35, 156–191.

Maciver, M. A., Sharabash, N. M., and Nelson, M. E. (2001). Prey-capture behavior in gymnotid electric fish: motion analysis and effects of water conductivity. *J. Exp. Biol.* 204, 543–557.

Payne, P. (2007). *The Diplomatic Gardener: Richard Schomburgk, Explorer and Garden Director*. North Adelaide, Australia: Jeffcott Press.

Pedersen, K. K., Nielsen, O. B., and Overgaard, K. (2013). Effects of high-frequency stimulation and doublets on dynamic contractions in rat soleus muscle exposed to normal and high extracellular [K^+]. *Physiol. Rep.* 1:e00026. doi: 10.1002/phy2.26

Piccolino, M., and Bresadola, M. (2002). Drawing a spark from darkness: john Walsh and electric fish. *Trends Neurosci.* 25, 51–57. doi: 10.1016/s0166-2236(00)02003-8

Roth, W. E. (1922). Richard Schomburgk's travels in british guiana, 1840–1844: translated and Edited, with Geographical and General Indices and Route Maps, by Walter E. Roth. "Daily Chronicle" Office, 1922 p. 22.

Schomburgk, R. H. (1843). "Ichthyology," in *Fishes of Guiana, Part II.*, (Vol. XL) ed. W.B. Jardine (London: The Naturalists Library), 1–214.

Schomburgk, R. H. (1838). Letter dated new amstrdam, berbice, April 8, 1837. *Ann. Nat. Hist.* 1, 63–67.

Stoddard, P. K. (2002). Electric signals: predation, sex, and environmental constraints. *Adv. Study Behav.* 31, 201–242. doi: 10.1016/s0065-3454(02)80009-2

Stoddard, P. K. (1999). Predation enhances complexity in the evolution of electric fish signals. *Nature* 400, 254–256. doi: 10.1038/22301

Stoddard, P. K., and Markham, M. R. (2008). Signal cloaking by electric fish. *Bioscience* 58, 415–425. doi: 10.1641/b580508

Sweeney, J. D. (2009). "Transcutaneous muscle stimulation," in *TASER® Conducted Electrical Weapons: Physiology, Pathology, and Law*, eds J. Ho and M. Kroll (Boston, MA: Springer), 51–62.

von Humboldt, A. (1806). Versuche über die electrischen Fische. *Ann. Phys.* 22, 1–13. doi: 10.1002/andp.18060220102

von Humboldt, A. (1807). Jagd und Kampf der electrischen Aale mit Pferden. Aus den Reiseberichten des Hrn. Freiherrn Alexander v. Humboldt. *Ann. Phys.* 25, 34–43. doi: 10.1002/andp.18070250103

Westby, G. M. (1988). The ecology, discharge diversity and predatory behaviour of gymnotiforme electric fish in the coastal streams of French Guiana. *Behav. Ecol. Sociobiol.* 22, 341–354.

Wu, C. H. (1984). Electric fish and the discovery of animal electricity: the mystery of the electric fish motivated research into electricity and was instrumental in the emergence of electrophysiology. *Am. Sci.* 72, 598–607.

Zajac, F. E., and Young, J. L. (1980a). Properties of stimulus trains producing maximum tension-time area per pulse from single motor units in medial *gastrocnemius* muscle of the cat. *J. Neurophysiol.* 43, 1206–1220. doi: 10.1152/jn.1980.43.5.1206

Zajac, F. E., and Young, J. L. (1980b). Discharge properties of hindlimb motoneurons in decerebrate cats during locomotion induced by *mesencephalic* stimulation. *J. Neurophysiol.* 43, 1221–1235. doi: 10.1152/jn.1980.43.5.1221

Conflict of Interest Statement: The author declares that the research was conducted in the absence of any commercial or financial relationships that could be construed as a potential conflict of interest.

frontiers in Integrative Neuroscience

ORIGINAL RESEARCH
published: 31 July 2019
doi: 10.3389/fnint.2019.00036

Electrosensory Contrast Signals for Interacting Weakly Electric Fish

Na Yu[1,2], *Ginette Hupe*[3], *André Longtin*[2,4]* *and John E. Lewis*[3,4]

[1]Department of Mathematics and Computer Science, Lawrence Technological University, Southfield, MI, United States, [2]Department of Physics, University of Ottawa, Ottawa, ON, Canada, [3]Department of Biology, University of Ottawa, Ottawa, ON, Canada, [4]Brain and Mind Research Institute, University of Ottawa, Ottawa, ON, Canada

Active sensory systems have evolved to properly encode natural stimuli including those created by conspecifics, yet little is known about the properties of such stimuli. We consider the electrosensory signal at the skin of a fixed weakly electric fish in the presence of a swimming conspecific. The dipole recordings are obtained in parallel with video tracking of the position of the animals. This enables the quantification of the relationships between the recording dipole and the positions of the head, midbody and tail of the freely swimming fish. The contrast of the signal at the skin is shown to be well-fitted by a decreasing exponential function of distance. It is thus anti-correlated with distance; it is also correlated with the second envelope (i.e., the envelope of the envelope) of the raw recorded signal. The variance of the contrast signal is highest at short range. However, the coefficient of variation (CV) of this signal increases with distance. We find a range of position and associated contrast patterns under quasi-2D swimming conditions. This is quantified using global measures of the visit times of the free fish within measurable range, with each visit causing a bump in contrast. The durations of these bumps as well as the times between these bumps are well reproduced by a doubly stochastic process formed by a dichotomous (two-state) noise with Poisson statistics multiplying a colored noise [Ornstein-Uhlenbeck (OU) process]. Certain rapid body movements such as bending or turning are seen to produce contrast drops that may be part of cloaking strategies.

Keywords: electrosensation, envelope, contrast, dichotomous noise, Hilbert transform, swimming behavior, active sensing

OPEN ACCESS

Edited by:
Maurice Chacron, McGill University, Canada

Reviewed by:
Michael Georg Metzen, McGill University, Canada
Jacob Engelmann, Bielefeld University, Germany

***Correspondence:**
André Longtin
alongtin@uottawa.ca

Received: *17 May 2019*
Accepted: *16 July 2019*
Published: *31 July 2019*

Citation:
Yu N, Hupe G, Longtin A and Lewis JE (2019) Electrosensory Contrast Signals for Interacting Weakly Electric Fish. Front. Integr. Neurosci. 13:36. doi: 10.3389/fnint.2019.00036

INTRODUCTION

Wave-type weakly electric fish generate electric organ discharges (EODs) to sense their environment and communicate with conspecifics in the dark. Individual fish have a signature EOD (carrier) frequency. Amplitude modulations (AMs) of this carrier provide sources of sensory information: the frequency and phase content of AMs (i.e., beat frequency) can provide information about the EOD frequency and identity of conspecifics (Yu et al., 2012; Shifman and Lewis, 2018); and the amplitude content of AMs (i.e., contrast or second envelope) can represent motion and conspecific location (Yu et al., 2012; Fotowat et al., 2013). The focus of this article is on the latter, i.e., the relationship between contrast and motion. In particular, we study how

the relative motion of two interacting fish affects the EOD modulations that provide sensory information about conspecific location. Motion perception is influenced by both object motion and observer motion. As a first step, we consider an intermediate situation in which one fish (the observer) is restrained to a stationary mode while another fish (the object) swims freely. This allows us to characterize the specific contributions of object (conspecific) motion to the contrast in EOD modulations. The associated signal is also relevant to the context in which a stationary fish in the wild, perhaps hiding in plants, images other fish swimming in its neighborhood.

Previous work has investigated how contrast signals vary with the distance between interacting electric fish (Yu et al., 2012; Fotowat et al., 2013; Metzen and Chacron, 2014). As expected from Coulomb's Law and the dipole nature of the electric fields generated by these fish (Babineau et al., 2006), contrast signals fall off quickly with inter-fish distance. By recording transdermal potential in freely swimming fish, Fotowat et al. (2013) clearly demonstrated this general trend but also showed that additional factors (besides distance) have an influence on signal contrast. These factors include relative orientation and pose (degree of body bending) of the fish. Here, we describe these relationships in more detail, as well as swimming patterns and their associated contrasts as a function of the distance between a patch of skin on the fixed fish to the head, mid-body and tail of the moving fish. We also provide a quantitative description, in the form of a mathematical model, that reproduces the dynamics of contrast variations during our experiments. Such a model can be used to experimentally or computationally mimic the presence of a moving conspecific.

The article is organized as follows. In "Materials and Methods" section, we outline the experimental and computational methods used for our work. "Results" section describes the experimental results, their analysis and the proposed doubly stochastic model for interactions of two fish under the conditions of our experiment. The article ends with a discussion and outlook onto future work.

MATERIALS AND METHODS

Experiments

This study was approved by the animal care committee of the University of Ottawa (BL-229; BL-1773) and carried out in accordance with the guidelines of Canadian Council on Animal Care. Mature male and female *A. leptorhynchus* were obtained from a tropical fish supplier. Fish were kept in large flow-through community tanks on a 12:12 h light:dark cycle with 0–4 tank mates, and fed thawed blood worms three times weekly. All experiments were performed within the first few hours of the dark phase of the light cycle in a tank measuring 30 × 40 cm with a depth of either 4 cm or 10 cm.

To characterize the contrasts produced while one fish is stationary and the other fish freely swims, we restrained one fish in a hammock (the restrained fish or reference fish, "Rfish," which acts as an observer) in the center of the tank while a second fish (the free-swimming fish, "Ffish," which acts as an observed object) was allowed to swim freely in the tank around it (Yu et al., 2012). All experiments were performed in the dark. The hammocks were created using rectangular tulle holders measuring 15 cm long and 6 cm deep, closed along the top edge with Velcro; while in these hammocks, the fish showed no signs of discomfort, and produced chirps readily. We recorded the electrical potential using a pair of electrodes attached to the hammock and positioned adjacent to the head of the Rfish near the operculum with the tips of the electrodes positioned 1 cm apart, perpendicular to the axis of the Rfish. The position of this pair of electrodes was chosen to sample the composite electrical image received near the rostral surface of the Rfish's body (i.e., available to nearby electroreceptors) during conspecific movements. The recorded signals were primarily composed of the Rfish's EOD, with the influence of the Ffish's EOD increasing whenever the Ffish moved closer to the Rfish.

Electrical recordings sampled at 50 kHz were acquired using Teflon-coated silver wire electrodes, a differential amplifier (AM Systems, Sequim, WA, USA), and a D1104 A/D system (dSpace Inc., Wixom, MI, USA). Electrical recordings were collected from a total of 12 randomly chosen pairs of fish for 5 min. In four of these trials, we also videotaped the interactions using an infrared (IR) video camera positioned above the tank (with the tank illuminated from below using an IR light panel) to record physical behaviors of the Ffish over the course of the interaction while simultaneously acquiring electrical recordings.

Data Analysis and Definitions

All data analyses and numerical simulations were carried out in MATLAB (The MathWorks, Inc., Natick, MA, USA). We calculated first- and second-order envelopes as well as instantaneous contrast time series (defined below) from electrical recordings in all 12 trials. The position and distance data (defined below) were calculated based on the video recordings of four fish pairs.

The First-Order Envelope (E1) and the Second-Order Envelope (E2)

The AM (i.e., the first-order envelope, E1) of the recorded signal, s (i.e., EOD) can be calculated as $E1 = \sqrt{s^2 + \hat{s}^2}$, where $\hat{s}$ is the Hilbert transform of s, i.e., $\hat{s} = \frac{1}{\pi t} * s$ where $*$ denotes convolution. The AM of E1 (i.e., the second order envelope, E2) can also be obtained by applying the above method on E1, i.e., $E2 = \sqrt{E1^2 + \widehat{E1}^2}$, where $\widehat{E1}$ is the Hilbert transform of $E1$ Examples of E1 and E2 are shown in **Figure 1A**.

Instantaneous Contrast

The sum of the two EODs at the recording dipole against a patch of skin on Rfish was recorded. From these recordings, the time-varying contrasts and envelopes were calculated. In the presence of one another, the fish each experience a beating EOD pattern (e.g., Yu et al., 2012). The beat frequency is equal to the difference between the individual EOD frequencies of the two fish. The amplitude of this beating pattern at the recording dipole is time-dependent, as it depends on the relative distance and orientation of the two fish (Kelly et al., 2008; Fotowat et al., 2013). This complicates the quantification of contrast. Instead of reporting a contrast at every sampling

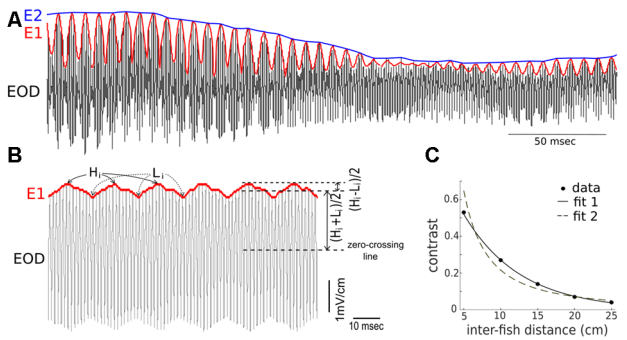

FIGURE 1 | Summary of the terms used to describe the composite recorded electric signal produced during conspecific interactions. **(A)** Shown are depictions of the electric organ discharge (EOD; black), the first-order envelope (E1, red), and the second-order amplitude (E2, blue) in a signal recorded during an interaction of two fish (one restrained "Rfish" and one free-swimming "Ffish"). The frequency of the E1 modulation is a consequence of the difference in the EODf of the interacting fish. The magnitude of E2 is related to the distance separating the two fish, and E2 modulations result from changes in the position and orientation of the fish. **(B)** Instantaneous values of contrasts indicate the magnitude of E2 and are determined by calculating, over time, the size of the modulation depth relative to the amplitude of the recorded signal. The heights of the E1 peaks are denoted by H1, while the heights of the troughs are denoted by L1.
"Contrast" = $[(H_i - L_i)/2]/[(H_i + L_i)/2]$, and varies between 0 and 1. **(C)** When two fish are restrained oriented parallel to one another, an electrical recording sampled adjacent to the skin of one of the fish, shows the contrast increases as the distance between the fish decreases. The inverse relationship can be fitted as: contrast = 0.9977 $e^{-(13.04*\ \text{distance})}$ with R^2 = 0.9989 (fit 1). It can also be fitted, although slightly less well, by a power law as: contrast = 0.56 $(\text{distance})^{-1.586}$ with R^2 = 0.9555 (fit 2). Note that the parameters in the fitting curve could take different values for another pair of fish.

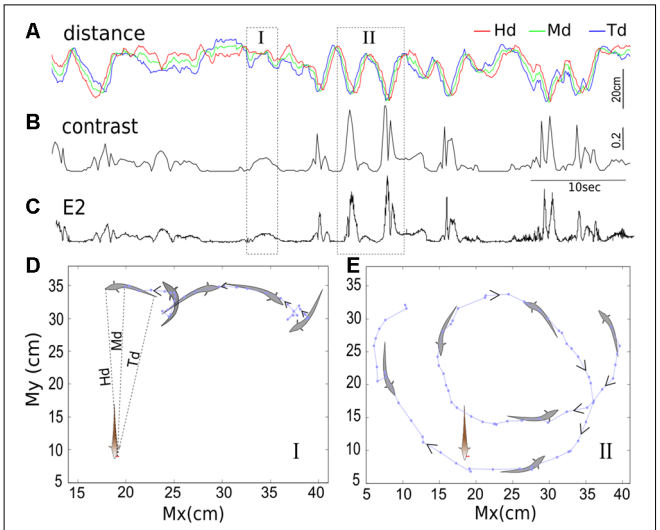

FIGURE 2 | The temporal relationships between inter-fish distances **(A)**, contrast **(B)** and second envelope E2 **(C)**. The distance separating the free-swimming fish and the recording electrodes positioned next to the operculum of the restrained fish are depicted in the top trace. The red, green and blue lines indicate the distance from the recording electrodes to the free-swimming fish's head, middle of the body, and end of the tail, denoted by Hd, Md and Td, respectively. The instantaneous contrast and E2 calculated over time are shown in the second and third traces, respectively; both are inversely correlated with inter-fish distance. The position of the free-swimming fish in epochs indicated by boxes I and II are shown in (**D,E**; in 100 ms increments), with the arrows indicating the direction of movement over time. During epoch I, the fish swims backward towards the recording electrodes and then changes direction, and this results in a contrast bump. In epoch II, the fish swims backward, looping twice around the tank, passing close to the recording electrodes each time. These movements are evident in the distance minima and corresponding contrast peaks. Each point indicates the position of the middle of the fish's body (Mx, My) measured at 100 ms increments.

point of the EODs, we compute one contrast value per beat cycle using the following method. We collected the highest points and lowest points of E1. As shown in **Figure 1B**, H_i and L_i denote i-th highest and lowest points, respectively. The "instantaneous" contrast during one beat cycle is defined by the ratio of the half-difference between H_i and L_i to the average of H_i and L_i, that is, contrast $= \frac{(H_i - L_i)/2}{(H_i + L_i)/2}$. This quantity ranges from 0 to 1, and is thus a dimensionless measure of contrast. Examples of instantaneous contrast are shown in **Figure 2B**. This peak-to-peak contrast is the same as the Michelson contrast used in the field of vision research (Michelson, 1927).

Representation of Video Recording

The position of the Ffish's head, midbody, and tail was extracted with 100 ms resolution from the video recordings using Videopoint Capture tracking software. The three pairs of points (Hx, Hy), (Mx, My) and (Tx, Ty) are used to denote the coordinates of Ffish's head, midbody and tail position in a 2D plane, respectively. The position of the electrodes beside the Rfish was also extracted from the video recording. We then calculated three measures of inter-fish distance (separating Ffish and Rfish): from the head, the midbody, and the tail of Ffish to the electrodes next to Rfish (**Figure 2**). These distances are denoted as HD, MD and TD, respectively.

RESULTS

Instantaneous Contrast Is Anti-correlated With Inter-Fish Distance

When two fish are stationary (e.g., experimentally restrained with a fixed distance and parallel to one another), the contrast of the composite electrical signal that one fish receives (for example, at a skin position near our recording dipole) is a constant. The value of this constant depends on the distance between the animals and their relative orientation. The contrast vs. inter-fish distance is well-fitted from 5 cm to 25 cm by an exponential, as shown in **Figure 1C**.

When two fish freely swim, the dynamic inter-fish distance causes a time-varying contrast. Based on Coulomb's law, we expect the EOD amplitude to drop off quickly with distance from the fish given the dipolar nature of the field. Thus, changes in the distance separating two fish (inter-fish distance) are expected to be negatively correlated with the EOD contrast. We examined the temporal relationship between the inter-fish distance, the instantaneous contrast and the second envelope E2. The inter-fish distance and the contrast generally exhibit the expected negative correlation (**Figures 2A,B**). We also first observe that the contrast and E2, although resulting from

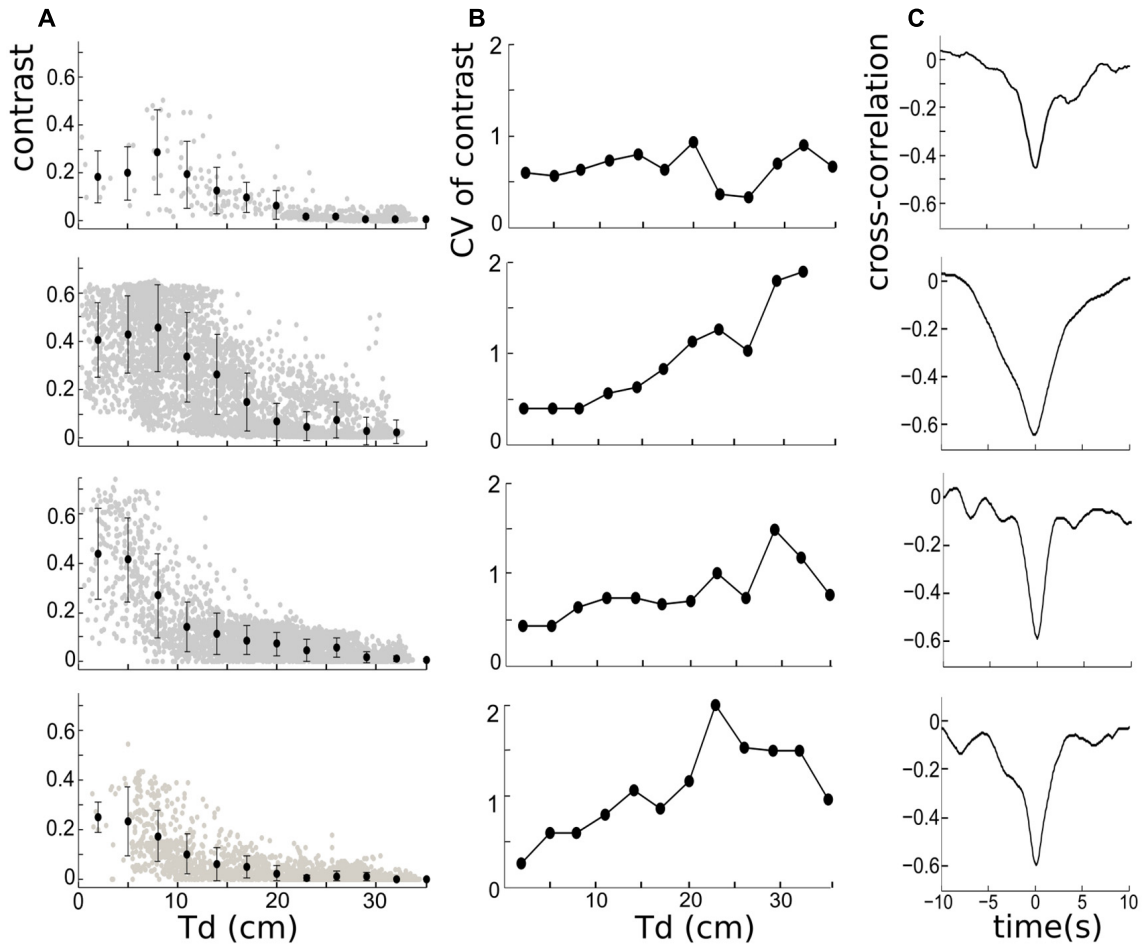

FIGURE 3 | (A) Left column: the negative relationship between instantaneous contrast and inter-fish distances measured from the tail of the free-swimming fish to the electrodes (Td), for four trials over 300 s. The errors bars on the mean contrasts correspond to ± 1 standard deviation, and reveal that the contrast variability is larger when mean distances are small. The mean contrast is calculated based on the bin-width of 10/3 cm. **(B)** Middle column: the corresponding coefficient of variation (CV) of contrast for four trials. The CV is largest at larger distances for three out of the four cases shown. **(C)** Right column: the cross-correlation functions depicting the relationship between contrast and Td. The significant negative correlation is present in all trials. The width of the trough and shape of the correlation vary across trials.

different computational methods as stated in "Materials and Methods" section, are both caused by the movement of Ffish, and are proportional to one another (**Figures 2B,C**). This observation is consistent with previous studies that fish movement can produce E2 (Yu et al., 2012; Fotowat et al., 2013; Metzen and Chacron, 2014), and specifically in an anti-correlated pattern (Stamper et al., 2013). Meanwhile, we are also aware of the fluctuations on the contrast and E2 (more obvious in E2). There are many factors that are able to generate contrast variability, for example, the occurrence of chirps, tail-bending and sudden changes in swimming orientation. Weakly electric fish tend to chirp more when they are in close proximity, often resulting in a transient (∼50 ms) decrease in E1, and a further decrease in E2 and contrast (Hupé and Lewis, 2008; Henninger et al., 2018).

In order to better understand how the movement of Ffish is projected to the instantaneous contrast (or E2), we reconstructed the swimming trajectories of Ffish from video-recordings. **Figures 2D,E** highlight two brief epochs during one experiment (denoted I and II). During epoch I (**Figure 2D**), Ffish hovers laterally, then turns and swims in reverse before turning again and swimming forward in the same direction. Note that the swim reversal results in a small change in Hd, but an obvious change in Td (**Figure 2A**), along with a contrast peak (**Figure 2B**). During epoch II (**Figure 2E**), Ffish swims in reverse following a looping trajectory and passing by Rfish very closely twice, resulting in two major peaks in contrast and E2 (**Figures 2B,C**).

The anti-correlation between inter-fish distance and instantaneous contrast was then quantified. The inter-fish distance is represented by Td here because the field strength is highest in the tail region (e.g., Shifman and Lewis, 2018). The mean of the instantaneous contrast associated with different Td (every 0.03 cm) decays with increasing Td for all four fish pairs (**Figure 3A**), which is consistent with our previous

observation of their temporal relationship. This negative relationship can also be quantitatively measured by the cross-correlation, which shows rather large negative correlation coefficients (−0.4 to −0.65) for the four fish pairs (**Figure 3C**). Using other inter-fish distances (Hd or Md) leads to the same conclusion (data not shown). The width and depth of the cross-correlation trough vary over trials. The most active fish pair (**Figure 3** second row—pair 2) has a higher contrast variability than other pairs, resulting in a larger width of the cross-correlation trough. We also found that the bottom of the trough, corresponding to the most negative correlation, occurs for 0 lag between the signals; and although the standard deviation of contrast appears to be higher when Td is small (**Figure 3A**), the relative variability of the contrast, measured by the coefficient of variation (CV, defined by the ratio of the standard deviation and the mean), is actually smaller when Td is smaller (**Figure 3B**). This suggests that changes in contrast may convey distance information even at relatively low absolute levels.

Spatial Distribution of the Contrast

We now consider the spatial distribution of the contrast during these interactions. In general, the contrast is high (≥0.3) when Ffish is within a radius of approximately 15 cm around Rfish (**Figures 4**, **5**). As expected, the closer two fish are, the higher the contrast, but body movements can produce brief decreases. As a consequence, we then examined whether swimming orientation is also represented in the local contrast signals. Here swimming orientation is approximately measured by the difference between the distances from RFish to the head and tail of Ffish, i.e., Hd-Td. When two fish are in a static state, contrast is larger if the tail is closer to Rfish (positive "Hd-Td"). However, this is not always true in the free-swimming state (bottom rows in **Figures 5A–D**). This is because chirps, turning or tail-bending can easily change the contrast and further cause high variability in contrast. This suggests that the electric image over a large region of the fish body is needed to identify the orientation of a neighboring fish and trace their movement (Pedraja et al., 2018).

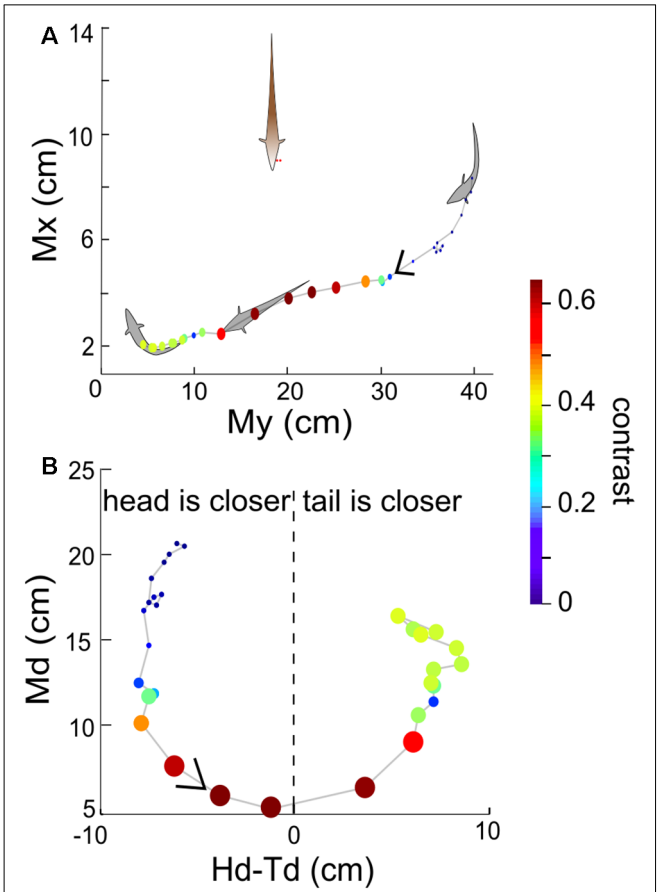

FIGURE 4 | (A) Example recorded time course of free-swimming fish movements and the associated contrast in 3 s. Each point indicates Mx and My of the free-swimming fish, measured at 100 ms increments. The size and color of the point indicate the contrast at that instant. The arrow indicates the direction of movement over time. **(B)** Md vs. Hd-Td for the same behavioral sequence as shown in **(A)**. The value Hd-Td provides information about the orientation and curvature of the free-swimming fish relative to the recording electrodes. Negative (positive) values of Hd-Td correspond to the head of Ffish being closer to (farther from) the recording electrodes. The orientation of the fish's body changes as the fish swims around and influences the calculated value of contrast.

Contrast Bumps and Their Temporal Distribution

The time-varying contrast exhibits random occurrences of bumps because of the looming (i.e., approaching) and receding (i.e., departure) behaviors of Ffish (**Figures 2A,B**, **6A**). Our working definition of contrast bump is any time interval during which the contrast remains over 0.04 for two or more consecutive 100 ms bins. We calculated the duration of the contrast bumps (bump duration, BD), the intervals separating two adjacent bumps (inter-bump duration or IBD), and the average of the instantaneous contrast within each BD and IBD for all interactions (**Figures 6B,C**). The contrast tends to increase with longer BDs but decrease with longer IBDs. To get a more comprehensive picture, we calculated mean BD, mean IBD and the means of all average contrasts over BDs and IBDs for each pair of fish (**Figures 6D,E**); each dot represents one pair of fish and is color-coded as in **Figures 6B,C**. This averaged contrast information indicates that longer BD and shorter IBD are related to higher mean contrast, for 11 out of 12 pairs. The brown dot in **Figure 6D** comes from a pair in which the Ffish was often relatively immobile at a certain distance from Rfish.

The start and end of a contrast bump reflect the "arrival" and "departure" respectively of Ffish, therefore contrast bumps can be used to characterize the interaction times between fish. The mean probability density function (PDF) of inter-arrival intervals (IAIs) averaged over 12 fish pairs is found to be well fitted by an exponential distribution with mean of 8.07 s (**Figure 7A**). Similarly, the mean inter-departure intervals (IDIs) is also well fitted to an exponential process with mean of 8.18 s, which is also the mean of IDIs (**Figure 7B**). The statistical analysis indicates that the looming and receding events of Ffish occur in a random pattern over

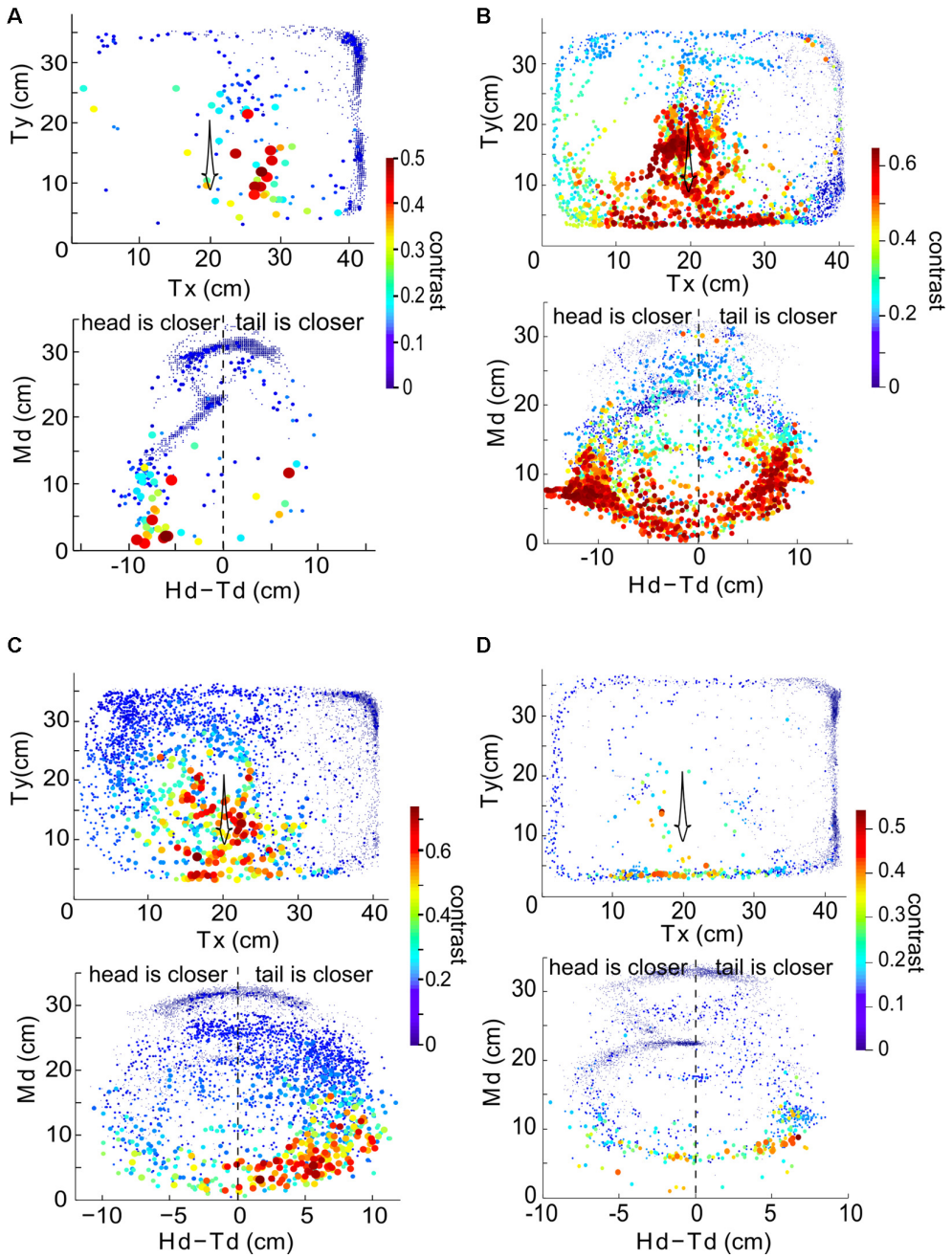

FIGURE 5 | The relationship between instantaneous contrast and the position of the free-swimming fish in the experimental tank over 300 s for the same four fish as in **Figure 3**. Data from a given pair of fish is plotted in each of the four panels. Top row in each panel: Tx and Ty indicate the position of the tail of the free-swimming fish in the tank relative to the bottom left corner of the tank, in centimeters. Each point indicates the position of the fish (averaged over a 100 ms time bin), and the size and color of each point (as shown in the color bar) denotes the value of the instantaneous contrast determined at that point in time. Bottom row in each panel: Md plotted against Hd-Td reveal orientation information. Panel **(A)** uses data from the fish pair in the first row of **Figure 3**, panel **(B)** to the second row of **Figure 3**, panel **(C)** to the third row of **Figure 3** and panel **(D)** to the fourth row of **Figure 3**.

time, which can be approximately described by Poisson processes with means 1/8.07 s and 1/8.18 s, respectively. **Figure 7C** shows that BDs and IBDs are again well characterized by an exponential distribution with 4.4 s and here the mean BD is 3.2 ± 0.7 s.

We then defined the Bump Fraction as the sum of all BDs divided by the trial time. A larger bump fraction implies that the Ffish stays at relatively close range to Rfish for a longer time. But a large bump fraction does not necessarily lead to a high average contrast; comparing **Figure 7D** with **Figure 6B**, one sees

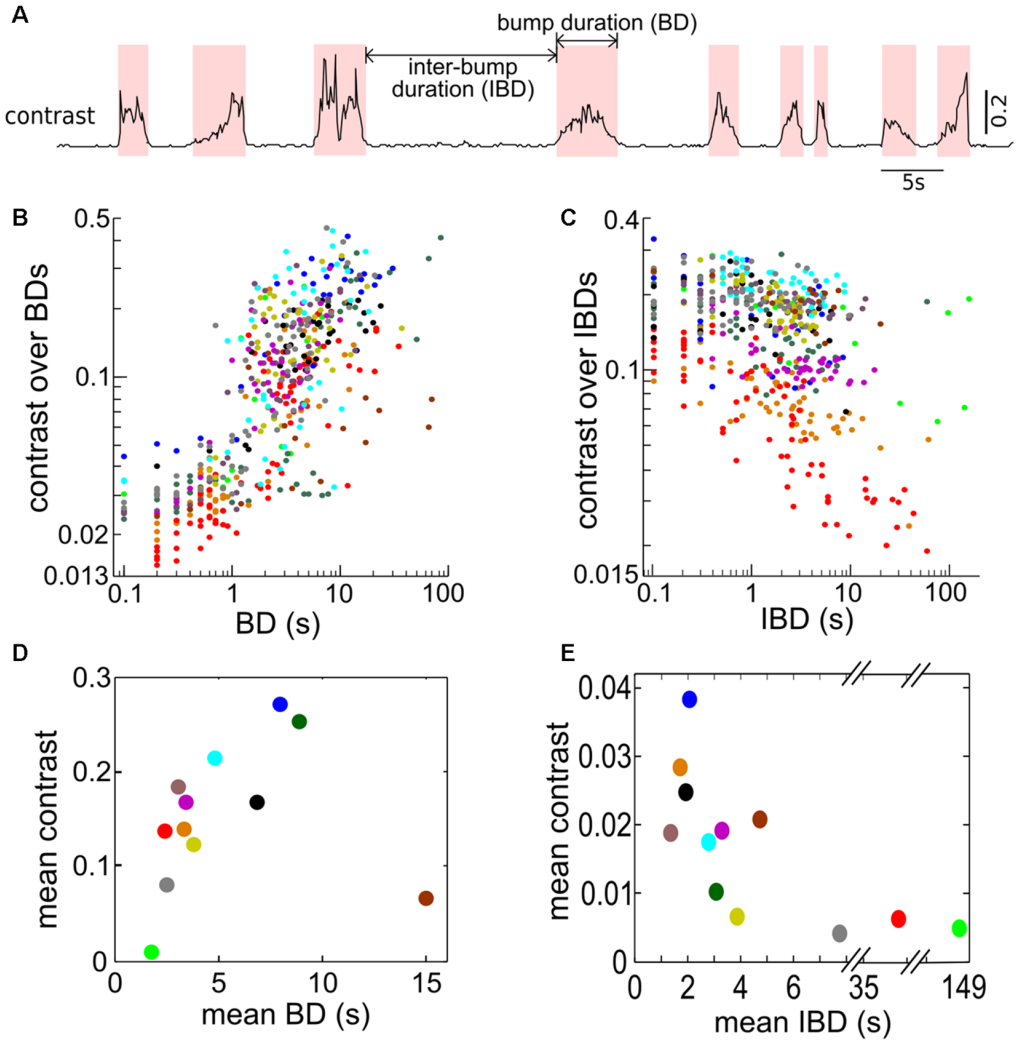

FIGURE 6 | Bumps in contrasts are associated with approach behaviors. **(A)** Trace showing instantaneous contrast calculated for one recording over 70 s demonstrating the occurrence of contrast bumps. Contrast bumps were defined as any time period in which the contrast remained above a value of 0.04 for two or more consecutive time bins (i.e., for 200 ms or longer). The contrast bump and inter-bump intervals are denoted as bump duration (BD) and inter-bump duration (IBD), respectively. **(B)** The average contrast calculated over each BD vs. the corresponding BD. **(C)** The average contrast calculated over each IBD vs. the corresponding IBD. **(D)** The relationship between the mean contrast calculated over all BDs plotted against the mean BD (in seconds). Each dot indicates one fish pair; 12 fish pairs are used. In general, longer BIs (i.e., longer duration when free-swimming fish is in the proximity of restrained fish) are associated with larger contrasts except the brown dot representing a fish pair where they kept a certain distance quietly most of the time. **(E)** The relationship between the mean contrast calculated during IBDs plotted against the mean IBD. For longer IBDs, the free-swimming fish tends to be further away from the restrained fish, resulting in lower contrasts. Panels **(D,E)** are color coded as **(B,C)** for each pair of fish.

for example that large bump fractions can occur for a mean BD around 5 s (**Figure 7D**), which correspond only to contrasts around 0.2 (**Figure 6B**). This is due in part to the threshold value of 0.04 that we used to define a contrast bump.

Stochastic Model for Long-Term Dynamic Contrast

We next seek a quantitative description with which to model the movement patterns under the conditions of our experiments. Such a quantitative description (i.e., simulated signal) has general usages in various experimental paradigms, including creating an artificial weakly electric fish capable of mimicking naturalistic signals, producing pseudo-natural stimuli to study neuronal processing and simulating natural inputs to computational models of the sensory pathway. The goal is to quantify the stochastic movement patterns with a small number of stochastic processes and parameters.

Our results so far enable us to extend the model of long-term instantaneous contrasts associated with movement that we developed in a previous study of movement encoding using envelopes (Yu et al., 2012). Specifically, we can write:

$$\text{Contrast} = \xi\,(A + \sigma\,\eta) \tag{1}$$

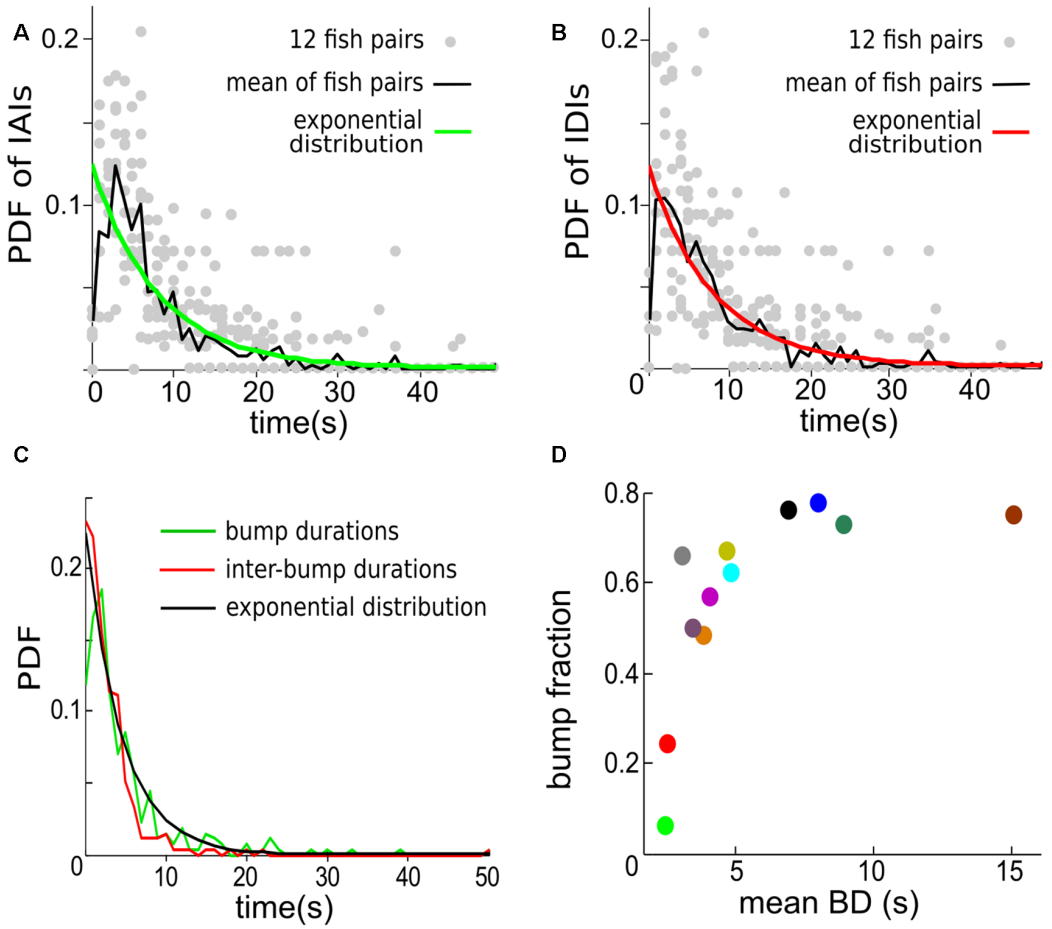

FIGURE 7 | The temporal distribution of contrast bumps across 12 individual fish pairs. **(A)** The probability density functions (PDFs) for individual trials (gray dots) and for the mean calculated across trials (green curve) of the intervals separating the start times of consecutive contrast bumps, i.e., inter-"arrival" intervals (IAIs). The mean IAI calculated over trials is 8.07 s. The PDF of an exponential distribution with mean rate λ equal to 8.07 s (black curve) is shown to fit well the observed mean IAI density. **(B)** The PDF for individual trials (gray dots) and for the mean calculated across trials (red curve) of the intervals separating the end times of consecutive contrast bumps, i.e., inter-departure intervals (IDIs). The mean IDI across trials is 8.18 s. The PDF of an exponential distribution with λ equal to 8.18 s (black curve) is again in good agreement with the observed mean IDI density. **(C)** The mean PDF of BDs and IBDs. The mean BD is 3.2 $\pm$ 0.7 s. An exponential distribution with λ equal to 4.44 s approximates the density of both BDs and IBDs. A bin width of 1 s is used for estimating the PDFs. **(D)** The bump fraction (fraction of time the contrast spends above chosen value of 0.04) vs. the mean BD for each fish pair. The data are color coded as in **Figures 6D,E**.

where we smooth out the variations from beat cycle to beat cycle, i.e., the contrast is a coarser representation of the movement envelope. In our previous study, ξ was simply a constant factor. Here however, to account for the looming and receding activities that lead to contrast bumps, we define ξ as a dichotomous noise, i.e., a two-state noise with Poisson-distributed (i.e., exponentially distributed) residence time in each state. It is also referred to as random telegraph noise. This dichotomous noise describes the random switching between contrast bump states (the high state of the dichotomous noise) and inter-bump states (the low state). The parameters A and σ are the mean and standard deviation of contrast bumps; η is Ornstein-Uhlenbeck process (OU) which is a simple type of lowpass-filtered Gaussian white noise with a cutoff frequency equal to the reciprocal of the autocorrelation time. The OU process has an exponentially decaying auto-correlation function, with correlation time of 1 s (Yu et al., 2012); it generates the fluctuations within contrast bump intervals.

Mean BD and mean IBD vary broadly in interactions between Rfish and Ffish (**Figures 6B,C**). We can now design artificial time series for instantaneous contrast statistics similar to those seen in interactions between most fish pairs. Three sample realizations of time-varying contrast are demonstrated in **Figure 8** with different mean BDs and mean IBDs, along with the contrasts arising from a real interaction.

DISCUSSION

In this study, we show that the dynamic contrast (or the second envelope, E2) of natural signals received by weakly electric fish reflects the motion of neighboring fish by analyzing simultaneous electrical and video recordings of multiple pairs

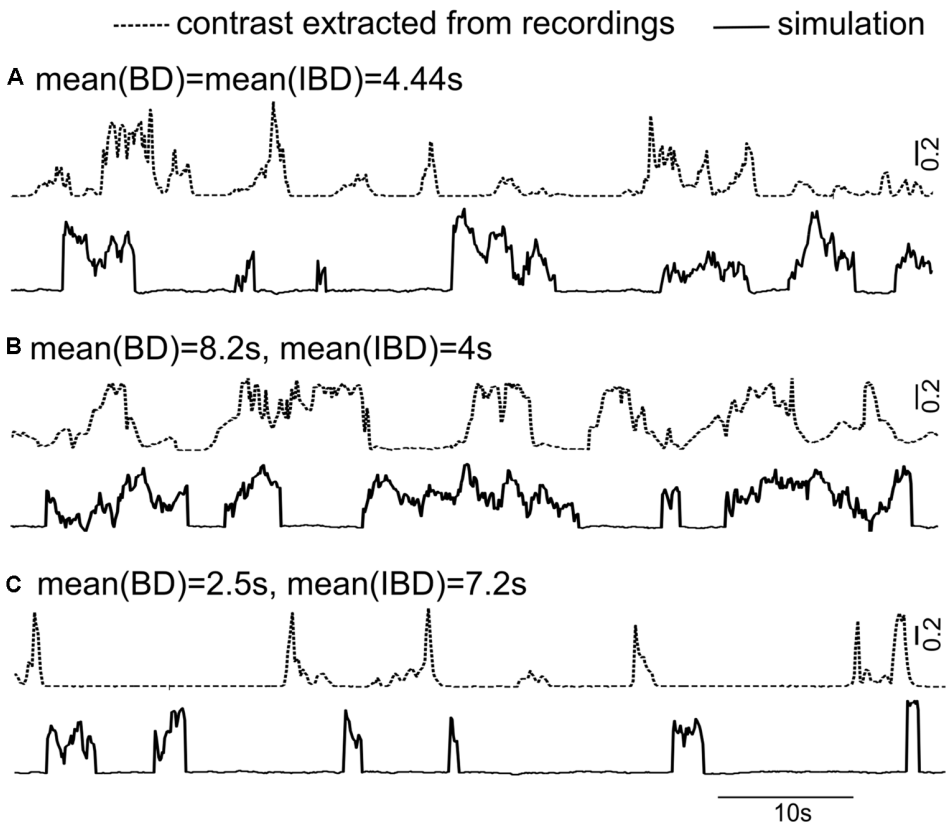

FIGURE 8 | The doubly stochastic model Contrast $= \xi\,(A + \sigma\,\eta)$ (see Equation 1) is used to simulate the long-term instantaneous contrasts. One noise term, ξ (dichotomous), causes the discrete transitions between a bump state (with the value of 1) and an inter-bump state (with the value of 0.02). A second noise term, η, is an exponentially correlated Ornstein-Uhlenbeck (OU) process with auto-correlation time of 1 s. This OU produces the contrast variability seen within contrast bump intervals. The instantaneous contrasts calculated from the recording (dashed lines) and representations of the model (solid lines) are shown in three cases: **(A)** mean(BD) = mean(IBD) = 4.4 s; **(B)** mean(BD) > mean(IBD); and **(C)** mean(BD) < mean(IBD). The parameters A and σ are the mean contrast value and the strength of the OU process η; here they take values of 0.2 and 0.1, respectively.

of fish. Specifically, the instantaneous contrast is anti-correlated with the time-varying inter-fish distance when two fish are in close proximity. Further, the contrast seen on longer time scales occurs as a sequence of stochastic bumps triggered by the random looming and receding visits of the freely swimming fish. The diverse interactions of conspecifics produce distinct characteristics of natural contrast (e.g., mean, standard deviation, contrast BDs). We then propose a stochastic model to simulate movement-generated contrasts with similar characteristics to those measured in our experiments.

Our study demonstrated that, in the context of two weakly electric fish, the major factor leading to the varying contrast of EOD-based signals received by a fish (the observer) is the distance separating the fish, as shown in **Figures 1C**, **2**. This distance determines the average values of the dynamic contrast (**Figure 3A**). Different patterns of swimming and associated contrast are seen to depend on the particular fish pair chosen (**Figures 3**, **5**). We have not investigated whether these different patterns are tied more to the identity of the swimming fish as opposed to the pair *per se*—this question could be explored in future work.

Besides the inter-fish distance, there are many other factors contributing to the contrast. These include the various swimming movements (e.g., turning or tail-bending), the angles and the phases of two superimposed electric fields (Kelly et al., 2008), and the occurrence of social signals such as chirps or the jamming avoidance response (Allen and Marsat, 2018; Henninger et al., 2018; Shifman and Lewis, 2018; Thomas et al., 2018). As a result, these factors could lead to the variance of contrast from a statistical point of view (**Figure 3A**). The variations of the contrast are magnified with shorter inter-fish distance, as was seen in our previous study (Yu et al., 2012). For instance, weakly electric fish tend to chirp more when they are in close proximity, normally resulting in transient (∼50 ms) decreases in the first envelope E1 and the contrast (e.g., Hupé and Lewis, 2008).

We note that contrast decays exponentially with distance under our experimental conditions (**Figure 1C**). This is different from the power-law relationships that have been fitted to experimental data for the EOD modulations due to small objects (with fractional power-law exponents e.g., Chen et al., 2005; Babineau et al., 2006). From a mathematical point of view, within a small distance scale, an exponential function (contrast

vs. distance) can be approximated by a power function (contrast vs. distance), and *vice versa*. Nevertheless, the exponential relationship could be used for modeling and to generate experimental stimuli.

Our work supports the notion that contrast can provide useful information to electrolocate conspecifics and guide the behaviors of the observer fish (e.g., navigation, collision avoidance). Meanwhile, the dynamic variations, in contrast, degrade this information and suggest that fast body movements (e.g., rapid turning, bending) or chirps could be used as disruptive or cloaking strategies, perhaps to confuse a conspecific or even an electroreceptive predator. Indeed, a fast body twist produced a pronounced and rapid decrease (or notch) on the second contrast peak in **Figure 2** box II. Such a change, in contrast, could mimic an approach, for example, without a change in inter-fish distance. More studies are required to determine whether fish actively use such strategies.

It is important to note that EOD-based signals recorded in our experiment will be encoded by electroreceptors located in an anterior region of Rfish. Previous studies reported that these electroreceptors can extract envelopes that contain movement information, and project them to target pyramidal cells in the electrosensory lateral line lobe (ELL) that respond to the movement envelopes (e.g., Middleton et al., 2006; Longtin et al., 2008; Huang and Chacron, 2016). Our results suggest that the sensory circuitry of a receiving fish has access to contrast envelopes, from which estimates of distance to the other fish are presumably derived. This is so in spite of the variability in contrast as a function of Td (and likely the other body markers too) observed across different swimming trajectories (**Figure 3**). This raises interesting questions about how the information is gathered across receptive fields to extract more precise information about the position and orientation of conspecifics.

To our knowledge, our work provides the first characterization of long-term instantaneous contrast time series as sequences of bumps with stochastic amplitudes resulting from approach behaviors (**Figure 6**). The occurrences of contrast bumps, representing approaches ("arrivals" of Ffish), are well accounted for by a Poisson distribution. The average inter-arrival time is 8.07 s in our experiments. The inter-arrival time of a Poisson process is memoryless, meaning one cannot predict better than the mean what the next arrival time will be based on the most recent arrival time. Such a memory-less process is a good first-order guess of the behavior at least in this experimental context; different behavioral and social contexts could result in different behavioral dynamics. Nevertheless, it will be interesting to determine the neural mechanisms that control such apparently random behavior.

Our model for long-term contrast (Equation 1) provides a reliable and efficient way to construct a naturalistic behaviorally-relevant stimulus to mimic free-swimming conspecifics in the laboratory. It could be used to study the neural responses to a moving conspecific and different approach behaviors. It can also be used to explore the multiple time scales of adaptation in the electroreceptors (Clarke et al., 2013) and the ELL evoked by a short-term stimulus (within one contrast bump) and long-term stimuli (a sequence of contrast bumps), similar to studies in the visual system (Ulanovsky et al., 2004).

While the form of the stochastic process we have chosen does justice to the main features of the signal, namely within bump variability as well as abrupt increases and decreases in overall amplitude, it is nevertheless an approximation. The electric field does decrease sharply with distance due to its dipolar nature, and this is approximated by a discrete switching process. Thus, we do not expect that the data will be well fitted by this model near the switches since there the overall signal amplitude varies continuously. The additive lowpass-filtered noise (OU process) on top of the dichotomous noise blurs out the associated discrepancies. Further, it is difficult to conceive of a simple stochastic process that would exhibit the strong nonlinearity imposed by the approximately dipolar relation between field strength and distance from the body. One could invoke a single non-Gaussian process, obtained e.g., by filtering a Gaussian process with a suitably designed or fitted static nonlinearity. One could also attempt to modify the spectral properties of a Gaussian noise process to fit the complete autocorrelation function of the signal; other kinds of noises such as fractal Brownian motions could have been used. But our goal was to provide a first picture of the interactions we observed in the context of our experiments and design a computationally simple model in terms of standard and easily implementable stochastic processes.

The close proximity of fish triggers not only dynamic contrasts but also communication signals (i.e., chirps). Preliminary results indicate that contrast bumps are temporally positively correlated with the bursting patterns of chirps (not shown; see also Allen and Marsat, 2018; Henninger et al., 2018). As chirps can also generate dramatic transient changes, in contrast, it would be very interesting to investigate the interplay among these three concurrent events, namely, the motion of the fish, the dynamic contrast and the chirps. The relative orientation of the interacting animals will also be an important factor, as well as the recent history of chirp emission.

One cannot expect purely random behavior from any animal, yet we have shown that at some level, certain features of the behavior are well-accounted for by assuming random processes—and specifically, the product of two standard noise processes. It is clear that the above results need to be submitted to other tests such as very long recordings, different tank sizes and depths, and eventually, to the case of two freely moving fish. The results of those future studies will, we hope, be contrasted to those reported here to reveal where and how pure randomness fails to explain significant features of the behavior.

DATA AVAILABILITY

The datasets generated for this study are available on request to the first author.

ETHICS STATEMENT

The animal study was reviewed and approved by University of Ottawa Animal Care Committee.

AUTHOR CONTRIBUTIONS

All authors contributed to the design of the experiments. NY and GH carried out the experiments and data analyses. The modeling analyses were performed by NY. NY wrote the article with input from JL and AL, who also supervised the whole project.

FUNDING

This research was supported by Natural Sciences and Engineering Research Council (NSERC) Canada.

REFERENCES

Allen, K. M., and Marsat, G. (2018). Task-specific sensory coding strategies are matched to detection and discrimination performance. *J. Exp. Biol.* 221:jeb170563. doi: 10.1242/jeb.170563

Babineau, D., Longtin, A., and Lewis, J. E. (2006). Modeling the electric field of weakly electric fish. *J. Exp. Biol.* 209, 3636–3651. doi: 10.1242/jeb.02403

Chen, L., House, J. L., Krahe, R., and Nelson, M. E. (2005). Modeling signal and background components of electrosensory scenes. *J. Comp. Physiol. A Neuroethol. Sens. Neural Behav. Physiol.* 191, 331–345. doi: 10.1007/s00359-004-0587-3

Clarke, S. E., Naud, R., Longtin, A., and Maler, L. (2013). Speed-invariant encoding of looming object distance requires power law spike rate adaptation. *Proc. Natl. Acad. Sci. U S A* 110, 13624–13629. doi: 10.1073/pnas.1306428110

Fotowat, H., Harrison, R. R., and Krahe, R. (2013). Statistics of the electrosensory input in the freely swimming weakly electric *fish Apteronotus leptorhynchus*. *J. Neurosci.* 33, 13758–13772. doi: 10.1523/JNEUROSCI.0998-13.2013

Henninger, J., Krahe, R., Kirschbaum, F., Grewe, J., and Benda, J. (2018). Statistics of natural communication signals observed in the wild identify important yet neglected stimulus regimes in weakly electric fish. *J. Neurosci.* 38, 5456–5465. doi: 10.1523/JNEUROSCI.0350-18.2018

Huang, C. J., and Chacron, M. J. (2016). Optimized parallel coding of second-order stimulus features by heterogeneous neural populations. *J. Neurosci.* 36, 9859–9872. doi: 10.1523/JNEUROSCI.1433-16.2016

Hupé, G. J., and Lewis, J. E. (2008). Electrocommunication signals in free swimming brown ghost knifefish, *Apteronotus leptorhynchus*. *J. Exp. Biol.* 211, 1657–1667. doi: 10.1242/jeb.013516

Kelly, M., Babineau, D., Longtin, A., and Lewis, J. E. (2008). Electric field interactions in pairs of electric fish: modeling and mimicking naturalistic input. *Biol. Cybern.* 98, 479–490. doi: 10.1007/s00422-008-0218-0

Longtin, A., Middleton, J. W., Cieniak, J., and Maler, L. (2008). Neural dynamics of envelope coding. *Math. Biosci.* 214, 87–99. doi: 10.1016/j.mbs.2008.01.008

Metzen, M. G., and Chacron, M. J. (2014). Weakly electric fish display behavioral responses to envelopes naturally occurring during movement: implications for neural processing. *J. Exp. Biol.* 217, 1381–1391. doi: 10.1242/jeb.098574

Michelson, A. (1927). *Studies in Optics*. Chicago, IL: The University of Chicago Press.

Middleton, J. W., Longtin, A., Benda, J., and Maler, L. (2006). The cellular basis for parallel neural transmission of a high-frequency stimulus and its low-frequency envelope. *Proc. Natl. Acad. Sci. U S A* 103, 14596–14601. doi: 10.1073/pnas.0604103103

Pedraja, F., Hofmann, V., Lucas, K. M., Young, C., Engelmann, J., and Lewis, J. E. (2018). Motion parallax in electric sensing. *Proc. Natl. Acad. Sci. U S A* 115, 573–577. doi: 10.1073/pnas.1712380115

Shifman, A. R., and Lewis, J. E. (2018). The complexity of high-frequency electric fields degrades electrosensory inputs: implications for the jamming avoidance response in weakly electric fish. *J. R. Soc. Interface* 15:20170633. doi: 10.1098/rsif.2017.0633

Stamper, S. A., Fortune, E. S., and Chacron, M. J. (2013). Perception and coding of envelopes in weakly electric fishes. *J. Exp. Biol.* 216, 2393–2402. doi: 10.1242/jeb.082321

Thomas, R. A., Metzen, M. G., and Chacron, M. J. (2018). Weakly electric fish distinguish between envelope stimuli arising from different behavioral contexts. *J. Exp. Biol.* 221:jeb.178244. doi: 10.1242/jeb.178244

Ulanovsky, N., Las, L., Farkas, D., and Nelken, I. (2004). Multiple time scales of adaptation in auditory cortex neurons. *J. Neurosci.* 24, 10440–10453. doi: 10.1523/JNEUROSCI.1905-04.2004

Yu, N., Hupé, G., Garfinkle, C., Lewis, J. E., and Longtin, A. (2012). Coding conspecific identity and motion in the electric sense. *PLoS Comput. Biol.* 8:e1002564. doi: 10.1371/journal.pcbi.1002564

Conflict of Interest Statement: The authors declare that the research was conducted in the absence of any commercial or financial relationships that could be construed as a potential conflict of interest.

The reviewer JE declared a past co-authorship with one of the authors JL to the handling Editor.

frontiers in Integrative Neuroscience

ORIGINAL RESEARCH
published: 13 August 2019
doi: 10.3389/fnint.2019.00037

Preoptic Area Activation and Vasotocin Involvement in the Reproductive Behavior of a Weakly Pulse-Type Electric Fish, *Brachyhypopomus gauderio*

Paula Pouso[1,2], *Álvaro Cabana*[3], *James L. Goodson*[4] *and Ana Silva*[1,5]*

[1]Departamento de Histología y Embriología, Facultad de Medicina, Universidad de la República, Montevideo, Uruguay, [2]Unidad Bases Neurales de la Conducta, Departamento de Neurofisiología Celular y Molecular, IIBCE, Montevideo, Uruguay, [3]Centro de Investigación Básica en Psicología (CIBPsi) and Instituto de Fundamentos y Métodos, Facultad de Psicología, Universidad de la República, Montevideo, Uruguay, [4]Department of Biology, Indiana University, Bloomington, IN, United States, [5]Laboratorio de Neurociencias, Facultad de Ciencias, Universidad de la República, Montevideo, Uruguay

OPEN ACCESS

Edited by:
Michael R. Markham,
University of Oklahoma,
United States

Reviewed by:
Raul Aguilar-Roblero,
Institute of Cellular Physiology,
National Autonomous University of Mexico, Mexico
Martin Ralph,
University of Toronto, Canada

***Correspondence:**
Ana Silva
asilva@fcien.edu.uy

Received: 29 April 2019
Accepted: 19 July 2019
Published: 13 August 2019

Citation:
Pouso P, Cabana Á, Goodson JL and Silva A (2019) Preoptic Area Activation and Vasotocin Involvement in the Reproductive Behavior of a Weakly Pulse-Type Electric Fish, Brachyhypopomus gauderio. Front. Integr. Neurosci. 13:37. doi: 10.3389/fnint.2019.00037

Social behavior exhibits a wide diversity among vertebrates though it is controlled by a conserved neural network, the social behavior network (SBN). The activity of the SBN is shaped by hypothalamic nonapeptides of the vasopressin-oxytocin family. The weakly electric fish *Brachyhypopomus gauderio* emits social electrical signals during courtship. Three types of vasotocin (AVT) cells occur in the preoptic area (POA), one of the SBN nodes. In this study, we aimed to test if POA neurons of the nucleus preopticus ventricularis anterior (PPa) and posterior (PPp), and in particular AVT+ cells, were activated by social stimuli using a 2-day behavioral protocol. During the first night, male-female dyads were recorded to identify courting males. During the second night, these males were divided in two experimental conditions: isolated and social (male with a female). Both AVT cells and the cellular activation of the POA neurons (measured by FOS) were identified. We found that the PPa of social males showed more FOS+ cells than the PPa of isolated males, and that the PPa had more AVT+ cells in social males than in isolated males. The double-immunolabeling for AVT and FOS indicated the activation of AVT+ neurons. No significant differences in the activation of AVT+ cells were found between conditions, but a clear association was observed between the number of AVT+ cells and certain behavioral traits. In addition, a different activation of AVT+ cell-types was observed for social vs. isolated males. We conclude that the POA of *B. gauderio* exhibits changes induced by social stimuli in reproductive context, involving an increase in AVT production and a different profile activation among AVT+ cell populations.

Keywords: preoptic area, electric fish, FOS, vasotocin, social behavior

INTRODUCTION

Social behavior in vertebrates arises as an emergent property of the social behavior network (SBN), a network of brain nuclei that includes the medial preoptic area (POA), lateral septum, anterior hypothalamus, ventromedial hypothalamus, periaqueductal gray, medial amygdala, and bed nucleus of the stria terminalis (Newman, 1999; Nelson and Trainor, 2007). It is accepted that the diversity in social behavior, within a given species and across vertebrates, would be achieved by changes in the distributed pattern of neural activity among the interconnected nodes of the SBN (Newman, 1999; Goodson and Kabelik, 2009). These neural circuits, initially described in mammals, appear to be highly conserved among all classes of vertebrates (Goodson, 2005; O'Connell and Hofmann, 2011). Multiple neuromodulators shape the spatio-temporal pattern of activity of the SBN controlling the emergence of environmental, ontogenic, social context, and phenotype-dependent behaviors (Newman, 1999; Goodson et al., 2012; Johnson and Young, 2017).

One effective way to approach the neural circuits underlying complex social behavior is the use of immediate early genes (IEGs) as neural activity markers (Clayton, 2000; Kovács, 2008). Across vertebrates, several studies report an increased expression of IEGs in specific nodes of the SBN in association to courtship (Kollack-Walker and Newman, 1995; Curtis and Wang, 2003; Okuyama et al., 2011), parental care (O'Connell et al., 2012; Zhong et al., 2014; Kasper et al., 2018; Kent and Bell, 2018), territorial behavior (Kollack-Walker and Newman, 1995; Goodson and Evans, 2004; Teles et al., 2015) and grouping (Goodson et al., 2005a; Cabrera-Álvarez et al., 2017; Wilson et al., 2018). The use of IEGs as a proxy for visualizing the activation of brain areas associated with social behavior has also implicated the activation of hypothalamic neurons involved in the production of nonapeptides of the vasopressin/oxytocin family during these behaviors (Goodson and Wang, 2006; Goodson and Kabelik, 2009; O'Connell et al., 2012; Loveland and Fernald, 2017; Wilson et al., 2018). Only two previous studies in teleosts have found a differential activation between isolated and social animals of isotocin (oxytocin homolog) neurons associated with parental care (O'Connell et al., 2012) and of vasotocin (AVT, vasopressin homolog) neurons involved in courtship and aggression (Loveland and Fernald, 2017). However, these studies failed to find the general pattern of increased expression of IEGs in social animals in the brain areas in which these nonapeptidergic neurons occur.

Weakly electric fish are traditional neuroethological model systems that exhibit both locomotor and electric displays in their behavior. These fish emit an electric organ discharge (EOD) generated by a very well-known electromotor circuit. The EOD rate and waveform contain information about an individual's species identity, sex, and physiological state (Stoddard, 2002; Caputi et al., 2005). *Brachyhypopomus gauderio* (Giora and Malabarba, 2009), former *Brachyhypopomus pinnicaudatus* (Hopkins, 1991) is a south American freshwater weakly electric fish that belongs to the Order Gymnotiformes. This species is gregarious, has a polygynous breeding system, and exhibits during the breeding season a strong morphological and electrophysiological sexual dimorphism (Caputi et al., 1998; Silva et al., 2003).

The behavioral displays of both courting (male-female) and agonistic (male-male) dyadic interactions are well understood in this species (Perrone et al., 2009; Zubizarreta et al., 2012). It is also clear that the electrical signaling of social behavior in this species is modulated by AVT in a context-dependent manner. For example, the nocturnal increase in EOD rate is AVT-dependent in courting breeding pairs (Silva et al., 2007; Perrone et al., 2010) but not in isolated individuals (Migliaro and Silva, 2016). In addition, males *B. gauderio* signal dominance by an AVT-dependent increase in EOD rate that is not observed in subordinates (Perrone and Silva, 2016). Further, as in other teleosts (Batten et al., 1990; Holmqvist and Ekström, 1995; Goodson and Kabelik, 2009; Ramallo et al., 2012), the typical three types of AVT+ cells [parvocells (pPOA), magnocells (mPOA), and gigantocells (gPOA)], have been exclusively reported within the POA of this species projecting to several brain areas including those related to the control of electromotor behavior (Pouso et al., 2017). In weakly electric fish, AVT+ cells are organized in two nuclei within the POA described by Maler et al. (1991): the preopticus periventricularis anterior (PPa) and the preopticus periventricularis posterior (PPp).

In this study, we aimed to evaluate how social stimulation (the presence of the female) affected the activation of POA neurons in general, and of AVT cells in particular, in courting males of *B. gauderio*. For the first time in electric fish, we double-immunolabeled POA neurons with AVT and FOS and showed that: (a) the PPa of chirping males shows increased transcription for FOS after the social stimulus of the female; (b) the number of AVT cells is higher in social males with respect to isolated ones in the PPa; and (c) the activation profile of AVT cells types is different between social and isolated males.

MATERIALS AND METHODS

Animals

In this study, we used 24 breeding adult males of *Brachyhypopomus gauderio* (Giora and Malabarba, 2009), with body-length ranging from 14.5 to 19.3 cm and body-weight from 5.2 to 8.9 g. Fish were detected and collected during the breeding season (November-February) in a freshwater lagoon in Laguna Lavalle (31°48′S, 55°13′W, Department of Tacuarembó, Uruguay) using a "fish detector," an electronic audio amplifier connected to a pair of electrodes, as previously described (Silva et al., 2003).

Fish were housed for at least 10 days before the behavioral experiments in 500-L outdoor communal tanks with two males and six females, which replicate the sex ratio of a natural breeding population (Miranda et al., 2008). All environmental variables were kept within the normal range observed in the natural breeding habitat (Silva et al., 2003). Water conductivity was maintained below 200 μS/cm by the addition of deionized

water. Water temperature in the tanks ranged from 18 to 33°C and the natural photoperiod ranged from LD14:10 to LD13:11. The surface of the water was covered with aquatic plants (*Eichhornia crassipes, Pistia stratiotes, Salvinia sp.*) that provided shelter for the fish. Fish were fed *Tubifex tubifex*. The fish collection, transportation, housing, and recording conditions were adjusted in order to minimize stress and to achieve reliable and repeatable behaviors. All experiments were performed in accordance with institutional and national guidelines and regulations for animal welfare. This study was reviewed and approved by an ethics committee (Comisión Honoraria de Experimentación Animal, Universidad de la República, Protocol Number 008/002).

Behavior

Behavioral Recording Station

Fish simultaneous video and electric recordings were performed in an experimental setup previously described (Silva et al., 2007). Four experimental tanks (50-l glass aquaria, 55 × 40 × 25 cm) were fitted with two pairs of orthogonal electrodes attached to each tank wall. The physicochemical parameters (water temperature, conductivity, and pH) and the day–night cycle of indoor tanks matched those of the outdoor housing tanks. All the experiments were performed in total darkness illuminated by an array of infrared LEDs (L-53F3BT) located above the tank and an infrared-sensitive video camera (SONY CCD-Iris and RoHS CCD Digital Video Camera) focused on the bottom of the tank. The detection of electric signals of freely moving fish was done by two pairs of fixed electrodes, connected to two high-input impedance amplifiers (FLA-01, Cygnus Technologies Inc.). Images and electric signals were captured by a video card (Pinnacle Systems, PCTV HD pro stick) and stored in the computer for further analysis. Fish were placed for 6 h in the recording tank at constant temperature (27–29°C) before the beginning of the behavioral experiments.

Behavioral Paradigm

All males used in this study were tested in a 2-day protocol. The courting behavior of male-female dyads (originally housed in the same tank) was tested during the first night. To proceed to the second night of the experiment, we selected the dyads that displayed locomotor and electric courting behavior as previously described in this species (Perrone et al., 2009). In other words, we only selected the dyads in which males chirped and females turned off their electric discharges. Both males and females were isolated for more than 24 h in individual tanks after the first night experiment. In the second night (**Figure 1**), the chirping males were randomly assigned to two experimental conditions: social (n = 8) and isolated (n = 6). Isolated males were recorded 150 min after artificial sunset. Social males were also recorded 150 min after artificial sunset, first in isolation until the same female used in the first night (immobilized in a net) was added to the tank 30 min after artificial sunset and removed 60 min later (**Figure 1**). Both isolated and social males were simultaneously anesthetized 120 min after the female was removed, intracardiac-perfused and brains were dissected for immunohistochemistry. In another control experiment, we carried out the same 2-day protocol to test, in the second night, isolated males vs. isolated males plus the addition of the empty net.

Behavioral Data Processing

We measured the following behavioral parameters in courting males in all the experiments: the time of movement of animals (measured in percentage), the number of approaches towards female, total time with female and the number of chirps emitted. Data for one male-female dyad was lost due to corruption of the output video file. Hence, behavior analyses are only shown for only seven animals.

Tissue Collection and Processing

Double Immunolabeling for FOS and AVT

Fish were anesthetized by immersion in 0.05% 2-phenoxy-ethanol (Sigma, P-1126) and then perfused with saline followed by 4% paraformaldehyde in phosphate buffered saline (PBS, 25–35 ml; pH = 7.4). Coded brains were processed by an observer blinded to treatment. Brains were dissected, post-fixed overnight in the same fixative at 4°C, rinsed in 0.1 M PBS and cryoprotected in 30% sucrose for 24 h at 4°C before embedding in Cryomatrix (Thermo Scientific) and storage at −80°C until processing. Brains were then sectioned on a cryostat into three series of 50 μm sections. The first series was double immunolabeling for FOS and AVT. Free-floating sections were rinsed in PBS, and non-specific binding sites were blocked with normal 10% donkey serum (DS, Jackson Immunoresearch) + 0.3% Triton (Sigma) in PBS 0, 1 M; PH 7, 4 for 1 h. Sections were incubated for 36 h in primary antibodies (anti- FOS, 1:500, goat, custom from Bethyl Labs) ; anti-AVP, 1:500, rabbit, Immunostar, dissolved in 0.1 M PBS + 0.3% Triton X-100 + 5% DS with sodium azide 0.01%. After incubation with the primary antibodies, sections were rinsed (3 × 10 min in PBS) and incubated for 2 h at room temperature with secondary antibodies [Alexa Fluor 594 (red) donkey anti-goat IgG (H + L), 1:200, Invitrogen, Cat#A11058, and Alexa Fluor 680 (false color green) donkey anti-rabbit IgG (H + L), 1:200, Invitrogen, Cat#A21109] dissolved in 0.1 M PBS + 0.3% Triton X-100 + 5% DS with Sodium Azide 0.01%. All sections were then rinsed (3 × 10 min in PBS) and mounted with a nuclear stain (ProLong Gold Antifade Mountant with DAPI, Molecular Probes, 'Cat#P3693).

AVT+ cells are only present in the POA forming a large band extended from behind the anterior commissure to the posterior POA, above the optic chiasm (Pouso et al., 2017, **Figures 2F,G**). Maler et al. (1991) identified two nuclei within the POA in which AVT+ cells were later reported to occur: the PPa (**Figures 2A–F**) and the PPp (**Figures 2G,H**). Parvocellular AVT cells (pPOA) were exclusively identified in the PPa, gigantocellular AVT cells (gPOA) were exclusively in the PPp while magnocellular (mPOA) cells occur in both PPa and PPp (Pouso et al., 2017).

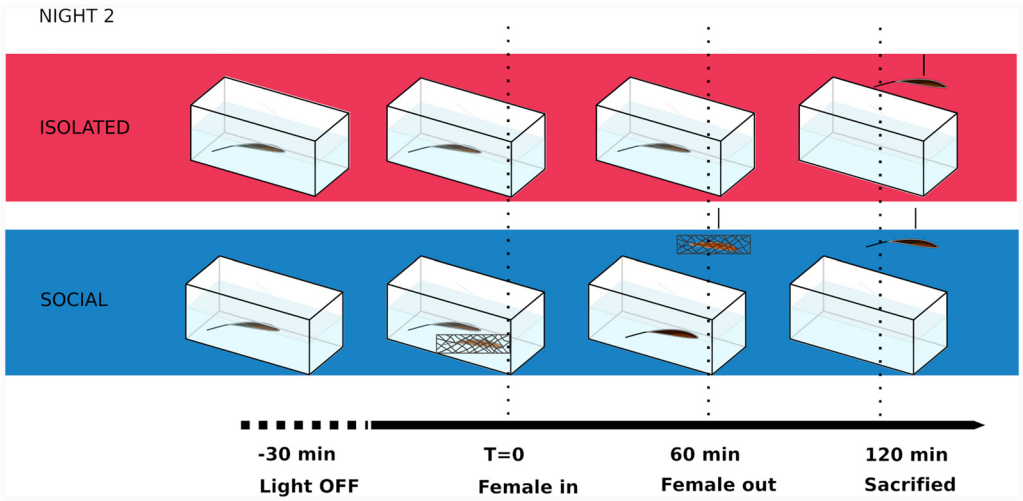

FIGURE 1 | Schematic of behavioral paradigm during the second night in courting males of *Brachyhypopomus gauderio*. T, time.

Double-immunolabeling for FOS and AVT was performed and quantified in PPa and PPp sections of the POA in both experimental conditions and an example is shown in a PPa section of a social male (**Figures 2A–D**). Control sections were incubated with the primary antiserum (anti-AVP) pre-absorbed with an excess of AVT (1 μg/ml; Cat. 66-0-09, American Peptide Company Inc., Sunnyvale, CA, USA) and no labeling was present. On the other hand, the preabsorption of anti AVP with an excess of IST (10 μM, 1:500, Bachem) showed a labeling that did not differ with plain AVP antibody staining (data not shown). Control sections were incubated with the primary antiserum (anti-FOS) pre-absorbed with an excess of FOS (1 mg/ml) for 3 h at room temperature and no labeling was observed (data not shown). Control experiments omitting the primary and secondary antibody were routinely performed.

Image Acquisition and Cell Counting

Images were generated at 10× using a Zeiss AxioImager microscope outfitted with an AxioCam HRm, z-drive, and an Apotome optical dissector (Carl Zeiss Inc.). We used standardized methods to quantify FOS+ cells (Goodson et al., 2005b; O'Connell et al., 2012; Lin et al., 2018). To measure the density of FOS+ cells, the counts of FOS+ nuclei were conducted within standardized polygons or boxes (100 μm^2) that were superimposed on the digital photomicrographs using Gimp 2.8.16 software. Dots were placed over each labeled cell (in a separate Gimp layer) and the dots were then counted using ImageJ software (National Institutes of Health, Bethesda, MD, USA). The raw cell counts were ultimately converted into the number of FOS+ nuclei per 100 μm^2 of tissue.

We also quantified the total number of AVT+ cells per slice following Pouso et al. (2017). Only somata with a distinct perimeter and at least one neurite were measured. Given that AVT immunostaining was conducted on 50 μm thickness slices and that soma size of these cells is ∼12–20 μm in diameter, it is unlikely to count them twice. Further, we avoided this possibility by not using adjacent slices. To quantify double labeling cells for FOS and AVT we use monochrome photomicrographs for each fluorophore at 10 and then quantification was subsequently conducted from layered monochrome images using Gimp 2.8.16 and ImageJ software (National Institutes of Health, Bethesda, MD, USA). We also quantify the proportion of these neurons co-labeled with FOS using methods previously described (Goodson and Evans, 2004; Goodson and Wang, 2006).

Statistical Analysis

Immunohistochemical quantification data were analyzed using general and generalized linear mixed models (Faraway, 2016). These models (also known as nested, hierarchical or multilevel models) explicitly consider the existence of correlations of observational units coming from the same individual, extend the applicability of linear models beyond the case of normally distributed outcomes, and are being increasingly used in ecology and neuroscience (for instance see Boisgontier and Cheval, 2016; Harrison et al., 2018; Fischer et al., 2019). Experimental condition (isolated, social), anatomical or morphological descriptors such as POA section (PPa or PPp) or cell type (gPOA, mPOA or pPOA), and behavioral predictors were introduced as fixed effects, while individual was included as random intercept effects. In some cases, the significance of main effects and interactions was assessed through analysis of variance (or deviance). *Post hoc* pairwise comparison of *p*-values were adjusted using the multivariate-*t*-test (mvt) method. Cell counts (AVT+ or FOS+ cells) for each slice were analyzed using generalized linear mixed models with Poisson distributions using the logarithmic link. Proportions (AVT+ cells that are also FOS+) for each slice were analyzed using generalized linear mixed models with binomial distributions using the logit link. The relationship between total movement and experimental condition was explored using a

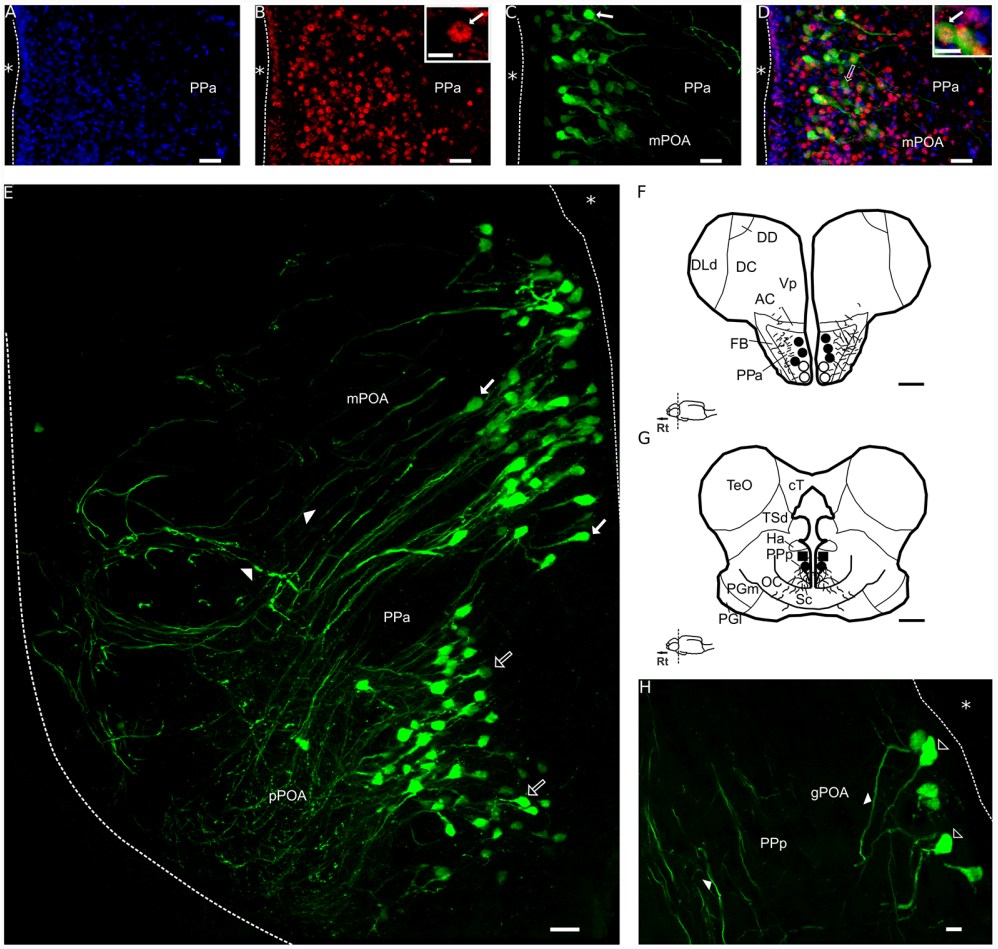

FIGURE 2 | Double immunolabeling for FOS and AVT in a transverse section of the POA of a social male of *Brachyhypopomus gauderio*. **(A)** Immunolabeling for DAPI (blue). **(B)** Immunolabeling for FOS (red). Inset in **(B)**: the arrow shows the nuclear label for FOS. **(C)** Immunolabeling for AVT (green). The arrow indicates an AVT+ cell. **(D)** Merge of **(A–C)**. Blank arrow indicates an AVT+ cell. Inset in **(D)**: the arrow shows a double-immunolabeled cell for FOS and AVT (yellow). **(E)** PPa section of the POA immunolabeled for AVT (false color green), blank arrows indicate pPOA cells and filled arrows indicate mPOA cells. Arrowheads indicate AVT+ fibers. **(F,G)** Diagrams of AVT+ cells; pPOA (dots), mPOA (black dots), gPOA (squares) and fibers (lines) in a rostral **(F)** and caudal **(G)** transverse sections. **(H)** PPp section of the POA immunolabeled for AVT (false color green). Blank arrowheads indicate gPOA cells somata and filled arrowheads indicate fibers. *, ventricle all levels; Rt, rostral; AVT, vasotocin; pPOA, parvocells; mPOA, magnocells; gPOA, gigantocells; PPa, nucleus preopticus ventricularis, anterior subdivision; PPp, nucleus preopticus ventricularis, posterior subdivision; AC, anterior commissure; cT, tectal commissure; DC, central division of dorsal forebrain; DD, dorsal division of the dorsal forebrain; Dld, dorsolateral telencephalon, dorsal subdivision; FB, forebrain bundle; Ha, hypothalamus anterioris; OC, optic chiasm; PGl, preglomeriular nucleus, lateral subdivison; PGm, preglomerular nucleus, medial subdivison; nucleus; PPa, nucleus preopticus periventricularis, anterior subdivision; Sc, suprachiasmatic nucleus; TeO, optic tectum; TSd, torus semicircularis, dorsal subdivision; Vp, ventral telencephalon, posterior subdivision. Bar scale: **(A–D)**: 20 μm; **(E)**: 20 μm; **(F,G)**: 500 μm; **(H)**: 10 μm. Inset in **(B)**: 5 μm. Inset in **(D)**: 10 μm.

general linear model with experimental condition as a fixed effect. All analyses were programmed in the R statistical programming language.

RESULTS

The double immunolabeling for AVT and FOS was performed in PPa and PPp sections of the POA in social and isolated males. An example of a PPa section is shown in a social male in **Figures 2A–D**. The nuclei of cells were stained with DAPI (**Figure 2A**), which allows the clear identification of double immunostained cells (**Figure 2D**, inset). The nuclear labeling for FOS is shown in the PPa (**Figure 2B**); the labeling is distributed as a "ring" inside the nucleus of the cell (inset in **Figure 2B**). AVT labeling was present in somata and fibers of cells in the PPa (**Figure 2C**) as well as the double labeling for FOS and AVT (**Figure 2D**). In accordance to the previous description of the POA of this species (Pouso et al., 2017), the distribution of AVT pPOA and mPOA cells is more rostral and ventral while gPOA cells are only located in the most caudal and dorsal portions of the POA (**Figures 2E–H**).

We assessed whether locomotor activity affected FOS labeling (Montag-Sallaz et al., 1999) and we quantified the percentage

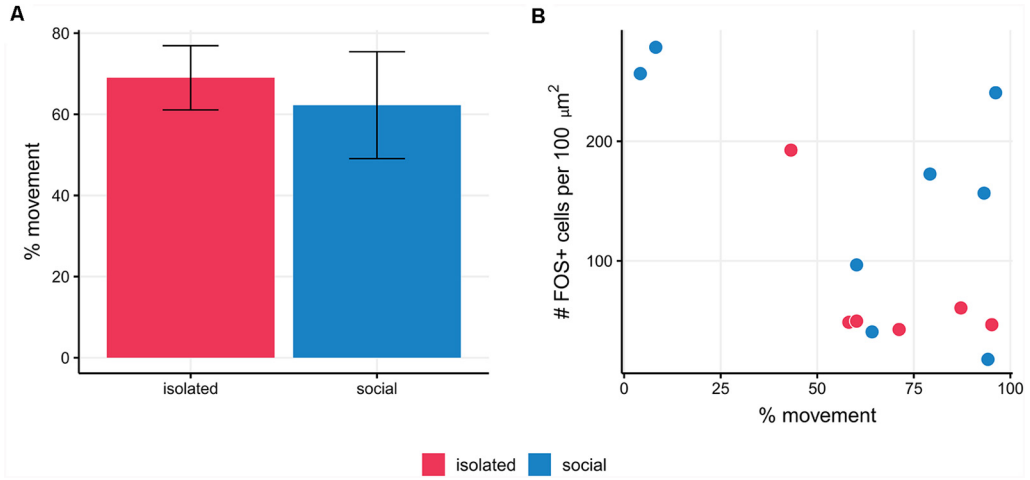

FIGURE 3 | (A) The percentage of movement in social males and isolated ones was similar ($p = 0.69$). **(B)** The mean number of FOS+ cells per slice is not correlated with the percentage of movement in social and isolated males of *B. gauderio* ($p = 0.18$).

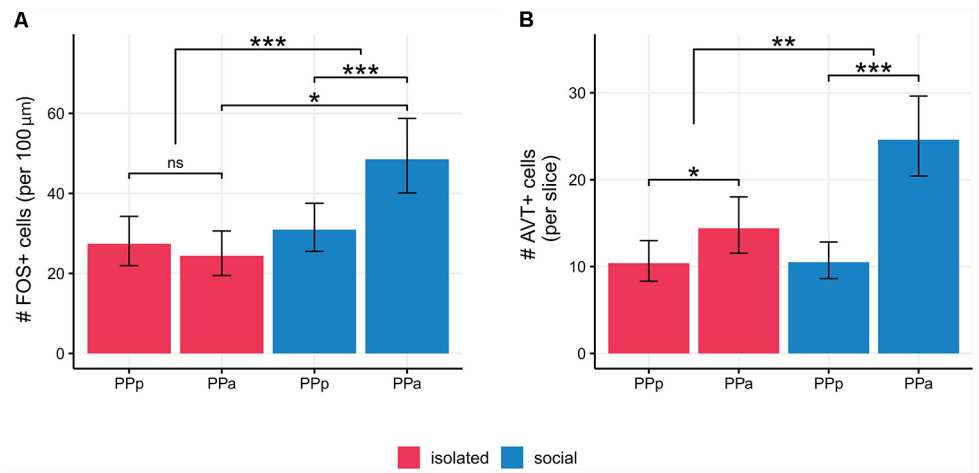

FIGURE 4 | (A) Social males show higher number of FOS+ cells/100 μm^2 in PPa sections with respect to PPp ones ($p < 0.001$) and as compared to PPa sections in isolated males ($p = 0.02$). **(B)** Isolated males show a higher number of AVT+ cells in PPa sections compared to PPp sections. ($p = 0.01$). Social males also show a higher number of AVT+ cells in PPa sections compared to PPp section ($p < 0.001$). The difference between PPa and PPp cell AVT+ cells was larger for social males ($p = 0.003$). POA, preoptic area; PPa, nucleus preopticus ventricularis, anterior subdivision; PPp, nucleus preopticus ventricularis, posterior subdivision. $^*p < 0.05$, $^{**}p < 0.01$, $^{***}p < 0.001$; ns, non-significant.

of time in which social and isolated males displayed locomotor activity. We found no correlation between the number of FOS+ immunolabeled cells and the percentage of time in which social and isolated males display locomotor activity [Generalized linear mixed model (Poisson): Wald's $\chi^2_{(1)} = 2.03$, $p = 0.15$]. Moreover, the percentage of movement in social males and isolated ones was similar (isolated: 69%; social: 62.25%; $t_{(12)} = -0.4$; $p = 0.69$; **Figure 3A**). We also validated the evaluation of the presence of the female (inside the net) as the actual social stimulus by checking that the net itself was not a relevant stimulus for FOS expression in isolated courting males [mean number of FOS+ cells per 100 μm^2 in isolated males, vs. isolated males with empty net; Generalized linear mixed model (Poisson): Wald's $\chi^2_{(1)} = 1.79$; $p = 0.18$].

Social Stimuli Increase FOS Expression in the Preoptic Area of *B. gauderio* Courting Males

We quantified the number of FOS+ cells per 100 μm^2 in PPa and PPp sections of the POA in social and isolated males (**Figure 4A**, **Table 1**). The density of FOS+ cells in PPa and PPp is different between experimental conditions [Generalized linear mixed model (Poisson). Interaction term: condition × POA section: Wald's $\chi^2_{(1)} = 23.99$; $p = 9.7 \times 10^{-7}$; **Figure 4A**, **Table 1**].

In the POA of isolated males, no differences were found between the mean number of FOS+ cells in PPa and PPp sections (paired contrast: $z = 1.23$, $p = 0.21$, **Figure 4A**, **Table 1**). In contrast, within the POA of social males, the mean number of FOS+ cells is higher in PPa sections compared to PPp ones ($z = -6.68$; $p = 2.37 \times 10^{-11}$, **Figure 4A**, **Table 1**). Furthermore, within the PPa sections of the POA, the mean number of FOS+ cells was higher in social males as compared to isolated males ($z = 2.32$; $p = 0.02$, **Figure 4A**, **Table 1**).

Social Males Exhibit Changes in the Number of AVT+ Cells

We quantified the number of AVT+ cells per slice in PPa and PPp sections of the POA both in social and isolated males (**Figure 4B**, **Table 1**). In both experimental conditions, we found a higher number of AVT+ cells per slice in the POA in PPa sections, as compared to the PPp (isolated: $z = 2.53$, $p = 0.01$; social: $z = 7.07$ $p = 1.52 \times 10^{-12}$, **Figure 4B**, **Table 1**). However, the difference between PPa and PPp cell counts was larger for social males than for isolated males [Generalized linear mixed model (Poisson). Interaction term: condition × POA section: Wald's $\chi^2_{(1)} = 8.78$, $p = 0.003$; **Supplementary Table S1**]. This difference seems to be due to an increase in the number of PPa AVT+ cells in the social condition when compared to the isolated condition ($z = 1.8$, $p = 0.06$), rather than to a change in PPp cell counts between conditions ($z = 0.04$, $p = 0.97$).

The Proportion of AVT+/FOS+ Cell Types Is Different Between Social and Isolated Males

We found no differences in the proportion of double labeled (AVT+/FOS+) cells in the PPa and PPp of isolated and social males [Generalized linear mixed model (Binomial): Wald's $\chi^2_{(1)} = 1.93$, $p = 0.16$; Interaction term, condition × POA section: Wald's $\chi^2_{(1)} = 0.6$, $p = 0.44$; **Supplementary Table S1**]. Nor was the activation of each AVT+ cell type different between experimental conditions (pairwise contrasts: gPOA: $z = -1.16$, $p = 0.24$; mPOA: $z = 1.42$, $p = 0.15$; pPOA: $z = 0.51$, $p = 0.61$). However, the pattern of activation of AVT+ cell types was different between isolated and social males (**Figure 5**, **Table 1**). Isolated males showed no significant differences in the proportion of FOS+/AVT+ cells between the different POA cell types (gPOA-mPOA: $z = 0.04$, $p = 0.99$; gPOA-pPOA: $z = 1.62$, $p = 0.39$; mPOA-pPOA: $z = 2.15$, $p = 0.14$). In contrast, in social males the proportion of FOS+/AVT+ was significantly higher for gPOA cells than for mPOA cells ($z = 2.78$, $p = 0.02$), and pPOA cells ($z = 3.41$, $p = 0.003$). This difference in the activation profile of gPOA and mPOA cell types between both experimental conditions is statistically significant (interaction contrast: $z = 2.11$, $p = 0.03$).

TABLE 1 | Summary of main results for FOS+, AVT+ and FOS+/AVT+ cells quantification in POA sections per experimental conditions.

Exp. condition	POA section or POA cell type	Mean (per slice)	95%CI
#FOS+ cells			
isolated	PPp	27.42	(17.71–42.43)
isolated	PPa	24.42	(15.68–38.04)
social	PPp	30.95	(21.2–45.18)
social	PPa	48.54	(33.39–70.57)
#AVT+ cells			
isolated	PPp	10.39	(6.71–16.09)
isolated	PPa	14.41	(9.3–22.33)
social	PPp	10.52	(7.12–15.54)
social	PPa	24.6	(17.09–35.42)
Proportion of FOS+/AVT+ cells			
isolated	gPOA	0.34	(0.11–0.67)
isolated	mPOA	0.33	(0.17–0.54)
isolated	pPOA	0.1	(0.03–0.34)
social	gPOA	0.63	(0.27–0.89)
social	mPOA	0.18	(0.1–0.31)
social	pPOA	0.07	(0.02–0.2)

**POA, preoptic area; PPa, nucleus preopticus ventricularis, anterior subdivision; PPp, nucleus preopticus ventricularis, posterior subdivision.*

Social Males' AVT Cellular Changes Correlate With Behavioral Traits

The number of AVT+ cells in PPa sections showed a positive correlation with the number of chirps displayed by social males [Generalized linear model (Poisson): β =0.19, Wald's $\chi^2_{(1)} = 10.47$, $p = 0.0001$, **Figure 6A**, **Supplementary Table S1**], the number of approaches towards female (β =0.21 Wald's $\chi^2_{(1)} = 12.03$, $p = 0.0005$, **Figure 6B**, **Supplementary Table S1**) and the total time spent with the female (β =0.29, Wald's $\chi^2_{(1)} = 10.07$, $p = 0.001$, **Figure 6C**, **Supplementary Table S1**). Meanwhile, in PPp sections of the POA, the number of AVT+ cells showed a negative correlation with chirp number ($\beta = -1.0$, Wald's $\chi^2_{(1)} = 12.85$, $p = 0.0003$, **Figure 6A**, **Supplementary Table S1**) and with the total time spent with the female ($\beta = -0.26$, Wald's $\chi^2_{(1)} = 4.61$, $p = 0.03$, **Figure 6C**, **Supplementary Table S1**), and a marginal negative correlation with the number of approaches towards female ($\beta = -0.22$, Wald's $\chi^2_{(1)} = 2.99$, $p = 0.08$, **Figure 6B**, **Supplementary Table S1**).

DISCUSSION

In this study, we confirmed for the first time in electric fish that the neuronal transcriptional FOS activity in the PPa portion of the POA, a node of the SBN, was significantly higher in courting males exposed to a social stimulus than in isolated males, as reported in other vertebrates (Kollack-Walker and Newman, 1995; Curtis and Wang, 2003; Okuyama et al., 2011). In addition, social males had more AVT+ cells in the PPa than isolated males, and the number of AVT+ cells in social males correlated with electric and locomotor courting traits. Furthermore, the profile of activation of the different AVT+ cell types differed between social and isolated males.

To confirm that the observed differences in FOS expression between experimental conditions were due only to the presence/absence of the female, the following precautions were taken. First, as FOS expression can be induced by animal movement (Montag-Sallaz et al., 1999), we confirmed that FOS expression was not correlated with the amount of movement (**Figure 3**). Second, it could be argued that because the experimental conditions differed in the presence or absence

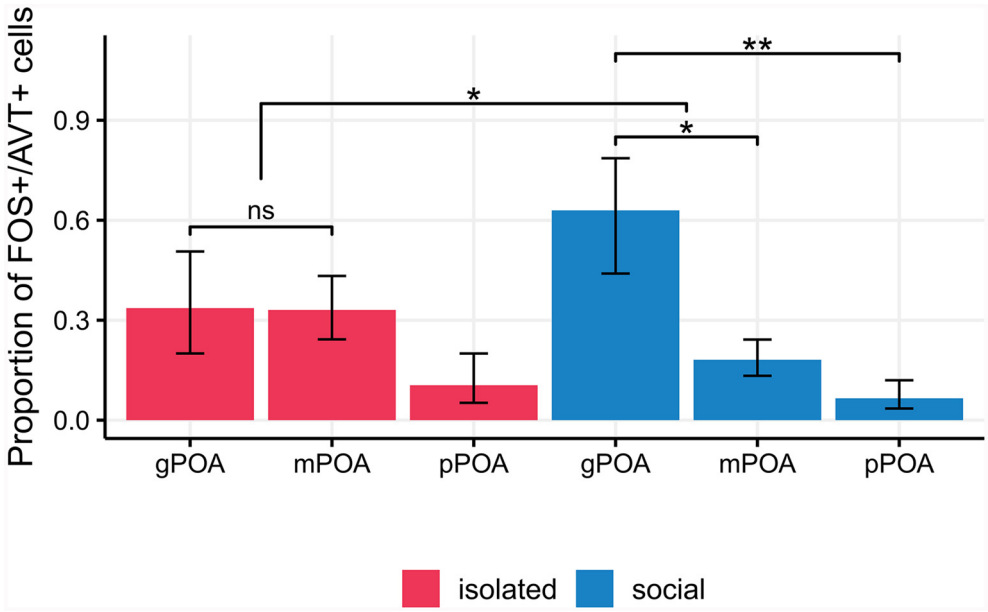

FIGURE 5 | Isolated males show no significant differences in the proportion of FOS+/AVT+ cells between the different POA cell types (pairwise p-values > 0.14). In social males, the proportion of FOS+/AVT+ is significantly higher for gPOA cells than for mPOA cells ($p = 0.02$), and pPOA cells ($p = 0.003$). This difference in the activation profile of gPOA and mPOA cell types between experimental conditions is statistically significant ($p = 0.03$). pPOA, parvocells; mPOA, magnocells; gPOA, gigantocells. *$p < 0.05$, **$p < 0.01$, ***$p < 0.001$; ns, non-significant.

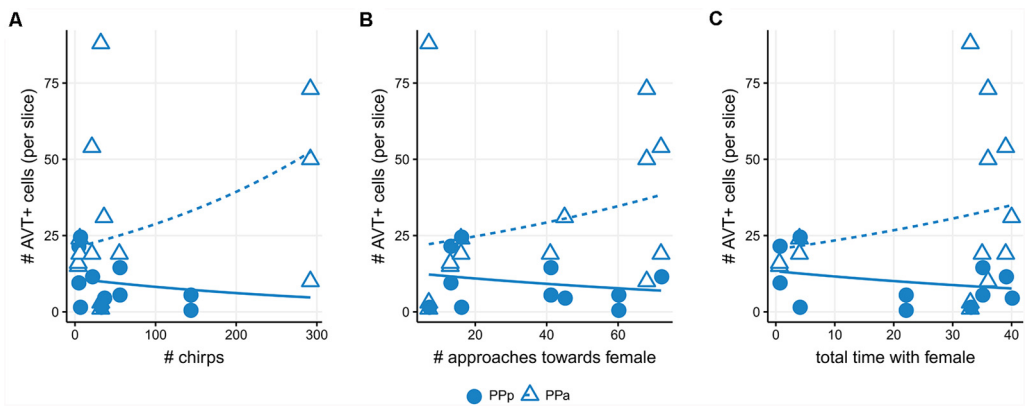

FIGURE 6 | Number of AVT+ cells correlate with behavioral traits in social males. **(A)** Positive correlation between the number of AVT+ cells in PPa sections and chirp number (triangles; $p < 0.001$). Negative correlation between the number of AVT+ cells in PPp sections and chirp number (dots; $p < 0.001$). **(B)** Positive correlation between the number of AVT+ cells in PPa sections and approaches towards a female (triangles; $p < 0.001$). Negative correlation trend between the number of AVT+ cells in PPp sections and approaches towards a female (dots; $p = 0.08$). **(C)** Positive correlation between the number of AVT+ cells in PPa sections and total time with the female (triangles; $p = 0.001$). Negative correlation between the number of AVT+ cells in sections and total time with the female (dots; $p = 0.03$).

of both the female and the holding net, the possibility that the observed differences in FOS expression were simply due to the presence of the net could not be completely ruled out. However, in a control experiment, we found no differences in FOS expression between isolated males and males that were placed near an empty net. Hence, the net can be considered as a neutral stimulus, not inducing substantial FOS expression. Finally, although the differences found between experimental conditions could be due in part to individual differences in AVT cell counts, the inclusion of random intercepts for each animal in the regression models reduces this possibility.

We showed for the first time in an electric fish that social interaction promotes the activation of POA cells as previously described across vertebrates (**Figure 4**; Kollack-Walker and Newman, 1995; O'Connell et al., 2012; Wilson et al., 2018). Among teleosts, other reports showed this expected result (Teles et al., 2015; Cabrera-Álvarez et al., 2017), while others failed to find differences between social males and controls in

the activation of POA cells (O'Connell et al., 2012; Loveland and Fernald, 2017). Hence, this work supports the idea of a conserved role of the POA in the modulation of social behavior in vertebrates.

Numerous studies have identified a role for both AVP and AVT in stimulating sexual, affiliative and communicative behaviors across vertebrates (Goodson and Bass, 2001; De Vries and Panzica, 2006). Particularly in teleosts, changes in the number and size of AVT cells have been reported in association with reproductive behavior (Ota et al., 1999; Grober et al., 2002; Maruska et al., 2007). In this study, we confirmed that the number of AVT cells in both social and isolated males is higher in the PPa of the POA respect to the PPp as expected from the differential rostro-caudal distribution of AVT cells in this species (**Figure 2**; Pouso et al., 2017). In addition, the number of PPa AVT+ cells is higher in social males than in isolated males (**Figure 4B**). This observation cannot be interpreted as the results of the generation of new AVT cells induced by the social stimulus, but rather as the consequence of an increase in AVT production that leads to the increase in the number of AVT cells that reach the threshold of AVT immunoreactive detection (Milo and Phillips, 2016). The presence of the female, as a sensory input, can regulate early gene expression (Ball and Balthazar, 2001) and also may activate AVT gene-related peptide release as occur with other peptides (Morton and Hutchison, 1989). Therefore, in line with the knowledge of neuropeptidergic physiology (Thompson and Walton, 2004), we interpret that the production and further liberation of AVT is involved in the reproductive behavior of *B. gauderio*.

The association of the behavioral and cellular data strongly reinforces this interpretation as we were able to find a positive correlation between the number of PPa AVT+ cells and both locomotor and electric displays of social courting males (**Figure 6**). On the other hand, since the number of PPp AVT+ cells is negatively correlated with chirps and locomotor traits, it is possible that cells in this portion of the POA may have a different functional role. In teleost fish, there is little information regarding the projection targets of different AVT POA cell populations. In general terms, it is known that rostral portions project to the telencephalon, thalamus and hypophysis, while caudal portions project to the telencephalon (Schreibman and Halpern, 1980; Holmqvist and Ekström, 1995; Saito et al., 2004; Dewan et al., 2008). In electric fish, anatomical and functional connections between PPa and areas that modulate the EOD have been established (Wong, 1997, 2000; Perrone et al., 2010; Pouso et al., 2017). This could indicate that different portions of the POA could project to areas that modulate different behaviors (Maruska et al., 2007), hence showing inverse correlation patterns with reproductive behavior traits.

We failed to find significant differences in activation of the different AVT cell-types between social and isolated males, probably due to the low number of slices from each animal that were processed for this experiment. However, we found differences in the activation profile of AVT cell types between both experimental conditions (**Figure 5**). In particular, in social males, gPOA cells turn out to be more activated with respect to mPOA and pPOA cells. Although gPOA cells are the less abundant AVT cell-type within the POA, previous reports have also emphasized the role of gPOA cells in the modulation of aggressive, reproductive and cooperative behaviors (Greenwood et al., 2008; Dewan and Tricas, 2011; Mendonça et al., 2013).

While the increased activation of the neurons in the PPa portion of the POA of courting males is very clear, this cannot be solely explained by an increased activation of AVTergic neurons. Although our results indicate that the number of AVTergic cells differs between experimental conditions and suggest that social interaction increases the activation of gPOA cells, they also suggest that other (AVT negative) cellular types of the POA are also significantly activated. These non-AVT cell populations may be more closely related to the responsiveness of the POA in a reproductive context.

DATA AVAILABILITY

The datasets generated for this study are available on request to the corresponding author.

ETHICS STATEMENT

Comisión Honoraria de Experimentación Animal, Universidad de la República, Protocol Number 008/002.

AUTHOR CONTRIBUTIONS

PP, JG and AS: conceptualization, investigation and resources. PP, ÁC, JG and AS: methodology. PP and AS: writing—original draft and funding acquisition. PP, ÁC and AS: writing—review and editing. JG and AS: supervision.

FUNDING

This research was partially supported by PEDECIBA.

ACKNOWLEDGMENTS

The preparation of the manuscript was completed after Dr. Goodson's passing, with the permission of his wife and colleague, Marcy Kingsbury. We strongly thank Marcy Kingsbury for her kindness, generous discussion and comments on the manuscript. We are also grateful to Laura Quintana and Rossana Perrone for their assistance in the behavioral experiments, Sara Schrock for her technical assistance, Jorge Pouso for his statistical counseling and Erik Zornik for his critical reading of this manuscript.

SUPPLEMENTARY MATERIAL

The Supplementary Material for this article can be found online at: https://www.frontiersin.org/articles/10.3389/fnint.2019.00037/full#supplementary-material

TABLE S1 | Detail of the main statistical analyses reported in the text.

REFERENCES

Ball, G. F., and Balthazar, J. (2001). Ethological concepts revisited: immediate early gene induction in response to sexual stimuli in birds. *Brain Behav. Evol.* 57, 252–270. doi: 10.1159/000047244

Batten, T. F., Cambre, M. L., Moons, L., and Vandesande, F. (1990). Comparative distribution of neuropeptide-immunoreactive systems in the brain of the green molly, *Poecilia latipinna*. *J. Comp. Neurol.* 302, 893–919. doi: 10.1002/cne.903020416

Boisgontier, M. P., and Cheval, B. (2016). The anova to mixed model transition. *Neurosci. Biobehav. Rev.* 68, 1004–1005. doi: 10.1016/j.neubiorev.2016.05.034

Cabrera-Álvarez, M. J., Swaney, W. T., and Reader, S. M. (2017). Forebrain activation during social exposure in wild-type guppies. *Physiol. Behav.* 182, 107–113. doi: 10.1016/j.physbeh.2017.10.012

Caputi, A. A., Carlson, B. A., and Macadar, O. (2005). "Electric organs and their control," in *Electroreception. Springer Handbook of Auditory Research*, eds T. H. Bullock C. D. Hopkins and A. N. Popper (New York, NY: Springer), 410–451.

Caputi, A. A., Silva, A. C., and Macadar, O. (1998). The electric organ discharge of *brachyhypopomus pinnicaudatus*. The effects of environmental variables on waveform generation. *Brain Behav. Evol.* 52, 148–158. doi: 10.1159/000006559

Clayton, D. F. (2000). The genomic action potential. *Neurobiol. Learn. Mem.* 74, 185–216. doi: 10.1006/nlme.2000.3967

Curtis, J. T., and Wang, Z. (2003). Forebrain c-*fos* expression under conditions conducive to pair bonding in female prairie voles (*Microtus ochrogaster*). *Physiol. Behav.* 80, 95–101. doi: 10.1016/s0031-9384(03)00226-9

De Vries, G. J., and Panzica, G. C. (2006). Sexual differentiation of central vasopressin and vasotocin systems in vertebrates: different. *Neuroscience* 138, 947–955. doi: 10.1016/j.neuroscience.2005.07.050

Dewan, A. K., Maruska, K. P., and Tricas, T. C. (2008). Arginine vasotocin neuronal phenotypes among congeneric territorial and shoaling reef butterflyfishes: species, sex and reproductive season comparisons. *J. Neuroendocrinol.* 20, 1382–1394. doi: 10.1111/j.1365-2826.2008.01798.x

Dewan, A. K., and Tricas, T. C. (2011). Arginine vasotocin neuronal phenotypes and their relationship to aggressive behavior in the territorial monogamous multiband butterflyfish, *Chaetodon multicinctus*. *Brain Res.* 1401, 74–84. doi: 10.1016/j.brainres.2011.05.029

Faraway, J. J. (2016). *Extending the Linear Model with R: Generalized Linear, Mixed Effects and Nonparametric Regression Models*. Boca Raton, FL: Chapman and Hall/CRC.

Fischer, E. K., Roland, A. B., Moskowitz, N. A., Tapia, E. E., Summers, K., Coloma, L. A., et al. (2019). The neural basis of tadpole transport in poison frogs. *bioRxiv* [Preprint] doi: 10.1101/630681

Giora, J., and Malabarba, L. R. (2009). *Brachyhypopomus gauderio*, new species, a new example of underestimated species diversity of electric fishes in the southern south america (Gymnotiformes: Hypopomidae). *Zootaxa* 2093, 60–68.

Goodson, J. L. (2005). The vertebrate social behavior network: evolutionary themes and variations. *Horm. Behav.* 48, 11–22. doi: 10.1016/j.yhbeh.2005.02.003

Goodson, J. L., and Bass, A. H. (2001). Social behavior functions and related anatomical characteristics of vasotocin/vasopressin systems in vertebrates. *Brain Res. Rev.* 35, 246–265. doi: 10.1016/s0165-0173(01)00043-1

Goodson, J. L., and Evans, A. K. (2004). Neural responses to territorial challenge and nonsocial stress in male song sparrows: segregation, integration, and modulation by a vasopressin V1 antagonist. *Horm. Behav.* 46, 371–381. doi: 10.1016/j.yhbeh.2004.02.008

Goodson, J. L., Evans, A. K., Lindberg, L., and Allen, C. D. (2005a). Neuro-evolutionary patterning of sociality. *Proc. R. Soc. B Biol. Sci.* 272, 227–235. doi: 10.1098/rspb.2004.2892

Goodson, J. L., Evans, A. K., and Soma, K. K. (2005b). Neural responses to aggressive challenge correlate with behavior in nonbreeding sparrows. *Neuroreport* 16, 1719–1723. doi: 10.1097/01.wnr.0000183898.47160.15

Goodson, J. L., and Kabelik, D. (2009). Dynamic limbic networks and social diversity in vertebrates: from neural context to neuromodulatory patterning. *Front. Neuroendocrinol.* 30, 429–441. doi: 10.1016/j.yfrne.2009.05.007

Goodson, J. L., Kelly, A. M., and Kingsbury, M. A. (2012). Evolving nonapeptide mechanisms of gregariousness and social diversity in birds. *Horm. Behav.* 61, 239–250. doi: 10.1016/j.yhbeh.2012.01.005

Goodson, J. L., and Wang, Y. (2006). Valence-sensitive neurons exhibit divergent functional profiles in gregarious and asocial species. *Proc. Natl. Acad. Sci. U S A* 103, 17013–17017. doi: 10.1073/pnas.0606278103

Greenwood, A. K., Wark, A. R., Fernald, R. D., and Hofmann, H. A. (2008). Expression of arginine vasotocin in distinct preoptic regions is associated with dominant and subordinate behaviour in an African cichlid fish. *Proc. R. Soc. B Biol. Sci.* 275, 2393–2402. doi: 10.1098/rspb.2008.0622

Grober, M. S., George, A. A., Watkins, K. K., Carneim, L. A., and Oliveira, R. F. (2002). Forebrain AVT and courtship in a fish with male alternative reproductive tactics. *Brain Res. Bull.* 57, 423–425. doi: 10.1016/s0361-9230(01)00704-3

Harrison, X. A., Donaldson, L., Correa-Cano, M. E., Evans, J., Fisher, D. N., Goodwin, C. E., et al. (2018). A brief introduction to mixed effects modelling and multi-model inference in ecology. *PeerJ* 6:e4794. doi: 10.7717/peerj.4794

Holmqvist, B. I., and Ekström, P. (1995). Hypophysiotrophic systems in the brain of the Atlantic salmon. Neuronal innervation of the pituitary and the origin of pituitary dopamine and nonapeptides identified by means of combined carbocyanine tract tracing and immunocytochemistry. *J. Chem. Neuroanat.* 8, 125–145. doi: 10.1016/0891-0618(94)00041-q

Hopkins, C. D. (1991). Hypopomus pinnicaudatus (Hypopomidae), a new species of gymnotiform fish from french guiana. *Copeia* 1991, 151–161. doi: 10.2307/1446259

Johnson, Z. V., and Young, L. J. (2017). Oxytocin and vasopressin neural networks: implications for social behavioral diversity and translational neuroscience. *Neurosci. Biobehav. Rev.* 76, 87–98. doi: 10.1016/j.neubiorev.2017.01.034

Kasper, C., Colombo, M., Aubin-Horth, N., and Taborsky, B. (2018). Brain activation patterns following a cooperation opportunity in a highly social cichlid fish. *Physiol. Behav.* 195, 37–47. doi: 10.1016/j.physbeh.2018.07.025

Kent, M., and Bell, A. M. (2018). Changes in behavior and brain immediate early gene expression in male threespined sticklebacks as they become fathers. *Horm. Behav.* 97, 102–111. doi: 10.1016/j.yhbeh.2017.11.002

Kollack-Walker, S., and Newman, S. W. (1995). Mating and agonistic behavior produce different patterns of FOS immunolabeling in the male syrian hamster brain. *Neuroscience* 66, 721–736. doi: 10.1016/0306-4522(94)00563-k

Kovács, K. J. (2008). Measurement of immediate-early gene activation- c-*fos* and beyond. *J. Neuroendocrinol.* 20, 665–672. doi: 10.1111/j.1365-2826.2008.01734.x

Lin, X., Itoga, C. A., Taha, S., Li, M. H., Chen, R., Sami, K., et al. (2018). c-Fos mapping of brain regions activated by multi-modal and electric foot shock stress. *Neurobiol. Stress* 8, 92–102. doi: 10.1016/j.ynstr.2018.02.001

Loveland, J. L., and Fernald, R. D. (2017). Differential activation of vasotocin neurons in contexts that elicit aggression and courtship. *Behav. Brain Res.* 317, 188–203. doi: 10.1016/j.bbr.2016.09.008

Maler, L., Sas, E., Johnston, S., and Ellis, W. (1991). An atlas of the brain of the electric fish Apteronotus leptorhynchus. *J. Chem. Neuroanat.* 4, 1–38. doi: 10.1016/0891-0618(91)90030-g

Maruska, K. P., Mizobe, M. H., and Tricas, T. C. (2007). Sex and seasonal co-variation of arginine vasotocin (AVT) and gonadotropin-releasing hormone (GnRH) neurons in the brain of the halfspotted goby. *Comp. Biochem. Physiol. Part A Mol. Integr. Physiol.* 147, 129–144. doi: 10.1016/j.cbpa.2006.12.019

Mendonça, R., Soares, M. C., Bshary, R., and Oliveira, R. F. (2013). Arginine vasotocin neuronal phenotype and interspecific cooperative behaviour. *Brain Behav. Evol.* 82, 166–176. doi: 10.1159/000354784

Migliaro, A., and Silva, A. (2016). Melatonin regulates daily variations in electric behavior arousal in two species of weakly electric fish with different social structures. *Brain Behav. Evol.* 87, 232–241. doi: 10.1159/000445494

Milo, R., and Phillips, R. (2016). *Cell Biology by the Numbers*. New York, NY: Taylor and Francis Group.

Miranda, M., Silva, A. C., and Stoddard, P. K. (2008). Use of space as an indicator of social behavior and breeding systems in the gymnotiform electric fish brachyhypopomus pinnicaudatus. *Environ. Biol. Fishes* 83, 379–389. doi: 10.1007/s10641-008-9358-2

Montag-Sallaz, M., Welzl, H., Kuhl, D., Montag, D., and Schachner, M. (1999). Novelty-induced increased expression of immediate-early genes c-*fos* and arg

3.1 in the mouse brain. *J. Neurobiol.* 38, 234–246. doi: 10.1002/(sici)1097-4695(19990205)38:2<234::aid-neu6>3.3.co;2-7

Morton, C. R., and Hutchison, W. D. (1989). Release of sensory neuropeptides in the spinal cord: studies with calcitonin gene-related peptide and galanin. *Neuroscience* 31, 807–815. doi: 10.1016/0306-4522(89)90443-0

Nelson, R. J., and Trainor, B. C. (2007). Neural mechanisms of aggression. *Nat. Rev. Neurosci.* 8, 536–546. doi: 10.1038/nrn2174

Newman, S. W. (1999). The medial extended amygdala in male reproductive behavior. A node in the mammalian social behavior network. *Ann. N Y Acad. Sci.* 877, 242–257. doi: 10.1111/j.1749-6632.1999.tb09271.x

O'Connell, L. A., and Hofmann, H. A. (2011). The vertebrate mesolimbic reward system and social behavior network: a comparative synthesis. *J. Comp. Neurol.* 519, 3599–3639. doi: 10.1002/cne.22735

O'Connell, L. A., Matthews, B. J., and Hofmann, H. A. (2012). Isotocin regulates paternal care in a monogamous cichlid fish. *Horm. Behav.* 61, 725–733. doi: 10.1016/j.yhbeh.2012.03.009

Okuyama, T., Suehiro, Y., Imada, H., Shimada, A., Naruse, K., Takeda, H., et al. (2011). Induction of c-fos transcription in the medaka brain (*Oryzias latipes*) in response to mating stimuli. *Biochem. Biophys. Res. Commun.* 404, 453–457. doi: 10.1016/j.bbrc.2010.11.143

Ota, Y., Ando, H., Ueda, H., and Urano, A. (1999). Differences in seasonal expression of neurohypophysial hormone genes in ordinary and precocious male masu salmon. *Gen. Comp. Endocrinol.* 116, 40–48. doi: 10.1006/gcen.1999.7344

Perrone, R., Batista, G., Lorenzo, D., Macadar, O., and Silva, A. (2010). Vasotocin actions on electric behavior: interspecific, seasonal, and social context-dependent differences. *Front. Behav. Neurosci.* 4:52. doi: 10.3389/fnbeh.2010.00052

Perrone, R., Macadar, O., and Silva, A. (2009). Social electric signals in freely moving dyads of brachyhypopomus pinnicaudatus. *J. Comp. Physiol. A Neuroethol. Sens. Neural Behav. Physiol.* 195, 501–514. doi: 10.1007/s00359-009-0427-6

Perrone, R., and Silva, A. (2016). Vasotocin increases dominance in the weakly electric fish brachyhypopomus gauderio. *J. Physiol. Paris* 110, 119–126. doi: 10.1016/j.jphysparis.2016.12.004

Pouso, P., Radmilovich, M., and Silva, A. (2017). An immunohistochemical study on the distribution of vasotocin neurons in the brain of two weakly electric fish, *Gymnotus omarorum* and *Brachyhypopomus gauderio*. *Tissue Cell* 49, 257–269. doi: 10.1016/j.tice.2017.02.003

Ramallo, M. R., Grober, M., Cánepa, M. M., Morandini, L., and Pandolfi, M. (2012). Arginine-vasotocin expression and participation in reproduction and social behavior in males of the Cichlid fish *cichlasoma dimerus*. *Gen. Comp. Endocrinol.* 179, 221–231. doi: 10.1016/j.ygcen.2012.08.015

Saito, D., Komatsuda, M., and Urano, A. (2004). Functional organization of preoptic vasotocin and isotocin neurons in the brain of rainbow trout: central and neurohypophysial projections of single neurons. *Neuroscience* 124, 973–984. doi: 10.1016/j.neuroscience.2003.12.038

Schreibman, M. P., and Halpern, L. R. (1980). The demonstration of neurophysin and arginine vasotocin by immunocytochemical methods in the brain and pituitary gland of the platyfish, *Xiphophorus maculatus*. *Gen. Comp. Endocrinol.* 40, 1–7. doi: 10.1016/0016-6480(80)90089-1

Silva, A., Quintana, L., Galeano, M., and Errandonea, P. (2003). Biogeography and breeding in gymnotiformes from uruguay. *Environ. Biol. Fishes* 66, 329–338. doi: 10.1023/A:1023986600069

Silva, A., Perrone, R., and Macadar, O. (2007). Environmental, seasonal, and social modulations of basal activity in a weakly electric fish. *Physiol. Behav.* 90, 525–536. doi: 10.1016/j.physbeh.2006.11.003

Stoddard, P. K. (2002). The evolutionary origins of electric signal complexity. *J. Physiol. Paris* 96, 485–491. doi: 10.1016/s0928-4257(03)00004-4

Teles, M. C., Almeida, O., Lopes, J. S., and Oliveira, R. F. (2015). Social interactions elicit rapid shifts in functional connectivity in the social decision-making network of zebrafish. *Proc. Biol. Sci.* 282:20151099. doi: 10.1098/rspb.2015.1099

Thompson, R. R., and Walton, J. C. (2004). Peptide effects on social behavior: effects of vasotocin and isotocin on social approach behavior in male goldfish (*Carassius auratus*). *Behav. Neurosci.* 118, 620–626. doi: 10.1037/0735-7044.118.3.620

Wilson, L. C., Goodson, J. L., and Kingsbury, M. A. (2018). Neural responses to familiar conspecifics are modulated by a nonapeptide receptor in a winter flocking sparrow. *Physiol. Behav.* 196, 165–175. doi: 10.1016/j.physbeh.2018.09.002

Wong, C. J. H. (1997). Afferent and efferent connections of the diencephalic prepacemaker nucleus in the weakly electric fish, *Eigenmannia virescens*: interactions between the electromotor system and the neuroendocrine axis. *J. Comp. Neurol.* 383, 18–41. doi: 10.1002/(sici)1096-9861(19970623)383:1<18::aid-cne2>3.0.co;2-o

Wong, C. J. H. (2000). Electrical stimulation of the preoptic area in eigenmannia: evoked interruptions in the electric organ discharge. *J. Comp. Physiol. A* 186, 81–93. doi: 10.1007/s003590050009

Zhong, J., Liang, M., Akther, S., Higashida, C., Tsuji, T., and Higashida, H. (2014). c-*fos* expression in the paternal mouse brain induced by communicative interaction with maternal mates. *Mol. Brain* 7:66. doi: 10.1186/s13041-014-0066-x

Zubizarreta, L., Perrone, R., Stoddard, P. K., Costa, G., and Silva, A. C. (2012). Differential serotonergic modulation of two types of aggression in weakly electric fish. *Front. Behav. Neurosci.* 6:77. doi: 10.3389/fnbeh.2012.00077

Conflict of Interest Statement: The authors declare that the research was conducted in the absence of any commercial or financial relationships that could be construed as a potential conflict of interest.

frontiers in Integrative Neuroscience

MINI REVIEW
published: 20 August 2019
doi: 10.3389/fnint.2019.00039

Encoding and Perception of Electro-communication Signals in *Apteronotus leptorhynchus*

*Michael G. Metzen**

Department of Physiology, McGill University Montreal, Montreal, QC, Canada

Animal communication plays an essential role in triggering diverse behaviors. It is believed in this regard that signal production by a sender and its perception by a receiver is co-evolving in order to have beneficial effects such as to ensure that conspecifics remain sensitive to these signals. However, in order to give appropriate responses to a communication signal, the receiver has to first detect and interpret it in a meaningful way. The detection of communication signals can be limited under some circumstances, for example when the signal is masked by the background noise in which it occurs (e.g., the cocktail-party problem). Moreover, some signals are very alike despite having different meanings making it hard to discriminate between them. How the central nervous system copes with these tasks and problems is a central question in systems neuroscience. Gymnotiform weakly electric fish pose an interesting system to answer these questions for various reasons: (1) they use a variety of communication signals called "chirps" during different behavioral encounters; (2) the central physiology of the electrosensory system is well known; and (3) most importantly, these fish give reliable behavioral responses to artificial stimuli that resemble natural communication signals, making it possible to uncover the neural mechanisms that lead to the observed behaviors.

Keywords: electro-communication, chirps, weakly electric fish, coding, perception

OPEN ACCESS

Edited by:
Michael R. Markham, University of Oklahoma, United States

Reviewed by:
Elias Manjarrez, Meritorious Autonomous University of Puebla, Mexico
Felix Scholkmann, University Hospital Zürich, Switzerland

***Correspondence:**
Michael G. Metzen
michael.metzen@mcgill.ca

Received: *29 May 2019*
Accepted: *31 July 2019*
Published: *20 August 2019*

Citation:
Metzen MG (2019) Encoding and Perception of Electro-communication Signals in Apteronotus leptorhynchus. Front. Integr. Neurosci. 13:39. doi: 10.3389/fnint.2019.00039

INTRODUCTION

The gymnotiform weakly electric fish, *Apteronotus leptorhynchus* uses active electroreception by means of a self-generated field (electric organ discharge, EOD) surrounding its body to navigate and communicate with conspecifics (Bennett, 1971; Zupanc et al., 2001). The EOD in this species can be described by a sinusoidal waveform of a specific frequency within the range of about 700–1,000 Hz. It has been shown that the individual EOD frequency is highly constant over long periods of time (i.e., hours), giving rise to a coefficient of variation of the EOD cycle period as low as 10^{-4}. This makes the mechanism generating the EOD the most regular biological oscillator known (Moortgat et al., 1998). The meaningful stimulus for these fish is thus the modulations of their own EOD caused either by objects (electro-location) or during social interactions (electro-communication; MacIver et al., 2001; Kelly et al., 2008). Perturbations of the electric field due to objects or conspecifics are sensed by an array of cutaneous electroreceptors and are further processed downstream to finally elicit appropriate behaviors.

Abbreviations: AM, amplitude modulation; dF, delta frequency; EAs, electrosensory afferents; ELL, electrosensory lateral line lobe; EOD, electric organ discharge; PCells, pyramidal cells; TS, torus semicircularis.

A specific type of electro-communication signal occurs when nearby fish briefly modulate their EOD frequencies. These signals are known as "chirps" and have been the focus of research for many years in terms of behavioral relevance (Hagedorn and Heiligenberg, 1985; Zupanc et al., 2006; Hupé and Lewis, 2008; Gama Salgado and Zupanc, 2011; Henninger et al., 2018) as well as their encoding across different stages of the central nervous system (Benda et al., 2005, 2006; Hupé et al., 2008; Marsat et al., 2009; Vonderschen and Chacron, 2009; Marsat and Maler, 2010; Metzen et al., 2016; Metzen and Chacron, 2017; Allen and Marsat, 2018). Because chirps can occur in different social settings, they must be reliably detected within complex backgrounds. No less important is the distinction of chirps in different situations within the same social encounter. As such, the production of chirps, as well as their perception and central processing by the members of the same species, must co-evolve in order to ensure that conspecifics remain sensitive and responsive to these signals (Allen and Marsat, 2019).

In the following, I will review the current advances about the central processing and perception of chirp signals in the weakly electric fish, *Apteronotus leptorhynchus*. I will first write about social communication signals in this species in general before briefly explaining the electrosensory pathway involved in signal processing. I will then give a brief overview about chirp encoding in different stages of sensory processing and finally give some insights on chirp production and chirp perception on the behavioral level.

SOCIAL COMMUNICATION SIGNALS IN *APTERONOTUS LEPTORHYNCHUS*

Social communication signals in *A. leptorhynchus* can be classified into different types, depending on the social context. **Figure 1** describes different types of electrosensory stimuli and shows examples of stimulus waveforms associated with electro-communication signals under different conditions. The simplest signal in this regard occurs when two fish are in close proximity (<1 m). Then the interference of their EODs creates an amplitude modulation (AM) or beat that oscillates at the difference frequency (*dF*) between the two individual EOD frequencies (**Figure 1A**). Since *A. leptorhynchus* have been reported to display a sexual dimorphism in baseline EOD frequency (males tend to have higher EOD frequencies than females; Meyer et al., 1987), the *dF* contains important information about the sexual identity of a conspecific: same sex-encounters typically result in a low beat frequency (<50 Hz), whereas opposite-sex encounters result in higher beat frequencies (>50 Hz; Benda et al., 2006).

Although the EOD of *A. leptorhynchus* displays a high degree of constancy (Bullock, 1969), transient modulations of the frequency and/or amplitude occur spontaneously or during social interactions. A huge variety of EOD modulations have been described (Hagedorn and Heiligenberg, 1985; Engler and Zupanc, 2001). Some of these modulations are known as "chirps" and represent commutation signals that are actively generated by the fish during social interactions and different types of chirps have been identified (see Zakon et al., 2002). During a chirp event, one fish increases its EOD frequency for a short amount of time (**Figure 1B**). Although the behavioral meaning of chirps is still not entirely clear, two chirp types (type I, or "big chirps" and type II, or "small chirps") have been the focus of extensive research on both, the behavioral level as well as on the encoding of them at several stages of sensory processing (Benda et al., 2005, 2006; Marsat et al., 2009; Marsat and Maler, 2010; Vonderschen and Chacron, 2011; Aumentado-Armstrong et al., 2015; Metzen et al., 2016; Metzen and Chacron, 2017; Allen and Marsat, 2018; Henninger et al., 2018).

A clear distinction between chirp types can be made based on two features: the increase in EOD frequency during a chirp and its duration (**Figure 1B**, red). While big chirps are characterized by large frequency increases (up to 1,000 Hz) that last between 20 and 30 ms, small chirps have smaller frequency increases (30–150 Hz) and shorter durations (10–18 ms). Big chirps are further accompanied by a significant drop in amplitude (up to 75%), whereas only negligible changes in amplitude (about 2%) have been reported for small chirps (Hagedorn and Heiligenberg, 1985; Zupanc and Maler, 1993; Bastian et al., 2001; Triefenbach and Zakon, 2003). Furthermore, big and small chirps occur at all phases of the beat with uniform probability (Aumentado-Armstrong et al., 2015). As such, chirp stimuli can display very heterogeneous waveforms (Zupanc and Maler, 1993; Benda et al., 2006). Especially for small chirps, the beat phase at which a chirp occurs can have huge effects on the resulting waveform (**Figure 1C**), whereas the waveforms of big chirps appear more self-similar across beat phases (**Figure 1D**; Aumentado-Armstrong et al., 2015). Similar effects on the chirp waveforms are obvious for different background beat frequencies (**Figures 1E,F**) and different combinations of frequency increase and duration most likely will impact the stimulus waveform as well.

Sociologically, big chirps occur most likely in behaviors associated with courtship contexts (Bastian et al., 2001; Engler and Zupanc, 2001) with more distant *dF*s (Zupanc et al., 2006; Hupé et al., 2008; Fugère and Krahe, 2010). In contrast, small chirps are commonly seen as aggressive intraspecific communication signals occurring on small *dFs* (Hagedorn and Heiligenberg, 1985; Bastian et al., 2001; Hupé and Lewis, 2008). It is well known that small chirps serve as a predictor of attacks during antagonistic encounters. As such, they are positively correlated with the overall expressed aggression of an animal, thus supporting the dominance hypothesis (Triefenbach and Zakon, 2008). In this regard, small chirps have been also shown to play an important role in mediating conspecific aggression (Hupé and Lewis, 2008). However, a recent field study showed that small chirps are also emitted during courtship behaviors between nearby fish of opposite sex (Henninger et al., 2018).

As for communication signals in other modalities and species (Allee et al., 2008, 2009; Gutzler et al., 2011; Beis et al., 2015; Wohr et al., 2015), processing of chirps by central neurons as well as chirping behavior has been shown to be regulated by serotonin (Deemyad et al., 2013; Larson et al., 2014) or steroid hormones (Dunlap et al., 2013; Smith, 2013).

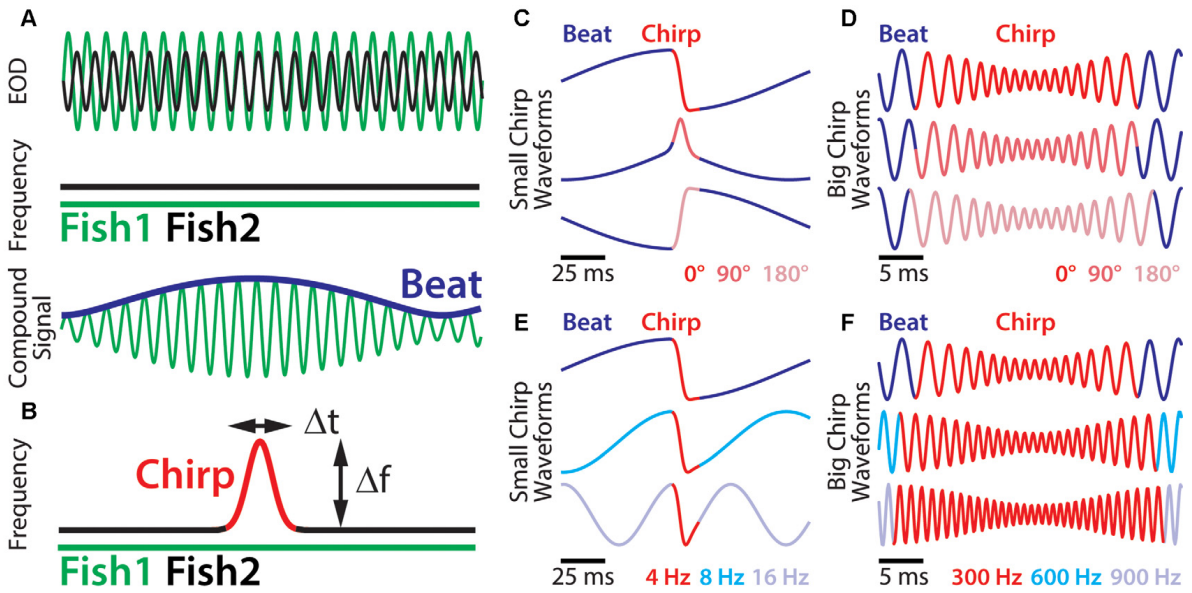

FIGURE 1 | Small chirp stimuli are more heterogeneous than big chirps. **(A)** When two fish are in close proximity, their individual electric organ discharges (EODs; top green and black traces) create alternating regions of constructive and destructive interference. This interference results in a sinusoidal amplitude modulation (AM; i.e., a beat, bottom blue trace) of the summed signal (bottom green trace) that oscillates at the difference EOD frequency. **(B)** During a chirp (red), the emitter fish transiently increases its EOD frequency (black trace), while the receiver fish's EOD frequency (top green trace) remains constant. A chirp can thus be characterized by its frequency increase and duration. **(C)** Resulting waveforms of small chirp stimuli (red) with fixed duration (14 ms) and frequency increase (60 Hz) within a 4 Hz beat (blue) occurring at different phases (dark red: 0°; light red: 90°; pink: 180°). **(D)** Resulting waveforms of big chirp stimuli (red) with fixed duration (25 ms), frequency increase (600 Hz) and amplitude drop (70%) within a 300 Hz beat (blue) occurring at different phases (dark red: 0°; light red: 90°; pink: 180°). **(E)** Resulting waveforms of small chirp stimuli (red) with fixed duration (14 ms) and frequency increase (60 Hz) occurring at the same beat phase (0°), but within different beat frequencies (dark blue: 4 Hz; cyan: 8 Hz; light blue: 16 Hz). **(F)** Resulting waveforms of big chirp stimuli (red) with fixed duration (25 ms) and frequency increase (600 Hz) occurring at the same beat phase (0°), but within different beat frequencies (dark blue: 300 Hz; cyan: 600 Hz; light blue: 900 Hz). Figures are adapted from Aumentado-Armstrong et al. (2015) and Metzen and Chacron (2017).

ELECTROSENSORY PATHWAY

Gymnotiform weakly electric fish possess a specialized electric organ whose discharges generate an oscillating electric field around the animal's body. The electric organ is composed of so-called electrocytes. In members of the family Apteronotidae, the electrocytes are derived from motor axons, whereas the electric organ of all other weakly electric fish species is composed of derived muscle cells (Bennett, 1971). The synchronous activity, as well as the organization of the electrocytes within the electric organ, thus defines the EOD in terms of frequency and amplitude. Electrocytes receive command pulses from neurons located in the pacemaker nucleus in the medulla oblongata (Bennett, 1971), making the EOD frequency a direct consequence of the oscillation frequency of the pacemaker nucleus. A detailed description of the neural control of the electric organ can be found elsewhere (Bennett, 1971).

Figure 2A shows the feedforward electrosensory pathway across different stages of sensory processing, leading to behavior (black arrows), as well as an important feedback pathway (red). Perturbations of the electric field due to objects (i.e., electro-location) or the EODs of conspecifics (i.e., electro-communication) in the vicinity are sensed by peripheral P-type tuberous electroreceptors (electrosensory afferents, EAs; Bullock, 1969; Nelson et al., 1997; **Figure 2A**). Each EA trifurcates and projects topographically to three maps within the hindbrain electrosensory lateral line lobe (ELL): the centro-medial (CMS), centro-lateral (CLS) and lateral (LS) segments (Carr et al., 1982; Heiligenberg and Dye, 1982; Krahe and Maler, 2014). The ELL contains two main types of pyramidal cells (PCells): ON- and OFF-type cells (Clarke et al., 2015). ON-type cells respond to increases in EOD amplitude with increased spiking activity, whereas OFF-type cells respond with decreased spiking activity to increases in EOD amplitude. Based on physiological, morphological and molecular criteria, ON- and OFF-type PCells can be further subdivided into deep, intermediate and superficial cell types (Maler, 2009). The apical dendrites of superficial and intermediate PCells reach into the molecular layer and receive feedback signals from higher-order brain areas (**Figure 2A**). This feedback originates from the deep PCells. Furthermore, PCells are the sole output of the ELL and thus project to the torus semicircularis (TS), a midbrain nucleus. TS neurons project to higher brain areas such as the nucleus electrosensorius (nE), which projects to the prepacemaker nucleus (PPn). The PPn projects to the pacemaker nucleus (Pn), which then sends command signals to the electric organ, thereby completing the sensorimotor loop.

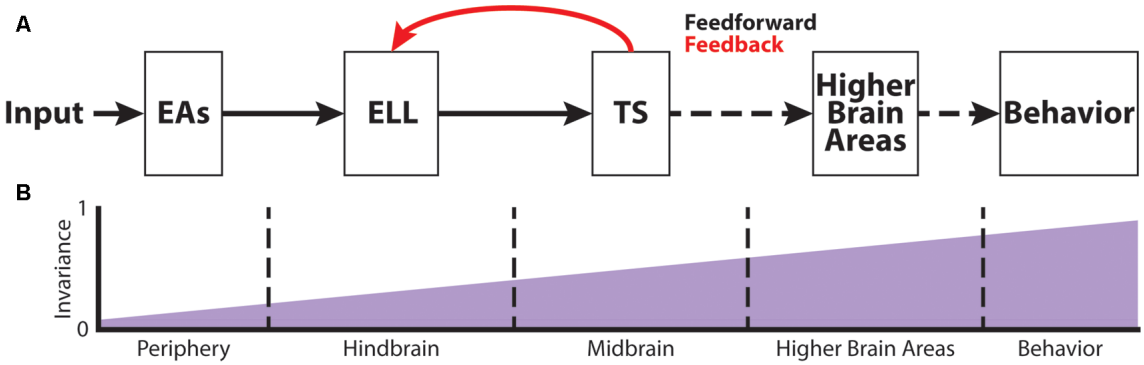

FIGURE 2 | The phase invariance representation of small chirps increases across successive brain areas. **(A)** Schematic showing the different stages of sensory processing in the electrosensory system. **(B)** Schematic showing the increase in phase invariance across successive stages of electrosensory processing. Figures are modified from Metzen et al. (2016) and Metzen et al. (2018).

CHIRP CODING AT THE SENSORY PERIPHERY

Peripheral EAs respond to AMs of the fish's own EOD with phase-locking (Hopkins, 1976; Bastian, 1981; Nelson et al., 1997). Hence, the probability of firing an action potential depends on the amplitude as well as the frequency of the AM (Nelson et al., 1997). As such, phase-locking tends to be greater for either higher amplitudes or higher frequencies, which is a direct consequence of their high-pass frequency tuning characteristics (Bastian, 1981; Xu et al., 1996; Chacron et al., 2005). Because EAs also display strong spike-frequency adaptation, their responses to low-frequency AMs are reduced (Benda et al., 2005). However, this adaptation can be overcome by a chirp stimulus, because chirps transiently increase the AM frequency, thus increasing EA responses (Benda et al., 2005).

The transient increase in frequency together with the resulting phase-reset leads to synchronous spiking activity in the EA population (Benda et al., 2006). This spiking synchronization can be categorized into two events: synchronous excitation in EAs due to small chirps that occur at a beat phase $<180°$ ("+ chirps"), and synchronous inhibition in EAs due to small chirps that occur at a beat phase $>180°$ ("− chirps"; Metzen et al., 2016). This correlated activity appears to be more similar for different patterns of small chirp waveforms than the firing rate modulations of single units, allowing for the emergence of an invariant representation of small chirps early in the nervous system (Metzen et al., 2016). However, due to their high-pass tuning properties, EAs also display a considerable amount of phase-locking to higher beat frequencies (Xu et al., 1996; Nelson et al., 1997; Chacron et al., 2005; Metzen and Chacron, 2017), which then decreases phase invariant coding by correlated afferent activity (Metzen and Chacron, 2017). Big chirps, in contrast, desynchronize EA responses, because of the large frequency increase as well as the significant drop in amplitude (Benda et al., 2006).

Because EAs are broadly tuned to stimuli associated with electro-location and -communication, studying the processing of electro-communication signals in weakly electric fish has some limitations: the electrosensory system is exposed to interferences among these two categories of signals (Benda et al., 2013). This is because electro-communication signals of low amplitude can be obscured by distortions of the electric field due to objects in its vicinity. However, it has been shown that the electrosensory system actually uses intrinsic stochastic resonance (i.e., neuronal noise) in order to enhance information processing for weak signals (Benda et al., 2013).

CHIRP CODING AT THE LEVEL OF THE HINDBRAIN

EAs project to the ELL in the hindbrain of *A. leptorhynchus* (**Figure 2A**) where they trifurcate to the different ELL maps, LS, CLS, and CMS (Carr et al., 1982; Krahe and Maler, 2014). As mentioned earlier, each segment is composed of superficial, intermediate and deep PCells that respond with excitation (ON-type) or inhibition (OFF-type) to increasing AMs (Bastian and Nguyenkim, 2001). Chirp encoding in ELL is strongly affected by feedback input (Marsat and Maler, 2012). While superficial and intermediate PCells receive large amounts of feedback on their apical dendrites, deep PCells only receive minimal feedback, but rather serve as the source of these feedback projections (Bastian et al., 2002, 2004). Due to the feedback input as well as different tuning properties across PCells (Krahe et al., 2008), big and small chirps are not processed within the same maps. While big chirps are encoded by PCells of all maps, LS turns out to be the most sensitive map for processing sensory information related to small chirps (Metzner and Juranek, 1997; Marsat et al., 2009). Moreover, ON-type PCells have been shown to encode the presence of a small chirp with a stereotyped burst response due to the feedback input (Marsat et al., 2009). Although the presence of either big or small chirps can be reliably detected by ELL PCells, the discrimination of AM waveforms associated with small chirps with different attributes is difficult (Marsat and Maler, 2010). Furthermore, it has been shown

that the encoding strategy of ELL PCells makes it difficult to discriminate between the different chirp waveforms of small chirps if they occur on a low-frequency beat (Marsat et al., 2009; Allen and Marsat, 2018). In contrast, if occurring on top of a high-frequency beat, both small and big chirps produce heterogeneous responses, and variations in the chirp waveform can be accurately discriminated (Marsat and Maler, 2010; Allen and Marsat, 2018). However, it has been shown that PCell responses to small chirps occurring at different phases of the beat are more invariant than the responses of single EAs (**Figure 2B**; Metzen et al., 2016). This is because ON-type PCells respond with similar excitation to "+ chirps," whereas OFF-type PCells respond with similar excitation to "− chirps" (Metzen et al., 2016).

CHIRP CODING AT THE LEVEL OF THE MIDBRAIN

The target region of ELL PCells is the midbrain TS (**Figure 2A**). TS neurons receive direct excitatory synaptic input from ELL PCells (Carr and Maler, 1985; McGillivray et al., 2012). Although TS consists a large number of different neuron types (∼50), they can be divided into dense and sparse coders based on their baseline firing rate and response properties to electrosensory stimuli (Chacron et al., 2011; Vonderschen and Chacron, 2011). Dense TS neurons respond to electrosensory stimulation similarly to ELL PCells. In contrast, sparse TS neurons respond selectively to preferred stimulus attributes and are mostly silent to other stimuli (Vonderschen and Chacron, 2011; Sproule et al., 2015). It is indeed these sparse coders that have been shown to have a higher degree of phase invariance compared to EAs and ELL PCells (**Figure 2B**) as they selectively respond to "+ chirps" as well as to "− chirps" with excitation but will not respond to the beat (Vonderschen and Chacron, 2011; Metzen et al., 2016). These neurons most likely correspond to previously characterized "ON-OFF" neurons that respond to both increase and decreases in the stimulus (Partridge et al., 1981; Rose and Call, 1993) because they receive balanced input from ON- and OFF-type ELL PCells (Aumentado-Armstrong et al., 2015). However, it is expected that further refinement of the observed phase invariance occurs in more downstream brain areas such as the nucleus electrosensorius in the diencephalon that receives direct input from TS (Carr et al., 1981). Both categories of TS neurons project to higher brain areas (Sproule et al., 2015). As such, the two categories of TS neurons could hold complementary functions within the processing of electro-communication signals: sparse neurons would simply detect the occurrence of a chirp, whereas dense neurons would instead transmit contextual information about the chirp identity (Metzen et al., 2016).

CHIRP PRODUCTION AND PERCEPTION

Behavioral responses to chirp stimuli have been mostly quantified through a behavioral paradigm in where the fish is restrained within a tube. There, it has been shown that chirp production in *A. leptorhynchus* decreases for increasing beat frequencies (Bastian et al., 2001; Engler and Zupanc, 2001) and that males respond with increased chirp production to increasing stimulus intensities (Zupanc and Maler, 1993; Engler and Zupanc, 2001). Furthermore, chirps naturally occur at all beat phases (Zupanc and Maler, 1993; Walz et al., 2013; Aumentado-Armstrong et al., 2015). Moreover, it has been shown that chirps generated by one individual follow those of another with a preferred latency of approximately 500–1,000 ms (Zupanc et al., 2006). These so-called "echo responses" can be also elicited by using artificial signals consisting of frequency modulations with different durations and thus can be used to study the neural bases of chirping behaviors under different experimental conditions (Gama Salgado and Zupanc, 2011; Metzen et al., 2016; Metzen and Chacron, 2017). Echo responses to small chirps have been shown to be similar if chirps where delivered at random beat phases on a low beat frequency resulting in a high degree of phase invariance on the organismal level (**Figure 2B**; Metzen et al., 2016), but phase invariant perception decreases for increasing beat frequencies (Metzen and Chacron, 2017). However, this phase invariant perception of small chirps indicates that *A. leptorhynchus* actually perceives different waveforms associated with small chirps as belonging to the same category if they occur on low beat frequencies. The decreased chirp detectability on the behavioral level at high beat frequencies is most likely due to increased phase-locking seen in EAs to higher background beat frequencies. This, in turn, synchronizes the responses of EAs irrespective of the chirp attributes, which is then decoded downstream.

Interestingly, in close proximity, fish tend to rather emit chirps instead of biting one another (Hupé and Lewis, 2008). It is therefore hypothesized that antagonistic chirps are primarily used to temporarily "blind" the opponent as they suppress electrosensory neural responses to other relevant stimuli (Zakon et al., 2002; Hupé and Lewis, 2008).

CONCLUSION

Electro-communication in weakly electric fish has been the focus of research for many years. However, most of these studies were conducted under laboratory conditions where the fish was restrained in a chirp chamber. Thereby, a lot of knowledge has been gained regarding the central processing of chirps and behavioral responses to them. However, how related behaviors such as chirp production and perception is affected under more natural conditions and with interacting individuals is not well understood to date. More studies are needed to identify the underlying mechanisms as well as to link these with observable behaviors. Moreover, a recent study revealed that there are robust behavioral responses in stimulus regimes that have been not considered in electrophysiological studies so far (Henninger et al., 2018). The reason for this is mainly due to the fact that such stimuli mainly occur in freely behaving animals within their natural habitats. The entire stimulus ensemble these fish are exposed to in their natural environment has thus not been sufficiently characterized. More

field studies are needed in order to fully understand the natural stimulus dynamics.

Apteronotus leptorhynchus is particularly well suited for studying sensory processing of and behavioral responses to electro-communication signals for various reasons. First, due to the neurogenic nature of its electric organ, the EOD persists after injecting the animal with curare-like drugs. This allows a preparation in which the animal is awake and behaving allowing a direct link of neuronal responses to chirp stimuli with behavioral responses. This is different in weakly electric fish species that possess a myogenic derived electric organ like *Eigenmannia* sp. because injection of curare-like drugs will basically silence the EOD due to inhibition of acetylcholine receptors at the neuromuscular junction (Hitschfeld et al., 2009). Second, *A. leptorhynchus* has been shown to give reliable behavioral responses (i.e., echo responses) during various social interactions (Zupanc, 2009). Furthermore, studying the limits of central processing and perception of electro-communication signals using for example highly unnatural chirp stimuli is feasible, as it is easy to elicit neuronal and behavioral responses to artificial chirp stimuli. Last, distinct chirp waveforms (or types) can be associated with different behaviors in *A. leptorhynchus*, whereas chirping in *Eigenmannia* sp. has been observed mainly in the context of reproduction (Zupanc and Bullock, 2005). However, since *Eigenmannia* sp. chirps contain both low- and high-frequency components that drive different types of electroreceptors, facilitating the study of parallel processing of different chirp attributes in *Eigenmannia*, but not in *Apteronotus* (Stöckl et al., 2014).

SIGNIFICANCE FOR THE FIELD

The study of electro-communication signals (chirps) in terms of behavioral relevance as well as the central encoding mechanisms has a long history in weakly electric fish research. Scientists were able to characterize a huge variety of different stimulus waveforms associated with chirp signals of different kinds and discovered various behaviors related to chirps. Over the last years, studies uncovered more and more details about the behavioral circumstances in which different chirp types occur. Moreover, neurophysiological experiments revealed how single units as well as populations of neurons at different stages of sensory processing encode the stimulus waveforms associated with different chirp types and identities. The use of more naturalistic experimental settings in order to study behavioral and neuronal responses to chirps has become more important in recent years and led to a more fundamental understanding of how chirps are centrally processed and perceived on the organismal level.

AUTHOR CONTRIBUTIONS

The author confirms being the sole contributor of this work and has approved it for publication.

FUNDING

This work was supported by the Canadian Institutes of Health Research.

REFERENCES

Allee, S. J., Markham, M. R., Salazar, V. L., and Stoddard, P. K. (2008). Opposing actions of 5HT1A and 5HT2-like serotonin receptors on modulations of the electric signal waveform in the electric fish Brachyhypopomus pinnicaudatus. *Horm. Behav.* 53, 481–488. doi: 10.1016/j.yhbeh.2007.12.001

Allee, S. J., Markham, M. R., and Stoddard, P. K. (2009). Androgens enhance plasticity of an electric communication signal in female knifefish, Brachyhypopomus pinnicaudatus. *Horm. Behav.* 56, 264–273. doi: 10.1016/j.yhbeh.2009.05.005

Allen, K. M., and Marsat, G. (2018). Task-specific sensory coding strategies are matched to detection and discrimination performance. *J. Exp. Biol.* 221:jeb170563. doi: 10.1242/jeb.170563

Allen, K. M., and Marsat, G. (2019). Neural processing of communication signals: the extent of sender-receiver matching varies across species of *Apteronotus*. *eNeuro* 6:ENEURO.0392-18.2019. doi: 10.1523/ENEURO.0392-18.2019

Aumentado-Armstrong, T., Metzen, M. G., Sproule, M. K., and Chacron, M. J. (2015). Electrosensory midbrain neurons display feature invariant responses to natural communication stimuli. *PLoS Comput. Biol.* 11:e1004430. doi: 10.1371/journal.pcbi.1004430

Bastian, J. (1981). Electrolocation. I. How the electroreceptors of *Apteronotus albifrons* code for moving-objects and other electrical stimuli. *J. Comp. Physiol. A Neuroethol. Sens. Neural Behav. Physiol.* 144, 465–479. doi: 10.1007/bf01326832

Bastian, J., Chacron, M. J., and Maler, L. (2002). Receptive field organization determines pyramidal cell stimulus-encoding capability and spatial stimulus selectivity. *J. Neurosci.* 22, 4577–4590. doi: 10.1523/jneurosci.22-11-04577.2002

Bastian, J., Chacron, M. J., and Maler, L. (2004). Plastic and nonplastic pyramidal cells perform unique roles in a network capable of adaptive redundancy reduction. *Neuron* 41, 767–779. doi: 10.1016/s0896-6273(04)00071-6

Bastian, J., and Nguyenkim, J. (2001). Dendritic modulation of burst-like firing in sensory neurons. *J. Neurophysiol.* 85, 10–22. doi: 10.1152/jn.2001.85.1.10

Bastian, J., Schniederjan, S., and Nguyenkim, J. (2001). Arginine vasotocin modulates a sexually dimorphic communication behavior in the weakly electric fish *Apteronotus leptorhynchus*. *J. Exp. Biol.* 204, 1909–1923.

Beis, D., Holzwarth, K., Flinders, M., Bader, M., Wohr, M., and Alenina, N. (2015). Brain serotonin deficiency leads to social communication deficits in mice. *Biol. Lett.* 11:20150057. doi: 10.1098/rsbl.2015.0057

Benda, J., Grewe, J., and Krahe, R. (2013). "Neural noise in electrocommunication: from burden to benefits," in *Animal Communication and Noise*, ed. H. Brumm (Berlin, Heidelberg: Springer), 331–372.

Benda, J., Longtin, A., and Maler, L. (2005). Spike-frequency adaptation separates transient communication signals from background oscillations. *J. Neurosci.* 25, 2312–2321. doi: 10.1523/JNEUROSCI.4795-04.2005

Benda, J., Longtin, A., and Maler, L. (2006). A synchronization-desynchronization code for natural communication signals. *Neuron* 52, 347–358. doi: 10.1016/j.neuron.2006.08.008

Bennett, M. V. L. (1971). Electric organs. *Fish Physiol.* 5, 347–491. doi: 10.1016/s1546-5098(08)60051-5

Bullock, T. H. (1969). Species differences in effect of electroreceptor input on electric organ pacemakers and other aspects of behavior in electric fish; pp. 102–118. *Brain Behav. Evol.* 2:85. doi: 10.1159/000125816

Carr, C. E., and Maler, L. (1985). A Golgi study of the cell types of the dorsal torus semicircularis of the electric fish Eigenmannia: functional and morphological diversity in the midbrain. *J. Comp. Neurol.* 235, 207–240. doi: 10.1002/cne.902350206

Carr, C. E., Maler, L., Heiligenberg, W., and Sas, E. (1981). Laminar organization of the afferent and efferent systems of the torus semicircularis

of Gymnotiform fish: morphological substrates for parallel processing in the electrosensory system. *J. Comp. Neurol.* 203, 649–670. doi: 10.1002/cne.902030406

Carr, C. E., Maler, L., and Sas, E. (1982). Peripheral organization and central projections of the electrosensory nerves in gymnotiform fish. *J. Comp. Neurol.* 211, 139–153. doi: 10.1002/cne.902110204

Chacron, M. J., Longtin, A., and Maler, L. (2011). Efficient computation *via* sparse coding in electrosensory neural networks. *Curr. Opin. Neurobiol.* 21, 752–760. doi: 10.1016/j.conb.2011.05.016

Chacron, M. J., Maler, L., and Bastian, J. (2005). Electroreceptor neuron dynamics shape information transmission. *Nat. Neurosci.* 8, 673–678. doi: 10.1038/nn1433

Clarke, S. E., Longtin, A., and Maler, L. (2015). Contrast coding in the electrosensory system: parallels with visual computation. *Nat. Rev. Neurosci.* 16, 733–744. doi: 10.1038/nrn4037

Deemyad, T., Metzen, M. G., Pan, Y., and Chacron, M. J. (2013). Serotonin selectively enhances perception and sensory neural responses to stimuli generated by same-sex conspecifics. *Proc. Natl. Acad. Sci. U S A* 110, 19609–19614. doi: 10.1073/pnas.1314008110

Dunlap, K. D., Chung, M., and Castellano, J. F. (2013). Influence of long-term social interaction on chirping behavior, steroid levels and neurogenesis in weakly electric fish. *J. Exp. Biol.* 216, 2434–2441. doi: 10.1242/jeb.082875

Engler, G., and Zupanc, G. K. (2001). Differential production of chirping behavior evoked by electrical stimulation of the weakly electric fish, *Apteronotus leptorhynchus*. *J. Comp. Physiol. A* 187, 747–756. doi: 10.1007/s00359-001-0248-8

Fugère, V., and Krahe, R. (2010). Electric signals and species recognition in the wave-type gymnotiform fish *Apteronotus leptorhynchus*. *J. Exp. Biol.* 213, 225–236. doi: 10.1242/jeb.034751

Gama Salgado, J. A., and Zupanc, G. K. H. (2011). Echo response to chirping in the weakly electric brown ghost knifefish (*Apteronotus leptorhynchus*): role of frequency and amplitude modulations. *Can. J. Zool.* 89, 498–508. doi: 10.1139/z11-014

Gutzler, S. J., Karom, M., Erwin, W. D., and Albers, H. E. (2011). Seasonal regulation of social communication by photoperiod and testosterone: effects of arginine-vasopressin, serotonin and galanin in the medial preoptic area-anterior hypothalamus. *Behav. Brain Res.* 216, 214–219. doi: 10.1016/j.bbr.2010.07.042

Hagedorn, M., and Heiligenberg, W. (1985). Court and spark: electric signals in the courtship and mating of gymnotoid fish. *Anim. Behav.* 33, 254–265. doi: 10.1016/s0003-3472(85)80139-1

Heiligenberg, W., and Dye, J. (1982). Labeling of electroreceptive afferents in a gymnotoid fish by intracellular injection of HRP: the mystery of multiple maps. *J. Comp. Physiol.* 148, 287–296. doi: 10.1007/bf00679013

Henninger, J., Krahe, R., Kirschbaum, F., Grewe, J., and Benda, J. (2018). Statistics of natural communication signals observed in the wild identify important yet neglected stimulus regimes in weakly electric fish. *J. Neurosci.* 38, 5456–5465. doi: 10.1523/Jneurosci.0350-18.2018

Hitschfeld, É. M., Stamper, S. A., Vonderschen, K., Fortune, E. S., and Chacron, M. J. (2009). Effects of restraint and immobilization on electrosensory behaviors of weakly electric fish. *ILAR J.* 50, 361–372. doi: 10.1093/ilar.50.4.361

Hopkins, C. D. (1976). Stimulus filtering and electroreception: tuberous electroreceptors in three speies of gymnotid fish. *J. Comp. Physiol. A Neuroethol. Sens. Neural Behav. Physiol.* 111, 171–207. doi: 10.1007/bf00605531

Hupé, G., and Lewis, J. (2008). Electrocommunication signals in free swimming brown ghost knifefish, *Apteronotus leptorhynchus*. *J. Exp. Biol.* 211, 1657–1667. doi: 10.1242/jeb.013516

Hupé, G. J., Lewis, J. E., and Benda, J. (2008). The effect of difference frequency on electrocommunication: chirp production and encoding in a species of weakly electric fish, *Apteronotus leptorhynchus*. *J. Physiol. Paris* 102, 164–172. doi: 10.1016/j.jphysparis.2008.10.013

Kelly, M., Babineau, D., Longtin, A., and Lewis, J. E. (2008). Electric field interactions in pairs of electric fish: modeling and mimicking naturalistic inputs. *Biol. Cybern.* 98, 479–490. doi: 10.1007/s00422-008-0218-0

Krahe, R., Bastian, J., and Chacron, M. (2008). Temporal processing across multiple topographic maps in the electrosensory system. *J. Neurophysiol.* 100, 852–867. doi: 10.1152/jn.90300.2008

Krahe, R., and Maler, L. (2014). Neural maps in the electrosensory system of weakly electric fish. *Curr. Opin. Neurobiol.* 24, 13–21. doi: 10.1016/j.conb.2013.08.013

Larson, E. A., Metzen, M. G., and Chacron, M. J. (2014). Serotonin modulates electrosensory processing and behavior *via* 5-HT2-like receptors. *Neuroscience* 271, 108–118. doi: 10.1016/j.neuroscience.2014.04.033

MacIver, M. A., Sharabash, N. M., and Nelson, M. E. (2001). Prey-capture behavior in gymnotid electric fish: motion analysis and effects of water conductivity. *J. Exp. Biol.* 204, 543–557.

Maler, L. (2009). Receptive field organization across multiple electrosensory maps. I. Columnar organization and estimation of receptive field size. *J. Comp. Neurol.* 516, 376–393. doi: 10.1002/cne.22124

Marsat, G., and Maler, L. (2010). Neural heterogeneity and efficient population codes for communication signals. *J. Neurophysiol.* 104, 2543–2555. doi: 10.1152/jn.00256.2010

Marsat, G., and Maler, L. (2012). Preparing for the unpredictable: adaptive feedback enhances the response to unexpected communication signals. *J. Neurophysiol.* 107, 1241–1246. doi: 10.1152/jn.00982.2011

Marsat, G., Proville, R. D., and Maler, L. (2009). Transient signals trigger synchronous bursts in an identified population of neurons. *J. Neurophysiol.* 102, 714–723. doi: 10.1152/jn.91366.2008

McGillivray, P., Vonderschen, K., Fortune, E. S., and Chacron, M. J. (2012). Parallel coding of first and second order stimulus attributes by midbrain electrosensory neurons. *J. Neurosci.* 32, 5510–5524. doi: 10.1523/JNEUROSCI.0478-12.2012

Metzen, M. G., and Chacron, M. J. (2017). Stimulus background influences phase invariant coding by correlated neural activity. *Elife* 6:e24482. doi: 10.7554/eLife.24482

Metzen, M. G., Hofmann, V., and Chacron, M. J. (2016). Neural correlations enable invariant coding and perception of natural stimuli in weakly electric fish. *Elife* 5:e12993. doi: 10.7554/eLife.12993

Metzen, M. G., Huang, C. G., and Chacron, M. J. (2018). Descending pathways generate perception of and neural responses to weak sensory input. *PLoS Biol.* 16:e2005239. doi: 10.1371/journal.pbio.2005239

Metzner, W., and Juranek, J. (1997). A sensory brain map for each behavior? *Proc. Natl. Acad. Sci. U S A* 94, 14798–14803. doi: 10.1073/pnas.94.26.14798

Meyer, J. H., Leong, M., and Keller, C. H. (1987). Hormone-induced and maturational changes in electric organ discharges and electroreceptor tuning in the weakly electric fish *Apteronotus*. *J. Comp. Physiol. A* 160, 385–394. doi: 10.1007/bf00613028

Moortgat, K. T., Keller, C. H., Bullock, T. H., and Sejnowski, T. J. (1998). Submicrosecond pacemaker precision is behaviorally modulated: the gymnotiform electromotor pathway. *Proc. Natl. Acad. Sci. U S A* 95, 4684–4689. doi: 10.1073/pnas.95.8.4684

Nelson, M. E., Xu, Z., and Payne, J. R. (1997). Characterization and modeling of P-type electrosensory afferent responses to amplitude modulations in a wave-type electric fish. *J. Comp. Physiol. A Sens. Neural Behav. Physiol.* 181, 532–544. doi: 10.1007/s003590050137

Partridge, B. L., Heiligenberg, W., and Matsubara, J. (1981). The neural basis of a sensory filter in the Jamming avoidance response: no grandmother cells in sight. *J. Comp. Physiol. A* 145, 153–168. doi: 10.1007/bf00605030

Rose, G. J., and Call, S. J. (1993). Temporal filtering properties of midbrain neurons in an electric fish: implications for the function of dendritic spines. *J. Neurosci.* 13, 1178–1189. doi: 10.1523/jneurosci.13-03-01178.1993

Smith, G. T. (2013). Evolution and hormonal regulation of sex differences in the electrocommunication behavior of ghost knifefishes (*Apteronotidae*). *J. Exp. Biol.* 216, 2421–2433. doi: 10.1242/jeb.082933

Sproule, M. K., Metzen, M. G., and Chacron, M. J. (2015). Parallel sparse and dense information coding streams in the electrosensory midbrain. *Neurosci. Lett.* 607, 1–6. doi: 10.1016/j.neulet.2015.09.014

Stöckl, A., Sinz, F., Benda, J., and Grewe, J. (2014). Encoding of social signals in all three electrosensory pathways of Eigenmannia virescens. *J. Neurophysiol.* 112, 2076–2091. doi: 10.1152/jn.00116.2014

Triefenbach, F., and Zakon, H. (2003). Effects of sex, sensitivity and status on cue recognition in the weakly electric fish *Apteronotus leptorhynchus*. *Anim. Behav.* 65, 19–28. doi: 10.1006/anbe.2002.2019

Triefenbach, F., and Zakon, H. (2008). Changes in signalling during agonistic interactions between male weakly electric knifefish, *Apteronotus leptorhynchus*. *Anim. Behav.* 75, 1263–1272. doi: 10.1016/j.anbehav.2007.09.027

Vonderschen, K., and Chacron, M. J. (2009). Sparse coding of natural communication signals in midbrain neurons. *BMC Neurosci.* 10:O3. doi: 10.1186/1471-2202-10-s1-o3

Vonderschen, K., and Chacron, M. J. (2011). Sparse and dense coding of natural stimuli by distinct midbrain neuron subpopulations in weakly electric fish. *J. Neurophysiol.* 106, 3102–3118. doi: 10.1152/jn.00588.2011

Walz, H., Hupé, G. J., Benda, J., and Lewis, J. E. (2013). The neuroethology of electrocommunication: how signal background influences sensory encoding and behaviour in *Apteronotus leptorhynchus*. *J. Physiol. Paris* 107, 13–25. doi: 10.1016/j.jphysparis.2012.07.001

Wohr, M., van Gaalen, M. M., and Schwarting, R. K. (2015). Affective communication in rodents: serotonin and its modulating role in ultrasonic vocalizations. *Behav. Pharmacol.* 26, 506–521. doi: 10.1097/FBP.0000000000000172

Xu, Z., Payne, J. R., and Nelson, M. E. (1996). Logarithmic time course of sensory adaptation in electrosensory afferent nerve fibers in a weakly electric fish. *J. Neurophysiol.* 76, 2020–2032. doi: 10.1152/jn.1996.76.3.2020

Zakon, H., Oestreich, J., Tallarovic, S., and Triefenbach, F. (2002). EOD modulations of brown ghost electric fish: JARs, chirps, rises and dips. *J. Physiol. Paris* 96, 451–458. doi: 10.1016/S0928-4257(03)00012-3

Zupanc, G. K. H. (2009). "Electrocommunication," in *Encyclopedia of Neuroscience*, ed. L. R. Squire (Oxford: Academic Press), 839–848.

Zupanc, G. K. H., and Bullock, T. H. (2005). "From electrogenesis to electroreception: an overview," in *Electroreception*, eds T. H. Bullock, C. D. Hopkins, E. N. Popper and R. R. Fay (New York, NY: Springer Verlag), 5–46.

Zupanc, M. M., Engler, G., Midson, A., Oxberry, H., Hurst, L. A., Symon, M. R., et al. (2001). Light-dark-controlled changes in modulations of the electric organ discharge in the teleost *Apteronotus leptorhynchus*. *Anim. Behav.* 62, 1119–1128. doi: 10.1006/anbe.2001.1867

Zupanc, G. K. H., and Maler, L. (1993). Evoked chirping in the weakly electric fish *Apteronotus leptorhynchus*: a quantitative biophysical analysis. *Can. J. Zool.* 71, 2301–2310. doi: 10.1139/z93-323

Zupanc, G. K., Sîrbulescu, R. F., Nichols, A., and Ilies, I. (2006). Electric interactions through chirping behavior in the weakly electric fish, *Apteronotus leptorhynchus*. *J. Comp. Physiol. A Neuroethol. Sens. Neural Behav. Physiol.* 192, 159–173. doi: 10.1007/s00359-005-0058-5

Conflict of Interest Statement: The author declares that the research was conducted in the absence of any commercial or financial relationships that could be construed as a potential conflict of interest.

frontiers in Integrative Neuroscience

MINI REVIEW
published: 13 September 2019
doi: 10.3389/fnint.2019.00052

Novel Functions of Feedback in Electrosensory Processing

Volker Hofmann and Maurice J. Chacron*

Department of Physiology, McGill University, Montreal, QC, Canada

Environmental signals act as input and are processed across successive stages in the brain to generate a meaningful behavioral output. However, a ubiquitous observation is that descending feedback projections from more central to more peripheral brain areas vastly outnumber ascending feedforward projections. Such projections generally act to modify how sensory neurons respond to afferent signals. Recent studies in the electrosensory system of weakly electric fish have revealed novel functions for feedback pathways in that their transformation of the afferent input generates neural firing rate responses to sensory signals mediating perception and behavior. In this review, we focus on summarizing these novel and recently uncovered functions and put them into context by describing the more "classical" functions of feedback in the electrosensory system. We further highlight the parallels between the electrosensory system and other systems as well as outline interesting future directions.

Keywords: descending pathways, weakly electric fish, response synthesis, neural coding, electrolocation, electrocommunication

OPEN ACCESS

Edited by:
Thomas W. James,
Indiana University Bloomington, United States

Reviewed by:
Angel Nunez,
Autonomous University of Madrid, Spain
Gary Marsat,
West Virginia University, United States
Andre Longtin,
University of Ottawa, Canada

****Correspondence:***
Volker Hofmann
volker.hofmann@mail.mcgill.ca

Received: *14 June 2019*
Accepted: *26 August 2019*
Published: *13 September 2019*

Citation:
Hofmann V and Chacron MJ (2019) Novel Functions of Feedback in Electrosensory Processing. Front. Integr. Neurosci. 13:52. doi: 10.3389/fnint.2019.00052

INTRODUCTION

How sensory information is processed by the brain to give rise to behavior remains an important yet poorly understood question in systems neuroscience. This is due in part to the fact that, along a given sensory pathway, descending connections from higher brain areas ("feedback") vastly outnumber ascending connections from the periphery ("feedforward"; Cajal, 1911; Holländer, 1970; Perkel et al., 1986; Sherman and Guillery, 2002; Markov et al., 2014; Salin and Bullier, 2017) and modify how sensory neurons respond to feedforward input. Previous studies have revealed multiple functions for such feedback pathways such as gain control (Treue and Martínez Trujillo, 1999), enhancing neural responses to particular stimuli (Hupé et al., 1998), or predictive coding (Bastos et al., 2012). Recent research in the electrosensory system of weakly electric fish has revealed novel, qualitatively different functions for feedback pathways in that their transformations of feedforward signals can generate neural responses that mediate behavioral responses to sensory input. Here, we review these novel functions and provide context for these results, particularly with regards to other previously established functions of feedback in the electrosensory as well as in other systems.

THE ELECTRIC SENSE: RELEVANT NEURAL CIRCUITRY AND SENSORY INPUT

Weakly electric fish as a model system benefit from well-characterized anatomy, natural stimuli, as well as feedback circuits that are easily accessible for pharmacological manipulation. We note that

all these features have been extensively reviewed elsewhere (Bastian, 1999; Berman and Maler, 1999; Bell and Maler, 2005; Chacron et al., 2011; Marsat et al., 2012; Krahe and Maler, 2014; Metzen et al., 2017).

To sense their surroundings and communicate with conspecifics, Gymnotiform weakly electric fish actively generate an electric field by emitting a quasi-sinusoidal electric organ discharge (EOD). Objects with a conductivity different from that of the surrounding water (e.g., prey) as well as interactions with the EOD of a conspecific will modulate the amplitude of the animal's EOD. These changes in amplitude are detected by electroreceptors scattered on the animal's skin (Scheich et al., 1973) that synapse onto pyramidal cells (P-cells) within the electrosensory lateral line lobe (ELL; Maler, 1979; Maler et al., 1981; **Figure 1A**). Specifically, each afferent fiber trifurcates to make synaptic contact with P-cells within three parallel segments: the centromedial (CMS), centrolateral (CLS) and the lateral (LS) segments (**Figure 1B**) that are organized in columns (**Figure 1C**) and display large differences in terms of receptive field organization (Shumway, 1989; Krahe et al., 2008; Hofmann and Chacron, 2017), ion channel composition (Ellis et al., 2008; Motipally et al., 2019), and responses to electrosensory stimuli (for review, see Krahe and Maler, 2014). There are two main types of P-cells: ON- and OFF-type that respond to increases and decreases in EOD amplitude, respectively (Maler, 1979; Maler et al., 1981; Saunders and Bastian, 1984). All P-cells project directly to the midbrain Torus semicircularis (TS) and, from there, indirectly to higher brain areas. There are large morphological and functional heterogeneities in the P-cell population (Maler, 2009a,b). In particular, so-called "deep" P-cells display small apical dendrites and receive little feedback, whereas "superficial" P-cells instead display large apical dendrites and receive large amounts of feedback.

P-cells receive large amounts of feedback from higher brain centers (Sas and Maler, 1983, 1987) that consist of three major pathways. Neurons within TS project back to stellate cells within the nucleus praeminentialis (nP) that then in turn project back to ELL P-cells with direct excitation and indirect inhibition through local interneurons (**Figure 1D**, blue). This feedback pathway forms a closed loop and is part of the "direct feedback pathway" (Bratton and Bastian, 1990; Berman and Maler, 1999). Bipolar and multipolar cells, as well as other cell types within nP, receive input from deep P-cells (i.e., only a sub-set of ELL output). While bipolar cells project back to ELL pyramidal cells in an inhibitory fashion forming the other part of the "direct pathway" (**Figure 1D**, magenta), multipolar cells instead project indirectly to ELL *via* granule cells of the eminentia granularis posterior (EGp; Bastian and Bratton, 1990). The ELL is a cerebellar-like structure, as EGp granule cell axons form parallel fibers that contact the apical dendrites of superficial P-cells (Bastian et al., 2004; **Figure 1D**, green). This open-loop feedback is known as the "indirect pathway." It should be noted that ELL pyramidal cells also receive other sources of neuromodulatory feedback (e.g., serotonergic, cholinergic; for review, see Márquez et al., 2013).

Electrosensory stimuli comprise of EOD amplitude modulations caused by prey or inanimate objects which are spatially localized (i.e., they impinge only upon a fraction of the animal's skin surface; Nelson and MacIver, 1999; Pedraja et al., 2018) or those caused by interactions with conspecifics that are spatially diffuse (i.e., they impinge on most if not all the animal's skin surface). In the latter case, interactions between the EODs of two conspecifics give rise to a sinusoidal amplitude modulation (i.e., a beat) whose frequency depends on the difference between the two individual EOD frequencies. The beat amplitude, termed the envelope, depends on the relative distance and orientation between both fish (Yu et al., 2012; Fotowat et al., 2013).

FUNCTIONS OF FEEDBACK INPUT ONTO ELL PYRAMIDAL CELLS

In this section, we will briefly summarize some of the established functions of feedback pathways on electrosensory processing towards modifying how P-cells respond to feedforward input from the periphery (e.g., response enhancement or attenuation). In the following section (see "Recently Uncovered Novel Functions for Electrosensory Feedback" section), we will then focus on recently uncovered novel functions of electrosensory feedback, that is the generation of neural responses which mediate perception and behavior.

Gain Control and Adaptive Cancelation of Sensory Stimuli

The first reported *in vivo* manipulations of electrosensory feedback pathways consisted of pharmacological inactivation as well as of lesioning the indirect feedback pathway (Bastian, 1986a,b). These manipulations made pyramidal cells more sensitive to changes in beat amplitude (i.e., increased the gain, which constitutes divisive gain control). This phenomenon has been studied in great theoretical detail (Lewis and Maler, 2004; Mejias et al., 2014) and a careful analysis revealed that there appears to be both divisive and subtractive (i.e., a shift in the sensitivity curve) gain control features.

Further studies have shown that the indirect pathway cancels predictable (i.e., redundant) sensory input *via* the formation of a "negative image" whose amplitude can be modulated to match that of the feedforward sensory input through plasticity at feedback synapses (for review, see Bastian, 1999). Moreover, investigators have focused on how recently-uncovered synaptic plasticity rules mediate the formation of the negative image (Bol et al., 2011; Harvey-Girard and Maler, 2013), thereby making neural responses more invariant with respect to stimulus amplitude (Mejias et al., 2013). The indirect feedback pathway is diffuse in nature and is primarily activated by spatially diffuse but not by spatially localized stimuli (Chacron et al., 2003, 2005b; Bastian et al., 2004; Chacron, 2006). It most likely originates from the so-called "non-classical" receptive field (i.e., the area of sensory space in which impinging stimuli do not by themselves affect the neural response but can modulate the response to stimuli impinging upon other areas of sensory space). Through this feedback input ELL pyramidal cells responses to low frequency stimuli are attenuated (Chacron et al., 2003, 2005a) and the responsiveness to spatially localized

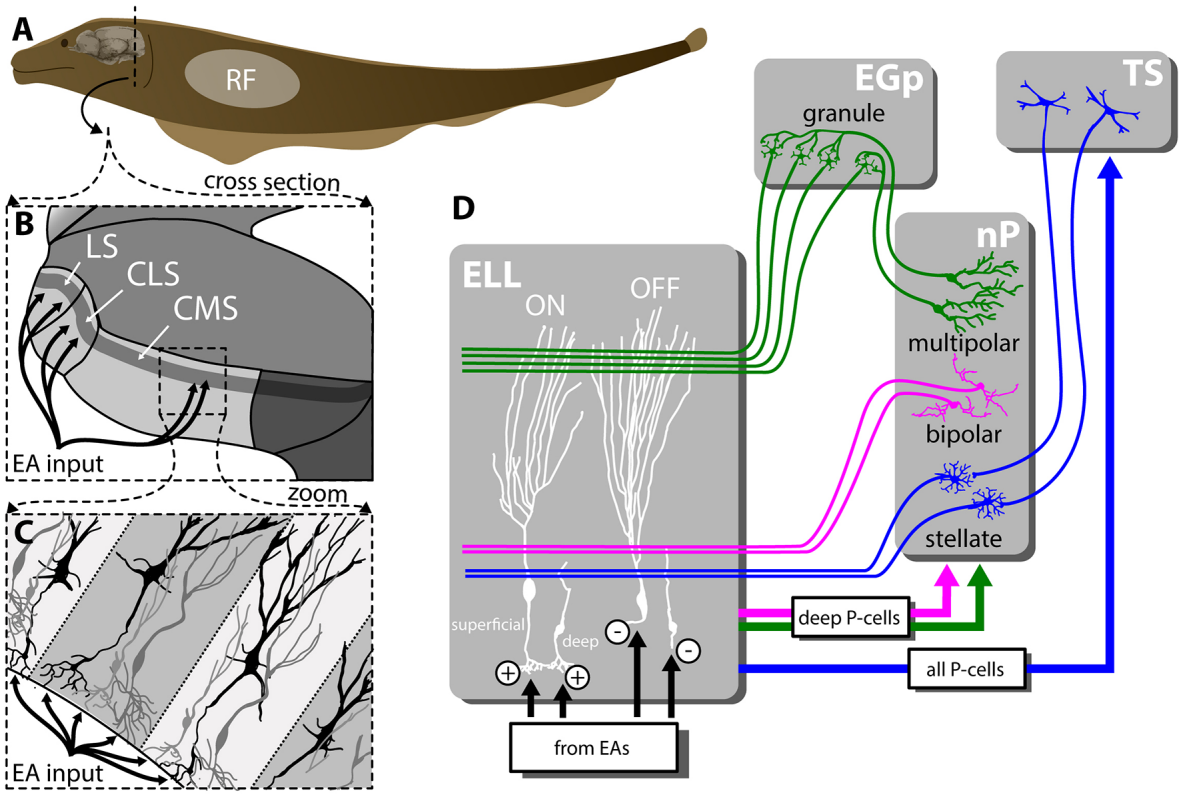

FIGURE 1 | Feedforward and feedback connectivity of the ELL. **(A)** Electroreceptors distributed across the body surface encode electrosensory stimuli and project to pyramidal cells (P-cells) within the hindbrain ELL. **(B)** The ELL is organized in three parallel segments (LS, CLS and CMS), each of which is a somatotopic representation of the body surface. All segments receive the same feedforward input from EAs. **(C)** Pyramidal cells (P-cells) within all ELL segments are organized in columns. P-cells receive feedforward input at their basal sites whereas feedback inputs project to the apical dendrites. **(D)** While ON-type P-cells receive direct excitatory ("+") input from peripheral electroreceptors, OFF-type P-cells instead receive indirect inhibitory input *via* local interneurons ("−"). While all P-cells project to the midbrain TS, only a subset of P-cells whose somata are located deep within the pyramidal cell layer (i.e., "deep" P-cells) project to the nP. There are several sources of feedback onto ELL P-cells: one of the pathways forms a closed-loop and is topographically ordered. It consists of ascending projections from all P-cells to TS from where descending projections project onto stellate cells within nP that then project back to ELL P-cells with direct excitation and indirect inhibition *via* local interneurons (blue). The second pathway consists of feedforward projections from deep P-cells to bipolar cells within nP that then project back to ELL P-cells in a diffuse manner and in an inhibitory fashion (magenta). The third pathway is termed "indirect" and consists of feedforward projections from deep P-cells to multipolar cells within nP that then project to granule cells within the EGP which make parallel fiber connections to ELL P-cells. It should be noted that such parallel fibers make little if any synaptic contact with deep P-cells. As such, this indirect pathway forms an open loop. Abbreviations: EA, electrosensory afferents; EGP, eminentia granularis posterior; ELL, electrosensory lateral line lobe; CLS, centrolateral segment; CMS, centromedial segment; LS, lateral segments; nP, nucleus praeminentialis; RF, receptive field; TS, torus semicircularis.

(e.g., prey) stimuli is increased (Litwin-Kumar et al., 2012). Moreover, as the indirect feedback pathway is primarily activated by low-frequency stimuli (Chacron et al., 2005b), another function is the enhancement of responses to high-frequency electrocommunication stimuli (Chacron et al., 2003, 2005b; Bastian et al., 2004; Chacron, 2006; Marsat and Maler, 2012; Marsat et al., 2012; Metzen, 2019) and the cancelation of re-afferent sensory input that is self-generated during tail motion (Bastian, 1995, 1996; Lewis et al., 2007). Most recently, it was shown that the indirect pathway is also involved in attenuating responses to low frequency envelopes (Huang et al., 2018), which is consistent with the above-mentioned fact that feedback makes neural responses to first-order stimuli more invariant with respect to stimulus amplitude (Mejias et al., 2013). It should be emphasized here that the indirect feedback pathway forms an open loop in that it originates from deep P-cells and primarily terminates on superficial P-cells. Modeling studies suggest that such a configuration is necessary for adaptive cancelation to occur (Bastian et al., 2004).

Similar functions have also been uncovered in other species of weakly electric fish (Enikolopov et al., 2018) and also show striking parallels to both the auditory and the visual system: the enhancement of responses to high-frequency stimuli through the attenuation of responses to low frequency stimuli is similar to what is seen in the auditory system. Here, feedback signals from the corticofugal system modulate frequency tuning of auditory subcortical neurons *via* synaptic plasticity (Chowdhury and Suga, 2000; Gao and Suga, 2000; Ma and Suga, 2001). Also, feedback was shown to effectively cancel responses to self-generated sounds in the dorsal

cochlear nucleus (Singla et al., 2017). The fact that electrosensory feedback originates from a "non-classical" part of the receptive field and modulates responses of target neurons (see above), is reminiscent to the visual system. Their stimulation outside of the receptive field was shown to effectively enhance the responses of neurons within the primary visual cortex to visual edges (i.e., high-spatial frequency stimulus features) in natural visual scenes (Vinje and Gallant, 2000, 2002), presumably through feedback signals. Similarly, stimulation of feedback to thalamic neurons was shown to effectively enhance their classical surround, thereby increasing sensitivity to high-spatial frequency stimuli (Murphy and Sillito, 1987; Sillito et al., 1993; Cudeiro and Sillito, 1996; Jones et al., 2000; Webb et al., 2003).

Generation of Gamma-Range Oscillations

Oscillatory neural activity within the gamma band (20–80 Hz) is seen ubiquitously across systems and species and is thought to play an important role in information processing (Uhlhaas et al., 2011; Buzsáki and Wang, 2012). During diffuse stimulation, inhibitory input from nP bipolar cells (**Figure 1D**, magenta) was shown to generate a gamma oscillation which can be seen in the activities of single ELL pyramidal cells (Doiron et al., 2003). Specifically, the transmission delay associated with this feedback pathway (∼15 ms) gives rise to a peak in spectral power (∼30 Hz). No such oscillations were seen when spatially localized stimuli mimicking prey were used instead. Subsequent studies have shown that the induced oscillations not only require spatially diffuse stimulation but also that the stimuli need to be spatially correlated with one another (Doiron et al., 2004; Lindner et al., 2005).

Further theoretical studies have highlighted potential issues with the original modeling as it did not specifically account for the fact that there are both ON- and OFF-type ELL pyramidal cells that respond to increases and decreases in the stimulus, respectively (Lefebvre et al., 2009; Payeur et al., 2013). If the feedback pathways simply integrate input from both cell types, then the power of gamma band oscillations would be weak, which is unlike what is observed experimentally. Based on these studies, several predictions regarding the anatomical organization of the feedback pathway were made: the feedback should be strongly asymmetric or segregated between ON- and Off-type responses. An oscillation resulting from stellate cell feedback seems however unlikely given that blocking excitatory feedback from nP stellate cells *in vivo* did not alter this oscillation (Doiron et al., 2003). Another alternative is that these oscillations result from a combination of feedforward excitatory and delayed feedforward inhibitory inputs that can mimic weak oscillatory states (Payeur et al., 2015).

Functionally, gamma-oscillations might enable the animal to distinguish between prey and conspecific-related stimuli (Doiron et al., 2003), or to enhance the ability of TS neurons to encode motion direction (Ramcharitar et al., 2005). Such functions are similar to those found in mammalian systems, where cortico-thalamic feedback loops generate multiple rhythms that drive neocortical neurons to fire in synchrony and thus presumably better encode specific stimulus features (for review, see Nuñez and Malmierca, 2007). Whether gamma-range oscillations synchronize the ELL pyramidal cell network remains to be shown experimentally. While only a limited number of studies has recorded from ELL pyramidal cell pairs so far (Chacron and Bastian, 2008; Litwin-Kumar et al., 2012; Simmonds and Chacron, 2015; Hofmann and Chacron, 2018b), answering the above question will require recordings from even greater population sizes. Such studies should also investigate if and how such synchronization enables the ELL pyramidal cell network to better encode behaviorally relevant stimuli.

Sensory Searchlight

While clear functional roles for both the indirect feedback as well as the direct feedback (bipolar component) were uncovered, the functional role of direct feedback pathway emanating from nP stellate cells has remained elusive. This is despite the fact that multiple studies have characterized how stellate cells respond to relevant electrosensory stimuli *in vivo* (Bratton and Bastian, 1990), characterized synaptic plasticity at stellate to P-cell synapses both *in vitro* (Oswald et al., 2002) and *in vivo* (for review, see Bastian, 1999). Because this pathway is topographic in nature, it was hypothesized that it should be primarily activated by spatially localized stimuli. Moreover, because of the strong potentiation observed at synapses, it was thought that this pathway acts as a "sensory searchlight" by enhancing P-cell responses to spatially localized stimuli (Berman and Maler, 1999). While it is true that stellate cells respond to stimuli mimicking prey (Bratton and Bastian, 1990), there has been, at least until very recently, no direct demonstration of a function for the direct feedback pathway *in vivo*. We next describe recently uncovered functions for this pathway.

RECENTLY UNCOVERED NOVEL FUNCTIONS FOR ELECTROSENSORY FEEDBACK

Generation of Bursting Neuronal Responses to Moving Objects

A recent study has investigated how electrosensory feedback pathways affect P-cell responses to moving objects (Clarke and Maler, 2017). While previous studies have investigated how electrosensory neurons respond to objects moving along the animal's rostro-caudal axis (Bastian, 1981a,b; Saunders and Bastian, 1984; Chacron et al., 2009; Khosravi-Hashemi et al., 2011). Clarke and Maler (2017) have instead investigated how electrosensory neurons responded to looming and receding objects. Such stimuli are experienced by the animal during the electromotor response (Heiligenberg, 1973; i.e., when animals seek to maintain a constant lateral position to large moving objects such as root masses of plants). Their stimulation paradigm consisted of a looming object that would then remain stationary close to the animal's skin surface. After a few seconds, the object was again receded from the skin surface. The authors used both metal as well as plastic objects that will increase and decrease EOD amplitude, respectively. They found that peripheral electroreceptors displayed strong adaptation to both

looming and receding objects (i.e., their firing rates returned to values seen in the absence of stimulation; Clarke et al., 2013). Interestingly and unlike afferents, an increase in firing rate due to burst firing was also observed when an "inverted-contrast" paradigm was used for receding motion (i.e., OFF-type cells with a metal object or ON-type cells with a plastic object). This burst response was seen even after the object remained stationary close to the animal's skin for several seconds during which the firing rate of peripheral electroreceptors almost fully adapted (Clarke et al., 2014).

How can P-cells give such a strong burst response even though the peripheral electroreceptors that provide feedforward input do not? Clarke and Maler (2017) investigated the role of ELL feedback pathways towards generating responses to both looming and receding objects. To do so, they blocked descending input from TS onto nP stellate cells (**Figure 1D**, blue). While such a manipulation only moderately affected responses to looming objects, they found that burst responses to receding objects were abolished. How can closed-loop feedback from TS to nP stellate cells to ELL generate bursting responses in P-cells to receding objects? P-cells display a burst mechanism that relies on somato-dendritic interactions (Lemon and Turner, 2000; Krahe and Gabbiani, 2004; Metzen et al., 2016). Generally burst firing serves to signal specific stimulus features (Oswald et al., 2004; Maler, 2009a; Avila-Akerberg et al., 2010; for review, see Krahe and Gabbiani, 2004). Here, the authors propose that feedback input from nP stellate cells is far more effective at eliciting burst firing from P-cells because these synapses display strong potentiation (Oswald et al., 2002). In contrast, the feedforward input from peripheral electroreceptors will be too weak to elicit a burst response by itself. Thus, this mechanism requires feedforward input to elicit feedback that then generates the neural burst response through a transformation of the feedforward input. Specifically, electroreceptor responses elicit P-Cell isolated spikes (i.e., no bursts) which then trigger bursting *via* feedback. Interestingly, further studies have shown that serotonergic modulation can enhance P-cells burst responses to improve the detectability of receding but not looming objects (Marquez and Chacron, 2018). Further experiments are needed to fully understand the mechanisms by which feedback pathways generate responses to moving objects.

Generating Neural Responses to Envelopes

In a series of experiments, Metzen et al. (2018) have found that, for low enough beat amplitudes (i.e., envelopes), feedback pathways are necessary to generate both neural and behavioral responses. Such stimuli would occur when both animals are located far away from each other (Stamper et al., 2013). The authors used sinusoidal beat stimuli whose amplitude (i.e., envelope) increased linearly over time and measured both neural and behavioral detection thresholds (i.e., the stimulus amplitude for which the neural or behavioral response became significantly different from that seen in the absence of stimulation). Responses were quantified by either the mean firing rate or the strength of phase locking to the beat.

Behaviorally, animals respond to very faint envelope stimuli (i.e., $<$10% contrast) through modulation of their EOD frequency. When investigating the neural underpinnings of these behavioral responses, it was found that, although ELL P-cells could detect faint envelope stimuli through increases in firing rate, peripheral electroreceptors did not. Their firing rates only showed significant increases at much higher ($>$30%) stimulus amplitudes. This finding is almost paradoxical: how can ELL P-cells respond through changes in firing rate to stimuli, even though their input does not? The answer lies beyond firing rate: if one considers detection thresholds based on phase locking, then both peripheral electroreceptors and P-cells actually respond to faint envelope signals (i.e., contrasts of less than 10%). Thus, a simple explanation for the observed behavioral responses is that information transmitted in a feedforward fashion *via* phase locking elicits behavioral responses. However, when eliminating feedback from nP stellate cells *via* injection of the sodium channel antagonist lidocaine, this explanation was proven wrong: both behavioral and P-cell firing rate responses to faint envelope signals were abolished. Interestingly, feedback manipulation did not affect phase locking in P-cells and as such, it is the P-cell firing rate response rather than phase locking that is decoded in order to give rise to behavior.

Other control experiments showed that blocking the indirect pathway did not affect P-cell responses and that injecting lidocaine into TS gave rise to the same effects on P-cell responses as those obtained after injecting lidocaine in nP. Recordings from stellate cells in nP showed an increase in firing rate to faint envelope signals. Both of these controls strongly suggest that the phase locking responses of P-cells are inherited from those of their afferent (i.e., feedforward) inputs and that these are transformed into a firing-rate response within the closed-loop feedback of the direct topographic pathway. A further study has shown that this pathway increases P-cell firing rate responses to envelopes independently of temporal frequency (Huang et al., 2018). Thus, phase locking from peripheral receptors induces phase locking in P-cells that presumably triggers an increase in the firing rate of nP stellate cells, which in turn increases P-cell firing rate response which is decoded downstream to give rise to behavior. Further studies are however needed to fully understand the mechanism that transforms phase locking to firing rate and generates P-cell firing rates responses to faint envelope signals. It should be noted that, in this case, ELL pyramidal cell phase locking responses (i.e., temporal code) are preserved and used to generate firing rate responses (i.e., a rate code). This shares similarities with the somatosensory system of rodents where cortical feedback transforms an incoming temporal code into a rate code (Ahissar et al., 2000).

SUMMARY AND FUTURE DIRECTIONS

In this review, we have summarized the classical functions of electrosensory feedback to highlight recently uncovered novel

TABLE 1 | Functions of feedback in the electrosensory system.

"classical" functions				
Function	**Pathway**	**Type**	**Effective transformation**	**Studies**
Cancelation of redundant LF input	Indirect, diffuse	Open loop	Generation and scaling of a negative image	Bastian (1995, 1999) and Bastian et al. (2004)
Control of frequency tuning	Indirect, diffuse	Open loop	Generation and scaling of a negative image for low frequency stimuli.	Chacron et al. (2003, 2005b), Chacron (2006); Huang et al. (2016, 2018) and Huang and Chacron (2017)
Induction of oscillation in gamma range	Direct, diffuse	Open loop	Delayed inhibitory feedback, interaction with STSP of ELL efferents	Doiron et al. (2003, 2004) and Lindner et al. (2005)
Sensory searchlight (?)	Direct, topographic	Closed loop	Excitatory input triggering burst firing	Berman and Maler (1999)
"novel" functions				
Generation of responses to receding objects	Direct, topographic	Closed loop	Excitatory input triggering burst firing	Clarke and Maler (2017)
Generation of envelope responses at low contrasts	Direct, topographic	Closed loop	Transformation of phase locking to firing rate.	Huang et al. (2018) and Metzen et al. (2018)

functions of the closed-loop direct pathway towards generating neural and behavioral responses. The functions of feedback in the ELL are summarized in **Table 1**.

It is likely that similar roles of feedback can be found in other systems. This is because the electrosensory system shares many similarities with both the visual (for review, see Clarke et al., 2015) as well as auditory and vestibular systems (Metzen et al., 2015). On top of examples mentioned above, recent studies have shown that feedback is necessary to complete the perception of touch (Manita et al., 2015; Kwon et al., 2016; Takahashi et al., 2016). Specifically, such feedback terminates on the apical dendrites of cortical neurons to generate a burst response, which is conceptually similar to the results of Clarke and Maler (2017). In neurons of the cochlear nucleus, detection thresholds to envelopes are thought to emerge through feedforward integration of input from auditory fibers. However, based on the results of Metzen et al. (2018), further studies should investigate how feedback contributes to determining auditory envelope detection thresholds.

In the electrosensory system, a better understanding of the mechanisms underlying the described feedback transformations will only be achieved by investigating how TS neurons respond to electrosensory stimuli (Khosravi-Hashemi et al., 2011; Vonderschen and Chacron, 2011; McGillivray et al., 2012; Sproule et al., 2015). Also, further studies will require the characterization of responses in nP using stimuli like those in Clarke and Maler (2017) and Metzen et al. (2018). In addition to that, further studies are needed to understand the interplay between neuromodulatory feedback and the feedback inputs described here and how this optimizes neural responses based on behavioral context. Beyond that, it is clear that, in the electrosensory as in other systems, behavior is determined by integrating the activities of large neural populations. However, only a few studies have begun to unravel the impact of feedback on population coding (Chacron and Bastian, 2008; Litwin-Kumar et al., 2012; Simmonds and Chacron, 2015; Hofmann and Chacron, 2018b). This research direction is particularly interesting and timely as feedback has been shown to impact population coding in other systems (Bondy et al., 2018; Merrikhi et al., 2018).

Finally, it should be noted that most studies have investigated the impact of feedback onto neuronal coding in immobilized and thus, at least partly, behaviorally restrained animals. Nonetheless, animals in general and weakly electric fish in particular are known to display a rich repertoire of sensory-related behaviors termed "active sensing movements" (for review, see e.g., Schroeder et al., 2010; Wachowiak, 2011; Hofmann et al., 2013; Grant et al., 2014). It was shown that active control of the re-afferent sensory input can enhance (Stamper et al., 2012; Hofmann et al., 2017) or even generate sensory information (Biswas et al., 2018; Hofmann and Chacron, 2018a; Pedraja et al., 2018). Recent technological advances made it possible to record neuronal activity in freely moving animals (Fotowat et al., 2019) and thus to investigate the role of feedback under active conditions. Such studies focus on how feedback is involved in differentiating between ex- and re-afferent input, and in shaping neuronal tuning in an activity-based manner. It is likely that such mechanisms are similar to those encountered in the somatosensory system of whisking rodents, where cortical feedback unto thalamic neurons can, for example, alter receptive field size thereby enhancing sensory information (Malmierca and Nuñez, 2004).

AUTHOR CONTRIBUTIONS

VH and MC conceptualized the review and revised the manuscript to its final version. VH prepared the figure, table and wrote the initial draft.

FUNDING

This research was supported by the Deutsche Forschungsgemeinschaft, DFG (VH; HO5912/1-1) and the Canadian Institutes of Health Research (MC).

REFERENCES

Ahissar, E., Sosnik, R., and Haldarilu, S. (2000). Transformation from temporal to rate coding in a somatosensory thalamocortical pathway. *Nature* 406, 302–306. doi: 10.1038/35018568

Avila-Akerberg, O., Krahe, R., and Chacron, M. J. (2010). Neural heterogeneities and stimulus properties affect burst coding *in vivo*. *Neuroscience* 168, 300–313. doi: 10.1016/j.neuroscience.2010.03.012

Bastian, J. (1981a). Electrolocation I. How the electrorecetor of Apteronotus albifrons code for moving objects and other electrical stimuli. *J. Comp. Physiol.* 144, 465–479. doi: 10.1007/bf01326832

Bastian, J. (1981b). Electrolocation II. The effects of moving objects and other electrical stimuli on the activities of two categories of posterior lateral line lobe cells in Apteronotus albifrons. *J. Comp. Physiol.* 144, 481–494. doi: 10.1007/bf01326833

Bastian, J. (1986a). Gain control in the electrosensory system: a role for the descending projections to the electrosensory lateral line lobe. *J. Comp. Physiol. A* 158, 505–515. doi: 10.1007/bf00603796

Bastian, J. (1986b). Gain control in the electrosensory system mediated by descending inputs to the electrosensory lateral line lobe. *J. Neurosci.* 6, 553–562. doi: 10.1523/jneurosci.06-02-00553.1986

Bastian, J. (1995). Pyramidal-cell plasticity in weakly electric fish: a mechanism for attenuating responses to reafferent electrosensory inputs. *J. Comp. Physiol. A* 176, 63–73. doi: 10.1007/bf00197753

Bastian, J. (1996). Plasticity in an electrosensory system. I. General features of a dynamic sensory filter. *J. Neurophysiol.* 76, 2483–2496. doi: 10.1152/jn.1996.76.4.2483

Bastian, J. (1999). Plasticity of feedback inputs in the apteronotid electrosensory system. *J. Exp. Biol.* 202, 1327–1337.

Bastian, J., and Bratton, B. (1990). Descending control of electroreception. I. Properties of nucleus-praeeminentialis neurons projecting indirectly to the electrosensory lateral line lobe. *J. Neurosci.* 10, 1226–1240. doi: 10.1523/jneurosci.10-04-01226.1990

Bastian, J., Chacron, M. J., and Maler, L. (2004). Plastic and nonplastic pyramidal cells perform unique roles in a network capable of adaptive redundancy reduction. *Neuron* 41, 767–779. doi: 10.1016/s0896-6273(04)00071-6

Bastos, A. M., Usrey, W. M., Adams, R. A., Mangun, G. R., Fries, P., and Friston, K. J. (2012). Canonical microcircuits for predictive coding. *Neuron* 76, 695–711. doi: 10.1016/j.neuron.2012.10.038

Bell, C., and Maler, L. (2005). "Central neuroanatomy of electrosensory system in fish," in *Electroreception*, eds H. B. Bullock, C. D. Hopkins, A. N. Popper and R. R. Fay (Berlin, Heidelberg, New York: Springer Verlag), 68–111.

Berman, N., and Maler, L. (1999). Neural architecture of the electrosensory lateral line lobe: adaptations for coincidence detection, a sensory searchlight and frequency-dependent adaptive filtering. *J. Exp. Biol.* 202, 1243–1253.

Biswas, D., Arend, L. A., Stamper, S. A., Vágvölgyi, B., Fortune, E. S., and Cowan, N. J. (2018). Closed-loop control of active sensing movements regulates sensory slip. *Curr. Biol.* 28, 4029–4036. doi: 10.1016/j.cub.2018.11.002

Bol, K., Marsat, G., Harvey-Girard, E., Longtin, A., and Maler, L. (2011). Frequency-tuned cerebellar channels and burst-induced LTD lead to the cancellation of redundant sensory inputs. *J. Neurosci.* 31, 11028–11038. doi: 10.1523/jneurosci.0193-11.2011

Bondy, A. G., Haefner, R. M., and Cumming, B. G. (2018). Feedback determines the structure of correlated variability in primary visual cortex. *Nat. Neurosci.* 21, 598–606. doi: 10.1038/s41593-018-0089-1

Bratton, B., and Bastian, J. (1990). Descending control of electroreception. II. Properties of nucleus praeeminentialis neurons projecting directly to the electrosensory lateral line lobe. *J. Neurosci.* 10, 1241–1253. doi: 10.1523/jneurosci.10-04-01241.1990

Buzsáki, G., and Wang, X.-J. (2012). Mechanisms of gamma oscillations. *Annu. Rev. Neurosci.* 35, 203–225. doi: 10.1146/annurev-neuro-062111-150444

Cajal, R. S. (1911). *Histologie du Système Nerveux de l'Homme et des Vertebres.* Paris: Maloine.

Chacron, M. J. (2006). Nonlinear information processing in a model sensory system. *J. Neurophysiol.* 95, 2933–2946. doi: 10.1152/jn.01296.2005

Chacron, M. J., and Bastian, J. (2008). Population coding by electrosensory neurons. *J. Neurophysiol.* 99, 1825–1835. doi: 10.1152/jn.01266.2007

Chacron, M. J., Doiron, B., Maler, L., Longtin, A., and Bastian, J. (2003). Non-classical receptive field mediates switch in a sensory neuron's frequency tuning. *Nature* 423, 77–81. doi: 10.1038/nature01590

Chacron, M. J., Longtin, A., and Maler, L. (2005a). Delayed excitatory and inhibitory feedback shape neural information transmission. *Phys. Rev. E Stat. Nonlin. Soft Matter Phys.* 72:051917. doi: 10.1103/physreve.72.051917

Chacron, M. J., Maler, L., and Bastian, J. (2005b). Feedback and feedforward control of frequency tuning to naturalistic stimuli. *J. Neurosci.* 25, 5521–5532. doi: 10.1523/jneurosci.0445-05.2005

Chacron, M. J., Longtin, A., and Maler, L. (2011). Efficient computation *via* sparse coding in electrosensory neural networks. *Curr. Opin. Neurobiol.* 21, 752–760. doi: 10.1016/j.conb.2011.05.016

Chacron, M. J., Toporikova, N., and Fortune, E. S. (2009). Differences in the time course of short-term depression across receptive fields are correlated with directional selectivity in electrosensory neurons. *J. Neurophysiol.* 102, 3270–3279. doi: 10.1152/jn.00645.2009

Chowdhury, S. A., and Suga, N. (2000). Reorganization of the frequency map of the auditory cortex evoked by cortical electrical stimulation in the big brown bat. *J. Neurophysiol.* 83, 1856–1863. doi: 10.1152/jn.2000.83.4.1856

Clarke, S. E., Longtin, A., and Maler, L. (2014). A neural code for looming and receding motion is distributed over a population of electrosensory ON and OFF contrast cells. *J. Neurosci.* 34, 5583–5594. doi: 10.1523/jneurosci.4988-13.2014

Clarke, S. E., Longtin, A., and Maler, L. (2015). Contrast coding in the electrosensory system: parallels with visual computation. *Nat. Rev. Neurosci.* 16, 733–744. doi: 10.1038/nrn4037

Clarke, S. E., and Maler, L. (2017). Feedback synthesizes neural codes for motion. *Curr. Biol.* 27, 1356–1361. doi: 10.1016/j.cub.2017.03.068

Clarke, S. E., Naud, R., Longtin, A., and Maler, L. (2013). Speed-invariant encoding of looming object distance requires power law spike rate adaptation. *Proc. Natl. Acad. Sci. U S A* 110, 13624–13629. doi: 10.1073/pnas.1306428110

Cudeiro, J., and Sillito, A. M. (1996). Spatial frequency tuning of orientation-discontinuity-sensitive corticofugal feedback to the cat lateral geniculate nucleus. *J. Physiol.* 490, 481–492. doi: 10.1113/jphysiol.1996.sp021159

Doiron, B., Chacron, M. J., Maler, L., Longtin, A., and Bastian, J. (2003). Inhibitory feedback required for network oscillatory responses to communication but not prey stimuli. *Nature* 421, 539–543. doi: 10.1038/nature01360

Doiron, B., Lindner, B., Longtin, A., Maler, L., and Bastian, J. (2004). Oscillatory activity in electrosensory neurons increases with the spatial correlation of the stochastic input stimulus. *Phys. Rev. Lett.* 93:048101. doi: 10.1103/physrevlett.93.048101

Ellis, L. D., Maler, L., and Dunn, R. J. (2008). Differential distribution of SK channel subtypes in the brain of the weakly electric fish *Apteronotus leptorhynchus*. *J. Comp. Neurol.* 507, 1964–1978. doi: 10.1002/cne.21597

Enikolopov, A. G., Abbott, L. F., and Sawtell, N. B. (2018). Internally generated predictions enhance neural and behavioral detection of sensory stimuli in an electric fish. *Neuron* 99, 135.e3–146.e3. doi: 10.1016/j.neuron.2018.06.006

Fotowat, H., Harrison, R. R., and Krahe, R. (2013). Statistics of the electrosensory input in the freely swimming weakly electric fish *Apteronotus leptorhynchus*. *J. Neurosci.* 33, 13758–13772. doi: 10.1523/jneurosci.0998-13.2013

Fotowat, H., Lee, C., Jun, J. J., and Maler, L. (2019). Neural activity in a hippocampus-like region of the teleost pallium is associated with active sensing and navigation. *Elife* 8:e44119. doi: 10.7554/eLife.44119

Gao, E., and Suga, N. (2000). Experience-dependent plasticity in the auditory cortex and the inferior colliculus of bats: role of the corticofugal system. *Proc. Natl. Acad. Sci. U S A* 97, 8081–8086. doi: 10.1073/pnas.97.14.8081

Grant, R. A., Itskov, P. M., Towal, R. B., and Prescott, T. J. (2014). Active touch sensing: finger tips, whiskers, and antennae. *Front. Behav. Neurosci.* 8:50. doi: 10.3389/fnbeh.2014.00050

Harvey-Girard, E., and Maler, L. (2013). Dendritic SK channels convert NMDA-R-dependent LTD to burst timing-dependent plasticity. *J. Neurophysiol.* 110, 2689–2703. doi: 10.1152/jn.00506.2013

Heiligenberg, W. (1973). "Electromotor" response in the electric fish Eigenmannia (Rhamphichichthydiae, Gymnotoidei). *Nature* 243, 301–302. doi: 10.1038/243301a0

Hofmann, V., and Chacron, M. J. (2017). Differential receptive field organizations give rise to nearly identical neural correlations across three parallel sensory maps in weakly electric fish. *PLoS Comput. Biol.* 13:e1005716. doi: 10.1371/journal.pcbi.1005716

Hofmann, V., and Chacron, M. J. (2018a). Active sensing: constancy requires change. *Curr. Biol.* 28, R1391–R1394. doi: 10.1016/j.cub.2018.10.060

Hofmann, V., and Chacron, M. J. (2018b). Population coding and correlated variability in electrosensory pathways. *Front. Integr. Neurosci.* 12:56. doi: 10.3389/fnint.2018.00056

Hofmann, V., Sanguinetti-Scheck, J. I., Gomez-Sena, L., and Engelmann, J. (2017). Sensory flow as a basis for a novel distance cue in freely behaving electric fish. *J. Neurosci.* 37, 302–312. doi: 10.1523/JNEUROSCI.1361-16.2016

Hofmann, V., Sanguinetti-Scheck, J. I., Künzel, S., Geurten, B., Gómez-Sena, L., and Engelmann, J. (2013). Sensory flow shaped by active sensing: sensorimotor strategies in electric fish. *J. Exp. Biol.* 216, 2487–2500. doi: 10.1242/jeb.082420

Holländer, H. (1970). The projection from the visual cortex to the lateral geniculate body (LGB) an experimental study with silver impregnation methods in the Cat. *Exp. Brain Res.* 10, 219–235. doi: 10.1007/bf00235047

Huang, C. G., and Chacron, M. J. (2017). SK channel subtypes enable parallel optimized coding of behaviorally relevant stimulus attributes: a review. *Channels* 11, 281–304. doi: 10.1080/19336950.2017.1299835

Huang, C. G., Metzen, M. G., and Chacron, M. J. (2018). Feedback optimizes neural coding and perception of natural stimuli. *Elife* 7:e38935. doi: 10.7554/elife.38935

Huang, C. G., Zhang, Z. D., and Chacron, M. J. (2016). Temporal decorrelation by SK channels enables efficient neural coding and perception of natural stimuli. *Nat. Commun.* 7:11353. doi: 10.1038/ncomms11353

Hupé, J. M., James, A. C., Payne, B. R., Lomber, S. G., Girard, P., and Bullier, J. (1998). Cortical feedback improves discrimination between figure and background by V1, V2 and V3 neurons. *Nature* 394, 784–787. doi: 10.1038/29537

Jones, H. E., Andolina, I. M., Oakely, N. M., Murphy, P. C., and Sillito, A. M. (2000). Spatial summation in lateral geniculate nucleus and visual cortex. *Exp. Brain Res.* 135, 279–284. doi: 10.1007/s002210000574

Khosravi-Hashemi, N., Fortune, E. S., and Chacron, M. J. (2011). Coding movement direction by burst firing in electrosensory neurons. *J. Neurophysiol.* 106, 1954–1968. doi: 10.1152/jn.00116.2011

Krahe, R., Bastian, J., and Chacron, M. J. (2008). Temporal processing across multiple topographic maps in the electrosensory system. *J. Neurophysiol.* 100, 852–867. doi: 10.1152/jn.90300.2008

Krahe, R., and Gabbiani, F. (2004). Burst firing in sensory systems. *Nat. Rev. Neurosci.* 5, 13–23. doi: 10.1038/nrn1296

Krahe, R., and Maler, L. (2014). Neural maps in the electrosensory system of weakly electric fish. *Curr. Opin. Neurobiol.* 24, 13–21. doi: 10.1016/j.conb.2013.08.013

Kwon, S. E., Yang, H., Minamisawa, G., and O'Connor, D. H. (2016). Sensory and decision-related activity propagate in a cortical feedback loop during touch perception. *Nat. Neurosci.* 19, 1243–1249. doi: 10.1038/nn.4356

Lefebvre, J., Longtin, A., and LeBlanc, V. G. (2009). Dynamics of driven recurrent networks of ON and OFF cells. *Phys. Rev. E Stat. Nonlin. Soft Matter Phys.* 80:041912. doi: 10.1103/physreve.80.041912

Lemon, N., and Turner, R. (2000). Conditional spike backpropagation generates burst discharge in a sensory neuron. *J. Neurophysiol.* 84, 1519–1530. doi: 10.1152/jn.2000.84.3.1519

Lewis, J. E., Lindner, B., Laliberté, B., and Groothuis, S. (2007). Control of neuronal firing by dynamic parallel fiber feedback: implications for electrosensory reafference suppression. *J. Exp. Biol.* 210, 4437–4447. doi: 10.1242/jeb.010322

Lewis, J. E., and Maler, L. (2004). Synaptic dynamics on different time scales in a parallel fiber feedback pathway of the weakly electric fish. *J. Neurophysiol.* 91, 1064–1070. doi: 10.1152/jn.00856.2003

Lindner, B., Doiron, B., and Longtin, A. (2005). Theory of oscillatory firing induced by spatially correlated noise and delayed inhibitory feedback. *Phys. Rev. E Stat. Nonlin. Soft Matter Phys.* 72:061919. doi: 10.1103/physreve.72.061919

Litwin-Kumar, A., Chacron, M. J., and Doiron, B. (2012). The spatial structure of stimuli shapes the timescale of correlations in population spiking activity. *PLoS Comput. Biol.* 8:e1002667. doi: 10.1371/journal.pcbi.1002667

Ma, X., and Suga, N. (2001). Corticofugal modulation of duration-tuned neurons in the midbrain auditory nucleus in bats. *Proc. Natl. Acad. Sci. U S A* 98, 14060–14065. doi: 10.1073/pnas.241517098

Maler, L. (1979). The posterior lateral line lobe of certain gymnotoid fish: quantitative light microscopy. *J. Comp. Neurol.* 183, 323–363. doi: 10.1002/cne.901830208

Maler, L. (2009a). Receptive field organization across multiple electrosensory maps. I. Columnar organization and estimation of receptive field size. *J. Comp. Neurol.* 516, 376–393. doi: 10.1002/cne.22124

Maler, L. (2009b). Receptive field organization across multiple electrosensory maps. II. Computational analysis of the effects of receptive field size on prey localization. *J. Comp. Neurol.* 516, 394–422. doi: 10.1002/cne.22120

Maler, L., Sas, E. K. B., and Rogers, J. (1981). The cytology of the posterior lateral line lobe of high-frequency weakly electric fish (gymnotidae): dendritic differentiation and synaptic specificity in a simple cortex. *J. Comp. Neurol.* 195, 87–139. doi: 10.1002/cne.901950107

Malmierca, E., and Nuñez, A. (2004). Primary somatosensory cortex modulation of tactile responses in nucleus gracilis cells of rats. *Eur. J. Neurosci.* 19, 1572–1580. doi: 10.1111/j.1460-9568.2004.03256.x

Manita, S., Suzuki, T., Homma, C., Matsumoto, T., Odagawa, M., Yamada, K., et al. (2015). A top-down cortical circuit for accurate sensory perception. *Neuron* 86, 1304–1316. doi: 10.1016/j.neuron.2015.05.006

Markov, N. T., Vezoli, J., Chameau, P., Falchier, A., Quilodran, R., Huissoud, C., et al. (2014). Anatomy of hierarchy: feedforward and feedback pathways in macaque visual cortex. *J. Comp. Neurol.* 522, 225–259. doi: 10.1002/cne.23458

Marquez, M. M., and Chacron, M. J. (2018). Serotonin selectively increases detectability of motion stimuli in the electrosensory system. *eNeuro* 5:ENEURO.0013–18.2018. doi: 10.1523/eneuro.0013-18.2018

Márquez, B. T., Krahe, R., and Chacron, M. J. (2013). Neuromodulation of early electrosensory processing in gymnotiform weakly electric fish. *J. Exp. Biol.* 216, 2442–2450. doi: 10.1242/jeb.082370

Marsat, G., Longtin, A., and Maler, L. (2012). Cellular and circuit properties supporting different sensory coding strategies in electric fish and other systems. *Curr. Opin. Neurobiol.* 22, 686–692. doi: 10.1016/j.conb.2012.01.009

Marsat, G., and Maler, L. (2012). Preparing for the unpredictable: adaptive feedback enhances the response to unexpected communication signals. *J. Neurophysiol.* 107, 1241–1246. doi: 10.1152/jn.00982.2011

McGillivray, P., Vonderschen, K., Fortune, E. S., and Chacron, M. J. (2012). Parallel coding of first- and second-order stimulus attributes by midbrain electrosensory neurons. *J. Neurosci.* 32, 5510–5524. doi: 10.1523/JNEUROSCI.0478-12.2012

Mejias, J. F., Marsat, G., Bol, K., Maler, L., and Longtin, A. (2013). Learning contrast-invariant cancellation of redundant signals in neural systems. *PLoS Comput. Biol.* 9:e1003180. doi: 10.1371/journal.pcbi.1003180

Mejias, J. F., Payeur, A., Selin, E., Maler, L., and Longtin, A. (2014). Subtractive, divisive and non-monotonic gain control in feedforward nets linearized by noise and delays. *Front. Comput. Neurosci.* 8:19. doi: 10.3389/fncom.2014.00019

Merrikhi, Y., Clark, K., and Noudoost, B. (2018). Concurrent influence of top-down and bottom-up inputs on correlated activity of Macaque extrastriate neurons. *Nat. Commun.* 9:5393. doi: 10.1038/s41467-018-07816-4

Metzen, M. G. (2019). Encoding and perception of electro-communication signals in *Apteronotus leptorhynchus*. *Front. Integr. Neurosci.* 13:39. doi: 10.3389/fnint.2019.00039

Metzen, M. G., Fortune, E. S., and Chacron, M. J. (2017). "Physiology of tuberous electrosensory systems," in *Reference Module in Life Sciences*, eds E. S. Fortune, M. J. Chacron and A. P. Farrell (Amsterdam: Elsevier), 366–374.

Metzen, M. G., Huang, C. G., and Chacron, M. J. (2018). Descending pathways generate perception of and neural responses to weak sensory input. *PLoS Biol.* 16:e2005239. doi: 10.1371/journal.pbio.2005239

Metzen, M. G., Jamali, M., Carriot, J., Ávila-Åkerberg, O., Cullen, K. E., and Chacron, M. J. (2015). Coding of envelopes by correlated but not single-neuron activity requires neural variability. *Proc. Natl. Acad. Sci. U S A* 112, 4791–4796. doi: 10.1073/pnas.1418224112

Metzen, M. G., Krahe, R., and Chacron, M. J. (2016). Burst firing in the electrosensory system of gymnotiform weakly electric fish: mechanisms and functional roles. *Front. Comput. Neurosci.* 10:81. doi: 10.3389/fncom.2016.00081

Motipally, S. I., Allen, K. M., Williamson, D. K., and Marsat, G. (2019). Differences in sodium channel densities in the apical dendrites of pyramidal cells of the

electrosensory lateral line lobe. *Front. Neural Circuits* 13:41. doi: 10.3389/fncir.2019.00041

Murphy, P. C., and Sillito, A. M. (1987). Corticofugal feedback influences the generation of length tuning in the visual pathway. *Nature* 329, 727–729. doi: 10.1038/329727a0

Nelson, M. E., and MacIver, M. A. (1999). Prey capture in the weakly electric fish Apteronotus albifrons: sensory acquisition strategies and electrosensory consequences. *J. Exp. Biol.* 202, 1195–1203.

Nuñez, A., and Malmierca, E. (2007). "Corticofugal modulation of sensory information," in *Advances in Anatomy Embryology and Cell Biology*, eds F. F. Beck, M. Frotscher, H.-W. Korf, R. Putz and T. H. Schiebler (Berlin, New York, NY, Tokyo: Springer Verlag), 1–74.

Oswald, A.-M. M., Chacron, M. J., Doiron, B., Bastian, J., and Maler, L. (2004). Parallel processing of sensory input by bursts and isolated spikes. *J. Neurosci.* 24, 4351–4362. doi: 10.1523/JNEUROSCI.0459-04.2004

Oswald, A.-M. M., Lewis, J. E., and Maler, L. (2002). Dynamically interacting processes underlie synaptic plasticity in a feedback pathway. *J. Neurophysiol.* 87, 2450–2463. doi: 10.1152/jn.00711.2001

Payeur, A., Lefebvre, J., Maler, L., and Longtin, A. (2013). Linear response theory for two neural populations applied to gamma oscillation generation. *Phys. Rev. E* 87, 1–14. doi: 10.1103/physreve.87.032703

Payeur, A., Maler, L., and Longtin, A. (2015). Oscillatory like behavior in feedforward neuronal networks. *Phys. Rev. E* 92:012703. doi: 10.1103/PhysRevE.92.012703

Pedraja, F., Hofmann, V., Lucas, K. M., Young, C., Engelmann, J., and Lewis, J. E. (2018). Motion parallax in electric sensing. *Proc. Natl. Acad. Sci. U S A* 115, 573–577. doi: 10.1073/pnas.1712380115

Perkel, D. J., Bullier, J., and Kennedy, H. (1986). Topography of the afferent connectivity of area 17 in the macaque monkey: a double-labelling study. *J. Comp. Neurol.* 253, 374–402. doi: 10.1002/cne.902530307

Ramcharitar, J. U., Tan, E. W., and Fortune, E. S. (2005). Effects of global electrosensory signals on motion processing in the midbrain of Eigenmannia. *J. Comp. Physiol. A Neuroethol. Sens. Neural Behav. Physiol.* 191, 865–872. doi: 10.1007/s00359-005-0008-2

Salin, P. A., and Bullier, J. (2017). Corticocortical connections in the visual system: structure and function. *Physiol. Rev.* 75, 107–154. doi: 10.1152/physrev.1995.75.1.107

Sas, E., and Maler, L. (1983). The nucleus praeeminentialis: a Golgi study of a feedback center in the electrosensory system of gymnotid fish. *J. Comp. Neurol.* 221, 127–144. doi: 10.1002/cne.902210202

Sas, E., and Maler, L. (1987). The organization of afferent input to the caudal lobe of the cerebellum of the gymnotid fish *Apteronotus leptorhynchus*. *Anat. Embryol.* 177, 55–79. doi: 10.1007/bf00325290

Saunders, J., and Bastian, J. (1984). The physiology and morphology of two types of electrosensory neurons in the weakly electric fish *Apteronotus leptorhynchus*. *J. Comp. Physiol. A* 154, 199–209. doi: 10.1007/bf00604985

Scheich, H., Bullock, T. H., and Hamstra, R. H. Jr. (1973). Coding properties of two classes of afferent nerve fibers: high-frequency electroreceptors in the electric fish, of Two Classes of Afferent Electroreceptors. *J. Neurophysiol.* 36, 39–60. doi: 10.1152/jn.1973.36.1.39

Schroeder, C. E., Wilson, D. A., Radman, T., Scharfman, H., and Lakatos, P. (2010). Dynamics of active Sensing and perceptual selection. *Curr. Opin. Neurobiol.* 20, 172–176. doi: 10.1016/j.conb.2010.02.010

Sherman, S. M., and Guillery, R. W. (2002). The role of the thalamus in the flow of information to the cortex. *Philos. Trans. R. Soc. B Biol. Sci.* 357, 1695–1708. doi: 10.1098/rstb.2002.1161

Shumway, C. A. (1989). Multiple electrosensory maps in the medulla of weakly electric gymnotiform fish. I. Physiological differences. *J. Neurosci.* 9, 4388–4399. doi: 10.1523/JNEUROSCI.09-12-04388.1989

Sillito, A. M., Cudeiro, J., and Murphy, P. C. (1993). Orientation sensitive elements in the corticofugal influence on centre-surround interactions in the dorsal lateral geniculate nucleus. *Exp. Brain Res.* 93, 6–16. doi: 10.1007/bf00227775

Simmonds, B., and Chacron, M. J. (2015). Activation of parallel fiber feedback by spatially diffuse stimuli reduces signal and noise correlations *via* independent mechanisms in a cerebellum-like structure. *PLoS Comput. Biol.* 11:e1004034. doi: 10.1371/journal.pcbi.1004034

Singla, S., Dempsey, C., Warren, R., Enikolopov, A. G., and Sawtell, N. B. (2017). A cerebellum-like circuit in the auditory system cancels responses to self-generated sounds. *Nat. Neurosci.* 20, 943–950. doi: 10.1038/nn.4567

Sproule, M. K. J., Metzen, M. G., and Chacron, M. J. (2015). Parallel sparse and dense information coding streams in the electrosensory midbrain. *Neurosci. Lett.* 607, 1–6. doi: 10.1016/j.neulet.2015.09.014

Stamper, S. A., Fortune, E. S., and Chacron, M. J. (2013). Perception and coding of envelopes in weakly electric fishes. *J. Exp. Biol.* 216, 2393–2402. doi: 10.1242/jeb.082321

Stamper, S. A., Roth, E., Cowan, N. J., and Fortune, E. S. (2012). Active sensing *via* movement shapes spatiotemporal patterns of sensory feedback. *J. Exp. Biol.* 215, 1567–1574. doi: 10.1242/jeb.068007

Takahashi, N., Oertner, T. G., Hegemann, P., and Larkum, M. E. (2016). Active cortical dendrites modulate perceptron. *Science* 354, 1159–1165. doi: 10.1126/science.aah6066

Treue, S., and Martínez Trujillo, J. C. (1999). Feature-based attention influencesmotionprocessing gain inmacaquevisual cortex. *Science* 399, 575–579.

Uhlhaas, P. J., Pipa, G., Neuenschwander, S., Wibral, M., and Singer, W. (2011). A new look at gamma? High- (>60 Hz) γ-band activity in cortical networks: function, mechanisms and impairment. *Prog. Biophys. Mol. Biol.* 105, 14–28. doi: 10.1016/j.pbiomolbio.2010.10.004

Vinje, W. E., and Gallant, J. L. (2000). Sparse coding and decorrelation in primary visual cortex during natural vision. *Science* 287, 1273–1276. doi: 10.1126/science.287.5456.1273

Vinje, W. E., and Gallant, J. L. (2002). Natural stimulation of the nonclassical receptive field increases information transmission efficiency in V1. *J. Neurosci.* 22, 2904–2915. doi: 10.1523/JNEUROSCI.22-07-02904.2002

Vonderschen, K., and Chacron, M. J. (2011). Sparse and dense coding of natural stimuli by distinct midbrain neuron subpopulations in weakly electric fish. *J. Neurophysiol.* 106, 3102–3118. doi: 10.1152/jn.00588.2011

Wachowiak, M. (2011). All in a sniff: olfaction as a model for active sensing. *Neuron* 71, 962–973. doi: 10.1016/j.neuron.2011.08.030

Webb, B. S., Tinsley, C. J., Barraclough, N. E., Parker, A., and Derrington, A. M. (2003). Gain control from beyond the classical receptive field in primate primary visual cortex. *Vis. Neurosci.* 20, 221–230. doi: 10.1017/s0952523803203011

Yu, N., Hupé, G., Garfinkle, C., Lewis, J. E., and Longtin, A. (2012). Coding conspecific identity and motion in the electric sense. *PLoS Comput. Biol.* 8:e1002564. doi: 10.1371/journal.pcbi.1002564

Conflict of Interest Statement: The authors declare that the research was conducted in the absence of any commercial or financial relationships that could be construed as a potential conflict of interest.

frontiers in Integrative Neuroscience

ORIGINAL RESEARCH
published: 02 October 2019
doi: 10.3389/fnint.2019.00055

A JAR of Chirps: The Gymnotiform Chirp Can Function as Both a Communication Signal and a Jamming Avoidance Response

*Caitlin E. Field[1,2], Thiago Alexandre Petersen[3], José A. Alves-Gomes[3] and Christopher B. Braun[1]**

[1] Department of Psychology, Hunter College, The City University of New York, New York, NY, United States, [2] New York City Department of Parks and Recreation, New York, NY, United States, [3] Laboratório de Fisiologia Comportamental e Evolução, Instituto Nacional de Pesquisas da Amazônia, Manaus, Brazil

The weakly electric gymnotiform fish produce a rhythmic electric organ discharge (EOD) used for communication and active electrolocation. The EOD frequency is entrained to a medullary pacemaker nucleus. During communication and exploration, this rate can be modulated by a pre-pacemaker network, resulting in specific patterns of rate modulation, including stereotyped communication signals and dynamic interactions with conspecifics known as a Jamming Avoidance Response (JAR). One well-known stereotyped signal is the chirp, a brief upward frequency sweep usually lasting less than 500 ms. The abrupt change in frequency has dramatic effects on phase precession between two signalers. We report here on chirping in *Brachyhypopmus* cf. *sullivani*, *Microsternarchus* cf. *bilineatus* Lineage C, and *Steatogenys* cf. *elegans* during conspecific playback experiments. *Microsternarchus* also exhibits two behaviors that include chirp-like extreme frequency modulations, EOD interruptions with hushing silence and tumultuous rises, and these are described in terms of receiver impact. These behaviors all have substantial impact on interference caused by conspecifics and may be a component of the JAR in some species. Chirps are widely used in electronic communications systems, sonar, and other man-made active sensing systems. The brevity of the chirp, and the phase disruption it causes, makes chirps effective as attention-grabbing or readiness signals. This conforms to the varied assigned functions across gymnotiforms, including pre-combat aggressive or submissive signals or during courtship and mating. The specific behavioral contexts of chirp expression vary across species, but the physical structure of the chirp makes it extremely salient to conspecifics. Chirps may be expected in a wide range of behavioral contexts where their function depends on being noticeable and salient. Further, in pulse gymnotiforms, the chirp is well structured to comprise a robust jamming signal to a conspecific receiver if specifically timed to the receiver's EOD cycle. *Microsternarchus* and *Steatogenys* exploit this feature and include chirps in dynamic jamming avoidance behaviors. This may be an evolutionary re-use of a circuitry for a specific signal in another context.

Keywords: electric fish, jamming avoidance response, hindbrain circuit, electric organ discharge, communication signals, pacemaker nucleus

OPEN ACCESS

Edited by:
Maurice Chacron, McGill University, Canada

Reviewed by:
John E. Lewis, University of Ottawa, Canada
Masashi Kawasaki, University of Virginia, United States

****Correspondence:***
Christopher B. Braun
cbraun@hunter.cuny.edu

Received: *14 May 2019*
Accepted: *09 September 2019*
Published: *02 October 2019*

Citation:
Field CE, Petersen TA, Alves-Gomes JA and Braun CB (2019) A JAR of Chirps: The Gymnotiform Chirp Can Function as Both a Communication Signal and a Jamming Avoidance Response. Front. Integr. Neurosci. 13:55. doi: 10.3389/fnint.2019.00055

INTRODUCTION

Gymnotiform fishes of South America produce rhythmic electric organ discharges (EODs) and can detect these fields with a specialized cutaneous electrosensory system (Zupanc and Bullock, 2005). The electric fields they generate are used in two ways: As a modality of intra-specific communication important for territoriality, courtship, and mating; and as the carrier signal for an active electrosensory system capable of imaging nearby objects (Caputi et al., 2002; Caputi and Budelli, 2006; Moller, 2006). These two functions, electrocommunication and electrolocation, may not be simultaneously compatible. The distortions to the carrier field used for electrolocation can be masked or otherwise degraded by the field of a nearby conspecific, a phenomenon known as jamming (Heiligenberg, 1986). Gymnotiforms first rose to prominence as an important model system because some species possess a stereotyped jamming avoidance response (JAR). Watenabe and Takeda (1963) and Bullock et al. (1972) described the JAR of *Eigenmannia* as a response to the presence of a nearby conspecific wherein the responding fish alters the rate of their ongoing EODs to minimize the impairment created by the conspecific's discharge. This reliable and experimentally tractable behavior has been used to determine and understand the circuitry of electrosensory analysis and the premotor and control circuits responsible for the resultant changes in ongoing EOD rate (Metzner, 1999; Rose, 2004).

In addition to the JAR, a wide range of patterned changes in EOD rate have been observed across gymnotiform species (Carlson, 2006). These electromotor behaviors are used as signals in a wide variety of communicative contexts, i.e., as adaptive stereotypic displays with specific signal functions. The best studied of these signals is the chirp, a very large transitory increase in frequency (Hopkins, 1974; Hagedorn, 1986, 1988; Dye, 1988; Shumway and Zelick, 1988; Kawasaki and Heiligenberg, 1989). The earliest observations of chirps were recorded during aggressive encounters (Bullock, 1969), but subsequent observations of chirps have shown them to occur also in reproductive and spawning behaviors as well (Hagedorn and Heiligenberg, 1985; Hagedorn, 1988). A large literature now contains a wealth of information and signal structure and functions in the gymnotiform family Apteronotidea (see Turner et al., 2007 for a systematic review), but there have been fewer studies in pulse-discharging gymnotiforms. Westby (1975) showed that the chirp is a signal mainly given by dominant *Gymnotus carapo*, and appears to often presage further aggression and can elicit submissive responses from a receiver. The more recent work on pulse gymnotiforms has elegantly demonstrated that there are specific functions for several structurally distinct chirp types in agonistic and territorial conflicts in *Gymnotus omarum* (Batista et al., 2012), and during reproductive courtship and male-male aggression in *Brachyhypopomus gauderio* (Perrone et al., 2009). This is consistent with the much larger literature on chirps in wave-type gymnotiforms, which documents a great deal of species variation in stereotyped chirp structure and their specific functions in intraspecific communication (Smith, 2013).

There is a deep phylogenetic and systematic split of gymnotiform fishes reflecting two modes of operation of the electric organ and electrosensory system (Zupanc and Bullock, 2005). The families Eigenmanniidae, Apteronotidae, and Sternopygidae are wave-type fish, with EODs that consist of roughly sinusoidal voltage modulations that are equal in duration to the length of the pacemaker cycle, creating a continuous discharge. The other gymnotiform families, Electrophoridae, Gymnotidae, Hypopomidae, and Rhamphichthyidae, are pulse-type fishes, with an EOD much shorter than the duration of the pacemaker cycle. There is great diversity across both wave and pulse type families (Crampton and Albert, 2006). In the Rhamphichthyidae, which includes the genus *Steatogenys*, EODs are generally short, around 1–2 ms, with very stable resting EOD rates between 40 and 80 Hz, although individual species typical rates may be as low as 20 Hz or as high as 120 Hz. The genera *Brachyhypopomus* and *Microsternarchus* are within the Hypopomidae, which also contains a wider diversity of EOD durations and pacemaker frequencies. The two species reported herein (*Microsternarchus bilineatus* lineage C (Maia and Alves-Gomes, 2012) and *Brachyhypopomus* sp. cf. *sullivani*) have EOD durations of ∼2–3 ms, with pacemaker frequencies between ca. 20–40 Hz in this species of *Brachyhypopomus* and 40–80 Hz in this lineage of *Microsternarchus*.

Since the majority of the EOD period is silent in pulse species, jamming interference by conspecifics is most detrimental when EODs coincide. Pulse species therefore modulate both the frequency and the relative timing of their EODs to minimize interference (Heiligenberg et al., 1978). Indeed, a major component of the pulse-type JAR is a brief rate increase that begins just before expected coincidence with the partner, resulting in fewer near-coincident EODs (Heiligenberg, 1980). Although evidence is limited to a few species, detection of other nearby objects is most impaired when a conspecific signal is presented immediately before or coincident with the animal's own EOD (Heiligenberg, 1974; Schuster, 2002). Conspecific EODs presented immediately after the animal's EOD have very little effect on electrolocation and this immunity to jamming persists through most of the silent inter-pulse interval (IPI). As conspecific EODs approach the later phases of the EOD cycle (just prior to the next EOD), the jamming interference again increases. This means that the most effective JAR behaviors minimize the time spent with detrimental phase relations. Effective JAR behaviors also likely depend on the ongoing pattern of phase precession to predict or judge the best time for a rate increase (Heiligenberg, 1980). This patterned phasic sensitivity to interference results (at least in part) from phasic changes in electrosensitivity (Westby, 1975; Castelló et al., 1998; Nogueira et al., 2006). The electrosensory system is most sensitive at the time of the animals' own EOD, with a sharp decline in sensitivity immediately afterward and throughout the middle of the cycle. Sensitivity gradually recovers to a peak levels a short time prior to the next EOD. This is congruent with the observation that the time immediately prior to the EOD and

perhaps briefly afterward is the most impacted by jamming interference (Heiligenberg, 1974). Conversely, the period of time after the EOD and continuing into the middle of the cycle is the least sensitive epoch and therefore most immune to jamming.

Electromotor behaviors that alter the phase precession immediately prior to or after a conspecific EOD are behaviors that manipulate jamming interference. This could also include specific signals (such as chirps) that are timed to maximize (or minimize) jamming interference or detectability based on phasic changes in receiver sensitivity. The exact duration of this sensitive time window is likely to be species specific, but we propose that discharges that occur within a 120° window surrounding coincidence are highly salient events for one or both members of a dyad. Prolonged periods of discharges within the window constitute jamming interferences. For a 50 Hz fish, 120° is equivalent to 6.7 ms. Events within the 60° window prior to a fish's own EOD are the most salient or potentially interfering and a time window beginning shortly after the EOD is the epoch most immune to interference. In a dyad, this is clearly reciprocal, fish A discharging just before fish B (in its most sensitive window) obviously means that fish B discharged immediately after fish A (in its least sensitive window). If this phase relationship were maintained over time, we would infer that Fish A is "jamming" fish B. Electromotor behaviors that minimize discharges in that time window can be interpreted as part of a JAR, while those that increase repeated discharges within the partner's most sensitive window may be active jamming maneuvers.

This phasic variation in sensitivity are important for understanding the impact of chirps on the receiver. The abrupt nature of chirps has large impact on phase precession between two fish. The immediate effect is a sharp change in the rather orderly phase precession between two close frequency partners. Regardless of chirp structure, this is likely to be very salient to the receiver, particularly if it results in the skipping of expected coincidences or consecutive EODs within the sensitive window. Further, if chirps result in EODs within the sensitive window of the receiver, this is likely to increase their salience.

In a series of studies on jamming avoidance behaviors, we observed chirps in *M. bilineatus* (lineage C) and in an undescribed species of *Steatogenys* (cf. *elegans*) obtained from the pet trade. This species of *Steatogenys* was unusual in that it occasionally exhibited small chirp-like behaviors spontaneously during isolated free exploration and more frequently during experiments where we presented synthetic conspecific EOD recordings. *Steatogenys* and *Microsternarchus* also showed clear evidence of chirps timed to specific phases of the stimulus cycle, and we present these in the context of putative jamming interactions. The present report describes the structure of chirps observed during conspecific playbacks in these two species as well as three individuals of a high-frequency species of *Brachyhypopomus* (cf. *sullivani)* from Amazonas state, Brazil. We describe the range of chirp structure observed, focusing especially on the resulting effects these chirps had in terms of the phase relationship with the synthetic conspecific partner.

MATERIALS AND METHODS

The subjects used in this study were hand collected in Amazonas state, Brazil, or imported through the pet trade in the United States, using exporters from Iquitos, Peru. Two different groups of *Steatogenys* were acquired through the pet trade, using the same US importers and Peruvian exporters, and were presumed to have been collected in similar localities. The first group was used in the experiments with varying playback frequencies and the second group was used in another experiment where stimulus EOD duration was manipulated. Subjects purchased from exporters were allowed to acclimate in group tanks at Hunter College for at least 2 weeks prior to testing. Subjects were also captured by hand net along the margins and banks of the Rio Negro and its tributaries in accordance with Brazilian laws and under ICMBIO permit #14833-1 to JA-G. Following capture, subjects were transported to the Laboratory of Behavioral Physiology and Evolution (LFCE) at INPA. These subjects were also maintained in group housing and tested between 2 and 4 weeks following capture. Sex and other aspects of physical condition are summarized in **Table 1**. All experiments were conducted in accordance with the Institutional Animal Care and Use Committee of Hunter College, CUNY, and the Ethical Committee for Animal Research of INPA.

The data presented in this report are selected from a larger database of responses to conspecific playback in pulse gymnotiform species. In this report we include only individuals that displayed a behavior known as chirping and will confine our analysis to those chirps. A fuller treatment of all behaviors exhibited in these experiments is forthcoming.

Behavioral Testing Apparatus

Animals were placed in a small plastic mesh cylinder and suspended centrally in a rectangular glass tank (25 × 40 × 20 cm) filled with roughly 14 cm of water. Subjects generally remained motionless in the tube, but the tube was sometimes closed with cloth screening if animals did not settle immediately in the tube. The recording electrodes were 8 cm carbon rods (5 mm diameter) or five loops of silver wire around a 5 mm plastic rod, located at opposite ends of the tank in parallel to the longitudinal axis of the subject. The stimulating electrode was a dipole electrode composed of either two carbon rod nubs, approximately 5 mm each, separated by 3 cm or a pair of silver electrodes separated by one half the subject body length. This stimulating electrode pair was suspended from above the tank and could be placed above the shelter, 2–4 cm from the subject's head. During calibration of the stimulus, the electrode was rotated to parallel the recording electrodes and the subject fish, just below or above the center of mass of the subject (usually 3–4 cm behind the tip of the nose). After calibration, the electrode was kept in the same position, but rotated to approximately 15–20 from perpendicular to reduce but not eliminate the S2 recording. The entire aquarium and electrode assembly was mounted within a grounded aluminum box or a grounded single-walled sound attenuating chamber. The signal from the recording electrodes was amplified 50–500× (CWE BMA-200 or AM Systems 3000) and digitized at 48828.125 kHz

TABLE 1 | Subject data.

Subject	Sex	Resting *F* in Hz (SE)	Length (cm)
Steat_012	M	56.11(0.08)	18.0
Steat_014	M	49.16(.09)	17.5
Steat_015	F	55.59(0.25)	17.0
Steat_003	NA	63.73(0.24)	17.0
Steat_029	F	57.48(0.09)	19.0
Steat_036	M	59.98(0.19)	18.5
Steat_042	F	51.41(0.16)	15.5
Steat_040	NA	53.19(0.16)	18.0
Steat_017	NA	57.37(0.28)	16.0
Steat_024	NA	62.67(0.16)	16.0
Steat_018	F	52.14(0.29)	15.0
Steat_044	F	48.18(0.28)	17.5
Steat_001	F	54.56(0.26)	17.0
Steat_011	F	65.11(0.15)	16.0
SteatYC_1	F	52.05(0.39)	21.5
SteatYC_2	M	55.86(0.59)	19.0
SteatYC_3	F	59.74(0.16)	20.0
SteatYC_4	M	57.62(0.31)	21.5
SteatYC_5	M	64.44(0.46)	18.0
SteatYC_6	M	48.72(0.09)	15.5
SteatYC_7	M	58.62(0.59)	22.6
SteatYC_8	M	66.29(0.71)	21.0
Micro_01	M	62.31(0.46)	9.7
Micro_02	F	73.57(1.06)	8.6
Micro_03	M	55.04(0.78)	7.2
Micro_05	F	44.1(0.11)	7.5
Micro_06	F	48.98(0.32)	8
Micro_07	F	55.91(0.29)	8.5
Micro_09	F	58.31(0.13)	7.5
Micro_10	M	86.4(0.34)	8
Micro_11	F	58.6(0.69)	7.6
Micro_12	M	49.44(0.3)	10.5
Micro_13	F	66.57(0.31)	12
Micro_15	M	57.19(0.24)	12.4
Micro_16	F	58.01(0.37)	11.7
Micro_17	F	57.31(0.21)	10.6
Micro_18	F	40.62(0.16)	7.5
Micro_19	F	52 9 (0.14)	11
Micro_21	F	74.1(0.29)	11
Micro_22	M	58.85(0.15)	7.5
Micro_23	F	56.44(0.1)	7
Micro_24	F	56.80(0.19)	7.5
Micro_25	M	43.05(0.11)	8
Micro_26	F	52.4(0.09)	8
Micro_27	F	54.7(0.09)	7.5
Micro_28	F	49.10(0.11)	7.5
Brachy_06	NA	28.23(0.08)	8
Brachy_08	NA	22.52(0.21)	8
Brachy_09	NA	21.46(0.13)	8
Brachy_10	NA	46.36(1.03)	7
Brachy_11	NA	27.23(0.17)	7
Brachy_12	NA	37.71(0.28)	9
Brachy_13	NA	24.56(0.17)	9.5

Tabular presentation of subject characteristics. Resting EOD frequency was measured during inter-trial intervals of stimulation experiments (see text).

using a Signal Processor (Tucker-Davis Technologies, Aluacha, FL, United States: either RM2.1, RP2.1, or RX6) connected to a windows computer. An isolation transformer was placed between all other equipment and the stimulus electrodes. All experiments and data analyses were conducted with custom routines in Visual Design Studio (Tucker-Davis Technologies) and Matlab (Mathworks, MA, United States). The signal processing system recorded both the analog waveform of the EODs during the experiment and determined the interpulse interval (IPI) of each EOD of the subject using spike timing algorithms and a voltage trigger. For measurements reported here, we measured the EOD timings directly from the analog waveform using spike detection routines in Matlab. EOD timings were collected by the signal processing computer as a record of IPIs during the pre- and post-trial periods.

As soon as visible agitation ceased and the subject (S1) began to acclimate to their surroundings (usually within 5–10 min), a recording of the animal's EOD was digitized to be used as the synthetic conspecific, or S2. Software settings were manually adjusted to calibrate delays and amplification of the S2 during single S2 presentations at the midpoint of the subject's IPI. The amplitude of the S2 was adjusted to 80–100% of the subjects EOD peak-peak amplitude (recorded through the same electrodes with the same amplification). The precise timing of the S2 was adjusted while shorting the stimulus electrode circuit (preventing delivery to the tank) and monitoring the timing of the recorded S1 and synthetic S2 on an oscilloscope. Equivalent phases of the S1 and S2 were matched to within 10 μs during testing at zero latency. Finally, the circuit was re-completed and the electrode position was rotated to minimize the recorded amplitude of the S2 stimulus artifact. The subject was allowed to continue acclimation for at least 15 min after calibration.

This study describes responses that occurred during S2 playback at a fixed frequency. For each trial, the S2 frequency was set relative to the subject's frequency at the start of the trial. This initial frequency difference (dF) ranged from −16 to +16 Hz from the subject baseline and playback lasted either 10 or 15 s.

In a subset of the *Steatogenys* individuals, the S2 EOD duration was manipulated and tested at several dFs. Subjects were exposed to six different EOD durations at each tested dF, including two EODs shorter than their own and three longer EOD lengths. Individuals of *Brachyhypopomus* were exposed to three replications of each stimulus type, and individuals of *Microsternarchus* and *Steatogenys* were tested with five replications of each stimulus type. Stimulus presentation order was randomized and included inter-trial breaks of 1–3 min.

Baseline Measurements

All trials were conducted during the subjects' quiescent daytime period. We did not systematically control for time of day, but most experiments were conducted in a period from 4 h after lights-on to 2 h before lights-out. This was done primarily of convenience, but also because animals are extremely active during night hours and would resist confinement and present movement artifacts. While behavioral differences may be expected during more active periods, there was no shortage of electromotor responses from these quiescent subjects. It

is notable that all three species tolerate large groups and probably rest in closely packed groups during the day. We used approximately 1 min of IPI recordings from each intertrial period during all experiments to estimate baseline frequency and IPI variability measurements for all subjects at the time of testing (reported in **Supplementary Table S1**). For each subject, we averaged all 1 min samples.

Data Analysis

All data analysis was performed in Matlab version 2018b (Mathworks) or R (R Core Team, 2014) using publicly available packages and custom routines. We utilized the circular statistics toolbox available from the Matlab File Exchange (Berens, 2009) and PMCMR (Pohlert, 2014) for non-parametric and repeated measurements. Data with non-normal or heterogeneous variance were ln-transformed or analyzed with non-parametric tests. Multiple pairwise comparisons were performed with Bonferroni corrections.

Prior to all measurements, we digitally removed the S2 stimulus artifact using an inverted S2 waveform and the programmed S2 timings. We then used peak detection to measure the occurrence of each S1 EOD and its latency to the preceding S2. All phase angle measures were expressed relative to the fixed S2 period. The S1 timings were also converted to instantaneous measures of S1 frequency and dF (which varied from the constant initial dF as the subject altered their own EOD rate). From the S1 frequency, we derived the instantaneous change in IPI duration for each EOD interval, expressed as a percent reduction in duration for each interval relative to the interval before (rIPI). This measure is generally quite small ($<1\%$, see section "Results") and is useful for locating abrupt changes in pacemaker rhythm lasting for only a few intervals, such as chirps.

Chirp Measurements

Chirps were recognized by large instantaneous increases in EOD rate. We analyzed all instances where rIPI was greater than 10%, that is all cases where the IPI decreased by more than 10% from one interval to the next (25% for *Brachyhypopomus*). For each chirp, we measured the phase angle of the first EOD in the chirp and its latency to the first delivered S2. We defined the start of the chirp as the first un-distorted EOD that begins an IPI that is at least 10% shorter than the preceding IPI. After recognition of the chirp, rIPI and amplitude reductions were measured against a baseline of the mean of three EODs prior to the chirp, or following the chirp if it occurred in the first five intervals of the trial (as was often the case in *Steatogenys*). In *Brachyhypopomus*, nearly all chirps were followed by a prolonged period of stable high frequency discharges (higher than the frequency prior to the chirp, but still much lower than frequencies achieved during the chirp). Subjects returned to a new stable frequency 20–100 ms after the last very high frequency intervals. We defined the end of the chirp as the moment when S1 frequency declined to within 10% of the post-chirp rate (measured at steady-state, at least 50 ms later). As illustrated in **Figure 1A**, we based our subsequent analyses on chirp duration (both number of pulses and time), maximum reduction in IPI, maximum reduction in EOD amplitude and the time to each of these latter two measures.

Tumultuous Rise Definition

Some chirps in *Microsternarchus* occurred in the context of a large rise in baseline frequency. Algorithmically, we recognized tumultuous rises when the time-averaged coefficient of variation (CV) was greater than 5 (reflecting many chirp-like intervals) and the baseline frequency increased by more than 25%, with both conditions remaining true for more than 500 ms. The baseline frequency was averaged in windows of 20 intervals and CV was measured in blocks of 200 ms, with 50% overlap between blocks. The end of the rise was marked at the point the frequency returned to within 5 standard deviations (SD) of the pretest frequency.

Jamming Index

To quantify the relative interference between the S1 and S2, we computed a jamming index that reflects asymmetry in the reciprocal phase relations between two fish. The jamming index was calculated by subtracting the proportion of S1 EODs that occur within 60° after the S2 from those S1 EODs occurring 60° prior to the S2 (using the total number of S1s within 120 of the S2 as the denominator in both cases). This results in an index from −1 to 1, with 0 reflecting an even distribution of S1s prior or subsequent to the S2. A jamming score of −1 indicates that all S1s in the critical window of −60° to 60° are subsequent to the S2s, meaning S1 is suffering great potential interference, while S2 is free of it. A score of 1, conversely indicates that all S1s are occurring prior to the S2, so S1 is free of interference and S2 is being jammed. We calculated jamming ratios for all trials that contained repetitive chirp-like intervals and tumultuous rises, using a sliding 400 ms measurement window, with 50% overlap between windows. To assess the statistical significance of this index, we generated 10000 uniform distributions of phase angles for matching numbers of S1 pulses in each time window. The standard deviation of the resulting shuffled jamming indices was used to convert each measured jamming index to Z-scores. Jamming indices with Z-scores greater than 1.96 were interpreted as significant measures of non-reciprocal jamming interference.

RESULTS

We observed chirps in a range of controlled and uncontrolled settings. The following description is based on recordings from two distinct behavioral experiments, one in which only the frequency of the stimulus fish (S2) was systematically varied, and one in which the duration of the S2 EOD was systematically varied and presented at a range of fixed S2 frequencies (dF = 0, ±0.5, ±1, ±5, ±8, ±16 Hz). All observations of *Microsternarchus* (subject N = 12, chirp N = 2555) and *Brachyhypopomus* (N = 3 and 58) were recorded during the S2 frequency experiments. Observations of *Steatogenys* chirps were taken from two groups of subjects, one group tested in the S2 duration experiments (subject N = 7) and another group tested in S2 frequency experiments (N = 14). In the presentation of chirps in *Steatogenys* in comparison to the other two species, the individuals from both experiments were pooled (N = 21; chirp N = 1314). Analysis of responses as a function of S2 frequency or duration, as well

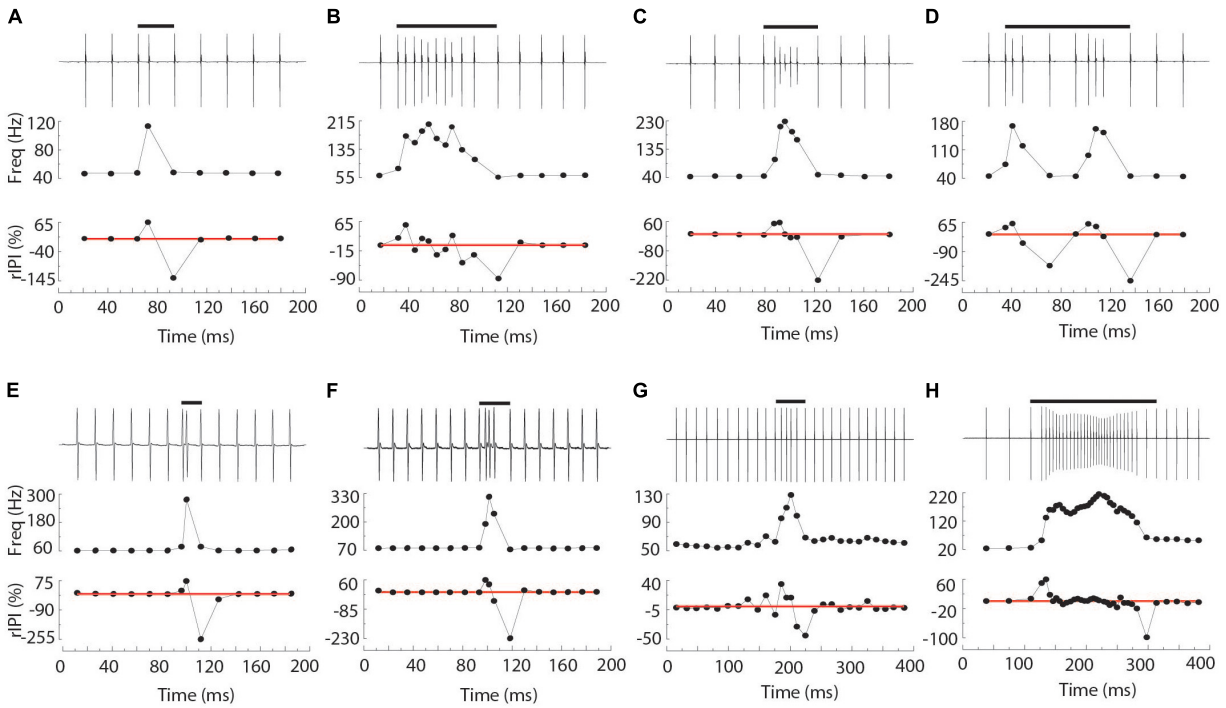

FIGURE 1 | Representative chirps from *Steatogenys* **(A–D)**, *Microsternarchus* **(E,F)**, and *Brachyhypopomus* **(G,H)**. In all panels, the upper trace shows the recordings of the chirp and several preceding and subsequent intervals. The total chirp duration is marked by the horizontal black bars. The lower subpanels show the instantaneous frequency of all intervals shown and their relative reduction from baseline (IPI r) as a percentage. The thin red lines are plotted to highlight the axis position of 0% changes from baseline.

as other behavioral responses to conspecific stimuli, will be presented in a subsequent publication.

Chirp Structure

Chirps are distinct from other electromotor behaviors in their abruptness. That is, chirps contain dramatic modulations that reach their maximum within a very small number of EOD intervals. We recognized chirps by the magnitude of interval-to-interval reduction in duration (rIPI). In baseline measurements (in the absence of chirps), the *Steatogenys* subjects had a mean rIPI of 0.0062%, with a standard deviation of 0.27. *Microsternarchus* subjects had a mean rIPI of 0.0022% (SD = 0.005). *Brachyhypopomus* subjects had a mean rIPI of 0.0297%, with a SD of 0.01. A large frequency shift during jamming avoidance or a startle response may have a peak rIPI of ca. 5%, with the majority of electromotor behaviors comprised of changes of less than 1 or 2% and persisting over more than 10 intervals. This is especially true for highly regular species like *Microsternarchus* and *Steatogenys*. Chirps were easily recognizable because they included extremely sudden instantaneous changes (rIPI > 10%). Large gradual frequency shifts in *Brachyhypopomus* may include rIPI values of 5–10%, so we used a higher chirp threshold of 25% rIPI in this species.

We observed chirps in a subset of individuals in all three species (S: 21 of 30 individuals tested in similar conditions; M: 12 of 24; B: 3 of 7). The three chirping individual *Brachyhypopomus* were undifferentiated and sex could not be determined. The majority of individuals were immature (stage 1 or 2), and only one male *Steatogenys* (SteatYC2) was stage 3 mature (following Crampton and Hopkins, 2005). Males, females and immature individuals of *Microsternarchus* and *Steatogenys* all chirped. We found no detectable statistical difference between sexes in numbers of chirps, chirp duration or reduction in either IPI or amplitude (Wilcoxon rank sum, all $p > 0.05$). In *Microsternarchus*, we also failed to find any significant correlation between chirp numbers, duration or modulation of IPI and amplitude with subject length (Spearman Rank, all $p > 0.05$). We had a greater range of size and maturity in *Steatogenys* and the most mature males (SteatYC2 and SteatYC7) were prolific chirpers, but there was no correlation between animal size and numbers or chirps or chirp durations in this species either. There was, however, a modest relationship between the amount of modulation within the chirp and animal size. Reduction of IPI was significantly correlated with animals size ($r^2 = 0.28$, $p < 0.05$), as was peak frequency ($r^2 = 0.48$, $p < 0.01$), and rAMP ($r^2 = 0.25$, $p < 0.05$).

Chirps in both *Microsternarchus* and *Steatogenys* were short, with two to six EODs comprising a chirp in *Microsternarchus* and two to 11 EODs in *Steatogenys* (**Figure 1**). *Microsternarchus* chirps were more stereotyped, with the majority (67.5%) comprised of a single interval shortened by an average of 44.1% (**Figures 2**, **3**). Reduction of EOD amplitude during the chirp was generally small, with a maximum of 17.3% (**Table 2**). The shortened chirp intervals were immediately followed by a

period of stable discharge rates similar to the preceding baseline frequency. Chirps in *Steatogenys* were also mostly short, with 45.8% comprised of a single interval shortened by an average of 27.9% from the preceding interval. As in *Microsternarchus*, shortened chirp intervals in *Steatogenys* are immediately followed by a resumption of regular discharges similar to the preceding rate (**Figure 1**). In the combined sample of *Steatogenys*, there was a relationship between chirp length and individual size, with the largest individuals displaying longer chirps with more complex patterns of amplitude and interval reduction (**Table 2** and **Figure 2**). In **Figure 2**, which shows the relationship between the numbers of EODs in a chirp and other chirp metrics, the group of smaller individuals (S2 dF experiment) was plotted as red dots. Chirps recorded from these individuals were generally smaller in all metrics we applied, but it should be noted that all individuals displayed an overlapping range of chirp intensities. Similar plots separated by individuals are shown in **Supplementary Figure S1**.

Brachyhypopomus chirps were longer, with at least six shortened intervals, usually with modest EOD amplitude reduction that increased gradually to a maximum near the midpoint of the chirp and gradually returned to full amplitude by the end of the chirp. Following the chirp, subjects gradually returned to a new baseline rate substantially higher than the preceding rate. IPI modulations were much greater in this species, with a mean IPI decrease of 82.3% and mean amplitude reduction of 27.5%.

The duration of each chirp is a product of the number of modulated EOD cycles, the underlying base frequency, and the degree of IPI reduction. This complicates comparison across species that differ in typical rates, as is the case for the three species herein. Since all of the chirps we analyzed were recorded during interactions with a synthetic conspecific, we translated chirp duration to a measure that reflects the perceptual experience of the chirp recipient. That is, we divided the chirp duration (in seconds), by the duration of a single S2 interval and converted the result to degrees of phase. This measure allows the comparison of chirps in units of S2 cycles (i.e., 360° per cycle), and these results are shown in **Figure 3**. In these terms, each chirp generally interacts with a small number of S2 cycles, from 1 or 2 in *Microsternarchus*, 1–5 *Steatogenys*, and 1–9 in *Brachyhypopomus* (although most chirps interact with fewer than five S2 cycles in this species as well).

Regardless of units, chirp durations were significantly different across individuals of these three species. A Kruskal–Wallis test found significant differences between all three species ($\chi^2(2) = 69.386$, $p < 0.001$), with significant pairwise differences between all pairs ($p < 0.001$). Predictably, the same result was found when this test was applied to chirp durations expressed as either S2 cycles ($\chi^2(2) = 111.928$, $p < 0.001$) or as EODs per chirp ($\chi^2(2) = 75.364$, $p < 0.001$), again with all pairwise comparisons being significantly different ($p < 0.001$).

The most prominent feature of chirps is the IPI reduction, but the magnitude differed greatly across species ($\chi^2(2) = 40.44578$, $p < 0.001$). *Brachyhypopomus* chirps had a greater reduction of IPI than chirps in either of the other two species ($p < 0.001$), but the distributions of rIPI were overlapping in *Microsternarchus* and *Steatogenys* and not statistically distinct. In frequency terms, however, the peak frequency (i.e., the inverse of the shortest chirp interval) did differ in all pairwise comparisons ($\chi^2(2) = 44.709$, $p < 0.001$: *Steatogenys* vs. *Microsternarchus* $p < 0.05$; *Brachyhypopomus* vs. either species $p < 0.001$).

In all three species, the individual EODs within a chirp were often reduced in amplitude (see **Figures 1**, **2**). Median EOD amplitude reduction was greatest in *Brachyhypopomus* (27.4%), and substantially less dramatic in both *Microsternarchus* (0.89%) and *Steatogenys* (1.8%). Although the median amplitude drop was similar in these two species, there was a much greater variability of EOD reduction in *Steatogenys*, possibly reflecting a wider range of subject maturity in those subjects All pairwise comparisons of amplitude reduction were significantly different between species ($\chi^2(2) = 44.670$, $p < 0.001$).

All three of these aspects of chirp structure, duration (regardless of units), IPI reduction (and max frequency), and EOD amplitude reduction, are tightly interdependent (**Figure 2**).

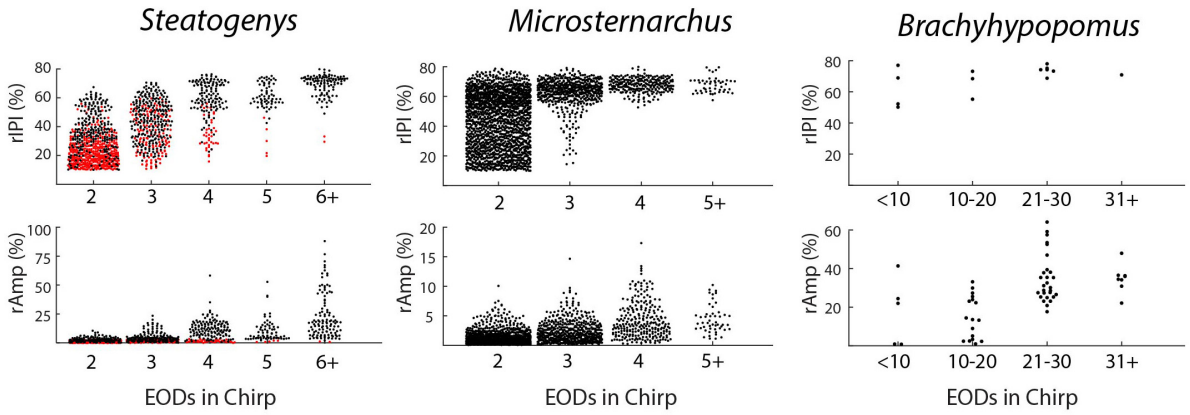

FIGURE 2 | Beeswarm plots of chirp parameters for all three species. The **upper** and **lower** panels depict the distributions of maximum IPI reduction and EOD amplitude reduction, respectively, each plotted as separate distributions according to the number of EODs comprising the chirp. In the *Steatogenys* panels, red circles indicate chirps recorded from the dF experiment group and black circles indicate chirps recorded from the EOD duration experiment group.

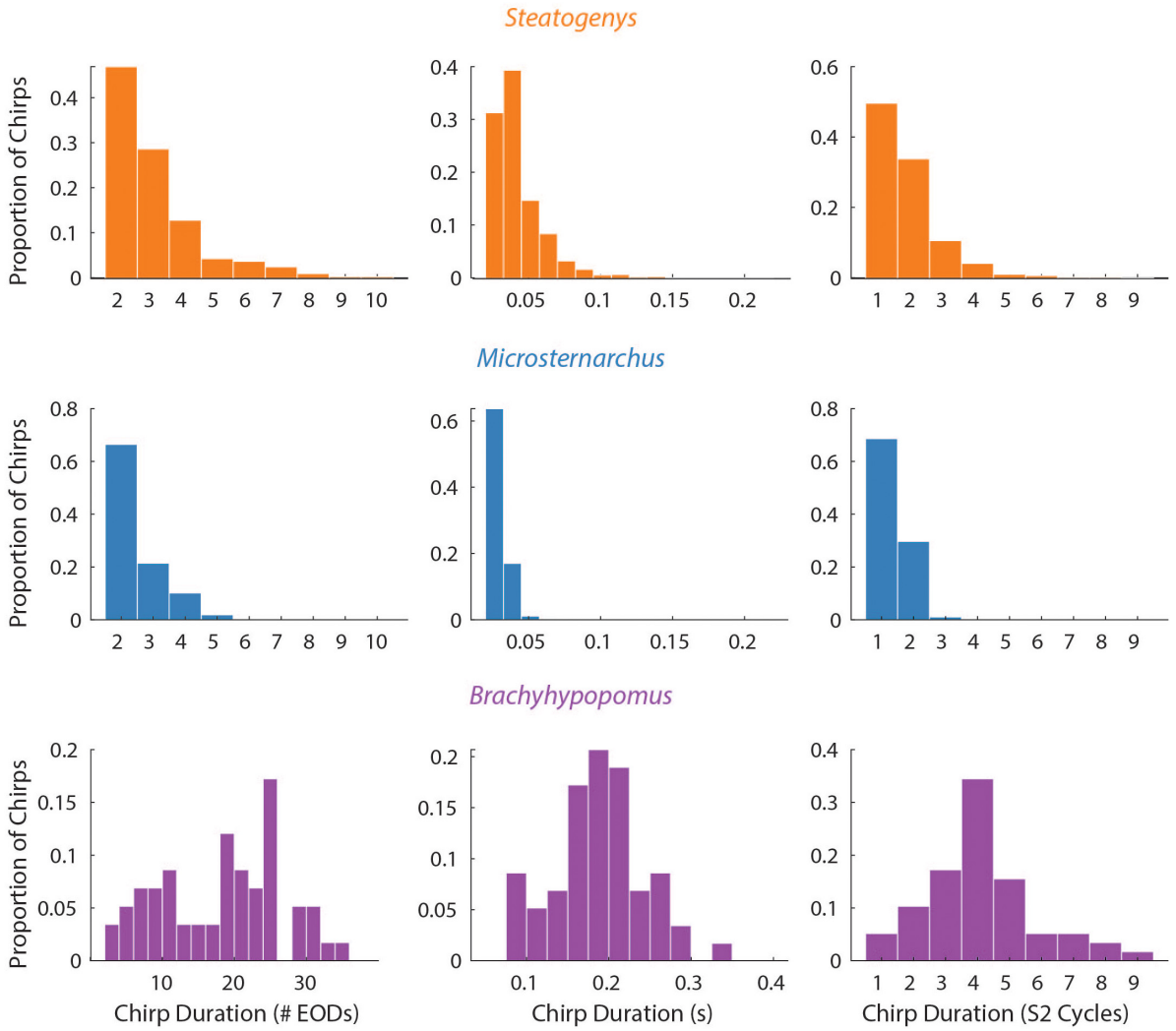

FIGURE 3 | Probability histograms of all chirps (pooled) in all three species, plotted in terms of three measures of chirp duration: number of EODs (left), time (middle), and number of S2 cycles affected (right). Chirp duration expressed as S2 cycles were the only metric that allows comparison across species on the same scale.

Both IPI reduction and amplitude reduction increased as chirps got longer, but the distribution of amplitude reductions also widened. Many long chirps had little or no amplitude reduction and some short chirps had greatly reduced EOD amplitudes (see **Figures 1B,D** for examples, and **Figure 2**).

The Chirp and Disruption of Phase Precession

The interference pattern of two individuals with closely matched frequencies consists of a stable precession of phase relationships, particularly in gymnotiforms with very regular rates, like *Microsternarchus* and *Steatogenys*. The large abrupt changes of chirps created particularly prominent breaks in phase precession (**Figure 4**). This was especially true of longer chirps, during which each successive EOD in the chirp occurred at scattered (and presumably unpredictable) phases across multiple S2 cycles. In *Microsternarchus*, with the shortest and most stereotyped chirps, the break in phase precession was the most prominent effect of the chirp. In *Steatogenys* chirps, with some variability of IPI within a chirp, this resulted in a scattering of S1 EODs across a few S2 cycles (**Figures 4B,C**). In *Brachyhypopomus*, which had more consistent rates during the chirp, the phase precession during the chirp appears regularized, reflecting a typical precession between partners with a large frequency difference (**Figure 4D**). This also had the effect of increasing the number of consecutive EODs within the partner's sensitive jamming window.

Chirp Occurrence Patterns and Timings Relative to the S2

In *Brachyhypopomus*, chirps occurred as single events (sometimes multiple times in a single trial) or in groups with an extended period of high frequency baseline between chirps. Of 58 chirps observed, 18 (31%) occurred as single

TABLE 2 | Summary statistics of chirp metrics in the three genera.

	# Chirps	Chirp metrics Mean (SD) (min–max)						
		Duration						
		EODs in chirp	Time (s)	# S2 cycles	Starting phase (°)	rIPI (%)	pkF (Hz)	rAmp (%)
Steatogenys	62.571 (62.092) (1–203)	2.610 (0.718) (2–4.537)	0.038 (0.007) (0.025–0.057)	2.158 (0.317) (1.629–2.906)	214.918 (85.798) (22.254–320.040)	31.421 (14.855) (13.266–69.737)	91.636 (27.519) (68.794–159.787)	3.161 (5.241) (0.323–23.0523)
Microsternarchus	212.917 (358.350) (5–1232)	2.231 (0.237) (2.044–2.825)	0.031 (0.005) (0.023–0.041)	1.748 (0.181) (1.438–1.983)	233.317 (126.746) (43.336–359.853)	41.961 (9.522) (23.499–58.810)	121.195 (39.619) (67.749–224.623)	1.503 (1.380) (0.499–5.609)
Brachyhypopomus	19.333 (18.037) (2–38)	21.135 (1.540) (19.667–22.737)	0.193 (0.023) (0.170–0.217)	4.619 (0.670) (4.160–5.388)	150.762 (82.553) (100.903–246.052)	83.598 (4.017) (79.813–87.812)	196.370 (14.188) (187.872–212.748)	25.541 (8.924) (15.678–33.057)

For each genus, the table provides the mean, standard deviation, and range for numbers of chirps recorded per individual, with combined averages for all other chirp metrics. The individual subject means are given in ***Supplementary Table S1****.*

events in a trial. The remainder of chirp observations occurred in trials with more than one chirp, with an average of 2.5 chirps per trial (0.17 chirps/second). Chirps did not occur uniformly throughout the trials, but rather in clusters of 2–6 chirps, with an average spacing of 2.7 s between chirps. In trials with several chirps, they often occurred at consistent phase angles throughout the trial (the mean SD of phase angles within a trial was 62.5°). The distribution of mean phase angles in these 34 trials is shown in **Figure 5**.

This distribution had a mean starting angle of 104.5° (SD = 93.6°), but could not be distinguished from a null hypothesis of uniform distribution (Rayleigh test $r = 0.26$, $p > 0.05$).

In the other two species, subjects chirped in a number of distinct patterns through the 10 or 15 s stimulus presentations. In both *Microsternarchus* and *Steatogenys*, it was common for a trial to contain multiple repetitive chirps with inter-chirp intervals roughly equal to the S1–S2 beat cycle duration. In both species, chirps often occurred once per beat cycle, with consistent phase timing for each chirp (**Figure 6**). The specific phase angle of chirps within a trial differed between trials, and varied from moment to moment within a trial, but repeated chirps often occurred at consistent phase angles for each beat cycle for a periods of 1–3 s of these trials. The duration of the beat cycle is the inverse of the frequency difference between the two signals, so inter-chirp intervals were dynamically matched to the frequency difference between the two signals, despite variation in S2 frequencies across trials.

In *Microsternarchus*, chirps nearly always occurred in multiples. Of 2555 chirps observed, only 34 (0.01%) occurred as single events in a 15 s stimulus presentation. Multiple chirps occurred in 169 stimulus trials, with a mean of 14.9 chirps per trial (range = 2–118). In many instances, chirps occurred at consistent phase angles, with chirps at the same phase of every beat cycle (**Figure 6B**) for periods of several seconds (mean SD within trials was 64.7°). The distribution of mean phase angles per trial (**Figure 5**) was significantly concentrated around a mean vector 358.4° (SD = 92.9°, Rayleigh test $r = 0.27$, $p < 0.001$), or just prior to the next S2. The dispersion indicates that the mean phase angles of most trials clustered either immediately before or after the S2.

The number of chirps in individual trials was too low to apply inferential statistics, but we analyzed the distribution of chirp angles for each individual, pooled across all trials. Six individual *Microsternarchus* had a significant concentration of phase angles ($p < 0.05$) and these distributions are shown in **Supplementary Figure S2**. The concentration of these distributions was weak ($r < 0.41$), but show a general tendency to avoid mid-cycle chirps, with a mean of 341.5° (SD 44.6) (**Supplementary Figure S2**).

Several individual *Microsternarchus* also produced chirps in rapid succession, with multiple chirp-like intervals per S2 cycle separated by only a few "normal" intervals between chirps (**Figure 7B**). This occurred with sometimes with minimal change to baseline frequency or with large increases. These events will

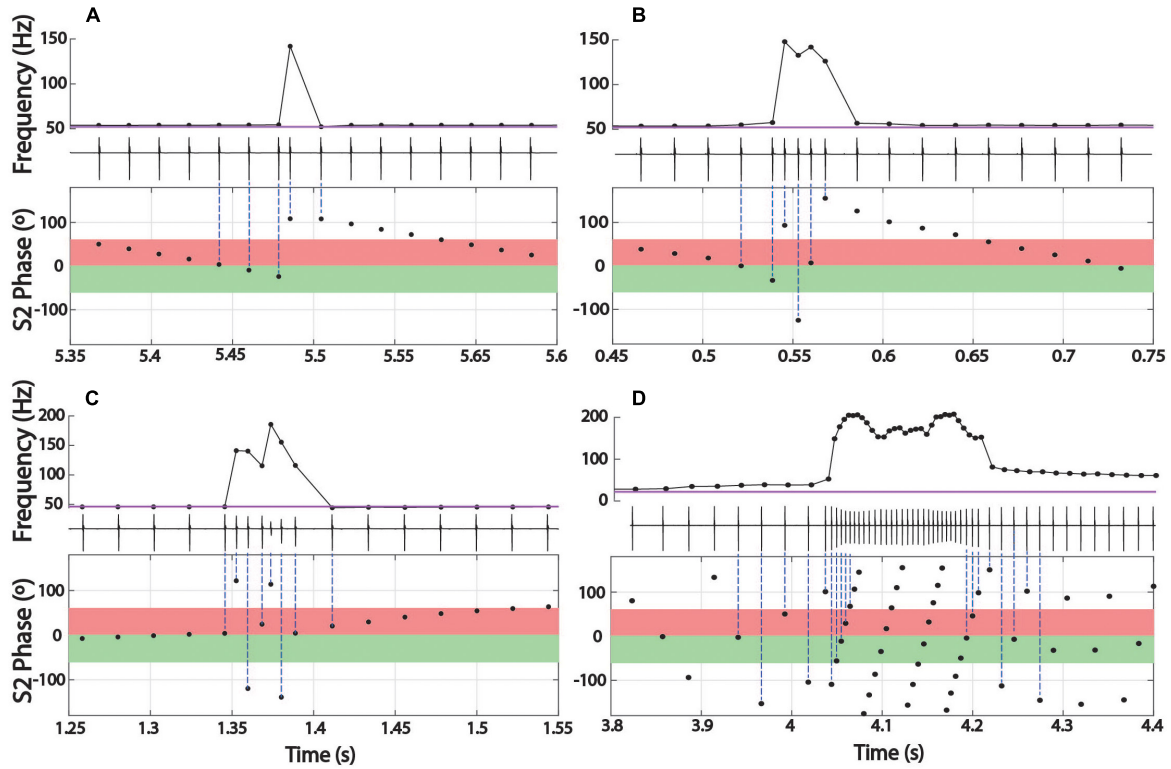

FIGURE 4 | Phase precession during chirps. Three representative chirps in *Steatogenys* are shown, simple **(A)**, long **(B)**, and complex **(C)**. A representative chirp from *Brachyhypomous* is shown in **D**. In each panel, the top subplot shows the instantaneous frequency, with the oscillogram trace directly below. The bottom subplot shows the phase of each S1 EOD with respect to the stimulus (S2). Each EOD is represented by a black circle, with dotted lines connecting to the chirp EODs for reference. The S2 frequency is depicted in the frequency plots by the horizontal purple line. In the phase plots, the 60° window before and after the S2 EODs is indicated by green and red boxes, respectively.

be described below, as burst-chirping and tumultuous rises, respectively. *Steatogenys* did not display burst-like repetitive chirping, although some long chirps could be interpreted as multiple chirps with very little time separation between them (e.g., **Figure 1D**) or possibly as an immature example of a longer chirp.

Aside from the absence of rapid repetitive chirping, *Steatogenys* chirping behavior was similar to *Microsternarchus* in that multiple chirps in a single trial were matched to the beat frequency and frequently occurred at similar phase angles (mean SD of individual trials was 52.2°). Of the 1314 chirps included in this analysis, 529 (40.2%) occurred as a single chirp in a 10 s stimulus presentation. The remaining 59.8% of chirps occurred as repeated events within a single trial (232 trials). These trials contained a mean of 3.4 chirps per trial (range: 2–11). The mean starting phase of chirps across trials in *Steatogenys* was directed around a mid-cycle mean of 218.4° (SD = 117.0°), but the concentration was weak (Rayleigh test $r = 0.12$, $p < 0.001$). In trials that only contained a single chirp (**Figure 5D**), the distribution of phase angles was uniform ($r = 0.07$, $p > 0.05$). For trials that contained multiple chirps, however, the mean start phases were more narrowly directed around a mean of 229.5° (SD = 93.6°, $r = 0.26$, $p < 0.001$, **Figure 5E**), or slightly past the mid-point of the S2 cycle. This tendency was also apparent in the chirp angles pooled across trials for each individual (**Supplementary Figure S2**). Fifteen individual *Steatogenys* (of 21 that chirped) exhibited a significant concentration of phase angles across trials (**Supplementary Figure S2**). Unlike the late-cycle chirps of *Microsternarchus*, most *Steatogenys* subjects chirped closer to mid-cycle, with a mean concentration of these chirps were concentrated just after the mid-point of the cycle, with a mean S2 angle of 233.2° (SD = 49.8°).

We also noticed that many *Steatogenys* trials included a short latency chirp, very quickly following the first S2 presentation. Of trials that contained chirps, 22.8% had a chirp within 100 ms following the first S2 (mean latency = 49.7 ms). In many cases, the chirp occurred immediately, with only one "normal" interval between the first S2 and the start of the chirp. Two examples of very short latency chirps are shown in **Figure 5F**). This was not observed in the other two species. Behavioral responses did occasionally occur within the first 100 ms in the other two species, but these were infrequent and there were none that occurred earlier than 50 ms after the first S2.

Steatogenys was also unique among the species studied in that we observed isolated individuals chirp without an apparent eliciting stimulus. We have observed some

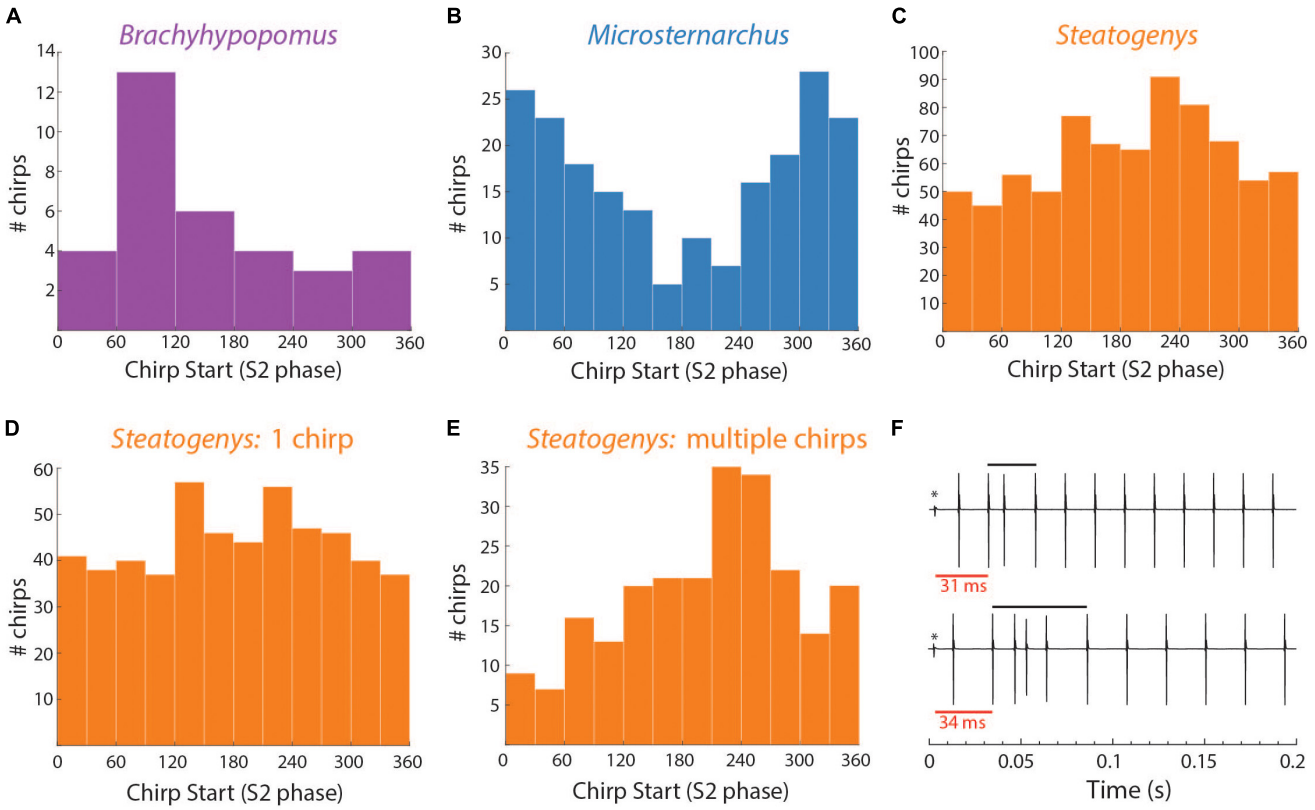

FIGURE 5 | Distributions of chirp starts in terms of S2 phase **(A–E)** and examples of early latency chirps in *Steatogenys* **(F)**. **(A–C)** Overall distribution of mean chirp starting phases for *Brachyhypopomus*, *Microsternarchus*, and *Steatogenys*. **(D,E)** The distribution of chirp phase angles in *Steatogenys* subdivided by trials that contain only a single chirp **(D)** vs. the distribution of chirp phase angles in trials where there is more than one chirp **(E)**, showing a significant concentration of phase angles around 240°. **(F)** Examples of short latency chirps in *Steatogenys*. For illustrative purposes, the first S2 stimulus artifact was not digitally removed from these records (*). The red bars show the latency from the first S2 to the start of the first chirp intervals. Black bars indicate the total chirp duration.

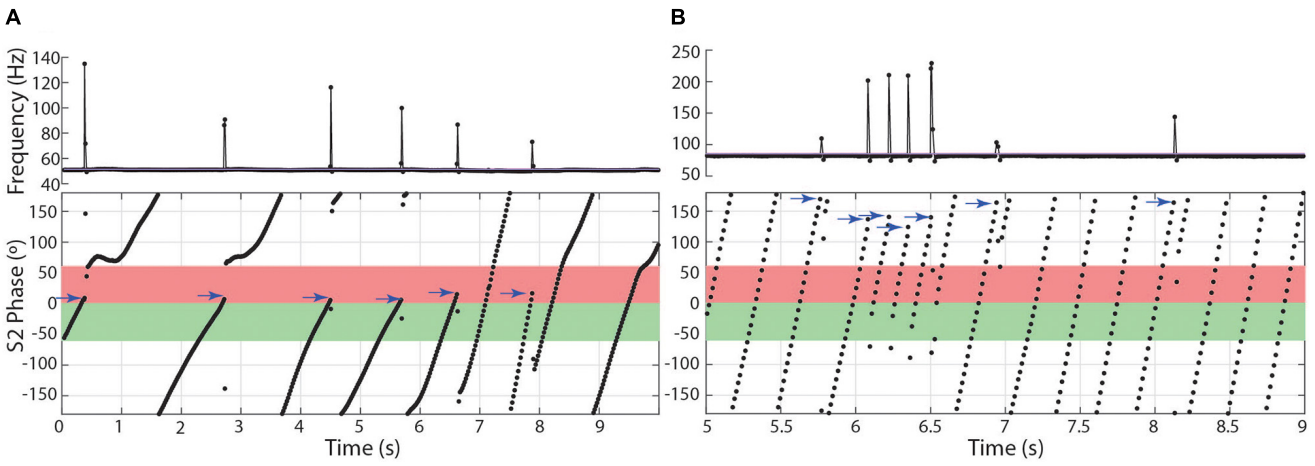

FIGURE 6 | Patterns of chirp occurrence during stimulus trials. **(A)** *Steatogenys*, **(B)** *Microsternarchus*. In trials with multiple chirps, successive chirps often occur at consistent phase angles (blue arrows).

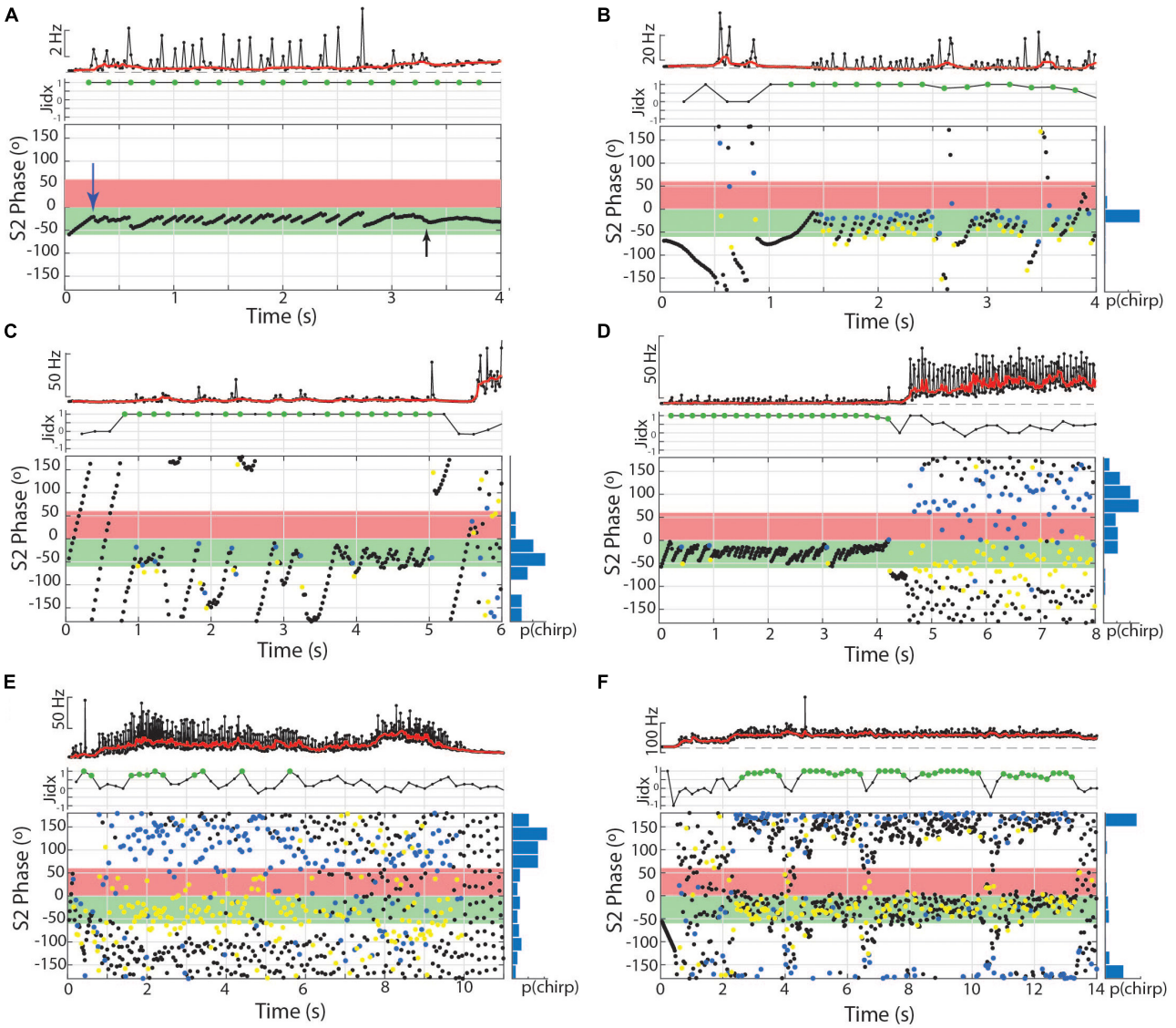

FIGURE 7 | Chirps and chirp-like intervals manipulate phase angle during burst-like chirping and tumultuous rises in *Microsternarchus*. **(A)** Subthreshold chirp-like intervals are timed to occur repeatedly at S2 phase angles very late in the S2 cycle (the first one is indicated by the blue arrow) at approximately –5°, equal to 355°. At 2.75 s, the chirp-like intervals are no longer expressed, but the subject switched to a steady matched frequency with a consistent phase of ∼–10° (black arrow). In this and subsequent panels, the jamming index is plotted, with significant positive values shown as green circles. **(B)** Burst-like chirping (these spikes are well above chirp-threshold of 10% rIPI) produced chirps every 2–6 intervals to maintain jamming avoidance and to fill the critical window of the S2 with EODs. In this and subsequent panels, the normalized chirp probability is shown as a histogram to the right of the phase plot. In all phase plots, the blue circles indicate the start of each chirp and yellow circles mark the location of the next EOD (within the chirp). **(C)** Another exemplary burst-like chirp episode. In this case, the timing between chirps was matched to a multplie of the S2 frequency, resulting in fewer, more widely spaced chirps, particularly during seconds 1–3. During this period, the S1 avoids being jammed but does not fill the critical phases of the S2 with EODs as occurred with the shorter, more frequent chirps in **(B)**. **(D)** Jamming by burst-like chirping followed by a tumultuous rise that does not include well matched inter-chirp timings. In the final 4 s of this example, there is no specific asymmetry of jamming interactions, but S1 EODs mostly avoid the critical windows. **(E)** Example of a tumultuous rise that produced some asymettric jamming but with less specificity than in **(D)** or **(F)**. **(F)** Example of a tightly matched tumultuous rise resulting in nearly 12 s of jamming the S2.

individuals chirping dozens of times per 24H of EOD recordings in isolation. Further, all individuals that displayed chirps did so within the first 100 ms in at least one trial, and six individuals chirped within the first 100 ms on more than 10% of trials, with a range of 2–80% of trials containing short latency chirps (mean = 14.7%, SD = 22) across individuals. Kruskal–Wallis analysis of the minimum latencies observed in these three species revealed a significant difference ($\chi^2(2) = 25.715$, $p < 0.001$), with significant pairwise differences between *Steatogenys* and both of the other species, but no significant difference found between *Microsternarchus* and *Brachyhypopomus*.

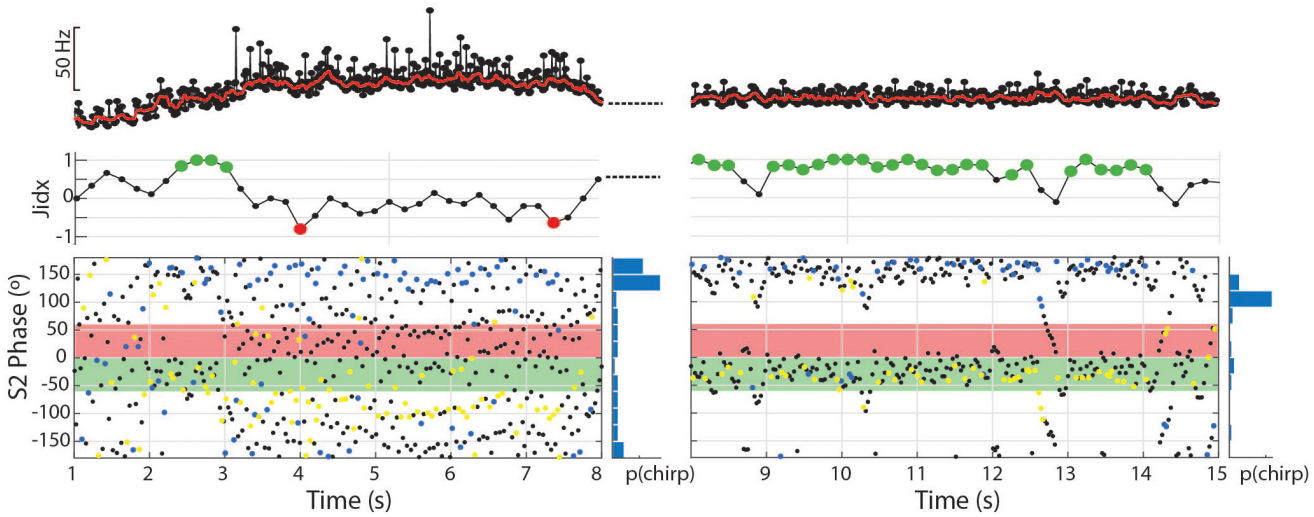

FIGURE 8 | The dynamic nature of the tumultuous rise allows subjects to find matching chirp intervals and jam the S2. In the first 7 s depicted, 81 chirps occurred with a mean phase angle of 160.8° ($r = 0.49$, $p < 0.01$). In the second 7 s depicted, the subject shifts to a stable frequency and continues to produce chirps timed to the S2 period, but fewer and with greater consistency (56 chirps, mean = 168.5°, $r = 0.72$, $p < 0.01$).

Other Behaviors With Large Instantaneous Interval Reductions: Burst-Like Chirping and Tumultuous Rises

We observed two other electromotor behavior patterns in *Microsternarchus* that contain the abrupt changes in IPI and EOD distortion seen in chirps: burst-like chirping and tumultuous rises. Twelve individuals (nine males and three females) displayed burst-like repetitive chirping, with chirp-like intervals (i.e., $>\sim$10% shorter than baseline) repeated almost continuously with fewer than three "normal" intervals between them (**Figures 7**, **8**). These events ranged from 0.63 to 12.9 s, with a mean duration of 5.9 s (SD 4.3). Burst-like chirping episodes contained from seven to 123 chirp-like intervals for an average of 34.0 chirp-like intervals per episode, or 5.8 chirps per second (range: 0.16–17.9 chirps per second).Examples of burst-like chirping are shown in **Figures 7B–D**.

The same twelve individuals, as well as two others (10 females and 4 males) also exhibited a repetitive chirping behavior paired with a very large increase in baseline frequency (**Figures 7D–F**, **8**, **9A,B**). We term this behavior tumultuous rise due to its similarity to the tumultuous rise described by Kawasaki and Heiligenberg (1989). Tumultuous rise events lasted from 0.68 to 15.78 s, with a mean duration of 6.65 s (SD 3.6). The average frequency rise from baseline was 34.3 Hz (SD 18.73), measured at the midpoint of the rise. The peak frequency of the baseline during the rise was an average of 62.54 Hz (SD 32.77) above the frequency prior to the rise (max = 187.73 Hz). Throughout the frequency rise, subjects exhibited closely packed chirp-like intervals. Individual tumultuous rise events contained between five and 245 chirp-like intervals for an average of 99.34 (SD 56.42) chirps per rise, or 15.61 chirps per second during rises (SD 6.23).

Tumultuous rises occurred more often when the starting dF was negative (167 instances where the initial S2 frequency was lower, vs. 78 instances with a higher starting S2: Mann–Whitney $U = 1182.5$, $p < 0.001$), but it should be noted that the large frequency rise resulted in negative dFs (S2 lower frequency) during all tumultuous rises.

Both bouts of burst-like chirping and tumultuous rises often contained periodic structure that resulted in consistent placement of S1 EODs across the S2 cycle (**Figures 7**, **8**). In some cases, repeated chirps at high phase angles (just prior to the S2) resulted in consecutive runs of closely spaced EODs within the sensitive window of the S2 (**Figures 7B,D**). Larger and less frequent chirps resulted in successive short blocks of interference separated by periods of neutral phase relations (as in **Figure 7C**). A similar pattern also occurred in the absence of chirps, but with repeated interspersed short intervals below the 10% rIPI chirp threshold, as in **Figure 7A**. Thus it is possible that there is a continuum of behaviors from jamming maintained by burst-like chirp intervals to smooth jamming by fixed frequency matching (as in the last $\sim$1.25 s of **Figure 7A**). Unlike these repetitive chirp behaviors, smooth jamming by matched frequency was generally infrequent, but was seen in at least one trial for 7 of 24 individuals tested.

During tumultuous rises, the high frequency of the S1 resulted in many more EODs distributed throughout the S2 cycle. If the fish interspersed chirp-like intervals specifically timed to the S2, the S1 EODs could be concentrated at specific phase angles. That is, with a fixed S2, if the time between chirps is equal to the S2 duration, or some whole multiple of it, the chirps will occur at consistent phase angles. The timing of EODs within the chirps will depend on chirp structure and the difference in frequency from the S2. In most trials, the phase of chirp-like intervals was roughly consistent within a bout, and coordinated with the harmonic relationship between S1 and S2 such that a majority S1

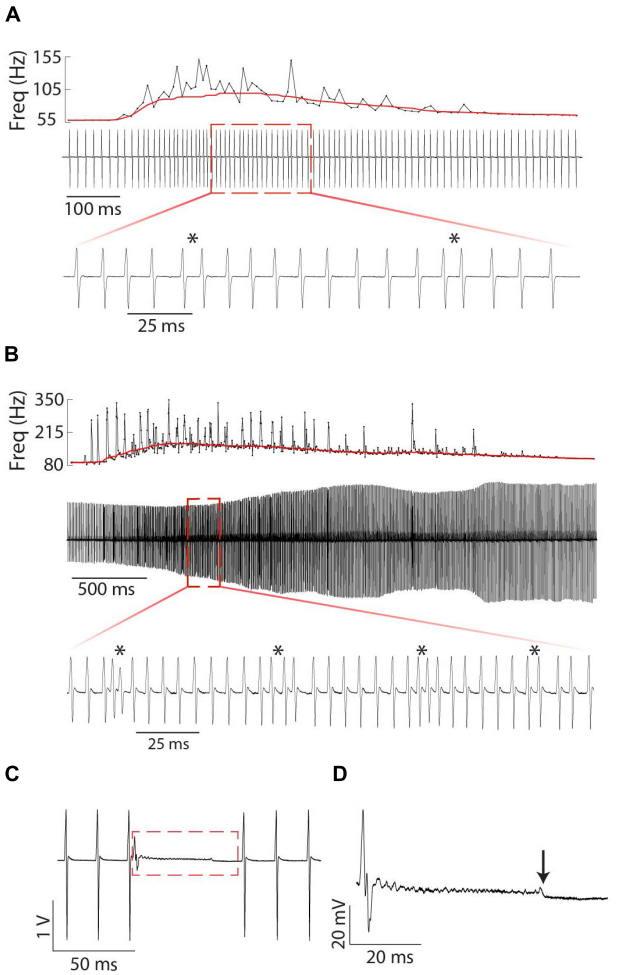

FIGURE 9 | Fine structure of tumultuous rises and interruptions in *Microsternarchus*: Relatively small **(A)** and large **(B)** Tumultuous Rises. In each panel, the top plot shows the instantaneous frequency of every EOD during the entire duration of the tumultuous rise, with a solid red line depicting the ongoing baseline after filtering with a moving window of 250 ms. The middle plot of each panel shows an oscillogram of EODs during the same time period. The expanded bottom plots show a smaller segment of time to illustrate individual chirp-like events, marked by asterisks. The interruption in **(C)** occurs abruptly, with no change to the ongoing EOD frequency. There is some apparent recovery in EOD amplitude following the interruption, but the frequency is unchanged. **(D)** Expanded view of the red rectangle in **(C)**. Interruptions always began with a very shortened IPI and a greatly reduced EOD, followed by a noisy hash. The hash typically ends midway through the interruption (downward arrow). Voltage and time scales for both panels illustrate scale directly. Note that the amplitude modulation of **(B)** is caused by animal motion relative to the electrodes.

EODs occurred within specific windows of the S2 cycle. These windows occurred at a range of values, with the first EOD per S2 cycle occurring before, simultaneously with, or after the S2. This appeared to be a dynamic process where subjects adjusted their own base frequency, the timing and consistency of chirps, and perhaps the chirp structure to match the stimulus. This is illustrated in **Figure 8**. In this example, as the subject began a tumultuous rise, it briefly passed through a dF that aligned the chirps and resulting EODs to the S2 cycle (between second 2 and 3). As the frequency increased further, the alignment of S1s to the S2 cycle degrades. Although the inter-chirp timing was matched to the S2 (as can be seen in the phase histogram), the duration of S1 intervals, both within the chirps and between them, was not coordinated and the subsequent EODs within and following each chirp arrived at a range of S2 phases as the S1 frequency shifted. At the 8th second, the fish abruptly shifted its frequency downward and regularized its interchirp timing, producing chirps with nearly every S2 cycle. This pattern was sustained for the next 6 s.

To examine the matching of chirp timing to the S2, we applied the Rayleigh test to each individual trial containing tumultuous rises. Of the 210 trials that contained tumultuous rises or burst-like chirping, 144 had significantly directed concentrations of chirp phase angles (mean angle = 227.8°, SD 51.3). For individual animals, the percentage of phase-locked trials ranged from 25 to 93% (one subject produced only two tumultuous rises, and both were significantly phase locked). Most of these events resulted in the pattern shown in 7F, with a high concentration of S1 EODs placed immediately prior to the S2 and resulting in clusters of S1 EODs within the critical window of S2, with a very small number falling in the S2 phases most detrimental to the S1.

To further characterize the effect of this behavior on jamming interactions in a dyad, we calculated a jamming ratio in 400 ms windows throughout these trials. The jamming ratio is a ratio of the number of EODs prior to the S2 relative to the number after the S2, with scores close to +1 indicating jamming of the S2 and scores close to −1 reflecting jamming of the S1. For these individuals, 12.5–74.1% of trials analyzed contained significant periods of jamming, with a positive jamming index indicating that the S1 was actively jamming the S2. Periods of significant jamming indices ranged from 400 ms to 6.4 s. Epochs with significantly negative jamming indices were rare in comparison, occurring only 14 times in 11 trials from seven of these individuals. The longest of these negative jamming epochs was 800 ms and most lasted only 400 ms (a single measurement window).

Interruptions

In three individual female *Microsternarchus*, we observed 22 interruptions in EOD rhythm lasting from 39.5 to 91.1 ms. This behavior began with a sudden EOD deformation and massive frequency increase, typically followed by a period of high-frequency hash. The high-frequency hash generally persisted for only a portion of the silent period, followed by a low-noise pause before an abrupt return to baseline EOD production (**Figure 9C**). All three individuals displayed interruptions during both negative and positive S2 stimulus presentations, although more interruptions occurred when the S2 stimulus was higher frequency at the start of the trial.

DISCUSSION

We found that three species of high-frequency pulse gymnotiforms produce chirp-like modulations of their EOD

frequency that could function as communication signals or as jamming avoidance behaviors, or both. In our laboratories, we have conducted similar experiments and had similar opportunities to observe chirps in seven other genera (including more than ten species), but we only observed chirps in these particular species of *Steatogenys*, *Microsternarchus,* and *Brachyhypopomus*. In our samples of *Microsternarchus* and *Brachyhypomus*, chirping was individual specific and possibly unusual. In *Brachyhypomus,* only three individuals produced chirps in these experiments. In *Microsternarchus*, a majority of individuals tested here chirped, but we have also examined several closely related species without ever observing chirps. In all three species studied here, there was great individual variation in chirp proclivity, with some fish chirping only a few times and others chirping hundreds of times over the course of a 1 or 2 h experiment.

Among pulse fishes, this species of *Steatogenys* is unusual for its frequent use of chirps. We have observed chirps in casual observation of fish housed in solitary tanks, with estimates of spontaneous chirping in these individuals ranging from 1 to 15 chirps per 24 h of observation (Field, 2016). Chirps have been observed in males and females and become common in individuals larger than 15 cm of either sex. In many of the trials reported here, the chirp appears similar to a startle or orienting response in its latency and repeatability, especially when presented with higher absolute dF stimuli. This possibility requires continued investigation, but it is also clear that chirps are a common feature of jamming interactions and are most often observed in interactions with low absolute dF stimuli. This is also true of our observations of chirping in *Brachyhypopmus* and *Microsternarchus*.

Sex and Maturity of the Individuals Observed

The present findings are constrained by the lack of diversity in our sample. Several individuals were too immature to assign to a sex. None of our subjects were in breeding condition and the most mature fish in our sample were only stage 2 or 3 on Crampton and Hopkins (2005) scale of maturity (=maturing-mature). This does not change the finding that *Steatogenys* chirps frequently and that all three species sometimes chirp when presented with conspecific stimuli, but it does limit our interpretations of these findings. We cannot yet comment on the specific behavioral context for chirp expression (e.g., reproductive, agonistic) or any specific correlations between chirp structure and behavioral usage.

Comparison of Chirps Presented Here and Those of Other Species in the Literature

The chirps we reported for *Brachyhypopomus* sp. are similar to those described for other *Brachyhypopomus* species, with perhaps the greatest similarity to type-M as described by Perrone et al. (2009). The type-M chirp was only observed in male-male interactions, but our subjects were not mature enough to be differentiated. Kawasaki and Heiligenberg (1989) distinguished "strong" and "weak" chirps in *Brachyhypopomus brevirostris*, but the analysis of Perrone et al. (2009) suggests that there may be several subtypes of chirps subsumed by Kawaski and Heiligenberg's title of "strong" chirps. The type-M and the chirp reported here are both somewhat intermediate between strong and weak, in that they are longer and have greater modulations than weak chirps, but have little deformation of the EOD waveform within the chirp, other than a 20–30% reduction in amplitude.

The weak chirps in Kawasaki and Heiligenberg (1989) and the decrement bursts of *Brachyhypopomus occidentalis* described by Hagedorn (1988) are very interesting in relation to the chirps seen in *Microsternarchus* and *Steatogenys*. In all cases, the modulations were short, consisting of a small number of intervals. In *B. brevirostris* and *B. occidentalis,* and in *Microsternarcus*, weak chirps were reported in sequences of many interspersed chirps or decrement bursts. Kawasaki and Heiligenberg (1989) did not report on the phase relations with the receiver, but it is possible that the weak chirps they observed were timed to specific phase relations, as the chirps were in *Microsternachus*. The tumultuous rise reported in that paper differed from that in *Microsternarchus* defined here, in that *B. brevirostris* did not intersperse chirps in the tumultuous rise, although they do report "frequency-dependent decrements in EOD pulse amplitude" (p. 734) and their examples come from freely moving individuals, complicating detection. These authors only detected tumultuous rises during courtship interactions.

Chirps as Signals vs. Chirps as Phase Manipulation for Jamming Avoidance

In the existing literature, chirps have been treated as signals, with specific structure presumably selected for specific responses from a receiver (e.g., Perrone et al., 2009). It is possible that at least some of the chirps reported here should be interpreted as specific communication signals. The repetitive chirping reported here, particularly when synchronized to the S2 frequency, suggests a different function. Rather than stereotyped signals, we suggest that chirp-like frequency shifts are a component of dynamic jamming interactions. Dramatically short intervals, like those that comprise chirp signals, may be dynamically interspersed and combined with shifts in baseline frequency to sustain long periods of specific phase relationships between fish EODs.

In our limited sample of *Brachyhypopomus* chirps, we found no evidence that the chirps are specifically timed to the S2 playback. In both *Steatogenys* and *Microsternarchus,* however, dynamic changes in base frequency and inter-chirp intervals altered the phase interactions between conspecifics in structured ways that reduced jamming for the S1 and increased it for the S2. The examples shown in **Figures 6–8** illustrate that specifically timed chirps can effectuate jamming (**Figure 7**) or jamming avoidance, although jamming was much more frequent.

This use of chirps or chirp-like behaviors as a jamming behavior has never been reported and it is not clear if we should consider these chirps reported here to be jamming avoidance behaviors, stereotyped signals or some combination of the two. To be clear, these chirps were not observed in specific interactions

(i.e., courtship or male-male conflict) and the artificiality of robotic playback complicates interpretation of chirp function. It is also possible, even likely, that signal chirps occurring in a natural context are timed to the same phase relations described here. This would enhance their salience, given the low responsiveness seen during the middle of the EOD cycle. Existing descriptions of chirps in pulse species do not address this question, but we hope that future reports will examine the timing of chirps with respect to receiver phase.

The Chirp as Startle Response in *Steatogenys*

The short latency chirp seen frequently in *Steatogenys* is striking. Chirps often occurred with the very next interval following stimulus onset, with the very first chirp EOD occurring as soon as 18-ms following the presentation of a single S2. This short latency makes it possible that the control of these chirps is not via a thalamic prepacemaker nucleus, but rather through intrinisic hindbrain circuitry. Falconi et al. (1995) described a Mauthner cell mediated abrupt frequency increase that they interpreted as an orienting response in *G. omarum*. The so-called M-AIR (Mauthner-initiated Abrupt Increase in Rate) resembles the natural orienting response of most pulse gymnotiforms: a brief frequency increase lasting some tens of intervals. Orienting responses are the most common electromotor behaviors seen in all species of pulse gymnotiforms and are thought to provide enhanced electroreception for brief periods of attention. The overall frequency increase of orienting responses is much smaller than that of chirps, usually <25% (occurring gradually relative to chirps) over 5 or more intervals, with a longer gradual return to baseline. Curti et al. (2006) showed that Mauthner neurons initiate the M-AIR by stimulation of NMDA activation of pacemaker neurons. Based on the timing and geometry of field potentials recorded in the pacemaker nucleus, these authors inferred that the M-cell activates pacemaker cells through local medullary interneurons, possibly components of the larger M-cell circuit or a previously unrecognized medullary pre-pacemaker network described by Comas and Borde (2010). *Steatogenys* also displays a typical gymnotiform orienting response, but the short latency chirp is dramatic and is possibly related to the spontaneous chirps we have observed in isolated exploration (Field, 2016). We suggest that the Mauthner neurons of *Steatogenys*, like those of *G. omarum*, are capable of short-latency influence over the pacemaker nucleus, possibly through medullary interneurons. This may be a convergent evolution in these distantly related genera, although the medullary pre-pacemaker inputs to the pacemaker nucleus reported by Comas and Borde (2010) suggest that there may be greater complexity of inputs to the pacemaker in pulse fishes or in species that have not yet been studied. Inputs to the M-cell system are typically reflective of the sensory complement of each species (Canfield and Rose, 1996), so it should be expected that electrosensory information is part of the M-cell system inputs. Canfield and Rose (1993) showed that electrosensory inputs can modulate the directionality of typical M-cell mediated behavior (acoustically stimulated escape), so it is likely that M-cell networks in all gymnotiforms receive electroreceptive input of some form. The possibility that the M-cell network can influence pacemaker activity deserves further exploration.

Circuit Considerations

There are two main features of chirps, a dramatic, but short-lived increase in rate, and a deformation or reduction of the EOD waveform. Both of these effects can be understood in relation to the EOD control circuit. The neuronal network (**Figure 10**) controlling the modulations of the EOD rate in Gymnotiformes is well characterized generally (Dye and Meyer, 1986; Metzner, 1999; Caputi et al., 2005) and consists of an unpaired medullary pacemaker nucleus (PN) containing two cell types: pacemaker (P) and relay cells (R). Apteronotid species also have a third PN cell type, but this has not been found in other gymnotiforms (Quintana et al., 2011). P-cells are smaller (50–100 μm) and have an intrinsically rhythmic activity (Bennett, 1968). These cells are electrotonically coupled by gap junctions and are the driver of electric organ rhythm (Bennett et al., 1967). The P cells have their cell bodies and axons restrained within the PN, and their dendrites mostly occupy the dorsal portion of nucleus (Kennedy and Heiligenberg, 1994), where they are contacted by axons from pre-pacemaker nuclei in the thalamus (CP-PPN). P cell axons project to R cells, where they make mixed chemical and electrical synapses. The R cells are larger (200–300 μm) than P cells and their cell bodies are also restricted to the nucleus. Their dendrites reach the surrounding regions of the PN, where they are also contacted by pre-pacemaker axons from both CP-PPN and a sub-lemniscal prepacemaker (SP-PPN). The R cell axons descend into the spinal cord and contact local motor neurons that drive electrocyte groups within the electric organ. Under ordinary circumstances, the P and R cells are electrotonically coupled and each P action potential drives a single action potential in R cells, in turn eliciting a single discharge from a unit of spinal motor neurons and their associated electrocytes. It is well known that P cells are electronically coupled via gap junctions, but relay cells are often also inter-connected with gap junctions, albeit with large and mostly unexplored species differences (Bennett et al., 1967). A more recent anatomical study (Quintana et al., 2011) of *B. gauderio* also suggested that there may be multiple populations of relay cells, allowing for network specializations that increase the diversity of outputs (rate changes). Relay cell differentiation might also be important for the coordination of electrocyte sub-populations in patterned activation patterns (e.g., Caputi, 1999). Future comparative studies of PN organization are needed to explore these questions.

Two pre-pacemaker nuclei directly contact the PN and their synaptic actions are well studied (Kawasaki and Heiligenberg, 1988, 1989, 1990; Kennedy and Heiligenberg, 1994; Spiro, 1997). The thalamic prepacemaker nucleus (CP-PPN) is a complex of cell groups within the central posterior thalamus that sends axons to the PN where they synapse on P cell dendrites. The PPN in pulse-species is subdivided into three regions, the PPN-G, -I, and -C. Stimulation of PPN-G activates NMDA receptors on P cells and causes a smooth increase in EO frequency, with coupled R cell activity. Similarly, stimulation of PPN-I causes a smooth decrease in EO frequency (Kawasaki and Heiligenberg, 1989),

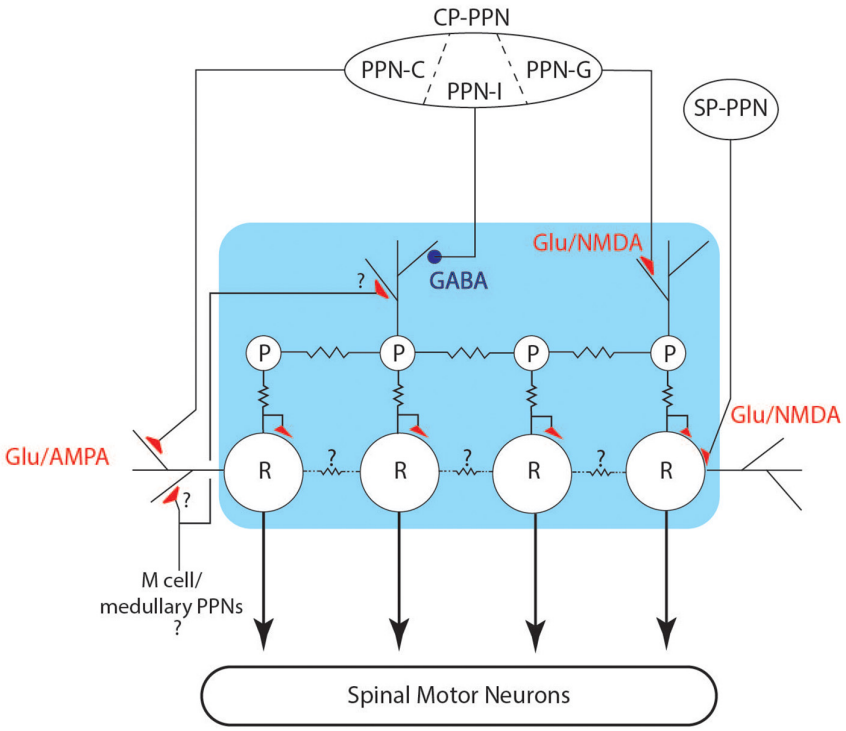

FIGURE 10 | Schematic of the pacemaker control circuit. The connections between pre-pacemaker nuclei and cells of the pacemaker (blue box) are shown, including inhibitory (blue circles) and excitatory (red triangles) connections. Electrotonic coupling is indicated by the jagged lines between cells.

in this case by activation of GABA receptors on P cells. Gymnotiform species have different dynamics to these smooth frequency changes, with frequency increases generally occurring more abruptly than decreases. Higher levels of stimulation of PPN-I lead to complete inhibition of P cell firing, resulting in silencing of relay cells and an interruption of EOD rhythm (Kawasaki and Heiligenberg, 1989, 1990; Spiro, 1997). These interruptions are different from those we recorded here, in that PPN-I stimulated interruptions begin with a smooth decrease in rate and have little or noise during the interruption. When the EOD resumes following PPN-I stimulation, EODs are fully formed as normal, and the rate gradually increases back to baseline. PPN-I stimulation does not appear to cause disruption in the coordination of R cell action potentials.

Stimulation of PPN-C causes AMPA activation on R cell receptors, and causes sustained depolarization and co-ordinated ringing in relay cells, resulting in abrupt EOD frequency increases resembling chirps (Kawasaki and Heiligenberg, 1989). With stronger stimulation of PPN-C, relay cell synchronization deteriorates; leading to amplitude and waveform modulation of the EODs within the chirp as electrocyte firing coordination degrades (Kawasaki and Heiligenberg, 1989; Spiro, 1997). Spiro (1997) reported on a limited set of simultaneous recordings from two R cells during AMPA activation and showed that some amount of R cell synchrony is maintained during early stages of the R cell depolarization. This could explain the gradual decrease of EOD amplitude through the time course of a chirp, as relay cell coordination fails with prolonged AMPA activation. The structure of chirps, tumultuous rises and interruptions all suggest that relay cell depolarization and/or ringing may contribute to the control of these behaviors.

The second major input to PN is the sublemniscal pre-pacemaker nucleus (SP-PPN) located in the midbrain. SP-PPN cells extend axons to the dendritic fields of R cells, and NMDA receptor activation of R cells causes prolonged depolarization in relay cell populations, leading to an abrupt cessation of EODs. During the depolarization, R cells fire bursts of low amplitude action potentials, leading to unsynchronized firing of the electrocytes and resulting in high frequency hash or "hushing silence," from the electric organ (**Figure 9**; Spiro, 1997). P cells continue firing relatively unchanged, although back-propagated action potentials from R cells can insert extraneous R cell action potentials (Spiro, 1997). When R cells repolarize, normal firing patterns resume and the EOD rate returns at very close to the rate prior to the interruption. This pattern matches the interruptions we observed in *Microsternarchus*.

Comas and Borde (2010) also described medullary neurons retrogradely labeled following biocytin injection to the pacemaker nucleus. They described these neurons as part of medullary pre-pacemaker network, but this possibility has not been pursued in the literature. The short latency of some *Steatogenys* chirps is consistent with more local control and the high-speed dynamic nature of jamming interactions (personal

observations) also suggests that local networks may play a larger role in pulse fish pacemaker modulations.

With respect to the behaviors reported here, chirps are almost certainly a result of PPN-C activation of AMPA receptors on relay cells, leading to coordinated high frequency EODs. Amplitude reduction of EODs may occur from a breakdown in synchrony between R cells. An important topic for future study is the question of R cell subpopulations and possible intra-PN mechanisms of regulating EOD amplitude during chirps (see Quintana et al., 2011). These mechanisms may lead to motivational coding in chirp expression, i.e., greater AMPA activation is specifically correlated to R cell desynchronization. Alternatively, there is also the possibility that selective recruitment of R cell sub populations could lead to patterned changes in EOD amplitude. There is no experimental evidence for the mechanism leading to specifically timed chirps or chirp like intervals, but it presumably relies on precise time-coded inputs to the PPN-C or direct connection to the pacemaker nucleus.

The short latency chirps of *Steatogenys* and the M-AIR of *Gymnotus* indicate that other inputs to the PN could exist, presumably within the hindbrain. In the case of *Gymnotus* M-AIR, these hindbrain prepacemakers exert their influence over P cells (Curti et al., 2006; Comas and Borde, 2010), but the short latency chirps in *Steatogenys* are indistinguishable from other chirps and presumably result from R cell activation. Integration of the PN with other hindbrain circuits, including the escape circuit, should be the subject of future investigation.

Interruptions reported here resemble those seen in other species and are likely to result from SPPN activation of AMPA receptors on relay cells. The tumultuous rise is the most unusual behavior and has not been reported as an outcome in physiological recordings. We speculate that it results from a combined PPN-C and PPN-G activation of both R and P cells. The frequency increase (generated by PPN-G activation of R cells) is larger than typical PPN-G mediated rate increases, but the smooth increase and sustained and steady high rate suggests changes to P cell rhythm.

The Functions of Chirps

In this report, we have shown that chirps in *Steatogenys* and *Microsternarchus* have a wide range of EOD rate and waveform modulations. This variation in structure could reflect multiple specific types (each with some range of motivational and expressional variation), as has been shown from many Apteronotid species and more recently for *G. omarum* (Batista et al., 2012) and *B. gauderio* (Perrone et al., 2009). This variation could also reflect an absence of specificity, with chirp-like intervals dynamically used in JAR interactions or as part of a larger communication and influence system that is not based solely on specifically evolved signals (Rendall et al., 2009). The function of a communication signal is best understood from the regularity of response elicited from conspecifics and the context of the interaction between communicators. For instance, if chirps are most often displayed by the larger of a pair and the production of chirps predicts increased aggressive behavior, as in *G. carapo* (Westby, 1975) or *B. gauderio* (Perrone et al., 2009), the chirp is clearly an attack warning by the dominant partner. Or, if chirps are often displayed by the loser of a contest following retreat, as in *G. omarum* (Batista et al., 2012), then the chirp can be interpreted as a signal of submission. Perrone et al. (2009) detail the specific context of multiple chirp types in *B. gauderio* using controlled context and field observations, and more studies of this sort will be greatly informative. Their results indicate that not only can chirps vary in function between closely related species, but also multiple structural types might be deployed with distinct meanings in a single species. In addition to specifically evolved behavioral contexts, the structure of communication signals creates constraints and affordances for their functional deployment. With respect to the current findings, several possibilities exist. We list these here as possibilities, to be explored with future experimental data. Chirps in *Steatogenys* may be a component of orienting behavior, mediated by hindbrain startle and escape circuits. The chirp itself in this context could have either sensory consequences (improved sampling) or even function as an alarm signal to conspecifics. Chirps in *Steatogenys* may contain an unambiguous signal of reproductive or androgenic state and could be used in agonistic and reproductive contexts as honest indicators of state (e.g., larger chirps signal higher testosterone levels). Chirps and chirp-like intervals are used in both *Microsternarchus* and *Steatogenys* during jamming interactions and can manipulate phase relations between partners for extended periods. It is not yet clear whether this manipulation itself has signal value (i.e., is jamming an agonistic behavior?), or if the chirps involved are themselves signals as well. We look forward to future studies of chirp significance, control, and diversity across pulse gymnotiforms. The jamming avoidance interactions described here suggest that jamming interactions comprise a dynamic communication system that is both a mechanism of preserving private electrolocation abilities and also system of intraspecific influence and communication.

DATA AVAILABILITY STATEMENT

The datasets generated for this study are available on request to the corresponding author.

ETHICS STATEMENT

The animal study was reviewed and approved by Hunter College Institutional Animal Care and Use Committee and the Ethical Committee for Animal Research of INPA.

AUTHOR CONTRIBUTIONS

All authors contributed to the design of the experiments, led by CB. CF and TP conducted the experiments and collected the data. CB, JA-G, and TP developed the ethographic framework for the description of specific electromotor behaviors like the chirp and tumultuous rise. CB and TP designed and conducted the statistical analysis. CB prepared the final version of the

manuscript and illustrations, with contributions and comments from all authors.

FUNDING

This work was supported by grants from the Professional Staff Congress of CUNY (65638-00 43) and CNPq (384980/2011-2 and 402441/2008-7) to CB, and INPA (PRJ-12.307) JA-G. TP was supported by fellowships from FAPEAM (P. 32143.UNI614.4510.05042016-44250) and CAPES (PDSE – 88881.189704/2018-01).

ACKNOWLEDGMENTS

The authors thank Peter Moller for comments on an earlier draft of the manuscript. Hunter College students, Baiyang Chen and Michelle Garcia-Lopez processed some of the chirp data from *Steatogenys*.

SUPPLEMENTARY MATERIAL

The Supplementary Material for this article can be found online at: https://www.frontiersin.org/articles/10.3389/fnint.2019.00055/full#supplementary-material

FIGURE S1 | Beeswarm plots of the three most prolific chirpers in *Steatogenys* in dF experiments **(A)** and S2 duration experiments **(B)**. The three most prolific chirpers in *Microsternarchus* are shown in **(C)**. As in **Figure 2**, the top plot of each panel shows the reduction of IPI as a function of position within the chirp and the bottom plot shows the reduction of amplitude for each successive EOD within the chirp.

FIGURE S2 | Distributions of trial mean chirp starts grouped by the individuals with significant overall distributions. **(A)** Six individual *Microsternarchus* had significantly concentrated distributions of chirp start angles. **(B)** Fifteen individual *Steatogenys* had significantly directed distributions. In all panels, the number of chirps, mean vector, and r-score are shown above the histograms. $P < 0.05$ for all instances shown.

TABLE S1 | Summary statistics of chirp metrics for each subject. **(a)** *Steatogenys*. **(b)** *Microsternarchus*. **(c)** *Brachyhypopomus*.

REFERENCES

Batista, G., Zubizarreta, L., Perrone, R., and Silva, A. (2012). Non-sex-biased dominance in a sexually monomorphic electric fish: fight structure and submissive signalling. *Ethology* 118, 398–410. doi: 10.1111/j.1439-0310.2012.02022.x

Bennett, M. B. (1968). "Neural control of electric organs," in *The Central Nervous System and Fish Behavior*, ed. D. Ingle (Chicago, IL: Chicago University Press), 147–169.

Bennett, M. B., Pappas, G. D., Giménez, M., and Nakajima, Y. (1967). Physiology and ultrastructure of electrotonic junctions. IV. Medullary electromotor nuclei in gymnotid fish. *J. Neurophysiol.* 30, 236–300. doi: 10.1152/jn.1967.30.2.236

Berens, P. (2009). CircStat: a MATLAB toolbox for circular statistics. *J. Stat. Softw.* 31, 1–21.

Bullock, T. H. (1969). Species differences in effect of electroreceptor input on electric organ pacemakers and other aspects of behavior in electric fish. *Brain Behav. Evol.* 2, 85–118.

Bullock, T. H., Hamstra, R. H., and Scheich, H. (1972). The jamming avoidance response of high frequency electric fish. *J. Comp. Physiol. A* 77, 1–48.

Canfield, J., and Rose, G. (1993). Activation of Mauthner neurons during prey capture. *J. Comp. Physiol. A.* 172, 611–618. doi: 10.1007/bf00213683

Canfield, J. G., and Rose, G. J. (1996). Hierarchical sensory guidance of Mauthner-mediated escape responses in goldfish (Carassius auratus) and cichlids (*Haplochromis burtoni*). *Brain Behav. Evol.* 48, 137–156. doi: 10.1159/000113193

Caputi, A. (1999). The electric organ discharge of pulse gymnotiforms: the transformation of a simple impulse into a complex spatio-temporal pattern. *J. Exp. Biol.* 202, 1229–1241.

Caputi, A., Carlson, B. A., and Macadar, O. (2005). "Electric organs and their control," in *Electroreception*, eds T. H. Bullock, C. D. Hopkins, A. N. Popper, and R. R. Fay (New York, NY: Springer), 410–451. doi: 10.1007/0-387-28275-0_14

Caputi, A. A., and Budelli, R. (2006). Peripheral electrosensory imaging by weakly electric fish. *J. Comp. Physiol. A* 192, 587–600. doi: 10.1007/s00359-006-0100-2

Caputi, A. A., Castello, M. E., Aguilera, P., and Trujillo-Cenoz, O. (2002). Electrolocation and electrocommunication in pulse gymnotids: signal carriers, pre-receptor mechanisms and the electrosensory mosaic. *J. Physiol.* 96, 493–505. doi: 10.1016/s0928-4257(03)00005-6

Carlson, B. A. (2006). "A neuroethology of electrocommunication: senders, receivers and everything in between," in *Communication in Fishes*, eds F. Ladich, S. P. Collin, P. Moller, and B. G. Kapoor (Enfield, NJ: Science Publishers), 805–848.

Castelló, M. E., Caputi, A., and Trujillo-Cenoz, O. (1998). Structural and functional aspects of the fast electrosensory pathway in the electrosensory lateral line lobe of the pulse fish, *Gymnotus carapo*. *J. Comp. Neurol.* 401, 549–563. doi: 10.1002/(sici)1096-9861(19981130)401:4<549::aid-cne7>3.3.co;2-8

Comas, V., and Borde, M. (2010). Neural substrate of an increase in sensory sampling triggered by a motor command in a gymnotid fish. *J. Neurophys.* 104, 2147–2157. doi: 10.1152/jn.00076.2010

Crampton, W. G. R., and Albert, J. S. (2006). "Evolution of electric signal diversity in gymnotiform fishes," in *Communication in Fishes*, eds F. Ladich, S. P. Collin, P. Moller, and B. G. Kapoor (Enfield, NJ: Science Publishers), 647–732.

Crampton, W. G. R., and Hopkins, C. D. (2005). Nesting and paternal care in the weakly electric fish Gymnotus (Gymnotiformes : Gymnotidae) with descriptions of larval and adult electric organ discharges of two species. *Copeia* 2005, 48–60. doi: 10.1643/ci-04-056r1

Curti, S., Comas, V., Rivero, C., and Borde, M. (2006). Analysis of behavior-related excitatory inputs to a central pacemaker nucleus in a weakly electric fish. *Neuroscience* 140, 491–504. doi: 10.1016/j.neuroscience.2006.02.037

Dye, J. (1988). An in vitro physiological preparation of a vertebrate communicatory behavior: Chirping in the weakly electric fish, *Apteronotus*. *J. Comp. Physiol. A* 163, 445–458. doi: 10.1007/bf00604899

Dye, J., and Meyer, J. H. (1986). "Central control of the electric organ discharge in weakly electric fish," in *Electroreception*, eds T. H. Bullock and W. Heiligenberg (New York, NY: John Wiley and sons), 71–102.

Falconi, A., Borde, M., Henandezcruz, A., and Morales, F. R. (1995). Mauthner cell-initiated abrupt increase of the electric organ discharge in the weakly electric fish Gymnotus carapo. *J Comp. Physiol. A* 176, 679–689. doi: 10.1007/bf01021588

Field, C. E. (2016). *Signaling and the Characterization of a Chirp-Like Signal in the Weakly Electric Fish Steatogenys Elegans*. Ph.D. thesis, City University of New York, New York, NY.

Hagedorn, M. (1986). "The ecology, courtship, and mating of gymnotiform electric fish," in *Electroreception*, eds T. H. Bullock and W. Heiligenberg (New York, NY: John Wiley and sons), 497–526.

Hagedorn, M. (1988). Ecology and behavior of a pulse-type electric fish, *Hypopomus* occidentalis (Gymnotiformes, Hypopomidae), in a fresh-water stream in Panama. *Copeia* 1988, 324–335.

Hagedorn, M., and Heiligenberg, W. (1985). Court and spark: electric signals in the courtship and mating of gymnotid fish. *Anim. Behav.* 33, 254–265. doi: 10.1016/s0003-3472(85)80139-1

Heiligenberg, W. (1974). Electrolocation and jamming avoidance in a *Hypopygus* (Rhamphichthyidae, Gymnotoidei), an electric fish with pulse-type discharges. *Comp. Physiol.* 91, 223–240. doi: 10.1007/bf00698054

Heiligenberg, W. (1980). The evaluation of electroreceptive feedback in a gymnotoid fish with pulse-type electric organ discharges. *J. Comp. Physiol. A* 138, 173–185. doi: 10.1007/bf00680441

Heiligenberg, W. (1986). "Jamming avoidance responses: model systems for neuroethology," in *Electroreception*, eds T. H. Bullock and W. Heiligenberg (New York, NY: John Wiley and Sons), 613–649.

Heiligenberg, W., Baker, C., and Bastian, J. (1978). The jamming avoidance response in gymnotoid pulse-species: a mechanism to minimize the probability of pulse-train coincidence. *J. Comp. Physiol. A* 124, 211–224. doi: 10.1007/bf00657053

Hopkins, C. D. (1974). Electric communication: functions in the social behavior of *Eigenmannia virescens*. *Behavior* 50, 270–305.

Kawasaki, M., and Heiligenberg, W. (1988). Individual pacemaker neurons can modulate the pacemaker cycle of the gymnotiform electric fish, *Eigenmannia*. *J. Comp. Physiol. A* 162, 13–21. doi: 10.1007/bf01342699

Kawasaki, M., and Heiligenberg, W. (1989). Distinct mechanisms of modulation in a neuronal oscillator generate different social signals in the electric fish *Hypopomus*. *J. Comp. Physiol. A* 165, 731–741. doi: 10.1007/bf00610872

Kawasaki, M., and Heiligenberg, W. (1990). Different classes of glutamate receptors and GABA mediate distinct modulations of a neuronal oscillator, the medullary pacemaker of a gymnotiform electric fish. *J. Neurosci.* 10, 3896–3904. doi: 10.1523/jneurosci.10-12-03896.1990

Kennedy, G., and Heiligenberg, W. (1994). Ultrastructural evidence of GABA-ergic inhibition and glutamatergic excitation in the pacemaker nucleus of the gymnotiform electric fish *Hypopomus*. *J. Comp. Physiol. A* 174, 267–280.

Maia, C., and Alves-Gomes, J. A. (2012). "Utilização do código de barras de DNA na estimativa de diversidade de peixes elétricos do gênero Microsternarchus (Ostariophysi: Gymnotiformes) na bacia do Rio Negro, Amazonas," in *Projeto Fronteira – desvendando as fronteiras do conhecimento na região Amazônica do Alto Rio Negro*, eds L. Souza and E. Castellón (Manaus: INPA), 185–201.

Metzner, W. (1999). Neural circuitry for communication and jamming avoidance in gymnotiform electric fish. *J. Exp. Biol.* 202, 1365–1375.

Moller, P. (2006). "Electrocommunication: history, insights, and new questions," in *Communication in Fishes*, Vol. 2, eds F. Ladich, S. P. Collin, P. Moller, and B. G. Kapoor (Enfield, NH: Science Publishers), 579–598.

Nogueira, J., Castelló, M. E., and Caputi, A. (2006). The role of single spiking spherical neurons in a fast sensory pathway. *J. Exp. Biol* 209, 1122–1134. doi: 10.1242/jeb.02080

Perrone, R., Macadar, O., and Silva, A. (2009). Social electric signals in freely moving dyads of *Brachypopomus pinnicaudatus*. *J. Comp. Physiol. A* 195, 501–514. doi: 10.1007/s00359-009-0427-6

Pohlert, T. (2014). *The Pairwise Multiple Comparison of Mean Ranks Package (PMCMR). R Package*. Available at: https://cran.r-project.org/package=PMCMR (accessed September 17, 2019).

Quintana, L., Pouso, P., Fabbiani, G., and Macadar, O. (2011). A central pacemaker that underlies the production of seasonal and sexually dimorphic social signals: anatomical and electrophysiological aspects. *J. Comp. Physiol. A* 197, 75–88. doi: 10.1007/s00359-010-0588-3

R Core Team (2014). *R: A Language and Environment For Statistical Computing*. Vienna, Austria: R Foundation for Statistical Computing. Available at: http://www.R-project.org/

Rendall, D., Owren, M. J., and Ryan, M. J. (2009). What do animal signals mean? *Anim. Behav.* 78, 233–240. doi: 10.1016/j.anbehav.2009.06.007

Rose, G. J. (2004). Insights into neural mechanisms and evolution of behaviour from electric fish. *Nat. Rev. Neurosci.* 5, 943–951. doi: 10.1038/nrn1558

Schuster, S. (2002). Behavioral evidence for post-pause reduced responsiveness in the electrosensory system of Gymnotus carapo. *J. Exp. Biol.* 205, 2525–2533.

Shumway, C. A., and Zelick, R. D. (1988). Sex recognition and neuronal coding of electric organ discharge waveform in the pulse-type weakly electric fish, *Hypopomus* occidentalis. *J. Comp. Physiol. A* 163, 465–478. doi: 10.1007/bf00604901

Smith, G. T. (2013). Evolution and hormonal regulation of sex differences in the electrocommunication behavior of ghost knifefishes (Apteronotidae). *J. Exp. Biol.* 216, 2421–2433. doi: 10.1242/jeb.082933

Spiro, J. E. (1997). Differential activation of glutamate receptor subtypes on a single class of cells enables a neural oscillator to produce distinct behaviors. *J. Neurophysiol.* 78, 835–847. doi: 10.1152/jn.1997.78.2.835

Turner, C. R., Derylo, M., De Santana, C. D., Alves-Gomes, J. A., and Smith, G. T. (2007). Phylogenetic comparative analysis of electric communication signals in ghost knifefishes (Gymnotiformes: Apteronotidae). *J. Exp. Biol.* 210, 4104–4122. doi: 10.1242/jeb.007930

Watenabe, A., and Takeda, K. (1963). The change in discharge frequency by A.C. stimulus in a weak electric fish. *J. Exp. Biol.* 40, 57–66.

Westby, G. W. M. (1975). Has the latency dependent response of *Gymnotus carapo* to discharge-triggered stimuli a bearing on electric fish communication. *J. Comp. Physiol. A* 96, 307–341. doi: 10.1007/bf00619223

Zupanc, G. K. H., and Bullock, T. H. (2005). "From electrogenesis to electroreception: an overview," in *Electroreception*, eds T. H. Bullock, C. D. Hopkins, A. N. Popper, and R. R. Fay (New York, NY: Springer New York), 5–46. doi: 10.1007/0-387-28275-0_2

Conflict of Interest: The authors declare that the research was conducted in the absence of any commercial or financial relationships that could be construed as a potential conflict of interest.

frontiers in Integrative Neuroscience

ORIGINAL RESEARCH
published: 07 July 2020
doi: 10.3389/fnint.2020.00038

Serotonergic Modulation of Sensory Neuron Activity and Behavior in *Apteronotus albifrons*

*Mariana M. Marquez and Maurice J. Chacron**

Computational Systems Neuroscience Laboratory, Department of Physiology, McGill University, Montreal, QC, Canada

Organisms must constantly adapt to changes in their environment to survive. It is thought that neuromodulators such as serotonin enable sensory neurons to better process input encountered during different behavioral contexts. Here, we investigated how serotonergic innervation affects neural and behavioral responses to behaviorally relevant envelope stimuli in the weakly electric fish species *Apteronotus albifrons*. Under baseline conditions, we found that exogenous serotonin application within the electrosensory lateral line lobe increased sensory neuron excitability, thereby promoting burst firing. We found that serotonin enhanced the responses to envelope stimuli of pyramidal cells within the lateral segment of the electrosensory lateral line lobe (ELL) by increasing sensitivity, with the increase more pronounced for stimuli with higher temporal frequencies (i.e., >0.2 Hz). Such increases in neural sensitivity were due to increased burst firing. At the organismal level, bilateral serotonin application within the ELL lateral segment enhanced behavioral responses to sensory input through increases in sensitivity. Similar to what was observed for neural responses, increases in behavioral sensitivity were more pronounced for higher (i.e., >0.2 Hz) temporal frequencies. Surprisingly, a comparison between our results and previous ones obtained in the closely related species *A. leptorhynchus* revealed that, while serotonin application gave rise to similar effects on neural excitability and responses to sensory input, serotonin application also gave rise to marked differences in behavior. Specifically, behavioral responses in *A. leptorhynchus* were increased primarily for lower (i.e., ≤0.2 Hz) rather than for higher temporal frequencies. Thus, our results strongly suggest that there are marked differences in how sensory neural responses are processed downstream to give rise to behavior across both species. This is even though previous results have shown that the behavioral responses of both species to envelope stimuli were identical when serotonin is not applied.

Keywords: neuromodulation, weakly electric fish, sensory processing, envelope, comparative

Edited by:
Pedro E. Maldonado, University of Chile, Chile

Reviewed by:
Eric Fortune, New Jersey Institute of Technology, United States
Angel Nunez, Autonomous University of Madrid, Spain

****Correspondence:***
Maurice J. Chacron
maurice.chacron@mcgill.ca

Received: *22 April 2020*
Accepted: *15 June 2020*
Published: *07 July 2020*

Citation:
Marquez MM and Chacron MJ (2020) Serotonergic Modulation of Sensory Neuron Activity and Behavior in Apteronotus albifrons. Front. Integr. Neurosci. 14:38. doi: 10.3389/fnint.2020.00038

INTRODUCTION

Organisms must detect and perceive natural stimuli efficiently and adaptively to survive in ever-changing environments (Wark et al., 2007; Sharpee et al., 2014). Serotonergic fibers originating from the raphe nuclei are found across sensory brain areas in all vertebrate species (Parent, 1981; Hurley et al., 2004) and are thought, in part, to help mediate adaptive sensory

neural responses to changes in input (Marder, 2012). Here, we used a comparative approach to better understand the function of the serotonergic system in sensory systems. Specifically, we investigated how serotonin application affects neural and behavioral responses to sensory input in the weakly electric fish species *Apteronotus albifrons* using the same paradigms used previously by our group (Marquez and Chacron, 2020b) in the closely related species *Apteronotus leptorhynchus*.

Gymnotiform weakly electric fish generate a quasi-sinusoidal electric field through their electric organ discharge (EOD) and can sense amplitude modulations of this field through an array of electroreceptor afferents embedded in their skin (Turner et al., 1999). Electroreceptor afferents make synaptic contact with pyramidal cells within the electrosensory lateral line lobe (ELL), which in turn project to higher brain centers mediating behavioral responses (Rose, 2004). Natural electrosensory stimuli comprise those caused by conspecifics. Specifically, when two fish are located close to one another (i.e., <1 m apart), interference between their EODs gives rise to sinusoidal amplitude modulation (AM) whose frequency is given by the difference between the EOD frequencies. Changes in the relative orientation and distance between both animals give rise to changes in the amplitude (i.e., the envelope) of the sinusoidal amplitude modulation (Yu et al., 2012; Fotowat et al., 2013; Metzen and Chacron, 2014; Huang et al., 2019). As such, the frequency components of the envelope are directly associated with the statistics of the relative movement between fish. The responses of ELL pyramidal cells to envelope stimuli have been well-characterized in both *A. leptorhynchus* (Huang and Chacron, 2016; Huang et al., 2016, 2018; Metzen et al., 2018; for review see Huang and Chacron, 2017; Metzen and Chacron, 2019) and *A. albifrons* (Martinez et al., 2016). Particularly, it has been shown that the tuning of ELL pyramidal cells to envelope stimuli is similar in both species. Notably, both *A. leptorhynchus* and *A. albifrons* display identical behavioral responses to envelope stimuli in that the animal's EOD frequency follows the detailed timecourse of the envelope in an almost one-to-one fashion (Metzen and Chacron, 2014, 2015; Huang et al., 2016; Martinez et al., 2016; Thomas et al., 2018).

ELL pyramidal cells also receive large amounts of descending input (for review see Hofmann and Chacron, 2019) including serotonergic innervation (Johnston et al., 1990; Deemyad et al., 2011; Fotowat et al., 2016; for review see Márquez et al., 2013; Marquez and Chacron, 2020a). Previous studies carried out in *A. leptorhynchus* have shown that serotonin increases pyramidal neuron excitability by promoting burst firing through inhibition of potassium channels (Deemyad et al., 2011, 2013; Larson et al., 2014; Marquez and Chacron, 2020b). In the case of envelopes, it was shown in *A. leptorhynchus* that serotonin application increases neural sensitivity to these stimuli, with greater increases in sensitivity for higher temporal frequencies, due to an increase in burst firing during stimulation. At the organismal level, it was shown that serotonin application increases behavioral sensitivity to envelopes, but that there was a greater increase in sensitivity for lower temporal frequencies (Marquez and Chacron, 2020b). In contrast, how serotonin affects neural and behavioral responses in *A. albifrons* has not been extensively characterized. Although it was recently shown that serotonin application increases pyramidal neuron excitability through increased burst firing, which enhances their responses to moving objects (Marquez and Chacron, 2018), how serotonin application affects neural and behavioral responses to envelope stimuli has not been investigated in *A. albifrons*.

Here, we used both electrophysiological recordings and behavioral assays to investigate how serotonin application alters ELL pyramidal cell and behavioral responses to envelope stimuli in *A. albifrons*. Our results show that serotonin application increases ELL pyramidal neuron excitability through increased burst firing under baseline conditions (i.e., in the presence of the animals unmodulated EOD). Serotonin application increased ELL pyramidal cell responses to envelope stimuli, with greater increases seen for high temporal frequencies. At the organismal level, serotonin application increased behavioral sensitivity, such that envelope stimuli gave rise to greater modulations in EOD frequency. Unexpectedly, such increases in behavioral sensitivity were greatest for higher temporal frequencies. We discuss the implications of our results in the context of previous ones obtained for *A. leptorhynchus*.

MATERIALS AND METHODS

We note that the purpose of this study was to investigate how serotonin affected both ELL pyramidal cell and behavioral responses in *A. albifrons* and to compare these results with those previously obtained in *A. leptorhynchus*. As such, the methodology used in this article is the same as that used previously (Marquez and Chacron, 2020b), except that the experiments were performed in a different species. We used wording similar to that found within the methods section of Marquez and Chacron (2020b) to facilitate the comparison between both studies.

Ethics Statement

All animal care and experimental procedures were reviewed and approved by McGill University's animal care committee under protocol number 5285.

Animals

We used a total of $N = 26$ *A. albifrons* specimens of either sex in this study. Animals were acquired from tropical fish suppliers and acclimated to laboratory conditions according to published guidelines (Hitschfeld et al., 2009).

Surgery and Recordings

Surgical procedures have been described in detail previously (Deemyad et al., 2013; Marquez and Chacron, 2018). Briefly, tubocurarine chloride hydrate (0.1–0.5 mg) was injected to immobilize animals ($N = 26$). These were then transferred to an experimental tank and we used a constant flow of water over the gills (∼10 ml/min) for respiration. A portion of the animal's head was kept out of the water and anesthetized locally with lidocaine ointment (5%). Then, to expose the hindbrain

for recording, a small craniotomy (∼5 mm^2) was made above the hindbrain for recordings. Extracellular recordings from pyramidal cells within the lateral segment (n = 16), based on recording depth and mediolateral positioning of the electrodes, were performed with micropipettes filled with Woods Metal alloy (LMA-117, Small Parts Inc) following standard methodology (Frank and Becker, 1964). The sample sizes are similar to those used in previous studies. Recordings were digitized at 10 kHz (CED Power 1401 and Spike 2 software, Cambridge Electronic Design) and stored on a computer for subsequent analysis. The population-averaged baseline (i.e., when the animal's EOD was not modulated) firing rate was 11.38 ± 5.78 Hz and was similar to that reported in previous studies (Martinez et al., 2016; Marquez and Chacron, 2018).

Action potential times were defined as the times at which the signal crossed a suitably chosen threshold value. Baseline statistics (e.g., firing rate) were obtained from 100 s of baseline activity before stimulus presentation. A burst threshold corresponding to the trough of the bimodal interspike interval (ISI) distribution (typically 10 ms) was used to separate the full spike train into the burst train and the isolated spike train, as done previously (Oswald et al., 2004; Ellis et al., 2007; Khosravi-Hashemi et al., 2011; Khosravi-Hashemi and Chacron, 2012, 2014; Deemyad et al., 2013; Marquez and Chacron, 2018). Specifically, if an ISI was less than the threshold, then the two action potentials were deemed to be part of a burst; if the next ISI was also less than the threshold, then the third action potential was also deemed to be part of the same burst. This process continues until the ISI is greater than the threshold. The isolated spike train consists of spikes that were not part of bursts. Burst fraction was defined as the ratio of the number of spikes that belong to a burst to the total number of spikes.

To visualize neural responses to envelopes, we created a binary sequence $R(t)$ with binwidth Δt = 0.1 ms from the spike time sequence and set the content of each bin to equal the number of spikes which fell within that bin. Time-dependent firing rates were obtained by low-pass filtering the binary sequences using a Kaiser filter whose cutoff frequency was 0.1% higher than the envelope frequency (see below).

To quantify neural responses to envelopes, we used linear systems identification techniques. Specifically, the neural gain is defined as the ratio of the amplitude of the modulated firing rate response and the amplitude of the stimulus obtained from a dipole in the water. To determine the firing rate modulation, we computed the phase histogram and fitted a sinewave to it as done previously (Marquez and Chacron, 2020b). The response phase was calculated as the average phase at which the fitted sinewave reached its maximum value relative to the maximum value of the stimulus waveform.

Stimulation

The neurogenic electric organ of *A. albifrons* is not affected by the injection of curare-like drugs. Stimuli consisted of amplitude modulations of the animal's own EOD and were produced by first detecting the EOD zero crossings, then generating a sinusoidal waveform train with a frequency slightly greater (20–30 Hz) than the EOD frequency that is triggered by the EOD zero crossings. This train is thus synchronized to the fish's EOD and will either increase or decrease the EOD amplitude based on polarity and intensity. This train is then multiplied (MT3 multiplier, Tucker Davis Technologies) with an amplitude modulated waveform (i.e., the stimulus). The resultant signal is then isolated from ground (A395 linear stimulus isolator, World Precision Instruments) and delivered to the experimental tank *via* two chloridized silver wire electrodes located ∼15 cm on each side of the animal (Bastian et al., 2002). To elicit neural and behavioral responses to envelopes, we used band-pass filtered noise (5–15 Hz, 4th order Butterworth) whose amplitude (i.e., the envelope) was modulated sinusoidally at 0.05, 0.1, 0.2, 0.5, 0.75, and 1 Hz. This stimulus structure is the same as that used previously in *A. leptorhynchus* (Marquez and Chacron, 2020b). We used a low pass filtered Gaussian white noise stimulus and zero mean (8th order Butterworth filter, 120 Hz cutoff frequency) to distinguish between cell types as described below. We also used a 4 Hz sinusoidal amplitude modulation to elicit behavioral responses (see below). Stimulus intensity was adjusted to produce changes in EOD amplitude that were ∼25% of the baseline level.

Behavior

We first recorded the jamming avoidance response (JAR) in response to a 4 Hz sinusoidal AM stimulation as mentioned above. The JAR magnitude was defined as the maximum EOD frequency elicited during stimulation relative to the EOD frequency baseline value (i.e., before stimulation). JAR responses were averaged across five stimulus presentations of 50 s each and compared before and after serotonin application as done previously (Deemyad et al., 2013; Marquez and Chacron, 2020b). Behavioral responses to sinusoidal envelopes were quantified using linear systems identifications techniques (Metzen and Chacron, 2014). Thus, the gain was defined as the ratio of the EOD frequency peak-to-peak amplitude to that of the envelope stimulus, the phase is the amount of time relative to the envelope cycle that EOD frequency must be shifted by to be in phase with the sinusoidal envelope stimulus, and the offset is the difference between the mean EOD frequency during stimulation and the EOD frequency baseline value.

Serotonin Application

Glutamate (1 mM; Sigma-Aldrich) and serotonin (1 mM; Sigma-Aldrich) were dissolved in saline (111 mM NaCl, 2 mM KCl, 2 mM $CaCl_2$, 1 mM $MgSO_4$, 1 mM $NaHCO_3$ and 0.5 mM NaH_2PO_4; Sigma-Aldrich) for application. Drug application electrodes were made using either two-barrel (for electrophysiology) or single-barrel (for behavior) glass micropipettes as described previously (Huang et al., 2018, 2019; Marquez and Chacron, 2018, 2020b; Metzen et al., 2018). For single neuron recordings, two-barrel pipettes were used for independent application of serotonin or glutamate in the vicinity of the neuron being recorded. We relied on glutamate-elicited excitatory responses to verify that the pipette was correctly placed next to the neuron we were recording from, as done previously (Bastian, 1993; Marquez and Chacron, 2020b). For behavioral experiments, single-barrel pipettes were used for the bilateral application of serotonin in the lateral segment of the ELL. Drugs

were delivered using a picospritzer at 15–25 p.s.i. during 100 ms, as done previously (Deemyad et al., 2013; Huang et al., 2018; Marquez and Chacron, 2018, 2020b). We note that previous studies have shown that the application of saline alone in this manner does not significantly alter either ELL pyramidal cell activity or behavior (Deemyad et al., 2013; Huang et al., 2016).

Classification of Cell Types

Previous studies have shown that there are two types of ELL pyramidal cells, while ON-type cells respond with excitation to increases in EOD amplitude, OFF-type cells instead respond with excitation to decreases in EOD amplitude (Saunders and Bastian, 1984; Martinez et al., 2016). We used a low pass filtered Gaussian white noise stimulus and zero mean (8th order Butterworth filter, 120 Hz cutoff frequency) as an amplitude modulation to distinguish between ON- and OFF-type ELL pyramidal cells, as described previously (Martinez et al., 2016). Specifically, we computed the spike-triggered average (STA) by averaging stimulus segments during 1 s windows centered at the action potential times. Thus, the STA is given by $\frac{1}{N}\sum_{(i=1)}^{N} S(t-t_i)$, where $S(t)$ is the 0–120 Hz stimulus, t_i is the ith spike time, and N is the total number of action potentials. The average STA slope within a time window of 10 ms centered at 7 ms before the action potential time was used to distinguish between ON- and OFF-type cells. The 7 ms accounts for the transmission delay from the skin surface to pyramidal cells within the ELL (Chacron et al., 2003). Cells for which slope was positive were classified as ON-type and cells for which the slope was negative were classified as OFF-type (Martinez et al., 2016). Confirming previous results by Martinez et al. (2016), we found no differences between the responses of ON- and OFF-type cells to envelope stimuli before serotonin application. Moreover, we found no differences in the effects of serotonin on either the baseline activity of ON- and OFF-type ELL pyramidal cells (change in burst fraction: ON-type 0.17 ± 0.16, OFF-type 0.22 ± 0.23, Kruskal–Wallis test, chi-square = 0.33, df = 1, P = 0.56; change in firing rate: ON-type 5.25 ± 5.05 Hz, OFF-type 4.71 ± 1.28 Hz, Kruskal–Wallis test, chi-square = 0.89, df = 1, P = 0.34), or the change in sensitivity (ON-type: change in sensitivity 3.03 ± 3.57 (spk/s)/(mV/cm); OFF-type change in sensitivity 4.74 ± 10.66 (spk/s)/(mV/cm); Kruskal–Wallis test, chi-square = 0.71, df = 1, P = 0.40), best-fit power law exponent to neural tuning curve (ON-type: change in α exponent 0.34 ± 0.33; OFF-type change in α exponent 0.17 ± 0.35; Kruskal–Wallis test, chi-square = 2.48, df = 1, P = 0.12) and phase (ON-type: change in phase −9.50 ± 16.09 deg; OFF-type change in phase −2.40 ± 20.22 deg; Kruskal–Wallis test, chi-square = 0.80, df = 1, P = 0.37) during stimulation. For these reasons, data from ON- and OFF-type cells were pooled.

Statistics

All values are reported as means ± SD throughout. Statistical significance was evaluated through either a parametric Student's t-test or a non-parametric Wilcoxon's signed-rank test for paired measurements at the P = 0.05 level. The choice of the test was based on: (1) whether the data followed a normal distribution (parametric test) or not (non-parametric test), as assessed by a Lilliefors test; and (2) whether the data had the same variance, as asses by an F-test. For multiple comparisons of phase and offset values, statistical significance was assessed through a Kruskal–Wallis test at the P = 0.05 level, since all the values followed a not normal distribution as assessed by a Lilliefors test. Correlations were calculated using Pearson's correlation coefficient. For the whisker boxplots, the central mark indicates the median, and the bottom and top edges indicate the 25th and 75th percentiles, respectively. Whiskers extend to the values that are not considered outliers. All data points including outliers are plotted. To improve the readability of data points in some figures, we plotted compact box plots that include the median, the bottom, and top edges only.

RESULTS

We investigated how serotonin altered both neural and behavioral responses to envelope stimuli. To do so, we recorded neural activity as well as behavioral responses, which consist of changes in the EOD frequency, from immobilized animals in a tank while presenting different stimuli (**Figure 1A**). Our recordings were from pyramidal cells within the lateral segment (LS) of ELL that receives neuromodulatory input from the raphe nuclei (**Figure 1B**).

Serotonin Application Increases ELL Pyramidal Cell Excitability Through Increased Burst Firing

We first investigated how serotonin application affected ELL pyramidal cell activity under baseline conditions (i.e., when the animal's EOD was not modulated). To do so, extracellular recordings from ELL pyramidal cells were obtained (see "Materials and Methods" section) while a double-barrel pipette containing both glutamate and serotonin was advanced independently (**Figure 2A**). We used glutamate to ascertain that the double-barrel pipette was in the vicinity of the cell recorded from, as ascertained from short-latency increases in spiking activity when glutamate is ejected *via* air pressure (see "Materials and Methods" section). Serotonin was then applied *via* air pressure. **Figure 2B** (top, black trace, and large arrows) shows the recorded spiking activity from a typical ELL pyramidal cell before serotonin application. Spiking activity typically consisted of isolated spikes (**Figure 2B**, top, small arrows) and occasional bursts (**Figure 2B**, top, vertical bars). However, after serotonin application, this same cell displayed an increased tendency to fire bursts of action potentials (**Figure 2B**, bottom, magenta; compare with top panel). The spike train consisted mostly of bursts with larger length and much fewer isolated spikes (**Figure 2B**, bottom, vertical bars, and small arrows; compare with top panel). This change in excitability was also seen when plotting the distribution of ISIs (the time between consecutive action potentials; **Figure 2C**). We found that the ISI distribution was bimodal before (**Figure 2C**, black) and after (**Figure 2C**, magenta) and used the ISI corresponding to the trough between both modes as a threshold to separate the spike train into bursts and isolated spikes (see "Materials

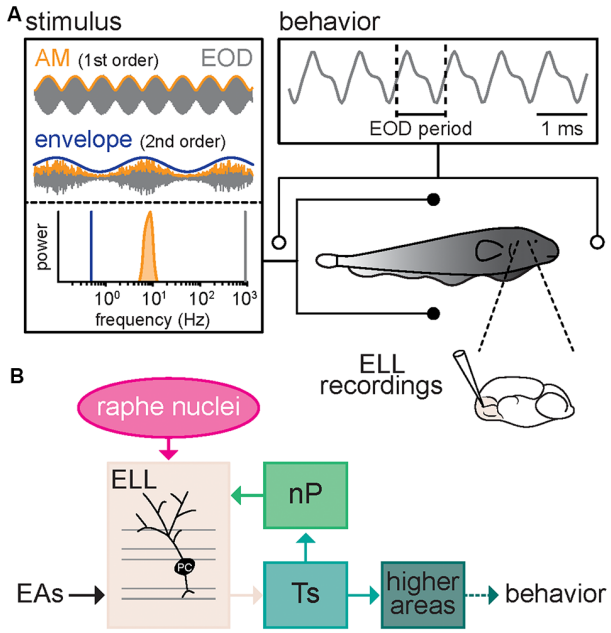

FIGURE 1 | Schematic of the experimental setup. **(A)** Schematic showing the recording setup. A fish is placed in a tank while its electric organ discharge (EOD) is being recorded *via* two electrodes located near the animal's head and tail. The neural responses consist of single-unit recordings from pyramidal neurons within the electrosensory lateral line lobe (ELL). The behavioral responses consist of changes in the frequency (i.e., the inverse of the period) of the quasi-sinusoidal EOD signal. The stimuli consist of amplitude modulations (AMs, orange) of the animal's own EOD (gray) that were either a 4 Hz sinewave (top, orange, AM or 1st order) or 5–15 Hz noise (bottom, orange, AM or 1st order) whose amplitude (bottom, blue, envelope or 2nd order) varied sinusoidally. Also shown are the frequency contents of the envelope (blue), AM (orange), and full signal (gray). **(B)** Schematic showing successive brain areas involved in the processing of electrosensory stimuli. Electroreceptor afferents (EAs) respond to EOD AMs and project to pyramidal cells (PC) within the ELL. ELL pyramidal cells in turn project to the midbrain Torus semicircularis (Ts) and indirectly to higher brain areas, thereby mediating behavioral responses. ELL pyramidal cells also receive descending projections from higher brain centers *via* the nucleus praeeminentialis (nP), as well as serotonergic fibers from the raphe nuclei (magenta).

and Methods" section). Qualitatively similar results were seen across our dataset. Overall, serotonin application significantly increased both the mean firing rate (**Figure 2D**; control: 11.38 ± 5.78 Hz; serotonin: 16.36 ± 7.42 Hz; Wilcoxon's signed-rank test, $P < 0.001$) and the burst fraction (i.e., the fraction of action potentials belonging to bursts; **Figure 2E**; control: 0.18 ± 0.15 Hz; serotonin: 0.37 ± 0.21 Hz; Wilcoxon's signed-rank test, $P < 0.01$). There was no significant correlation between the change in burst fraction due to serotonin application and the cell's firing rate before serotonin application ($r = 0.05$, $n = 16$, $p = 0.87$).

Serotonin Application Increases ELL Pyramidal Cell Responses to Envelope Stimuli

Next, we investigated how serotonin application affected ELL pyramidal cell responses to envelope stimuli. To do so, we used the same setup to apply serotonin except that the same envelope stimuli were presented to each neuron before (i.e., control) and after serotonin application (**Figure 3A**). Envelope stimuli consisted of sinewaves with frequencies 0.05 Hz, 0.1 Hz, 0.2 Hz, 0.5 Hz, 0.75 Hz, and 1 Hz (see "Materials and Methods" section). The response of a typical ELL pyramidal cell before serotonin application to a sinusoidal envelope stimulus is shown in **Figure 3B** (top, black). ELL pyramidal cells typically increased their spiking activity near the local maxima of the envelope, such that there was a noticeable modulation in the time-dependent firing rate (**Figure 3B**, black). After serotonin application, there was increased burst firing near the local maxima of the envelope, such that the modulation in firing rate was greater (**Figure 3B**, magenta). Indeed, there were significant increases in both burst fraction (**Figure 3C**) and firing rate (**Figure 3D**) for all envelope frequencies tested. As the neural responses followed the stimulus waveform in an almost one-to-one fashion during both conditions, we used linear systems analysis to quantify the responses of ELL pyramidal cells to envelope stimuli. Specifically, we computed both the neural gain, which is the ratio of the amplitude of the firing rate modulation to that of the envelope stimulus and the phase, which is the amount of time by which one must shift the envelope stimulus to be in phase with the firing rate response relative to the stimulus period (see "Materials and Methods" section). Before the serotonin application, we found that neural gain increased as a power law as a function of increasing envelope frequency (**Figure 3E**, black), which is consistent with previous results (Martinez et al., 2016). After serotonin application, the neural gain was increased primarily for higher envelope frequencies (**Figure 3E**, magenta). This change was quantified by computing the best-fit power-law exponent to the neural tuning curves (i.e., the neural gain as a function of envelope frequency) before (**Figure 3F**, black) and after (**Figure 3F**, magenta) serotonin application. We found that serotonin application significantly increased the power-law exponent (**Figure 3F**, compare black and magenta; control: 0.30 ± 0.33; serotonin: 0.55 ± 0.32 Hz; Student's t-test, $P < 0.05$). Overall, there was no significant correlation between the change in exponent due to serotonin application and the cell's baseline firing rate before serotonin application ($r = 0.27$, $n = 16$, $p = 0.32$). When analyzing the phase relationship between the envelope stimulus and the firing rate response, we observed that it remained relatively constant and that it was not significantly altered by serotonin application (**Figure 3G**, compare black and magenta; Kruskal–Wallis test, chi-square = 0.94, $df = 1$, $P = 0.01$).

Increased ELL Pyramidal Cell Responses to Envelope Stimuli Due to Serotonin Application Are Primarily Due to Increased Burst Firing

To gain a better understanding as to how serotonin application led to increased ELL pyramidal cell responses to envelope stimuli, we separated the spike train into the burst and isolated spike trains (see "Materials and Methods" section). Our results show that, when considering only the burst train, there was increased rate modulation after serotonin

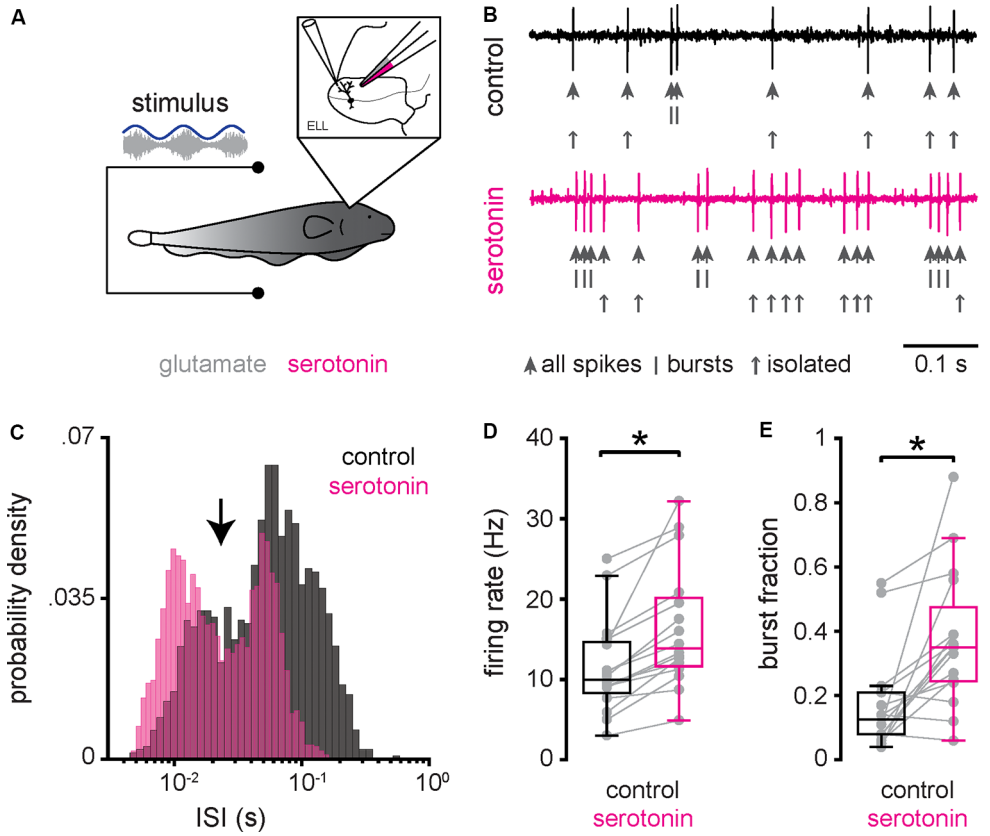

FIGURE 2 | Serotonin application increases ELL pyramidal neuron excitability and promotes burst firing under baseline conditions. **(A)** Schematic showing a pyramidal cell that is being recorded from extracellularly while a double-barrel pipette containing both glutamate and serotonin is located in the vicinity. Glutamate is used to ascertain that the double-barrel pipette is close to the pyramidal cell being recorded from as judged from short-latency increases in firing rate following glutamate release *via* air pressure (Bastian, 1993; Marquez and Chacron, 2018, 2020b). Serotonin is then applied *via* air pressure (see "Materials and Methods" section). **(B)** Extracellular recording from a typical pyramidal cell before (top, black) and after (bottom, magenta) application of serotonin. In each case, the action potentials are indicated by large vertical arrows, while the spikes belonging to bursts and isolated spikes (i.e., spikes not belonging to bursts) are indicated by vertical bars and small vertical arrows, respectively. **(C)** Interspike interval (ISI) distribution from this same example pyramidal neuron before (black) and after (magenta) serotonin application. Note the bimodal distribution. An ISI threshold corresponding to the trough between both modes (vertical arrow) was used to separate the spike train into bursts and isolated spikes (see "Materials and Methods" section). **(D)** Firing-rate before (left, black) was significantly lower than that after (right, magenta) serotonin application. **(E)** Burst fraction (i.e., the fraction of action potentials belonging to bursts; see "Materials and Methods" section) was significantly lower before (left, black) as compared to after (right, magenta) serotonin application. *Indicates a statistically significant difference at the $p = 0.05$ level as indicated by a Wilcoxon's signed-rank test.

application (**Figure 4A**), as observed for the full spike train. As such, neural gain computed from the burst train was increased after serotonin application primarily for higher envelope frequencies (**Figure 4B**, compare black and magenta). Thus, serotonin application led to a significant increase in the best-fit power-law exponent (**Figure 4C**, compare black and magenta, control: 0.20 ± 0.33 Hz; serotonin: 0.42 ± 0.32 Hz; Student's *t*-test, $P < 0.05$). Overall, serotonin application significantly increased the firing rate computed from the burst train (**Figure 4D**, compare black and magenta). We found no significant change in the phase (**Figure 4E**, compare black and magenta, Kruskal–Wallis test, chi-square = 1.45, $df = 1$, $P = 0.23$).

Qualitatively different results were observed when instead considering the isolated spike train (**Figure 4F**). Indeed, the rate computed from the isolated spike train displayed much weaker modulation before serotonin application than those obtained from the burst train or the full spike train (compare short-dashed black trace in **Figure 4F** to long-dashed black trace in **Figure 4A** and solid black trace in **Figure 3B**, respectively). Moreover, after serotonin application, there was no increase in modulation when considering the isolated spike train (**Figure 4F**, compare black and magenta short-dashed traces). As such, serotonin application did not lead to significant increases in either of neural gain (**Figure 4G**, compare black and magenta), best-fit power-law exponent (**Figure 4H**, compare black and magenta, control: 0.21 ± 0.31 Hz; serotonin: 0.35 ± 0.36 Hz; Student's *t*-test, $P = 0.12$), firing rate computed from the isolated spike train (**Figure 4I**, compare black and magenta), or phase (**Figure 4J**, compare black and magenta, Kruskal–Wallis test, chi-square = 0.78, $df = 1$, $P = 0.38$). We thus conclude that the changes in the neural gain observed after serotonin application

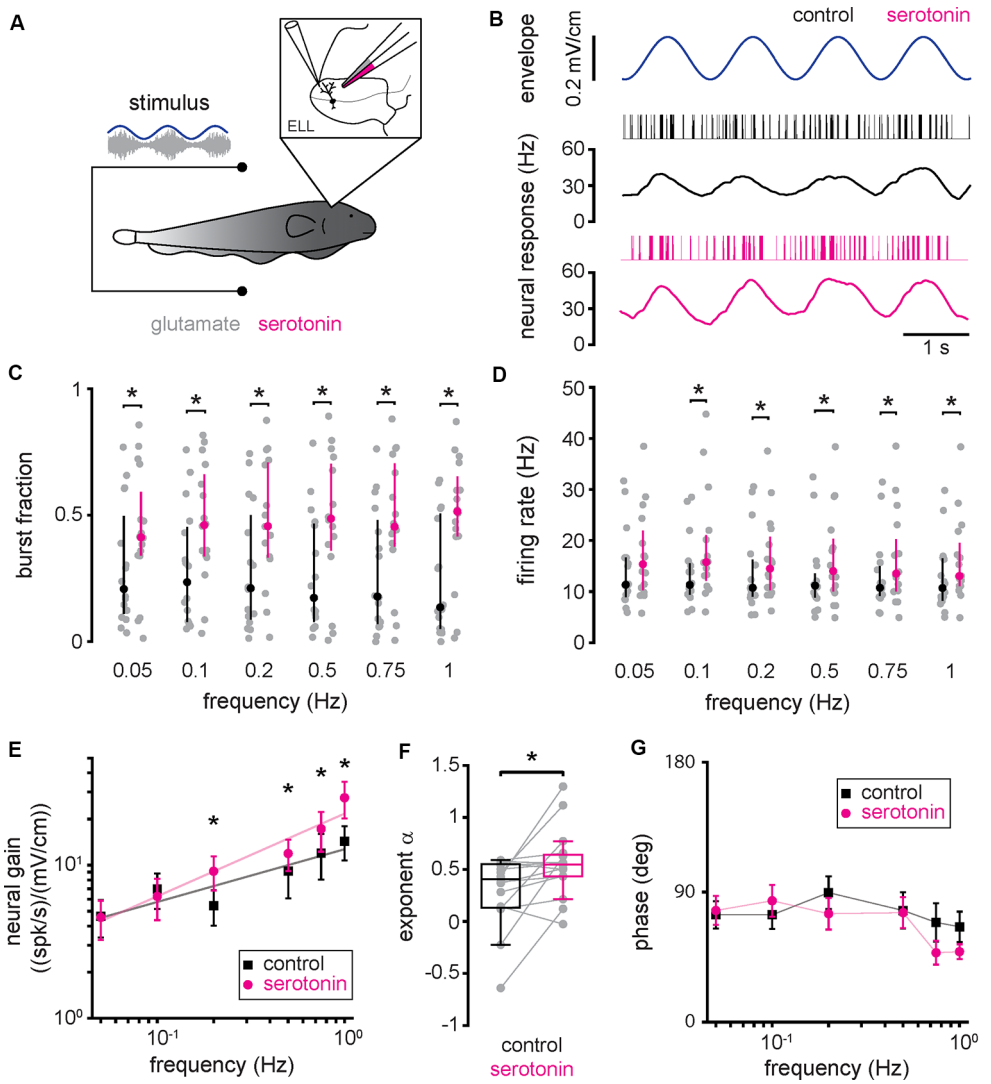

FIGURE 3 | Serotonin application increases pyramidal neuron responses to envelope stimuli through increased burst firing. **(A)** Schematic showing a pyramidal cell that is being recorded from extracellularly while a double-barrel pipette containing both glutamate as well as serotonin is located in the vicinity. **(B)** Spike train (black vertical bars) and firing rate (black trace) responses from a typical pyramidal cell to an envelope stimulus (blue, top) before serotonin application. Also shown are the spike train (magenta vertical bars) and firing rate (magenta trace) responses from this same pyramidal cell to the envelope stimulus (blue, top) after serotonin application. **(C)** Burst fraction before (black) and after (magenta) serotonin application for all envelope frequencies tested. **(D)** Firing-rate before (black) and after (magenta) serotonin application for all envelope frequencies tested. **(E)** Population averaged sensitivity (i.e., neural gain) between the envelope stimulus and the full spike train before (black) and after (magenta) serotonin application as a function of temporal frequency. **(F)** Best-fit power-law exponents before (left, black) and after (right, magenta) serotonin application to the neural gain as a function of temporal frequency curves shown in panel **(E)**. **(G)** Population averaged phase between the envelope stimulus and the full spike train before (black) and after (magenta) serotonin application as a function of temporal frequency. Throughout, "*" indicates a statistically significant difference at the $p = 0.05$ level using either a Wilcoxon's signed-rank test or a Student's *t*-test.

are primarily, if not exclusively, due to changes in the burst rather than isolated spike firing.

Serotonin Application Increases the Jamming Avoidance Response

Next, we investigated the effects of serotonin application on behavioral responses. To do so, serotonin was applied bilaterally into the ELL while the animal was being stimulated and behavioral responses recorded (**Figure 5A**; see "Materials and Methods" section). We first studied the effects of serotonin application in the extensively studied JAR. The JAR consists of an increase in EOD frequency during stimulation caused by interference of signals with similar frequencies (Hitschfeld et al., 2009; Deemyad et al., 2013) and it has been shown previously that serotonin increases the JAR magnitude in *A. leptorhynchus*. Thus, we compared the magnitude of the JAR before and after serotonin application using a 4 Hz sinusoidal AM stimulus (see "Materials and Methods" section). We found that serotonin

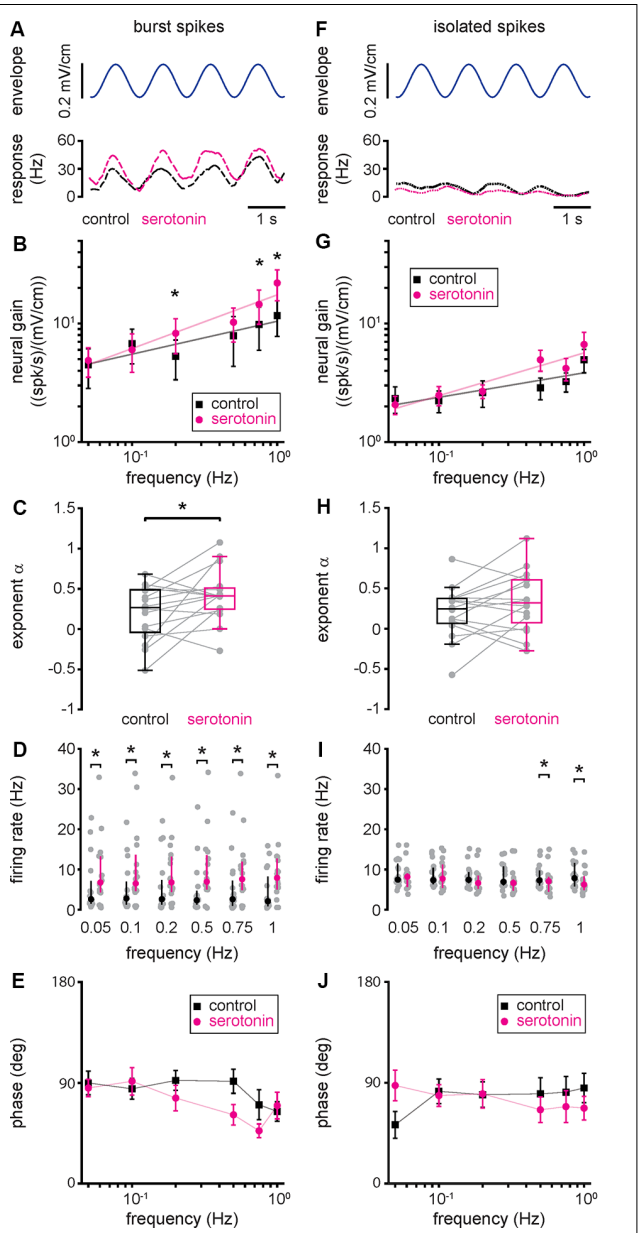

FIGURE 4 | Changes in neural responses to envelope stimuli due to serotonin application are due to changes in burst firing. **(A)** Envelope stimulus (top, blue) and the firing rate responses (bottom) of the burst (long-dashed) spike train before (black) and after (magenta) serotonin application. **(B)** Population averaged sensitivity (i.e., neural gain) between the envelope stimulus and the burst spike train before (black) and after (magenta) serotonin application as a function of temporal frequency. **(C)** Best-fit power-law exponents before (left, black) and after (right, magenta) serotonin application. **(D)** Firing-rate before (black) and after (magenta) serotonin application for all envelope frequencies tested when using the burst train. **(E)** Population averaged phase between the envelope stimulus and the burst spike train before (black) and after (magenta) serotonin application as a function of temporal frequency. **(F)** Same as **(A)**, but for the isolated spike train (short-dashed). **(G)** Same as **(B)**, but for the isolated spike train. **(H)** Same as **(C)**, but for the isolated spike train. **(I)** Same as **(D)**, but for the isolated spike train. **(J)** Same as **(E)**, but for the isolated spike train. Throughout, "*" indicates a statistically significant difference at the $p = 0.05$ level using either a Wilcoxon's signed-rank test or a Student's t-test.

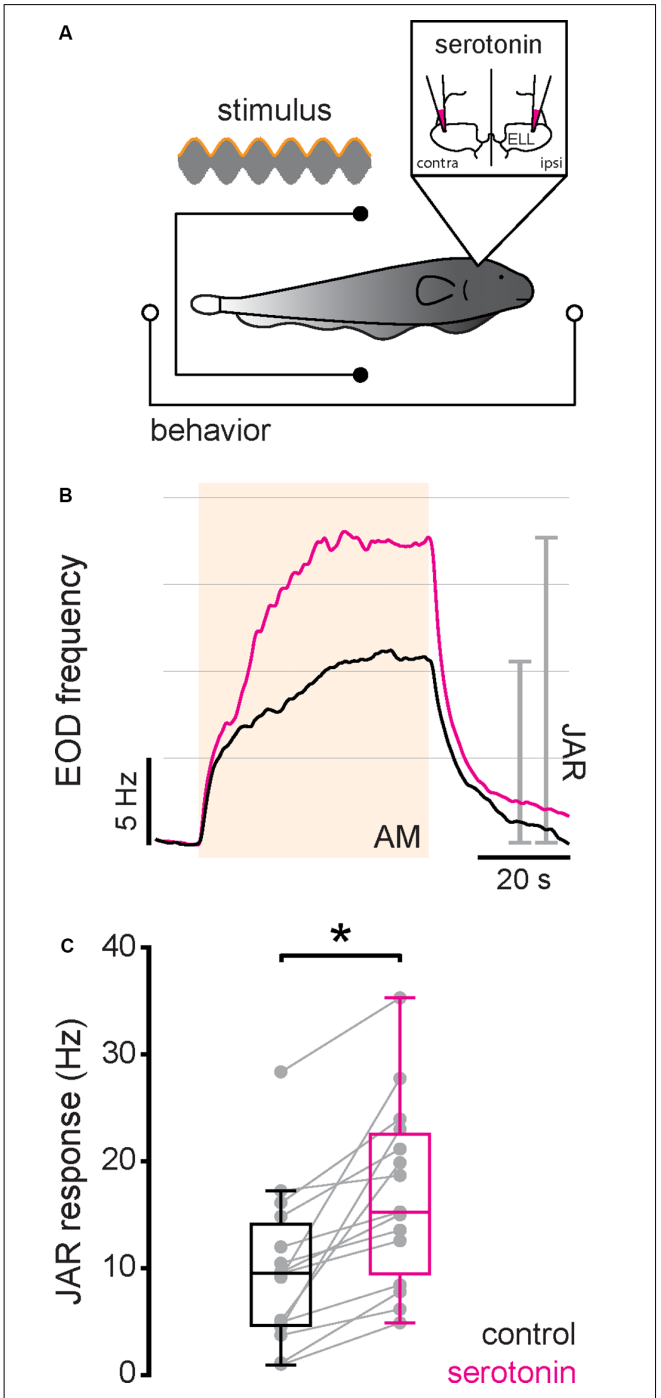

FIGURE 5 | Serotonin application increases the jamming avoidance response (JAR) response. **(A)** Schematic showing the setup in which the animal's behavior (EOD) was recorded while being stimulated and serotonin injected bilaterally in the ELL. **(B)** Time course of the EOD frequency for a typical fish before (black) and after (magenta) serotonin application. The stimulus was a 4 Hz sinusoidal AM (see "Materials and Methods" section). The shaded band indicates the period during which the stimulus was applied. The JAR magnitude is measured as the change in EOD frequency from immediately before the stimulus onset to immediately before stimulus offset (gray lines). **(C)** Jar magnitude before (black) and after (magenta) serotonin application. Serotonin application significantly increased the JAR magnitude (Student's t-test, $P < 0.001$) as indicated by the "*".

application was indeed effective, as the JAR magnitude was increased after serotonin application in both an example fish (**Figure 5B**, compare black and magenta) and significantly across our dataset (**Figure 5C**, compare black and magenta, control: 9.87 ± 6.99 Hz; serotonin: 16.90 ± 8.26 Hz; Student's *t*-test, $P < 0.001$).

Serotonin Application Increases Behavioral Responses to Envelope Stimuli

We next tested whether and, if so, how serotonin application affects behavioral responses to envelope stimuli. To do so, we presented the same envelope stimuli used for electrophysiology before and after applying serotonin bilaterally into the ELL (**Figure 6A**). **Figure 6B** shows a representative EOD frequency change (bottom) in response to the envelope stimulus (top, blue) before (black) and after (magenta) serotonin application. Before the serotonin application, the behavioral response consisted of an overall increase in the EOD frequency which was modulated quasi-sinusoidally (**Figure 6B**, black), consistent with previous results (Metzen and Chacron, 2014; Martinez et al., 2016). After serotonin application, we found that the EOD frequency was greater overall during stimulation and displayed greater quasi-sinusoidal modulations that follow the stimulus waveform (**Figure 6B**, magenta). As such, we used linear systems identification techniques to quantify the behavioral response. Specifically, we computed the behavioral gain as the ratio of the EOD frequency modulation amplitude (i.e., "A_{output}") to that of the stimulus (i.e., "A_{input}"). We also computed the phase, which is the amount of time by which the envelope stimulus must be shifted to be in phase with the EOD frequency, as well as the offset, which was computed as the difference between the mean EOD frequency during the stimulus and that before stimulus onset (see **Figure 6B** and "Materials and Methods" section). Before the serotonin application, the behavioral gain decreased as a power law with increasing envelope frequency (**Figure 6C**, black), consistent with previous results (Martinez et al., 2016). However, serotonin application led to a greater increase in behavioral gain for higher envelope frequencies (**Figure 6C**, compare black and magenta). As such, the best-fit power-law exponent increased after serotonin application (**Figure 6D**, compare black and magenta; control: −0.99 ± 0.19 Hz; serotonin: −0.80 ± 0.25 Hz; Student's *t*-test, $P < 0.05$), such that the behavioral gain decreased less steeply with increasing envelope frequency (**Figure 6C**, compare black and magenta). We observed no significant change in phase (**Figure 6E**, compare black and magenta; Kruskal–Wallis test, chi-square = 0.41, $df = 1$, $P = 0.52$) and an overall increased offset (**Figure 6F**, compare black and magenta; Kruskal–Wallis test, chi-square = 8.31, $df = 1$, $P < 0.05$) after serotonin application.

Changes in Burst Firing Due to Serotonin Application Best Correlate With the Resulting Changes in Behavior

Finally, we investigated the relationship between changes in neural and behavioral responses due to serotonin application. To do so, we computed the relative change in behavioral gain for the different envelope frequencies and correlated this quantity with the relative change in neural gain when considering all spikes (**Figure 7A**; $r = 0.54$, $n = 6$, $p = 0.27$), burst spikes (**Figure 7B**; $r = 0.90$, $n = 6$, $p < 0.05$), and isolated spikes (**Figure 7C**; $r = 0.28$, $n = 6$, $p = 0.59$). Overall, we found a significant correlation only for burst spikes, which suggests that bursts rather than isolated spikes are being decoded downstream to help generate behavioral responses. This is further discussed below.

DISCUSSION

Summary of Results

We investigated the effects of serotonin on both lateral segment ELL pyramidal cell and behavioral responses to envelope stimuli in the weakly electric fish *A. albifrons*. Serotonin application increased ELL pyramidal cell excitability and promoted burst firing under baseline conditions. In response to envelope stimuli, serotonin application increased the response gain, such that the envelope stimulus gave rise to greater modulation in firing rate. There was a greater increase in gain for high envelope frequencies, such that neural gain increased more steeply as a function of envelope frequency, as quantified by a greater power-law exponent. Such changes in responsiveness were primarily, if not exclusively, due to increased burst firing. This is because serotonin application did not lead to significant changes in responsiveness when considering the isolated spike train. Finally, we investigated the effects of serotonin application on behavioral responses. Serotonin application increased behavioral gain, such that envelope stimuli gave rise to greater modulations in EOD frequency. There was a greater increase in behavioral gain for greater envelope frequencies, such that behavioral gain decreased less steeply as a function of increasing frequency after serotonin application, as quantified by a power-law exponent with decreased magnitude. Overall, changes in behavioral gain as a function of frequency were best correlated with changes in neural gain when considering bursts, rather than the full spike train or isolated spikes.

Effects of Serotonin on Sensory Processing: Comparison Between *A. albifrons* and *A. leptorhynchus*

Our results have shown that serotonin application increased lateral segment ELL pyramidal cell burst activity in *A. albifrons*, such that the neural gain increased more steeply with increasing frequency as characterized by a greater exponent. Previous results have shown that, before serotonin application, the tuning curves of lateral segment ELL pyramidal cells to envelope stimuli were essentially identical in both *A. albifrons* and *A. leptorhynchus* (Huang and Chacron, 2016; Huang et al., 2016; Martinez et al., 2016). The effects of serotonin application on ELL pyramidal cell responses to envelope stimuli have been recently characterized by us in *A. leptorhynchus* (Marquez and Chacron, 2020b). In *A. leptorhynchus*, serotonin application also increases ELL pyramidal cell excitability and responses to envelope stimuli, primarily through increased burst firing. The changes in neural gain observed for *A. albifrons* in the

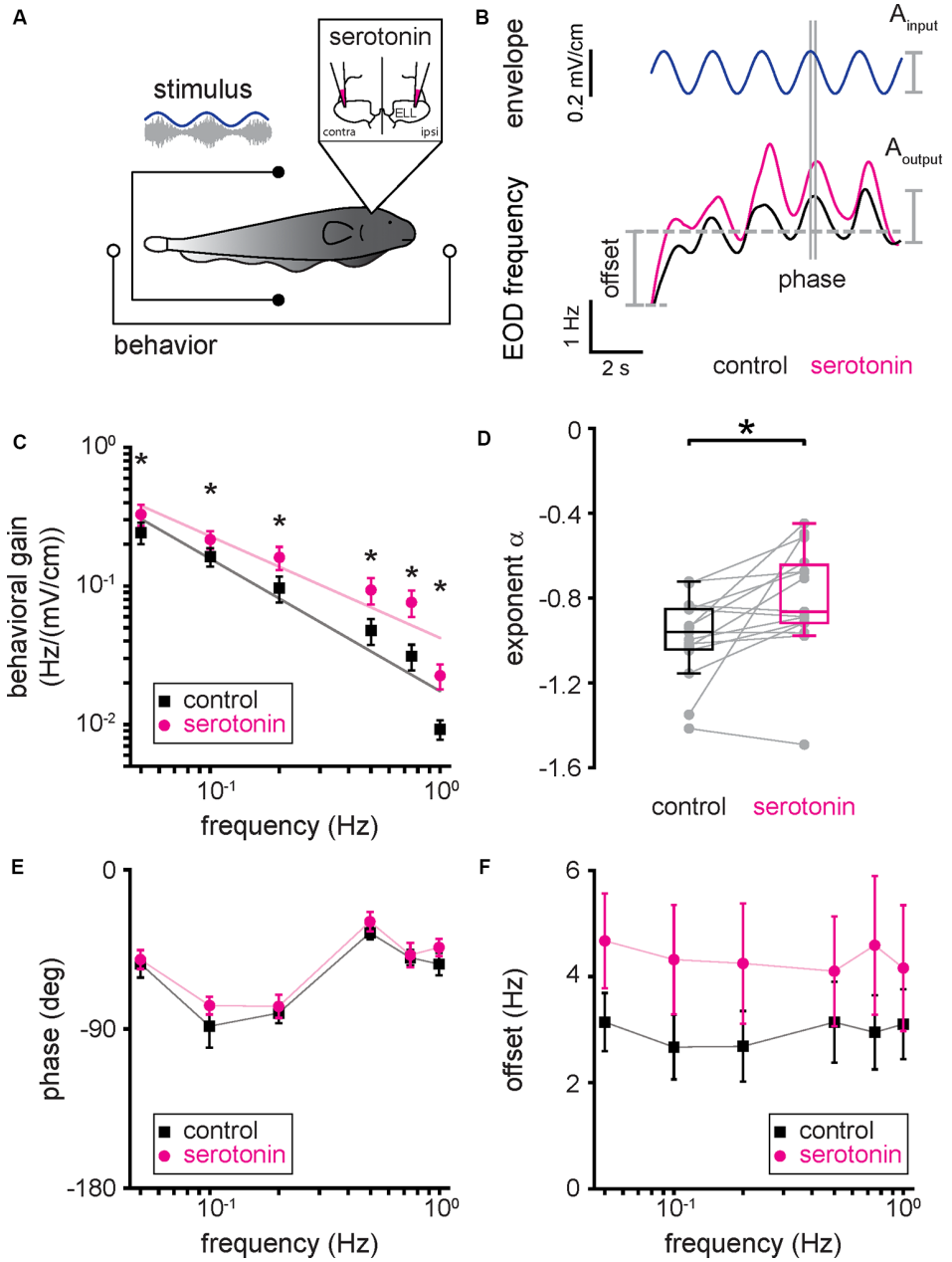

FIGURE 6 | Serotonin application increases behavioral responses to envelope stimuli. **(A)** Schematic showing the setup in which the animal's behavior (EOD frequency) was recorded while being stimulated and serotonin injected bilaterally in the ELL. **(B)** EOD frequency from a typical fish before (bottom, black) and after (bottom, magenta) serotonin application to the same envelope stimulus (top, blue). The behavioral response was quantified using the behavioral gain, which is the ratio of the EOD frequency modulation A_{output} to that of the stimulus A_{input}. The behavioral response was also quantified using the phase, which is the time by which the behavioral response is shifted concerning the envelope stimulus normalized by the stimulus cycle, and the offset, which is the increase in the mean EOD frequency during stimulation. **(C)** Population averaged behavioral gain between the envelope stimulus and the EOD frequency before (black) and after (magenta) serotonin application as a function of envelope frequency. **(D)** Best-fit power-law exponents before (left, black) and after (right, magenta) serotonin application to the behavioral gain as a function of temporal frequency curves shown in panel **(C)**. **(E)** Population averaged phase between the envelope stimulus and the EOD frequency before (black) and after (magenta) serotonin application as a function of temporal frequency. **(F)** Population averaged offset between the envelope stimulus and the EOD frequency before (black) and after (magenta) serotonin application as a function of temporal frequency. Throughout, "*" indicates a statistically significant difference at the $p = 0.05$ level using either a Wilcoxon's signed-rank test or a Student's t-test.

current study were similar to those previously observed for *A. leptorhynchus* (compare **Figures 3E**, **4B,G** with **Figures 4D–F** of Marquez and Chacron, 2020b, respectively). As such, we hypothesize that serotonin increases ELL pyramidal cell excitability and responsiveness through the same mechanisms in both *A. albifrons* and *A. leptorhynchus*. Specifically, serotonin

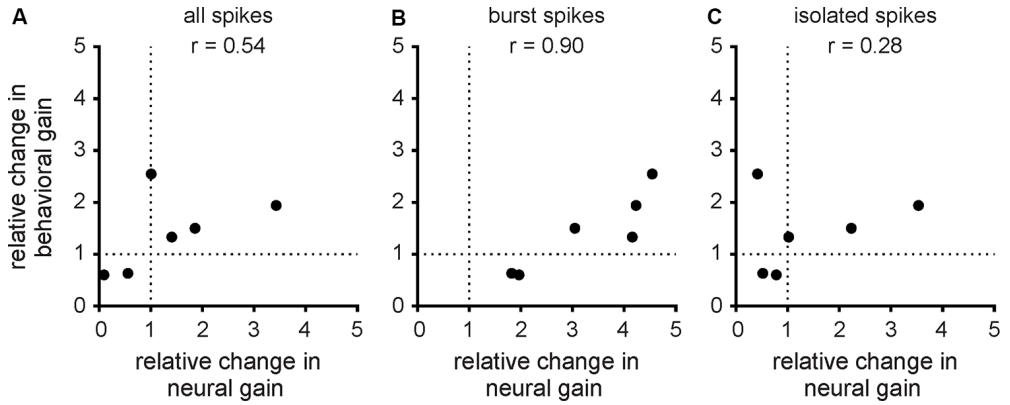

FIGURE 7 | Changes in behavioral gain best correlate with changes in the neural gain of bursts. **(A)** Population-averaged relative change in behavioral gain as a function of the population-averaged relative change in neural gain from the all spike train. The data points correspond to the different envelope frequencies. There was no significant correlation between both quantities ($r = 0.54$, $n = 6$, $p = 0.27$). **(B)** Same as **(A)**, but for the burst spike train. There was a significant correlation between both quantities ($r = 0.90$, $n = 6$, $p < 0.05$). **(C)** Same as **(A)**, but for the isolated spike train. There was no significant correlation between both quantities ($r = 0.28$, $n = 6$, $p = 0.59$).

increases ELL pyramidal neuron excitability in *A. leptorhynchus* by inhibiting potassium channels, namely small conductance calcium-activated and M-type channels, that both give rise to an afterhyperpolarization after the action potential (Deemyad et al., 2011, 2013; for review see Márquez et al., 2013; Huang and Chacron, 2017). The removal of this afterhyperpolarization allows for the depolarizing afterpotential, which is critical for burst generation in ELL pyramidal cells, to potentiate during the burst, thereby increasing the number of spikes during the burst (Lemon and Turner, 2000; Krahe et al., 2008; Toporikova and Chacron, 2009; for review see Metzen et al., 2016). Further studies carried out in *A. albifrons* are however needed to verify these predictions.

Our results have shown that serotonin application increases the power-law exponent characterizing the relationship between neural gain and envelope frequency (i.e., the "neural exponent") in *A. albifrons*. Previous studies carried out in *A. leptorhynchus* have shown that the neural exponent is closely matched to the statistics of natural envelope stimuli such as to optimally encode them *via* temporal whitening (Huang and Chacron, 2016; Huang et al., 2016; for review see Huang and Chacron, 2017; Metzen and Chacron, 2019). Specifically, this is because the power-law increase in neural sensitivity compensates for the decaying spectral power of natural envelope stimuli with increasing envelope frequency, such that the resulting response power is independent of frequency (i.e., "temporally whitened"). Further studies have shown that descending pathways play a critical role in shaping the envelope tuning curve of ELL pyramidal cells (Huang et al., 2018). Most recently, it was shown that serotonin was critical in mediating adaptive optimization of envelope stimuli in *A. leptorhynchus* (Huang et al., 2019). Specifically, when the statistics of the envelope stimulus change, processes occur that cause changes in the response properties of ELL pyramidal cells, such that their responses to the new envelope stimulus become more temporally whitened over time. Huang et al. (2019) showed that serotonin is necessary to achieve such sensory adaptation. Moreover, sensory adaptation is seen ubiquitously across systems and species (Wark et al., 2007; Sharpee et al., 2014). Thus, we hypothesize that similar mechanisms are found in *A. albifrons*. However, further studies are needed to ascertain whether natural envelope stimulus statistics (i.e., how does spectral power decay with increasing envelope frequency) are similar in both *A. albifrons* and *A. leptorhynchus* to validate this hypothesis.

Effects of Serotonin on Behavioral Responses: Comparison Between *A. albifrons* and *A. leptorhynchus*

Previous studies have shown that both *A. leptorhynchus* and *A. albifrons* display nearly identical responses to envelopes (Metzen and Chacron, 2014, 2015; Martinez et al., 2016; Thomas et al., 2018). Specifically, in both species, the EOD frequency tracks the detailed timecourse of the envelope stimulus. Such behavioral responses habituate to repeated stimulus presentations and are thus thought to be mediated by higher brain centers. In both species, behavioral gain decays as a power-law with increasing envelope frequency. In *A. leptorhynchus*, the power-law exponent is the same as that describing how the stimulus spectral power decays with increasing envelope frequency (Metzen and Chacron, 2014). This match between behavioral gain and stimulus spectral power is thought to optimize behavioral responses to maximize responses to the frequency components that are most prevalent in the stimulus. This is supported by results showing that, in response to envelope stimuli with different statistics (i.e., different power-law exponents), behavioral responses in *A. leptorhynchus* adapt such that the behavioral exponent better matches that of the stimulus (Huang et al., 2019). The fact that both *A. leptorhynchus* and *A. albifrons* display nearly identical behavioral responses to envelope stimuli before serotonin application suggests that these

responses serve a similar function and that they are mediated by similar mechanisms in the brain.

However, a comparison of our results and previous ones obtained for *A. leptorhynchus* reveals an important difference. Indeed, while our results have shown that serotonin application increases behavioral gain more for high envelope frequencies than for low envelope frequencies (**Figure 6C**), previous results have shown that, for *A. leptorhynchus*, behavioral gain increases more for low envelope frequencies than for high envelope frequencies (see Figure 7E in Marquez and Chacron, 2020b). Thus, after serotonin application, the behavioral gain decreases less steeply with increasing envelope frequency in *A. albifrons* but more steeply for *A. leptorhynchus*. Indeed, while the behavioral exponent increases for *A. albifrons* (**Figure 6D**), this same exponent decreases for *A. leptorhynchus* (see inset of Figure 7E in Marquez and Chacron, 2020b). Because serotonin application gave rise to similar effects on ELL pyramidal cell activity in both species, these qualitative differences on behavior cannot be ascribed to differences in the spiking activities of ELL pyramidal cells. Rather, we hypothesize that the observed differences in behavior result from differences in decoding of ELL pyramidal cell activity by higher brain areas in both species. In particular, the behavioral responses to envelope stimuli are likely in part mediated by the forebrain, which has recently been the focus of intense investigation in *A. leptorhynchus* (Giassi et al., 2012a,b,c; Trinh et al., 2016; Wallach et al., 2018; Fotowat et al., 2019). Further comparative studies carried out in *A. albifrons* are needed to ascertain as to whether and, if so, how the envelope responses of ELL pyramidal cells are decoded differentially by higher brain centers.

Future studies should also focus on how midbrain neurons, which receive input from ELL neurons, respond to envelope stimuli. Such responses have been investigated in part in *A. leptorhynchus* (McGillivray et al., 2012) but not at all in *A. albifrons*. However, based on the relative similarity of midbrain neural responses observed in *A. leptorhynchus* (Chacron et al., 2009; Chacron and Fortune, 2010) and in *Eigenmannia virescens* (Fortune and Rose, 1997a,b, 2001, 2003; Rose and Fortune, 1999), we would expect that midbrain neurons would respond similarly to the envelope in both *A. leptorhynchus and A. Albifrons*. In particular, we hypothesize that the subthreshold membrane conductances displayed by midbrain neurons (Fortune and Rose, 1997a; Rose and Fortune, 1999; Chacron and Fortune, 2010) enable them to better detect coincident burst firing from ELL pyramidal cell populations after serotonin application. Indeed, burst firing from ELL pyramidal cells would serve to generate a stronger signal that would better counteract the depression observed at ELL-midbrain synapses (Rose and Fortune, 1999; Chacron et al., 2009). Further studies are however needed to test this prediction.

What are the functional implications of serotonin primarily increasing behavioral responses to envelopes for low temporal frequencies in *A. leptorhynchus* and primarily for higher temporal frequencies in *A. albifrons*? As mentioned above, these give rise to behavioral sensitivities that are characterized by different exponents. We hypothesize that these might be better matched to different envelope statistics in both species. Indeed, a recent study has shown that the level of activity in *A. leptorhynchus* strongly influences the exponent at which the envelope stimulus power decays (Huang et al., 2019). As such, it is conceivable that different movement strategies in *A. leptorhynchus* and *A. albifrons* would give rise to different statistics (i.e., envelope stimulus power decays with different exponents), and that serotonin would attempt to better match behavioral sensitivity with these differing statistics, thereby explaining the different effects on behavior. Further studies are however needed to test this hypothesis.

Our results have shown that serotonin application increased JAR magnitude in *A. albifrons*. Overall, our results were similar to those obtained previously for *A. leptorhynchus* (Deemyad et al., 2013; Marquez and Chacron, 2020b). At first glance, this would suggest that the effects of serotonin on the JAR would serve a similar function in both species. It has been observed that EOD frequency is a signal of social dominance in *A. leptorhynchus* and other apteronotid species, with males having EOD frequencies higher than females and more dominant males having higher EOD frequencies than less dominant ones (Triefenbach and Zakon, 2008; Fugère and Krahe, 2010; Fugère et al., 2011; Henninger et al., 2018; Raab et al., 2019). Indeed, injection of androgens such as 11-ketotestosterone will increase EOD frequency in *A. leptorhynchus* (Meyer et al., 1987; Schaefer and Zakon, 1996). Results showing that serotonin application increased JAR magnitude in *A. leptorhynchus* are thus consistent with the JAR as a means of establishing social hierarchy in a group of fish (for review see Rose, 2004). More submissive male individuals tend to display greater levels of serotonin following aggressive encounters (Larson and Summers, 2001), and these greater levels would be expected to give rise to a larger JAR when encountering another conspecific, thereby making that submissive individual appear stronger.

However, the situation appears to be qualitatively different when considering *A. albifrons*. This is because, contrary to *A. leptorhynchus*, male *A. albifrons* tend to have lower EOD frequencies than females (Zakon and Dunlap, 1999) and because androgen treatment actually decreases EOD frequency (Dunlap et al., 1998). These results suggest that, in male *A. albifrons*, a lower EOD frequency is a signal of increased dominance. As such, our results showing that serotonin application increased the magnitude of the JAR in *A. albifrons* are a bit counterintuitive in light of the interpretation made above for *A. leptorhynchus*. This is because increased serotonin levels in a submissive male would then make this individual appear even more submissive when encountering another conspecific. Thus, it is conceivable that the function of serotonin towards determining JAR behavior is qualitatively different in *A. albifrons* and *A. leptorhynchus*. Alternatively, it is important to recall that both these species are not very gregarious, as they tend to be found by themselves most of the time (Stamper et al., 2010). As such, the JAR might not play an important role in establishing social dominance. Further studies are needed to better understand the functional role of the JAR in both species.

Implications for Other Systems

Here we used a comparative approach to gain a better understanding as to the function of the serotonergic system on sensory processing. Such approaches have proven useful to distinguish brain coding strategies that can be generalized from those that are species-specific (Carlson, 2012; Hale, 2014; Brenowitz and Zakon, 2015). In the case of the serotonergic system, the remarkable conservation across vertebrate species suggests a common function (Parent, 1981). While this may be true in general, our results show that even when comparing two very closely related species such as *A. leptorhynchus* and *A. albifrons*, application of serotonin in the same brain area can give rise to opposite effects on behavioral responses. It is thus likely that the serotonergic system will serve species-specific functions. Further studies are needed to ascertain whether this hypothesis holds across different sensory systems and species.

DATA AVAILABILITY STATEMENT

All datasets presented in this study are included in the article.

ETHICS STATEMENT

The animal study was reviewed and approved by McGill University Downtown facility B animal care committee.

AUTHOR CONTRIBUTIONS

MM and MC: conceptualization, methodology, validation, writing—review, and editing. MM: data curation, formal analysis, investigation, and visualization. MC: funding acquisition, project administration, resources, software, supervision and writing—original draft.

FUNDING

This research was supported by CoNaCyT (MM) and the Canadian Institutes of Health Research (MC). The funders had no role in the study design, data collection and analysis, decision to publish, or preparation of the manuscript.

REFERENCES

Bastian, J. (1993). The role of amino acid neurotransmitters in the descending control of electroreception. *J. Comp. Physiol. A* 172, 409–423. doi: 10.1007/bf00213523

Bastian, J., Chacron, M. J., and Maler, L. (2002). Receptive field organization determines pyramidal cell stimulus-encoding capability and spatial stimulus selectivity. *J. Neurosci.* 22, 4577–4590. doi: 10.1523/jneurosci.22-11-04577.2002

Brenowitz, E. A., and Zakon, H. H. (2015). Emerging from the bottleneck: benefits of the comparative approach to modern neuroscience. *Trends Neurosci.* 38, 273–278. doi: 10.1016/j.tins.2015.02.008

Carlson, B. A. (2012). Diversity matters: the importance of comparative studies and the potential for synergy between neuroscience and evolutionary biology. *Arch. Neurol.* 69, 987–993. doi: 10.1001/archneurol.2012.77

Chacron, M. J., Doiron, B., Maler, L., Longtin, A., and Bastian, J. (2003). Non-classical receptive field mediates switch in a sensory neuron's frequency tuning. *Nature* 423, 77–81. doi: 10.1038/nature01590

Chacron, M. J., and Fortune, E. S. (2010). Subthreshold membrane conductances enhance directional selectivity in vertebrate sensory neurons. *J. Neurophysiol.* 104, 449–462. doi: 10.1152/jn.01113.2009

Chacron, M. J., Toporikova, N., and Fortune, E. S. (2009). Differences in the time course of short-term depression across receptive fields are correlated with directional selectivity in electrosensory neurons. *J. Neurophysiol.* 102, 3270–3279. doi: 10.1152/jn.00645.2009

Deemyad, T., Maler, L., and Chacron, M. J. (2011). Inhibition of SK and M channel-mediated currents by 5-HT enables parallel processing by bursts and isolated spikes. *J. Neurophysiol.* 105, 1276–1294. doi: 10.1152/jn.00792.2010

Deemyad, T., Metzen, M. G., Pan, Y., and Chacron, M. J. (2013). Serotonin selectively enhances perception and sensory neural responses to stimuli generated by same-sex conspecifics. *Proc. Natl. Acad. Sci. U S A* 110, 19609–19614. doi: 10.1073/pnas.1314008110

Dunlap, K. D., Thomas, P., and Zakon, H. H. (1998). Diversity of sexual dimorphism in electrocommunication signals and its androgen regulation in a genus of electric fish, Apteronotus. *J. Comp. Physiol. A* 183, 77–86. doi: 10.1007/s003590050236

Ellis, L. D., Krahe, R., Bourque, C. W., Dunn, R. J., and Chacron, M. J. (2007). Muscarinic receptors control frequency tuning through the downregulation of an A-type potassium current. *J. Neurophysiol.* 98, 1526–1537. doi: 10.1152/jn.00564.2007

Fortune, E. S., and Rose, G. J. (1997a). Passive and active membrane properties contribute to the temporal filtering properties of midbrain neurons *in vivo*. *J. Neurosci.* 17, 3815–3825. doi: 10.1523/jneurosci.17-10-03815.1997

Fortune, E. S., and Rose, G. J. (1997b). Temporal filtering properties of ampullary electrosensory neurons in the torus semicircularis of Eigenmannia: Evolutionary and computational implications. *Brain Behav. Evol.* 49, 312–323. doi: 10.1159/000113000

Fortune, E. S., and Rose, G. J. (2001). Short-term synaptic plasticity as a temporal filter. *Trends Neurosci.* 24, 381–385. doi: 10.1016/s0166-2236(00)01835-x

Fortune, E. S., and Rose, G. J. (2003). Voltage-gated Na^+ channels enhance the temporal filtering properties of electrosensory neurons in the torus. *J. Neurophysiol.* 90, 924–929. doi: 10.1152/jn.00294.2003

Fotowat, H., Harrison, R. R., and Krahe, R. (2013). Statistics of the electrosensory input in the freely swimming weakly electric fish *Apteronotus leptorhynchus*. *J. Neurosci.* 33, 13758–13772. doi: 10.1523/jneurosci.0998-13.2013

Fotowat, H., Harvey-Girard, E., Cheer, J. F., Krahe, R., and Maler, L. (2016). Sub-second sensory-evoked serotonin dynamics and its relation to ongoing communication behavior. *eNeuro* 3:ENEURO.0115-16.2016. doi: 10.1523/eneuro.0115-16.2016

Fotowat, H., Lee, C., Jun, J. J., and Maler, L. (2019). Neural activity in a hippocampus-like region of the teleost pallium is associated with active sensing and navigation. *eLife* 8:e44119. doi: 10.7554/elife.44119

Frank, K., and Becker, M. C. (1964). "Microelectrodes for recording and stimulation," in *Physical Techniques in Biological Research*, ed. W. L. Nastuk (New York, NY: Academic), 23–84.

Fugère, V., and Krahe, R. (2010). Electric signals and species recognition in the wave-type gymnotiform fish *Apteronotus leptorhynchus*. *J. Exp. Biol.* 213, 225–236. doi: 10.1242/jeb.034751

Fugère, V., Ortega, H., and Krahe, R. (2011). Electrical signalling of dominance in a wild population of electric fish. *Biol. Lett.* 7, 197–200. doi: 10.1098/rsbl.2010.0804

Giassi, A. C., Duarte, T. T., Ellis, W., and Maler, L. (2012a). Organization of the gymnotiform fish pallium in relation to learning and memory: II. Extrinsic connections. *J. Comp. Neurol.* 520, 3338–3368. doi: 10.1002/cne.23109

Giassi, A. C., Ellis, W., and Maler, L. (2012b). Organization of the gymnotiform fish pallium in relation to learning and memory: III. Intrinsic connections. *J. Comp. Neurol.* 520, 3369–3394. doi: 10.1002/cne.23108

Giassi, A. C., Harvey-Girard, E., Valsamis, B., and Maler, L. (2012c). Organization of the gymnotiform fish pallium in relation to learning and memory: I. Cytoarchitectonics and cellular morphology. *J. Comp. Neurol.* 520, 3314–3337. doi: 10.1002/cne.23097

Hale, M. E. (2014). Mapping circuits beyond the models: integrating connectomics and comparative neuroscience. *Neuron* 83, 1256–1258. doi: 10.1016/j.neuron.2014.08.032

Henninger, J., Krahe, R., Kirschbaum, F., Grewe, J., and Benda, J. (2018). Statistics of natural communication signals observed in the wild identify important yet neglected stimulus regimes in weakly electric fish. *J. Neurosci.* 38, 5456–5465. doi: 10.1523/jneurosci.0350-18.2018

Hitschfeld, E. M., Stamper, S. A., Vonderschen, K., Fortune, E. S., and Chacron, M. J. (2009). Effects of restraint and immobilization on electrosensory behaviors of weakly electric fish. *ILAR J.* 50, 361–372. doi: 10.1093/ilar.50.4.361

Hofmann, V., and Chacron, M. J. (2019). Novel functions of feedback in electrosensory processing. *Front. Integr. Neurosci.* 13:52. doi: 10.3389/fnint.2019.00052

Huang, C. G., and Chacron, M. J. (2016). Optimized parallel coding of second-order stimulus features by heterogeneous neural populations. *J. Neurosci.* 36, 9859–9872. doi: 10.1523/jneurosci.1433-16.2016

Huang, C. G., and Chacron, M. J. (2017). SK channel subtypes enable parallel optimized coding of behaviorally relevant stimulus attributes: a review. *Channels* 11, 281–304. doi: 10.1080/19336950.2017.1299835

Huang, C. G., Metzen, M. G., and Chacron, M. J. (2018). Feedback optimizes neural coding and perception of natural stimuli. *Elife* 7:e38935. doi: 10.7554/elife.38935

Huang, C. G., Metzen, M. G., and Chacron, M. J. (2019). Descending pathways mediate adaptive optimized coding of natural stimuli in weakly electric fish. *Sci. Adv.* 5:eaax2211. doi: 10.1126/sciadv.aax2211

Huang, C. G., Zhang, Z. D., and Chacron, M. J. (2016). Temporal decorrelation by SK channels enables efficient neural coding and perception of natural stimuli. *Nat. Commun.* 7:11353. doi: 10.1038/ncomms11353

Hurley, L. M., Devilbiss, D. M., and Waterhouse, B. D. (2004). A matter of focus: monoaminergic modulation of stimulus coding in mammalian sensory networks. *Curr. Opin. Neurobiol.* 14, 488–495. doi: 10.1016/j.conb.2004.06.007

Johnston, S. A., Maler, L., and Tinner, B. (1990). The distribution of serotonin in the brain of *Apteronotus leptorhynchus*: an immunohistochemical study. *J. Chem. Neuroanat.* 3, 429–465.

Khosravi-Hashemi, N., and Chacron, M. J. (2012). Bursts and isolated spikes code for opposite movement directions in midbrain electrosensory neurons. *PLoS One* 7:e40339. doi: 10.1371/journal.pone.0040339

Khosravi-Hashemi, N., and Chacron, M. J. (2014). Motion processing across multiple topographic maps in the electrosensory system. *Physiol. Rep.* 2:e00253. doi: 10.1002/phy2.253

Khosravi-Hashemi, N., Fortune, E. S., and Chacron, M. J. (2011). Coding movement direction by burst firing in electrosensory neurons. *J. Neurophysiol.* 106, 1954–1968. doi: 10.1152/jn.00116.2011

Krahe, R., Bastian, J., and Chacron, M. J. (2008). Temporal processing across multiple topographic maps in the electrosensory system. *J. Neurophysiol.* 100, 852–867. doi: 10.1152/jn.90300.2008

Larson, E. A., Metzen, M. G., and Chacron, M. J. (2014). Serotonin modulates electrosensory processing and behavior *via* 5-HT2-like receptors. *Neuroscience* 271, 108–118. doi: 10.1016/j.neuroscience.2014.04.033

Larson, E. T., and Summers, C. H. (2001). Serotonin reverses dominant social status. *Behav. Brain Res.* 121, 95–102. doi: 10.1016/s0166-4328(00)00393-4

Lemon, N., and Turner, R. W. (2000). Conditional spike backpropagation generates burst discharge in a sensory neuron. *J. Neurophysiol.* 84, 1519–1530. doi: 10.1152/jn.2000.84.3.1519

Marder, E. (2012). Neuromodulation of neuronal circuits: back to the future. *Neuron* 76, 1–11. doi: 10.1016/j.neuron.2012.09.010

Marquez, M. M., and Chacron, M. J. (2018). Serotonin selectively increases detectability of motion stimuli in the electrosensory system. *eNeuro* 5:ENEURO.0013–0018.2018. doi: 10.1523/eneuro.0013-18.2018

Marquez, M. M., and Chacron, M. J. (2020a). "Serotonin and sensory processing," in *Handbook of the Behavioral Neurobiology of Serotonin*, eds C. Muller and K. Cunningham (New York, NY: Academic Press), 449–459.

Marquez, M. M., and Chacron, M. J. (2020b). Serotonin modulates optimized coding of natural stimuli through increased neural and behavioural responses via enhanced burst firing. *J. Physiol.* 598, 1573–1589. doi: 10.1113/jp278940

Márquez, B. T., Krahe, R., and Chacron, M. J. (2013). Neuromodulation of early electrosensory processing in gymnotiform weakly electric fish. *J. Exp. Biol.* 216, 2442–2450. doi: 10.1242/jeb.082370

Martinez, D., Metzen, M. G., and Chacron, M. J. (2016). Electrosensory processing in Apteronotus albifrons: implications for general and specific neural coding strategies across wave-type weakly electric fish species. *J. Neurophysiol.* 116, 2909–2921. doi: 10.1152/jn.00594.2016

McGillivray, P., Vonderschen, K., Fortune, E. S., and Chacron, M. J. (2012). Parallel coding of first- and second-order stimulus attributes by midbrain electrosensory neurons. *J. Neurosci.* 32, 5510–5524. doi: 10.1523/jneurosci.0478-12.2012

Metzen, M. G., and Chacron, M. J. (2014). Weakly electric fish display behavioral responses to envelopes naturally occurring during movement: implications for neural processing. *J. Exp. Biol.* 217, 1381–1391. doi: 10.1242/jeb.098574

Metzen, M. G., and Chacron, M. J. (2015). Neural heterogeneities determine response characteristics to second-, but not first-order stimulus features. *J. Neurosci.* 35, 3124–3138. doi: 10.1523/jneurosci.3946-14.2015

Metzen, M. G., and Chacron, M. J. (2019). "Envelope coding and processing: implications for perception and behavior," in *Electroreception: Fundamental Insights from Comparative Approaches*, eds B. Carlson, J. Sisneros, A. Popper and R. Fay (Cham: Springer), 251–277.

Metzen, M. G., Huang, C. G., and Chacron, M. J. (2018). Descending pathways generate perception of and neural responses to weak sensory input. *PLoS Biol.* 16:e2005239. doi: 10.1371/journal.pbio.2005239

Metzen, M. G., Krahe, R., and Chacron, M. J. (2016). Burst firing in the electrosensory system of gymnotiform weakly electric fish: mechanisms and functional roles. *Front. Comput. Neurosci.* 10:81. doi: 10.3389/fncom.2016.00081

Meyer, J. H., Leong, M., and Keller, C. H. (1987). Hormone-induced and maturational changes in electric organ discharges and electroreceptor tuning in the weakly electric fish Apteronotus. *J. Comp. Physiol. A* 160, 385–394. doi: 10.1007/bf00613028

Oswald, A. M. M., Chacron, M. J., Doiron, B., Bastian, J., and Maler, L. (2004). Parallel processing of sensory input by bursts and isolated spikes. *J. Neurosci.* 24, 4351–4362. doi: 10.1523/JNEUROSCI.0459-04.2004

Parent, A. (1981). Comparative anatomy of the serotoninergic systems. *J. Physiol.* 77, 147–156.

Raab, T., Linhart, L., Wurm, A., and Benda, J. (2019). Dominance in habitat preference and diurnal explorative behavior of the weakly electric fish *Apteronotus leptorhynchus*. *Front. Integr. Neurosci.* 13:21. doi: 10.3389/fnint.2019.00021

Rose, G. J. (2004). Insights into neural mechanisms and evolution of behaviour from electric fish. *Nat. Rev. Neurosci.* 5, 943–951. doi: 10.1038/nrn1558

Rose, G. J., and Fortune, E. S. (1999). Frequency-dependent PSP depression contributes to low-pass temporal filtering in Eigenmannia. *J. Neurosci.* 19, 7629–7639. doi: 10.1523/jneurosci.19-17-07629.1999

Saunders, J., and Bastian, J. (1984). The physiology and morphology of two classes of electrosensory neurons in the weakly electric fish *Apteronotus leptorhynchus*. *J. Comp. Physiol. A* 154, 199–209. doi: 10.1007/bf00604985

Schaefer, J., and Zakon, H. H. (1996). Opposing actions of androgen and estrogen on in vitro firing frequency of neuronal oscillators in the electromotor system. *J. Neurosci.* 16, 2860–2868. doi: 10.1523/jneurosci.16-08-02860.1996

Sharpee, T. O., Calhoun, A. J., and Chalasani, S. H. (2014). Information theory of adaptation in neurons, behavior and mood. *Curr. Opin. Neurobiol.* 25, 47–53. doi: 10.1016/j.conb.2013.11.007

Stamper, S. A., Carrera, G. E., Tan, E. W., Fugere, V., Krahe, R., and Fortune, E. S. (2010). Species differences in group size and electrosensory interference in weakly electric fishes: implications for electrosensory processing. *Behav. Brain Res.* 207, 368–376. doi: 10.1016/j.bbr.2009.10.023

Thomas, R. A., Metzen, M. G., and Chacron, M. J. (2018). Weakly electric fish distinguish between envelope stimuli arising from different behavioral contexts. *J. Exp. Biol.* 221:jeb178244. doi: 10.1242/jeb.178244

Toporikova, N., and Chacron, M. J. (2009). Dendritic SK channels gate information processing *in vivo* by regulating an intrinsic bursting mechanism seen *in vitro*. *J. Neurophysiol.* 102, 2273–2287. doi: 10.1152/jn.00282.2009

Triefenbach, F. A., and Zakon, H. H. (2008). Changes in signalling during agonistic interactions between male weakly electric knifefish, *Apteronotus leptorhynchus*. *Anim. Behav.* 75, 1263–1272. doi: 10.1016/j.anbehav.2007.09.027

Trinh, A. T., Harvey-Girard, E., Teixeira, F., and Maler, L. (2016). Cryptic laminar and columnar organization in the dorsolateral pallium of a weakly electric fish. *J. Comp. Neurol.* 524, 408–428. doi: 10.1002/cne.23874

Turner, R. W., Maler, L., and Burrows, M. (1999). Electroreception and electrocommunication. *J. Exp. Biol.* 202, 1167–1458.

Wallach, A., Harvey-Girard, E., Jun, J. J., Longtin, A., and Maler, L. (2018). A time-stamp mechanism may provide temporal information necessary for egocentric to allocentric spatial transformations. *eLife* 7:e36769. doi: 10.7554/elife.36769

Wark, B., Lundstrom, B. N., and Fairhall, A. (2007). Sensory adaptation. *Curr. Opin. Neurobiol.* 17, 423–429. doi: 10.1016/j.conb.2007.07.001

Yu, N., Hupe, G., Garfinkle, C., Lewis, J. E., and Longtin, A. (2012). Coding conspecific identity and motion in the electric sense. *PLoS Comput. Biol.* 8:e1002564. doi: 10.1371/journal.pcbi.1002564

Zakon, H. H., and Dunlap, K. D. (1999). Sex steroids and communication signals in electric fish: a tale of two species. *Brain Behav. Evol.* 54, 61–69. doi: 10.1159/000006612

Conflict of Interest: The authors declare that the research was conducted in the absence of any commercial or financial relationships that could be construed as a potential conflict of interest.

frontiers in Integrative Neuroscience

REVIEW
published: 29 July 2020
doi: 10.3389/fnint.2020.00042

A History of Corollary Discharge: Contributions of Mormyrid Weakly Electric Fish

*Matasaburo Fukutomi and Bruce A. Carlson**

Department of Biology, Washington University in St. Louis, St. Louis, MO, United States

Corollary discharge is an important brain function that allows animals to distinguish external from self-generated signals, which is critical to sensorimotor coordination. Since discovery of the concept of corollary discharge in 1950, neuroscientists have sought to elucidate underlying neural circuits and mechanisms. Here, we review a history of neurophysiological studies on corollary discharge and highlight significant contributions from studies using African mormyrid weakly electric fish. Mormyrid fish generate brief electric pulses to communicate with other fish and to sense their surroundings. In addition, mormyrids can passively locate weak, external electric signals. These three behaviors are mediated by different corollary discharge functions including inhibition, enhancement, and predictive "negative image" generation. Owing to several experimental advantages of mormyrids, investigations of these mechanisms have led to important general principles that have proven applicable to a wide diversity of animal species.

OPEN ACCESS

Edited by:
Michael R. Markham, The University of Oklahoma, United States

Reviewed by:
Romulo Fuentes Flores, University of Chile, Chile
Elias Manjarrez, Meritorious Autonomous University of Puebla, Mexico

***Correspondence:**
Bruce A. Carlson
carlson.bruce@wustl.edu

Received: *14 May 2020*
Accepted: *08 July 2020*
Published: *29 July 2020*

Citation:
Fukutomi M and Carlson BA (2020) A History of Corollary Discharge: Contributions of Mormyrid Weakly Electric Fish. Front. Integr. Neurosci. 14:42. doi: 10.3389/fnint.2020.00042

Keywords: efference copy, sensorimotor integration, electrosensory, electrolocation, communication, prediction, comparative physiology

INTRODUCTION

When we move our eyes to shift our gaze, a drastic change happens in our retinal image, but we still perceive a static visual scene. When we tickle ourselves, we hardly feel tickled. Thus, we must discriminate between environmental change-driven sensory input (exafference) and self-generated sensory input (reafference). These signals cannot be distinguished by sensory receptors. Instead, exafferent and reafferent stimuli are distinguished within the central nervous system using a corollary discharge or efference copy, which are internal copies of motor command signals that influence central sensory processing.

The concepts of corollary discharge and efference copy were proposed by Sperry (1950) and von Holst and Mittelstaedt (1950), respectively. Corollary discharge refers to any motor-related timing signal that influences sensorimotor processing. Efference copy has a narrower sense, referring to a subtractive signal for canceling predictable reafferent input. Since their discovery, neurobiologists have sought to identify mechanisms using diverse animal species. Studies of mormyrid weakly electric fish have contributed substantially to understanding the neural circuitry and mechanisms underlying corollary discharge. These fish generate stereotyped electric pulses termed electric organ discharges (EODs) from an electric organ located at the base of the tail. The EODs are used for two different behaviors. One is electrocommunication, in which fishes communicate their identities and behavioral states to each other (Hopkins, 1986a). The other is active electrolocation, in

which fish can sense the environment by detecting distortions in their self-generated EOD (von der Emde, 1999). In addition, mormyrids can detect the external electric fields generated by all aquatic organisms, which is referred to as low-frequency passive electrolocation (Kalmijn, 1974). Importantly, self-generated EODs have different implications for these three behaviors (**Figure 1**). Reafferent inputs are noise for communication and passive electrolocation, whereas they are signal for active electrolocation. By contrast, exafferent input is noise for active electrolocation. The sensory processing related to these behaviors is performed by separate sensory pathways, each having a different type of sensory receptor (Bell, 1989; Perks and Sawtell, 2019). In these dedicated sensory pathways, corollary discharges differently modulate sensory processing to extract behaviorally relevant information (Bell, 1989; Perks and Sawtell, 2019).

Mormyrids have several advantages for studying neural mechanisms of corollary discharge. (1) In freely behaving fish, the motor command signal from spinal electromotor neurons is linked 1:1 with EOD output. (2) It is easy to record this motor command signal as a fictive EOD when the fish is immobilized and electrically silenced. (3) This recording of command signals is not invasive. (4) The recording site for motor commands is distant from the brain, which allows for simultaneous electrophysiological recording from the brain. (5) Stimuli that mimic reafferent EOD input can be delivered with arbitrary waveform and timing. Owing to these advantages, mormyrids have provided novel general insights into corollary discharge mechanisms in sensory processing.

There are numerous review papers describing mechanisms of corollary discharge in various sensory modalities and animals (e.g., Cullen, 2004; Poulet and Hedwig, 2007; Crapse and Sommer, 2008; Requarth and Sawtell, 2011; Schneider and Mooney, 2018; Straka et al., 2018). This review takes a historical perspective, emphasizing the critical contributions of research on mormyrids in advancing our understanding of corollary discharge mechanisms in sensory processing.

EMERGING CONCEPTS OF COROLLARY DISCHARGE AND EFFERENCE COPY

In 1950, corollary discharge and efference copy were proposed independently by research groups in the United States and Germany. von Holst and Mittelstaedt (1950), who were German researchers, published a landmark paper titled *Das Reafferenzprinzip* (The Reafference Principle). In that paper, they discussed why stimuli that trigger reflexive behavior under stationary conditions do not evoke such reflexes when those stimuli are self-generated during voluntary behavior, referencing the optokinetic response of blowflies, postural reflex of fish, and bending reflex of millipedes. They proposed that an "efference copy" acts to subtract self-generated sensory input, or "reafference," to distinguish from external sensory input, or "exafference." For example, the optokinetic response is a reflex in which animals shift their gaze by moving their eyes or body in response to rapid changes in visual input (**Figure 2A**). This gaze shifting works to maintain visual field stability. A change in visual input also occurs when an animal voluntarily moves, but animals do not show optokinetic responses during voluntary movement (**Figure 2B**). von Holst and Mittelstaedt performed an experiment that rotated the fly's head by 180 degrees about its longitudinal axis, which reversed its visual flow horizontally. They found that the head-rotated fly continuously circled after starting a voluntary movement in either direction (**Figure 2C**). This finding indicated that the optokinetic response was not simply inhibited during voluntary movements. Instead, they suggested the moving insect "expects" a specific visual stimulus due to its own movement, which is "neutralized" by an efference copy from the motor center. This could explain why the fly continued circling when the head rotation caused inverted visual flow, as the resulting reafferent sensory input would not be compensated, but instead enhanced by the efference copy.

Sperry, who was a neuropsychologist in the United States, first used the term "corollary discharge" (Sperry, 1950). Since "corollary" means something that is a direct or natural consequence of something else, Sperry used the term "corollary

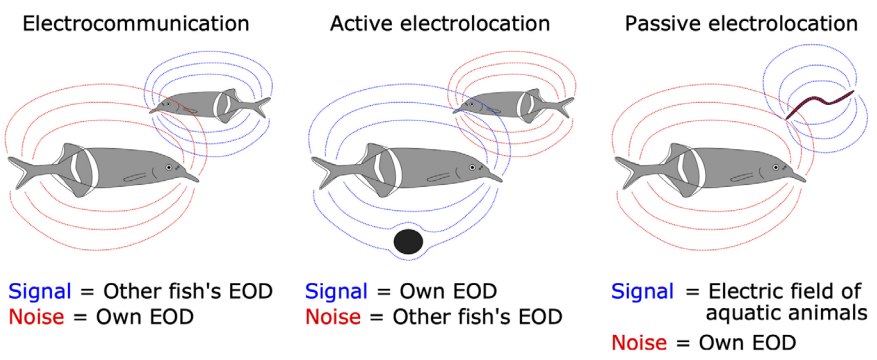

FIGURE 1 | Signal and noise are different among the three electrosensory-mediated behaviors. For electrocommunication, EODs generated from neighboring fish (dashed blue lines) are signal while self-generated EODs (dashed red lines) are noise **(left)**. For active electrolocation, self-generated EODs (blue) are signal while EODs from other fish (red) are noise **(middle)**. For passive electrolocation, low-frequency weak electric fields generated from aquatic animals (e.g., worm) are signal (blue) while self-generated EODs (red) are noise **(right)**.

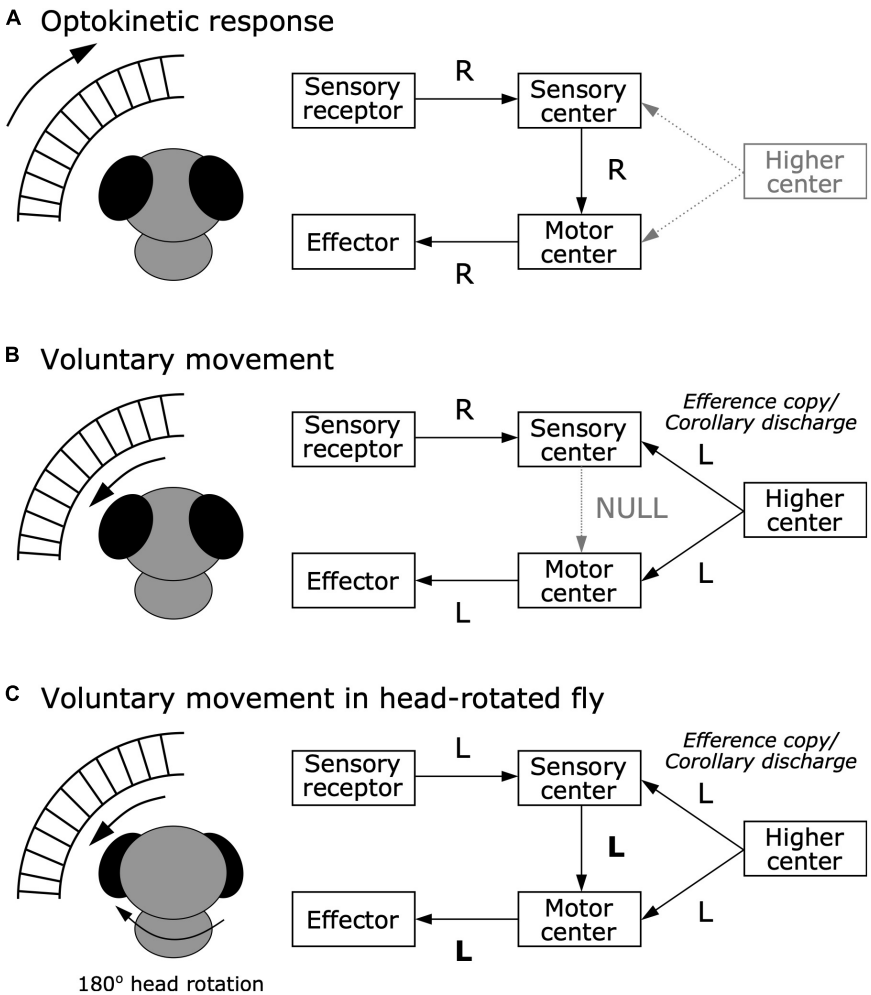

FIGURE 2 | Efference copy hypothesis from the optokinetic response in blowfly. **(A)** Optokinetic response. When the external world moves rightward (R), sensory receptors tells the sensory center about this information. In turn, to stabilize the visual scene, the sensory center sends information about the rightward movement to the motor center, which executes the effector to move toward the right to maintain a stable visual image. **(B)** Voluntary movement in a normal fly. When the fly voluntarily moves leftward (L), rightward visual flow occurs. While the higher center provides the motor center with a command to move leftward, it also provides the sensory center with an efference copy or corollary discharge about the leftward movement command. This efference copy or corollary discharge signal can nullify the reafferent sensory signal, resulting in inhibition of the optokinetic response. **(C)** Voluntary movement in a head-rotated fly. When the 180° head-rotated fly moves leftward, leftward visual flow occurs. While the higher center provides the motor center with a command to move leftward, it also provides the sensory center with an efference copy or corollary discharge about the leftward movement command. However, since visual flow in the head-rotated fly is to the left rather than to the right, the efference copy or corollary discharge cannot nullify the reafferent signal, and instead amplifies it, resulting in continuous circling movements due to the optokinetic response.

discharge" to refer to an internal signal that is the direct result of a motor command. Similar to the experiment by von Holst and Mittelstaedt, he focused on the optokinetic response of swellfish, *Sphaeroides spengleri.* He rotated one eyeball of the fish by 180 degrees, which also reversed its visual flow horizontally, while the other eyeball was covered with a foil blinder. He found a similar circling behavior in the eye-rotated fish. Further, he investigated the neural basis underlying this circling behavior by ablating vestibular organs or brain regions, including the optic tectum, forebrain, cerebellum, and/or inferior lobes. He found that ablation of the portion of the optic tectum that received input from the rotated eye abolished the circling behavior whereas ablation of the other regions had no effect. From these results, he predicted integration in the optic tectum between visual signals from the eye and corollary discharge signals of motor patterns that plays an important role in visual perception during voluntary movement.

Since emerging concurrently and independently, the terms corollary discharge and efference copy have often been used interchangeably. However, some previous reviews have described important differences between corollary discharge and efference copy (Crapse and Sommer, 2008; Straka et al., 2018). Efference copy, as its name suggests, is defined as a copy of an efferent motor command sent to the sensory pathway. The efference copy

contains a subtractive signal for canceling predictable sensory input caused by an animal's own behavior. In other words, if the reafferent input is regarded as a "positive image," the efference copy is a "negative image" of the reafferent input. By contrast, corollary discharge has a more general meaning: a motor-related timing signal that influences sensorimotor processing. A corollary discharge can have many different effects including inhibition, facilitation, and modulation. Thus, the term corollary discharge encompasses efference copies and additional effects of motor-related signals on sensorimotor processing.

EARLY PHYSIOLOGICAL EVIDENCE OF COROLLARY DISCHARGES

Although there is no consensus as to who obtained the first physiological evidence of a corollary discharge, supporting data began to be published around the end of the 1960s.

Possible Corollary Discharge Signals

The first evidence of a corollary discharge signal might have been found in goldfish (*Carassius auratus*), in relation to eye movement (Johnstone and Mark, 1969). Johnstone and Mark (1969) focused on the tectal commissure, which connects the left-right optic tecta, which directly receive inputs from retinal ganglion cells. They found that neurons in the tectal commissure showed two types of responses. One type of neuron exhibited regular discharge in the dark that was inhibited by applying light (Mark and Davidson, 1966). The other type had no spontaneous activity but exhibited high-frequency spikes in synchrony with flicking movements of the eyes (Johnstone and Mark, 1969). The authors interpreted the latter type of activity as a corollary discharge signal because: (1) stopping eye movements by paralyzing eye muscles did not affect this activity, suggesting it was not associated with sensory responses to eye movement; and (2) removal of the tectal commissure did not affect spontaneous eye movement, suggesting the commissure was not involved in the motor control of eye movement.

Another possible corollary discharge signal was found in the lateral-line system of the dogfish, *Scyliorhinus canicula*. The lateral-line hair cells monitor water flow surrounding the animal, which is drastically affected by self-generated sinuous movement during swimming. These hair cells are innervated by efferent fibers originating from the cerebellum (Hillman, 1969; Paul and Roberts, 1977). Roberts and Russell found that these efferent fibers were active when the fish was swimming, both spontaneously and when stimulated, whereas the fibers were silent when the fish was moved by the observer (Roberts and Russell, 1972). Because these efferent fibers provide inhibitory inputs to the hair cells, this system prevents the hair cells from being over-stimulated by self-generated movement.

Suppression of Sensory Processing by Own Behavior

Around the same time, suppressive effects of behavior on sensory processing were found in various sensory modalities and taxa, suggesting a role for corollary discharges. To our knowledge, the first evidence for corollary discharge inhibition was found in the electrosensory system of a mormyrid, as we discuss in detail in a later section (Bennett and Steinbach, 1969). Here, we review motor-related suppression effects in other sensory modalities reported in the 1970s.

Motor-related suppression in the visual system was found in a study of visual responses in optic fibers of crayfish (*Procambarus clarkii*) (Wiersma and Yamaguchi, 1967). Wiersma and Yamaguchi found optic fiber neurons that responded to moving visual stimuli but were unresponsive during active or passive (experimenter-induced) eye movements. Inhibition of visual responses during active eye movement might have been mediated by a corollary discharge (**Figure 3A**). However, inhibition during passive movement must have been mediated by sensory feedback about the eye movements (e.g., proprioception) because there was no internal motor command in this case (**Figure 3B**). Such feedback could also account for the inhibition observed during active eye movement (**Figure 3A**). As we will see, determining whether changes in sensory processing during behavior are due to sensory feedback or corollary discharge often requires experiments in which behavior is blocked such that central motor commands are decoupled from motor output (**Figure 3C**).

A similar kind of motor-related suppression was discovered in the superior colliculus of rhesus macaques, *Macaca mulatta* (Goldberg and Wurtz, 1972). Goldberg and Wurtz (1972) found that spontaneous activity of superior colliculus neurons was suppressed by eye movement in total darkness. In this case, because this suppression effect slightly preceded the eye movement, it was most likely due to a corollary discharge rather than sensory feedback.

Motor-related suppression was also found in the auditory system of the gray bat, *Myotis grisescens*. To navigate in a dark environment, bats emit ultrasound pulses and utilize information from the echo. Suga and Schlegel (1972) recorded auditory responses from the auditory nerve and the lateral lemniscus, which is a tract of axons relaying auditory information from the cochlear nuclei to the inferior colliculus. They found that the evoked potential response of the lateral lemniscus to self-vocalized sound was weaker than playback of the same sound, even though playback intensity was the same as the vocalization. Because auditory nerve responses were equivalent between these two sounds, this attenuation must have occurred between the auditory nerve and the inferior colliculus. In turn, Suga and Shimozawa (1974) explored where the attenuation actually occurs and identified it in the nucleus of the lateral lemniscus. This suppression mechanism likely acts to prevent habituation in response to the loud pulse and maintain sensitivity to the subsequent echo. However, these studies could not determine whether a corollary discharge or sensory feedback resulting from vocalization mediated this attenuation (see **Figure 3**).

Motor-related suppression was also found in the mechanosensory system. Crickets have organs called cerci at the rear of the abdomen, which have mechanosensory hairs that detect air flow (reviewed in Casas and Dangles, 2010). The cerci detect the rapid air flow that accompanies the approach of a predator, which triggers an escape response. However,

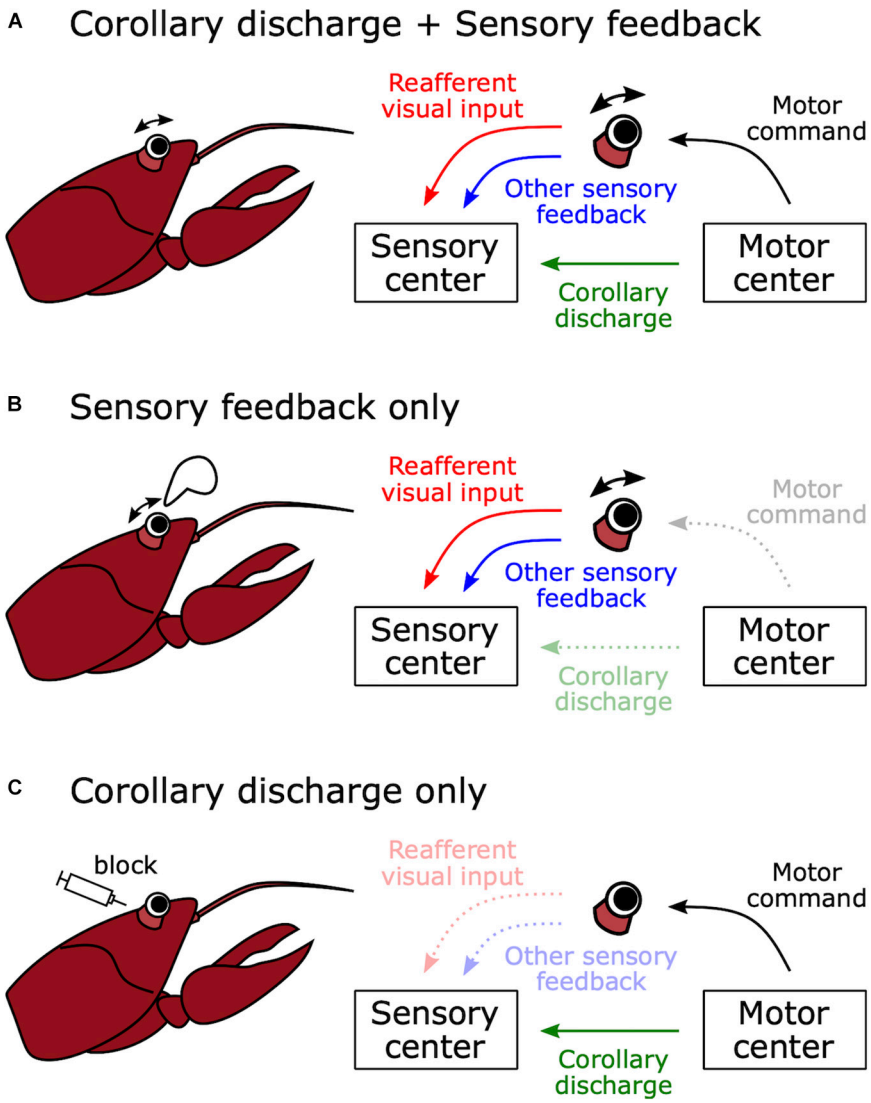

FIGURE 3 | How to distinguish between sensory feedback and corollary discharge in mediating motor-related effects on sensory processing. **(A)** Natural voluntary behavior. When a crayfish moves its eye stalk, visual sensory processing may be modulated by corollary discharge signals from the motor control center or sensory feedback, for example from vestibular, proprioceptive, or coherent wide field visual inputs. **(B)** Passive movement of sensory organ. When the eye stalk is passively moved by an experimenter, there is no motor command and no corollary discharge signal. Thus, any effects of eye motion on the processing of visual stimuli must be due to sensory feedback. **(C)** Immobilized preparation. When the muscles involved in eye movement are curarized, there is no eye movement in response to a motor command and there is no reafferent visual input or sensory feedback. Thus, any changes in the processing of visual stimuli in response to motor commands must be due to a corollary discharge signal. In this case, even though eye movement is blocked, motor command signals from the motor center can be monitored as fictive movements.

the cerci also respond to air flow caused by self-locomotion. Murphey and Palka (1974) found that second-order neurons were less responsive to mechanosensory stimuli during walking compared to resting. Further, they made intracellular recordings from an identified neuron (medial giant interneuron; MGI) in a restrained preparation while monitoring extracellular neural activity from the ipsilateral middle leg nerve. The MGI showed an inhibitory postsynaptic potential during spontaneous burst firing of the leg nerve. Note that, by eliminating actual movement and monitoring fictive movement from the leg nerve, these experiments succeeded in eliminating sensory feedback as a possible cue, thereby demonstrating that this inhibition was mediated by a corollary discharge (see **Figure 3C**).

Corollary Discharge Circuits Mediating Behaviors

How does corollary discharge govern an animal's natural behavior? Compared to vertebrates, invertebrates have a small number of identifiable neurons in the central nervous system, which attracts neurobiologists who seek to understand neural circuits underlying behavior at a cellular level. In the mid-1970s,

neural circuits involving corollary discharges were identified in sea slugs and crayfish.

Like swimming and walking, feeding behavior consists of rhythmic movements. Davis et al. (1973) examined neural circuits governing rhythmic feeding behavior in the sea slug *Pleurobranchaea californica*. While they identified motor neurons in the buccal ganglia that produced rhythmic oscillations during feeding, they also found neurons that send a corollary discharge associated with these oscillations to the brain (Davis et al., 1973; Siegler et al., 1974). Moreover, Gillette and Davis identified a command neuron in the brain, termed metacerebral giant (MCG), that triggers the rhythmic feeding behavior (Gillette and Davis, 1977). The MCG receives corollary discharge inhibition from the buccal ganglion, as well as tactile mechanosensory and chemosensory inputs related to food from the mouth. The corollary discharge feedback associated with feeding oscillations serves to amplify the rhythmic excitatory drive for feeding (Gillette and Davis, 1977). These studies were the first to demonstrate that corollary discharge governs rhythmic motor output during behavior.

A corollary discharge was also found to mediate behavioral choice in *Pleurobranchaea californica*. The sea slug normally exhibits a withdrawal response to vigorous tactile stimulation of the oral veil, whereas it starts rhythmic feeding behavior in response to chemical stimulation from food. When both stimuli are present, the sea slug shows feeding behavior, but does not exhibit the withdrawal response (Davis et al., 1973, 1977). Kovac and Davis (1977) identified one pair of corollary discharge interneurons from the feeding circuit that suppressed the activities of withdrawal motor neurons in response to tactile stimulation. Later, Kovac and Davis (1980) revealed this corollary discharge interneuron directly inhibited the withdrawal command neuron. This inhibition therefore acts to suppress withdrawal in response to self-generated tactile stimulation during feeding. More generally, these findings described a cellular basis for behavioral choice governed by corollary discharge inhibition.

The crayfish *Procambarus clarkii* exhibits a rapid escape response to mechanosensory stimuli. The neural circuit underlying this tail-flip escape behavior has been well characterized (Wiersma, 1947; Edwards et al., 1999): mechanosensory stimulation to the caudal body activates lateral giant (LG) fibers to elicit upward-jumping escape while stimulation to the rostral body activates medial giant (MG) fibers to elicit backward escape. These giant fibers receive mechanosensory inputs via second-order sensory interneurons. Strong mechanosensory stimulation is generated from spontaneous movements, including the tail-flip, which would strongly activate many mechanosensory afferents. Krasne and Bryan (1973) examined how crayfish discriminate such self-generated stimuli from external mechanosensory stimuli. They found that a corollary discharge signal from the tail-flip motor circuit provides presynaptic inhibition to the synapse between the mechanosensory afferents and the interneurons, which can protect the animal from maladaptive habituation and prevent repeated activation of the escape circuit in response to the animal's own movement. Thus, this study also delineated a cellular-level circuit involving a corollary discharge that governs behavior.

COROLLARY DISCHARGE INHIBITION FOR COMMUNICATION

Many animals communicate with conspecifics by exchanging signals such as sounds. In communication, each sender is also a receiver of others' signals. The problem here is that the sender receives an intense stimulus from their own signal production, which represents a source of noise in processing other individuals' signals and may lead to desensitization through habituation (**Figure 1**). How does the central nervous system address this problem?

Electrocommunication in Mormyrid Weakly Electric Fish

Understanding corollary discharge mechanisms underlying communication began with the study of a mormyrid fish, *Gnathonemus petersii*. As mentioned in the introduction, mormyrid fish generate EODs from an electric organ, and distinct sensory pathways govern three different electrosensory behaviors: electrocommunication, active electrolocation, and low-frequency passive electrolocation. Before the discovery of a corollary discharge in mormyrids, it was thought that the neural pathway that mediates communication derives from a relatively large type of electroreceptor called the Knollenorgan (KO) (Bennett, 1965). The reasons why the KO was thought to mediate communication are (1) sensitivity to high-frequency signals characteristic of EODs, (2) a fixed-latency spike of primary afferents in response to EODs that is largely amplitude invariant, and (3) the greatest sensitivity among the three types of electroreceptors. Together, these properties suggested this receptor is specialized to detect electric signals from other fish.

Bennett and Steinbach published the idea that electrosensory processing needs information about when an EOD is produced to extract behaviorally relevant information (Bennett and Steinbach, 1969). They tested whether neural signals related to EOD production were observed in sensory areas across the brain. They used a preparation of curarized (muscle-inactivated) fish, in which the EOD is silenced but fish continue to produce fictive EODs from spinal electromotor neurons (**Figure 4A**). This preparation has the powerful advantage that silencing the EOD can isolate the effects of a corollary discharge on sensory processing by eliminating sensory feedback (see **Figure 3C**). They found that the cerebellum and the electrosensory lateral line lobe, in which the electrosensory afferents terminate, both received corollary discharges reflecting the timing of EOD production. In addition, they showed that sensory responses of the exterolateral nucleus in the midbrain torus semicircularis disappeared when electrosensory stimuli were delivered within a narrow window of time shortly after the fictive EOD (**Figure 4B**). Later, it was shown that the exterolateral nucleus appeared to receive electrosensory inputs from KO afferents via the hindbrain nucleus of the electrosensory lateral line lobe (nELL) (Enger et al., 1976a,b). Taken together, it was shown that the KO pathway

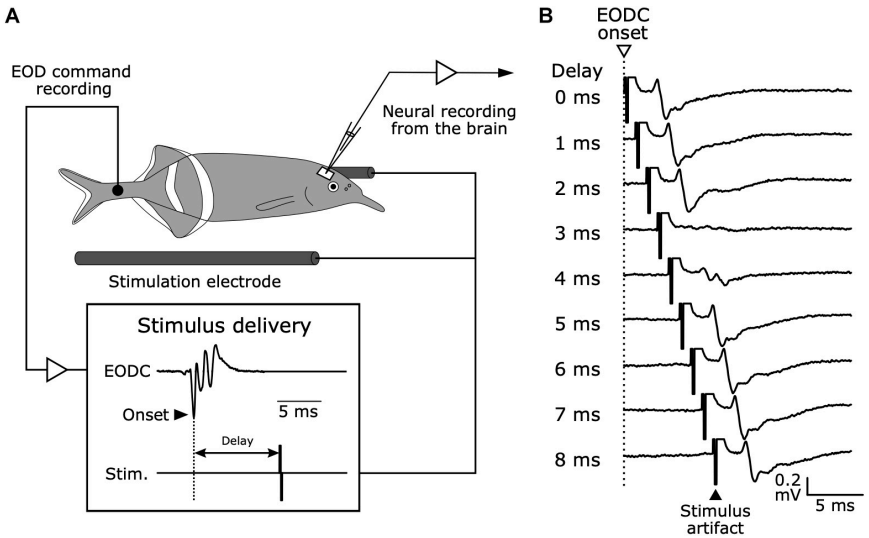

FIGURE 4 | Electrophysiology in mormyrid fish brains while monitoring EOD command signals and delivering time-locked stimuli. **(A)** Experimental setup. Although the fish is curarized to eliminate movement and silence EOD production, EOD commands (EODC) from spinal electromotor neurons can be recorded as fictive EODs using an extracellular electrode placed next to the tail. Electrosensory stimuli can be delivered at fixed delays relative to the EODC onset. This system allows for the examination of corollary discharge effects on electrosensory neurons in the brain and to separate corollary discharge effects from the effects of sensory feedback. Modified from Bell (1981). **(B)** Evoked potentials from the exterolateral nucleus anterior (ELa) in response to stimuli at varying delays following EOD command onset (0–8 ms) in *G. petersii*.

can efficiently extract communication signals from other fish by internally canceling responses to self-generated signals using a corollary discharge.

The question that followed was what neural pathways mediate this corollary discharge inhibition. Zipser and Bennett (1976) found that the corollary discharge inhibition occurred in the nELL, the first sensory center of the KO pathway (Zipser and Bennett, 1976). In turn, using horseradish peroxidase tracing, Bell et al. (1981) revealed that, in addition to input from KO primary afferents, the nELL also received inputs from a small group of cells, later named the sublemniscal nucleus (slem) (Mugnaini and Maler, 1987). Furthermore, Bell et al. (1983) described a corollary discharge pathway from the EOD command nucleus (CN) to the slem through the bulbar command-associated nucleus (BCA) and mesencephalic command-associated nucleus (MCA) (**Figure 5**). The input from the slem appeared to be GABAergic based on immunocytochemistry (Denizot et al., 1987; Mugnaini and Maler, 1987). Since the neural activity in the CN corresponds 1:1 to EOD production, this pathway was strongly suggested to provide corollary discharge inhibition to the nELL. Indeed, Bell and Grant performed intracellular recording from the nELL, including nELL neurons, KO primary afferents, and inhibitory inputs from slem, and revealed the neural circuit of corollary discharge inhibition physiologically (**Figure 6**; Bell and Grant, 1989).

These studies elucidated a corollary discharge circuit and mechanism underlying communication for the first time. In addition, they suggested that, since the corollary discharge inhibition of the nELL can preserve the temporal information of communication signals from other fish, the downstream pathway should analyze temporal features of the signal. Indeed, future studies demonstrated that the ELa extracts information about temporal features of the EOD waveform that reflect the identity of signaling fish (Friedman and Hopkins, 1998; Lyons-Warren et al., 2013), and that the posterior exterolateral nucleus (ELp), to which ELa sends its only output, extracts temporal patterns of inter-pulse intervals that reflect the behavioral state of signaling fish (Carlson, 2009b; Baker et al., 2016). Owing partly to this corollary discharge inhibition, mormyrid fishes provided a unique opportunity to study how the nervous system decodes temporal signals during communication (Xu-Friedman and Hopkins, 1999; Baker et al., 2013).

Acoustic Communication in Primates

Similar to electric communication in mormyrids, corollary discharge inhibition may mediate acoustic communication in primates, including humans. Like prior research on bats (Suga and Schlegel, 1972; Suga and Shimozawa, 1974), Müller-Preuss and Ploog (1981) compared sensory responses of auditory cortex to playback calls and self-vocalized calls in squirrel monkeys (*Saimiri scireus*) and found that the auditory response was absent during vocalization. A similar effect was subsequently found in human cortex (Creutzfeldt et al., 1989).

The anatomy of a possible corollary discharge pathway underlying communication in primates remains controversial today. One possible source seems to be the prefrontal cortex, because (1) there are reciprocal connections between the auditory cortex and prefrontal cortex (Müller-Preuss et al., 1980) and (2) electrical stimulation of the prefrontal cortex can suppress responsiveness in the auditory cortex (Alexander et al., 1976). However, the electrical stimulation in the latter case did not necessarily reproduce the same activity that results from real

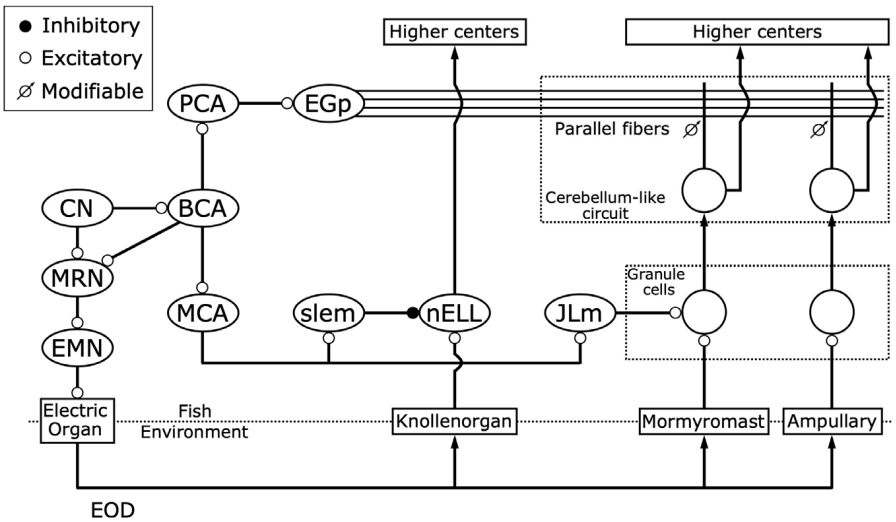

FIGURE 5 | Corollary discharge pathways interact with three distinct electrosensory pathways. While the command nucleus (CN) drives the electric organ to generate each EOD via the medullary relay nucleus (MRN) and spinal electromotor neurons (EMN), it also provides a corollary discharge via the bulbar command-associated nucleus (BCA). Knollenorgans, which are dedicated to communication, send their primary afferents to the nucleus of the electrosensory lateral line lobe (nELL), which receives corollary discharge inhibition from the BCA via the mesencephalic command-associated nucleus (MCA) and the sublemniscal nucleus (slem). Mormyromast and ampullary receptors, which are dedicated to active electrolocation and passive electrolocation, respectively, send their afferents to granule cells of the electrosensory lateral line lobe (ELL). Only granule cells that are innervated by mormyromast afferents receive corollary discharge enhancement from the BCA via the MCA and the medial juxtalobar nucleus (JLm). Both granule cells send their outputs to medium ganglion (MG) cells, which also receive inputs onto their apical dendrites from parallel fibers that come from the eminentia granularis posterior (EGp), forming cerebellum-like circuits. The EGp provides corollary discharge inputs to the MG cells via the BCA and the paratrigeminal command-associated nucleus (PCA). In these cerebellum-like circuits, a "negative image" of expected reafferent input is made through anti-Hebbian spike-timing-dependent plasticity at the synapses between parallel fibers and the apical dendrites of MG cells. Modified from Bell (1989); Perks and Sawtell (2019).

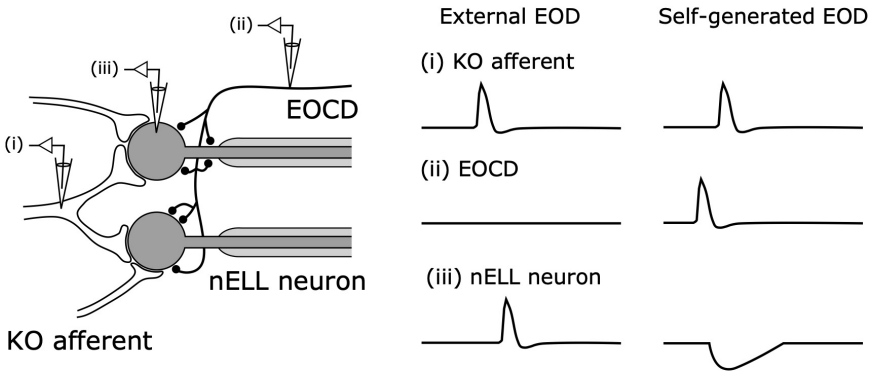

FIGURE 6 | Corollary discharge inhibition in the nucleus of the nELL. Primary Knollenorgan (KO) afferents form large excitatory synapses onto the soma of adendritic nELL neurons. The electric organ corollary discharge (EOCD) from the sublemniscal nucleus (slem) also provides inhibitory inputs onto the soma and initial segment of nELL neurons. In response to an external EOD, (i) KO afferents and (iii) nELL neurons produce spikes whereas (iii) the EOCD is not activated. In response to self-generated EODs, (ii) slem neurons produce a spike preceding (i) the KO afferent spike, resulting in: (iii) nELL neurons showing an inhibitory postsynaptic potential that blocks the spiking response to afferent input. Modified from Bell and Grant (1989); Carlson (2009a).

vocalization. In addition, it remains unclear whether a corollary discharge directly inhibits the auditory cortex. Vocalization-induced suppression was not observed in the inferior colliculus of monkeys (Pieper and Jürgens, 2003), in contrast to findings in bats (Suga and Shimozawa, 1974), and it is not known whether thalamic or thalamocortical mechanisms participate in the vocalization-induced suppression observed in auditory cortex. A recent review paper provides further discussion of corollary discharge mechanisms in the auditory system of primates (Eliades and Wang, 2019).

Acoustic Communication in Crickets

Male crickets produce song by rhythmically rubbing the forewings together to attract female crickets. The song is quite loud at the source (over 100 dB SPL) so that distant conspecifics can hear it (Nocke, 1972). This means that a singing cricket is

fully exposed to the loud self-generated sound, which strongly stimulates the auditory tympanal organs located on the front legs. Early behavioral evidence showed that crickets can respond to external sound during singing (Heiligenberg, 1969), suggesting the existence of a corollary discharge. A series of later studies by Poulet and Hedwig clearly delineated the neural circuit underlying corollary discharge inhibition of the auditory pathway at the level of identified cells in singing field crickets, *Gryllus bimaculatus* (Poulet and Hedwig, 2002, 2003a,b, 2006).

Compared to mormyrids, insects have a distinct experimental advantage: individual neurons can be identified. However, there were two challenges to be worked out. (1) It is rare for crickets to sing during electrophysiological experiments. (2) The forewing movement during singing is very fast, and a method to detect and quantify this movement was needed. Hedwig (2000a,b) addressed these problems. (1) They found that injection of acetylcholine and cholinergic agonists into the brain can reliably trigger singing through activation of a command neuron (Wenzel and Hedwig, 1999; Hedwig, 2000b). (2) Hedwig developed an opto-electronic system to record wing movement at a 5 kHz sampling rate (Hedwig, 2000a).

Using these methods and intracellular recording, Poulet and Hedwig recorded from auditory neurons in the prothoracic ganglion, where the auditory afferents terminate, during singing (Poulet and Hedwig, 2002, 2003a,b). First, they showed that the auditory neurons responded with bursts of spikes to a cricket's own singing sounds. However, the resulting spike rate was lower than the response to 100 dB SPL sound pulses at rest, suggesting inhibition of the auditory system during singing. Second, they prevented sound production while still allowing for wing movement by removing one forewing and directly showed inhibitory postsynaptic potentials (IPSPs) in phase with wing movement in the auditory neurons. Third, they isolated corollary discharge effects from sensory feedback (see **Figure 3C**) by cutting motor and sensory nerves except for auditory nerves and showed that the IPSPs continued to occur in phase with fictive singing as recorded from the wing motor nerve root. These results demonstrated that a singing-related corollary discharge inhibits the auditory neurons' responses and prevents self-induced desensitization.

In a follow-up study, Poulet and Hedwig identified a corollary discharge interneuron (CDI) responsible for this inhibition (Poulet and Hedwig, 2006). The CDI has its dendrites in the mesothoracic ganglion, where the motor neurons innervating the wing muscles are found. However, the CDI is not involved in generating song. With dual intracellular recordings from the CDI and auditory neurons, they showed that activation of CDI induced suppression of auditory neurons while inactivation of CDI removed the effects of inhibition on auditory neurons during singing. This suggested that the CDI is necessary and sufficient to provide corollary discharge inhibition. These studies described for the first time the cellular basis for corollary discharge inhibition underlying acoustic communication.

Around the same time, Weeg et al. (2005) recorded from efferent neurons that innervate the inner ear and lateral line of a sound-producing fish, the plainfin midshipman (*Porichthys notatus*). Most of these neurons showed an increase in activity that was time-locked to the fine temporal structure of evoked fictive vocalizations. In addition, the activity of efferents projecting to the inner ear was suppressed just after the end of each fictive vocalization. These findings suggest that a corollary discharge of vocalizations acts to modulate auditory sensitivity to self-generated sounds and maintain sensitivity to external sounds. This is similar to the findings in crickets, and suggests that similar mechanisms may be operating across vocalizing invertebrate and vertebrate species.

COROLLARY DISCHARGE ENHANCEMENT FOR ACTIVE SENSING

Active sensing is acquiring sensory inputs through overt sampling behaviors, which requires sensorimotor interactions in a different manner from communication. In the context of communication, corollary discharges act to inhibit sensory responses. In the context of active sensing, however, corollary discharges can act to enhance sensory processing. Only two study systems, mormyrids and bats, have been used to study corollary discharges or motor-related enhancement during active sensing. In both systems, motor-related signals serve to gate sensory responses to self-generated behavioral outputs through enhancement.

Active Electrolocation in Mormyrid Fish

Weakly electric fishes use EODs to sense their environment. Unlike sounds, electric signals do not propagate as traveling waves but exist as localized electrostatic fields (Hopkins, 1986b). This means that reflected echoes, which bats use during echolocation (Griffin, 1958), are not relevant to electric fish. Instead, objects near the fish alter the EOD-evoked current flow across receptors and project an "electrical image" onto the skin (reviewed in von der Emde and Bell, 2003). Objects with conductivity greater than the surrounding water project an electrical "brightspot" onto the skin, whereas objects with conductivity lower than the surrounding water project an electrical "darkspot" onto the skin.

Before discovering a corollary discharge underlying active sensing, researchers thought the mormyromast pathway has a major role in active electrolocation because the mormyromast receptors: (1) have high sensitivity to high-frequency signals characteristic of EODs; (2) show intensity dependencies in spike latency and number of spikes produced by the afferents, which could encode stimulus amplitude related to the size and location of objects; (3) are less sensitive than Knollenorgans (Bennett, 1965). In addition to these specialized features of mormyromasts, active electrolocation requires information regarding when the EODs were produced (Bennett and Steinbach, 1969).

Zipser and Bennett (1976) made intracellular recordings from neurons in the electrosensory lateral line lobe (ELL) that received inputs from the mormyromast afferents and found that neural responses were facilitated within a narrow time window (6–11 ms) with respect to EOD command onset. This suggested that a corollary discharge gated self-generated responses. In contrast to the nELL in the Knollenorgan pathway, the ELL cortex has a

laminar structure that includes various types of neurons (Maler, 1973). However, Zipser and Bennett did not determine what cell types were responsible for corollary discharge enhancement of electrosensory responses. With intracellular recording and morphological analysis, Bell et al. (1989) later identified granule cells as the convergent site of corollary discharge inputs and mormyromast afferents (**Figure 5**; Bell et al., 1989; Bell, 1990). Subsequently, Bell and colleagues found that excitatory corollary discharge inputs to granule cells come from the medial juxtalobar nucleus (JLm) located at the anterior ventral margin of the ELL (**Figure 5**; Bell and von der Emde, 1995; Bell et al., 1995). The JLm receives inputs from the MCA, which also sends corollary discharge output to the nELL, indirectly through the sublemniscal nucleus (**Figure 5**; Bell and von der Emde, 1995). In summary, a corollary discharge that arises from the command nucleus facilitates sensory inputs in the mormyromast pathway. This increases the gain of mormyromast responses to self-generated EODs, which provides information about the surrounding environment.

Echolocation in Bats

Do bats have a similar mechanism of corollary discharge that makes them more sensitive to the sounds they produce? In contrast to active electrolocation in mormyrids, in which they directly analyze self-generated electric pulses, bats do not use self-generated sounds directly, but rather compare information from the outgoing sound pulse and resulting echo to glean information about the surrounding environment.

Suga and Schlegel (1972) and Suga and Shimozawa (1974) demonstrated that the sensory response to a bat's own call during vocalization was attenuated compared to the response to playback of the call during no vocalization. By contrast, Schuller provided evidence that a corollary discharge may enhance auditory responses to echoes of self-generated vocalizations in the greater horseshoe bat, *Rhinolophus ferrumequinum* (Schuller, 1979). He performed extracellular single-unit recordings from the inferior colliculus (IC) and compared responses to (1) playback of a simulated echo occurring just after a self-generated vocalization and (2) playback of both a simulated vocalization and simulated echo at rest. He found that IC neurons responded more strongly to (1) than to (2). Furthermore, the facilitation of echo responses by self-generated vocalization vanished when the phantom echo was delivered at delays longer than 60 ms. This indicates that the enhancement of echo responses has a specific time window and that the bat might have a detection range limit of ∼10 m distance (Neuweiler, 2003).

The neural source of vocalization-related enhancement in bat echolocation remains to be determined. Suga and Shimozawa suggested sensory attenuation by vocalization occurred in the nucleus of the lateral leminiscus, but it is not known whether enhancement of echo processing also happens in this nucleus. In addition, Schuller noted that, because vocalization was elicited by electrical stimulation of the central gray matter of the midbrain, this facilitation by self-vocalization might be different from natural echolocation during free flight (Schuller, 1979; Nachtigal and Schuller, 2014). Recently, telemetry neural recording techniques were developed and used for recording from the hippocampus and the superior colliculus during free flight in bats (Yartsev and Ulanovsky, 2013; Kothari et al., 2018). In the future, these techniques may be used to reveal the nature of motor-related enhancement under more natural conditions. Also, it remains to be determined whether corollary discharge, sensory feedback, or both are involved in vocalization-related enhancement of echo responses (see **Figure 3**).

COROLLARY DISCHARGE IS USED TO GENERATE PREDICTIONS AND MEMORIES

Corollary discharges discussed so far are wired robustly to sensory circuits to suppress or facilitate sensory responses to self-generated stimuli. However, canceling predicted sensory inputs caused by own behavior does not always mean complete inhibition, especially when the motor act and the reafferent response patterns are complex and long lasting. In this case, complete inhibition would render the animal completely insensitive to sensory stimulation for a prolonged period of time. Instead, von Holst and Mittelstaedt suggested that an internal signal representing a "negative image" (i.e., efference copy) of the expected reafference would act to cancel the sensory consequences of own behavior while maintaining sensitivity to exafferent stimuli (von Holst and Mittelstaedt, 1950). Further, the internal prediction should be plastic so that it can be updated in response to environmental change because such change can alter the reafferent input in response to own behavior. Such a modifiable efference copy was first discovered in the passive electrosensory system of mormyrid fish.

Negative Image Predicts Reafferent Input in the Passive Electrosensory System of Mormyrids

Mormyrid fish can detect and orient to the low-frequency electric signals generated by aquatic organisms such as insects and worms (**Figure 1**). This behavior is called passive electrolocation, and is shared with other animals that have electrosensation such as sharks and rays (Kalmijn, 1971). However, mormyrid fish face a difficult task for such electrolocation because they produce EODs that are much larger in amplitude than the weak, low-frequency signals generated by their prey. Indeed, the primary afferents of ampullary receptors that detect low-frequency electric fields respond to self-generated EODs with a long-lasting (∼100 ms), complex, multiphasic response (Bell and Russell, 1978). If a corollary discharge completely inhibited self-generated responses as in the Knollenorgan pathway, it would mask behaviorally important signals for a prolonged period of time.

Bell examined how a corollary discharge solves this problem in the ampullary electrosensory pathway by obtaining unit recordings from the ampullary region of ELL (Bell, 1981). When an electric pulse stimulus triggered by the EOD command was delivered to a curarized fish (**Figure 4A**), ELL neurons initially responded with long-lasting, complex changes in spike rate similar to the responses of primary afferents (**Figure 7**).

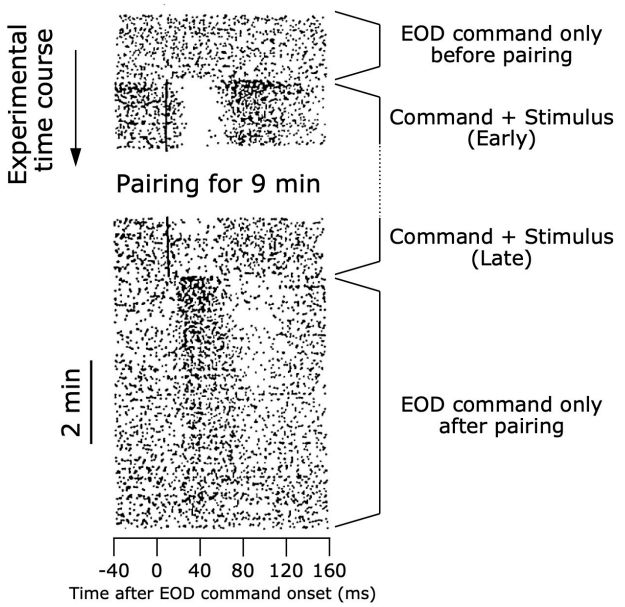

FIGURE 7 | Modifiable efference copy in an ELL neuron. Raster shows responses of a cell in the ampullary region of the ELL. Each dot represents a spike, and each row shows the spiking activity aligned to each EOD command onset (see also **Figure 4**). At the beginning of the experiment, the EOD command alone did not affect the spiking activity of the cell. When an electrosensory stimulus was paired with the EOD command, the stimulus initially evoked a pause-burst spiking response of the cell. After several minutes of paring, the response to the electrosensory stimulus decreased dramatically. Upon removal of the electrosensory stimulus, the cell then showed a response to the EOD command alone. The shape of this response to the EOD command just after pairing represented a negative image of the initial response to electrosensory stimulation at the beginning of pairing. As time passed, the cell no longer responded to the EOD command alone. Modified from Bell (1989).

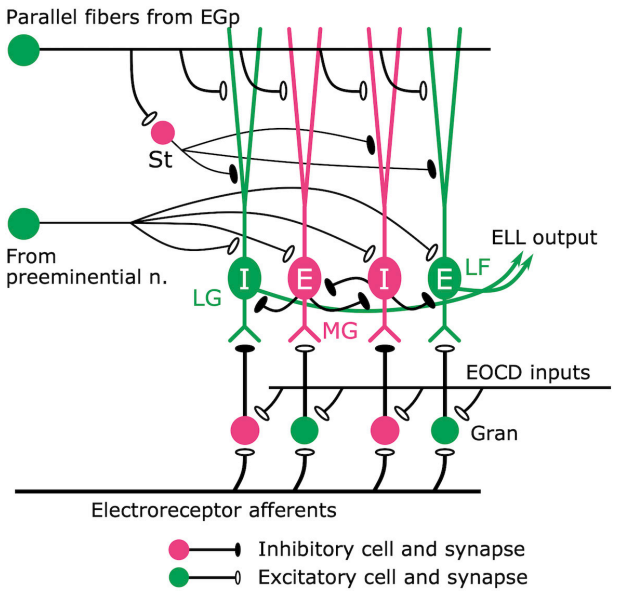

FIGURE 8 | Cerebellum-like circuit in the ELL cortex. Mormyromast and ampullary afferents terminate on granule cells (gran). In the mormyromast region of ELL, the granule cells receive precisely timed electric organ corollary discharge (EOCD) input. However, the ampullary region lacks this input (not shown here). The granule cells provide both excitatory and inhibitory outputs to the downstream neurons. The large fusiform (LF) cells and the lateral ganglion (LG) cells receive excitatory and inhibitory inputs from granule cells, respectively. Medium ganglion (MG) cells are Purkinje-like cells that receive sensory inputs from granule cells and provide major inhibitory inputs to the LF cells and LG cells, which send their outputs to higher centers. E cells are excited by an increase in afferent activity, while I cells are inhibited. Parallel fibers provide corollary discharge input to the apical dendrites of MG cells, LF cells, and LG cells directly and indirectly via inhibitory stellate (St) cells. In addition, the preeminential nucleus provides electrosensory feedback to MG cells, LF cells, and LG cells. Modified from Sawtell et al. (2005).

After repeated presentation of the stimulus, however, the sensory responses of ELL neurons decreased markedly (**Figure 7**). Next, Bell removed the paired electric pulse stimulus and observed the ELL neurons' responses to the EOD command alone (**Figure 7**). The ELL neurons now showed a response to the EOD command, even though they showed no response to the command before presenting the paired stimulus (**Figure 7**). Remarkably, the shape of this response to the EOD command after removal of the stimulus was similar to an inverted version of the initial sensory response to the electric pulse stimulus (**Figure 7**). This result strongly indicated that a corollary discharge conveyed a negative image to subtract the predicted reafferent responses to the fish's own EOD, and that this negative image was generated through plasticity. Indeed, the strong responses of ELL neurons to the command alone that was observed just after removing the paired stimulus gradually dissipated with time, reflecting a constant process of updating the negative image as the sensory consequences of behavior changed.

What is the neural circuit mediating this efference copy? Maler first pointed out an interesting anatomical feature of the ELL: similarities to the cerebellum of mammals (Maler, 1973; **Figure 8**). The ELL has Purkinje-like GABAergic neurons (called MG cells) that receive inputs from primary electrosensory afferents via granule cells in a deep layer, as well as inputs from parallel fibers in a superficial molecular layer (**Figure 8**). Libouban and Szabo (1977) described a pathway from the paratrigeminal command-associated nucleus (PCA) to the eminentia granularis posterior (EGp), whose axons form the parallel fibers in the ELL (**Figure 5**). In addition, Bell, Libouban, and Szabo found that the PCA receives inputs from BCA (Bell et al., 1983; **Figure 5**). These anatomical studies suggested that the parallel fibers convey corollary discharge information and that the MG cells integrate inputs from primary electrosensory afferents and this corollary discharge pathway.

Bell et al. (1993, 1997) investigated how negative images emerge in this cerebellum-like circuit. Using intracellular recording, they found that MG cells produce two types of spikes: broad spikes that occur in the apical dendrites that receive corollary-discharge input and narrow spikes that occur in axons (Bell et al., 1993). They found that paring a broad spike evoked by current injection with the EOD command could induce synaptic plasticity at the parallel fiber synapses (Bell et al., 1993). Further

in vitro study revealed an anti-Hebbian rule to this synaptic plasticity: excitatory postsynaptic potentials (EPSPs) evoked by electric stimulation of parallel fibers preceding broad spikes induced synaptic depression, whereas EPSPs following broad spikes induced synaptic potentiation (Bell et al., 1997). These results demonstrated that negative images were generated at the synapses between parallel fibers and Purkinje-like cells through spike-timing-dependent plasticity with an anti-Hebbian learning rule. This was among the first demonstrations of spike-timing-dependent plasticity in any neural circuit (Markram et al., 2011).

In order to form a negative image that lasts long enough to cancel reafferent inputs from ampullary afferents, parallel fibers need to provide temporally variable inputs that cover the duration of afferent responses. This property of parallel fibers had been assumed for a long time, but it had not been directly tested, and the underlying mechanisms for temporal dispersion remained unknown. Sawtell, Kennedy et al. (2014) found that EGp received a brief corollary discharge input and that the parallel fibers indeed provide such a temporal basis, which was mediated by relaying interneurons in EGp called unipolar brush cells. This finding linked the corollary discharge circuit to synaptic plasticity to describe the formation of long-lasting negative images.

Note that a similar cancelation of predictive signals was also found in the mormyromast pathway (Bell and Grant, 1992). While afferents from ampullary receptors and mormyromast receptors innervate different regions of the ELL cortex, MG cells of both regions receive corollary discharge inputs from parallel fibers and afferent inputs from granule cells (**Figure 5**). It is thought that the same process mediating negative image formation in the ampullary region of ELL cortex is also occurring in the cerebellum-like circuit of the mormyromast region of ELL cortex. This serves to cancel predicted reafferent responses in the active electrolocation pathway, so that the system only responds to novel, unexpected sensory inputs.

Cerebellum-Like Circuits Mediate Subtraction of Self-Generated Inputs

After the discovery of modifiable internal predictions was made in the mormyrid ELL, many similar mechanisms were found in other cerebellum-like structures across various sensory modalities and species (reviewed in Bell et al., 2008). For example, the skate *Raja erinacea* is a cartilaginous fish that has a low-frequency, passive electrosensory system. Similar to mormyrid fish, own movements such as respiration strongly affect electrosensory processing. This reafference problem is solved by a cerebellum-like circuit in the dorsal octovolateral nucleus (DON) where primary electrosensory afferents terminate (Bodznick and Northcutt, 1980; Montgomery, 1984; New and Bodznick, 1990). Furthermore, similar to the passive electrosensory system in mormyrids, this cancelation appears to be modifiable through learning as shown by an experiment using paired stimulation (Montgomery and Bodznick, 1994). A similar cancelation phenomenon was found in the medial octovolateral nucleus (MON) of scorpion fish, *Scorpoena papillosus*, which is the first sensory center with a cerebellum-like structure in the mechanosensory lateral line system (Montgomery and Bodznick, 1994).

Another example of a cerebellum-like circuit is the dorsal cochlear nucleus (DCN) in the auditory pathway of mammals. Own behaviors including vocalization, chewing, licking, and other movements of body parts have predictable auditory consequences that may disrupt auditory processing. The DCN directly receives primary auditory afferents from the cochlea in the deep layer and also receives motor-related inputs including corollary discharge information via parallel fibers in the molecular layer (Oertel and Young, 2004). Like MG cells in the mormyrid ELL, *in vitro* studies showed plasticity at the synapse between the parallel fibers and the GABAergic Purkinje-like cells (called cartwheel cells) that follows an anti-Hebbian rule (Tzounopoulos et al., 2004, 2007). Until recently, whether the cerebellum-like circuit in the DCN works to subtract predictable signals was untested. Singla et al. (2017) developed a unique experiment with mice to directly test this hypothesis, in which they delivered auditory stimulation paired with licking behavior. They found that DCN neurons reliably encoded external auditory stimuli even during licking. Moreover, DCN neurons reduced responsiveness to auditory stimuli that were repeatedly temporally correlated with licking, suggesting that the DCN circuit creates adaptive filters for canceling self-generated sound through learning, much like the generation of negative images in the ELL of mormyrids.

Modifications that adapt to the sensory consequences of own behavior in the cerebellum-like circuits discussed here are not necessarily due to corollary discharges, and could be due to sensory feedback (see **Figure 3**). However, these studies highlight how the cerebellum-like circuit in mormyrid ELL provided general insight into how various circuits solve the problem of canceling the predictable sensory consequences of own behavior.

Subtraction of Expected Signals in Primate Vestibular Processing

Using vestibular organs of the inner ear, the vestibular system can detect head motion, including rotational and translational velocities relative to space. This sensory information is used for maintaining posture, perceiving self-motion, and computing spatial orientation. As with other sensory modalities, distinguishing self-generated from external stimuli is important for these functions.

All afferent fibers from the vestibular organs project to the vestibular nucleus and terminate on two categories of neurons: vestibulo-ocular reflex (VOR) neurons and vestibular-only (VO) neurons (reviewed in Cullen, 2012). While the vestibular afferents encode vestibular stimuli caused by both external and self-generated changes in a similar way, VO neurons do not provide reliable information about active head movements (Boyle et al., 1996; McCrea et al., 1999; Roy and Cullen, 2001; Cullen and Minor, 2002). This suggested that a corollary discharge from the neck motor command directly inhibits the VO neurons, but this was not supported experimentally (Roy and Cullen,

2004). Alternatively, Roy and Cullen proposed a more interesting mechanism: an inhibitory neck proprioceptive signal is gated in only when the actual activation of neck proprioceptors matches an internal prediction (corollary discharge) of the consequence of head motion (Roy and Cullen, 2004).

Next, Cullen et al. (2011) were interested in where and how internal predictions and actual neck proprioceptive signals meet. They focused on the rostral fastigial nucleus (rFN) in the deep cerebellum. The rFN receives descending projections from the anterior vermis, a region of the cerebellum that receives direct projections from cortical structures involved in producing head and neck movement (Batton et al., 1977; Yamada and Noda, 1987; Alstermark et al., 1992a,b; Cullen et al., 2011). That is, the rFN would receive a corollary discharge of neck motor commands. In addition, the rFN integrates vestibular and proprioceptive inputs and contains unimodal neurons (vestibular only) and bimodal neurons (vestibular and proprioceptive) (Brooks and Cullen, 2009). Furthermore, Brooks and Cullen showed, during active movement, that unimodal neurons encode unexpected head motions whereas bimodal neurons encode unexpected body motion (Brooks and Cullen, 2013). This result indicated that information of expected motion was subtracted in the rFN. Moreover, Brooks et al. (2015) found that loading the monkey's movement, which resulted in a difference between estimated sensory consequences of own behavior and actual sensory consequences, altered this internal prediction. Trial-by-trial changes in the neuronal response were gradual and consistent with the resultant behavioral learning. This describes a similar process to generating negative images in mormyrid fish.

Predictive Visual Representation During Saccades in Primates

A milestone in the study of corollary discharge in predictive sensory coding would be a series of studies on visual representation during saccades in primates. Duhamel et al. (1992) addressed how eye movement affects the receptive fields of neurons, i.e., the region of space that can elicit a visual response. They recorded neural activities from the lateral intraparietal area (LIP) of rhesus macaques, *Maccaca mulatta*. They found that LIP neurons respond to a visual stimulus in their receptive field with a 70 ms latency. Next, a visual stimulus was positioned so that it would be in the receptive field after the monkey completed a saccade. Although the neurons would be expected to start firing 70 ms after the eye movement brought the stimulus into the receptive field, Duhamel et al. (1992) found that the cells started responding 80 ms before the saccade was initiated. That is, the receptive field location shifted before the eye movement. A similar receptive field shift was also found in the frontal eye field (FEF) of the frontal cortex (Umeno and Goldberg, 1997). These results suggest that a corollary discharge conveying internal predictions accurately adjusts the receptive field of LIP and FEF visual neurons in anticipation of intended eye movements.

Sommer and Wurtz investigated the neural pathway that mediates visual stability by corollary discharge. The candidate source of corollary discharge was the superior colliculus (SC) because the SC contains neurons that fire just before initiating a saccade, suggesting it is a motor control center for eye movement (Sparks and Hartwich-Young, 1989). Anatomical research showed a neural pathway from the SC to the FEF via the mediodorsal nucleus (MD) of the thalamus, suggesting this pathway could convey corollary discharges related to eye movement (Lynch et al., 1994). Sommer and Wurtz (2002, 2004) found that this pathway encoded the vector of upcoming eye movements and that inactivation of this pathway impaired a corollary discharge-related behavioral task (double-step saccade task). Furthermore, they found that the shift of receptive field in the FEF neurons before upcoming eye movements was impaired by interrupting the corollary discharge signal from the MD (Sommer and Wurtz, 2006). This result demonstrated the causality of corollary discharge input from the MD in signaling the vector of intended eye movement to shift the receptive fields of FEF neurons.

Internal Prediction Mediates Sensorimotor Learning in Songbirds

Songbirds acquire specific song patterns through vocal learning during development. Vocal learning consists of three phases including (1) sensory learning: modifying the internal template of own song based on the songs of one or more tutors; (2) sensorimotor learning: matching own song performance to the internal template; and (3) crystallization: establishment of fixed, mature song patterns (Marler, 1964; Konishi, 1965). The neural mechanisms underlying vocal learning in songbirds have attracted many neuroscientists because of striking similarities to the development of human speech (Doupe and Kuhl, 1999).

An important question in vocal learning was how the nervous system can compare auditory feedback from own song with the internal template during sensorimotor learning. Using modeling studies, Troyer and Doupe proposed that a corollary discharge plays an essential role in comparing the tutor's song stored in its memory to actual auditory feedback (Troyer and Doupe, 2000a,b). According to this hypothesis, when the bird vocalizes, a corollary discharge representing an internal prediction of the template was emitted and compared with the actual feedback. The errors between the template and the sensory consequences of vocalization were thought to be corrected by a repeating cycle including vocal production and adjustment of the motor program. To date, however, the nature of this corollary discharge remains controversial.

The neural pathways mediating bird song production and learning have been well characterized (Nottebohm, 2005). The telencephalic nucleus called the high vocal center (HVC) plays an important role in both song production and learning and is a source of two important pathways: (1) posterior descending pathway (PDP) necessary for both learning and production, and (2) anterior forebrain pathway (AFP) necessary for learning only (Nottebohm, 2005). Prather et al. (2008) found that the first projection neuron in the AFP (i.e., HVC–>Area X) responds both to own song production and auditory feedback with the same latency. This feature is similar to mirror neurons (Gallese et al., 1996) and also suggested this might be a suitable site

for comparing feedback of own vocalization with the internal template. Furthermore, in recent years, a candidate corollary discharge pathway was identified (Roberts et al., 2017). Roberts et al. (2017) focused on another pathway from HVC to a small cluster of neurons (Avalanche, Av) embedded in the caudal mesopallium (CM), analog of the mammalian secondary auditory cortex (Akutagawa and Konishi, 2010). They identified a new type of projection neuron (HVC–>Av) that receives inputs from premotor neurons and transmits motor-related activity during song production. In addition, genetically ablating this type of neuron in juveniles disrupted vocal learning. Future studies should examine how the downstream circuit integrates internal predictions represented by a corollary discharge and actual sensory inputs and how the error signals are used to adjust motor programs.

COROLLARY DISCHARGE IN THE PATTERNING OF BEHAVIOR

Although we have mostly discussed effects of corollary discharges on sensory processing thus far, corollary discharges have also been found to influence motor systems. For example, as discussed previously, corollary discharge inhibition regulates the temporal pattern generation of feeding behavior in sea slugs (Davis et al., 1973; Siegler et al., 1974; Gillette and Davis, 1977). Similar to this case, a corollary discharge pathway in mormyrid fish is also involved in generating rhythmic temporal patterns of EOD production.

Temporal Pattern Generation of EOD Production in Mormyrids

Similar to other rhythmic behaviors such as locomotion and feeding, EOD production by mormyrid fish consists of variably rhythmic temporal patterns, which play an important role in communicating behavioral state (Carlson, 2002a). What neural circuitry governs EOD production? Bell et al. (1983) first identified the medullary command nucleus (CN) that controls EOD production, as well as corollary discharge pathways, using neuronal tracing with horseradish peroxidase. The CN projects to the medullary relay nucleus (MRN), which sends its output to the spinal electromotor neurons that innervate the electrocytes in the electric organ (EO), which produce the EOD (Bennett et al., 1967; Bell et al., 1983). The reasons why this nucleus was identified as a "command" nucleus are (1) its output is time-locked in a one-to-one manner with EOD generation, (2) it integrates major inputs from the mesencephalic precommand nucleus (PCN), minor inputs from the mesencephalic ventroposterior nucleus (VP), and unspecified inputs to the adjacent medial reticular formation, and (3) its neurons are interconnected by complex electronic coupling, resulting in the first occurrence of neuronal synchronization in the pathway (Bell et al., 1983; Elekes and Szabo, 1985; Grant et al., 1986).

How does the electromotor circuit generate variable temporal patterns of EOD production? The CN itself is not a pacemaker, rather it integrates descending inputs to decide whether or not to generate an EOD. von der Emde et al. (2000) first recorded neural activities from the PCN, and discovered two types of neurons. Neurons of one type fired in the moments leading up to fictive EOD production, but were inhibited immediately after each fictive EOD. Neurons of the second type fired bursts of spikes immediately after each fictive EOD, during the silent period of the first neuron type. This suggested that the first type of neuron was providing descending excitatory input to the CN, whereas the second type of neuron was relaying corollary discharge inhibition to the first type of neuron.

Carlson further studied the neuroanatomy of the electromotor system in the species *Brienomyrus brachyistius* (Carlson, 2002b). Carlson confirmed that the anatomical pathway was similar to that of *G. petersii* (Bell et al., 1983), and added important new findings: (1) In addition to PCN, the dorsal posterior nucleus of the thalamus (DP) also provides a major input to the CN; (2) VP has two distinct subdivisions, one dorsal (VPd) and one ventral (VPv); (3) VPv projects to the CN, DP, and PCN, whereas VPd projects only to DP and PCN; (4) VPd receives input from the corollary discharge pathway via MCA (**Figure 9**). These findings suggested that VPd neurons were the source of corollary discharge inhibition of PCN neurons first identified by von der Emde et al. (2000). Indeed, using single-unit extracellular recordings and pharmacological stimulation, Carlson and Hopkins demonstrated that VPd provides corollary discharge inhibition to DP and PCN and that disinhibition increases the EOD rate (Carlson, 2003; Carlson and Hopkins, 2004). Thus, recurrent inhibition of premotor circuits by a corollary discharge can act to regulate rhythmic motor output.

Both DP and VPd are connected reciprocally with the optic tectum (Wullimann and Northcutt, 1990; Carlson, 2002b), which is considered a primary sensorimotor hub (Meek and Nieuwenhuys, 1998). This suggests that the EOD command

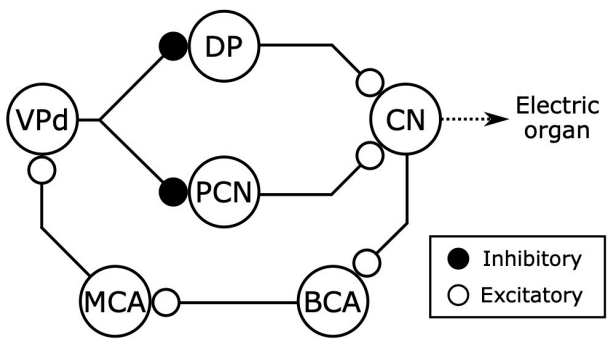

FIGURE 9 | Electromotor network of mormyrids receives inhibitory feedback from the electric organ corollary discharge pathway. The command nucleus (CN) controls the timing of EOD production and also gives rise to a corollary discharge pathway including the bulbar command-associated nucleus (BCA) and mesencephalic command-associated nucleus (MCA) (see also **Figure 5**). The CN receives excitatory inputs from the thalamic dorsal posterior nucleus (DP) and the mesencephalic precommand nucleus (PCN). The DP and PCN both receive inhibitory input from the dorsal ventroposterior nucleus (VPd) of the torus semicircularis, which receives corollary discharge excitation from the MCA. Thus, the main sources of excitatory input to the CN receive inhibitory feedback from the corollary discharge pathway immediately following each EOD. Modified from Carlson (2003).

network integrates sensory information and inhibitory feedback from a corollary discharge to generate rhythmic EOD patterns, much like the feeding circuit found in the sea slug *Pleurobranchea* (Davis et al., 1973; Gillette and Davis, 1977). Thus, a similar integration of corollary discharge feedback and sensory input may shape rhythmic motor output across invertebrate and vertebrate species.

Corollary Discharge Mediates Motor Coupling in Larval Tadpoles

Another important finding on the role of corollary discharge in governing behavioral pattern generation comes from a series of studies on the link between spinal locomotion circuits and eye-movement circuits in larval tadpoles. Locomotion such as swimming results in both body movements and head movements, which may greatly disrupt visual perception. To stabilize their visual world, aquatic animals move their eyes in conjunction with tail movements to minimize retinal image slip (Lyon, 1900; Harris, 1965; Easter and Johns, 1974; Chagnaud et al., 2012). This motor coupling could be explained by the concerted actions of visuo-vestibular and proprioceptive reflexes (Angelaki and Hess, 2005). However, earlier behavioral studies suggested that such sensorimotor transformations would be relatively slow due to the filtering characteristics of the sensory periphery (Lyon, 1900; Harris, 1965; Easter and Johns, 1974; Chagnaud et al., 2012). Instead, central, motor-related signals may inform eye-movement circuits about ongoing locomotor patterns.

Stehouwer first demonstrated this possibility using a preparation of an isolated central nervous system including only the nerves innervating extraocular muscles of the eyes of a larval bullfrog (*Rana catesbeiana*) (Stehouwer, 1987). The reduced *in vitro* preparation enabled recording from motor neurons that innervate extraocular muscles during fictive swimming, which was indicated by burst activity of axial motor neurons in the spinal cord. By isolating the central nervous system and eliminating movement, the effects of sensory feedback, such as vestibular and proprioceptive inputs, were eliminated (see **Figure 3C**). He found that burst activities from motor neurons mediating eye movement were phase-locked to burst activities associated with fictive swimming. This result suggested that motor coupling between swimming and eye movement depends on intrinsic communication between the brain and spinal cord.

Lambert et al. (2012) later examined the link between spinal swimming circuitry and eye-movement circuitry using larval *Xenopus laevis*. They removed other supraspinal areas such as the midbrain reticular formation, cerebellum, or vestibular nucleus from the *in vitro* preparation, and found that this motor coupling remained intact. In addition, they delineated an ascending pathway from the spinal cord to eye-movement circuitry based on anatomical evidence. These results demonstrated that a corollary discharge from the spinal swimming circuit directly regulates the eye-movement used for gaze stabilization.

These studies established the novel concept that corollary discharges can affect other motor circuits in addition to sensory processing (reviewed in Straka et al., 2018). Such corollary discharge function is not likely limited to swimming-extraocular motor coupling in tadpoles. For example in cats, there are pathways that convey motor information during scratching from the spinal cord to the cerebellum (Arshavsky et al., 1978a,b; Martínez-Silva et al., 2014). It is speculated that the corollary discharge feedback may be used to compare and adjust the precision of movements according to environmental demands (Morton and Bastian, 2004), although there is no behavioral evidence as of yet. In addition, in mormyrid fish, corollary discharge related potentials are also found in the cerebellum (Bennett and Steinbach, 1969), but their function remains unknown.

EVOLUTION OF COROLLARY DISCHARGE FUNCTION

As we have described, corollary discharge is found across various sensory modalities and species. While mechanisms underlying corollary discharge have been extensively studied in select species, little is known about the evolution of corollary discharge circuits and mechanisms. How have animals acquired novel corollary discharge functions through evolution? How have corollary discharges evolved along with evolutionary change in behavior? Comparative studies of weakly electric mormyrid fish may provide answers to these questions.

Does acquiring electrogenesis mean emergence of corollary discharge function? The answer seems to be no. The ability of electrogenesis has evolved at least 6 times independently in fish (Gallant et al., 2014). The electric fishes can be categorized into two groups: wave-type fish that generate continuous, quasi-sinusoidal EODs in which the interval between each EOD is approximately equal to the duration of each EOD; and pulse-type fish that generate discrete EODs with longer periods of silence between them. While all mormyrids generate pulse-type EODs, the closest relative to mormyrids, *Gymnarchus niloticus*, generates a wave-type EOD. Recently, we demonstrated that an electric organ corollary discharge seems to exist in all species of mormyrids (Vélez and Carlson, 2016), but *Gymnarchus* appears to lack an electric organ corollary discharge pathway (Kawasaki, 1993, 1994). This suggests that an electric organ corollary discharge pathway evolved with the origin of pulse-type EODs in mormyrids. However, in the distantly related gymnotiform electric fish, it appears that neither wave-type nor pulse-type species have an electric organ corollary discharge pathway (Kawasaki and Heiligenberg, 1990; Keller et al., 1990; Heiligenberg, 1991; Heiligenberg and Kawasaki, 1992; Kennedy and Heiligenberg, 1994). Mormyrids generate EODs at much more variable rates than pulse-type gymnotiforms (Kawasaki and Heiligenberg, 1990; Carlson, 2002a). It may be that a corollary discharge is important for signaling the timing of EOD production in fish that generate EODs with greater irregularity, that is with less predictability. Regardless, these findings reveal that evolving electrogenesis does not always mean acquiring a novel electric organ corollary discharge pathway.

Nearly all detailed studies of corollary discharge circuitry and mechanisms in mormyrids have focused on one species, *Gnathonemus petersii*. However, EODs have diversified extensively across the mormyrid family, especially in duration, which varies across species from 0.1 to over 10 ms (Hopkins,

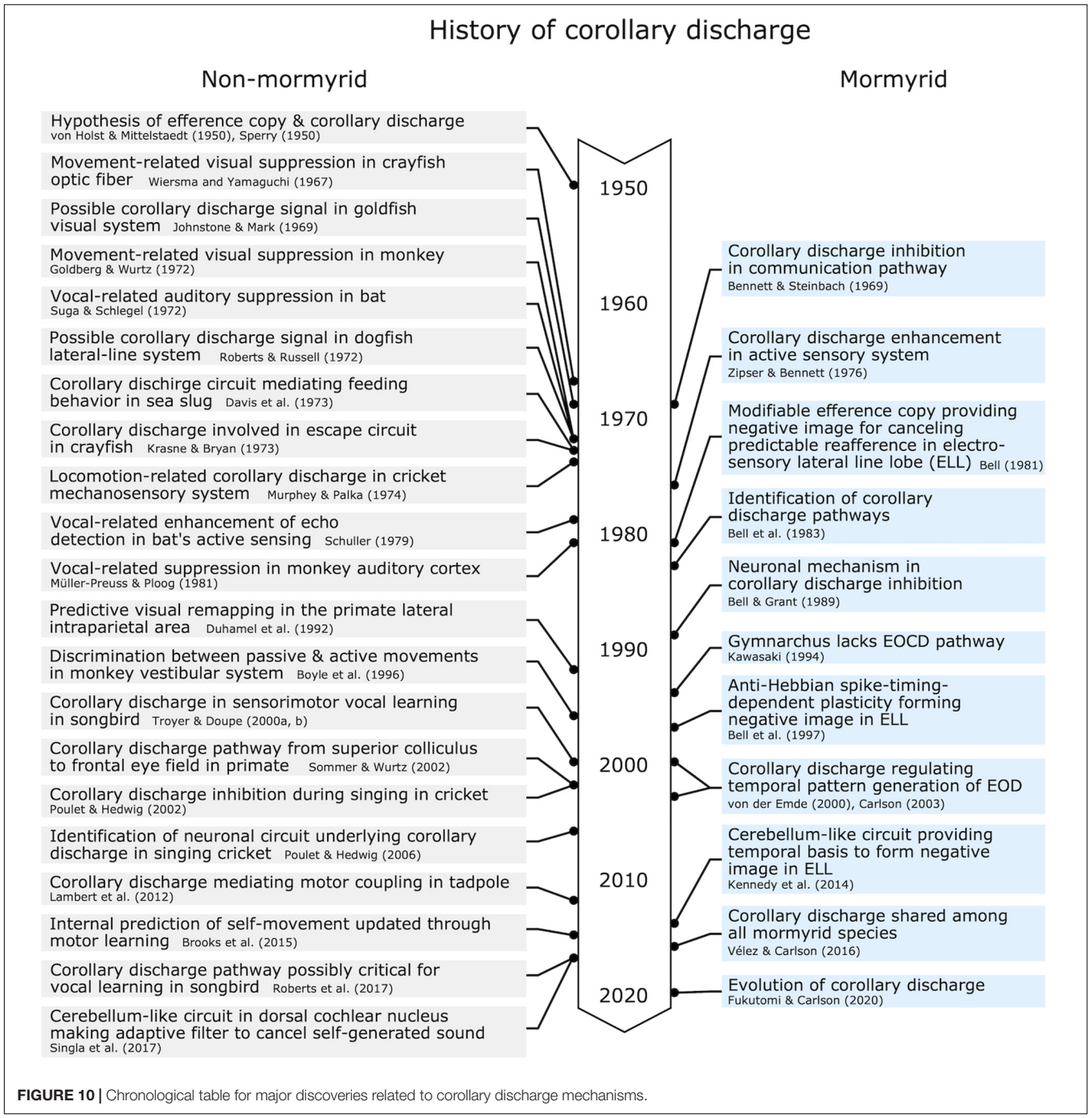

FIGURE 10 | Chronological table for major discoveries related to corollary discharge mechanisms.

1999). How does corollary discharge function vary with these electric signals? Recently, our group compared corollary discharge inhibition in the communication pathway among several species with varying EOD durations (Fukutomi and Carlson, 2020). We found that fish with long-duration EODs have delayed corollary discharge inhibition of the nELL and that this time-shifted corollary discharge optimally blocks electrosensory responses to the fish's own EOD (Fukutomi and Carlson, 2020). This suggests that corollary discharge mechanisms coevolve along with the evolution of communication signals, but the underlying mechanisms for shifting this inhibitory delay remain unknown.

CONCLUDING REMARK

Here, we discussed how corollary discharge mechanisms have been understood in a historical context, with a focus on the study of mormyrid weakly electric fish (**Figure 10**). Because dysfunction of corollary discharge may be related to

psychiatric diseases such as schizophrenia in humans (Ford et al., 2001), studying corollary discharge mechanisms is important in medical science as well as basic science. Since the concepts of corollary discharge and efference copy were proposed in 1950, studies in mormyrids have pioneered our understanding of the underlying circuitry and mechanisms. Although many animals including humans have neither electrosensory systems nor the ability to actively generate electric fields, these findings in mormyrids have provided insights that have led to general principles of corollary discharge function and mechanism, including inhibition in communication, enhancement in active sensing, modifiable efference copies involved in learning and sensorimotor integration, and feedback to premotor centers for regulating behavioral output. The generality of these principals has been supported by numerous studies on a diversity of species and sensory systems.

AUTHOR CONTRIBUTIONS

Both authors conceptualized the review and wrote the manuscript.

FUNDING

This work was supported by the National Science Foundation (IOS-1755071 to BC) and the Uehara Memorial Foundation (to MF).

REFERENCES

Akutagawa, E., and Konishi, M. (2010). New brain pathways found in the vocal control system of a songbird. *J. Comp. Neurol.* 518, 3086–3100. doi: 10.1002/cne.22383

Alexander, G. E., Newman, J. D., and Symmes, D. (1976). Convergence of prefrontal and acoustic inputs upon neurons in the superior temporal gyrus of the awake squirrel monkey. *Brain Res.* 116, 334–338. doi: 10.1016/0006-8993(76)90913-6

Alstermark, B., Pinter, M. J., and Sasaki, S. (1992a). Descending pathways mediating disynaptic excitation of dorsal neck motoneurones in the cat: facilitatory interactions. *Neurosci. Res.* 15, 32–41. doi: 10.1016/0168-0102(92)90015-5

Alstermark, B., Pinter, M. J., and Sasaki, S. (1992b). Descending pathways mediating disynaptic excitation of dorsal neck motoneurones in the cat: brain stem relay. *Neurosci. Res.* 15, 42–57. doi: 10.1016/0168-0102(92)90016-6

Angelaki, D. E., and Hess, B. J. M. (2005). Self-motion-induced eye movements: effects on visual acuity and navigation. *Nat. Rev. Neurosci.* 6, 966–976. doi: 10.1038/nrn1804

Arshavsky, I., Gelfand, I. M., Orlovsky, G. N., and Pavlova, G. A. (1978a). Messages conveyed by spinocerebellar pathways during scratching in the cat. I. Activity of neurons of the lateral reticular nucleus. *Brain Res.* 151, 479–491. doi: 10.1016/0006-8993(78)91081-8

Arshavsky, I., Gelfand, I. M., Orlovsky, G. N., and Pavlova, G. A. (1978b). Messages conveyed by spinocerebellar pathways during scratching in the cat. II. Activity of neurons of the ventral spinocerebellar tract. *Brain Res.* 151, 493–506. doi: 10.1016/0006-8993(78)91082-x

Baker, C. A., Kohashi, T., Lyons-Warren, A. M., Ma, X., and Carlson, B. A. (2013). Multiplexed temporal coding of electric communication signals in mormyrid fishes. *J. Exp. Biol.* 216, 2365–2379. doi: 10.1242/jeb.082289

Baker, C. A., Ma, L., Casareale, C. R., and Carlson, B. A. (2016). Behavioral and single-neuron sensitivity to millisecond variations in temporally patterned communication signals. *J. Neurosci.* 36, 8985–9000. doi: 10.1523/JNEUROSCI.0648-16.2016

Batton, R. R., Jayaraman, A., Ruggiero, D., and Carpenter, M. B. (1977). Fastigial efferent projections in the monkey: an autoradiographic study. *J. Comp. Neurol.* 174, 281–305. doi: 10.1002/cne.901740206

Bell, C., Dunn, K., Hall, C., and Caputi, A. (1995). Electric organ corollary discharge pathways in mormyrid fish. *J. Comp. Physiol. A* 177, 449–462. doi: 10.1007/bf00187481

Bell, C., and von der Emde, G. (1995). Electric organ corollary discharge pathways in mormyrid fish. *J. Comp. Physiol. A* 177, 463–479. doi: 10.1007/bf00187482

Bell, C. C. (1981). An efference copy which is modified by reafferent input. *Science* 214, 450–453. doi: 10.1126/science.7291985

Bell, C. C. (1989). Sensory coding and corollary discharge effects in mormyrid electric fish. *J. Exp. Biol.* 146, 229–253.

Bell, C. C. (1990). Mormyromast electroreceptor organs and their afferent fibers in mormyrid fish. II. Intra-axonal recordings show initial stages of central processing. *J. Neurophysiol.* 63, 303–318. doi: 10.1152/jn.1990.63.2.303

Bell, C. C., Caputi, A., Grant, K., and Serrier, J. (1993). Storage of a sensory pattern by anti-Hebbian synaptic plasticity in an electric fish. *Proc. Natl. Acad. Sci. U.S.A.* 90, 4650–4654. doi: 10.1073/pnas.90.10.4650

Bell, C. C., Finger, T. E., and Russell, C. J. (1981). Central connections of the posterior lateral line lobe in mormyrid fish. *Exp. Brain Res.* 42, 9–22. doi: 10.1007/BF00235724

Bell, C. C., and Grant, K. (1989). Corollary discharge inhibition and preservation of temporal information in a sensory nucleus of mormyrid electric fish. *J. Neurosci.* 9, 1029–1044. doi: 10.1523/jneurosci.09-03-01029.1989

Bell, C. C., and Grant, K. (1992). Sensory processing and corollary discharge effects in mormyromast regions of mormyrid electrosensory lobe. II. Cell types and corollary discharge plasticity. *J. Neurophysiol.* 68, 859–875. doi: 10.1152/jn.1992.68.3.859

Bell, C. C., Han, V., and Sawtell, N. B. (2008). Cerebellum-like structures and their implications for cerebellar function. *Annu. Rev. Neurosci.* 31, 1–24. doi: 10.1146/annurev.neuro.30.051606.094225

Bell, C. C., Han, V. Z., Sugawara, Y., and Grant, K. (1997). Synaptic plasticity in a cerebellum-like structure depends on temporal order. *Nature* 387, 278–281. doi: 10.1038/387278a0

Bell, C. C., Libouban, S., and Szabo, T. (1983). Pathways of the electric organ discharge command and its corollary discharges in mormyrid fish. *J. Comp. Neurol.* 216, 327–338. doi: 10.1002/cne.902160309

Bell, C. C., and Russell, C. J. (1978). Effect of electric organ discharge on ampullary receptors in a mormyrid. *Brain Res.* 145, 85–96. doi: 10.1016/0006-8993(78)90798-9

Bell, C. C., Zakon, H., and Finger, T. E. (1989). Mormyromast electroreceptor organs and their afferent fibers in mormyrid fish: I. Morphology. *J. Comp. Neurol.* 286, 391–407. doi: 10.1002/cne.902860309

Bennett, M. V., Pappas, G. D., Aljure, E., and Nakajima, Y. (1967). Physiology and ultrastructure of electrotonic junctions. II. Spinal and medullary electromotor nuclei in mormyrid fish. *J. Neurophysiol.* 30, 180–208. doi: 10.1152/jn.1967.30.2.180

Bennett, M. V. L. (1965). Electroreceptors in mormyrids. *Cold. Spring Harb. Sym.* 30, 245–262. doi: 10.1101/sqb.1965.030.01.027

Bennett, M. V. L., and Steinbach, A. B. (1969). "Influence of electric organ control system on electrosensory afferent pathways in Mormyrids," in *Neurobiology of Cerebellar Evolution and Development*, ed. R. Llinás (Chicago, IL: American Medical Association), 207–214.

Bodznick, D., and Northcutt, R. G. (1980). Segregation of electro- and mechanoreceptive inputs to the elasmobranch medulla. *Brain Res.* 195, 313–321. doi: 10.1016/0006-8993(80)90067-0

Boyle, R., Belton, T., and McCrea, R. A. (1996). Responses of identified vestibulospinal neurons to voluntary eye and head movements in the squirrel monkey. *Ann. N.Y. Acad. Sci.* 781, 244–263. doi: 10.1111/j.1749-6632.1996.tb15704.x

Brooks, J. X., Carriot, J., and Cullen, K. E. (2015). Learning to expect the unexpected: rapid updating in primate cerebellum during voluntary self-motion. *Nat. Neurosci.* 18, 1310–1317. doi: 10.1038/nn.4077

Brooks, J. X., and Cullen, K. E. (2009). Multimodal integration in rostral fastigial nucleus provides an estimate of body movement. *J. Neurosci.* 29, 10499–10511. doi: 10.1523/jneurosci.1937-09.2009

Brooks, J. X., and Cullen, K. E. (2013). The primate cerebellum selectively encodes unexpected self-motion. *Curr. Biol.* 23, 947–955. doi: 10.1016/j.cub.2013.04.029

Carlson, B. A. (2002a). Electric signaling behavior and the mechanisms of electric organ discharge production in mormyrid fish. *J. Physiol. Paris* 96, 405–419. doi: 10.1016/S0928-4257(03)00019-6

Carlson, B. A. (2002b). Neuroanatomy of the mormyrid electromotor control system. *J. Comp. Neurol.* 454, 440–455. doi: 10.1002/cne.10462

Carlson, B. A. (2003). Single-unit activity patterns in nuclei that control the electromotor command nucleus during spontaneous electric signal production in the mormyrid *Brienomyrus brachyistius*. *J. Neurosci.* 23, 10128–10136. doi: 10.1523/jneurosci.23-31-10128.2003

Carlson, B. A. (2009a). "Reafferent control in electric communication," in *Encyclopedia of Neuroscience*, eds M. D. Binder, N. Hirokawa, U. Windhorst, and M. C. Hirsch (Berlin: Springer). doi: 10.1007/978-3-540-29678-2_4945

Carlson, B. A. (2009b). Temporal-pattern recognition by single neurons in a sensory pathway devoted to social communication behavior. *J. Neurosci.* 29, 9417–9428. doi: 10.1523/JNEUROSCI.1980-09.2009

Carlson, B. A., and Hopkins, C. D. (2004). Central control of electric signaling behavior in the mormyrid *Brienomyrus brachyistius*: segregation of behavior-specific inputs and the role of modifiable recurrent inhibition. *J. Exp. Biol.* 207, 1073–1084. doi: 10.1242/jeb.00851

Casas, J., and Dangles, O. (2010). Physical ecology of fluid flow sensing in arthropods. *Annu. Rev. Entomol.* 55, 505–520. doi: 10.1146/annurev-ento-112408-085342

Chagnaud, B. P., Simmers, J., and Straka, H. (2012). Predictability of visual perturbation during locomotion: implications for corrective efference copy signaling. *Biol. Cybern.* 106, 669–679. doi: 10.1007/s00422-012-0528-0

Crapse, T. B., and Sommer, M. A. (2008). Corollary discharge across the animal kingdom. *Nat. Rev. Neurosci.* 9, 587–600. doi: 10.1038/nrn2457

Creutzfeldt, O., Ojemann, G., and Lettich, E. (1989). Neuronal activity in the human lateral temporal lobe. *Exp. Brain Res.* 77, 476–489. doi: 10.1007/bf00249601

Cullen, K. E. (2004). Sensory signals during active versus passive movement. *Curr. Opin. Neurobiol.* 14, 698–706. doi: 10.1016/j.conb.2004.10.002

Cullen, K. E. (2012). The vestibular system: multimodal integration and encoding of self-motion for motor control. *Trends Neurosci.* 35, 185–196. doi: 10.1016/j.tins.2011.12.001

Cullen, K. E., Brooks, J. X., Jamali, M., Carriot, J., and Massot, C. (2011). Internal models of self-motion: computations that suppress vestibular reafference in early vestibular processing. *Exp. Brain Res.* 210, 377–388. doi: 10.1007/s00221-011-2555-9

Cullen, K. E., and Minor, L. B. (2002). Semicircular canal afferents similarly encode active and passive head-on-body rotations: implications for the role of vestibular efference. *J. Neurosci.* 22:RC226. doi: 10.1523/jneurosci.22-11-j0002.2002

Davis, W. J., Mpitsos, G. J., Pinneo, J. M., and Ram, J. L. (1977). Modification of the behavioral hierarchy of *Pleurobranchaea*. *J. Comp. Physiol.* 117, 99–125. doi: 10.1007/bf00605525

Davis, W. J., Siegler, M. V. S., and Mpitsos, G. J. (1973). Distributed neuronal oscillators and efference copy in the feeding system of *Pleurobranchaea*. *J. Neurophysiol.* 36, 258–274. doi: 10.1152/jn.1973.36.2.258

Denizot, J. P., Clausse, S., Elekes, K., Geffard, M., Grant, K., Libouban, S., et al. (1987). Convergence of electrotonic club endings, GABA- and serotoninergic terminals on second order neurons of the electrosensory pathway in mormyrid fish, *Gnathonemus petersii* and *Brienomyrus niger* (Teleostei). *Cell Tissue Res.* 249, 301–309. doi: 10.1007/bf00215512

Doupe, A. J., and Kuhl, P. K. (1999). Birdsong and human speech: common themes and mechanisms. *Annu. Rev. Neurosci.* 22, 567–631. doi: 10.1146/annurev.neuro.22.1.567

Duhamel, J. R., Colby, C. L., and Goldberg, M. E. (1992). The updating of the representation of visual space in parietal cortex by intended eye movements. *Science* 255, 90–92. doi: 10.1126/science.1553535

Easter, S. S., and Johns, P. R. (1974). Horizontal compensatory eye movements in goldfish (*Carassius auratus*). *J. Comp. Physiol.* 92, 37–57. doi: 10.1007/bf00696525

Edwards, D., Heitler, W., and Krasne, F. (1999). Fifty years of a command neuron: the neurobiology of escape behavior in the crayfish. *Trends Neurosci.* 22, 153–161. doi: 10.1016/S0166-2236(98)01340-X

Elekes, K., and Szabo, T. (1985). The mormyrid brainstem—III. Ultrastructure and synaptic organization of the medullary "pacemaker" nucleus. *Neuroscience* 15, 431–443. doi: 10.1016/0306-4522(85)90224-6

Eliades, S. J., and Wang, X. (2019). Corollary discharge mechanisms during vocal production in marmoset monkeys. *Biol. Psychiatry Cogn. Neurosci. Neuroimaging* 4, 805–812. doi: 10.1016/j.bpsc.2019.06.008

Enger, P. S., Libouban, S., and Szabo, T. (1976a). Fast conducting electrosensory pathway in the mormyrid fish, *Gnathonemus petersii*. *Neurosci. Lett.* 2, 133–136. doi: 10.1016/0304-3940(76)90004-5

Enger, P. S., Libouban, S., and Szabo, T. (1976b). Rhombo-mesencephalic connections in the fast conducting electrosensory system of the mormyrid fish, *Gnathonemus peters*ii. An HRP study. *Neurosci. Lett.* 3, 239–243. doi: 10.1016/0304-3940(76)90049-5

Ford, J. M., Mathalon, D. H., Heinks, T., Kalba, S., Faustman, W. O., and Roth, W. T. (2001). Neurophysiological evidence of corollary discharge dysfunction in Schizophrenia. *Am. J. Psychiat.* 158, 2069–2071. doi: 10.1176/appi.ajp.158.12.2069

Friedman, M. A., and Hopkins, C. D. (1998). Neural substrates for species recognition in the time-coding electrosensory pathway of mormyrid electric fish. *J. Neurosci.* 18, 1171–1185. doi: 10.1523/JNEUROSCI.18-03-01171.1998

Fukutomi, M., and Carlson, B. A. (2020). Signal diversification is associated with corollary discharge evolution in weakly electric fish. *J. Neurosci.* (in press). doi: 10.1523/JNEUROSCI.0875-20.2020

Gallant, J. R., Traeger, L. L., Volkening, J. D., Moffett, H., Chen, P.-H., Novina, C. D., et al. (2014). Genomic basis for the convergent evolution of electric organs. *Science* 344, 1522–1525. doi: 10.1126/science.1254432

Gallese, V., Fadiga, L., Fogassi, L., and Rizzolatti, G. (1996). Action recognition in the premotor cortex. *Brain* 119, 593–609. doi: 10.1093/brain/119.2.593

Gillette, R., and Davis, W. J. (1977). The role of the metacerebral giant neuron in the feeding behavior of *Pleurobranchaea*. *J Comp. Physiol.* 116, 129–159. doi: 10.1007/bf00605400

Goldberg, M. E., and Wurtz, R. H. (1972). Activity of superior colliculus in behaving monkey. I. Visual receptive fields of single neurons. *J. Neurophysiol.* 35, 542–559. doi: 10.1152/jn.1972.35.4.542

Grant, K., Bell, C. C., Clausse, S., and Ravaille, M. (1986). Morphology and physiology of the brainstem nuclei controlling the electric organ discharge in mormyrid fish. *J. Comp. Neurol.* 245, 514–530. doi: 10.1002/cne.902450407

Griffin, D. R. (1958). *Listening in the Dark*. New Haven, CT: Yale University Press.

Harris, A. J. (1965). Eye movements of the dogfish *Squalus acanthias* L. *J. Exp. Biol.* 43, 107–138.

Hedwig, B. (2000b). Control of cricket stridulation by a command neuron: efficacy depends on the behavioral state. *J. Neurophysiol.* 83, 712–722. doi: 10.1152/jn.2000.83.2.712

Hedwig, B. (2000a). A highly sensitive opto-electronic system for the measurement of movements. *J. Neurosci. Meth.* 100, 165–171. doi: 10.1016/s0165-0270(00)00255-7

Heiligenberg, W. (1969). The effect of stimulus chirps on a cricket's chirping (*Acheta domesticus*). *Z. Vergl. Physiologie* 65, 70–97. doi: 10.1007/bf00297990

Heiligenberg, W., and Kawasaki, M. (1992). An internal current source yields immunity of electrosensory information processing to unusually strong jamming in electric fish. *J. Comp. Physiol. A* 171, 309–316. doi: 10.1007/bf00223961

Heiligenberg, W. F. (1991). *Neural Nets in Electric Fish*. Cambridge, MA: MIT Press.

Hillman, D. E. (1969). Light and electron microscopical study of the relationships between the cerebellum and the vestibular organ of the frog. *Exp. Brain Res.* 9, 1–15. doi: 10.1007/bf00235448

Hopkins, C. D. (1986a). "Behavior of mormyridae," in *Electroreception*, eds T. H. Bullock and W. Heilgenberg (New York, NY: John Wiley & Sons), 527–576.

Hopkins, C. D. (1986b). Temporal structure of non-propagated electric communication signals. *Brain Behav. Evol.* 28, 43–59. doi: 10.1159/000118691

Hopkins, C. D. (1999). Design features for electric communication. *J. Exp. Biol.* 202, 1217–1228.

Johnstone, J. R., and Mark, R. F. (1969). Evidence for efference copy for eye movements in fish. *Comp. Biochem. Physiol.* 30, 931–939. doi: 10.1016/0010-406x(69)90048-6

Kalmijn, A. J. (1971). The electric sense of sharks and rays. *J. Exp. Biol.* 55, 371–383.

Kalmijn, A. J. (1974). "The detection of electric fields from inanimate and animate sources other than electric organs," in *Electroreceptors and Other Specialized Receptors in Lower Vertrebrates. Handbook of Sensory Physiology*, ed. A. Fessard (Berlin: Springer), 147–200. doi: 10.1007/978-3-642-65926-3_5

Kawasaki, M. (1993). Independently evolved jamming avoidance responses employ identical computational algorithms: a behavioral study of the African electric fish, *Gymnarchus niloticus*. *J. Comp. Physiol. A* 173, 9–22. doi: 10.1007/bf00209614

Kawasaki, M. (1994). The African wave-type electric fish, *Gymnarchus niloticus*, lacks corollary discharge mechanisms for electrosensory gating. *J. Comp. Physiol. A* 174, 133–144. doi: 10.1007/bf00193781

Kawasaki, M., and Heiligenberg, W. (1990). Different classes of glutamate receptors and GABA mediate distinct modulations of a neuronal oscillator, the medullary pacemaker of a gymnotiform electric fish. *J. Neurosci.* 10, 3896–3904. doi: 10.1523/jneurosci.10-12-03896.1990

Keller, C. H., Maler, L., and Heiligenberg, W. (1990). Structural and functional organization of a diencephalic sensory-motor interface in the gymnotiform fish, *Eigenmannia*. *J. Comp. Neurol.* 293, 347–376. doi: 10.1002/cne.902930304

Kennedy, A., Wayne, G., Kaifosh, P., Alviña, K., Abbott, L., and Sawtell, N. B. (2014). A temporal basis for predicting the sensory consequences of motor commands in an electric fish. *Nat. Neurosci.* 17, 416–422. doi: 10.1038/nn.3650

Kennedy, G., and Heiligenberg, W. (1994). Ultrastructural evidence of GABA-ergic inhibition and glutamatergic excitation in the pacemaker nucleus of the gymnotiform electric fish, *Hypopomus*. *J. Comp. Physiol. A* 174, 267–280. doi: 10.1007/bf00240210

Konishi, M. (1965). The role of auditory feedback in the control of vocalization in the white-crowned sparrow. *Z. Tierpsychol.* 22, 770–783.

Kothari, N. B., Wohlgemuth, M. J., and Moss, C. F. (2018). Dynamic representation of 3D auditory space in the midbrain of the free-flying echolocating bat. *eLife* 7:e29053. doi: 10.7554/eLife.29053

Kovac, M. P., and Davis, W. J. (1977). Behavioral choice: neural mechanisms in *Pleurobranchaea*. *Science* 198, 632–634. doi: 10.1126/science.918659

Kovac, M. P., and Davis, W. J. (1980). Neural mechanism underlying behavioral choice in *Pleurobranchaea*. *J. Neurophysiol.* 43, 469–487. doi: 10.1152/jn.1980.43.2.469

Krasne, F. B., and Bryan, J. S. (1973). Habituation: regulation through presynaptic inhibition. *Science* 182, 590–592. doi: 10.1126/science.182.4112.590

Lambert, F. M., Combes, D., Simmers, J., and Straka, H. (2012). Gaze stabilization by efference copy signaling without sensory feedback during vertebrate locomotion. *Curr. Biol.* 22, 1649–1658. doi: 10.1016/j.cub.2012.07.019

Libouban, S., and Szabo, T. (1977). An integration centre of the mormyrid fish brain: the *Auricula cerebelli*. An HRP study. *Neurosci. Lett.* 6, 115–119. doi: 10.1016/0304-3940(77)90005-2

Lynch, J. C., Hoover, J. E., and Strick, P. L. (1994). Input to the primate frontal eye field from the substantia nigra, superior colliculus, and dentate nucleus demonstrated by transneuronal transport. *Exp. Brain Res.* 100, 181–186. doi: 10.1007/bf00227293

Lyon, E. P. (1900). Compensatory motions in fishes. *Am. J. Physiol.* 4, 77–82. doi: 10.1152/ajplegacy.1900.4.2.77

Lyons-Warren, A. M., Kohashi, T., Mennerick, S., and Carlson, B. A. (2013). Detection of submillisecond spike timing differences based on delay-line anticoincidence detection. *J. Neurophysiol.* 110, 2295–2311. doi: 10.1152/jn.00444.2013

Maler, L. (1973). The posterior lateral line lobe of a mormyrid fish — a golgi study. *J. Comp. Neurol.* 152, 281–298. doi: 10.1002/cne.901520305

Mark, R. F., and Davidson, T. M. (1966). Unit responses from commissural fibers of optic lobes of fish. *Science* 152, 797–799. doi: 10.1126/science.152.3723.797

Markram, H., Gerstner, W., and Sjöström, P. J. (2011). A history of spike-timing-dependent plasticity. *Front. Syn. Neurosci.* 3:4. doi: 10.3389/fnsyn.2011.00004

Marler, P. (1964). "Inheritance and learning in the development of animal vocalization," in *Acoustic Behavior of Animals*, ed. M. C. Busnel (Amsterdam: Elsevier), 228–243.

Martínez-Silva, L., Manjarrez, E., Gutiérrez-Ospina, G., and Quevedo, J. N. (2014). Electrophysiological representation of scratching CPG activity in the cerebellum. *PLoS One* 9:e109936. doi: 10.1371/journal.pone.0109936

McCrea, R. A., Gdowski, G. T., Boyle, R., and Belton, T. (1999). Firing behavior of vestibular neurons during active and passive head movements: vestibulo-spinal and other non-eye-movement related neurons. *J. Neurophysiol.* 82, 416–428. doi: 10.1152/jn.1999.82.1.416

Meek, J., and Nieuwenhuys, R. (1998). "Holosteans and teleosts," in *The Central Nervous System of Vertebrates*, eds R. Nieuwenhuys, H. J. Donkelaar, and C. Nicholson (New York: Springer), 759–937. doi: 10.1007/978-3-642-18262-4_15

Montgomery, J. C. (1984). Noise cancellation in the electrosensory system of the thornback ray; common mode rejection of input produced by the animal's own ventilatory movement. *J. Comp. Physiol. A* 155, 103–111. doi: 10.1007/bf00610935

Montgomery, J. C., and Bodznick, D. (1994). An adaptive filter that cancels self-induced noise in the electrosensory and lateral line mechanosensory systems of fish. *Neurosci. Lett.* 174, 145–148. doi: 10.1016/0304-3940(94)90007-8

Morton, S. M., and Bastian, A. J. (2004). Cerebellar control of balance and locomotion. *Neuroscientist* 10, 247–259. doi: 10.1177/1073858404263517

Mugnaini, E., and Maler, L. (1987). Cytology and immunocytochemistry of the nucleus of the lateral line lobe in the electric fish *Gnathonemus petersii* (mormyridae): evidence suggesting that GABAergic synapses mediate an inhibitory corollary discharge. *Synapse* 1, 32–56. doi: 10.1002/syn.890010107

Müller-Preuss, P., Newman, J. D., and Jürgens, U. (1980). Anatomical and physiological evidence for a relationship between the 'cingular' vocalization area and the auditory cortex in the squirrel monkey. *Brain Res.* 202, 307–315. doi: 10.1016/0006-8993(80)90143-2

Müller-Preuss, P., and Ploog, D. (1981). Inhibition of auditory cortical neurons during phonation. *Brain Res.* 215, 61–76. doi: 10.1016/0006-8993(81)90491-1

Murphey, R. K., and Palka, J. (1974). Efferent control of cricket giant fibres. *Nature* 248, 249–251. doi: 10.1038/248249a0

Nachtigal, P. E., and Schuller, G. (2014). "Hearing during echolocation in whales and bats," in *Biosonar*, eds A. Surlykke, P. E. Nachtigal, R. R. Fay, and A. N. Popper (New York, NY: Springer), 143–168. doi: 10.1007/978-1-4614-9146-0_5

Neuweiler, G. (2003). Evolutionary aspects of bat echolocation. *J. Comp. Physiol. A* 189, 245–256. doi: 10.1007/s00359-003-0406-2

New, J. G., and Bodznick, D. (1990). Medullary electrosensory processing in the little skate. *J. Comp. Physiol. A* 167, 295–307. doi: 10.1007/bf00188121

Nocke, H. (1972). Physiological aspects of sound communication in crickets (*Gryllus campestris* L.). *J. Comp. Physiol.* 80, 141–162. doi: 10.1007/bf00696487

Nottebohm, F. (2005). The neural basis of birdsong. *PLoS Biol.* 3:e164. doi: 10.1371/journal.pbio.0030164

Oertel, D., and Young, E. D. (2004). What's a cerebellar circuit doing in the auditory system? *Trends Neurosci.* 27, 104–110. doi: 10.1016/j.tins.2003.12.001

Paul, D. H., and Roberts, B. L. (1977). Studies on a primitive cerebellar cortex I. The anatomy of the lateral-line lobes of the dogfish, *Scyliorhinus canicula*. *Proc. R. Soc. B* 195, 453–466. doi: 10.1098/rspb.1977.0020

Perks, K., and Sawtell, N. B. (2019). "Influences of motor systems on electrosensory processing," in *Electroreception: Fundamental Insights form Comparative Approaches*, eds B. A. Carlson, J. A. Sisneros, A. N. Popper, and R. R. Fay (New York, NY: Springer), 315–338. doi: 10.1007/978-3-030-29105-1_11

Pieper, F., and Jürgens, U. (2003). Neuronal activity in the inferior colliculus and bordering structures during vocalization in the squirrel monkey. *Brain Res.* 979, 153–164. doi: 10.1016/s0006-8993(03)02897-x

Poulet, J. F., and Hedwig, B. (2003a). A corollary discharge mechanism modulates central auditory processing in singing crickets. *J. Neurophysiol.* 89, 1528–1540. doi: 10.1152/jn.0846.2002

Poulet, J. F., and Hedwig, B. (2003b). Corollary discharge inhibition of ascending auditory neurons in the stridulating cricket. *J. Neurosci.* 23, 4717–4725. doi: 10.1523/JNEUROSCI.23-11-04717.2003

Poulet, J. F., and Hedwig, B. (2006). The cellular basis of a corollary discharge. *Science* 311, 518–522. doi: 10.1126/science.1120847

Poulet, J. F., and Hedwig, B. (2007). New insights into corollary discharges mediated by identified neural pathways. *Trends Neurosci.* 30, 14–21. doi: 10.1016/j.tins.2006.11.005

Poulet, J. F. A., and Hedwig, B. (2002). A corollary discharge maintains auditory sensitivity during sound production. *Nature* 418, 872–876. doi: 10.1038/nature00919

Prather, J. F., Peters, S., Nowicki, S., and Mooney, R. (2008). Precise auditory–vocal mirroring in neurons for learned vocal communication. *Nature* 451, 305–310. doi: 10.1038/nature06492

Requarth, T., and Sawtell, N. B. (2011). Neural mechanisms for filtering self-generated sensory signals in cerebellum-like circuits. *Curr. Opin. Neurobiol.* 21, 602–608. doi: 10.1016/j.conb.2011.05.031

Roberts, B. L., and Russell, I. J. (1972). The activity of lateral-line efferent neurones in stationary and swimming dogfish. *J. Exp. Biol.* 57, 435–448.

Roberts, T. F., Hisey, E., Tanaka, M., Kearney, M. G., Chattree, G., Yang, C. F., et al. (2017). Identification of a motor-to-auditory pathway important for vocal learning. *Nat. Neurosci.* 20, 978–986. doi: 10.1038/nn.4563

Roy, J. E., and Cullen, K. E. (2001). Selective processing of vestibular reafference during self-generated head motion. *J. Neurosci.* 21, 2131–2142. doi: 10.1523/jneurosci.21-06-02131.2001

Roy, J. E., and Cullen, K. E. (2004). Dissociating self-generated from passively applied head motion: neural mechanisms in the vestibular nuclei. *J. Neurosci.* 24, 2102–2111. doi: 10.1523/jneurosci.3988-03.2004

Sawtell, N. B., Williams, A., and Bell, C. C. (2005). From sparks to spikes: information processing in the electrosensory systems of fish. *Curr. Opin. Neurobiol.* 15, 437–443. doi: 10.1016/j.conb.2005.06.006

Schneider, D. M., and Mooney, R. (2018). How movement modulates hearing. *Annu. Rev. Neurosci.* 41, 553–572. doi: 10.1146/annurev-neuro-072116-031215

Schuller, G. (1979). Vocalization influences auditory processing in collicular neurons of the CF-FM-bat, *Rhinolophus ferrumequinum*. *J. Comp. Physiol.* 132, 39–46. doi: 10.1007/bf00617730

Siegler, M. V., Mpitsos, G. J., and Davis, W. J. (1974). Motor organization and generation of rhythmic feeding output in buccal ganglion of *Pleurobranchaea*. *J. Neurophysiol.* 37, 1173–1196. doi: 10.1152/jn.1974.37.6.1173

Singla, S., Dempsey, C., Warren, R., Enikolopov, A. G., and Sawtell, N. B. (2017). A cerebellum-like circuit in the auditory system cancels responses to self-generated sounds. *Nat. Neurosci.* 20, 943–950. doi: 10.1038/nn.4567

Sommer, M. A., and Wurtz, R. H. (2002). A pathway in primate brain for internal monitoring of movements. *Science* 296, 1480–1482. doi: 10.1126/science.1069590

Sommer, M. A., and Wurtz, R. H. (2004). What the brain stem tells the frontal cortex. II. Role of the SC-MD-FEF pathway in corollary discharge. *J. Neurophysiol.* 91, 1403–1423. doi: 10.1152/jn.00740.2003

Sommer, M. A., and Wurtz, R. H. (2006). Influence of the thalamus on spatial visual processing in frontal cortex. *Nature* 444, 374–377. doi: 10.1038/nature05279

Sparks, D. L., and Hartwich-Young, R. (1989). The deep layers of the superior colliculus. *Rev. Oculomot. Res.* 3, 213–255.

Sperry, R. W. (1950). Neural basis of the spontaneous optokinetic response produced by visual inversion. *J. Comp. Physiol. Psychol.* 43, 482–489. doi: 10.1037/h0055479

Stehouwer, D. J. (1987). Compensatory eye movements produced during fictive swimming of a deafferented, reduced preparation in vitro. *Brain Res.* 410, 264–268. doi: 10.1016/0006-8993(87)90323-4

Straka, H., Simmers, J., and Chagnaud, B. P. (2018). A new perspective on predictive motor signaling. *Curr. Biol.* 28, R232–R243. doi: 10.1016/j.cub.2018.01.033

Suga, N., and Schlegel, P. (1972). Neural attenuation of responses to emitted sounds in echolocating bats. *Science* 177, 82–84. doi: 10.1126/science.177.4043.82

Suga, N., and Shimozawa, T. (1974). Site of neural attenuation of responses to self-vocalized sounds in echolocating bats. *Science* 183, 1211–1213. doi: 10.1126/science.183.4130.1211

Troyer, T. W., and Doupe, A. J. (2000a). An associational model of birdsong sensorimotor learning I. Efference copy and the learning of song syllables. *J. Neurophysiol.* 84, 1204–1223. doi: 10.1152/jn.2000.84.3.1204

Troyer, T. W., and Doupe, A. J. (2000b). An associational model of birdsong sensorimotor learning II. Temporal hierarchies and the learning of song sequence. *J. Neurophysiol.* 84, 1224–1239. doi: 10.1152/jn.2000.84.3.1224

Tzounopoulos, T., Kim, Y., Oertel, D., and Trussell, L. O. (2004). Cell-specific, spike timing–dependent plasticities in the dorsal cochlear nucleus. *Nat. Neurosci.* 7, 719–725. doi: 10.1038/nn1272

Tzounopoulos, T., Rubio, M. E., Keen, J. E., and Trussell, L. O. (2007). Coactivation of pre- and postsynaptic signaling mechanisms determines cell-specific spike-timing-dependent plasticity. *Neuron* 54, 291–301. doi: 10.1016/j.neuron.2007.03.026

Umeno, M. M., and Goldberg, M. E. (1997). Spatial processing in the monkey frontal eye field. I. predictive visual responses. *J. Neurophysiol.* 78, 1373–1383. doi: 10.1152/jn.1997.78.3.1373

Vélez, A., and Carlson, B. A. (2016). Detection of transient synchrony across oscillating receptors by the central electrosensory system of mormyrid fish. *eLife* 5:e16851. doi: 10.7554/eLife.16851

von der Emde, G. (1999). Active electrolocation of objects in weakly electric fish. *J. Exp. Biol.* 202, 1205–1215.

von der Emde, G., and Bell, C. C. (2003). ""Active electrolocation and its neural processing in mormyrid,"," in *Sensory Processing in Aquatic Environments*, eds S. P. Collin and J. Marshall (New York, NY: Springer), 92–107. doi: 10.1007/978-0-387-22628-6_5

von der Emde, G., Sena, L. G., Niso, R., and Grant, K. (2000). The midbrain precommand nucleus of the mormyrid electromotor network. *J. Neurosci.* 20, 5483–5495. doi: 10.1523/jneurosci.20-14-05483.2000

von Holst, E., and Mittelstaedt, H. (1950). Das reafferenzprinzip. *Naturwissenschaften* 37, 464–476. doi: 10.1007/bf00622503

Weeg, M. S., Land, B. R., and Bass, A. H. (2005). Vocal pathways modulate efferent neurons to the inner ear and lateral line. *J. Neurosci.* 25, 5967–5974. doi: 10.1523/jneurosci.0019-05.2005

Wenzel, B., and Hedwig, B. (1999). Neurochemical control of cricket stridulation revealed by pharmacological microinjections into the brain. *J. Exp. Biol.* 202, 2203–2216.

Wiersma, C. A., and Yamaguchi, T. (1967). Integration of visual stimuli by the crayfish central nervous system. *J. Exp. Biol.* 47, 409–431.

Wiersma, C. A. G. (1947). Giant nerve fiber system of the crayfish. A contribution to comparative physiology of synapse. *J. Neurophysiol.* 10, 23–38. doi: 10.1152/jn.1947.10.1.23

Wullimann, M. F., and Northcutt, R. G. (1990). Visual and electrosensory circuits of the diencephalon in mormyrids: an evolutionary perspective. *J. Comp. Neurol.* 297, 537–552. doi: 10.1002/cne.902970407

Xu-Friedman, M., and Hopkins, C. (1999). Central mechanisms of temporal analysis in the knollenorgan pathway of mormyrid electric fish. *J. Exp. Biol.* 202, 1311–1318.

Yamada, J., and Noda, H. (1987). Afferent and efferent connections of the oculomotor cerebellar vermis in the macaque monkey. *J. Comp. Neurol.* 265, 224–241. doi: 10.1002/cne.902650207

Yartsev, M. M., and Ulanovsky, N. (2013). Representation of three-dimensional space in the hippocampus of flying bats. *Science* 340, 367–372. doi: 10.1126/science.1235338

Zipser, B., and Bennett, M. V. (1976). Interaction of electrosensory and electromotor signals in lateral line lobe of a mormyrid fish. *J. Neurophysiol.* 39, 713–721. doi: 10.1152/jn.1976.39.4.713

Conflict of Interest: The authors declare that the research was conducted in the absence of any commercial or financial relationships that could be construed as a potential conflict of interest.

The handling editor declared a past collaboration with one of the authors BC.

frontiers in Integrative Neuroscience

ORIGINAL RESEARCH
published: 22 October 2020
doi: 10.3389/fnint.2020.561524

Spooky Interaction at a Distance in Cave and Surface Dwelling Electric Fishes

Eric S. Fortune[1], Nicole Andanar[1], Manu Madhav[2], Ravikrishnan P. Jayakumar[2], Noah J. Cowan[2], Maria Elina Bichuette[3] and Daphne Soares[1]*

[1] Biological Sciences, New Jersey Institute of Technology, Newark, NJ, United States, [2] Department of Mechanical Engineering, Johns Hopkins University, Baltimore, MD, United States, [3] Departamento de Ecologia e Biologia Evolutiva, Universidade Federal de São Carlos, São Carlos, Brazil

Glass knifefish (*Eigenmannia*) are a group of weakly electric fishes found throughout the Amazon basin. Their electric organ discharges (EODs) are energetically costly adaptations used in social communication and for localizing conspecifics and other objects including prey at night and in turbid water. Interestingly, a troglobitic population of blind cavefish *Eigenmannia vicentespelea* survives in complete darkness in a cave system in central Brazil. We examined the effects of troglobitic conditions, which includes a complete loss of visual cues and potentially reduced food sources, by comparing the behavior and movement of freely behaving cavefish to a nearby epigean (surface) population (*Eigenmannia trilineata*). We found that the strengths of electric discharges in cavefish were greater than in surface fish, which may result from increased reliance on electrosensory perception, larger size, and sufficient food resources. Surface fish were recorded while feeding at night and did not show evidence of territoriality, whereas cavefish appeared to maintain territories. Surprisingly, we routinely found both surface and cavefish with sustained differences in EOD frequencies that were below 10 Hz despite being within close proximity of about 50 cm. A half century of analysis of electrosocial interactions in laboratory tanks suggest that these small differences in EOD frequencies should have triggered the "jamming avoidance response," a behavior in which fish change their EOD frequencies to increase the difference between individuals. Pairs of fish also showed significant interactions between EOD frequencies and relative movements at large distances, over 1.5 m, and at high differences in frequencies, often >50 Hz. These interactions are likely "envelope" responses in which fish alter their EOD frequency in relation to higher order features, specifically changes in the depth of modulation, of electrosocial signals.

Keywords: gymnotiformes, weakly electric fish, troglobitic, epigean, envelope, cavefish, jamming avoidance response, diceCT

OPEN ACCESS

Edited by:
Michael R. Markham, University of Oklahoma, United States

Reviewed by:
Thomas Preuss, Hunter College (CUNY), United States
Elias Manjarrez, Meritorious Autonomous University of Puebla, Mexico

****Correspondence:***
Eric S. Fortune
eric.fortune@njit.edu

Received: *12 May 2020*
Accepted: *07 September 2020*
Published: *22 October 2020*

Citation:
Fortune ES, Andanar N, Madhav M, Jayakumar RP, Cowan NJ, Bichuette ME and Soares D (2020) Spooky Interaction at a Distance in Cave and Surface Dwelling Electric Fishes. Front. Integr. Neurosci. 14:561524. doi: 10.3389/fnint.2020.561524

1. INTRODUCTION

Gymnotiformes are a group of nocturnal fishes characterized by a suite of adaptations that allow them to localize conspecifics (Davis and Hopkins, 1988; Crampton, 2019) and capture prey (Nelson and MacIver, 1999) in complete darkness. These fishes produce weak electric fields, typically <100 mV/cm (Assad et al., 1998), using an electric organ located along the sides of the animal and in the tail (Heiligenberg, 1991; Markham, 2013). This electric field, known as the electric organ discharge or EOD, is detected using specialized electroreceptors embedded in the skin (Metzen et al., 2017). These receptors encode modulations generated through interactions with the electric fields of conspecifics and by nearby objects. This system provides a mechanism for communication among conspecifics and for the detection and characterization of prey and other salient environmental features (Nelson and MacIver, 1999; Pedraja et al., 2018; Crampton, 2019; Yu et al., 2019) at night and in turbid water that reduce visual cues.

On one hand, the nocturnal life histories of Gymnotiform species, facilitated by their electrosensory systems, make them well-suited for life in caves. On the other hand, caves are often poor in nutrients: the generation of EODs is energetically costly, consuming up to one quarter of an individual's energy budget (Salazar et al., 2013; Markham et al., 2016). Interestingly, a single species of Gymnotiform fish, *Eigenmannia vicentespelaea*, has been discovered in a cave system in central Brazil (Triques, 1996; Bichuette and Trajano, 2006, 2017). These fish exhibit features that are commonly found in species adapted to life in caves, including reduced pigmentation and reduction and/or elimination of the eyes (Culver and Pipan, 2019). The population is estimated to be around only 300 individuals (Bichuette and Trajano, 2015).

To discover the potential consequences of adaptation for troglobitic life on electrosensory behavior, we compared the electric behavior and movement of the cavefish *Eigenmannia vicentespelea* to nearby epigean (surface) relatives, *Eigenmannia trilineata*, that live in the same river system (**Figure 1**). We used a recently developed approach for characterizing electric behaviors and locomotor movements of weakly electric fishes in their natural habitats (Madhav et al., 2018; Henninger et al., 2020). This approach, which uses a grid of electrodes placed in the water, permits an estimation of features of the electric field of each fish and an analysis of their concurrent movement (**Figure 2**).

We looked for differences between surface and cavefish populations in electrogenic behaviors and movement, and in previously-described electrosocial behaviors. Fish in the genus *Eigenmannia* produce quasi-sinusoidal electric signals that are maintained at frequencies between about 200 and 700 Hz (Heiligenberg, 1991). Individual *Eigenmannia* change their electric field frequencies in response to electrosocial signals produced by nearby conspecifics. The best described of these behaviors is the "Jamming Avoidance Response" (JAR) in which individuals raise or lower their electric field frequency to avoid differences of less than about 10 Hz (Watanabe and Takeda, 1963; Heiligenberg, 1991; Madhav et al., 2013). *Eigenmannia* also exhibit "envelope responses" in which individuals change their electric field frequencies in relation to relative movement between individuals, which is encoded in the amplitude envelope of their summed electric fields (Metzen and Chacron, 2013; Stamper et al., 2013; Huang and Chacron, 2016; Thomas et al., 2018). Envelope responses can also occur in groups of three or more fish when the pairwise differences of their electric field frequencies are close, within 1–8 Hz, of one another (Stamper et al., 2012). Finally, weakly electric fishes produce a variety of transient frequency and amplitude modulations, including "chirps," with durations on the order of 10s of milliseconds to 10s of seconds. These signals have roles in aggression, dominance hierarchies, and in other social interactions (Hupe and Lewis, 2008; Walz et al., 2013; Allen and Marsat, 2019; Metzen, 2019).

2. METHODS

These observational studies were reviewed and approved by the animal care and use committee of Rutgers University/New Jersey Institute of Technology, and follow guidelines for the use of animals in field research established by the National Research Council. Field research permits in Brazil were granted by the ICMBio and SEMARH/SECIMA.

2.1. Study Sites

The study sites were located in Terra Ronca State Park (46° 10′–46° 30′ S, 13° 30′–13° 50′ W), in the Upper Tocantins river basin, state of Goiás, central Brazil (**Figure 1A**). We measured the electric behavior of the cavefish *Eigenmannia vicentespelaea* in the São Vicente II cave (13° 58′37″ S, 46° 40′04″ W) in October of 2016 (**Figure 1B**). The electric behavior of the epigean species, *Eigenmannia trilineata*, was measured in the Rio da Lapa at the mouth of the Terra Ronca cave (13° 38′44″ S; 46° 38′ 08″ W) in April of 2016 (**Figure 1B**). These streams have moderate water currents, clear water with conductivity below 20 μS, and the substrate is composed of sand, rocks, and boulders.

2.2. Anatomy

Four alcohol fixed specimens from the collection at the Universidade Federal de São Carlos (Dr. Bichuette) were submerged in 11.25 Lugol's iodine (I2KI) solution for up to 36 h prior to diffusable iodine based contrast enhanced computer tomography (DiceCT). Stained specimens were removed from Lugol's solution, rinsed in water to remove excess stain and sealed in rubber sleeves to prevent dehydration. Samples were then loaded into 50 mL polypropylene centrifuge tubes for scanning.

Stained and unstained specimens were scanned at the Core Imaging Facility of the American Museum of Natural History (New York, NY), using a 2010 GE Phoenix v|tome|x s240CT high resolution microfocus computed tomography system (General Electric, Fairfield, CT, USA). DiceCT scanning permits visualization of soft tissue details of the head and the body. Scans were made at 125 kV, with an exposure time of 60 s. Voxel sizes was 20.0–25.9 μm. Volume reconstruction of raw X-ray images were achieved using a GE Phoenix datos|x.

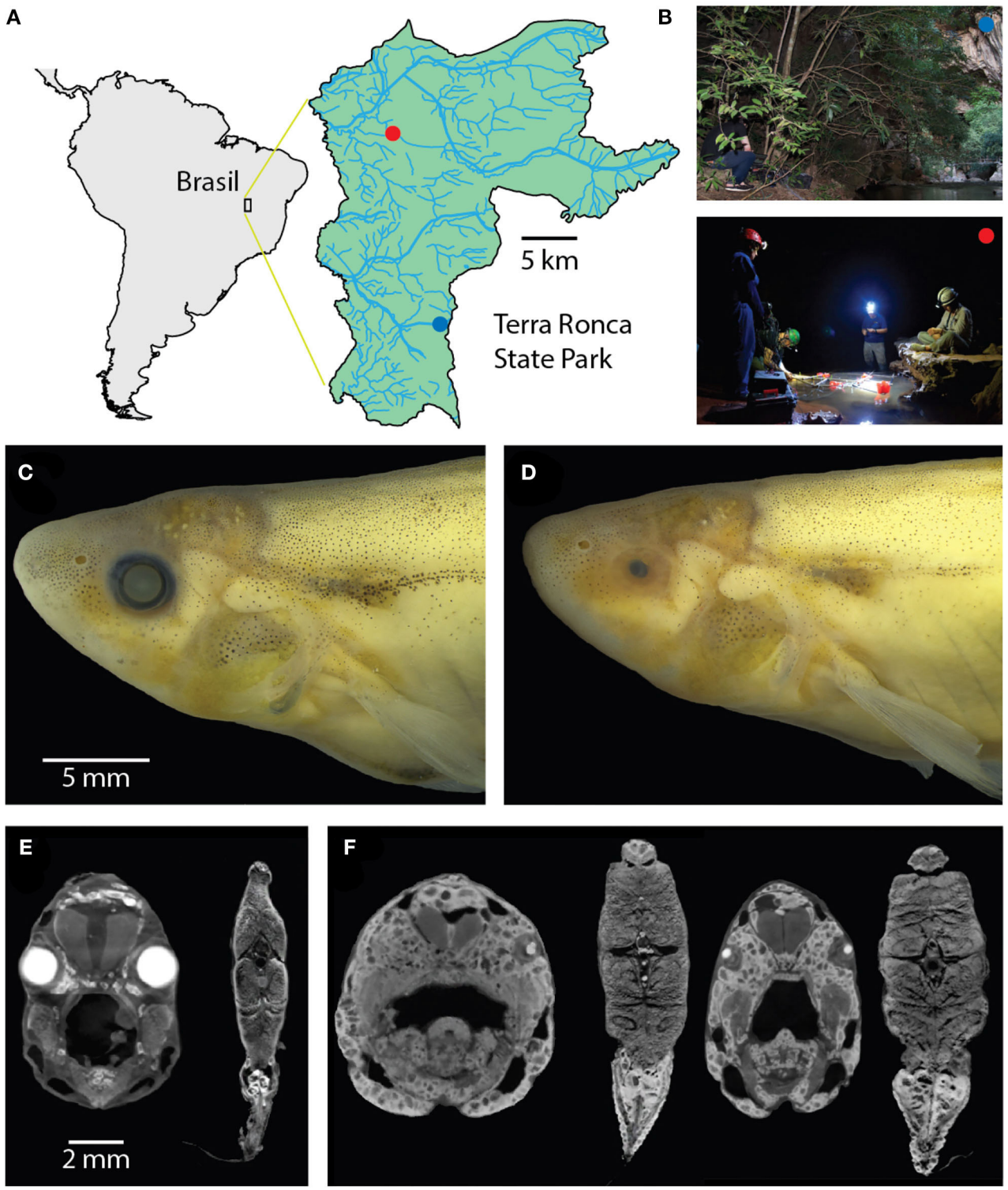

FIGURE 1 | Surface and cave *Eigenmannia*. **(A)** Study sites are in a clear water system in the Rio da Lapa karst region in Goiás, Brazil. **(B)** Top, the surface *Eigenmannia* site is in the entrance of the Rio da Lapa cave. Bottom, the cave *Eigenmannia* are found in the São Vicente II cave. **(C)** Surface *Eigenmannia* have well-developed eyes and distinctive markings. **(D)** Cave *Eigenmannia* have poorly developed or missing eyes and reduced pigmented features. diceCT imaging reveals the differences in eye sizes and a potential difference in the relative size of electric organs. **(E)** Coronal sections through the head and mid-body of a surface fish and **(F)** two cavefish (dorsal is up). Large, bright cells in the caudoventral coronal sections appear relatively larger in the cave vs. surface species.

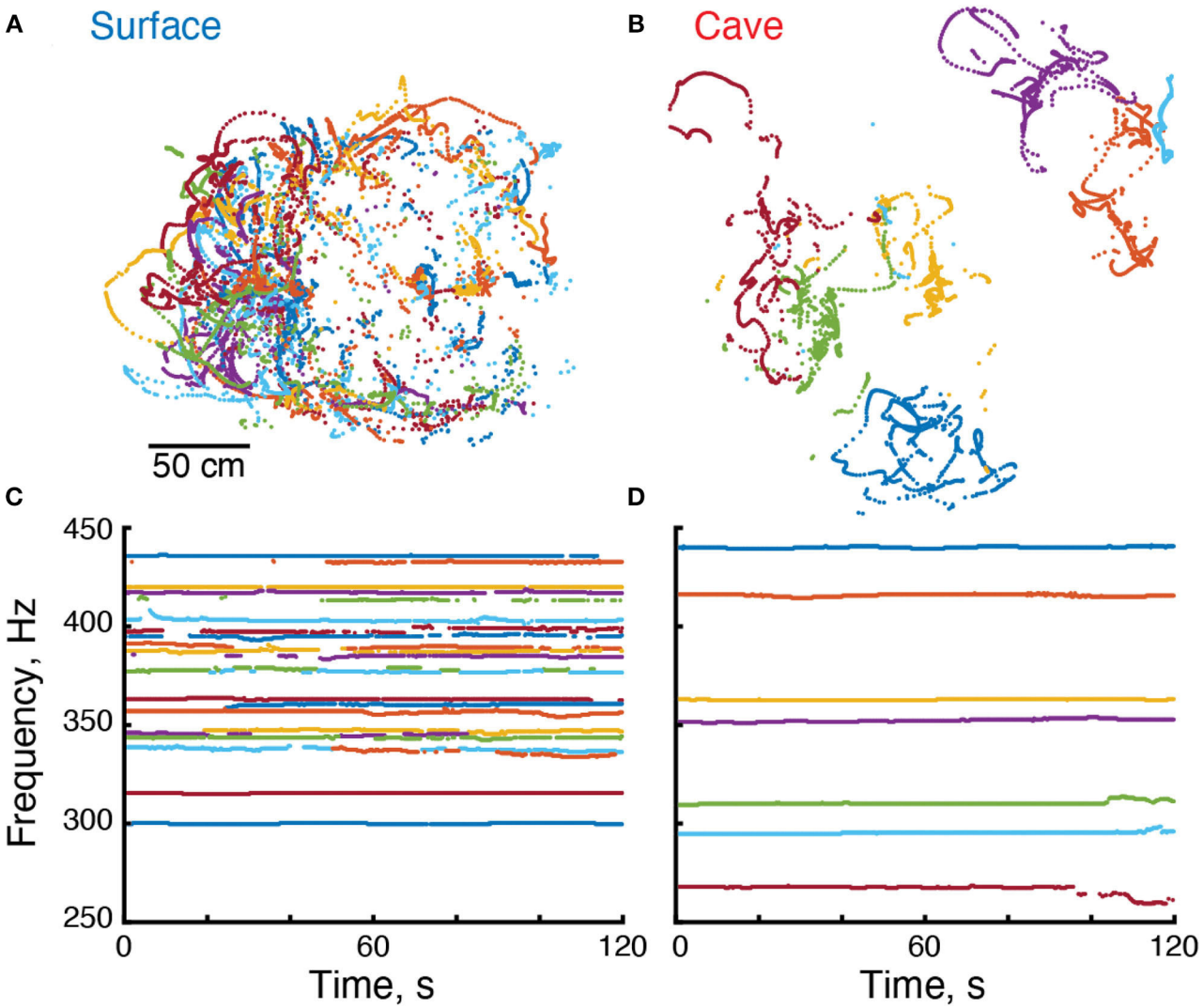

FIGURE 2 | Electrical and locomotor behavior of *Eigenmannia*. **(A,B)** Positions of surface and cave *Eigenmannia* over a period of 120 s. **(C,D)** EOD frequencies of these fish. Each color represents a unique fish in each recording.

2.3. Recordings of Electric Behavior at Field Sites

Eigenmannia were initially identified and located using hand-held single-electrode probes with a custom amplifier/speaker system. This river permits direct visualization of the animals—the water is sufficiently clear and free of debris to see fish by eye from above the surface of the water, and for underwater photography when the fish are swimming in open water (Hero Cam, GoPro 3, USA, see **Supplementary Videos 1**, **2**).

Electric recordings were made using a grid of active electrodes (50 cm spacing) (Madhav et al., 2018). For measurements of the epigean fish, an array of eight electrodes was placed along the edges of the Rio da Lapa stream after sundown when the fish were active. In the São Vicente II cave, an array of 16 electrodes was placed in eddies and side pools along the primary stream. The flow at the center of the stream was too strong for the grid array. Unfortunately, we were unable to use the larger grid on our second visit to the surface site due to a concurrent religious festival. As a result, the maximum XY range of the surface grid is about 100 cm diameter smaller than the cave grid. In all other respects, the measurements from both grids are identical.

We used an algorithm (Madhav et al., 2018) (code available at doi: 10.7281/T1/XTSKOW) to identify each *Eigenmannia* using its time-varying fundamental frequency (**Figure 2**). Position and pose were calculated in relation to the distribution of power at each EOD frequency across the grid of electrodes. In these recordings, which were made in shallow water of no more than 40 cm depth using a planar array of electrodes, the position estimates were restricted to the XY-plane (**Figures 2A,B**). We calculated an estimate of the strength of the electric field for each fish. Fish were considered to be ideal current dipoles—a source-sink pair of equal but time varying strength $I(t)$, separated

by a small distance d. The electric current dipole moment for the fish is defined as $p = Id$ which has the units of Ampere-meter or "Am".

Continuous recording sessions using the grid were made both at the cave site ($N = 14$) and surface site ($N = 5$). Each recording had a duration of at least 600 s, while others were over 1,200 s. Intervals between recording sessions ranged from 5 min to several hours. Because fish could not be tracked between recording sessions, it is likely that some individual fish were measured across sessions. The position and EOD frequency data were analyzed, unless otherwise described, in 300 s duration non-overlapping epochs.

2.4. Analysis of Position and EOD Frequency Data

All analyses were conducted using custom scripts in Matlab (Mathworks, Natick MA). These data and scripts are publically available (https://web.njit.edu/~efortune/Brasil). We estimated the XY region of movement for each fish for each epoch using a minimum convex polygon fitted to its positions. We then calculated the pairwise overlap between each convex polygon.

To assess the relations between pairs of EOD frequencies and their relative movement, we calculated Pearson correlations between (1) instantaneous distance between pairs of fish (distance) and (2) instantaneous difference in EOD frequency (dF). Euclidean distances between pairs of fish were computed as a function of time (4.9 measurements per second) during each 300 s epoch. dF was calculated as the absolute value of the difference in EOD frequencies of the pair of fish. The Pearson correlation was calculated between distance and dF for each 300 s epoch. These "dF/distance correlations" ranged from −0.93 to 0.90. Negative Pearson correlations represent an inverse relation between dF and distance, where positive Pearson correlations represent direct correlations between them. To estimate the rate of spontaneous correlations between dF and distance, we shuffled (Matlab randperm) the epochs of dF and distance measurements and again calculated Pearson correlations. We then compared the distribution of correlations in the shuffled data to the correlations in the original data.

3. RESULTS

3.1. General Observations

Eigenmannia at both the surface and cave sites were found in clear water streams with rock and sand substrates (Bichuette and Trajano, 2003, 2006, 2015, 2017). At the surface site, we observed a marked diurnal modulation of behavior. During the day, surface fish were found alone or in groups along the banks of the Rio da Lapa, typically below or around boulders and rocks. The grid system was not used to make recordings of surface fish during the day due to a local festival. Nevertheless, we used hand held probes to examine the distribution of surface *Eigenmannia* during the day, and the distribution appeared, by ear, to be similar to that described previously at sites in Ecuador (Tan et al., 2005). Unlike in previous measurements at other study sites (Stamper et al., 2010), no other Gymnotiform species were detected in our short survey. At night, we observed surface *Eigenmannia* swimming in open water in the center of the stream, typically near the bottom.

Using flashlights, we observed surface fish foraging in sandy substrates at night. Foraging behavior included hovering with slow forward or backward swimming punctuated by strikes into the substrate (see **Supplementary Video 1**). These strikes involved tilting of the head and body downwards with a rapid forward lunge to drive the mouth into the sand a few millimeters. These strikes differ from feeding behavior described in *Apteronotus albifrons* in which fish captured freely swimming *Daphnia*, typically from below the prey (Nelson and MacIver, 1999). We observed groups of *Eigenmannia* simultaneously foraging with inter-fish distances on the order of 10s of centimeters. These distances suggest that fish experience significant ongoing electrosensory interference from conspecifics. At other locations, we visually observed single fish foraging while swimming rather than hovering at a particular location.

Not surprisingly, we did not observe diurnal modulation of behavior in cave *Eigenmannia*. Cavefish were observed along the banks of the stream and in small eddies and pools. Fish were alone or in small groups of up to 10 individuals. Cavefish retreated to crevices and spaces within boulders and rocks when disturbed, forming temporary aggregates of individuals (see **Supplementary Video 2**). Videos show eyeless cavefish orienting face-to-face during social interactions. Such movements, in the absence of visual cues, are controlled, at least in part, using electrosensory signals. The distinctive substrate foraging behavior routinely seen in the surface fish was not observed in these cavefish.

3.2. Morphology

We observed that surface *Eigenmannia* had large eyes that were circumferential and of the same size (**Figures 1C,E**) whereas the cavefish had eyes in various states of degeneration, from microphthalmic to completely absent (**Figures 1D,F**). A preliminary review of CT scans of four fish showed potential differences in the size of the electric organ (**Figures 1E,F**), but additional material will be necessary for quantitative analysis of electric organ structure and physiology.

A prior study (Bichuette and Trajano, 2006) found that the surface *Eigenmannia* are smaller than the cavefish: mean length of the snout to the end of the anal fin base was reported to be 8.45 cm (sd = 2.67) in surface fish and 11.1 cm (sd = 2.47) in cavefish. Size is important as it likely impacts the strength of electric fields: larger fish typically can generate larger currents in their electric organs. Fish were not captured for similar measurements in the present study.

3.3. Electric Field Amplitudes

We used the grid recording system to estimate the strength of each individual's electric field using Fourier analysis. The mean strength of the electric fields (Ampere-meter, "A-m") of surface fish was 6.5×10^{-4} A-m ($n = 110$ EOD frequencies in 5 recordings) and 9.66×10^{-4} A-m for cavefish ($n = 82$ EODs in 14 recordings) (**Figure 3B**). The strengths of surface fish were significantly lower than cavefish (Wilcoxon rank sum, two-sided,

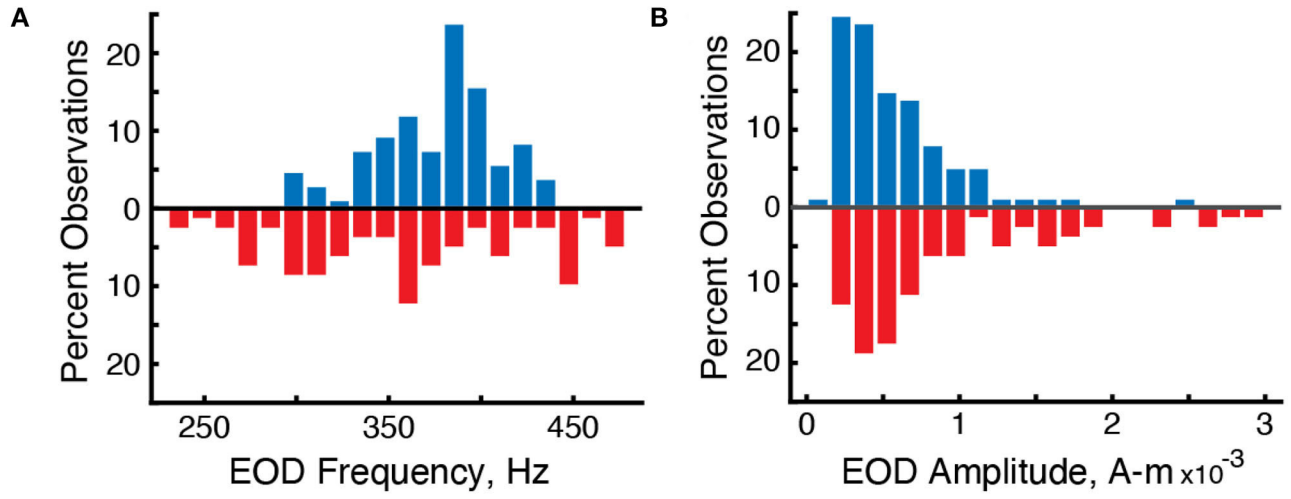

FIGURE 3 | Differences in the distribution of EOD frequencies and amplitudes in surface fish (blue, up) and cavefish (red, down). **(A)** Percent observations of EOD frequencies for surface fish and cavefish. **(B)** Percent observations of EOD amplitudes.

$z = 2.98, p = 0.0029$). The increase in EOD amplitude may be an energetically costly adaptation (Markham et al., 2016) to life in this cave: larger EOD amplitudes would increase the ability to detect objects and capture prey (Nelson and MacIver, 1999) in the absence of visual cues.

3.4. Electric Field Frequencies

We used the grid recording system to calculate the EOD frequency of each fish within the grid (**Figure 2**). EOD frequencies of surface fish were between 299.9 and 435.6 Hz ($n = 110$ EODs in five recordings) whereas EOD frequencies of cavefish were between 230.0 and 478.6 Hz ($n = 82$ EODs in 14 recordings) (**Figure 3A**). The mean and median frequencies of surface fish were 375.8 and 382.0 Hz, and for cavefish were 356.6 and 360.8 Hz. The distribution of EOD frequencies of surface and cavefish are significantly different (Wilcoxon sign-rank, two-sided, $z = 2.57, p = 0.0100$).

We observed variations in EOD frequencies that likely include social signals, such as chirps (**Figures 2C,D**). Although a detailed description of these social signals is beyond the scope of this report, we calculated the standard deviation of each EOD frequency as a simple proxy for the rate of production of social signals. Variation in EOD frequencies were calculated over 300 s duration epochs. The EOD frequencies of surface fish had a mean standard deviation of 0.64 Hz (184 epochs from 97 fish). Variation in EOD frequencies of cavefish had a mean standard deviation of 1.11 Hz (257 epochs from 72 fish). The variation of EOD frequencies in cavefish was significantly different from surface fish (Wilcoxon rank sum, two-sided, $z = 4.97, p = 0.000001$). We expect the variability of EOD frequencies in surface fish will differ during daylight hours, when the fish are hiding along the shores of the rivers, in relation to night hours when the fish are active. Additional recordings made during the day are needed to test this hypothesis.

The electric fields of some species of Gymnotiform fishes have been shown to have diurnal modulations in amplitude and frequency content (Stoddard et al., 2006; Markham et al., 2009; Sinnett and Markham, 2015; Migliaro et al., 2018). We did not observe diurnal modulation of EOD frequencies in cave *Eigenmannia*. Because we did not make daytime recordings at the surface site, we do not know whether or not such modulations are present in the surface *Eigenmannia*.

We recorded preliminary data which suggest that the fish's own movement can contribute to modulation of EOD frequencies. We placed three surface *Eigenmannia* in tubes as part of a calibration of the grid system. These tubes restricted the animal's movement to a few centimeters in the grid. Those fish had significantly less variability in their EOD frequencies than the freely-moving fish swimming around them (mean = 0.38 Hz, 29 epochs from three fish; Wilcoxon rank sum, two-sided, $z = -4.40, p = 0.000011$).

3.5. Differences in EOD Frequencies

The JAR is a behavior that, in laboratory settings, reduces the likelihood that pairs of fish will have a difference in EOD frequency (dF) of <10 Hz (Heiligenberg, 1991). For each pair of EOD frequencies, the mean dF was calculated over 300 s duration epochs in each recording. We then calculated the mean of these dFs: in surface fish the mean dF was 44.89 Hz (sd = 26.64 over 172 epochs) while in cavefish the mean dF was 78.39 Hz (sd = 47.92 over 938 epochs) (**Figure 4A**). Mean dFs in cavefish are significantly greater than in surface fish (Wilcoxon rank sum, two-sided, $z = 8.84, p \ll 0.0001$). These findings are consistent with a role of the JAR in maintaining larger dFs between most individuals, but may also simply reflect the greater density of fish that we observed at the surface site.

Interestingly, we routinely found nearby fish with sustained, lasting for hundreds of seconds, differences in electric field frequencies that were below 10 Hz (**Figure 4B**). In surface fish,

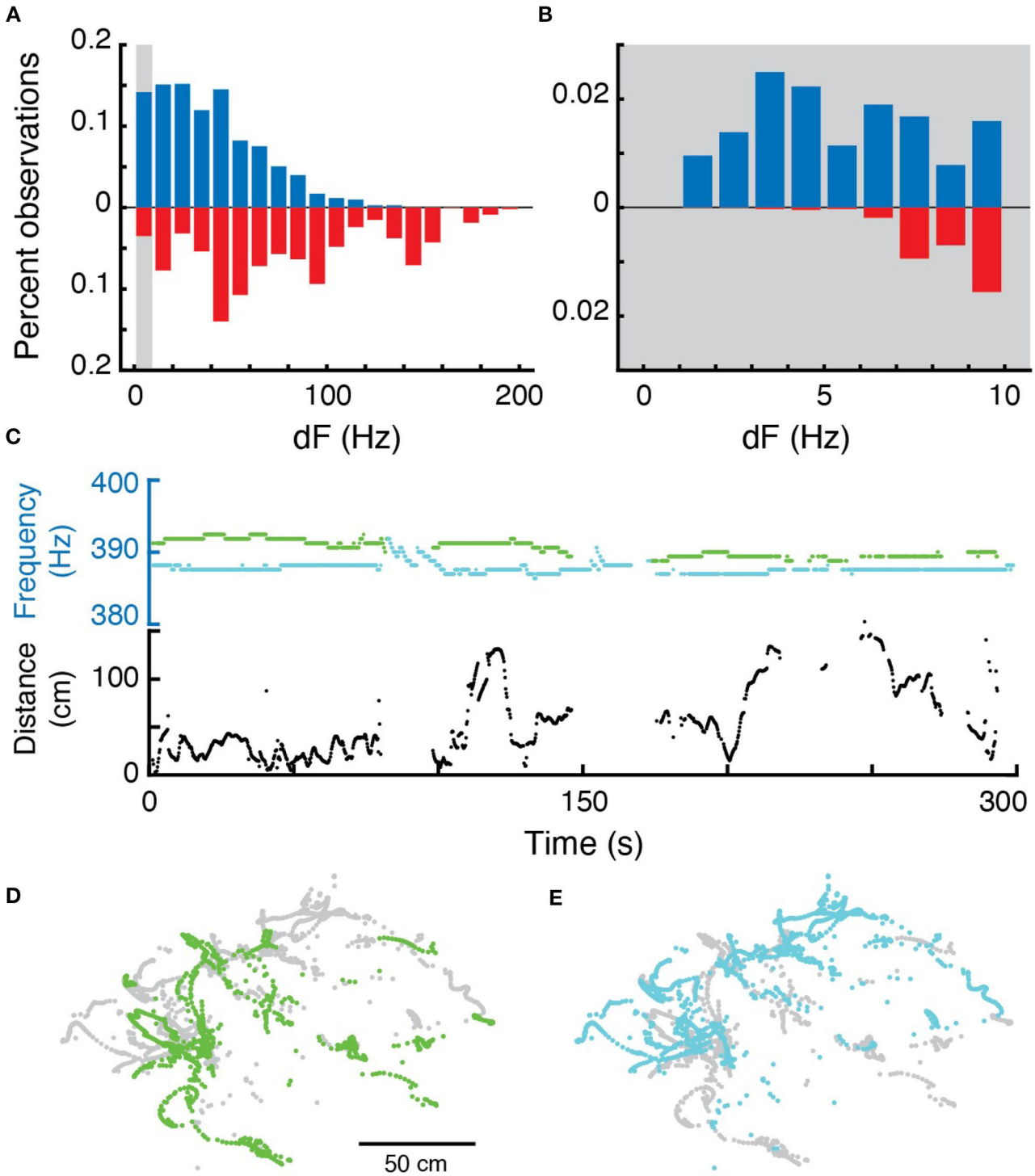

FIGURE 4 | Differences in EOD frequencies. **(A)** Percent observations of dFs for surface fish (blue, up) and cavefish (red, down). Gray bar highlights the low frequency region shown in **(B)**. **(B)** Same as **(A)**, but for dF frequencies of 10 Hz and below. **(C)** Example 300 second epoch of two fish with sustained low-frequency dF. Top, EOD frequencies each fish; bottom Euclidian distance over time. **(D,E)** X-Y positions of each fish during this epoch.

there were 294 pairs with mean dFs of <10 Hz over their entire recording sessions, and of those 142 pairs had mean dFs of <5 Hz (out of 1,119 potentially interacting pairs across five recording sessions). In cavefish, there were 18 pairs of fish with mean dFs that were <10 Hz over entire recording sessions, of which 4 were <5 Hz (out of total 2,356 potentially interacting pairs

across 14 recording sessions). Pairs of fish were often at distances <50 cm during these low dF encounters (**Figures 4C–E**).

3.6. Patterns of Movement in Surface and Cavefish

We estimated the position of each fish in and around the grid (Madhav et al., 2018) in our recordings. Cavefish appeared to swim within small regions or territories on the order of tens of centimeters in diameter (**Figure 2B**). In contrast, surface fish appeared to have widely overlapping swimming trajectories (**Figure 2A**). To examine the relative movements of fish, we divided the data into 300 s duration epochs and fitted a minimum convex polygon to each fish's positions.

Although there was no difference in the overall size of the convex polygons between surface and cavefish (Wilcoxon rank sum, two-sided, $z = 0.28, p = 0.7822$), we found significantly more overlap in the trajectories of surface fish. The overlap between convex polygons of pairs of surface fish (mean = 13.89% overlap, sd = 9.57, $n = 1,371$ comparisons) was significantly greater (Wilcoxon rank sum, two-sided, $z = 14.14, p \ll 0.0001$) than in cavefish (mean = 8.41%, sd = 9.08, $n = 950$ comparisons).

Our impression is that the cavefish are more territorial than surface fish, at least while the surface fish are feeding at night. The increased overlap in trajectories in surface fish may be a result of their lower amplitude electric fields, which could reduce the distance for detection of conspecifics, localized distribution of food resources in the substrate, or simply due to the larger numbers of surface fish at the study sites. We expect that the surface fish may defend territories during the day when hiding in refugia. The necessary grid recordings were not possible during the day—additional recordings are needed to explore the diurnal modulation of social behavior in the surface fish.

3.7. Correlations Between Movement and EOD Frequencies Suggest Envelope Responses in the Field

We examined the relations between relative movement and EOD frequency as fish interacted with conspecifics. We measured the dFs of all pairs of fish and their simultaneous pairwise distances over 300 s epochs (**Figure 5**). In many pairs of fish, dF and distance appeared to be strongly correlated—either changing in the same or opposite directions (**Figures 5A,B**). These correlations are likely "envelope" responses (Stamper et al., 2012, 2013; Metzen and Chacron, 2013; Huang and Chacron, 2016; Thomas et al., 2018). As *Eigenmannia* move closer together, the relative amplitudes of each fish's electric field increases (similar to moving closer to a sound source). Fish respond to these increases by shifting their electric field frequency either up or down (Metzen and Chacron, 2013; Stamper et al., 2013; Huang and Chacron, 2016; Thomas et al., 2018).

Correlations between two independently varying measurements may, however, occur spontaneously. To assess the rate of spontaneous correlations, we shuffled the distance and dF trajectories in time. We compared distributions of Pearson correlations between dF and distance in the shuffled and original data (**Figures 5C,D**).

In cavefish, we found both significantly more negative and positive correlations (Fisher's exact test, < -0.6: $p = 0.00005$, >0.6: $p = 0.0107$; 1,630 epochs). Interestingly, positive correlations were observed in fish with dFs of lower than 10 Hz (**Figure 5B**). Such positive correlations at low dFs are unexpected because of the impact of the JAR: the JAR is strongest at dFs of ∼2–8 Hz (Heiligenberg, 1991) and should increase dFs with nearby fish, generally resulting in negative correlations between distance and dF. These unexpected positive correlations may be a result of the production of social signals that "override" the JAR, or may be driven by social interactions with other nearby fish that have higher dFs.

We also found examples of strong Pearson correlations between dF and distance at dFs over 50 Hz and distances of over 100 cm (**Figure 5A**) in cavefish. This is interesting because these distances were previously believed to be beyond the boundary of the animal's ability to detect such signals (Bastian, 1981; Nelson et al., 1997; Henninger et al., 2018). These "spooky" interactions at large distances have also been seen in other species of weakly electric fishes, which demonstrates that individuals can detect and respond to each other via weak modulations of their electric fields (Henninger et al., 2018; Raab et al., 2019).

In contrast, correlations between EOD frequencies of surface fish were not significantly different from shuffled EODs (Fisher's exact test, < -0.6: p=0.814, >0.6: $p = 0.580$; 577 epochs; **Figure 5C**). The lack of envelope responses in the surface fish may result from the high densities of fish: competing simultaneous interactions with multiple fish may have diluted the strengths of the pairwise measurements that we used. There may be context-dependent changes in envelope responses, such as an elimination of envelope responses during feeding, or these surface fish may simply not generate envelope responses.

4. DISCUSSION

Weakly electric fishes rely on their electric fields for social interactions and localizing objects including prey, which reduce their reliance on visual cues for these functions. Electrogenic species, therefore, appear to be well-suited for life in caves in which there are no visual signals. However, electrogenesis is energetically costly; caves commonly have reduced food resources (Zepon and Bichuette, 2017; Pipan et al., 2018). As a first step in describing changes and adaptations for cave life in electrogenic fishes, we compared the electric behavior and locomotor movement of a population of troglobitic weakly electric fish *Eigenmannia vicentespelea* to a nearby population of epigean fish, *Eigenmannia trilineata*.

We found that the cavefish had stronger electric fields than the surface fish. The distributions of EOD frequencies was greater in the cavefish than in surface fish. These differences in EOD frequencies may result from differences in movement: the cavefish appeared to maintain territories whereas the surface fish did not at night. We also found a difference in the distribution of dFs between individuals. Cavefish had greater dFs than the surface fish. However, we found examples in both surface and cavefish in which pairs of nearby fish, within

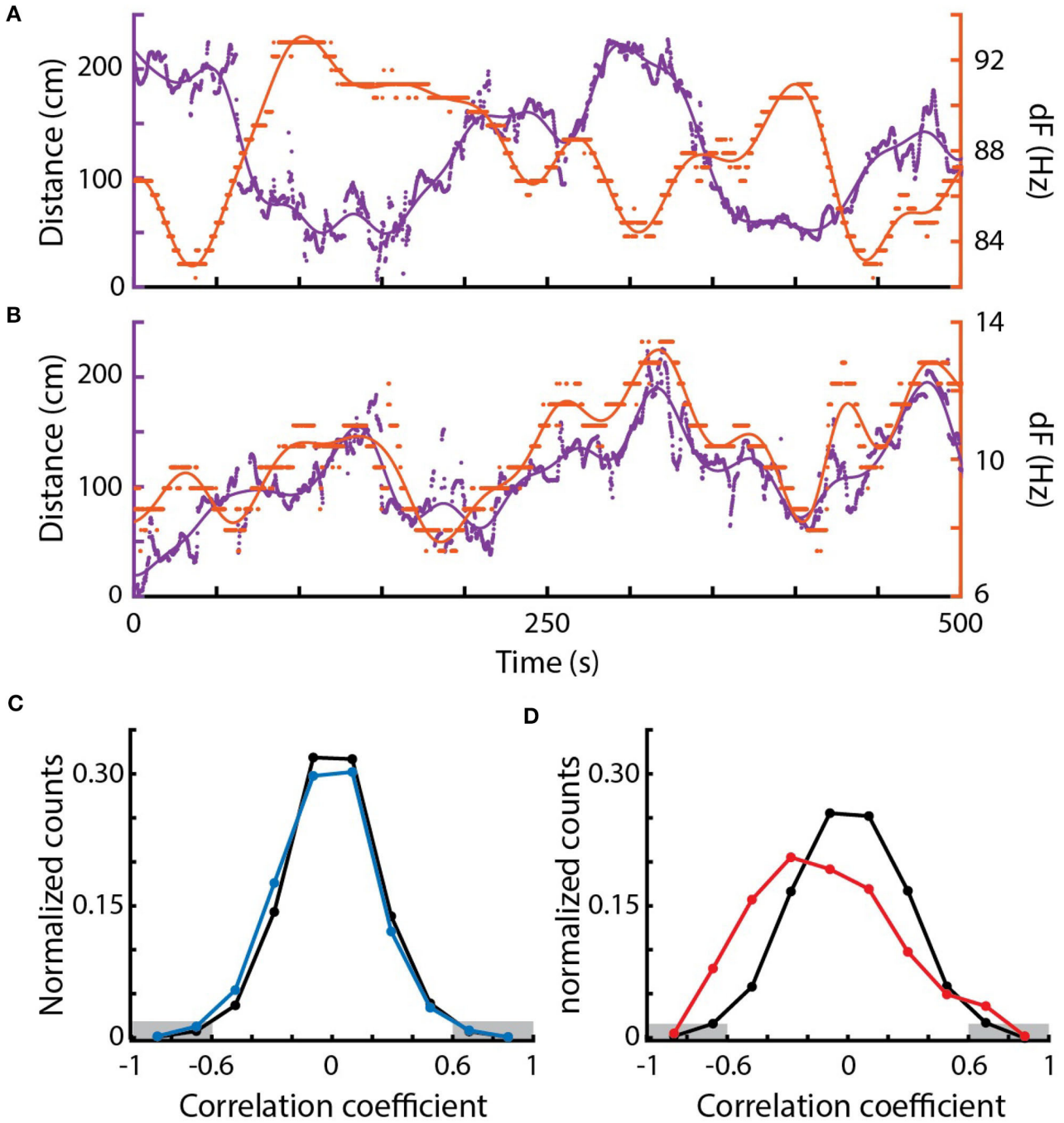

FIGURE 5 | Correlations between EOD frequency and movement. **(A)** Example of a strong negative correlation between distance (purple, left) and dF (orange, right) of a pair of *Eigenmannia* over a period of 500 s. Dots are measurements, lines are low-pass fits of the data. **(B)** Example of a strong positive correlation. **(C)** Distribution of Pearson correlations between distance and dF for surface fish (blue) and shuffled data (black). **(D)** Distribution of Pearson correlations between distance and dF for cavefish (red) and shuffled data (black). There were significantly more strong Pearson correlations, below −0.6 and above 0.6 (marked in gray) in the original data when compared to the shuffled data in cavefish but not surface fish.

about 50 cm, maintained dFs of below 10 Hz for minutes. Finally, cavefish but not surface fish exhibited strong correlations between relative movement and dF—a behavior known as an envelope response.

4.1. Energetics

The EOD amplitudes of the troglobitic *Eigenmannia* were, on average, higher than the nearby surface fish. This may be in part due to body size: a previous report (Bichuette and Trajano, 2006)

showed that the cavefish are generally larger than the surface fish. Further, our preliminary anatomical evidence from diceCT scans suggest that the electric organs of cavefish may also be relatively larger than in the surface fish. Irrespective of size, the energetic cost of generating electric fields is high, consuming up to one quarter of an individual's energy budget (Salazar et al., 2013; Markham et al., 2016). The fact that cave *Eigenmannia* produce such energetically costly electric fields suggests that sufficient food resources are available and accessible. The loss of eyes and pigment in these cavefish, therefore, is likely not under strong selection for energetic costs, but rather neutral selection (Jeffery, 2009).

Indeed, Gymnotiform fishes throughout the Amazon basin have relatively small eyes. Over the years, we have encountered many individual fish with missing or damaged eyes. Further, we routinely observe dense infestations of nematode parasites in the eyes of individuals from a related genus, *Apteronotus*. These anecdotal observations are consistent with the theory that Gymnotiform fishes rely more heavily on electric sensing than vision for survival and reproduction. Gymnotiform fishes, including the troglobitic weakly electric cavefish *Eigenmannia vicentespelea*, represent a unique opportunity to study evolutionary changes related to sensory perception and behavioral control.

4.2. EOD Frequencies

The distributions of EOD frequencies in both of these groups of *Eigenmannia* were not strongly bi-modal, which is similar to previous observations of *Eigenmannia* in Ecuador (Tan et al., 2005). Further, we were not able to identify any frequency-dependent signaling that might be correlated with sex. Sex differences in EOD frequencies are well-known in *Apteronotus* (Fugère et al., 2010; Raab et al., 2019) and *Sternopygus* (Hopkins, 1972), and there may be sex differences in EOD frequencies in *Eigenmannia* (Dunlap and Zakon, 1998).

There was a significant difference in the distributions of EOD frequencies between the cavefish and surface fish, but the meaning of these differences remains unclear. The larger range of frequencies seen in the cavefish may be due to sustained interactions related to territoriality—fish in adjacent territories may increase their dFs over time due to sustained stimulation of the neural circuitry that controls the JAR (Oestreich and Zakon, 2002, 2005).

Unexpectedly, we observed instances of sustained, low-frequency dFs in both surface and cavefish. In laboratory settings, in which artificial mimics of conspecific signals were presented to fish (Watanabe and Takeda, 1963; Heiligenberg, 1973), low frequency dFs activate the JAR, which results in higher dFs. For such experiments, fish are typically held in tubes or other restraints to reduce movement (Watanabe and Takeda, 1963; Hitschfeld et al., 2009). In the laboratory, low-frequency dFs have been shown to impair electrolocation (Heiligenberg, 1973; Ramcharitar et al., 2005). In the wild, fish could rely on JARs to avoid jamming, or could move further apart to lower the effects of jamming signals (Tan et al., 2005). There is some evidence, however, that fish actively match EOD frequencies or jam each other with similar EOD frequencies (Tallarovic and Zakon, 2002).

It seems unlikely that the surface fish were experiencing significant impairment of sensory function despite the ongoing low-frequency jamming: these fish were engaged in feeding on prey under the substrate in complete darkness. If the active electrosensory system was indeed impaired by the low-frequency jamming, it is possible that the fish were instead relying on their ampullary electroreceptors. Studies in *Apteronotus albifrons* demonstrates that fish may use ampullary receptors to detect exogenously generated electric fields for prey capture (Nelson and MacIver, 1999). In addition, elasmobranchs have also been shown to detect and discriminate signals from substrate-bound prey using passive electroreception mediated by ampullary electroreceptors (Kalmijn, 1971, 1982). Clearly, the relations between the JAR and jamming differ between laboratory and field settings, reflecting the richer social and environmental milieu.

4.3. Territoriality

Territoriality is a form of space-related dominance (Kaufmann, 1983). The most prominent function of having a territory is to provide the holder with a secured supply of resources. In the epigean streams outside of the Terra Ronca cave, food resources for *Eigenmannia* appear to be widely distributed in sandy substrates. Our guess is that the size and distribution of prey items precludes territorial defense of food resources. On the other hand, we expect to find evidence of territoriality during the day, as refugia likely vary in quality and are relatively small.

Why cavefish exhibit evidence of territoriality is unclear. There are no known predators of *Eigenmannia* in the cave, eliminating the value of protective refugia. Territoriality may occur as a result of uneven distribution of food resources in the cave, due to other physical features that impact the fish, or a consequence of plesiomorphic social and/or reproductive behaviors. Territoriality has been described in other genera, such as *Gymnotus* (Zubizarreta et al., 2020).

4.4. Spooky Interactions at a Distance

The strength of electric fields in water decay at a rate of approximately distance cubed (Henninger et al., 2018). As a result, the distances between fish determine the strength of the interaction of their electric fields: nearby fish will experience higher EOD voltages than from those of distant fish. Because the EODs of *Eigenmannia* are nearly sinusoidal, distance will have an effect on the amplitude of modulations caused by the summation of EODs: nearby fish will have large amplitude modulations near 100%, whereas distant fish will have far lower depths of modulation, below 10%. The relative movement between fish will cause concomitant changes in the strengths of EODs and depths of modulation that are proportional to distance. The changes are known as "envelopes"—the modulation of amplitude modulations. Envelope stimuli can elicit changes in electric field frequencies in *Eigenmannia* and other Gymnotiform species (Stamper et al., 2013; Thomas et al., 2018). In other animals, sensory envelopes are used in a wide array of behavioral contexts including speech perception (Ríos-López et al., 2017) and stereopsis (Tanaka and Ohzawa, 2006).

We found strong correlations between distance and pairwise differences in EOD frequencies at large distances

of over 1.5 m and dFs of over 50 Hz. These results are similar to reports from field studies that examined other Gymnotiform species (Henninger et al., 2018; Raab et al., 2019). These field studies suggest that electric fish are far more sensitive to electrosocial stimuli than previously appreciated, requiring a reexamination of the neural systems for their perception.

Negative correlations between distance and dF are likely driven by the amplitude envelope of electrical interference patterns, producing JAR-like behavioral responses (Stamper et al., 2012). These findings show that laboratory studies of envelope responses are ecologically relevant (Stamper et al., 2012, 2013; Metzen and Chacron, 2013; Huang and Chacron, 2016; Thomas et al., 2018). Cavefish also exhibited significantly more positive correlations between distance and dF. These positive correlations may be aggressive signals in which fish actively jam each other (Tallarovic and Zakon, 2002).

Changes is dF may also be mediated by the simultaneous interactions of EODs of more than two fish (Partridge and Heiligenberg, 1980; Stamper et al., 2012). Our analyses were limited to pairwise interactions. It is likely that the changes in EOD frequencies that we observed included responses to features of electrosensory signals, including "social envelopes" (Stamper et al., 2012), that emerged as a result of interactions between three or more fish. Weakly electric fish have been shown to discriminate between envelopes that are generated in different contexts (Thomas et al., 2018). Importantly, pairwise analyses like those used above do not capture higher order group dynamics (Miller et al., 2013). Such undiscovered emergent dynamics may have dramatic influences on both the movements and EOD frequencies of individuals within aggregations of freely moving *Eigenmannia*.

DATA AVAILABILITY STATEMENT

The raw data supporting the conclusions of this article will be made available by the authors, without undue reservation.

ETHICS STATEMENT

The animal study was reviewed and approved by Rutgers Newark Institutional Animal Care and Use Committee.

AUTHOR CONTRIBUTIONS

MB, DS, and EF conceived and executed the field research. NA, MM, RJ, and EF analyzed the electrical data. DS collected and analyzed the diceCT data. MM, RJ, and NC contributed to the design, use, and analysis of data from the grid system. All authors contributed to the preparation of the manuscript.

FUNDING

This work was supported by a collaborative National Science Foundation (NSF) Award to NC (1557895) and EF (1557858). The field work was supported by startup funds provided by the New Jersey Institute of Technology to DS. MB received funding from the CNPq (Awards 308557/2014-0).

ACKNOWLEDGMENTS

Field research permits were granted by the ICMBio and SEMARH/SECIMA. We would like to thank D. F. Torres, M. J. Rosendo, and C. C. P. de Paula for help in the field. Thanks to Dr. Jessica Ware for the use of the CT scanner. This manuscript has been released as a pre-print at Fortune et al. (2019).

SUPPLEMENTARY MATERIAL

The Supplementary Material for this article can be found online at: https://www.frontiersin.org/articles/10.3389/fnint.2020.561524/full#supplementary-material

Supplementary Video 1 | There are two scenes in the video. Several *Eigenmannia trilineata* feed on prey below the substrate. We can see that the fish are separated by distances on the order of single body lengths, between 10 and 20 cm, while foraging. The fish are mostly oriented head-first into the flow of the water. Visible light is provided by a handheld flashlight shone from above. As we have seen at other study sites in the Amazon basin, weakly electric fish often show little or no reaction to flashlights during dark nights. In the second scene, a solitary fish swims by the camera. The tail shows clear evidence of regrowth, possibly from a predation event or an injury caused by a conspecific.

Supplementary Video 2 | Eyeless *Eigenmannia vicentespelea* are seen swimming in tight groups under rocks, and as individuals along sandy substrates. Unlike the surface fish, the cavefish were disturbed by filming and retreated from the open areas where they were swimming into adjacent rocky outcrops. Social interactions include coordinated face-to-face swimming, which is likely mediated by their electric sense. The social interactions and movements of these fish are, to our eyes, as complex as those seen in sighted species of *Eigenmannia*. No foraging behavior similar to that seen in the surface fish was filmed.

REFERENCES

Allen, K. M., and Marsat, G. (2019). Neural processing of communication signals: the extent of sender–receiver matching varies across species of apteronotus. *Eneuro* 6:ENEURO.0392-18.2019. doi: 10.1523/ENEURO.0392-18.2019

Assad, C., Rasnow, B., Stoddard, P., and Bower, J. (1998). The electric organ discharges of the gymnotiform fishes: II. *Eigenmannia*. *J. Compar. Physiol. A* 183, 419–432. doi: 10.1007/s003590050268

Bastian, J. (1981). Electrolocation I. how electroreceptors of *Apteronotus albifrons* code for moving objects and other electrical stimuli. *J. Compar. Physiol. A* 144, 465–479. doi: 10.1007/BF01326832

Bichuette, M., and Trajano, E. (2003). Epigean and subterranean ichthyofauna from the São Domingos karst area, Upper Tocantins River basin, Central Brazil. *J. Fish Biol.* 63, 1100–1121. doi: 10.1046/j.1095-8649.2003.00227.x

Bichuette, M., and Trajano, E. (2006). Morphology and distribution of the cave knifefish *Eigenmannia vicentespelaea* triques, 1996 (gymnotiformes: Sternopygidae) from Central Brazil, with an expanded diagnosis and comments on subterranean evolution. *Neotrop. Ichthyol.* 4, 99–105. doi: 10.1590/S1679-62252006000100011

Bichuette, M., and Trajano, E. (2015). Population density and habitat of an endangered cave fish *Eigenmannia vicentespelaea* Triques, 1996 (Ostariophysi: Gymnotiformes) from a karst area in central Brazil. *Neotrop. Ichthyol.* 13, 113–122. doi: 10.1590/1982-0224-20140095

Bichuette, M., and Trajano, E. (2017). Biology and behavior of *Eigenmannia vicentespelaea*, a troglobitic electric fish from Brazil (Teleostei: Gymnotiformes: Sternopygidae): a comparison to the epigean species, *E. trilineata*, and the consequences of cave life. *Trop. Zool.* 30, 68–82. doi: 10.1080/03946975.2017.1301141

Crampton, W. G. R. (2019). Electroreception, electrogenesis and electric signal evolution. *J. Fish Biol.* 95, 92–134. doi: 10.1111/jfb.13922

Culver, D., and Pipan, T. (2019). *The Biology of Caves and Other Subterranean Habitats*. Oxford: Oxford University Press.

Davis, E., and Hopkins, C. (1988). Behavioural analysis of electric signal localization in the electric fish, *Gymnotus carapo* (Gymnotiformes). *Anim. Behav.* 36, 1658–1671. doi: 10.1016/S0003-3472(88)80106-4

Dunlap, K., and Zakon, H. (1998). Behavioral actions of androgens and androgen receptor expression in the electrocommunication system of an electric fish, *Eigenmannia virescens*. *Horm. Behav.* 34, 30–38. doi: 10.1006/hbeh.1998.1460

Fortune, E., Andanar, N., Madhav, M., Jayakumar, R., Cowan, N., Bichuette, M., et al. (2019). Spooky interaction at a distance in cave and surface dwelling electric fishes. *bioRxiv*. doi: 10.1101/747154

Fugère, V., Ortega, H., and Krahe, R. (2010). Electrical signalling of dominance in a wild population of electric fish. *Biol. Lett.* 7, 197–200. doi: 10.1098/rsbl.2010.0804

Heiligenberg, W. (1973). Electrolocation of objects in the electric fish *Eigenmannia* (rhamphichthyidae, gymnotoidei). *J. Compar. Physiol.* 87, 137–164. doi: 10.1007/BF01352158

Heiligenberg, W. (1991). *Neural Nets in Electric Fish (Computational Neuroscience)*. Cambridge, MA: MIT press.

Henninger, J., Krahe, R., Kirschbaum, F., Grewe, J., and Benda, J. (2018). Statistics of natural communication signals observed in the wild identify important yet neglected stimulus regimes in weakly electric fish. *J. Neurosci.* 38, 5456–5465. doi: 10.1523/JNEUROSCI.0350-18.2018

Henninger, J., Krahe, R., Sinz, F., and Benda, J. (2020). Tracking activity patterns of a multispecies community of gymnotiform weakly electric fish in their neotropical habitat without tagging. *J. Exp. Biol.* 223:jeb206342. doi: 10.1242/jeb.206342

Hitschfeld, E. M., Stamper, S. A., Vonderschen, K., Fortune, E. S., and Chacron, M. J. (2009). Effects of restraint and immobilization on electrosensory behaviors of weakly electric fish. *ILAR J.* 50, 361–372. doi: 10.1093/ilar.50.4.361

Hopkins, C. (1972). Sex differences in electric signaling in an electric fish. *Science* 176, 1035–1037. doi: 10.1126/science.176.4038.1035

Huang, C., and Chacron, M. (2016). Optimized parallel coding of second-order stimulus features by heterogeneous neural populations. *J. Neurosci.* 36, 9859–9872. doi: 10.1523/JNEUROSCI.1433-16.2016

Hupe, G., and Lewis, J. (2008). Electrocommunication signals in free swimming brown ghost knifefish, *Apteronotus leptorhynchus*. *J. Exp. Biol.* 211, 1657–1667. doi: 10.1242/jeb.013516

Jeffery, W. (2009). Regressive evolution in Astyanax cavefish. *Annu. Rev. Genet.* 43, 25–47. doi: 10.1146/annurev-genet-102108-134216

Kalmijn, A. (1971). The electric sense of sharks and rays. *J. Exp. Biol.* 55, 371–383.

Kalmijn, A. (1982). Electric and magnetic field detection in elasmobranch fishes. *Science* 218, 916–918. doi: 10.1126/science.7134985

Kaufmann, J. (1983). On the definitions and functions of dominance and territoriality. *Biol. Rev.* 58, 1–20. doi: 10.1111/j.1469-185X.1983.tb00379.x

Madhav, M., Jayakumar, R., Demir, A., Stamper, S., Fortune, E., and Cowan, N. (2018). High-resolution behavioral mapping of electric fishes in Amazonian habitats. *Sci. Rep.* 8:5830. doi: 10.1038/s41598-018-24035-5

Madhav, M., Stamper, S., Fortune, E., and Cowan, N. (2013). Closed-loop stabilization of the jamming avoidance response reveals its locally unstable and globally nonlinear dynamics. *J. Exp. Biol.* 216, 4272–4284. doi: 10.1242/jeb.088922

Markham, M., Ban, Y., McCauley, A., and Maltby, R. (2016). Energetics of sensing and communication in electric fish: a blessing and a curse in the anthropocene? *Integr. Compar. Biol.* 56, 889–900. doi: 10.1093/icb/icw104

Markham, M., McAnelly, L., Stoddard, P., and Zakon, H. (2009). Circadian and social cues regulate ion channel trafficking. *PLoS Biol.* 7:e1000203. doi: 10.1371/journal.pbio.1000203

Markham, M. R. (2013). Electrocyte physiology: 50 years later. *J. Exp. Biol.* 216, 2451–2458. doi: 10.1242/jeb.082628

Metzen, M., and Chacron, M. (2013). Weakly electric fish display behavioral responses to envelopes naturally occurring during movement: implications for neural processing. *J. Exp. Biol.* 217, 1381–1391. doi: 10.1242/jeb.098574

Metzen, M., Fortune, E., and Chacron, M. (2017). "Physiology of tuberous electrosensory systems," in *Reference Module in Life Sciences* (Elsevier), 1–13. doi: 10.1016/B978-0-12-809633-8.03045-4

Metzen, M. G. (2019). Encoding and perception of electro-communication signals in apteronotus leptorhynchus. *Front. Integra. Neurosci.* 13:39. doi: 10.3389/fnint.2019.00039

Migliaro, A., Moreno, V., Marchal, P., and Silva, A. (2018). Daily changes in the electric behavior of weakly electric fish naturally persist in constant darkness and are socially synchronized. *Biol. Open* 7:bio036319. doi: 10.1242/bio.036319

Miller, N., Garnier, S., Hartnett, A. T., and Couzin, I. D. (2013). Both information and social cohesion determine collective decisions in animal groups. *Proc. Natl. Acad. Sci. U.S.A.* 110, 5263–5268. doi: 10.1073/pnas.1217513110

Nelson, M., and MacIver, M. (1999). Prey capture in the weakly electric fish *Apteronotus albifrons*: sensory acquisition strategies and electrosensory consequences. *J. Exp. Biol.* 202, 1195–1203.

Nelson, M., Xu, Z., and Payne, J. (1997). Characterization and modeling of P-type electrosensory afferent responses to amplitude modulations in a wave-type electric fish. *J. Compara. Physiol. A* 181, 532–544. doi: 10.1007/s003590050137

Oestreich, J., and Zakon, H. H. (2002). The long-term resetting of a brainstem pacemaker nucleus by synaptic input: a model for sensorimotor adaptation. *J. Neurosci.* 22, 8287–8296. doi: 10.1523/JNEUROSCI.22-18-08287.2002

Oestreich, J., and Zakon, H. H. (2005). Species-specific differences in sensorimotor adaptation are correlated with differences in social structure. *J. Compar. Physiol. A* 191, 845–856. doi: 10.1007/s00359-005-0006-4

Partridge, B. L., and Heiligenberg, W. (1980). Three's a crowd? Predicting eigenmannia's responses to multiple jamming. *J. Compar. Physiol. A* 136, 153–164. doi: 10.1007/BF00656909

Pedraja, F., Hofmann, V., Lucas, K., Young, C., Engelmann, J., and Lewis, J. (2018). Motion parallax in electric sensing. *Proc. Natl. Acad. Sci. U.S.A.* 115, 573–577. doi: 10.1073/pnas.1712380115

Pipan, T., Culver, D. C., Papi, F., and Kozel, P. (2018). Partitioning diversity in subterranean invertebrates: the epikarst fauna of Slovenia. *PLoS ONE* 13:e0195991. doi: 10.1371/journal.pone.0195991

Raab, T., Linhart, L., Wurm, A., and Benda, J. (2019). Dominance in habitat preference and diurnal explorative behavior of the weakly electric fish *Apteronotus leptorhynchus*. *Front. Integr. Neurosci.* 13:21. doi: 10.3389/fnint.2019.00021

Ramcharitar, J., Tan, E., and Fortune, E. (2005). Effects of global electrosensory signals on motion processing in the midbrain of *Eigenmannia*. *J. Compar. Physiol. A* 191, 865–872. doi: 10.1007/s00359-005-0008-2

Ríos-López, P., Molnar, M. T., Lizarazu, M., and Lallier, M. (2017). The role of slow speech amplitude envelope for speech processing and reading development. *Front. Psychol.* 8:1497. doi: 10.3389/fpsyg.2017.01497

Salazar, V., Krahe, R., and Lewis, J. (2013). The energetics of electric organ discharge generation in gymnotiform weakly electric fish. *J. Exp. Biol.* 216, 2459–2468. doi: 10.1242/jeb.082735

Sinnett, P., and Markham, M. (2015). Food deprivation reduces and leptin increases the amplitude of an active sensory and communication signal in a weakly electric fish. *Horm. Behav.* 71, 31–40. doi: 10.1016/j.yhbeh.2015.03.010

Stamper, S., Carrera,-G., E., Tan, E., Fugere, V., Krahe, K., Fortune, E. S., et al. (2010). Species differences in group size and electrosensory interference in weakly electric fishes: implications for electrosensory processing. *Behav. Brain Res.* 207, 368–376. doi: 10.1016/j.bbr.2009.10.023

Stamper, S., Fortune, E., and Chacron, M. (2013). Perception and coding of envelopes in weakly electric fishes. *J. Exp. Biol.* 216, 2393–2402. doi: 10.1242/jeb.082321

Stamper, S., Madhav, M., Cowan, N., and Fortune, E. (2012). Beyond the jamming avoidance response: weakly electric fish respond to the envelope of social electrosensory signals. *J. Exp. Biol.* 215, 4196–4207. doi: 10.1242/jeb.076513

Stoddard, P., Zakon, H., Markham, M., and McAnelly, L. (2006). Regulation and modulation of electric waveforms in gymnotiform electric fish. *J. Compar. Physiol. A* 192, 613–624. doi: 10.1007/s00359-006-0101-1

Tallarovic, S., and Zakon, H. (2002). Electrocommunication signals in female brown ghost electric knifefish, *Apteronotus leptorhynchus*.

J. Compar. Physiol. A 188, 649–657. doi: 10.1007/s00359-002-0344-4

Tan, E., Nizar, J., Carrera,-G., E., and Fortune, E. (2005). Electrosensory interference in naturally occurring aggregates of a species of weakly electric fish, *Eigenmannia virescens*. *Behav. Brain Res.* 164, 83–92. doi: 10.1016/j.bbr.2005.06.014

Tanaka, H., and Ohzawa, I. (2006). Neural basis for stereopsis from second-order contrast cues. *J. Neurosci.* 26, 4370–4382. doi: 10.1523/JNEUROSCI.4379-05.2006

Thomas, R., Metzen, M., and Chacron, M. (2018). Weakly electric fish distinguish between envelope stimuli arising from different behavioral contexts. *J. Exp. Biol.* 221:jeb178244. doi: 10.1242/jeb.178244

Triques, M. (1996). *Eigenmannia vicentespelaea*, a new species of cave dwelling electrogenic neotropical fish (Ostariophysi: Gymnotiformes: Sternopygidae). *Rev. Franc. Aquariol.* 23, 1–4.

Walz, H., Hupé, G. J., Benda, J., and Lewis, J. E. (2013). The neuroethology of electrocommunication: how signal background influences sensory encoding and behaviour in apteronotus leptorhynchus. *J. Physiol.* 107, 13–25. doi: 10.1016/j.jphysparis.2012.07.001

Watanabe, A., and Takeda, K. (1963). The change of discharge frequency by A.C. stimulus in a weak electric fish. *J. Exp. Biol.* 40, 57–66.

Yu, N., Hupe, G., Longtin, A., and Lewis, J. (2019). Electrosensory contrast signals for interacting weakly electric fish. *Front. Integr. Neurosci.* 13:36. doi: 10.3389/fnint.2019.00036

Zepon, T., and Bichuette, M. E. (2017). Influence of substrate on the richness and composition of neotropical cave fauna. *Anais Acad. Brasil. Ciênc.* 89, 1615–1628. doi: 10.1590/0001-3765201720160452

Zubizarreta, L., Quintana, L., Hernández, D., Teixeira de Mello, F., M, M., Honji, R., Guimarães Moreira, R., et al. (2020). Seasonal and social factors associated with spacing in a wild territorial electric fish. *bioRxiv*. doi: 10.1101/2020.01.29.924761

Conflict of Interest: The authors declare that the research was conducted in the absence of any commercial or financial relationships that could be construed as a potential conflict of interest.

Advantages of publishing in Frontiers

OPEN ACCESS
Articles are free to read for greatest visibility and readership

FAST PUBLICATION
Around 90 days from submission to decision

HIGH QUALITY PEER-REVIEW
Rigorous, collaborative, and constructive peer-review

TRANSPARENT PEER-REVIEW
Editors and reviewers acknowledged by name on published articles

Frontiers
Avenue du Tribunal-Fédéral 34
1005 Lausanne | Switzerland

Visit us: www.frontiersin.org
Contact us: frontiersin.org/about/contact

REPRODUCIBILITY OF RESEARCH
Support open data and methods to enhance research reproducibility

DIGITAL PUBLISHING
Articles designed for optimal readership across devices

FOLLOW US
@frontiersin

IMPACT METRICS
Advanced article metrics track visibility across digital media

EXTENSIVE PROMOTION
Marketing and promotion of impactful research

LOOP RESEARCH NETWORK
Our network increases your article's readership